Novel technologies for antibody hit discovery and engineering of antibody-like proteins with therapeutic relevance

TECHNISCHE UNIVERSITÄT DARMSTADT

Vom Fachbereich Chemie

der Technischen Universität Darmstadt

zur Erlangung des Grades

Doctor rerum naturalium (Dr. rer. nat.)

Dissertation

eingereicht von

Lukas Pekar, M. Eng.

aus Rüsselsheim

Referent: Prof. Dr. rer. nat. Harald Kolmar

Korreferent: Prof. Dr. rer. nat. Dr. med. h.c. Siegfried Neumann

Darmstadt 2020

Lukas Pekar:

Novel technologies for antibody hit discovery and engineering of antibody-like proteins with therapeutic relevance

Darmstadt, Technische Universität Darmstadt

Jahr der Veröffentlichung der Dissertation auf TUprints: 2021

Tag der mündlichen Prüfung: 07.12.2020

Die vorliegende Arbeit wurde unter der Leitung von Herrn Prof. Dr. Harald Kolmar am Clemens-Schöpf-Institut für Organische Chemie und Biochemie der Technischen Universität Darmstadt sowie bei Merck KGaA in Darmstadt von Juli 2017 bis Oktober 2020 angefertigt.

Publications and patents derived from this work

Parts of this work have been published or are currently under review.

Publications as first or shared first author:

- **Lukas Roth***, Julius Grzeschik*, Steffen C. Hinz, Stefan Becker, Lars Toleikis, Michael Busch, Harald Kolmar, Simon Krah and Stefan Zielonka
  Facile generation of antibody heavy and light chain diversities for yeast surface display by Golden Gate Cloning
  Biological Chemistry 2019

- Carolin Sellmann*, **Lukas Pekar***, Christina Bauer, Elke Ciesielski, Simon Krah, Stefan Becker, Lars Toleikis, Jonas Kügler, André Frenzel, Bernhard Valldorf, Michael Hust, Stefan Zielonka
  A One-Step Process for the Construction of Phage Display scFv and VHH Libraries
  Molecular Biotechnology 2020

- **Lukas Pekar**, Michael Busch, Bernhard Valldorf, Steffen C. Hinz, Lars Toleikis, Simon Krah, Stefan Zielonka
  Biophysical and biochemical characterization of a VHH-based IgG-like bi- and trispecific antibody platform
  mAbs 2020

- **Lukas Pekar***, Katja Klausz*, Michael Busch, Bernhard Valldorf, Harald Kolmar, Daniela Wesch, Hans-Heinrich Oberg, Steffen Krohn, Ammelie Boje, Carina-Lynn Gehlert, Lars Toleikis, Simon Krah, Tushar Gupta, Brian Rabinovich, Stefan Zielonka and Matthias Peipp
  Affinity maturation of B7-H6 translates into enhanced NK cell-mediated tumor cell lysis and improved proinflammatory cytokine release of bispecific immunoligands via NKp30 engagement
  Submitted (2020)

- Janina Klemm*, **Lukas Pekar***, Simon Krah and Stefan Zielonka
  Antibody Display Systems
  Accepted for publication in Introduction to Antibody Engineering (2020)

- **Lukas Roth**, Simon Krah, Ralf Guenther, Lars Toleikis, Michael Busch, Stefan Becker and Stefan Zielonka
  Isolation of antigen-specific VHH single domain antibodies by combining animal immunization with yeast surface display
  Methods in Molecular Biology 2020

Other publications:

- Julius Grzeschik, Desislava Yanakieva, **Lukas Roth**, Simon Krah, Steffen C. Hinz, Adrian Elter, Tina Zollmann, Gerhard Schwall, Stefan Zielonka, and Harald Kolmar
  Yeast Surface Display in Combination with Fluorescence-activated Cell Sorting Enables the Rapid Isolation of Antibody Fragments Derived from Immunized Chickens
  Biotechnology Journal 2019

- Bernhard Valldorf*, Steffen C. Hinz*, Giulio Russo, **Lukas Pekar***, Laura Mohr, Janina Klemm, Achim Doerner, Simon Krah, Michael Hust and Stefan Zielonka
  Antibody Display Technologies – Selecting the cream of the crop
  Submitted (2020)

Patent applications:

- Stefan Zielonka, **Lukas Pekar**, Simon Krah and Lars Toleikis
  Affinity optimized versions of B7-H6 for NK cell engagement
  European patent office reference EP20193930.3
  Patent application filed September 2020

- Stefan Zielonka, **Lukas Pekar**, Simon Krah and Lars Toleikis
  Anti-NKp30 VHHs for efficient NK cell engagement
  Technische Universität Darmstadt reference 2020/16, Merck KGaA reference I20-064
  Patent application in preparation, invention report listed September 2020

*These authors contributed equally to the respective publication.

Table of content

1 Zusammenfassung und wissenschaftlicher Erkenntnisgewinn

Im Jahr 1975 konnten die Wissenschaftler Köhler und Milstein erfolgreich B-Lymphozyten aus immunisierten Mäusen mit Myelomzellen fusionieren und mittels dieses, als Hybridoma Technologie bezeichneten Verfahrens, Zellen erzeugen die Vorteile beider Vorgängerzellen vereinten. Diese immortalisierten Hybridomazellen sind sowohl kultivierbar, als auch in der Lage Antigen spezifische Antikörper zu sezernieren. Ihre bahnbrechende Erfindung für die Herstellung von Antikörpern wurde 1984 mit dem Nobelpreis honoriert.

Allerdings stellt die Hybridoma Technologie einen langwierigen Prozess mit geringer Effizienz dar. Zusätzlich ergibt sich durch die murine Herkunft der Antikörper eine potenzielle Immungenitätsproblematik bei Applikation im Menschen.

Aus diesen Gründen wurden in den letzten Jahrzehnten verschiedene Technologien zur Überwindung dieser Limitationen entwickelt. Sie umfassen dabei die Nutzung von humanen naiven, semi- oder komplett synthetischen Antikörperdiversitäten (zur Vermeidung der Immungenitätsproblematik) in Verbindung mit zellulären oder nicht-zellulären in vitro Selektionssystemen zur Präsentation und Isolation von Antikörpern, wie z.B. das Phagen- oder Hefe-Display. Durch die Entwicklung dieser Methoden konnten große Repertoires bezüglich vorgegebener Eigenschaften durchmustert und spezifische Moleküle isoliert werden, was den heutigen, erfolgreichen Einsatz von monoklonalen Antikörpern in biotechnologischen und medizinischen Anwendungen unterstützte. Trotz aller Verbesserungen im Antikörperfindungsprozess stellt die Generierung der initialen Display-Bibliotheken immer noch einen aufwendigen und anspruchsvollen Prozess dar. Dieser ist oft mehrstufig und umfasst am Beispiel des Hefe-Displays verschiedene Klonierungsschritte, die Erstellung von getrennten Bibliotheken für schwere und leichte Ketten, sowie letztlich deren Paarung durch *Mating*.

Dieser Ablauf kann durch die Anwendung von *Golden Gate Cloning* (GGC) vereinfacht werden und in nur einer Reaktion erfolgen. Die Klonierungsreaktion im GGC beruht dabei auf der Nutzung von Typ IIs Restriktionsenzymen. Diese Enzyme schneiden DNA in einer definierten Distanz außerhalb ihrer Erkennungssequenzen und ermöglichen dadurch die Inkorporation von Überhängen mit gewünschter Signatur. Typ IIs Restriktionsenzyme erlauben somit einen gerichteten, einstufigen Klonierungsprozess, bei dem die Erkennungssequenzen während der Reaktion entfernt und das Reaktionsgleichgewicht auf die Seite des spezifischen Klonierungsproduktes verschoben wird.

In der vorliegenden Arbeit konnte anhand von drei unterschiedlichen Selektionskampagnen die Anwendbarkeit von GGC für die Bibliotheks-Generierung im Hefen- und Phagen-Display demonstriert werden.

Dabei wurden spezifische Fab Antikörper gegen CEACAM6, EGFR und hCG aus Immunrepertoiren von transgenen Ratten und Wildtyp Hühnern (Hefe-Display), sowie EGFR spezifische scFv und VHH Antikörper aus Immunrepertoiren von Hühnern und Kameliden (Phagen-Display) isoliert. GGC konnte dabei im

Vergleich zur klassischen Generierung von Antikörper-Bibliotheken bezüglich Verteilungen der Genrepertoires, der allgemeinen Bibliotheks-Größen, sowie biophysikalischer Charakteristika der isolierten Antikörper validiert werden. Der entwickelte, einstufige GGC Prozess ist in der Lage Antikörper Bibliotheken basierend auf kombinatorischen schweren und leichten Ketten Diversitäten mit gleicher Qualität gegenüber der traditionellen Methode zu generieren. Zusätzlich bietet er den Vorteil einer schnelleren und weniger aufwendigen Methodik, da er die multiplen Schritte des traditionellen Ansatzes parallelisiert.

Neben klassischen monoklonalen Antikörpern und Antikörperfragmenten bieten neue Antikörperformate Ansätze zur therapeutischen Anwendung. Dazu zählen Moleküle wie bispezifische Antikörper (bsAbs) und Immunoliganden, sowie andere Antikörperfragmente und -derivate, z.B. kamelide Einzeldomänenantikörper-Fc Fusionen.
Bei der Herstellung von IgG-basierten bispezifischen Antikörpern, bestehend aus zwei unterschiedlichen schweren und zwei unterschiedlichen leichten Ketten, müssen theoretisch vier unterschiedlichen Plasmide für deren Expression in der Zellkultur eingesetzt werden, was zu einer statistischen Ausbeute von lediglich 12.5 % des gewünscht assembliertem Proteins führt. Eine Möglichkeit die Heterogenität bei der Expression von mehreren gleichgearteten Polypeptidketten zu umgehen, ist die Nutzung der Strand-Exchange Engineered Domain (SEED) Technologie. Durch die Einfügung alternierender IgA und IgG β-Faltblatt Strukturen in den CH3 Domänen, entstehen anti-parallele Immunglobulinstrukturen, die eine Heterodimerisierung der schweren Ketten begünstigen. Zur Vermeidung von Homodimerisierung der schweren Ketten wurden neben SEED noch andere Technologien wie „knob-into-holes“, controlled Fab arm exchange oder gezielte Aminosäure-Austausche zur Einführung von konträren elektrostatischen Ladungen in den beiden schweren Ketten entwickelt.
Um darüber hinaus eine leichte Ketten-Fehlpaarung der Antikörper zu verhindern, wurden ebenfalls diverse Technologien entwickelt, wie z.B. CrossMab oder die Nutzung einer Common Light Chain. Eine weitere Möglichkeit hierfür besteht zusätzlich in der Verwendung von kameliden VHH Domänen. Diese nutzen nicht die für den kanonischen Antikörper notwendige leichte Kette, sondern stellen eine spezifische Antigen-Bindung ausschließlich über die variable Domäne der schweren Kette her.

In diesem Kontext war ein Ziel der vorliegenden Arbeit die Kombination der SEED Technologie mit einem 2013 von Baty und Kollegen konzeptionell beschriebenen Fab ähnlichen bispezifischen VHH Antikörper.
Dies ermöglichte die Generierung einer neuartigen bi- und trispezifischen, IgG-ähnlichen VHH basierten Antikörperplattform mit damit verbundenen variablen Valenzen im Rahmen dieser Promotion. Die Ergebnisse der Charakterisierung dieses Antikörperformats bezüglich ihrer biophysikalischen und biochemischen Eigenschaften, wie z.B. spezifischem, NK-Zell vermitteltem ADCC, belegten die Vielseitigkeit dieser generischen Plattform zur Expression voll funktioneller mono-, bi und trispezifischer Antikörper mit unterschiedlichen Valenzen als „plug-and-play“ Anwendung.
Darüber hinaus ist der Einsatz von bispezifischen Molekülen für die gerichtete NK-Zell Rekrutierung in heutiger Zeit von großem Interesse. Die spezifische NK-Zell Rekrutierung zu tumorösen oder infizierten

Zellen ermöglicht eine spezifische Zytolyse der Zielzellen und die gleichzeitige Immunmodulation durch eine NK-Zell vermittelte Zytokin-Freisetzung.

Eine Möglichkeit, um die Rekrutierung von NK-Zellen zu adressieren, bieten die von diesen Zellen umfassend exprimierten Natürlichen Cytotoxischen Rezeptoren (NCRs). In dieser Arbeit konnte mittels Hefe-Display die bindungsrelevante *N*-terminale IgV-ähnliche Domäne des natürliche Liganden B7-H6 für den NCR Rezeptor NKp30 affinitätsmaturiert werden. Mittels *Fluorescence Activated Cell Sorting* (FACS) basierter Selektion wurden B7-H6 Varianten mit signifikant erhöhter Affinität zu NKp30 erhalten. Auch zeigten diese Varianten bei der Anwendung im Format bispezifischer Immunoliganden signifikant gesteigerte NK-Zell vermittelte Zytotoxizitäten und Zytokin-Freisetzungen gegenüber dem parentalen B7-H6 Molekül.

Diese Erkenntnisse belegen die zu Grunde liegende Hypothese, dass eine gesteigerte Affinität von B7-H6 zu NKp30 in einer erhöhten NK-Zell basierten Tumorzell-Zytolyse und einer gesteigerten NK-Zell vermittelten Sekretion von proinflammatorischen Zytokinen resultiert. Eine Affinitätssteigerung von natürlichen Liganden aktivierender NK-Rezeptoren könnte somit zur Entwicklung potenzieller Immuntherapeutika zur Behandlung von Patienten mit unterschiedlichen Krebserkrankungen verwendet werden.

2 Scientific novelty and overview

In 1975, scientists Köhler and Milstein successfully fused B-lymphocytes from immunized mice with myeloma cells and, through this procedure entitled hybridoma technology, were able to combine the advantages of both precursor cells. These immortalized cells are culturable and able to secrete antigen-specific antibodies. The scientists' invention, revolutionary for the production of monoclonal antibodies, was awarded with a Nobel Prize in 1984.

It became apparent, however, that the hybridoma technology is a lengthy process with low efficiency. In addition, the murine origin of the antibodies causes a potential problem with immunogenicity when applied to humans.

Several new technologies have been developed in the last decades in order to overcome these limitations. These technologies include the use of human naïve, semi-synthetic or synthetic antibody diversities (to avoid the immunogenicity issue) in combination with cellular or non-cellular in vitro selection systems for the presentation and isolation of antibodies, such as Phage or Yeast Display. By the invention of these methods, large repertoires could be examined for predefined characteristics, thus enabling the isolation of specific molecules, which advanced today's successful use of monoclonal antibodies in biotechnological and medical applications. Despite all improvements in the finding process of antibodies, the generation of initial display libraries is still complex and laborious. It is often a multistage process which, as with Yeast Display, encompasses multiple cloning steps, the generation of separated libraries for heavy and light chains as well as, ultimately, their mating. This process can be simplified and condensed to only one reaction through the application of *Golden Gate Cloning* (GGC). The cloning reaction within GGC is based on the use of Type IIs restriction enzymes, which digest DNA in a defined distance from their recognition sequences and, thereby, allow for the incorporation of overhangs with requested signatures. Type IIs restriction enzymes enable a targeted, single-stage cloning process in which all recognition sequences are removed during the reaction, thereby causing an equilibrium shift towards the specific cloning product.

As part of this work, the feasibility of GGC for the generation of Yeast and Phage Display libraries could be demonstrated for three different selection campaigns. Specific Fab antibodies against CEACAM6, EGFR and hCG were isolated from the immune repertoires of transgenic rats and wild type chickens (Yeast Display), and EGFR-specific scFv and VHH antibodies were isolated from the immune repertoires of chickens and camelids (Phage Display). In comparison to the traditional generation of antibody libraries, GGC could be validated with regards to gene repertoire distribution, the overall size of libraries as well as to the biophysical characteristics of isolated antibodies. The developed single-stage GGC process is able to generate antibody libraries based on combinatorial heavy and light chain diversities with the same quality as the traditional method. In addition, the process is a faster and less laborious method, which parallels the multiple steps of the original approach.

Besides classical monoclonal antibodies and antibody fragments, new antibody formats can broaden the therapeutic space of new biological entities. Among these are molecules such as bispecific antibodies (bsAbs) and immunoligands, as wells as other antibody fragments and derivates - such as camelid single domain antibody Fc-fusions.

In theory, four different plasmids have to be used during the expression of IgG-based bispecific antibodies in cell culture, as they consist of two different heavy chains and two different light chains. This would lead to a statistical yield of only 12.5 % of the desired assembled protein. The Strand Exchange Engineered Domain (SEED) technology is one possibility to avoid heterogeneity during the expression of several similar polypeptide chains. Through the introduction of alternating IgA and IgG β-sheet structures in the CH3 domains, antiparallel immunoglobulin structures occur, which promote a heterodimerization of the heavy chains. In order to avoid heavy chain homodimerization, additional technologies, such as "knob-into-holes", controlled Fab arm exchange or targeted amino acid exchanges used to introduce contrary electrostatic charges into both heavy chains have been developed.

Moreover, mispairing of antibodies light chains can be prevented by technologies such as CrossMab or the use of a Common Light Chain. Another possibility is the utilization of camelid VHH domains. VHHs, compared to canonical antibodies, provide specific antigen binding exclusively via the variable domain of the heavy chain.

In this context, it was one of the goals of the present work to combine the SEED Technology with a bispecific Fab-like VHH antibody which was conceptionally described by Baty and coworkers in 2013. This combination enabled the generation of a novel bi- and trispecific, IgG-like VHH-based antibody platform with related variable valences.

The results of the characterization of this antibody format with regards to its biophysical and biochemical characteristics - such as the specific NK cell-mediated ADCC - verify the versatility of the generic platform in expressing fully functional mono-, bi- and trispecific antibodies with different valences as a "plug and play" application.

Furthermore, the use of bispecific molecules for a targeted NK cell recruitment is of substantial interest nowadays. The specific NK cell recruitment towards tumorous or infected cells enables a specific cytolysis of target cells and a simultaneous immune modulation through NK cell-mediated cytokine release.

One possibility to address the recruitment of NK cells are the Natural Cytotoxicity Receptors (NCRs), comprehensively expressed by NK cells. For this work, and through the use of Yeast Display, the *N*-terminal IgV-like domain of B7-H6 (natural ligand of NKp30), which is relevant for receptor binding, could be affinity matured. Via *Fluorescence Activated Cell Sorting* (FACS)-based selection, B7-H6 variants with significantly increased affinity to NKp30 were achieved. Additionally, these variants showed significantly increased NK cell mediated cytotoxicities and cytokine release when used in the format of bispecific immunoligands, compared to the parental B7-H6 molecule.

These results verify the underlying hypothesis that an increased affinity of B7-H6 to NKp30 results in an increased NK cell-based tumor cell cytolysis as well as in increased NK cell-mediated secretion of

proinflammatory cytokines. An increased affinity of activating NK cell receptors natural ligands could, therefore, be used in the development of potential immunotherapies for the treatment of patients with various cancerous diseases.

3 Introduction

3.1 Antibodies

Lymphocytes are the prime mediators of the adaptive immune system, eliminating invading pathogens. They recognize the foreign structures by their specific antigen receptors. During lymphocyte maturation, B cells and T cells undergo a unique rearrangement of germline encoded, antigen independent gene segments, finally forming a specific B cell (BCR) or T cell (TCR) receptor, which then allows recognition of foreign structures. This process involves different stages of maturation and comprises several steps of genetic diversification, explained in more detail in the following sections.
Antibodies can be termed as "final product" of maturated and activated plasma B cells and represent the humoral immune response of the adaptive immune system in vertebrates, recognizing and binding to structures of foreign proteins.

The humoral immune response was first described by van Behring and Kitasato in 1890, who discovered an antitoxic blood serum component in immunized rodents which could neutralize diphtheria toxin [1]. In the 1930s, this discovery was refined by other scientists like Heidelberger and Kendall, however, especially by Tiselius and Kabat in 1939 [2], [3]. They were able to separate serum via electrophoresis into alpha (α), beta (β) and gamma (γ)-globulin fractions and showed "that the antibody function migrated with the γ-globulin fraction only", paving the way for the present terminology immunoglobulin (*Ig*) and IgG. The γ-globulin portion was then fractionated by sizing columns into heavy fraction, containing IgM, and regular fraction, comprising IgA, IgD, IgE and IgG.

3.1.1 Structure of antibodies

Antibodies are large molecules secreted by matured, activated plasma B cells, forming in monomeric state a Y-shaped molecule consisting of two similar homodimerized heavy chains and two identical light chains (H_2L_2) covalently connected via disulfide bonds [4]. Each chain contains variable and constant regions, defining the antigen-binding specificity and the immune-mediated activities, referred to as effector functions. These two moieties, both consisting of Ig-like β-pleated sheets, can be further defined as Fab (antigen binding fragment), which is responsible for the antigen interaction, and Fc (crystallizable fragment), responsible for the effector functions. The largely conserved constant heavy chain regions (CH) are responsible for the antibodies effector functions and define the molecules isotype IgA, IgD, IgM, IgG or IgE. IgG and IgA can be further divided into subclasses IgA1 and IgA2 as well as IgG1-4. Each of these isotypes facilitate different immune-mediation mechanisms like antibody localization, polymerization or the interaction of the antibody with different immune cells by various Fc receptors [5]. In contrast to CHs, constant light chain domains (CL) which are divided into kappa (κ) and lambda (λ) domains increase the

diversification of the antibody repertoire and elevate the ratio of functional proteins during the B cell maturation rather than participate in immune-mediation activities. The Fab fragment consists of the *N*-terminal variable region of the heavy chain (VH), followed by the constant region 1 of the heavy chain (CH1) and the corresponding variable (VL) and CL chain domain. The variable regions are responsible for antigen recognition by interaction of three variable regions of the light and heavy chain, respectively, termed complementarity determining regions (CDRs) [6]. These regions are diversified within B cell maturation by a process called somatic recombination. The CDRs of the heavy chain consist of a variable (V) segment (completely encoding for CDR1 and CDR2) as well as a diversity (D) and a joining (J) segment. Since the junctions of V, D and J are located at the third CDR (CDR3) of the VH domain, this loop displays the region of highest diversity. Light chain genes are recombined by V and J segments only, yielding the three light chains CDRs. The combination of all six CDR loops together form the antibodies 3D-paratope, allowing for highly specific antigen interaction [4], [6].

The sophisticated mechanism responsible for antibody repertoire diversification is described in more detail in the following section.

3.1.2 B cell maturation

B cells begin to develop as pluripotent hematopoietic stem cells (HSC) in the bone marrow, where they differentiate i.a. into multipotent progenitor cells (MPPs), common lymphoid progenitor cells (CLP) and into pro-B cells due to stimuli of stroma cells [7]. These stimuli comprise interactions of specific surface receptors and cytokines as well as chemokines like FLT3-ligand, stem cell factor (SCF) and stromal cell-derived factor 1 (SDF-1), to name a few [8]–[10]. In the early pro-B cells, the expression of proteins responsible for the *Ig* gen rearrangement, e.g. recombination activation genes RAG1 and RAG2, initiates the somatic recombination [11]. Due to specific relocalization of the V, (D) and J segments with successive DNA cleavage resulting in DNA double-strand breaks, the segments are finally joined via non-homologous end joining (NHEJ) enzymes to the final BCR, referred to as somatic recombination or receptor editing process. By V(D)J-gene rearrangement a various number of different antibody coding sequences are formed. Human chromosomes 14, 2 and 22 encode for 38-46 V, 23 D and 6 J segments for the VH domain, 34-38 V and 5 J segments for VLκ as well as 29-33 V and 4-5 J segments for VLλ [12]. Considering a random combination of any V(D)J segment and pairing with either κ or λ, a minimum total number of around 1.5×10^6 distinct antibody sequences can be generated.

To further increase the diversity, within the single V(D)J recombination steps, nucleotide deletions as well as the addition of so called P (palindromic) or N (non-templated) nucleotides can occur, the latter being caused by maturating lymphocyte specific enzyme *terminal deoxynucleotidyl transferase* (TdT) [13].

This complex maturation process results in a vast diversity of different proteins. However, this is only a theoretical number. Many B cells receive apoptotic stimuli because of the random gene rearrangement leading to a non-functional BCR or because of them dying before they encounter their corresponding antigen. Furthermore, due to the random joining of V(D)J segments, BCRs recognizing self-antigens will

occur, which are mostly removed in the bone marrow by clonal deletion or by a secondary receptor re-arrangement to prevent self-reactive antibodies circulating in the host [14], [15]. Cells which pass the development checkpoints leave the bone marrow to enter peripheral circulation in secondary lymphoid tissues (SLTs), presenting membrane-bound IgM and IgD isotypes of their specific BCR as naïve B cells. To activate the B cells, an interaction with T helper cells specific for the same pathogen is necessary. Once a B cell encounters its specific antigen, the BCR antigen complex is taken up by endocytosis, degraded and followed by antigen peptide presentation on the surface via major histocompatibility complex (MHC)-II molecules [16]. Those peptide MHC-II complexes are again recognized by T helper cells with their specific T cell receptor (TCR), which respond with the expression of CD40-ligand on their surface as well as the secretion of specific cytokines [17], [18]. These agents promote stimuli for the proliferation, immunoglobulin class switch recombination, somatic hypermutations as well as the differentiation to antibody secreting or long-lasting memory B cells, maintaining the specific pathogen response for repeated infections.

Once differentiated into plasma cells, B cells are able to secrete antibody proteins equivalent to their membrane-bound BCR. These proteins thereby differ by the lack of the transmembrane and cytoplasmic domain but harbor a short amino acid sequence called the tailpiece, which facilitates the secretion of the antibodies.

3.1.3 Somatic hypermutation and class switching

As mentioned above, activation of mature B cells can result in a second stage of diversification, referred to as somatic hypermutations (SHM), comprising a molecular mechanism to further increase the antibody repertoire and to concurrently “affinity maturate” the antibodies aiming at a stronger antigen interaction [19]. The B lymphocyte specific activation-induced cytidine deaminase (AID) is thought to be the key enzyme for this process, deaminating cytidines to uracil (C to U) causing an uracil:guanine (U:G) mismatch [20]. This mismatch triggers Ig loci mutagenic processing by base excision repair and mismatch repair pathways evoking transition (C to T) or transversion mutations as well as mutations spread to nearby adenine:thymine (A:T) pairings [21]. However, this AID-mediated process seems not to be completely random but orientates itself to preferentially targeted DNA “hotspot” motifs consisting of several nucleotides, introducing more defined mutations [22].

Furthermore, there is evidence that AID is a crucial component for another DNA alternation process in B cells, changing the constant domain to another isotype, referred to as class switch recombination (CSR) [19], [20]. Within several rounds of cell division, at least partly due to the appropriate activation of AID, CSR as an intrachromosomal deletional recombination event can change the HC from IgM and IgD to other isotypes. To this end, AID deaminates cytidines in HC upstream switch (S) region, consisting of tandem repeats of short G-rich sequences. Deamination needs to occur in both, the S region of IgM as well as of the acceptor isotype, inducing repair processes finally leading to DNA double-strand breaks and NHEJ, explained elsewhere [23]. However, an AID overexpression induces class switch from IgM to IgA without

additional cytokine stimulation, whereas a lack of AID causes a class switch deficiency resulting in a hyper IgM syndrome [24].

The switch to different isotypes creates a variety of antibodies with equal specificity but distinct immune-mediation activities, helping to broaden the immune response against the pathogen and thereby steering function of the antibodies. Additionally, depending on the isotype, partially molecular components are added which support dimerization (IgA) or formation of pentamers and hexamers (IgM) and therefore showing additional effects on e.g. diffusion and avidity. Furthermore, the CH domain influences the stability of the protein, the capability of transcytosis and complement activation as well as the interaction with immune cells via different receptors showing varying affinities for the isotypes. These effector mechanisms are briefly described in the following section.

3.1.4 Effector functions

Upon binding their respective antigen with the Fab moiety, the Fc is accessible for other proteins or immune cells to attach and interact. As already mentioned, depending on the isotype, the interacting components and modes of action differ. Due to binding their complementary structures, antibodies cover the pathogen surface either mark it for immune cells to attack (opsonization), directly neutralize the pathogen, e.g. toxins or viruses, or activate a cascade of plasma proteins, the complement system, which again can directly lyse the pathogen or interact with immune cells [5]. For example, IgM, next to IgG, is primarily responsible for complement-dependent cytotoxicity (CDC). Although IgM, as first isotype of antibodies secreted after an infection, exhibits only moderate affinities, the multimeric structure compensates this issue by the inclusion of avidity effects, simultaneously acting as substantial activation unit for the complement cascade [25], [26]. In contrast, the dimeric IgA is the most predominant isotype in intestinal and respiratory outer mucus layer, crossing the epithelial cells by transcytosis capturing pathogens in mucus to prevent from infections [27], [28], whereas IgE plays a key role in defense against parasites and venoms by interaction with Fcε receptors triggering mast cell and granulocyte activation [29], [30]. However, the major isotype present in the human blood is monomeric IgG. Compared to other isotypes, IgGs exhibit a prolonged serum half-life of about three weeks. Reason for this special pharmacokinetic profile is the antibody recycling mechanism, elicited by interaction with the neonatal Fc receptor (FcRn) [31]. During this process, the IgG antibodies are internalized by cells via endo- or pinocytosis and bind to the FcRn receptor in the acidic environment of the endosomes. The FcRn:IgG complex is then transferred back to the surface where the antibody dissociates due to the physiological pH. Moreover, interactions with additional Fc receptors like FcγRI (CD64), FcγRII (CD32) and FcγRIII (CD16) highlights IgG as important isotype for the activation of innate immune cells resulting in antibody-dependent cellular phagocytosis (ADCP) and antibody-dependent cell cytotoxicity (ADCC) [32]. ADCC is e.g. mediated by natural killer (NK) cells, which express the activating receptor FcγRIIIa (CD16a), recognizing IgG-covered cells and resulting in the release of cytotoxic perforins and granzymes as well as

proinflammatory cytokines like interferon-γ (IFN-γ) and tumor necrosis factor α (TNF-α) [33]. Thus, NK cells are important mediators, acting between the innate immunity and the adaptive immune response of the host and will be explained in more detail in the following section.

3.2 Innate immunity

The human defense against invading pathogens is structured in two different, constantly interacting stages, referred to as innate and adaptive immunity, each comprising cellular and non-cellular components to recognize and neutralize foreign structures. Whereas the slower adaptive immune system provides a pathogen-specific, long-lasting response, the innate immune system is less specific but frequently encountered in multi-cellular organisms. It acts as the early stage against pathogen invasions and is constantly present in the organisms, therefore enabling a rapid immune response. Innate immunity comprises continual defense lines like physical barriers of the body and antimicrobial substances as well as inducible protection triggered by immune cells. Skin, respiratory and gastrointestinal epithelium impede pathogens from penetration and express antimicrobial agents as lysozyme and defensins tackling the intruder as a first defense line [34], [35]. Additionally, innate immune cells contribute substantially to the inflammatory response by directly combatting the pathogen as well as supplying crucial stimuli for the activation of the pathogen-specific adaptive immune response. However, in contrast to the highly variable BCR and TCR, innate immune cells like NK cells can bind foreign substances among others via multifarious germline-encoded receptors referred to as pattern recognition receptors (PRRs) These PRRs associate with similar molecular patterns exposed by large groups of pathogens (like polysaccharides in bacterial cell walls) and are named pathogen-associated molecular patterns (PAMPs) [36]. Consequently, the innate immune cells act less pathogen-specific than the adaptive immunity, however, much faster, enabling an immediate suppression of the pathogen.

NK cells, as part of the innate immunity, are also essentially involved in anti-tumor and anti-viral responses [37], [38]. Since the ability of NK cells to mediate strong anti-tumor responses is fundamental for a main part of this work, NK cells will be scrutinized in more detail in the following.

3.2.1 NK cell development

NK cells belong to the innate lymphoid cell (ILC) family and therefore to the lymphatic lineage, like B and T cells, developing from HSCs and MPPs, sharing e.g. functional characteristics but lack of the antigen-specific receptor. NK cells were thought to mature exclusively in the bone marrow, but more recent evidence suggests that SLTs like tonsils, spleen, and lymph nodes play an important role in the NK cell development as well [39]. However, the maturation of NK cells comprises several intermediate stages of development, each dictated by distinct surface markers and stimuli, described in detail by Yu et al. in 2013 and Abel et al. in 2018 [37], [40].

NK cells are classically assigned to the innate immunity because they can perform pathogen-cytotoxic and immune-mediating activities without prior antigen contact, however, they share many attributes to lymphocytes of the adaptive immunity, like education and selection during their maturation as well as the generation of long-lived memory cells following antigen exposure, hence providing the ability to create a secondary recall response, elegantly described elsewhere [41], [42]. An example for this intermediate status of NK cells is the ability to produce INF-γ like ILC1 cells but coincidently harboring granules releasing cytotoxic perforin and granzymes to lyse target cells, comparable to cytotoxic CD8+ T cells [43].
Therefore, NK cells act as discrete effector cells in the innate immunity, enhancing the signals of the early pathogen recognition and mediating an immune response [44]. Because of their multidimensional nature, either secreting proinflammatory cytokines or directly antagonizing altered cells, NK cells represent an important cell population in the immunosurveillance.

The first step to define CLP differentiation into lymphoid lineage is depicted by the expression of interleukin (IL)-7 receptor-alpha (IL-7Rα, CD127) in combination with other surface markers. Successive expression of IL-2 receptor β chain (CD122) and transcription factors like E4bp4 (Nfil3) result in the blockade of B cell and T cell differentiation by subsequent transcription factors expression like Id2, thus enabling development into cells of the ILC family [45]–[47]. ILCs do not possess somatic recombined receptors, but express IL-7 receptor, which is also crucial for B cell development. For further differentiation, survival and homeostasis, NK cells require cytokine signals, like IL-2, IL-7 and IL-15, mediated through the common receptor gamma-chain (γc) family members, as well as stimuli via distinct surface markers either transducing inhibitory or activating signals [40], [48]–[51]. IL-15 was also demonstrated to be crucial for the NK development process itself, since IL-15-deficient mice revealed a severe reduction of functional NK cells [52].
NK cell developmental steps are commonly divided into six linear stages, however, recent evidence suggests a partially more flexible chronology [53], [54]. Nevertheless, the classical description defines HSC, MPP and CLP as the first stages, followed by NK cell developmental intermediates (NKDI) committing the cells to the NK lineage. The single stages are characterized by specified variations of surface marker up- and down-regulation like different C-type lectin superfamily members, e.g. NKG2A and NKG2D, neural cell adhesion molecule (NCAM, CD56), natural cytotoxicity triggering receptor 1 (NKp46, CD335), FcγRIIIa (CD16a, for convenience only named further on CD16) and killer-cell immunoglobulin-like receptors (KIRs), to mention a few. Furthermore, CD56 expression levels provide an additional classification of the NK cells based on their functionality [55], [56]. In development stage 5, the NK cell majority downregulates CD56 expression, resulting in the $CD56^{dim}$ subset. About 90 % of the circulating NK cells are designated as $CD56^{dim}CD16^{high}$ and thought to be predominant in cytolytic activities, whereas the $CD56^{bright}$ subset is primarily located in SLTs showing lower levels of CD16 expression ($CD16^{low}$) and demonstrate superior immunoregulatory capabilities [44], [57], [58]. However, i.a. Fehniger and colleagues could show that the supposedly less-matured $CD56^{bright}$ subset exhibits potent antitumor responses after prior IL-15 sensitization, suggesting a more dynamic functionality classification of matured NK cells as supported by other findings as well [59], [60].

As previously mentioned, surface receptors indicate the various developmental stages of the NK cells. Additionally, members of the surface receptors contribute to NK cell homeostasis and activation by either signaling inhibitory or activating stimuli upon ligand binding, described in the next section.

3.2.2 NK cell homeostasis and activation

NK cells are orchestrated by the integration of signals through inhibitory and activating receptors, building a fine balance for homeostasis [61]–[63]. These stimuli can be triggered by either surface cell ligands, e.g. inhibitory MHC molecules or activating B7-H6, or soluble agents like cytokines and antibodies [64], [65].
Under physiological conditions, human NK cells receive inhibitory signals mainly through interaction of KIRs with self-antigens represented by MHC-I molecules on normal cells. This ability to recognize and therefore distinguish between self and non-self is commonly referred to as "education" or "licensing" of NK cells [66], [67]. The origin model describes the inhibitory signals as more powerful as positive stimuli, hence controlling the NK cell responsiveness. However, the model was modified by Raulet and Vance in 2006 to a "arming" and a "disarming" model [68]. They proposed the need for inhibitory signals via MHC-I interactions to promote NK cell development thereby being responsible for maturation and functionality. Therefore, NK cells lacking MHC-I specific receptors are "disarmed" and hyporesponsive to activating stimuli, as they are not fully matured, resulting in self-tolerance.
Additionally, different theories for the activation of matured NK cells developed. One of the three main theories for NK cell activation is referred to as "missing-self" hypothesis, by which NK cells are activated due to the absence of inhibitory signals provided by, e.g., MHC-I molecules [69]. However, more recent results indicate that additional activating signals are necessary for proper NK cell responses [70]. Moreover, the „non-self" recognition postulates another hypothesis of NK cell activation due to the identification of cell markers different from the host, e.g. differences in MHC-I molecules due to allogeneic tissue transplants. The third activation thesis is named "induced-self" recognition. Herein, NK cell response is commenced by enhanced activation stimuli with concurrent presence of MHC-I molecules due to the exhibition of a distinct cell surface ligand profile of pre-malignant or stressed cells, which differ from normal cells.
As an example, the "missing-self" recognition occurs within diverse tumors and viral infections, when the expression of MHC-I molecules is downregulated to avoid foreign peptide presentation resulting in cytotoxic T-cells recognition and cell lysis. However, this evading strategy results in an increased NK cell susceptibility, which benefits from the reduced MHC-I related inhibitory stimulus, in turn elevating the activating signals and resulting in an "missing-self" activation [71].
Furthermore, the "induced-self" mechanism is e.g. simulated in diverse therapeutic approaches using immunoconstructs or immunoligands for the NK cell recruitment, thereby mimicking an induced-self condition for a NK cell response [72]–[74].
This specific immune response in the context of NK cell activation comprises the secretion of proinflammatory cytokines INF-γ, TNF-α and granulocyte-macrophage colony stimulating factor (GM-CSF)

as well as lysis of the altered target cell, depending on the NK cell phenotype [56]. Cell lysis is either mediated by specific receptors inducing cell death, discussed in section Inhibitory receptors *FasL and TRAIL*, or via NK cell degranulation due to the release of granules containing lytic perforin and granzymes. However, the NK cell activation is only triggered if the activation stimuli exceed the inhibitory ones. To make sure the activation occurs only under specific circumstances like contact to an altered target cell, NK cell activation is tightly regulated by the interplay of a diverse set of distinct inhibitory and activating signals [65].

Because of the variety of different surface receptors on NK cells contributing to their homeostasis, only some of the probably most relevant receptors will be described briefly in the following.

3.2.3 Inhibitory receptors

Receptors contributing to NK cell homeostasis by the mediation of activation-suppressing signals are generally referred to as inhibitory receptors. They act as mediators of negative feedback to prevent from chronic NK activation and immunopathology by the differentiation of self and non-self antigens on autologous cell surfaces facilitating self-tolerance. Upon ligand binding, inhibitory receptors signal through immunoreceptor tyrosine-based inhibitory motifs (ITIMs) in their cytoplasmic tails, causing tyrosine phosphorylation and successive protein tyrosine phosphatases or lipid phosphatases recruitment, which can suppress activation pathway signaling [63], [75]–[77]. Inhibitory receptors on NK cells comprise i.a. programmed cell death protein 1 (PD-1), T cell immunoreceptor with Ig and ITIM domains (TIGIT), T cell surface protein tactile (tactile), NKG2A and several KIRs.

Inhibitory killer-cell immunoglobulin-like receptors (KIRs)

Several members of the KIR group interacting with MHC-I molecules function as important inhibitory receptors on NK cells, as the absence or downregulation of MHC enhances NK cell activation [78]. In more detail, human leucocyte antigen (HLA)-C associates with KIR2DL1, KIR2DL2 and KIR2DL3, while KIR2DL4 recognizes HLA-G. Furthermore, KIR3DL1 binds to HLA-B and KIR3DL2 associates with HLA-A [79]. The underlying nomenclature of the KIR receptors depends on whether two or three extracellular domains (2D or 3D) as well as short or long cytoplasmic tails (S or L) are present. While all inhibitory KIRs contain long cytoplasmatic tails bearing ITIM motifs, this description further reveals their functionality, except for KIR2DL4 [79], [80]. In short, inhibitory KIR receptors belong to the Type I transmembrane (TM) receptors possessing extracellular Ig-like domains and long cytoplasmatic tails harboring ITIM motifs enabling inhibitory signaling.

Although in vivo studies of the KIR2DL1-3 antibody Lirilumab demonstrated strong blocking effects on KIR interactions with HLA-C expressing tumor cells, clinical trials of acute myeloid leukemia failed to detect

any treatment benefits [81], [82]. A possible reason could be the expression of other essential inhibitory receptors, such as NKG2A.

Natural Killer Cell Receptor Group 2 Member A (NKG2A)

NKG2 lectin-like receptors are expressed as heterodimers with CD94 on NK cells and can either dimerize with NKG2A, forming an inhibitory receptor, or dimerize with NKG2C, leading to an activation signaling. Both receptors specifically recognize HLA-E, a non-classical MHC-I molecule [83]. HLA-E itself binds a restricted subset of peptides derived from classical MHC-I molecules signal peptides, which is necessary for its surface presentation [84]. Thus, employing CD94/NKG2A interacting with peptide complexed HLA-E, NK cells are able to indirectly monitor cell surface expression levels of classical MHC-I molecules. Additionally, besides broad expression on NK cells, NKG2A is present on some T cell subsets, including CD8+ T cells.

Due to the expression on diverse immune cells, the contrary nature of HLA-E as well as its upregulation in diverse tumors, the suppression of the HLA-E/NKG2A interaction represents a possible approach for cancer immunotherapy [85], [86]. Therefore, different xenografts models were developed, in which, e.g., adoptively transferred human NK cells lacking NKG2A expression improved the mouse immunity to human HLA-E expressing sarcoma cells [87]. In addition, preclinical trials with anti-NKG2A Monalizumab exhibited promising results [88], [89]. Therefore, ongoing clinical trials evaluate combinatorial effects of Monalizumab with anti-EGFR (epidermal growth factor receptor) Cetuximab or anti-PDL1 (programmed cell death protein 1 ligand 1) Durvalumab [90], [91].

3.2.4 Activating receptors

The counterparts to the inhibitory receptors are represented by a wide variety of activation-stimulating surface receptors on NK cells. Upon ligand binding, downstream signaling is mediated via different adapter molecules, either containing immunoreceptor tyrosine-based activating motifs (ITAM) like CD3ζ, FcεRIγ (FcRγ) and TYRO protein tyrosine kinase-binding protein (DAP-12, TYROBP or KARAP) or non-ITAM adapter proteins like DNAX-associated protein of 10 kDa (DAP-10) [76], [92]–[95]. As examples, the activation receptor NKG2D signals through its association with DAP10, which possesses YxxM non-ITAM motif, whereas signaling lymphocytic activation molecule (SLAM) family receptor members like 2B4 use immunoreceptor tyrosine-based switch motifs (ITSM) for signaling, distinct from DAP10 and ITAM YxxL/I motifs. The utilization of different signaling pathways by activating receptors could be a possible explanation for the presence of several members of activation signaling molecules, enabling the mediation of different responses by the NK cells [96]. However, for a sufficient cell response leading to a final NK cell activation, the combination of stimuli by manifold activating receptors are necessary, comprising cell interactions via membrane-bound ligands as well as cytokine stimulation, except for CD16 [65], [77], [97]. Apart from inhibitory receptors, NK cells employ a variety of different germline-encoded activating

receptors, such as, e.g., Fas ligand (FasL), TNF-related apoptosis-inducing ligand (TRAIL), CD16, 2B4, NKG2D or the natural cytotoxicity receptors (NCRs), equipping the NK cells to recognize a plethora of target cell alterations.

FasL and TRAIL

Fas ligand (FasL) and TNF-related apoptosis-inducing ligand (TRAIL), also known as 'death ligands', represent a perforin-independent mechanism of NK cells to kill tumor necrosis factor (TNF) receptor superfamily member, commonly known as 'death receptors', expressing target cells [98], [99]. Binding of NK cells via these receptors can induce target cells apoptosis, finally causing programmed cell death [100]. FasL expression is restricted to cytotoxic T cells and activated NK cells, whereas Fas is expressed on diverse tissues. Fas protein cross-linking initiates nuclear and cytoplasmic condensation, membrane blebbing, and caspase activation [101], [102].

It was shown that Fas is downregulated in many cancers during tumor progression reducing the susceptibility of tumor cells towards Fas-mediated apoptosis, however, more recent studies showed a selectively cytotoxic effect against oral cancer cells with a low FasL/Fas ratio using a Fas ligand-fused humanized bispecific fusion protein indicating the possibility to use Fas as apoptosis-inducing tumor target [103], [104].

Besides FasL, TRAIL represents another possibility for NK cells to induce target cell apoptosis. It is constitutively expressed by NK cells, either anchored as membrane-bound or released as secreted protein and was shown to mediate spontaneous cytotoxicity against TRAIL receptor (TRAILR1 and TRAILR2) expressing tumor cells due to the mediation of a pro-apoptotic signal through activation of caspases [105], [106].

While rodent tumor models showed promising results, TRAIL death receptor targeting in clinical studies was not able to exhibit satisfying anti-tumor efficacy up to now [107], [108].

NKG2D

NKG2D is a homodimeric activating receptor and member of the C-type lectin superfamily. It is expressed on subsets of T cells as well as on all NK cells and binds to cell surface glycoproteins MHC-I polypeptide-related sequence A (MICA) and MICB as well as UL16 binding proteins (ULBPs; ULBP1 to ULBP6). These ligands are scarcely expressed on healthy cells but can be induced by viral infection, oxidative stress, DNA damage and cell transformation [109], [110]. Upon ligand binding, NKG2D signals through its adapter molecule DAP10 in humans initiating the recruiting p85 subunit of phosphatidylinositol 3-kinase (PI3K) and a complex of growth factor receptor-bound protein 2 (GRB2) and VAV1, finally enabling NK cell degranulation and cytokine production [111].

However, tumors have developed different mechanisms to evade from recognition via NKG2D surface ligand expression. Thus, NKG2D is thought to be important for the early tumor surveillance, since NKG2D-

deficient mice tend to produce spontaneous malignancies, encouraging the suggestion of important early immunoediting events in NKG2D ligands in tumor [112]. Besides immunoediting events causing selection advantages of NKG2D low expressing tumor cells, NKG2D ligands can be shed from the surface. This reduces the expression on tumor cells helping to evade from immune recognition as well as facilitating the downregulation of NKG2D receptors on lymphocytes by endocytosis upon shed NKG2D ligand binding [113]. In contrast to that, evidence of NK activating functions of soluble ligands have emerged in mice promoting tumor control, indicating a more difficile role of shed NKG2D ligands [114].

To avoid shedding, approaches with inhibitor molecules interacting with a disintegrin and metalloproteinase domain-containing protein 10 (ADAM10) and matrix metalloproteinase (MMP) are investigated, aiming at the inhibition of NKG2D ligand shedding from tumor cells [115]. Additionally, recent studies using antibodies addressing the proteolytic site of MICA and MICB proteins, thus fixating the ligands on the cell surface, exhibited preclinical efficacy in diverse tumor models as well as a reduction of lung cancer metastasis [116].

FcγRIII (CD16)

Another important granule-mediated mechanism of NK cell-targeted killing is referred to as antibody-dependent cell-mediated cytotoxicity (ADCC). ADCC is based on the ligation of antibody Fc portions with cognate Fc receptors expressed on the NK cells, whereas the antibodies Fabs confer specificity and affinity towards their antigen. In contrast to other lymphocytes, NK cells express only activating Fc receptors, namely FcγRIIIa (CD16) and FcγRIIC (CD32c), and therefore are considered to be important ADCC effector cells [117]. While CD16 is expressed by most NK cells, CD32c is present on NK cells in only 7 to 15 % of healthy individuals (as a result of a single-nucleotide polymorphism (SNP)) [118]. A single SNP is also responsible for genotypic variations of the expressed FcRs on NK cells, for instance resulting in CD16 polymorphic variants either harboring a phenylalanine (F) or a valine (V) at amino acid position 158. This amino acid exchange influences the affinity of CD16 to immunoglobulins, leading to an improved clinical outcome for patients with homozygosity for the higher affinity V genotype compared to F/V heterozygous or F/F homozygous individuals if treated with therapeutic monoclonal IgGs [119]–[121].

ADCC was initially described as secretion of cytotoxic perforin and granzymes leading to the lysis antibody-coated target cells following ligation of CD16 by IgG target cells. Nowadays, ADCC is understood and used as a multi-tiered process involving coordinated immune cells with distinct functionalities. In case of NK cells, ADCC can induce different effector pathways including cytotoxic granule exocytosis and the release of proinflammatory cytokines, such as TNF-α and INF-γ without costimulation necessary for other receptors to sufficiently activate NK cells [122]. CD16 harbors only a short cytoplasmatic tail lacking ITAM motifs, thus depends on the association with homodimers or heterodimers of adaptor molecules CD3ζ or FcεRIγ within the cell membrane for appropriate activation signaling [123]. CD16 association with an immunoglobulin Fc portion thereby initiates the signal transduction mechanisms of NK cells comprising phosphorylation of the ITAM motifs on the adapter molecules cytoplasmic tails, binding of tyrosine kinases

ZAP-70 and Syk as well as activation of PI3K, NF-κB and ERK pathways, finally resulting in NK cell degranulation and cytokine secretion [124].

Until today, many monoclonal antibody therapies addressing distinct tumor targets like Rituximab (anti-CD20), Trastuzumab (anti-HER2), Cetuximab (anti-EGFR) and Daratumumab (anti-CD38) are used as standard of care treatments for tumors and hematological malignancies, emphasizing the important role of ADCC in mediating anti-tumor effects [33], [125]. Furthermore, different antibody-derived platforms like bispecific killer engagers (BiKEs) or trispecific killer engagers (TriKEs) have developed applying anti-CD16 moieties for ADCC mediation on NK cells, even with some proteins in ongoing clinical studies [126]–[128]. Analogous to NKG2D, CD16 was reported to be shed by NK cells due to activities of a disintegrin and metalloprotease, ADAM17. It was shown that inhibition of the metalloprotease and thereby consistent CD16 expression on NK cells resulted in a notable increase of intracellular cytokines. In contrast to that, the effect on degranulation and cytotoxicity was less [129]. This result was supported by Davis and colleagues in 2018, who revealed that CD16 shedding facilitates NK cell detachment from target cells, supporting NK cell motility and serial engagement of target cells [130]. Taken together, a higher expression of CD16 on NK cells seems to trigger more cytokine production, whereas lower surface expression of CD16 may be beneficial for NK cell serial killing.

Natural cytotoxicity receptors (NCRs)

The natural cytotoxicity receptors (NCRs), comprising three Type I TM receptors belonging to the immunoglobulin superfamily, were identified in the late nineties of the last century by their ability to recognize and lyse tumor cells by human NK cells [131]–[133]. The receptors NKp30 (NCR3; CD337) and NKp46 (NCR1; CD335) are constitutively expressed on resting NK cells, while NKp44 (NCR2; CD336) requires NK cell activation for its expression. Even though the NCRs belong to the same immunoglobulin superfamily and perform similar functions, crystallographic characterization of the NCRs revealed considerable differences between the three receptors regarding their amino acid sequence and structure [134]. While NKp46 contains two extracellular Ig-like domains, NKp30 and NKp44 possess only one Ig-like domain responsible for ligand binding. All three NCR ectodomains consist of a membrane-proximal stalk domain and the distal ligand-binding domain. The ectodomain is suggested to possess multiple interaction sites to explain how the NCRs can interact with structurally diverse ligands. Positively charged amino acid residues in their inherent C-terminal TM domains form a salt bridge with a corresponding residue in the associated TM domains of the ITAM adaptor molecules necessary for signal transduction. NKp44 is the only NCR which associates with DAP-12, whereas NKp46 and NKp30 attach to CD3ζ or FcεRIγ forming heterotrimeric structures for downstream signaling [124].

Although the NCRs have been known for over twenty years, their ligands are less well characterized than those of other receptors. Hence, a lot of efforts have been made in the last years to identify ligands for these three activating receptors. These comprise viral-, bacterial- and parasite-derived structures as well as cellular ligands on stressed or tumorous cells which are barely expressed on healthy tissue [135], [136].

This diverse ligand profile opens a wide field for possible therapeutic applications addressing NK cells due to their NCR receptors.

NKp46

The NKp46 encoding gene, NCR1, is located in the tail of the leucocyte receptor complex on chromosome 19, and the translated protein is the main NK cell lineage-defining activating receptor in mammals, whose triggering culminates in degranulation and the release of proinflammatory cytokines [136]. NKp46 was the first NCR identified and exists in several isoforms [137], [138]. Although NKp46 is primarily present on NK cells, some other cell populations were found expressing it as well. These include γδ T cells, ILC1 and a subset of group 3 ILCs as well as some other discrete T cell sets [139]–[143].

In contrast to NKp44 and NKp30, an NKp46 orthologue was identified in mice, allowing for in vivo assessments of this protein entitled NCR1 (mNKp46). Thus, Mandelboim and colleagues were able to generate NCR1 knockout mice by the replacement of NCR1 exons with a GFP reporter cassette. These mice died rapidly due to influenza virus infections and exhibited an increase in tumor metastasis [144], [145]. Additionally, other mutant mice were generated via random mutagenesis on this receptor, exhibiting increased resistance to viral infections due to hyperresponsive NK cells because of a mutation in the NCR1 gene [146]. These observations show the important role of NKp46 for the immunosurveillance. However, NKp46 is also associated with NK and T cell lymphomas and suggested to be involved in diabetes [147]–[149]. For these NKp46-dependent diseases, in vitro studies of anti-NKp46 antibodies were recently published, implying possible treatment options [150], [151].

To date, many distinct ligands from different pathogenic origins are described to associate with NKp46 in an NK cell-activating manner. It was shown that NKp46 binds hemagglutinin and hemagglutinin-neuraminidase of diverse viruses as well as bacterial structures like vimentin expressed on *mycobacterium tuberculosis*-infected cells, inducing a NK cell-mediated lysis of these cells [152]–[156]. Furthermore, NKp46 ligands have been reported to be expressed on different tumors [145], [157].

Therefore, NKp46 is used as a target for immunostimulatory approaches, by either expressing its ectodomains as chimeric antigen receptor on (CAR) T cells or by using an anti-NKp46 antibody entity as part of NK cell engagers (NKCEs) [158], [159].

NKp44

NKp44, in contrast to NKp30 and NKp46, is not constitutively expressed by resting NK cells, but is upregulated on NK cells if stimulated, e.g. with IL-2, IL-15 or IL-1β [160], [161].

NKp44 is encoded by the NCR2 gene located in the triggering receptors expressed on myeloid cells (TREM) receptor locus on chromosome 6 [162]. Transcription of the NCR2 gene translates into three expressed variants, termed NKp44-1, NKp44-2 and NKp44-3. Whereas NKp46, NKp30 and variants NKp44-2 and NKp44-3 harbor only short cytoplasmic tails lacking signaling motifs, only the cytoplasmic domain of

NKp44-1 contains an ITIM motif typical for NK cell inhibitory receptors. Thus, NKp44-1 provides the potential of imparting suppressing as well as activating signals as it can still couple with DAP-12 [135]. Like the other NCRs, NKp44 is also expressed on sets of distinct ILCs and diverse T cells.

Several ligands of NKp44 have been identified, comprising primary flavivirus-derived and cellular molecules. For example, NKp44 binds specifically to envelope proteins of the *West Nile virus* (WNV) and *Dengue virus*, since WNV-infected cells stimulated NK cell degranulation and IFN-γ secretion in an NKp44-dependent manner [163]. Furthermore, a new exon of the usually nuclear mixed-lineage leukemia protein-5 (MLL5) resulting in a protein variant with an altered C-terminal amino acid sequence, hence aberrantly expressed on tumors or virus-infected cells but not on healthy tissue, was identified and termed NKp44 ligand (NKp44L) [164]. As another NKp44 ligand, Nidogen-1 (NID1 or Entactin) usually functions as extracellular matrix linker, stabilizing and assembling the basement membrane. If present in soluble form, this ligand might impair NK cell function as seen in serum from patients with ovarian and lung cancer [165], [166].

NKp30

NKp30 is encoded by the NCR3 gene located in the highly polymorphic telomeric end of the class III region of human MHC locus. Its transcription generates several mRNA splice variants finally translated into three constitutively expressed isoforms NKp30a, NKp30b, and NKp30c, which differ in length of their cytoplasmic domain [135]. Out of all, NKp30a and NKp30b are the ones which act immunostimulating, whereas NKp30c is found to be immunosuppressive [167]. Although the isoforms are concurrently expressed on NK cells, the canonical role for the dominant splice variant is NK cell activation culminating in cytokine release and degranulation. Besides NK cells, NKp30 is expressed on other lymphocytes like a set of CD8+ T cells, expanded peripheral blood γδ T cells (Vδ1+) and umbilical cord blood T cells cultured in IL-15 [168]–[170].

To date, several ligands for NKp30 are known, comprising viral structures like hemagglutinin of human vaccinia virus or human cytomegalovirus protein pp65, both acting as antagonists, or the parasites Duffy binding-like-1 α domain of *Plasmodium falciparum* erythrocyte membrane protein-1, which mediates NK cell lysis of infected cells [171]–[173]. Furthermore, fungal structures such as β-1,3 glucan of *Cryptococcus neoformans* and *Candida albicans* as well as cellular ligands, e.g. B7-H6, which is upregulated in altered and stressed cells, induce direct killing by NK cells via NKp30 engagement [174]–[176].

Interestingly, there is evidence that the stalk domain of NKp30 contributes to the ligand binding and increases its affinity for cellular ligands BAG6 and B7-H6 [177], [178].

Furthermore, it has been shown that NKp30 is a promising receptor for immunostimulatory approaches, enhancing immune engagement by increased NK cell-mediated target cell cytotoxicity via combination of therapeutic antibodies with recombinant immunoligand B7-H6, generation of CAR T cells based on NKp30 receptor or, as recently published, incorporating anti-NKp30 antibody entities in TriKEs [179]–[183].

B7-H6 as natural ligand of NKp30 is another essential part of this work, therefore, this protein is described in more detail within the next section.

3.3 B7-H6

Natural cytotoxicity triggering receptor 3 ligand 1, also known as B7-H6 (or B7H6). is a natural ligand of NKp30. B7-H6 belongs to the B7 family and possesses two extracellular Ig-like domains similar to other members of this group, which can be divided into a membrane distal Ig variable-like domain and membrane proximal Ig constant-like domain [184]. For the association, the front and back β-sheets of the NCR interact with the cognate CDR-like loops of B7-H6 variable-like domain, thus engaging B7-H6 in an antibody-like manner.

Besides expression on a wide range of tumor cells and on a small set of proinflammatory monocytes and neutrophils upon stimulation with proinflammatory cytokines such as IL-1b and TNF-α or ligands of Toll-like receptors, B7-H6 expression on healthy cells is found to be neglectable [176], [185].

Additionally, B7-H6 expression is upregulated on cells as reaction to disfunctions such as endoplasmic reticulum stress or due to cancer treatment with chemotherapy, targeted therapy or radiation therapy after initial tumor evasion, to serve as mode of immunosurveillance, thereby turning immune-cold into immune-hot tumors [186], [187].

In contrast to the B7-H6 surface expression upregulation, mechanisms of NK cell evasion by B7-H6 downregulation have been found in virus infections like human cytomegalovirus and human herpesvirus 6 [188], [189]. Similarly, some tumors use metalloprotease-mediated shedding of B7-H6 from their surface to escape immune cell recognition, which is also associated with reduced NKp30 expression and dysfunction due to chronic engagement of NK cells, resulting in poor patients' overall survival [190], [191]. Furthermore, soluble B7-H6 was detected in the sera of patients with gram-negative sepsis suggesting a B7-H6-dependent NK cell inhibition during inflammation [185].

However, it was demonstrated that the engagement of NKp30 upon B7-H6 binding is sufficient for NK cell activation resulting in degranulation and secretion of proinflammatory cytokines, as shown by NKp30-dependent NK cell-mediated killing of B7-H6 expressing human erythroleukemic K562 cells [176].

For this reason and the aforementioned restricted expression on stressed cells, NKp30 engagement via B7-H6 seems to be a promising approach for possible immunotherapies. To this end, conceptual approaches were evaluated by Peipp and colleagues involving the fusion of B7-H6 ectodomain to an antibody single chain variable fragment (scFv) either addressing human epidermal growth factor 2 (HER2) on HER2-positive breast cancers or targeting CD20 on B cell lymphomas, revealing specific target-dependent cellular cytotoxicities [72], [179], [180].

Based on these results and the observations of Yili Li et al. [184], who determined a low affinity of B7-H6 to its cognate receptor NKp30 with a dissociation constant of approximately 1 μM, one major task of this study was to assess if an increased affinity of B7-H6 to NKp30 translates into an improved NK cell-mediated cytolyses using a bispecific antibody-like scaffold.

3.4 Surface display systems

A modified version of the following section has been submitted by our group and has recently been accepted for publication as book chapter in *Introduction to Antibody Engineering* Rüker & Wozniak-Knopp (eds) (see chapter 6.5 and 7.5)

Besides Hybridoma technology, which still remains state-of-the-art in antibody hit discovery, several display technologies have emerged during the last decades that were inspired by the work of Köhler and Milstein, who fused single antibody expressing B cells with immortal myeloma cells, resulting in culturable monoclonal antibody (mAb) expressing hybridoma cells [192].
Until now, distinct display systems have been described, comprising non-cellular systems like mRNA display, ribosomal display and DNA display, as well as cellular systems like phage display and yeast surface display. The most essential feature of these in vitro selection platforms relies on genotype phenotype coupling, allowing for backtracking of the represented protein selected by its biophysical properties to its genetic code. Thus, all display systems simulate the B cell maturation cycle in vivo, aiming at the amplification of desired candidates matching the requirements. Since display systems have been developed for more than thirty years, they can be applied for manifold and complex approaches like affinity maturation, screening for pH-sensitive binding or for peptides recognizing chemical modifications, small molecules or toxins [193]–[195]. However, the identification of appropriate proteins with prescribed properties via surface display methodologies still remains laborious and challenging, since large diversities created by either naïve, immunized or synthetic repertoires need to be screened [196].

3.4.1 Phage Display

Based on the idea of George P. Smith, who fused the genetic code of oligo-peptides to the minor coat protein III (pIII) gene of filamentous *E. coli* phage M13, Sir Gregory P. Winter refined this methodology for antibody engineering, thereby generating the first and still most frequently used in vitro selection system named phage display [197].
In the classical phage display approach, the initial step is the library construction. For this, the desired proteins, e.g. antibodies, are cloned as a protein::pIII fusion into a plasmid, referred to as “phagemid” in *Escherichia coli* (*E. coli*). By separating the protein::pIII fusion from other cis-acting elements for phage replication and packaging, a more flexible system was achieved. Most of the phage display systems available today still rely on the classical fusion to pIII, thus reflecting the robust and versatile system of the protein::pIII fusion [198].
After cloning, the resulting *E. coli* library is infected with helper phage providing the necessary components for final assembling of the phagemid into phage particles and subsequent protein display on their surface [198], [199]. This crucial step for protein presentation on the phage surface was significantly enhanced by Dübel and colleagues, who developed an improved helper phage system, the so-called “hyperphage” [200].

When the phagemid containing bacteriophages display the translated fusion proteins on their surface, the "panning" step is employed, meaning that the bacteriophages displaying the respective library candidates are incubated with immobilized antigen. While the antigen-specific variants associate with the target protein, the unspecific molecules are removed by washing steps. Within this process, chemical, biological and physical parameters, such as pH, competitor or temperature, can be adjusted, to force the isolation of protein with desired properties. After elution of the antigen-specific bacteriophages, *E. coli* cells are infected once more, enabling the amplification of the enriched protein candidates for iterative phage display rounds.

Phage display allows for the rapid generation of libraries in the range of more than 10^{11} variants and the utilization of different antibody scaffolds [201]–[206]. However, due to the utilization of a prokaryotic folding machinery in *E. coli*, the production of complex structures like full-length antibodies remains challenging.

Until today, phage display enabled the isolation of several biologics which are in clinical and preclinical stages or even been granted market approval [207]. As an example, the commercially most successful fully human antibody Adalimumab was engineered by phage display, as was the 2011 by FDA-approved B cell-activating factor inhibiting antibody Belimumab [208], [209].

3.4.2 Yeast Surface Display

The yeast surface display (YSD) technology was described for the first time by Boder and Wittrup in 1997. This process utilizes the eukaryotic yeast strain *Saccharomyces cerevisiae* for the cell surface display of the protein of interest (POI) [210]. The expression of the POI is mediated by the genetical fusion to surface anchor proteins like a-agglutinin of *S. cerevisiae*, which normally mediates cell adhesion contact to other yeast cells during the mating process [211], [212]. This glycoprotein consists of two subunits, of which Aga1p is linked to the cell membrane via a glycosylphosphatidylinositol (GPI) anchor and is covalently linked to subunit Aga2p by two disulfide bridges [213]. Fusion of the POI to subunit Aga2p consequently enables the surface presentation and attachment to the yeast cell surface. To reliably induce the expression of the POI on the yeast cell surface, Boder and Wittrup developed a system well established today, in which the expression of both Aga1p, integrated in the yeast genome, as well as Aga2p, linked to the POI and expressed from a display plasmid, is controlled by a galactose-inducible promotor.

Due to the eukaryotic background of yeast cells, which provides an adequate protein-folding machinery, even more complex structures like whole IgG1 antibodies can be displayed [214]. Additionally, other structures like antibody scFv, Fabs or Nanobodies can be presented on the cell surface [215].

Initially, a diversity of the POI is used for the transformation of yeast cells, followed by a cell metabolism switch due to a change of the carbon source glucose to galactose, thereby inducing the POI expression. Then, the yeast cells can be screened via FACS for cells displaying an POI with desired properties, which represents another advantage of YSD over classical biopanning. Typically, in FACS screenings, distinct fluorescence dyes are used for antigen labeling as well as dyes to check the protein display on the yeast

cells by, e.g., genetic implementation of a HA tag into the expression plasmid and the use of fluorescently labeled antibodies directed against it. These dyes can be detected simultaneously, thus allowing for the detection as well as quantification of the fluorescence signals from each yeast cell, further enabling the collection of double positive cells (antibody-presenting and antigen-binding) [216]. During several rounds of sorting, the antigen-specific diversity can be increased. Further, by adjusting the sorting stringency via, e.g., gating strategy or a decrease in antigen concentration, cells matching predefined characteristics such as high-affinities variants can be enriched [217]. The applicability of YSD for affinity maturation was already demonstrated by Boder and Wittrup in 1997 with studies on a fluorescein-binding scFv and further validated by Wittrup and colleagues in 2000 with the identification of an antibody with affinities among the highest reported so far [210], [218].

Besides the maturation of antibody affinities, YSD was utilized to enhance the affinity of ligands to their cognate receptors, such as epidermal growth factor (EGF) or interleukin-2 (IL-2) with affinities increased up to thirtyfold for EGF receptor and IL-2 receptor alpha subunit, respectively, or an affinity enhanced approximately up to 50,000-fold of a signal-regulatory protein α (SIRPα) variant to the integrin associated protein (IAP, CD47), giving clear evidence that YSD application is not restricted to antibody scaffolds [219]–[221].

3.5 Bispecific antibodies and immunoligands

As briefly mentioned in chapter 3.4, Köhler and Milstein provided the basis for modern immune therapies with their research on mAb production, paving the way for more than 80 antibody therapeutics which have been granted market approval until today [222].

However, due to their monospecific structure enabling the binding of only one target, mAbs provide only a constrained mode of action limiting their efficacy in complex, multifactorial-originated diseases [223], [224]. To this end, more flexible and multi-specific scaffolds, such as bispecific antibodies (bsAbs), were developed, of which three bsAbs have already been granted market access and over 85 are under clinical investigation (as of 2019) [225]–[227].

As another possible therapeutic approach, bispecific immunoligands emerged, comprising at least one natural ligand-derived entity, whereas bsAbs comprise two physically connected single-binding antibody moieties enabling the simultaneous binding of two different structures [74], [228]. The choice whether to employ a bsAb or bispecific immunoligand as well as the final molecule format thereby influences its properties regarding processability, pharmacokinetics and pharmacodynamics [226], [229]–[231]. The latter, for instance, is suggested to be influenced by size and affinity of the bispecific molecules, altering shape and duration of the immunological synapse. [232]–[234].

All these bispecific proteins allow applications like addressing of distinct epitopes, blocking of different disease mediators or recruitment of immune cells to a specific target, which was, e.g., shown to receive curative outcomes for patients with minimal residual disease B cell precursor acute lymphoblastic

leukemia by treatment with bispecific T cell engager Blinatumomab [235], [236]. Besides T cells, other immune cells like NK cells can be exerted for this approach of immune cell redirection, which was, e.g., utilized by Peipp and colleagues employing bispecific immunoligands, exhibiting promising in vitro results [72], [179], [180]. In these studies, tumor-associated antigens targeting scFv antibody moieties were physically connected to NK cell activation receptor binding ligands. The advantage of these "Fc-less" formats relies on their small size allowing better tissue penetration as well as facile manufacturability due to expression of a single polypeptide chain. But the lack of the Fc portion is yet the main drawback of these bispecifics, as they cannot provoke Fc-mediated effector functions like ADCC or FcRn recycling, thereby evincing shorter plasma half-life influencing their therapeutic activities [237]. In contrast, the IgG-based bispecific constructs incorporating antibody Fc portions show prolonged half-life but struggle with mispairing of heavy chains (HCs) and light chains (LCs) during expression. To bypass this issue, different techniques evolved, which are explained elsewhere [226], [227], [238].

To overcome HC homodimerization in IgG-based bispecific molecules consisting of two distinct "half" antibodies each comprising a single HC and cognate LC to form the specific paratope, strategies like "knobs-into-holes" (KiH) or Strand-Exchange Engineered Domain (SEED) were developed. To force HC heterodimerization, KiH utilizes the introduction of bulky amino acid residues to one HC to form a "knob" and smaller residues on the opposite chain creating the shape of the complementary "hole" [239]. In contrast, by engineering of alternating IgA and IgG segments in the CH3 domains of both HCs, the SEED technology allows for heterodimerization due to the assembly of the resulting anti-parallel CH3 domains [240], [241].

Besides the homodimerization of HC, the two different LC in classical Fab-derived IgG-like bispecific antibodies can lead to mispairings, resulting in loss of affinity or even abrogation of antigen binding. This issue can be addressed by the incorporation of artificial, non-native linker sequences, connecting the heavy and light chain, like in scFv or scFab formats [242]. Another approach is based on domain crossover of CH1 and CL in a Fab moiety to obtain correct LC pairing, referred to as CrossMab [243].

A more extensive technology employs transgenic rodents, e.g. OmniFlic® rats, harboring a full human antibody VH diversity but only a single functional "common" LC [244]. Consequently, a bispecific antibody can be produced with only one LC, bypassing the LC mispairing issue. Besides these briefly described examples, other technologies for correct LC pairing have been developed, which are described elsewhere [238].

Additionally, another approach circumventing HC homodimerization and LC mispairing is the utilization of camelid nanobodies (VHH)- or VH-based IgG-like bispecific antibody platforms [245], [246]. The exchange of the antibodies VH and VL by VHH domains creates a bispecific antibody without the need of VL contribution. Hence, if expressed as IgG-like protein, a bispecific bivalent molecule with an intact Fc portion is formed. It was recently shown by our group that even a one-armed molecule of this format, thereby possessing monovalent bispecificity, was able to recruit and activate NK cells [246].

4 Objectives

Since the groundbreaking invention of the hybridoma technology in 1975 by Köhler and Milstein, extensive studies have enabled the generation of antibodies for distinct applications, such as laboratory and diagnostic tools and as therapeutic entities. Nowadays, a plethora of possibilities is available for the creation of different antibody and antibody-like structures, regarding their origin, format and biophysical properties, to name a few. Alongside, technologies facilitating the identification of specific antibodies with desired properties evolved, allowing for screenings of diversities obtained from immune, naïve or (semi-)synthetic libraries. However, search for appropriate antibodies during the pre-clinical phase still remains laborious and challenging. One aim of this study was the expansion of the existing phage and yeast surface display technology to streamline the hit-discovery process by the implementation of an optimized library generation approach. For this purpose, the *Golden Gate Cloning* (GGC) methodology was utilized for the generation of a combinatorial antibody library in a one-step process, bypassing the classical multi-step process for library generation. In more detail, the common approaches for the generation of combined VH and VL repertoires for phage and yeast surface display rely on execution of several successive cloning steps. One objective of this work was the simplification of this process by the application of a "one-pot" GGC reaction, while maintaining quality standards such as library functionality and number of hits. Moreover, the applicability of this optimized library generation approach should be tested for the facile generation of distinct antibody formats as well as different diversity sources.

The discovery of unique camelid heavy chain antibodies (hcAb) and their binding domains, referred to as nanobodies or VHHs, enables the generation of mono- and bispecific antibody structures devoid of light chains. In this context, Baty and colleagues published a proof of concept bispecific VHH-based Fab-like format utilizing the constant domains Cκ and CH1 of IgG as natural dimerization domains in 2013. According to this, IgG-like SEED bispecific VHH-based antibodies were created within this work via the replacement of VH and VL by different VHH domains. This allows the generation of full-length bi- and trispecific antibodies with adjustable valences for their cognate antigens. The generation and assessment of this novel VHH-antibody platform regarding its processability and biophysical properties of antibodies created was another aim of this work. Furthermore, the applicability of these molecules in the context of immune cell recruitment towards tumor cells should be examined in this work with exemplarily chosen immune therapy-relevant NK cells.

With respect to immune cell recruitment, bispecific immunoligands have attracted continual interest besides bsAbs, especially for the redirection of NK cells in cancer indications. It has been shown by Peipp and colleagues that NK cells can be recruited and simultaneously activated by the engagement of NKp30 via its natural ligand B7-H6 if used as bispecific immunoligand. It was also described by other groups that YSD has been successfully applied for the affinity maturation of polypeptides different to antibody molecules. Another essential part of this study was the affinity maturation of B7-H6 via YSD and the

assessment of the hypothesis that increased affinity of B7-H6 for NKp30 may translate into an enhanced NK cell cytolysis as well as an augmented secretion of proinflammatory cytokines.

5 References

[1] E. v. Behring, "Zur Geschichte der antitoxischen Antikörper," *Einführung die Lehre von der Bekämpfung der Infekt.*, no. Zur Geschichte der antitoxischen Antikörper, pp. 93–101, 1912.

[2] A. Tiselius, "Electrophoresis of serum globulin: Electrophoretic analysis of normal and immune sera.," *Biochem. J.*, vol. 31, no. 9, pp. 1464–77, 1937.

[3] A. Tiselius and E. A. Kabat, "An electrophoretic study of immune sera and purified antibody preparations," *J. Exp. Med.*, vol. 69, no. 1, pp. 119–132, 1939.

[4] H. W. Schroeder, L. Cavacini, H. W. Schroeder Jr., L. Cavacini, H. W. Schroeder, and L. Cavacini, "Structure and function of immunoglobulins.," *J. Allergy Clin. Immunol.*, vol. 125, no. 2 Suppl 2, pp. S41-52, 2010.

[5] L. L. Lu, T. J. Suscovich, S. M. Fortune, and G. Alter, "Beyond binding: Antibody effector functions in infectious diseases," *Nat. Rev. Immunol.*, vol. 18, no. 1, pp. 46–61, 2018.

[6] M. L. Chiu, D. R. Goulet, A. Teplyakov, and G. L. Gilliland, "Antibody Structure and Function: The Basis for Engineering Therapeutics," *Antibodies*, vol. 8, no. 4, p. 55, 2019.

[7] P. E. Funk, P. W. Kincade, and P. L. Witte, "Native associations of early hematopoietic stem cells and stromal cells isolated in bone marrow cell aggregates," *Blood*, vol. 83, no. 2, pp. 361–369, Jan. 1994.

[8] R. J. Ray, C. J. Paige, C. Furlonger, S. D. Lyman, and R. Rottapel, "Flt3 ligand supports the differentiation of early B cell progenitors in the presence of interleukin-11 and interleukin-7.," *Eur. J. Immunol.*, vol. 26, no. 7, pp. 1504–1510, Jul. 1996.

[9] M. Ichii, K. Oritani, and Y. Kanakura, "Early B lymphocyte development: Similarities and differences in human and mouse," *World J. Stem Cells*, vol. 6, no. 4, pp. 421–431, Sep. 2014.

[10] M. D'Apuzzo *et al.*, "The chemokine SDF-1, stromal cell-derived factor 1, attracts early stage B cell precursors via the chemokine receptor CXCR4.," *Eur. J. Immunol.*, vol. 27, no. 7, pp. 1788–1793, Jul. 1997.

[11] D. G. Schatz and P. C. Swanson, "V(D)J Recombination: Mechanisms of Initiation," *Annu. Rev. Genet.*, vol. 45, no. 1, pp. 167–202, Nov. 2011.

[12] K. Murphy and C. Weaver, *Janeway Immunologie*. 2018.

[13] S. V Desiderio *et al.*, "Insertion of N regions into heavy-chain genes is correlated with expression of terminal deoxytransferase in B cells.," *Nature*, vol. 311, no. 5988, pp. 752–755, Oct. 1984.

[14] N. R. Rose, "Molecular mimicry and clonal deletion: A fresh look," *J. Theor. Biol.*, vol. 375, pp. 71–76, Jun. 2015.

[15] E. T. Luning Prak, M. Monestier, and R. A. Eisenberg, "B cell receptor editing in tolerance and autoimmunity.," *Ann. N. Y. Acad. Sci.*, vol. 1217, pp. 96–121, Jan. 2011.

[16] A. Lanzavecchia, "Antigen-specific interaction between T and B cells," *Nature*, vol. 314, no. 6011, pp. 537–539, 1985.

[17] R. Elgueta, M. J. Benson, V. C. de Vries, A. Wasiuk, Y. Guo, and R. J. Noelle, "Molecular mechanism and function of CD40/CD40L engagement in the immune system," *Immunol. Rev.*, vol. 229, no. 1, pp. 152–172, May 2009.

[18] D. C. Parker, "T cell-dependent B cell activation.," *Annu. Rev. Immunol.*, vol. 11, pp. 331–360, 1993.

[19] Z. Li, C. J. Woo, M. D. Iglesias-Ussel, D. Ronai, and M. D. Scharff, "The generation of antibody diversity through somatic hypermutation and class switch recombination," *Genes Dev.*, vol. 18, no. 1, pp. 1–11, 2004.

[20] C. Keim, D. Kazadi, G. Rothschild, and U. Basu, "Regulation of AID, the B-cell genome mutator," *Genes Dev.*, vol. 27, no. 1, pp. 1–17, 2013.

[21] M. Stratigopoulou, T. P. van Dam, and J. E. J. Guikema, "Base Excision Repair in the Immune System: Small DNA Lesions With Big Consequences," *Front. Immunol.*, vol. 11, no. May, 2020.

[22] M. Liu and D. G. Schatz, "Balancing AID and DNA repair during somatic hypermutation," *Trends Immunol.*, vol. 30, no. 4, pp. 173–181, 2009.

[23] C. E. Stavnezer, Janet; Guikema, Jeroen E.J.; Schrader, "Mechanism and Regulation of Class Switch Recombination," *Annu Rev Immunol.*, vol. 26, pp. 261–292., 2008.

[24] M. Muramatsu, K. Kinoshita, S. Fagarasan, S. Yamada, Y. Shinkai, and T. Honjo, "Class switch recombination and hypermutation require activation-induced cytidine deaminase (AID), a potential RNA editing enzyme," *Cell*, vol. 102, no. 5, pp. 553–563, 2000.

[25] R. Racine and G. M. Winslow, "IgM in microbial infections: Taken for granted?," *Immunol. Lett.*, vol. 125, no. 2, pp. 79–85, 2009.

[26] T. H. Sharp, A. L. Boyle, C. A. Diebolder, A. Kros, A. J. Koster, and P. Gros, "Insights into IgM-mediated complement activation based on in situ structures of IgM-C1-C4b," *Proc. Natl. Acad. Sci. U. S. A.*, vol. 116, no. 24, pp. 11900–11905, 2019.

[27] B. Mantis,Nicholas J.; Rol, Nicolas; Corthésy, "Secretory IgA's Complex Roles in Immunity and Mucosal Homeostasis in the Gut," *Mucosal Immunol.*, vol. 4, no. 6, pp. 603–611, 2011.

[28] Y. Li, L. Jin, T. Chen, and C. J. Pirozzi, "The Effects of Secretory IgA in the Mucosal Immune System," *Biomed Res. Int.*, vol. 2020, 2020.

[29] S. J. Mukai, Kaori; Tsai, Mindy; Starkl, Philipp; Marichal, Thomas; Galli, "IgE and mast cells in host defense against parasites and venoms," *Semin Immunopathol*, vol. 38, no. 5, pp. 581–603, 2016.

[30] B. T. Kelly and M. H. Grayson, "Immunoglobulin E, what is it good for?," *Ann. Allergy, Asthma Immunol.*, vol. 116, no. 3, pp. 183–187, 2016.

[31] L. Liu, "Pharmacokinetics of monoclonal antibodies and Fc-fusion proteins," *Protein Cell*, vol. 9, no. 1, pp. 15–32, 2018.

[32] G. Vidarsson, G. Dekkers, and T. Rispens, "IgG subclasses and allotypes: From structure to effector functions," *Front. Immunol.*, vol. 5, no. OCT, pp. 1–17, 2014.

[33] W. Wang, A. K. Erbe, J. A. Hank, Z. S. Morris, and P. M. Sondel, "NK cell-mediated antibody-dependent cellular cytotoxicity in cancer immunotherapy," *Front. Immunol.*, vol. 6, no. JUL, 2015.

[34] D. Yang, A. Biragyn, L. W. Kwak, and J. J. Oppenheim, "Mammalian defensins in immunity: more than just microbicidal," *Trends Immunol.*, vol. 23, no. 6, pp. 291–296, 2002.

[35] K. De Smet and R. Contreras, "Human antimicrobial peptides: defensins, cathelicidins and histatins.," *Biotechnol. Lett.*, vol. 27, no. 18, pp. 1337–1347, Sep. 2005.

[36] F. Souza-Fonseca-Guimaraes, M. Adib-Conquy, and J. M. Cavaillon, "Natural killer (NK) cells in antibacterial innate immunity: angels or devils?," *Mol. Med.*, vol. 18, no. 1, pp. 270–285, 2012.

[37] A. M. Abel, C. Yang, M. S. Thakar, and S. Malarkannan, "Natural killer cells: Development, maturation, and clinical utilization," *Front. Immunol.*, vol. 9, no. AUG, pp. 1–23, 2018.

[38] S. H. Lee, T. Miyagi, and C. A. Biron, "Keeping NK cells in highly regulated antiviral warfare," *Trends Immunol.*, vol. 28, no. 6, pp. 252–259, 2007.

[39] S. D. Scoville, A. G. Freud, and M. A. Caligiuri, "Modeling human natural killer cell development in the era of innate lymphoid cells," *Front. Immunol.*, vol. 8, no. MAR, pp. 4–11, 2017.

[40] M. A. Yu, Jianhua; Freud, Aharon G.; Caligiuri, "Location and cellular stages of NK cell development," *Trends Immunol.*, vol. 34, no. 12, 2013.

[41] T. E. O'Sullivan, J. C. Sun, and L. L. Lanier, "Natural Killer Cell Memory," *Immunity*, vol. 43, no. 4, pp. 634–645, 2015.

[42] G. Min-oo, Y. Kamimura, D. W. Hendricks, and T. Nabekura, "NK cells: walking three paths down memory lane," *Trends Immunol.*, vol. 34, no. 6, pp. 251–258, 2013.

[43] J. Rosenberg, Jillian; Huang, "CD8+ T Cells and NK Cells: Parallel and Complementary Soldiers of Immunotherapy," *Curr Opin Chem Eng.*, vol. 19, pp. 9–20, 2018.

[44] T. A. Fehniger *et al.*, "CD56bright natural killer cells are present in human lymph nodes and are activated by T cell-derived IL-2: A potential new link between adaptive and innate immunity," *Blood*, vol. 101, no. 8, pp. 3052–3057, 2003.

[45] E. E. Rosmaraki, I. Douagi, C. Roth, F. Colucci, A. Cumano, and J. P. Di Santo, "Identification of committed NK cell progenitors in adult murine bone marrow," *Eur. J. Immunol.*, vol. 31, no. 6, pp. 1900–1909, Jun. 2001.

[46] V. Male *et al.*, "The transcription factor E4bp4/Nfil3 controls commitment to the NK lineage and directly regulates Eomes and Id2 expression," *J. Exp. Med.*, vol. 211, no. 4, pp. 635–642, 2014.

[47] R. B. Delconte *et al.*, "The Helix-Loop-Helix Protein ID2 Governs NK Cell Fate by Tuning Their Sensitivity to Interleukin-15," *Immunity*, vol. 44, no. 1, pp. 103–115, Jan. 2016.

[48] A. Ma, R. Koka, and P. Burkett, "Diverse Functions of Il-2, Il-15, and Il-7 in Lymphoid Homeostasis," *Annu. Rev. Immunol.*, vol. 24, no. 1, pp. 657–679, 2006.

[49] J. C. Sun and L. L. Lanier, "NK cell development, homeostasis and function: parallels with CD8+ T cells," *Nat. Rev. Immunol.*, vol. 11, no. 10, pp. 645–657, 2011.

[50] N. S. Williams *et al.*, "Natural killer cell differentiation: Insights from knockout and transgenic mouse models and in vitro systems," *Immunol. Rev.*, vol. 165, pp. 47–61, 1998.

[51] C. A. J. Vosshenrich *et al.*, "Roles for Common Cytokine Receptor γ-Chain-Dependent Cytokines in the Generation, Differentiation, and Maturation of NK Cell Precursors and Peripheral NK Cells in Vivo," *J. Immunol.*, vol. 174, no. 3, pp. 1213–1221, 2005.

[52] M. K. Kennedy *et al.*, "Reversible defects in natural killer and memory CD8 T cell lineages in interleukin 15-deficient mice," *J. Exp. Med.*, vol. 191, no. 5, pp. 771–780, 2000.

[53] F. Cichocki, B. Grzywacz, and J. S. Miller, "Human NK cell development: One road or many?," *Front. Immunol.*, vol. 10, no. AUG, pp. 1–10, 2019.

[54] F. Bozzano, F. Marras, and A. De Maria, "Natural killer cell development and maturation revisited: Possible implications of a novel distinct Lin-CD34+DNAM-1brightCXCR4+ cell progenitor," *Front. Immunol.*, vol. 8, no. MAR, pp. 6–13, 2017.

[55] S. S. Farag and M. A. Caligiuri, "Human natural killer cell development and biology," *Blood Rev.*, vol. 20, no. 3, pp. 123–137, 2006.

[56] M. A. Cooper, T. A. Fehniger, and M. A. Caligiuri, "The biology of human natural killer-cell subsets," vol. 22, no. 11, pp. 633–640, 2001.

[57] M. A. Cooper *et al.*, "Human natural killer cells: A unique innate immunoregulatory role for the CD56BRIGHT SUBSET," *Blood*, vol. 96, no. 11 PART II, pp. 3146–3151, 2000.

[58] T. Michel *et al.*, " Human CD56 bright NK Cells: An Update ," *J. Immunol.*, vol. 196, no. 7, pp. 2923–2931, 2016.

[59] J. A. Wagner *et al.*, "CD56bright NK cells exhibit potent antitumor responses following IL-15 priming," *J. Clin. Invest.*, vol. 127, no. 11, pp. 4042–4058, 2017.

[60] S. M. Poznanski and A. A. Ashkar, "What defines NK cell functional fate: Phenotype or metabolism?," *Front. Immunol.*, vol. 10, no. JUN, pp. 1–12, 2019.

[61] L. L. Lanier, "Nk Cell Receptors," *Annu. Rev. Immunol.*, vol. 16, no. 1, pp. 359–393, 1998.

[62] P. Parham, "Immunogenetics of killer cell immunoglobulin-like receptors," *Mol. Immunol.*, vol. 42, no. 4 SPEC. ISS., pp. 459–462, 2005.

[63] N. Isakov, "ITIMs and ITAMs The Yin and Yang of Antigen and Fc Receptor-Linked Signaling Machinery Department," *Immunol. Res.*, vol. 16, pp. 85–100, 1997.

[64] C. Chester, K. Fritsch, and H. E. Kohrt, "Natural killer cell immunomodulation: Targeting activating, inhibitory, and co-stimulatory receptor signaling for cancer immunotherapy," *Front. Immunol.*, vol. 6, no. DEC, pp. 1–9, 2015.

[65] S. Paul and G. Lal, "The molecular mechanism of natural killer cells function and its importance in cancer immunotherapy," *Front. Immunol.*, vol. 8, no. SEP, 2017.

[66] S. Kim *et al.*, "Licensing of natural killer cells by host major histocompatibility complex class I molecules," *Nature*, vol. 436, no. 7051, pp. 709–713, 2005.

[67] M. M. Tu, A. B. Mahmoud, and A. P. Makrigiannis, "Licensed and Unlicensed NK Cells: Differential Roles in Cancer and Viral Control," *Front. Immunol.*, vol. 7, p. 166, May 2016.

[68] D. H. Raulet and R. E. Vance, "Self-tolerance of natural killer cells," *Nat. Rev. Immunol.*, vol. 6, no. 7, pp. 520–531, 2006.

[69] H. G. Ljunggren and K. Kärre, "In search of the 'missing self': MHC molecules and NK cell recognition.," *Immunol. Today*, vol. 11, no. 7, pp. 237–244, Jul. 1990.

[70] C. Guillerey, N. D. Huntington, and M. J. Smyth, "Targeting natural killer cells in cancer immunotherapy," *Nat. Immunol.*, vol. 17, no. 9, pp. 1025–1036, 2016.

[71] J. Bubeník, "Tumour MHC class I downregulation and immunotherapy (Review)," *Oncol Rep*, vol. 10, no. 6, pp. 2005–2008, 2003.

[72] C. Kellner *et al.*, "Mimicking an Induced Self Phenotype by Coating Lymphomas with the NKp30 Ligand B7-H6 Promotes NK Cell Cytotoxicity," *J. Immunol.*, vol. 189, no. 10, pp. 5037–5046, 2012.

[73] F. Souza-Fonseca-Guimaraes, J. Cursons, and N. D. Huntington, "The Emergence of Natural Killer Cells as a Major Target in Cancer Immunotherapy," *Trends Immunol.*, vol. 40, no. 2, pp. 142–158, 2019.

[74] M. Vyas, U. Koehl, M. Hallek, and E. P. von Strandmann, "Natural ligands and antibody-based fusion proteins: Harnessing the immune system against cancer," *Trends Mol. Med.*, vol. 20, no. 2, pp. 72–82, 2014.

[75] D. K. Tourdot, Benjamin E; Brenner, Michelle K.; Keough, Kathleen C.; Holyst, Trudy; Newman, Peter J.; Newman, "Immunoreceptor Tyrosine-based Inhibitory Motif (ITIM)-mediated Inhibitory Signaling is Regulated by Sequential Phosphorylation Mediated by Distinct Nonreceptor Tyrosine Kinases: A Case Study Involving PECAM-1," *Biochemistry*, vol. 52, no. 15, pp. 2597–2608, 2013.

[76] E. Vivier, "Natural killer cell signaling pathways," *Science (80-.).*, vol. 306, no. 5701, p. 1517—1519, 2004.

[77] E. O. Kim, Hun Sik; Das, Asmita; Gross, Catharina C.; Bryceson, Yenan T.; Long, "Synergistic Signals for Natural Cytotoxicity Are Required to Overcome Inhibition by c-Cbl," *Immunity*, vol. 32, no. February, pp. 175–186, 2010.

[78] E. O. Long, "Negative signaling by inhibitory receptors: The NK cell paradigm," *Immunol. Rev.*, vol. 224, no. 1, pp. 70–84, 2008.

[79] A. Moretta, D. Pende, F. Locatelli, and L. Moretta, "Activating and inhibitory killer immunoglobulin-like receptors (KIR) in haploidentical haemopoietic stem cell transplantation to cure high-risk leukaemias," *Clin. Exp. Immunol.*, vol. 157, no. 3, pp. 325–331, 2009.

[80] K. S. Campbell and A. K. Purdy, "Structure/function of human killer cell immunoglobulin-like receptors: lessons from polymorphisms, evolution, crystal structures and mutations," *Immunology*, vol. 132, no. 3, pp. 315–325, Mar. 2011.

[81] F. Romagné *et al.*, "Preclinical characterization of 1-7F9, a novel human anti-KIR receptor therapeutic antibody that augments natural killer-mediated killing of tumor cells," *Blood*, vol. 114, no. 13, pp. 2667–2677, Sep. 2009.

[82] U. N. L. of Medicine, "NCT01687387 @ www.clinicaltrials.gov," *ClinicalTrials.gov*, 2012. [Online]. Available: http://www.clinicaltrials.gov/ct2/show/NCT01687387.

[83] López-Botet Miguel, M. Llano, F. Navarro, and T. Bellon, "NK cell recognition of non-classical HLA class I molecules," *Semin. Immunol.*, vol. 12, no. 2, pp. 109–119, 2000.

[84] N. Lee, D. R. Goodlett, A. Ishitani, H. Marquardt, and D. E. Geraghty, "HLA-E surface expression depends on binding of TAP-dependent peptides derived from certain HLA class I signal sequences.," *J. Immunol.*, vol. 160, no. 10, pp. 4951–60, 1998.

[85] R. Huang *et al.*, "Loss of Fas expression and high expression of HLA-E promoting the immune escape of early colorectal cancer cells," *Oncol. Lett.*, vol. 13, no. 5, pp. 3379–3386, May 2017.

[86] D. A. Costa Arantes *et al.*, "Evaluation of HLA-G, HLA-E, and PD-L1 proteins in oral osteosarcomas," *Oral Surg. Oral Med. Oral Pathol. Oral Radiol.*, vol. 123, no. 6, pp. e188–e196, 2017.

[87] T. Kamiya, M. Robinson, and D. Campana, "Blocking expression of inhibitory receptor NKG2A overcomes tumor resistance to NK cells Graphical abstract The Journal of Clinical Investigation," *J Clin Invest*, vol. 129, no. 5, pp. 2094–2106, 2019.

[88] P. André *et al.*, "Anti-NKG2A mAb Is a Checkpoint Inhibitor that Promotes Anti-tumor Immunity by Unleashing Both T and NK Cells," *Cell*, vol. 175, no. 7, pp. 1731-1743.e13, 2018.

[89] E. M. McWilliams *et al.*, "Therapeutic CD94/NKG2A blockade improves natural killer cell dysfunction in chronic lymphocytic leukemia," *Oncoimmunology*, vol. 5, no. 10, pp. 1–9, 2016.

[90] U. N. L. of Medicine, "NCT02643550 @ www.clinicaltrials.gov," *ClinicalTrials.gov*, 2015. [Online]. Available: http://www.clinicaltrials.gov/ct2/show/NCT02643550.

[91] U. N. L. of Medicine, "NCT02671435 @ www.clinicaltrials.gov," *ClinicalTrials.gov*, 2016. [Online]. Available: http://www.clinicaltrials.gov/ct2/show/NCT02671435.

[92] L. L. Lanier, B. C. Corliss, J. Wu, C. Leong, and J. H. Phillips, "Immunoreceptor DAP12 bearing a tyrosine-based activation motif is involved in activating NK cells," *Nature*, vol. 391, pp. 703–707, 1998.

[93] M. J. Wilson, J. A. Lindquist, and J. Trowsdale, "DAP12 and KAP10 (DAP10)-novel transmembrane adapter proteins of the CD3zeta family," *Immunol. Res.*, vol. 10, no. 1, pp. 21–42, 2000.

[94] L. L. Lanier, "DAP10- and DAP12-associated receptors in innate immunity," *Immunol. Rev.*, vol. 227, no. 1, pp. 150–160, 2009.

[95] R. Takaki, S. R. Watson, and L. L. Lanier, "DAP12: An adapter protein with dual functionality," *Immunol. Rev.*, vol. 214, no. 1, pp. 118–129, 2006.

[96] S. Kumar, "Natural killer cell cytotoxicity and its regulation by inhibitory receptors," *Immunology*, vol. 154, no. 3, pp. 383–393, 2018.

[97] E. O. Long, H. Sik Kim, D. Liu, M. E. Peterson, and S. Rajagopalan, "Controlling NK Cell Responses: Integration of Signals for Activation and Inhibition," *Annu. Rev. Immunol.*, vol. 31, pp. 227–258, 2013.

[98] L. Zamai, M. Ahmad, I. M. Bennett, L. Azzoni, E. S. Alnemri, and B. Perussia, "Natural killer (NK) cell-mediated cytotoxicity: Differential use of TRAIL and Fas ligand by immature and mature primary human NK cells," *J. Exp. Med.*, vol. 188, no. 12, pp. 2375–2380, 1998.

[99] M. E. Guicciardi and G. J. Gores, "Life and death by death receptors," *FASEB J.*, vol. 23, no. 6, pp. 1625–1637, Jun. 2009.

[100] M. J. Smyth *et al.*, "Activation of NK cell cytotoxicity," *Mol. Immunol.*, vol. 42, no. 4 SPEC. ISS., pp. 501–510, 2005.

[101] A. R. Kerr, J. F. R.; Wyllie, A. H.; Currie, "APOPTOSIS: A BASIC BIOLOGICAL PHENOMENON WITH WIDE- RANGING IMPLICATIONS IN TISSUE KINETICS," *Br. J. Cancer*, vol. 26, no. 239, 1972.

[102] S. Elmore, "Apoptosis: A Review of Programmed Cell Death," *Toxicol. Pathol.*, vol. 35, no. 4, pp. 495–516, 2007.

[103] E. Reichmann, "The biological role of the Fas/FasL system during tumor formation and progression," *Semin. Cancer Biol.*, vol. 12, no. 4, pp. 309–315, 2002.

[104] M. H. Chien *et al.*, "A Fas Ligand (FasL)-fused humanized antibody against tumor-Associated glycoprotein 72 selectively exhibits the cytotoxic effect against oral cancer cells with a low FasL/Fas ratio," *Mol. Cancer Ther.*, vol. 16, no. 6, pp. 1102–1113, 2017.

[105] K. Takeda *et al.*, "Involvement of tumor necrosis factor-related apoptosis-inducing ligand in surveillance of tumor metastasis by liver natural killer cells," *Nat. Med.*, vol. 7, no. 1, pp. 94–100, 2001.

[106] A. Thorburn, "Tumor Necrosis Factor-Related Apoptosis-Inducing Ligand (TRAIL) Pathway Signaling," *J. Thorac. Oncol.*, vol. 2, no. 6, pp. 461–465, 2007.

[107] H. Wajant, "Molecular mode of action of TRAIL receptor agonists—Common principles and their translational exploitation," *Cancers (Basel).*, vol. 11, no. 7, 2019.

[108] K. Legler *et al.*, "The novel TRAIL-receptor agonist APG350 exerts superior therapeutic activity in pancreatic cancer cells," *Cell Death Dis.*, vol. 9, no. 5, 2018.

[109] S. Bauer *et al.*, "Activation of NK Cells and T Cells by NKG2D, a Receptor for Stress-Inducible MICA," *Science (80-.).*, vol. 285, no. 5428, pp. 727 LP – 729, Jul. 1999.

[110] S. Gasser, S. Orsulic, E. J. Brown, and D. H. Raulet, "The DNA damage pathway regulates innate immune system ligands of the NKG2D receptor," *Nature*, vol. 436, no. 7054, pp. 1186–1190, Aug. 2005.

[111] J. L. Upshaw, L. N. Arneson, R. A. Schoon, C. J. Dick, D. D. Billadeau, and P. J. Leibson, "NKG2D-mediated signaling requires a DAP10-bound Grb2-Vav1 intermediate and phosphatidylinositol-3-kinase in human natural killer cells.," *Nat. Immunol.*, vol. 7, no. 5, pp. 524–532, May 2006.

[112] N. Guerra *et al.*, "NKG2D-deficient mice are defective in tumor surveillance in models of spontaneous malignancy," *Immunity*, vol. 28, no. 4, pp. 571–580, Apr. 2008.

[113] V. Groh, J. Wu, C. Yee, and T. Spies, "Tumour-derived soluble MIC ligands impair expression of NKG2D and T-cell activation," *Nature*, vol. 419, no. 6908, pp. 734–738, 2002.

[114] W. Deng *et al.*, "A shed NKG2D ligand that promotes natural killer cell activation and tumor rejection," *Science (80-.).*, vol. 348, no. 6230, pp. 136–139, 2015.

[115] M. R. Zocchi *et al.*, "ADAM10 new selective inhibitors reduce NKG2D ligand release sensitizing Hodgkin lymphoma cells to NKG2D-mediated killing," *Oncoimmunology*, vol. 5, no. 5, pp. e1123367–e1123367, Dec. 2015.

[116] L. F. De Andrade *et al.*, "Antibody-mediated inhibition of MICA and MICB shedding promotes NK cell-driven tumor immunity," *Science (80-.).*, vol. 359, no. 6383, pp. 1537–1542, 2018.

[117] D. Metes *et al.*, "Ligand binding specificities and signal transduction pathways of Fc gamma receptor IIc isoforms: the CD32 isoforms expressed by human NK cells," *Eur. J. Immunol.*, vol. 29, no. 9, p. 2842—2852, Sep. 1999.

[118] X. Li *et al.*, "Allelic-dependent expression of an activating Fc receptor on B cells enhances humoral immune responses," *Sci. Transl. Med.*, vol. 5, no. 216, 2013.

[119] A. Musolino *et al.*, "Immunoglobulin G fragment C receptor polymorphisms and clinical efficacy of trastuzumab-based therapy in patients with HER-2/neu-positive metastatic breast cancer.," *J. Clin. Oncol. Off. J. Am. Soc. Clin. Oncol.*, vol. 26, no. 11, pp. 1789–1796, Apr. 2008.

[120] G. Cartron *et al.*, "Therapeutic activity of humanized anti-CD20 monoclonal antibody and polymorphism in IgG Fc receptor FcγrIIIa gene," *Blood*, vol. 99, no. 3, pp. 754–758, 2002.

[121] J. Rodríguez *et al.*, "Fc gamma receptor polymorphisms as predictive markers of Cetuximab efficacy in epidermal growth factor receptor downstream-mutated metastatic colorectal cancer," *Eur. J. Cancer*, vol. 48, no. 12, pp. 1774–1780, 2012.

[122] Y. T. Bryceson, M. E. March, H.-G. Ljunggren, and E. O. Long, "Synergy among receptors on resting NK cells for the activation of natural cytotoxicity and cytokine secretion," *Blood*, vol. 107, no. 1, pp. 159–166, Jan. 2006.

[123] A. Blázquez-Moreno, S. Park, W. Im, M. J. Call, M. E. Call, and H. T. Reyburn, "Transmembrane features governing Fc receptor CD16A assembly with CD16A signaling adaptor molecules," *Proc. Natl. Acad. Sci. U. S. A.*, vol. 114, no. 28, pp. E5645–E5654, 2017.

[124] C. Watzl and E. O. Long, "Signal transduction during activation and inhibition of natural killer cells," *Curr. Protoc. Immunol.*, vol. Chapter 11, pp. 10.1002/0471142735.im1109bs90-11.9B, Aug. 2010.

[125] C. Lo Nigro, M. Macagno, D. Sangiolo, L. Bertolaccini, M. Aglietta, and M. C. Merlano, "NK-mediated antibody-dependent cell-mediated cytotoxicity in solid tumors: biological evidence and clinical perspectives," *Ann. Transl. Med.*, vol. 7, no. 5, p. 105, Mar. 2019.

[126] N. C. Smits, T. A. Coupet, C. Godbersen, and C. L. Sentman, "Designing multivalent proteins based on natural killer cell receptors and their ligands as immunotherapy for cancer," *Expert Opin. Biol. Ther.*, vol. 16, no. 9, pp. 1105–1112, Sep. 2016.

[127] E. Sanseviero, "NK Cell-Fc Receptors Advance Tumor Immunotherapy," *J. Clin. Med.*, vol. 8, no. 10, p. 1667, Oct. 2019.

[128] U. N. L. of Medicine, "NCT02321592 @ www.clinicaltrials.gov," *ClinicalTrials.gov*, 2014. .

[129] R. Romee *et al.*, "NK cell CD16 surface expression and function is regulated by a disintegrin and metalloprotease-17 (ADAM17)," *Blood*, vol. 121, no. 18, pp. 3599–3608, May 2013.

[130] K. Srpan *et al.*, "Shedding of CD16 disassembles the NK cell immune synapse and boosts serial engagement of target cells," *J. Cell Biol.*, vol. 217, no. 9, pp. 3267–3283, 2018.

[131] S. Sivori *et al.*, "p46, a novel natural killer cell-specific surface molecule that mediates cell activation.," *J. Exp. Med.*, vol. 186, no. 7, pp. 1129–1136, Oct. 1997.

[132] M. Vitale *et al.*, "NKp44, a novel triggering surface molecule specifically expressed by activated natural killer cells, is involved in non-major histocompatibility complex-restricted tumor cell lysis.," *J. Exp. Med.*, vol. 187, no. 12, pp. 2065–2072, Jun. 1998.

[133] D. Pende *et al.*, "Identification and molecular characterization of NKp30, a novel triggering receptor involved in natural cytotoxicity mediated by human natural killer cells.," *J. Exp. Med.*, vol. 190, no. 10, pp. 1505–1516, Nov. 1999.

[134] M. G. Joyce and P. D. Sun, "The structural basis of ligand recognition by natural killer cell receptors.," *J. Biomed. Biotechnol.*, vol. 2011, p. 203628, 2011.

[135] A. D. Barrow, C. J. Martin, and M. Colonna, "The natural cytotoxicity receptors in health and disease," *Front. Immunol.*, vol. 10, no. MAY, pp. 1–20, 2019.

[136] P. H. Kruse, J. Matta, S. Ugolini, and E. Vivier, "Natural cytotoxicity receptors and their ligands," *Immunol. Cell Biol.*, vol. 92, no. 3, pp. 221–229, 2014.

[137] A. Pessino *et al.*, "Molecular cloning of NKp46: a novel member of the immunoglobulin superfamily involved in triggering of natural cytotoxicity.," *J. Exp. Med.*, vol. 188, no. 5, pp. 953–960, Sep. 1998.

[138] Y. Shemer-Avni *et al.*, "Expression of NKp46 Splice Variants in Nasal Lavage Following Respiratory Viral Infection: Domain 1-Negative Isoforms Predominate and Manifest Higher Activity," *Front. Immunol.*, vol. 8, p. 161, Feb. 2017.

[139] A. Diefenbach, M. Colonna, and S. Koyasu, "Development, differentiation, and diversity of innate lymphoid cells.," *Immunity*, vol. 41, no. 3, pp. 354–365, Sep. 2014.

[140] T. Verrier, N. Satoh-Takayama, N. Serafini, S. Marie, J. P. Di Santo, and C. A. J. Vosshenrich, "Phenotypic and Functional Plasticity of Murine Intestinal NKp46+ Group 3 Innate Lymphoid Cells," *J. Immunol.*, vol. 196, no. 11, pp. 4731–4738, Jun. 2016.

[141] C. A. Stewart, T. Walzer, S. H. Robbins, B. Malissen, E. Vivier, and I. Prinz, "Germ-line and rearranged Tcrd transcription distinguish bona fide NK cells and NK-like γδ T cells," *Eur. J. Immunol.*, vol. 37, no. 6, pp. 1442–1452, Jun. 2007.

[142] J. Ettersperger *et al.*, "Interleukin-15-Dependent T-Cell-like Innate Intraepithelial Lymphocytes Develop in the Intestine and Transform into Lymphomas in Celiac Disease.," *Immunity*, vol. 45, no. 3, pp. 610–625, Sep. 2016.

[143] B. Meresse *et al.*, "Reprogramming of CTLs into natural killer-like cells in celiac disease," *J. Exp. Med.*, vol. 203, no. 5, pp. 1343–1355, May 2006.

[144] R. Gazit *et al.*, "Lethal influenza infection in the absence of the natural killer cell receptor gene Ncr1.," *Nat. Immunol.*, vol. 7, no. 5, pp. 517–523, May 2006.

[145] A. Glasner *et al.*, "Recognition and Prevention of Tumor Metastasis by the NK Receptor NKp46/NCR1," *J. Immunol.*, vol. 188, no. 6, pp. 2509 LP – 2515, Mar. 2012.

[146] E. Narni-Mancinelli *et al.*, "Tuning of natural killer cell reactivity by NKp46 and Helios calibrates T cell responses.," *Science*, vol. 335, no. 6066, pp. 344–348, Jan. 2012.

[147] A. Bensussan, N. Remtoula, S. Sivori, M. Bagot, A. Moretta, and A. Marie-Cardine, "Expression and function of the natural cytotoxicity receptor NKp46 on circulating malignant CD4+ T lymphocytes of Sézary syndrome patients.," *J. Invest. Dermatol.*, vol. 131, no. 4, pp. 969–976, Apr. 2011.

[148] A. G. Freud *et al.*, "Expression of the activating receptor, NKp46 (CD335), in human natural killer and T-cell neoplasia.," *Am. J. Clin. Pathol.*, vol. 140, no. 6, pp. 853–866, Dec. 2013.

[149] Y. Wang, W. Yuan, H. Guo, and Y. Jiang, "High frequency of activated NKp46(+) natural killer cells in patients with new diagnosed of latent autoimmune diabetes in adults.," *Autoimmunity*, vol. 48, no. 4, pp. 267–273, Jun. 2015.

[150] R. Yossef *et al.*, "Targeting Natural Killer Cell Reactivity by Employing Antibody to NKp46: Implications for Type 1 Diabetes," *PLoS One*, vol. 10, no. 2, p. e0118936, Feb. 2015.

[151] O. Berhani *et al.*, "Human anti-NKp46 antibody for studies of NKp46-dependent NK cell function and its applications for type 1 diabetes and cancer research," *Eur. J. Immunol.*, vol. 49, no. 2, pp. 228–241, Feb. 2019.

[152] T. I. Arnon *et al.*, "The mechanisms controlling the recognition of tumor- and virus-infected cells by NKp46.," *Blood*, vol. 103, no. 2, pp. 664–672, Jan. 2004.

[153] O. Mandelboim *et al.*, "Recognition of haemagglutinins on virus-infected cells by NKp46 activates lysis by human NK cells.," *Nature*, vol. 409, no. 6823, pp. 1055–1060, Feb. 2001.

[154] M. Jarahian *et al.*, "Activation of Natural Killer Cells by Newcastle Disease Virus Hemagglutinin-Neuraminidase," *J. Virol.*, vol. 83, no. 16, pp. 8108 LP – 8121, Aug. 2009.

[155] R. Vankayalapati *et al.*, "Role of NK cell-activating receptors and their ligands in the lysis of mononuclear phagocytes infected with an intracellular bacterium.," *J. Immunol.*, vol. 175, no. 7, pp. 4611–4617, Oct. 2005.

[156] A. Garg *et al.*, "Vimentin expressed on Mycobacterium tuberculosis-infected human monocytes is involved in binding to the NKp46 receptor.," *J. Immunol.*, vol. 177, no. 9, pp. 6192–6198, Nov. 2006.

[157] E. Cagnano *et al.*, "Expression of Ligands to NKp46 in Benign and Malignant Melanocytes," *J. Invest. Dermatol.*, vol. 128, no. 4, pp. 972–979, 2008.

[158] Y. Tal *et al.*, "An NCR1-based chimeric receptor endows T-cells with multiple anti-tumor specificities," *Oncotarget*, vol. 5, no. 21, pp. 10949–10958, Nov. 2014.

[159] L. Gauthier *et al.*, "Multifunctional Natural Killer Cell Engagers Targeting NKp46 Trigger Protective Tumor Immunity," *Cell*, vol. 177, no. 7, pp. 1701-1713.e16, 2019.

[160] C. Cantoni *et al.*, "NKp44, a triggering receptor involved in tumor cell lysis by activated human natural killer cells, is a novel member of the immunoglobulin superfamily.," *J. Exp. Med.*, vol. 189, no. 5, pp. 787–796, Mar. 1999.

[161] I. Mattiola *et al.*, "Priming of Human Resting NK Cells by Autologous M1 Macrophages via the Engagement of IL-1β, IFN-β, and IL-15 Pathways," *J. Immunol.*, vol. 195, no. 6, pp. 2818–2828, 2015.

[162] R. J. N. Allcock, A. D. Barrow, S. Forbes, S. Beck, and J. Trowsdale, "The human TREM gene cluster at 6p21.1 encodes both activating and inhibitory single IgV domain receptors and includes NKp44.," *Eur. J. Immunol.*, vol. 33, no. 2, pp. 567–577, Feb. 2003.

[163] O. Hershkovitz *et al.*, "NKp44 receptor mediates interaction of the envelope glycoproteins from the West Nile and dengue viruses with NK cells.," *J. Immunol.*, vol. 183, no. 4, pp. 2610–2621, Aug. 2009.

[164] F. Baychelier, A. Sennepin, M. Ermonval, K. Dorgham, P. Debré, and V. Vieillard, "Identification of a cellular ligand for the natural cytotoxicity receptor NKp44.," *Blood*, vol. 122, no. 17, pp. 2935–2942, Oct. 2013.

[165] S. Gaggero *et al.*, "Nidogen-1 is a novel extracellular ligand for the NKp44 activating receptor," *Oncoimmunology*, vol. 7, no. 9, p. e1470730, Sep. 2018.

[166] N. Willumsen, C. L. Bager, D. J. Leeming, A. C. Bay-Jensen, and M. A. Karsdal, "Nidogen-1 Degraded by Cathepsin S can be Quantified in Serum and is Associated with Non–Small Cell Lung Cancer," *Neoplasia (United States)*, vol. 19, no. 4, pp. 271–278, 2017.

[167] N. F. Delahaye *et al.*, "Alternatively spliced NKp30 isoforms affect the prognosis of gastrointestinal stromal tumors," *Nat. Med.*, vol. 17, no. 6, pp. 700–707, 2011.

[168] D. V Correia, M. Fogli, K. Hudspeth, M. G. da Silva, D. Mavilio, and B. Silva-Santos, "Differentiation of human peripheral blood Vδ1+ T cells expressing the natural cytotoxicity receptor NKp30 for recognition of lymphoid leukemia cells.," *Blood*, vol. 118, no. 4, pp. 992–1001, Jul. 2011.

[169] M. P. Correia *et al.*, "Distinct human circulating NKp30(+)FcεRIγ(+)CD8(+) T cell population exhibiting high natural killer-like antitumor potential.," *Proc. Natl. Acad. Sci. U. S. A.*, vol. 115, no. 26, pp. E5980–E5989, Jun. 2018.

[170] Q. Tang *et al.*, "Umbilical cord blood T cells express multiple natural cytotoxicity receptors after IL-15 stimulation, but only NKp30 is functional.," *J. Immunol.*, vol. 181, no. 7, pp. 4507–4515, Oct. 2008.

[171] T. I. Arnon *et al.*, "Inhibition of the NKp30 activating receptor by pp65 of human cytomegalovirus.," *Nat. Immunol.*, vol. 6, no. 5, pp. 515–523, May 2005.

[172] M. Jarahian *et al.*, "Modulation of NKp30- and NKp46-mediated natural killer cell responses by poxviral hemagglutinin.," *PLoS Pathog.*, vol. 7, no. 8, p. e1002195, Aug. 2011.

[173] E. Mavoungou, J. Held, L. Mewono, and P. G. Kremsner, "A Duffy binding-like domain is involved in the NKp30-mediated recognition of Plasmodium falciparum-parasitized erythrocytes by natural killer cells.," *J. Infect. Dis.*, vol. 195, no. 10, pp. 1521–1531, May 2007.

[174] S. S. Li *et al.*, "The NK receptor NKp30 mediates direct fungal recognition and killing and is diminished in NK cells from HIV-infected patients.," *Cell Host Microbe*, vol. 14, no. 4, pp. 387–397, Oct. 2013.

[175] S. S. Li *et al.*, "Identification of the fungal ligand triggering cytotoxic PRR-mediated NK cell killing of Cryptococcus and Candida," *Nat. Commun.*, vol. 9, no. 1, p. 751, Feb. 2018.

[176] C. S. Brandt *et al.*, "The B7 family member B7-H6 is a tumor cell ligand for the activating natural killer cell receptor NKp30 in humans," *J. Exp. Med.*, vol. 206, no. 7, pp. 1495–1503, Jun. 2009.

[177] S. Memmer *et al.*, "The Stalk Domain of NKp30 Contributes to Ligand Binding and Signaling of a Preassembled NKp30-CD3ζ Complex," *J. Biol. Chem.*, vol. 291, no. 49, pp. 25427–25438, Dec. 2016.

[178] J. Hartmann *et al.*, "The stalk domain and the glycosylation status of the activating natural killer cell receptor NKp30 are important for ligand binding," *J. Biol. Chem.*, vol. 287, no. 37, pp. 31527–31539, Sep. 2012.

[179] C. Kellner *et al.*, "Enhancing natural killer cell-mediated lysis of lymphoma cells by combining therapeutic antibodies with CD20-specific immunoligands engaging NKG2D or NKp30," *Oncoimmunology*, vol. 5, no. 1, pp. 1–12, 2016.

[180] M. Peipp *et al.*, "HER2-specific immunoligands engaging NKp30 or NKp80 trigger NK-cell-mediated lysis of tumor cells and enhance antibody-dependent cell-mediated cytotoxicity," *Oncotarget*, vol. 6, no. 31, pp. 32075–32088, 2015.

[181] T. Zhang, M.-R. Wu, and C. L. Sentman, "An NKp30-based chimeric antigen receptor promotes T cell effector functions and antitumor efficacy in vivo," *J. Immunol.*, vol. 189, no. 5, pp. 2290–2299, Sep. 2012.

[182] M.-R. Wu, T. Zhang, L. R. DeMars, and C. L. Sentman, "B7H6-specific chimeric antigen receptors lead to tumor elimination and host antitumor immunity," *Gene Ther.*, vol. 22, no. 8, pp. 675–684, Aug. 2015.

[183] J. Watkins-Yoon *et al.*, "CTX-8573, an Innate-Cell Engager Targeting BCMA, is a Highly Potent Multispecific Antibody for the Treatment of Multiple Myeloma," *Blood*, vol. 134, no. Supplement_1, p. 3182, Nov. 2019.

[184] Y. Li, Q. Wang, and R. A. Mariuzza, "Structure of the human activating natural cytotoxicity receptor NKp30 bound to its tumor cell ligand B7-H6.," *J. Exp. Med.*, vol. 208, no. 4, pp. 703–714, Apr. 2011.

[185] J. Matta *et al.*, "Induction of B7-H6, a ligand for the natural killer cell-activating receptor NKp30, in inflammatory conditions.," *Blood*, vol. 122, no. 3, pp. 394–404, Jul. 2013.

[186] A. Obiedat *et al.*, "The integrated stress response promotes B7H6 expression," *J. Mol. Med.*, vol. 98, no. 1, pp. 135–148, 2020.

[187] G. Cao, J. Wang, X. Zheng, H. Wei, Z. Tian, and R. Sun, "Tumor Therapeutics Work as Stress Inducers to Enhance Tumor Sensitivity to Natural Killer (NK) Cell Cytolysis by Up-regulating NKp30 Ligand B7-H6.," *J. Biol. Chem.*, vol. 290, no. 50, pp. 29964–29973, Dec. 2015.

[188] Y. Charpak-Amikam *et al.*, "Human cytomegalovirus escapes immune recognition by NK cells through the downregulation of B7-H6 by the viral genes US18 and US20.," *Sci. Rep.*, vol. 7, no. 1, p. 8661, Aug. 2017.

[189] D. Schmiedel, J. Tai, F. Levi-Schaffer, S. Dovrat, and O. Mandelboim, "Human Herpesvirus 6B Downregulates Expression of Activating Ligands during Lytic Infection To Escape Elimination by Natural Killer Cells.," *J. Virol.*, vol. 90, no. 21, pp. 9608–9617, Nov. 2016.

[190] E. Schlecker *et al.*, "Metalloprotease-mediated tumor cell shedding of B7-H6, the ligand of the natural killer cell-activating receptor NKp30.," *Cancer Res.*, vol. 74, no. 13, pp. 3429–3440, Jul. 2014.

[191] S. Pesce *et al.*, "B7-H6-mediated downregulation of NKp30 in NK cells contributes to ovarian carcinoma immune escape.," *Oncoimmunology*, vol. 4, no. 4, p. e1001224, Apr. 2015.

[192] G. Köhler and C. Milstein, "Continuous cultures of fused cells secreting antibody of predefined specificity," *Nature*, vol. 256, 1975.

[193] H. Thie, B. Voedisch, S. Dübel, M. Hust, and T. Schirrmann, "Affinity maturation by phage display.," *Methods Mol. Biol.*, vol. 525, pp. 309–22, 2009.

[194] C. Schröter *et al.*, "A generic approach to engineer antibody pH-switches using combinatorial histidine scanning libraries and yeast display," *MAbs*, vol. 7, no. 1, pp. 138–151, 2015.

[195] A. R. M. Bradbury, S. Sidhu, J. Mccafferty, and L. Alamos, "Beyond natural antibodies: the power of in vitro display technologies," *Nat Biotechnol.*, vol. 29, no. 3, pp. 245–254, 2011.

[196] H. R. Hoogenboom, "Selecting and screening recombinant antibody libraries," *Nat. Biotechnol.*, vol. 23, no. 9, pp. 1105–1116, 2005.

[197] G. P. Smith, "Filamentous fusion phage: novel expression vectors that display cloned antigens on the virion surface," *Science (80-.).*, vol. 228, no. 4705, pp. 1315 LP – 1317, Jun. 1985.

[198] F. Breitling, S. Dübel, T. Seehaus, I. Klewinghaus, and M. Little, "A surface expression vector for antibody screening," *Gene*, vol. 104, no. 2, pp. 147–153, 1991.

[199] C. F. Barbas, A. S. Kang, R. A. Lerner, and S. J. Benkovic, "Assembly of combinatorial antibody libraries on phage surfaces: The gene III site," *Proc. Natl. Acad. Sci. U. S. A.*, vol. 88, no. 18, pp. 7978–7982, 1991.

[200] S. Rondot, J. Koch, F. Breitling, and S. Dübel, "A helper phage to improve single-chain antibody presentation in phage display," *Nat. Biotechnol.*, vol. 19, no. 1, pp. 75–78, 2001.

[201] M. Hust *et al.*, "A human scFv antibody generation pipeline for proteome research," *J. Biotechnol.*, vol. 152, no. 4, pp. 159–170, Apr. 2011.

[202] H. J. de Haard *et al.*, "A large non-immunized human Fab fragment phage library that permits rapid isolation and kinetic analysis of high affinity antibodies," *J. Biol. Chem.*, vol. 274, no. 26, pp. 18218–18230, Jun. 1999.

[203] C. Vincke, C. Gutiérrez, U. Wernery, N. Devoogdt, G. Hassanzadeh-Ghassabeh, and S. Muyldermans, "Generation of Single Domain Antibody Fragments Derived from Camelids and Generation of Manifold Constructs," in *Antibody Engineering*, vol. 907, P. Chames, Ed. Totowa, NJ: Humana Press, 2012, pp. 145–176.

[204] D. Könning *et al.*, "Camelid and shark single domain antibodies: structural features and therapeutic potential," *Curr. Opin. Struct. Biol.*, vol. 45, pp. 10–16, Aug. 2017.

[205] O. C. Ubah, C. J. Barelle, M. J. Buschhaus, and A. J. Porter, "Phage Display Derived IgNAR V Region Binding Domains for Therapeutic Development," *Curr. Pharm. Des.*, vol. 22, no. 43, pp. 6519–6526, 2016.

[206] Y. Mazor, T. Van Blarcom, R. Mabry, B. L. Iverson, and G. Georgiou, "Isolation of engineered, full-length antibodies from libraries expressed in Escherichia coli," *Nat. Biotechnol.*, vol. 25, no. 5, pp. 563–565, 2007.

[207] A. Frenzel, T. Schirrmann, and M. Hust, "Phage display-derived human antibodies in clinical development and therapy," *MAbs*, vol. 8, no. 7, pp. 1177–1194, 2016.

[208] R. Rau, "Adalimumab (a fully human anti-tumour necrosis factor α monoclonal antibody) in the treatment of active rheumatoid arthritis: The initial results of five trials," *Ann. Rheum. Dis.*, vol. 61, no. SUPPL. 2, pp. 70–73, 2002.

[209] K. P. Baker *et al.*, "Generation and Characterization of LymphoStat-B, a Human Monoclonal Antibody That Antagonizes the Bioactivities of B Lymphocyte Stimulator," *Arthritis Rheum.*, vol. 48, no. 11, pp. 3253–3265, 2003.

[210] E. T. Boder and K. D. Wittrup, "Yeast surface display for screening combinatorial polypeptide libraries," *Nat. Biotechnol.*, vol. 15, no. 6, pp. 553–557, 1997.

[211] C. Cappellaro, C. Baldermann, R. Rachel, and W. Tanner, "Mating type-specific cell-cell recognition of Saccharomyces cerevisiae: cell wall attachment and active sites of a- and alpha-agglutinin.," *EMBO J.*, vol. 13, no. 20, pp. 4737–4744, Oct. 1994.

[212] G. M. Cherf and J. R. Cochran, "Applications of yeast surface display for protein engineering," *Methods Mol. Biol.*, 2015.

[213] N. Gera, M. Hussain, and B. M. Rao, "Protein selection using yeast surface display," *Methods*, vol. 60, no. 1, pp. 15–26, 2013.

[214] J. A. Rakestraw, D. Aird, P. M. Aha, B. M. Baynes, and D. Lipovšek, "Secretion-and-capture cell-surface display for selection of target-binding proteins," *Protein Eng. Des. Sel.*, vol. 24, no. 6, pp. 525–530, Mar. 2011.

[215] E. T. Boder, M. Raeeszadeh-Sarmazdeh, and J. V. Price, "Engineering antibodies by yeast display," *Arch. Biochem. Biophys.*, vol. 526, no. 2, pp. 99–106, 2012.

[216] L. Roth *et al.*, "Isolation of Antigen-Specific VHH Single-Domain Antibodies by Combining Animal Immunization with Yeast Surface Display.," *Methods Mol Biol.*, 2019.

[217] G. Chao, W. L. Lau, B. J. Hackel, S. L. Sazinsky, S. M. Lippow, and K. D. Wittrup, "Isolating and engineering human antibodies using yeast surface display," *Nat. Protoc.*, vol. 1, no. 2, pp. 755–768, 2006.

[218] E. T. Boder, K. S. Midelfort, and K. D. Wittrup, "Directed evolution of antibody fragments with monovalent femtomolar antigen-binding affinity," *Proc. Natl. Acad. Sci. U. S. A.*, vol. 97, no. 20, pp. 10701–10705, 2000.

[219] J. R. Cochran, Y.-S. Kim, S. M. Lippow, B. Rao, and K. D. Wittrup, "Improved mutants from directed evolution are biased to orthologous substitutions," *Protein Eng. Des. Sel.*, vol. 19, no. 6, pp. 245–253, Mar. 2006.

[220] B. M. Rao, A. T. Girvin, T. Ciardelli, D. A. Lauffenburger, and K. D. Wittrup, "Interleukin-2 mutants with enhanced alpha-receptor subunit binding affinity.," *Protein Eng.*, vol. 16, no. 12, pp. 1081–1087, Dec. 2003.

[221] K. Weiskopf *et al.*, "Engineered SIRPα variants as immunotherapeutic adjuvants to anticancer antibodies," *Science*, vol. 341, no. 6141, pp. 88–91, Jul. 2013.

[222] H. Kaplon, M. Muralidharan, Z. Schneider, and J. M. Reichert, "Antibodies to watch in 2020," *MAbs*, vol. 12, no. 1, p. 1703531, 2020.

[223] C. Wu *et al.*, "Simultaneous targeting of multiple disease mediators by a dual-variable-domain immunoglobulin.," *Nat. Biotechnol.*, vol. 25, no. 11, pp. 1290–1297, Nov. 2007.

[224] R. E. Kontermann, "Dual targeting strategies with bispecific antibodies.," *MAbs*, vol. 4, no. 2, pp. 182–197, 2012.

[225] S. Stamova *et al.*, "Cancer Immunotherapy by Retargeting of Immune Effector Cells via Recombinant Bispecific Antibody Constructs," *Antibodies*, vol. 1, no. 2, pp. 172–198, 2012.

[226] U. Brinkmann and R. E. Kontermann, "The making of bispecific antibodies," *MAbs*, vol. 9, no. 2, pp. 182–212, 2017.

[227] A. F. Labrijn, M. L. Janmaat, J. M. Reichert, and P. W. H. I. Parren, "Bispecific antibodies: a mechanistic review of the pipeline," *Nat. Rev. Drug Discov.*, vol. 18, no. 8, pp. 585–608, 2019.

[228] U. H. Weidle, B. Schneider, G. Georges, and U. Brinkmann, "Genetically engineered fusion proteins for treatment of cancer.," *Cancer Genomics Proteomics*, vol. 9, no. 6, pp. 357–372, Nov. 2012.

[229] S. Muro, "Challenges in design and characterization of ligand-targeted drug delivery systems," *J. Control. Release*, vol. 164, no. 2, pp. 125–137, Dec. 2012.

[230] A. M. Scott, J. D. Wolchok, and L. J. Old, "Antibody therapy of cancer," *Nat. Rev. Cancer*, vol. 12, no. 4, pp. 278–287, 2012.

[231] Y. Chen and Y. Xu, "Pharmacokinetics of Bispecific Antibody," *Curr. Pharmacol. Reports*, vol. 3, May 2017.

[232] J. S. Orange, "Formation and function of the lytic NK-cell immunological synapse," *Nat. Rev. Immunol.*, vol. 8, no. 9, pp. 713–725, 2008.

[233] F. J. Culley *et al.*, "Natural killer cell signal integration balances synapse symmetry and migration," *PLoS Biol.*, vol. 7, no. 7, 2009.

[234] S. Dickopf, G. J. Georges, and U. Brinkmann, "Format and geometries matter: Structure-based design defines the functionality of bispecific antibodies," *Comput. Struct. Biotechnol. J.*, vol. 18, pp. 1221–1227, 2020.

[235] R. Bargou *et al.*, "Tumor Regression in Cancer Patients by Very Low Doses of a T Cell–Engaging Antibody," *Science (80-.).*, vol. 321, no. 5891, pp. 974 LP – 977, Aug. 2008.

[236] N. Gökbuget *et al.*, "Curative outcomes following blinatumomab in adults with minimal residual disease B-cell precursor acute lymphoblastic leukemia," *Leuk. Lymphoma*, pp. 1–9, Jul. 2020.

[237] R. E. Kontermann, "Strategies to Extend Plasma Half-Lives of Recombinant Antibodies," *BioDrugs*, vol. 23, no. 2, pp. 93–109, 2009.

[238] S. Krah, H. Kolmar, S. Becker, and S. Zielonka, "Engineering IgG-Like Bispecific Antibodies—An Overview," *Antibodies*, vol. 7, no. 3, p. 28, 2018.

[239] J. B. Ridgway, L. G. Presta, and P. Carter, "'Knobs-into-holes' engineering of antibody CH3 domains for heavy chain heterodimerization.," *Protein Eng.*, vol. 9, no. 7, pp. 617–621, Jul. 1996.

[240] J. H. Davis *et al.*, "SEEDbodies: Fusion proteins based on strand-exchange engineered domain (SEED) CH3 heterodimers in an Fc analogue platform for asymmetric binders or immunofusions and bispecific antibodies," *Protein Eng. Des. Sel.*, vol. 23, no. 4, pp. 195–202, 2010.

[241] M. Muda *et al.*, "Therapeutic assessment of SEED: A new engineered antibody platform designed to generate mono- and bispecific antibodies," *Protein Eng. Des. Sel.*, vol. 24, no. 5, pp. 447–454, 2011.

[242] M. Hust *et al.*, "Single chain Fab (scFab) fragment," *BMC Biotechnol.*, vol. 7, no. 1, p. 14, 2007.

[243] W. Schaefer *et al.*, "Immunoglobulin domain crossover as a generic approach for the production of bispecific IgG antibodies.," *Proc. Natl. Acad. Sci. U. S. A.*, vol. 108, no. 27, pp. 11187–11192, Jul. 2011.

[244] K. E. Harris *et al.*, "Sequence-Based Discovery Demonstrates That Fixed Light Chain Human Transgenic Rats Produce a Diverse Repertoire of Antigen-Specific Antibodies," *Front. Immunol.*, vol. 9, p. 889, Apr. 2018.

[245] A. Ljungars *et al.*, "A bispecific IgG format containing four independent antigen binding sites," *Sci. Rep.*, vol. 10, no. 1, p. 1546, 2020.

[246] L. Pekar *et al.*, "Biophysical and biochemical characterization of a VHH-based IgG-like bi- and trispecific antibody platform," *MAbs*, p. 1812210, Aug. 2020.

6 Cumulative section

6.1 Facile generation of antibody heavy and light chain diversities for yeast surface display by Golden Gate Cloning

Authors

Lukas Roth[+], Julius Grzeschik[+], Steffen C. Hinz, Stefan Becker, Lars Toleikis, Michael Busch, Harald Kolmar, Simon Krah and Stefan Zielonka

[+] These authors contributed equally to this work

Bibliographic information

Biological Chemistry

Volume 400, Issue 3, February 2019, Pages 383-393

DOI: https://doi.org/10.1515/hsz-2018-0347

Contributions by Lukas Pekar

- Project idea and project planning together with S. Zielonka
- Prepared GGC and YM library generation for transgenic rats
- Conducted rodent YSD selection of CEACAM6-specific antibodies
- Expression of all antibody derivatives
- Conducted all BLI experiments
- Wrote manuscript together with J. Grzeschik and S. Zielonka
- Prepared tables and figures together with J. Grzeschik and S. Zielonka
- Prepared the supplementary section

Lukas Roth[a], Julius Grzeschik[a], Steffen C. Hinz, Stefan Becker, Lars Toleikis, Michael Busch, Harald Kolmar, Simon Krah* and Stefan Zielonka*

Facile generation of antibody heavy and light chain diversities for yeast surface display by Golden Gate Cloning

https://doi.org/10.1515/hsz-2018-0347
Received August 15, 2018; accepted November 11, 2018; previously published online November 17, 2018

Abstract: Antibodies can be successfully engineered and isolated by yeast or phage display of combinatorial libraries. Still, generation of libraries comprising heavy chain as well as light chain diversities is a cumbersome process involving multiple steps. Within this study, we set out to compare the output of yeast display screening of antibody Fab libraries from immunized rodents that were generated by Golden Gate Cloning (GGC) with the conventional three-step method of individual heavy- and light-chain sub-library construction followed by chain combination via yeast mating (YM). We demonstrate that the GGC-based one-step process delivers libraries and antibodies from heavy- and light-chain diversities with similar quality to the traditional method while being significantly less complex and faster. Additionally, we show that this method can also be used to successfully screen and isolate chimeric chicken/human antibodies following avian immunization.

Keywords: antibody discovery; chimeric antibodies; gap repair cloning; Golden Gate Cloning; human antibodies; yeast mating.

[a]**Lukas Roth and Julius Grzeschik:** These authors contributed equally to this work.
***Corresponding authors: Simon Krah and Stefan Zielonka,** Protein Engineering and Antibody Technologies, Merck KGaA, Frankfurter Strasse 250, D-64293 Darmstadt, Germany, e-mail: Simon.Krah@merckgroup.com; Stefan.Zielonka@merckgroup.com
Lukas Roth, Julius Grzeschik, Steffen C. Hinz and Harald Kolmar: Institute for Organic Chemistry and Biochemistry, Technische Universität Darmstadt, Alarich-Weiss-Strasse 4, D-64287 Darmstadt, Germany
Stefan Becker and Lars Toleikis: Protein Engineering and Antibody Technologies, Merck KGaA, Frankfurter Strasse 250, D-64293 Darmstadt, Germany
Michael Busch: Discovery Pharmacology, Merck KGaA, Frankfurter Strasse 250, D-64293 Darmstadt, Germany

Introduction

Monoclonal antibodies are among the most successfully applied molecules for biomedical as well as biotechnological applications (Carter and Lazar, 2017; Kaplon and Reichert, 2018). Their high affinity and specificity towards an antigen combined with effector functions is rendering antibodies efficacious for the treatment of various diseases such as immunological disorders or cancer. Nowadays, more than 50 antibodies are clinically available and a multitude of different molecules is currently investigated in late stage clinical trials or is undergoing regulatory review (Chung, 2017; Kaplon and Reichert, 2018). With regards to antibody discovery, it has been known for quite some time that yeast surface display (YSD) is a powerful platform technology for the identification of antibodies and for engineering purposes (Boder and Wittrup, 1997; Feldhaus et al., 2003; Doerner et al., 2014; Yang et al., 2018). Consequently, a plethora of different antibodies and antibody-based constructs was engineered using YSD (Wozniak-Knopp et al., 2010; Zielonka et al., 2014; Schröter et al., 2015; Wang et al., 2016; Könning et al., 2017; Krah et al., 2017; McMahon et al., 2018). It was recently shown by Nozach and co-workers that in comparison to scFvs or single chain Fab moieties the Fab format is most efficient in expressing functional antibodies on the surface of the yeast, supporting the notion that Fab fragments more closely resemble the classical antibody structure (Sivelle et al., 2018). One prominent approach for the generation of YSD Fab libraries is the individual generation of heavy and light chain encoding plasmids in haploid yeast strains via a homologous recombination-based process referred to as gap repair cloning. Afterwards, these yeast cells are combined by yeast mating (YM) into diploid cells that display functional antibody fragments (Weaver-Feldhaus et al., 2004). We have previously described an alternative one-step strategy by utilizing Golden Gate Cloning (GGC) for library construction (Rosowski et al., 2018). Pioneered by Marillonnet and colleagues, this technology makes use of type IIs restriction enzymes that have non-palindromic recognition sites and cut outside of their recognition

sequence (Engler et al., 2008). Therefore, restriction site overhangs (herein termed signature sequences) can be designed by purpose, allowing for cloning in a one-pot reaction in a unidirectional manner with deletion of the recognition sites during the reaction. We showed that the heavy and light chain of a Fab can be simultaneously cloned into the final display vector in a single step, significantly reducing the complexity of library establishment (Rosowski et al., 2018). Subsequently, we demonstrated that this approach is versatile for the isolation of common light chain antibodies from heavy chain diversities only. However, the generation of classical antibody Fab libraries with adequate qualities is more sophisticated, as heavy as well as light chain diversities need to be incorporated properly. Such GGC-based libraries were recently constructed efficiently using phage display as the platform technology (Nelson and Valadon, 2017).

In this work we aimed at comparing the library construction process and selection output of the GGC-based methodology with the classical approach of YM. To this end, transgenic rats comprising a partial human VH and VL repertoire were immunized with CEACAM6, an antigen overexpressed in many tumors (Lewis-Wambi et al., 2008; Zhang et al., 2014; Rizeq et al., 2018). From the same starting material, GGC-based (Figure 1) as well as YM-based libraries were constructed and compared in terms of library size and immunoglobulin gene repertoire usage. In order to isolate antigen-specific clones, both libraries were sorted against recombinant CEACAM6 protein. Afterwards, the sorting output from both libraries was analyzed with respect to sequence diversity and representative clones identified were characterized in terms of affinity.

Additionally, we also set out to demonstrate a broader applicability of this GGC-based approach. For this, wild type chickens were immunized with epidermal growth factor receptor (EGFR) as well as human chorionic gonadotropin (hCG) and chimeric chicken/human antibody YSD libraries were constructed in which the chicken VH and VL repertoires were grafted onto human domains CH1 and CLλ. EGFR is overexpressed in many human cancers, such as colorectal and head and neck cancer (Sigismund et al., 2018). hCG is being used as earliest indicator of pregnancy by detection of this glycoprotein hormone in the urine (Braunstein et al., 1976). Due to their phylogenetic distance from humans, such chicken antibodies are interesting for biotechnological applications, as they allow for the generation of antigen-specific moieties recognizing conserved epitopes on mammalian targets (Davies et al., 1995; Abdiche et al., 2016). We show that a diverse set of

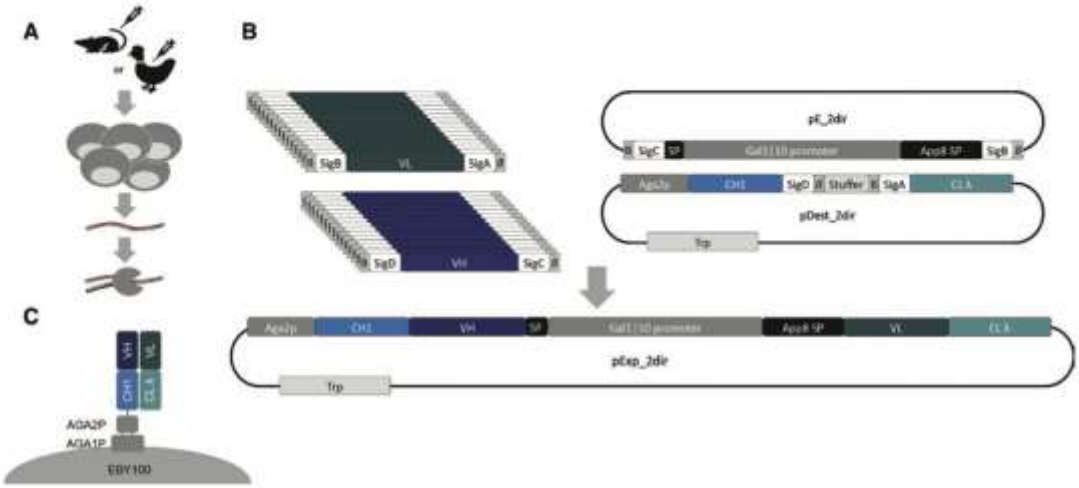

Figure 1: Workflow for the generation of GGC-based YSD libraries.
(A) Transgenic rats or wild type chickens were immunized with protein antigens. Afterwards, lymph node cells or splenocytes were resected followed by total RNA isolation and cDNA synthesis. (B) Components for GGC-derived Fab libraries and resulting bidirectional display plasmid after reaction. Destination plasmid (pDest), entry plasmid (pE) and PCR amplicons contain or are flanked by BsaI recognition sites in different orientations (B: ggtctcn, *B*: ngagacc). SP, Aga2p signal peptide. SigA-D, signature sequences i.e. restriction site overhangs that can be designed by purpose. APP8 SP, APP8 signal peptide. (C) Schematic illustration of Fab display on the surface of yeast cells. Fab fragments are fused to Aga2p via domain CH1. Display is mediated by covalent linkage of Aga2p to Aga1p.

antigen-specific chimeric antibodies can be obtained by library sorting against both antigens.

Results

Design of library components

In this study, we aimed at comparing the library generation process as well as the selection output of a GGC-based yeast surface display library approach with the conventional (YM) three-step method of individual heavy and light chain sub-library construction followed by YM. For the GGC-based library components, we decided to adopt the two-directional design as previously published by our group (Rosowski et al., 2018). Here, four different modules were utilized, a destination plasmid, an entry plasmid comprising GAL1/GAL10 promoters for bidirectional expression of heavy and light chains as well as signal sequences for antibody secretion and both, the heavy and light chain variable region modules, i.e. the PCR amplified VH and VL repertoire with flanking type IIs restriction sites (BsaI) and signature sequences for directional cloning. The destination plasmid was essentially composed of a tryptophan marker for vector selection, a CLλ domain as well as a CH1 region that is fused to Aga2p enabling Fab surface display. In general, signature sequences were part of antibody constant regions or signal sequences (Figure 1B). All restriction sites were designed to be removed during the restriction-ligation reaction, allowing for one-step cloning.

In order to compare the GGC-based method with the mating-based approach according to Weaver-Feldhaus et al. (Weaver-Feldhaus et al., 2004), a two-vector based system for heavy- and light chain expression was utilized. Expression of both chains was mediated by the GAL1 promoter. The heavy chain plasmid encoded for a signal peptide, followed by a stuffer for VH gap repair cloning as well as by domain CH1 fused to Aga2p. Additionally, this vector comprised a tryptophan auxotrophic marker. Akin to this, the light chain encoded for a signal peptide followed by a stuffer and CLλ as well as for a leucin marker gene (Krah et al., 2017).

Library construction, analysis and selection of CEACAM6-specific antibodies

Transgenic rats harboring human antibody variable regions, referred to as OmniRats (Osborn et al., 2013) were DNA-immunized with CEACAM6. After immunization, lymph nodes were resected, and total RNA was extracted followed by cDNA synthesis (Figure 1A). For both libraries, VH and VL repertoires were amplified in two consecutive PCRs. In the first PCR, the different forward primers annealed in the leader of heavy and light chain V-genes whereas the reverse primer annealed in region CH1 or CLλ. The resulting product served as template material for the GGC as well as the YM approach. The second PCR was carried out to incorporate BsaI sites and signature sequences for the GGC approach or to introduce homologous sites for gap repair cloning into the two-vector system of the YM approach.

With respect to GGC, a one-pot restriction-ligation reaction was performed and the resulting expression plasmid comprising heavy and light chain combinatorial diversities was transformed into *Saccharomyces cerevisiae* strain EBY100, yielding a calculated library size of approximately 2.9×10^9 independent clones. For the YM-based method, heavy and light chain variable regions were separately incorporated into linearized YSD plasmid in a homologous-repair mediated process named plasmid gap repair. The yeast strain EBY100 (haploid, mating type a, MATa) was utilized for gap repair cloning of the heavy chain repertoire, whereas BJ5464 cells (haploid, mating type α, MATα) were used for the incorporation of light chain diversities. Both libraries yielded about $1–2 \times 10^9$ clones after electroporation. Interestingly, the transformation procedure in this approach is facilitated with a linearized DNA for both, the PCR insert as well as the digested plasmid backbone. This is in contrast to the GGC-approach where a circular plasmid is utilized. Still, both approaches deliver library or sub-library sizes in the same range, supporting the notion that gap repair cloning is very efficient for library construction. Subsequently, YM was applied to generate Fab libraries comprising combined heavy and light chain diversities. This resulted into a calculated library size of about 2.2×10^9 independent clones. It should be noted that in the YM approach a simple analysis of heavy and light chain diversities cannot be made, as the final display library is a product of two sub-libraries, which have gone through several rounds of culturing prior to the final library generation. In comparison, the GGC-procedure results in the functional display library after a single step. Therefore, clone numbers obtained from dilution plating might be more comprehensive with respect of diversity in the case of the GGC-approach. In both approaches Fab fragments were displayed on the yeast cell surface *via* fusion to cell wall protein Aga2p, which is anchored to the cell wall by

covalent association with Aga1p (Figure 1C). From both libraries approximately 100 clones each were sent out for sequencing to analyze V-family representation. As shown in Figure 2A IgHV families were represented very similarly in both library generation procedures. With regards to IgLV region occurrence, the distribution in both libraries was also comparable (Figure 2B). Whereas families IgLV2-8 and IgVL2-11 seemed to be underrepresented in the GGC-based approach, regions IgLV3-10 as well as IgLV3-12 were found infrequently in YM library, indicating that no profound bias was observed by comparing both approaches. Furthermore, the functionality in both libraries, i.e. functional VH or VL domains without stop codons, frameshifts or deletions was very similar (Supplementary Table 1).

Moreover, the two resulting libraries were selected separately by FACS against recombinant human CEACAM6 protein. In order to analyze the sequence output more comprehensively without the risk of losing binders during library sorting, we decided to apply a low-stringency strategy by applying a fixed antigen concentration of 1 μM for all rounds of sorting. CEACAM6 binding was detected using an Alexa Fluor 647 conjugated anti-Penta-His antibody whereas Fab display was identified simultaneously by application of lambda light chain specific goat $F(ab')_2$ R-PE conjugate. Controls, in which cells were stained with secondary detection reagents only were applied to adjust the sorting gates to only consider target positive populations. In the first round of sorting approximately 3×10^8 cells were sorted for both approaches. In subsequent sorting rounds, a minimum cell oversampling by the factor of 10 with respect to the previously sorted cells was ensured. As shown in Figure 3, for both library generation approaches we were able to strongly enrich for antigen-binding populations within three rounds of FACS sorting. Enriched clones were then analyzed by sequencing (Supplementary Figures 1–4) and a clustering strategy was applied in which clones with less than three amino acid exchanges within CDR-H3 belong to the same family. Moreover, at least three sequences must fulfil this criterion to be considered as a cluster. Peculiarly, this revealed that whereas the sequence output of the GGC approach comprised five distinct clusters (Supplementary Figure 1, cluster 1–5), only two of those were present by evaluating the YM approach. Even more interestingly, those two

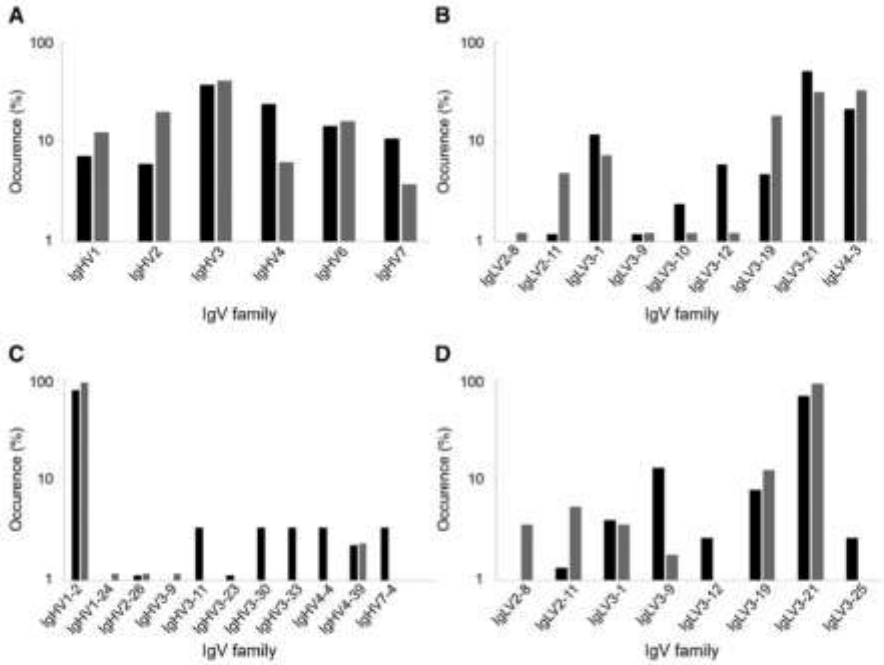

Figure 2: Analysis of IgV-gene occurrence in YSD Fab libraries constructed using GGC (black bars) or YM approach (gray bars). (A) IgHV and (B) IgLV frequencies as found by sequencing after library establishment. (C) IgHV and (D) IgLV occurance after FACS sorting against recombinant human CEACAM6 protein.

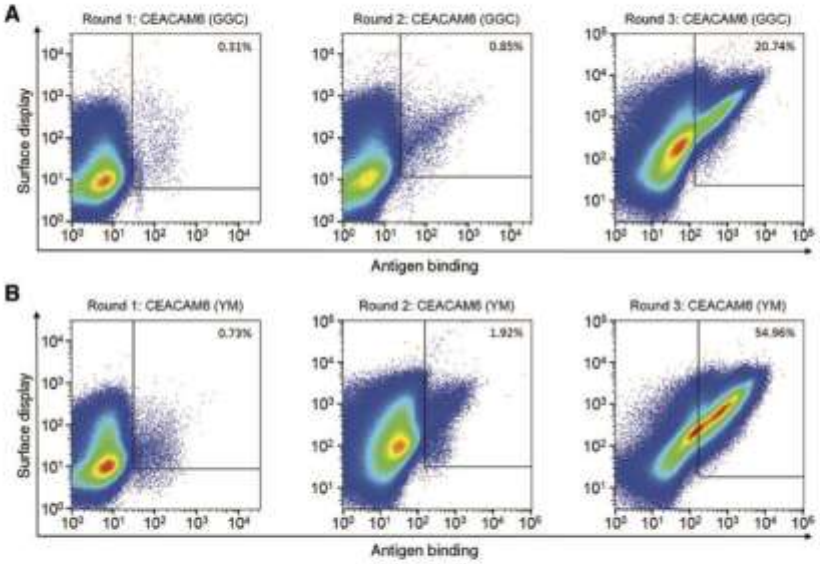

Figure 3: Screening of CEACAM6 YSD Fab immune libraries by FACS.
Yeast cells were consecutively incubated with 1 µM of His tagged recombinant human CEACAM6 protein followed by secondary labeling with Alexa Fluor 647 conjugated anti-Penta-His antibody and PE conjugated anti-lambda-antibody. (A) Sorting of GGC-based library. (B) Sorting of library based on YM approach.

clusters (Supplementary Figure 3, cluster 2 and 3) were also strongly represented in the GGC approach, indicating a considerable sampling of the immune diversity using this cloning technique for library establishment. These findings were also substantiated by evaluating the V-gene representation (Figure 2C and D). After library sorting, distinct IgHV (IgHV1-2) and IgLV (IgLV3-19 and IgLV3-21) families were represented most prevalent in both approaches, supporting the notion that no substantial liabilities were introduced using the GGC-approach.

From each of the five clusters, one representative clone was reformatted into plasmids enabling the production as full-length IgG moieties in Expi293 cells. After antibody expression and purification using Protein A chromatography, binding kinetics to recombinant human CEACAM6 were investigated via BLI (Table 1, Supplementary Figure 5). Specific antigen binding in the double-digit nanomolar range was observed for the clones from clusters 2 and 3, that were present by analyzing the sequence output in both approaches. Moreover, two out of three clones from the clusters that were only found in the GGC library showed specific binding to CEACAM6 in the picomolar to nanomolar range (clones obtained from clusters 1 and 4), demonstrating clear evidence that in this particular case the GGC approach enabled the isolation of rare but still antigen-specific clones.

Table 1: Kinetic analysis of clones reformatted as IgG.

Clones	Library	Antigen	K_{on} (1/Ms)	K_{off} (1/s)	KD (M)
C1	GGC	CEACAM6	5.78E+04	1.37E-03	2.37E-08
C2	GGC, YM	CEACAM6	4.60E+03	7.49E-05	1.63E-08
C3	GGC, YM	CEACAM6	4.82E+03	6.26E-05	1.30E-08
C4	GGC	CEACAM6	4.45E+05	1.21E-04	2.72E-10
C5	GGC	CEACAM6	–	–	–
E1	Chimeric GGC	EGFR	1.35E+05	1.36E-01	1.01E-06
E2	Chimeric GGC	EGFR	2.44E+05	1.38E-03	5.65E-09
H1	Chimeric GGC	hCG	1.11E+05	4.28E-02	3.85E-07
H2	Chimeric GGC	hCG	2.03E+04	8.06E-05	3.97E-09

Clone names are given as well as the libraries clones were obtained from, the target protein, on-rate, off-rate and KD as determined by BLI.

Chimeric chicken/human library construction and selection of EGFR- and hCG-specific antibodies

Within this study, we also wanted to figure out whether the GGC approach is applicable in a broader manner. To this end, we aimed at isolating chimeric chicken/human antibodies after avian immunization. Two specimens of *Gallus gallus domesticus* were immunized with EGFR and hCG, respectively. cDNA was prepared using total RNA collected

from spleen tissues with random hexamer primers and subsequently heavy as well as light chain variable regions were amplified in a one-step PCR. Those generated VH and VL modules were grafted onto human CH1 and CLλ regions using GGC. For this, the same entry and destination plasmids as described for the CEACAM6 study were utilized. Consequently, this resulted in two libraries with calculated library sizes of approximately 4×10^8 unique clones, respectively.

The generated libraries were screened separately by FACS for binders targeting recombinant human EGFR and human hCG protein. Target binding was monitored by indirect antigen fluorescence staining and Fab surface display levels were analyzed simultaneously by lambda light chain labeling. As shown in Figure 4, we were able to enrich for antigen-positive populations in two consecutive screening rounds by incubating cells with 1 µM or 500 nM antigen, for EGFR and hCG, respectively. Also, no binding against secondary detection reagents could be observed (data not shown). Flow cytometry analysis after library sorting revealed for both screening campaigns almost quantitative antigen binding populations with strong correlation between antigen binding and Fab display

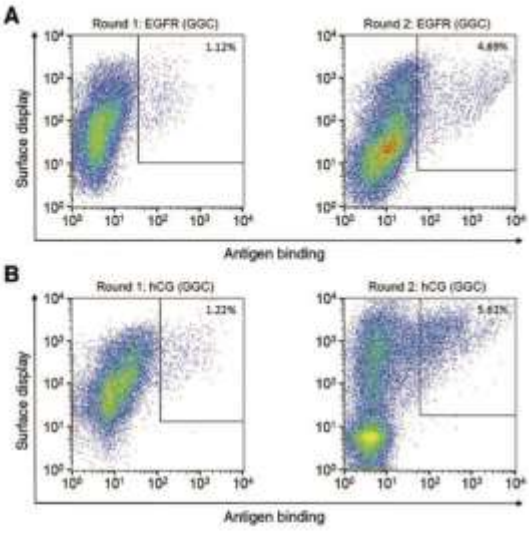

Figure 4: Screening of chimeric chicken/human YSD Fab immune libraries by FACS.
Antigen binding was monitored by indirect antigen fluorescence staining and Fab surface display levels were analyzed simultaneously by lambda light chain labeling. (A) Sorting of recombinant human EGFR GGC-based library using an antigen concentration of 1 µM. (B) Sorting of recombinant hCG GGC-based library with 0.5 µM target protein.

(Supplementary Figure 6). Sequence analysis of the enriched cells showed a very diverse output for heavy and light chain variable domains, respectively (Supplementary Figures 7–10). Notwithstanding, specific CDR3 sequence patterns were highly enriched in both domains. From each library two of the most abundant clones based on region CDR-H3 were reformatted into chimeric chicken/human IgGs, expressed in Expi293 cells and purified *via* Protein A chromatography. Binding kinetics were measured using BLI. All the clones showed specific binding towards their cognate antigen in the low nanomolar to micromolar range (Table 1, Supplementary Figure 5).

Discussion

Yeast surface display, as pioneered by Boder and Wittrup in 1997, emerged as a powerful platform technology for antibody engineering purposes (Colby et al., 2004; Cherf and Cochran, 2015; Grzeschik et al., 2017; Schröter et al., 2018). One benefit of YSD relies in its compatibility with FACS sorting, enabling real-time and on-line analysis of individual library candidates and consequently a fine discrimination of variants comprising desired prescribed properties. Moreover, complex proteins like antibodies are believed to be more properly folded due to the presence of sophisticated quality control machineries in the host *S. cerevisiae* (Doerner et al., 2014). Regarding antibody formats, multiple constructs can be displayed on the surface of the yeast, e.g. scFvs, Fab fragments or single chain Fabs (Boder and Wittrup, 1997; Weaver-Feldhaus et al., 2004; Walker et al., 2009). It was recently shown that functional antibodies are most efficiently displayed in the Fab format (Sivelle et al., 2018). Such Fab antibody libraries are typically constructed in a three-step process consisting of individual heavy and light chain sub-library generation in haploid yeast strains with opposite mating types followed by YM into diploid cells (Weaver-Feldhaus et al., 2004). Besides being very efficient for library creation and sampling (Schröter et al., 2015; Krah et al., 2017), this technique seems to be laborious and time-consuming. We recently presented an alternative strategy for the construction of Fab antibody YSD libraries using GGC (Rosowski et al., 2018). The charm of this cloning technique relies on the utilization of type IIs restriction enzymes cutting outside of their respective recognition sequence. By carefully designing restriction site overhangs, i.e. signature sequences, directional one-step cloning is amenable with elimination of the recognition sites during the reaction (Engler et al., 2008). It was shown

that this cloning principle is also applicable to generate and screen phage display libraries (Nelson and Valadon, 2017; Romão et al., 2018). In our previous work, we used GGC to generate antigen-specific antibodies from heavy chain repertoires only after immunization. For this, the heavy chain repertoire was paired with a fixed light chain and common light chain antibodies were readily isolated. Albeit proven to be a valid tool in this study, the generation of antibodies from both, heavy as well as light chain diversities is more sophisticated. In the present investigations we aimed at more thoroughly comparing the library construction process and selection output of a GGC-based library with that of the conventional three-step process involving YM. To this end, OmniRats were immunized with recombinant human CEACAM6 protein and libraries were constructed using both approaches. Calculated library sizes as well as IgV gene analysis demonstrated a similar quality for both individual approaches and library sorting by FACS enabled the strong enrichment of antigen binding populations. Surprisingly, sequencing of enriched antigen binding populations revealed a broader diversity using the GGC technique. Essentially, three additional sequence clusters were identified in this library and by reformatting and soluble expression of respective cluster representatives we could show that two out of those three clusters comprised additional functional, i.e. target-specific antibodies. However, we cannot exclude that those additional clusters were also present in the YM library and presumably those clones could be identified by more comprehensive sequencing such as next-generation sequencing (Friedensohn et al., 2018). Nevertheless, these findings are indicating that YSD libraries with adequate qualities can be generated by GGC, requiring significantly less hands-on-time compared to conventional methods for Fab library generation.

Nelson and Valadon described in their work BsaI restriction sites being present in a significant fraction of human IgV gene segments (Nelson and Valadon, 2017). With respect to library construction, this has also been described for standard type II restriction enzymes. For example, SpeI restriction sites, an enzyme often used for cloning of antibody genes into phage display plasmids are also found in notable amounts in human IGHV sets. Moreover, commonly used type II enzyme restriction sites such as SacI and XbaI are frequently found in murine antibody light chain variable regions (Barbas et al., 1991; Nelson and Valadon, 2017). Within our study we utilized BsaI for Fab fragment cloning. Interestingly, after library establishment, in approximately 22% of analyzed sequences BsaI sites were still present, even though during GGC the final reaction step comprised an elongated digestion in order to digest remaining destination plasmid for the sake of library quality. Consequently, it is tempting to speculate that in *S. cerevisae* DNA repair ligases of the non-homologous DNA end joining pathway facilitate the rescue of potential library candidates comprising BsaI sites (Wilson et al., 1997; Dudášová et al., 2004). Nonetheless, it remains elusive in a broader sense how GGC, i.e. the presence of type IIs restriction sites in immunoglobulin variable gene segments affects the gene usage of generated libraries. Hence, it will be interesting to investigate more meticulously the YSD library construction process as well as resulting biases using different type IIs restriction enzymes by next-generation sequencing.

Within this work, we also demonstrated that chimeric chicken/human antibodies can be isolated by YSD in combination with GGC after avian immunization. Chicken antibodies are of interest for biotechnological and biomedical applications. Due to their phylogenetic separation to mammals, human proteins are very often immunogenic to chickens, enabling the generation of antibody repertoires with a broader epitope coverage (Abdiche et al., 2016). Consequently, immune responses can be raised against conserved human proteins that are not immunogenic to mice (Ching et al., 2018). After immunization of two specimens with recombinant human EGFR and hCG, two GGC-based YSD libraries were constructed. Chicken heavy as well as light chain variable domain repertoires were grafted onto human constant domains CH1 and CLλ. Within two rounds of library sorting, we highly enriched antigen binding populations for both antigens, respectively. After sequence analysis we still obtained a large diversity in both libraries. Soluble expression of highly abundant clones in a chimeric chicken/human IgG format revealed high affinities for their cognate antigens, showing clear evidence that GGC is a valid method to generate YSD libraries with adequate qualities in the context of antibody discovery and engineering.

Materials and methods

Immunization of transgenic rats and wild-type chicken

OmniRats® (Osborn et al., 2013), transgenic for human antibody variable regions, were immunized by genetic immunization using vaccination vectors encoding for CEACAM6 (R&D Systems, Minneapolis, MN, USA) at Aldevron (Freiburg, Germany), as previously described elsewhere (Krah et al., 2017).

Additionally, two chickens (*G. gallus domesticus*) were immunized with protein antigens. One chicken was immunized with human EGFR (extracellular domain, produced and purified in-house) and another specimen with a cocktail of EGFR and hCG (BBI Solutions,

Cardiff, UK). Immunizations were performed at Davids Biotechnologie (Regensburg, Germany). In brief, two adult laying hens were immunized by intramuscularly injection of 150 µg of the respective antigens using AddaVax (InvivoGen, San Diego, CA, USA) as vaccine adjuvant. After initial injection, the birds received boosters after 2, 4, 5 and 8 weeks. After 9 weeks both animals were sacrificed followed by isolation of total splenic RNA using TriFast reagent (VWR, Radnor, PA, USA), as described elsewhere (Grzeschik et al., 2018).

All experimental procedures and animal care were in accordance with EU animal welfare protection laws and regulations.

Plasmids

Plasmids for GGC were designed in-house and synthesized at GeneArt (Thermo Fisher Scientific, Waltham, MA, USA). Genetic elements were deduced from pYD1 plasmid backbone (Yeast Display Vector Kit, version D, #V835-01, Thermo Fisher Scientific) as well as pESC vector series (Agilent, Santa Clara, CA, USA). The entry plasmid (pEntry) was designed with a kanamycin resistance gene, whereas the destination vector contained an ampicillin resistance cassette as well as a tryptophan selection marker for selection in yeast (Rosowski et al., 2018). Essential elements are given in Figure 1B.

Vectors used for the YM approach were also based on the pYD1 plasmid backbone. The heavy chain plasmid contained a tryptophan auxotrophic marker and an ampicillin resistance marker (Schröter et al., 2015; Krah et al., 2017). The light chain plasmid comprised leucine marker and kanamycin resistance genes. Moreover, the heavy chain plasmid encoded for the *AGA2* signal peptide, followed by the antibody VH region genetically fused to the CH1 region of IgG1, which allowed surface presentation of a VH-CH1-GS/Linker-Aga2p fusion protein. The light chain plasmid encoded for the *αMFpp8* signal sequence (Rakestraw et al., 2009) for soluble secretion, followed by the sequence for the constant lambda region. Expression of antibody heavy and light chain genes was under control of the galactose inducible promotor (*GAL1*).

Yeast strains and media

For GGC-derived yeast surface display, *S. cerevisiae* strain EBY100 (*MATa URA3-52 trp1 leu2Δ1 his3Δ200 pep4::HIS3 prb1Δ1.6R can1 GAL (pIU211:URA3)*) was employed (Thermo Fisher Scientific). This strain was also utilized for YM heavy chain sub-library construction. In addition, for light chain sub-library construction (YM) *S. cerevisiae* strain BJ5464 (*MATα URA3-52 trp1 leu2Δ1his3Δ200 pep4::HIS3 prb1Δ1.6R can1 GAL*) (American Type Culture Collection, Manassas, VA, USA) was used. Initially, strains were cultivated in YPD medium composed of 20 g/l peptone (Merck KGaA, Darmstadt, Germany), 20 g/l dextrose (Merck KGaA) and 10 g/l yeast extract supplemented with 10 ml/l penstrep (Gibco, Thermo Fisher Scientific). EBY100 cells harboring library plasmids (pDest) after GGC were cultivated in medium using minimal SD-base (Clontech, Mountain View, CA, USA) with commercially available dropout mix (Clontech) composed of all essential amino acids except for tryptophan, according to the manufacturer's instructions, supplemented with 5.4 g/l Na_2HPO_4 (Merck KGaA) and 8.6 g/l $NaH_2PO_4 \times H_2O$ (Merck KGaA). For YM-based library generation EBY100 cells were cultivated accordingly. BJ5464 cells were cultivated using a leucine dropout mix (Clontech). After YM, diploid yeast cells were cultivated in leucine and tryptophane double dropout mix (Clontech). For induction of antibody gene expression, cells were transferred into respective SG dropout medium wherein glucose was replaced by galactose containing SG-base (Clontech). Additionally, 10% (w/v) polyethylene glycol 8000 (PEG8000, Sigma Aldrich, St. Louis, USA) was incorporated. Furthermore, minimal Synthetic defined (SD) agar base (Clontech) supplemented with respective dropout mixes was used for preparation of agar plates.

Library construction

Total RNA was extracted from 1×10^7 lymph node cells of immunized OmniRats® using the RNeasy MiniKit (Qiagen, Venlo, Netherlands) according to the manufacturer's protocol. For cDNA synthesis from both, OmniRat® and chicken RNA, 50 µl RNA extract, 20 µl RT-buffer, 40 µl 25 mM $MgCl_2$, 20 µl 0.1 M DTT, 10 µl RNase Out and the 10 µl Superscript III reverse transcriptase (SuperScript III First-Strand Kit, Thermo Fisher Scientific) was used as well as random hexamer primers (Eurofins Scientific, Luxemburg) (Figure 1A). The reaction was treated as follows: 10 min at 25°C, 50 min at 50°C followed by heat inactivation for 5 min at 85°C. Afterwards, 1 µl RNase H (Thermo Fisher Scientific) was added followed by an incubation step at 37°C for 20 min.

Human heavy and light chain antibody variable regions from OmniRats® were amplified from cDNA in two consecutive PCR reactions for both approaches, respectively. First PCR was executed including 12 reactions for VH and 10 reactions for VLλ with 5 µl cDNA in a final volume of 50 µl using a Q5 High-Fidelity 2×Master Mix (New England Biolabs, Ipswich, MA, USA) and unique forward primers annealing to germline leader sequences and one reverse primer annealing to rat CH1 or CLλ. PCRs were performed at 95°C for 120 s, 30 cycles of 95°C for 15 s, 58°C for 30 s and 72°C for 90 s. The Wizard® SV Gel and PCR Clean-up System (Promega, Madison, WI, USA) was used for the purification of the PCR products, followed by equimolar pooling of the samples. With respect to the GGC-approach, in the second PCR, human VH and VLλ domains were amplified with primers incorporating BsaI recognition sequences for subsequent cloning. Reaction conditions were as follows: 98°C for 30 s, 15 cycles of 98°C for 10 s, 55°C for 10 s and 72°C for 30 s followed by 72°C for 120 s. In contrast, the second PCR for the YM-method was performed to amplify VH and VLλ domains with overlaps to their respective destination plasmids. Reaction conditions were: 98°C for 30 s, 30 cycles of 98°C for 10 s, 58°C for 20 s and 72°C for 45 s followed by 72°C for 120 s. The second PCRs for both approaches were performed with distinct primer set according to Saulquin et al. and Hust and co-workers (Kügler et al., 2015; Ouisse et al., 2017). Primer sequences are given in Supplementary Table 2. Nine forward and one reverse primer for VH regions as well as 11 forward and two reverse primers for VLλ regions were used to amplify antibody variable regions, respectively. PCR products were purified via the Wizard® SV Gel and PCR Clean-up System (Promega) and pooled in an equimolar ratio.

For chimeric chicken/human Fab library generation, for each animal VH and VL repertoires were amplified in one PCR reaction, respectively. For each reaction, 5 µl cDNA was utilized in a final volume of 50 µl using Taq polymerase (New England Biolabs) as well as primer sets given in Supplementary Table 2. Reaction conditions were as follows: 95°C for 30 s, 30 cycles of 20 s at 95°C, 30 s at 55°C and 30 s at 68°C, followed by 68°C for 5 min. After PCR purification

via the Wizard® SV Gel and PCR Clean-up System (Promega) samples were pooled for subsequent cloning.

Human as well as chicken antibody variable regions were incorporated simultaneously into a single destination vector for the GGC approach (Krah et al., 2018). Reactions were executed in a final volume of 100 µl using 1 µg of destination vector (Figure 1), 1.4 µg entry vector and approx. 160 ng of pooled VH PCR product, approx. 160 ng pooled VL product as well as 200 U BsaI (New England Biolabs), 800 U T4 DNA ligase (New England Biolabs) and 10 µl 10× T4 Ligase buffer (New England Biolabs). Reaction conditions were 30 cycles of 1 min at 37°C, 1 min at 16°C followed by 5 min at 55°C. After cloning, six reactions were pooled, purified using the Wizard® SV Gel and PCR Clean-up System (Promega) and eluted in a final volume of 30 µl which were subsequently used for one electroporation reaction into EBY100 as previously described by Benatuil et al. (Benatuil et al., 2010). Ten transformation reactions were performed for library establishment. Library sizes were calculated by dilution plating.

To accomplish library generation via homologous recombination (YM), the destination vectors were linearized with restriction enzymes BamHI (New England Biolabs) and NotI (New England Biolabs) for VLλ or restriction enzymes EcoRI (New England Biolabs) and NotI (New England Biolabs) for the antibody heavy chain. Transformation was performed using 4 µg digested destination vector as well as 12 µg purified PCR product within every transformation reaction according to Benatuil et al. (Benatuil et al., 2010). Ten reactions were performed for the generation of either antibody heavy chain library in EBY100 or antibody light chain library in BJ5464 cells. Library sizes were calculated from serial dilution plating of transformed cells. YM was applied to combine the generated diversities, as described by Weaver-Feldhaus et al. (Weaver-Feldhaus et al., 2004). The haploid cells harboring either antibody heavy or light chain diversity were grown in SD media, lacking tryptophan or leucine, at 30°C and 200 rpm for 24 h. Thereon, cells were pooled and incubated on YPD agar plates at 30°C for 24 h. After this incubation, cells were washed from the plates and used for the inoculation of SD-Trp-Leu double dropout medium. Library sizes were calculated by serial dilution plating on SD-Trp-Leu plates.

Library sorting

Recombinant human His-tagged CEACAM6 extracellular domain as well as Fc-tagged EGFR was purchased from R&D systems. hCG was purchased from BBI Solutions. Recombinant human his-tagged EGFR was produced in-house.

For library sorting, respective library cells were grown overnight in SD medium with adequate dropout mixes at 30°C and 200 rpm. Afterwards, cells were transferred to SG medium with appropriate dropout mix at 10^7 cells/ml followed by incubation at 20°C for 2 days. Antigen staining was performed either by utilizing biotinylated hCG employing EZ-Link Sulfo-NHS-LC-Biotin (Thermo Fisher Scientific) combined with Streptavidin conjugated to APC or PE (Affymetrix eBioscience, Thermo Fisher Scientific), or Penta-His Alexa Fluor 647 Conjugate antibody (Qiagen, diluted 1:20) for his-tagged EGFR and his-tagged CEACAM6 or anti-Human IgG Fc PE conjugate (SouthernBiotech, Birmingham, AL, USA) for Fc-tagged EGFR. Fab expression was monitored by incubation with light chain specific goat $F(ab')_2$ anti-human lambda R-phycoerythrin (R-PE) or Alexa Fluor 647 conjugate (SouthernBiotech, diluted 1:20).

Labeling of cells for FACS analysis or sorting was conducted by two consecutive washing steps of library candidates with PBS (Sigma Aldrich) followed by incubation with the respective antigen at a concentration of 1 µM. After incubation on ice for approx. 30 min an additional washing step was performed, followed by staining with secondary labeling reagents as described already. Finally, cells were washed with PBS (Sigma Aldrich). FACS-sorting rounds were either performed on a Sony SH800 cell sorter (Sony Biotechnology, San Jose, CA, USA), a MoFlo Legacy device (Beckman Coulter, Indianapolis, IN, USA) or on a BD Influx™ cell sorter (BD, San Jose, CA, USA).

Expression and purification of isolated library candidates

Human as well as chicken VH and VL regions were cloned into pTT5 for full-length IgG production (GeneArt/Thermo Fisher Scientific). For this, Expi293 cells were transiently transfected with expression vectors according to the manufacturer's instructions (Thermo Fisher Scientific). Five days post transfection, antibody-containing supernatants were harvested by centrifugation and purified via MabSelect antibody purification chromatography resin (GE Healthcare, Chicago, IL, USA). Finally, the buffer was exchanged to PBS (Sigma Aldrich) pH 6.8 using Amicon Ultra-4 Centrifugal Filters (EMD Millipore, Burlington, VT, USA).

Biolayer interferometry (BLI)

The Octet RED96 system (ForteBio, Pall Life Science, Fremont, CA, USA) was employed for binding kinetic measurements. All steps were performed in a final volume of 200 µl at 30°C and 1000 rpm agitation. Antibodies were loaded on anti-human Fc biosensors (ForteBio) at 5 µg/ml in PBS (Sigma Aldrich) for 300 s. Afterwards, tips were transferred to kinetics buffer [KB; PBS with 0.1% Tween-20 (Merck KGaA) and 1% bovine serum albumin, BSA (Merck KGaA)] for 60 s for sensor rinsing. Association to CEACAM6 (R&D Systems), EGFR (in-house) or hCG (BBI Solutions) (varying concentrations ranging from a minimum of 1.6 nM to a maximum 400 nM in KB) was measured for 300 s followed by dissociation for 600 s (in KB). In each experiment, one negative control was measured, wherein the captured antibody was incubated with KB instead of antigen. Data fitting and analysis was performed with ForteBio data analysis software using a 1:1 binding model after Savitzky-Golay filtering.

Acknowledgments: We are grateful to Ramona Gaa, Iris Willenbuecher, Kerstin Hallstein and Deniz Demir for experimental support.

References

Abdiche, Y.N., Harriman, R., Deng, X., Yeung, Y.A., Miles, A., Morishige, W., Boustany, L., Zhu, L., Izquierdo, S.M., and Harriman, W. (2016). Assessing kinetic and epitopic diversity across orthogonal monoclonal antibody generation platforms. MAbs *8*, 264–277.

Barbas, C.F., Kang, A.S., Lerner, R.A., and Benkovic, S.J. (1991). Assembly of combinatorial antibody libraries on phage surfaces: the gene III site. Proc. Natl. Acad. Sci. USA *88*, 7978–7982.

Benatuil, L., Perez, J.M., Belk, J., and Hsieh, C.-M. (2010). An improved yeast transformation method for the generation of very large human antibody libraries. Protein Eng. Des. Sel. PEDS *23*, 155–159.

Boder, E.T. and Wittrup, K.D. (1997). Yeast surface display for screening combinatorial polypeptide libraries. Nat. Biotechnol. *15*, 553–557.

Braunstein, G.D., Rasor, J., Danzer, H., Adler, D., and Wade, M.E. (1976). Serum human chorionic gonadotropin levels throughout normal pregnancy. Am. J. Obstet. Gynecol. *126*, 678–681.

Carter, P.J. and Lazar, G.A. (2017). Next generation antibody drugs: pursuit of the "high-hanging fruit." Nat. Rev. Drug Discov. *17*, 197–223.

Cherf, G.M. and Cochran, J.R. (2015). Applications of yeast surface display for protein engineering. In Yeast Surface Display, B. Liu, ed. (New York, NY: Springer), pp. 155–175.

Ching, K.H., Collarini, E.J., Abdiche, Y.N., Bedinger, D., Pedersen, D., Izquierdo, S., Harriman, R., Zhu, L., Etches, R.J., van de Lavoir, M.-C., et al. (2018). Chickens with humanized immunoglobulin genes generate antibodies with high affinity and broad epitope coverage to conserved targets. MAbs *10*, 71–80.

Chung, J. (2017). Special issue on therapeutic antibodies and biopharmaceuticals. Exp. Mol. Med. *49*, e304.

Colby, D.W., Kellogg, B.A., Graff, C.P., Yeung, Y.A., Swers, J.S., and Wittrup, K.D. (2004). Engineering antibody affinity by yeast surface display. Methods Enzymol. *388*, 348–358.

Davies, E.L., Smith, J.S., Birkett, C.R., Manser, J.M., Anderson-Dear, D.V., and Young, J.R. (1995). Selection of specific phage-display antibodies using libraries derived from chicken immunoglobulin genes. J. Immunol. Methods *186*, 125–135.

Doerner, A., Rhiel, L., Zielonka, S., and Kolmar, H. (2014). Therapeutic antibody engineering by high efficiency cell screening. FEBS Lett. *588*, 278–287.

Dudásová, Z., Dudás, A., and Chovanec, M. (2004). Non-homologous end-joining factors of *Saccharomyces cerevisiae*. FEMS Microbiol. Rev. *28*, 581–601.

Engler, C., Kandzia, R., and Marillonnet, S. (2008). A one pot, one step, precision cloning method with high throughput capability. PloS One *3*, e3647.

Feldhaus, M.J., Siegel, R.W., Opresko, L.K., Coleman, J.R., Feldhaus, J.M.W., Yeung, Y.A., Cochran, J.R., Heinzelman, P., Colby, D., Swers, J., et al. (2003). Flow-cytometric isolation of human antibodies from a nonimmune *Saccharomyces cerevisiae* surface display library. Nat. Biotechnol. *21*, 163–170.

Friedensohn, S., Lindner, J.M., Cornacchione, V., Iazeolla, M., Miho, E., Zingg, A., Meng, S., Traggiai, E., and Reddy, S.T. (2018). Synthetic standards combined with error and bias correction improve the accuracy and quantitative resolution of antibody repertoire sequencing in human naïve and memory B cells. Front. Immunol. *9*, 1401.

Grzeschik, J., Hinz, S.C., Könning, D., Pirzer, T., Becker, S., Zielonka, S., and Kolmar, H. (2017). A simplified procedure for antibody engineering by yeast surface display: Coupling display levels and target binding by ribosomal skipping. Biotechnol. J. *12*, 1600454.

Grzeschik, J., Yanakieva, D., Roth, L., Krah, S., Hinz, S.C., Elter, A., Zollmann, T., Schwall, G., Zielonka, S., and Kolmar, H. (2018). Yeast surface display in combination with fluorescence-activated cell sorting enables the rapid isolation of antibody fragments derived from immunized chickens. Biotechnol J. doi: 10.1002/biot.201800466.

Kaplon, H. and Reichert, J.M. (2018). Antibodies to watch in 2018. MAbs *10*, 183–203.

Könning, D., Rhiel, L., Empting, M., Grzeschik, J., Sellmann, C., Schröter, C., Zielonka, S., Dickgießer, S., Pirzer, T., Yanakieva, D., et al. (2017). Semi-synthetic vNAR libraries screened against therapeutic antibodies primarily deliver anti-idiotypic binders. Sci. Rep. *7*, 9676.

Krah, S., Schröter, C., Eller, C., Rhiel, L., Rasche, N., Beck, J., Sellmann, C., Günther, R., Toleikis, L., Hock, B., et al. (2017). Generation of human bispecific common light chain antibodies by combining animal immunization and yeast display. Protein Eng. Des. Sel. *30*, 291–301.

Krah, S., Grzeschik, J., Rosowski, S., Gaa, R., Willenbuecher, I., Demir, D., Toleikis, L., Kolmar, H., Becker, S., and Zielonka, S. (2018). A streamlined approach for the construction of large yeast surface display Fab antibody libraries. Methods Mol. Biol. Clifton NJ *1827*, 145–161.

Kügler, J., Wilke, S., Meier, D., Tomszak, F., Frenzel, A., Schirrmann, T., Dübel, S., Garritsen, H., Hock, B., Toleikis, L., et al. (2015). Generation and analysis of the improved human HAL9/10 antibody phage display libraries. BMC Biotechnol. *15*, 10.

Lewis-Wambi, J.S., Cunliffe, H.E., Kim, H.R., Willis, A.L., and Jordan, V.C. (2008). Overexpression of CEACAM6 promotes migration and invasion of oestrogen-deprived breast cancer cells. Eur. J. Cancer *44*, 1770–1779.

McMahon, C., Baier, A.S., Pascolutti, R., Wegrecki, M., Zheng, S., Ong, J.X., Erlandson, S.C., Hilger, D., Rasmussen, S.G.F., Ring, A.M., et al. (2018). Yeast surface display platform for rapid discovery of conformationally selective nanobodies. Nat. Struct. Mol. Biol. *25*, 289–296.

Nelson, R.S. and Valadon, P. (2017). A universal phage display system for the seamless construction of Fab libraries. J. Immunol. Methods *450*, 41–49.

Osborn, M.J., Ma, B., Avis, S., Binnie, A., Dilley, J., Yang, X., Lindquist, K., Ménoret, S., Iscache, A.-L., Ouisse, L.-H., et al. (2013). High-affinity IgG antibodies develop naturally in Ig-knockout rats carrying germline human IgH/Igκ/Igλ loci bearing the rat CH region. J. Immunol. *190*, 1481–1490.

Ouisse, L.-H., Gautreau-Rolland, L., Devilder, M.-C., Osborn, M., Moyon, M., Visentin, J., Halary, F., Bruggemann, M., Buelow, R., Anegon, I., et al. (2017). Antigen-specific single B cell sorting and expression-cloning from immunoglobulin humanized rats: a rapid and versatile method for the generation of high affinity and discriminative human monoclonal antibodies. BMC Biotechnol. *17*, 3.

Rakestraw, J.A., Sazinsky, S.L., Piatesi, A., Antipov, E., and Wittrup, K.D. (2009). Directed evolution of a secretory leader for the improved expression of heterologous proteins and full-length antibodies in *Saccharomyces cerevisiae*. Biotechnol. Bioeng. *103*, 1192–1201.

Rizeq, B., Zakaria, Z., and Ouhtit, A. (2018). Towards understanding the mechanisms of actions of carcinoembryonic antigen-related cell adhesion molecule 6 in cancer progression. Cancer Sci. *109*, 33–42.

Romão, E., Poignavent, V., Vincke, C., Ritzenthaler, C., Muyldermans, S., and Monsion, B. (2018). Construction of high-quality

camel immune antibody libraries. In Phage Display, M. Hust, and T.S. Lim, eds. (New York, NY: Springer), pp. 169–187.

Rosowski, S., Becker, S., Toleikis, L., Valldorf, B., Grzeschik, J., Demir, D., Willenbücher, I., Gaa, R., Kolmar, H., Zielonka, S., et al. (2018). A novel one-step approach for the construction of yeast surface display Fab antibody libraries. Microb. Cell Factories *17*, 3.

Schröter, C., Günther, R., Rhiel, L., Becker, S., Toleikis, L., Doerner, A., Becker, J., Schönemann, A., Nasu, D., Neuteboom, B., et al. (2015). A generic approach to engineer antibody pH-switches using combinatorial histidine scanning libraries and yeast display. MAbs *7*, 138–151.

Schröter, C., Beck, J., Krah, S., Zielonka, S., Doerner, A., Rhiel, L., Günther, R., Toleikis, L., Kolmar, H., Hock, B., et al. (2018). Selection of antibodies with tailored properties by application of high-throughput multiparameter fluorescence-activated cell sorting of yeast-displayed immune libraries. Mol. Biotechnol. *60*, 727–735.

Sigismund, S., Avanzato, D., and Lanzetti, L. (2018). Emerging functions of the EGFR in cancer. Mol. Oncol. *12*, 3–20.

Sivelle, C., Sierocki, R., Ferreira-Pinto, K., Simon, S., Maillere, B., and Nozach, H. (2018). Fab is the most efficient format to express functional antibodies by yeast surface display. MAbs *10*, 720–729.

Walker, L.M., Bowley, D.R., and Burton, D.R. (2009). Efficient recovery of high-affinity antibodies from a single-chain Fab yeast display library. J. Mol. Biol. *389*, 365–375.

Wang, B., Lee, C.-H., Johnson, E.L., Kluwe, C.A., Cunningham, J.C., Tanno, H., Crooks, R.M., Georgiou, G., and Ellington, A.D. (2016). Discovery of high affinity anti-ricin antibodies by B cell receptor sequencing and by yeast display of combinatorial V_a:V_t libraries from immunized animals. MAbs *8*, 1035–1044.

Weaver-Feldhaus, J.M., Lou, J., Coleman, J.R., Siegel, R.W., Marks, J.D., and Feldhaus, M.J. (2004). Yeast mating for combinatorial Fab library generation and surface display. FEBS Lett. *564*, 24–34.

Wilson, T.E., Grawunder, U., and Lieber, M.R. (1997). Yeast DNA ligase IV mediates non-homologous DNA end joining. Nature *388*, 495–498.

Wozniak-Knopp, G., Bartl, S., Bauer, A., Mostageer, M., Woisetschläger, M., Antes, B., Ettl, K., Kainer, M., Weberhofer, G., Wiederkum, S., et al. (2010). Introducing antigen-binding sites in structural loops of immunoglobulin constant domains: Fc fragments with engineered HER2/neu-binding sites and antibody properties. Protein Eng. Des. Sel. *23*, 289–297.

Yang, Z., Du, M., Wang, W., Xin, X., Ma, P., Zhang, H., and Lerner, R.A. (2018). Affinity maturation of an TpoR targeting antibody in full-length IgG form for enhanced agonist activity. Protein Eng. Des. Sel. *31*, 233–241.

Zhang, Y., Zang, M., Li, J., Ji, J., Zhang, J., Liu, X., Qu, Y., Su, L., Li, C., Yu, Y., et al. (2014). CEACAM6 promotes tumor migration, invasion, and metastasis in gastric cancer. Acta Biochim. Biophys. Sin. *46*, 283–290.

Zielonka, S., Weber, N., Becker, S., Doerner, A., Christmann, A., Christmann, C., Uth, C., Fritz, J., Schäfer, E., Steinmann, B., et al. (2014). Shark attack: High affinity binding proteins derived from shark vNAR domains by stepwise in vitro affinity maturation. J. Biotechnol. *191*, 236–245.

Supplementary Material: The online version of this article offers supplementary material (https://doi.org/10.1515/hsz-2018-0347).

6.2 A One-Step Process for the Construction of Phage Display scFv and VHH Libraries

Authors

Carolin Sellmann, **Lukas Pekar**, Christina Bauer, Elke Ciesielski, Simon Krah, Stefan Becker, Lars Toleikis, Jonas Kügler, André Frenzel, Bernhard Valldorf, Michael Hust, Stefan Zielonka

Carolin Sellmann and Lukas Pekar contributed equally to this work.

Bibliographic information

Molecular Biotechnology

Volume 62, Issue 4, January 2020, Pages 228–239

DOI: https://doi.org/10.1007/s12033-020-00236-0

Contributions by Lukas Pekar

- Coordinated the project together with C. Sellmann and S. Zielonka
- Planned and conducted in silico analysis and experiments together with C. Bauer, E. Ciesielski, B. Valldorf, L. Toleikis, S. Becker and S. Krah
- Conducted all expression and purifications of isolated library candidates in mammalian cells
- Conducted all BLI experiments
- Wrote the manuscript together with C. Sellmann and S. Zielonka
- Prepared the supplementary section together with C. Sellmann and S. Zielonka

Molecular Biotechnology (2020) 62:228–239
https://doi.org/10.1007/s12033-020-00236-0

ORIGINAL PAPER

A One-Step Process for the Construction of Phage Display scFv and VHH Libraries

Carolin Sellmann[1] · Lukas Pekar[1] · Christina Bauer[1] · Elke Ciesielski[1] · Simon Krah[1] · Stefan Becker[1] · Lars Toleikis[1] · Jonas Kügler[2] · André Frenzel[2] · Bernhard Valldorf[3] · Michael Hust[2,4] · Stefan Zielonka[1]

Published online: 24 January 2020

Abstract

In this work we present a one-step cloning approach for the establishment of antibody phage display libraries relying on type IIs restriction enzymes. We show that single chain variable fragment (scFv) libraries with adequate qualities can readily be cloned in a 'scar-less' manner and that the isolation of antigen-specific antibodies from immunized chickens is feasible within three selection rounds. Moreover, we demonstrate the general applicability of this method by rapidly constructing and panning VHH single domain antibody phage display libraries from immunized Llama repertoires.

Keywords Phage display · Golden gate cloning · Type IIs enzyme · Antibody · scFv · VHH · Single domain antibody

Abbreviations

BLI	Bio-layer interferometry
BSA	Bovine serum albumin
CDR	Complementarity-determining region
ECD	Extracellular domain
EGFR	Epidermal Growth Factor Receptor
ELISA	Enzyme-linked immunosorbent assay
Fab	Antigen-binding fragment
GGC	Golden Gate Cloning
IPTG	Isopropyl-beta-D-thiogalacto pyranoside
MTP	Microtiter plate
PBS	Phosphate-buffered saline
RT	Room temperature
ScFv	Single chain variable fragment
TMB	3,3′,5,5′-Tetramethylbenzidne
VH	Variable domain of the heavy chain
VHH	Variable domain of the heavy chain of a heavy chain only antibody
VL	Variable domain of the light chain

Carolin Sellmann and Lukas Pekar contributed equally to this work.

Electronic supplementary material The online version of this article (https://doi.org/10.1007/s12033-020-00236-0) contains supplementary material, which is available to authorized users.

✉ Stefan Zielonka
Stefan.Zielonka@merckgroup.com

[1] Protein Engineering and Antibody Technologies, Merck Healthcare KGaA, Frankfurter Strasse 250, 64293 Darmstadt, Germany

[2] YUMAB GmbH, Inhoffenstraße 7, 38124 Braunschweig, Germany

[3] Chemical and Pharmaceutical Development, Merck Healthcare KGaA, Frankfurter Strasse 250, 64293 Darmstadt, Germany

[4] Institut für Biochemie, Biotechnologie Und Bioinformatik, Technische Universität Braunschweig, Spielmannstr. 7, 38106 Braunschweig, Germany

Background

Monoclonal antibodies emerged as the most important class of biologics on the therapeutic market. The simple fact that over 80 therapeutics have been granted marketing approval as well as that more than 570 antibody-derived candidates are currently being investigated in clinical trials is corroborating their therapeutic and economical potential [1]. The most prominent approach for the generation of antigen-specific antibodies relies on the combination of animal immunization with hybridoma technology, as pioneered by Köhler and Milstein [2]. With the advent of transgenic animals, e.g., rats or mice endowed with partially human antibody gene repertoires [3–7], fully human antibodies can be isolated in this manner. Alternatively, in vitro selection technologies such as phage display, yeast surface display, or ribosomal display enable the isolation of antigen-specific entities from naïve, synthetic as well as immunized repertoires

[8–12]. Here, the key feature that enables the identification of desired candidates from antibody libraries is the linkage between the antibody variant to its coding genetic information. In this respect, phage display is the most established as well as most widely used platform technology. In 2016, six phage-derived antibodies, among them also the best-selling drug Adalimumab (Humira®) [13], were approved for therapy and several further were tested in clinical trials. Only three years later, already 12 antibodies discovered via the phage display platform have reached approval.

In the commonly applied phagemid format [14], the expression of the antibody fragment as fusion with phage envelope protein pIII is uncoupled from phage protein production and phage replication. A morphogenic signal is added for packaging as well as for phage replication. Correct phage assembly thus requires co-expression of other phage proteins, as provided by helper phage [14]. Phage display allows for the generation of huge antibody libraries in different formats such as scFv, Fab as well as single antibody domains [15-19]. However, cloning of libraries comprising heavy and light chain diversities is a tedious and laborious process, for instance, as it requires sequential cloning of the light and heavy chain repertoire into the phagemid [20]. We have previously shown that the process of yeast surface display library generation can be streamlined significantly [21–23]. Utilization of type IIs restriction enzymes allowed for efficient one-step cloning of heavy as well as light chain diversities into a single Fab display plasmid in a directional manner as well as the isolation of high-affinity antibodies. Similarly, it was demonstrated by Nelson and Valadon that this cloning principle, referred to as Golden Gate Cloning (GGC), is also valid for the construction of phage display Fab libraries [24].

In this present work, we set out to broaden the applicability of GGC for library establishment in the context of phage display by the facile generation of phage display chicken (Gallus gallus domesticus) scFv immune libraries as well as camelid (Lama glama) single domain VHH immune libraries. To this end, we analyzed the respective antibody germline repertoires for type IIs restriction enzymes having a minimal or neglectable frequency of recognition sites in antibody variable domain genes. Likewise, PCR-amplified VH-, VL-, and VHH-repertoires, respectively, were scrutinized in this manner, enabling the identification of optimal enzymes for library establishment with minimal restriction enzyme-based bias. A cloning strategy was designed, allowing for one-step library generation (Fig. 1, Fig. S1). Libraries with a high level of insert correctness could readily be constructed using either splenocytes from chicken or PBMCs from llamas immunized with human EGFR antigen (extracellular domain) as starting material, an important target in cancer therapy. Panning of libraries enabled the selection of antigen-specific antibodies with high affinities ultimately giving clear evidence that GGC is a versatile tool for phage display-derived library construction and antibody hit discovery.

Methods

Animal Immunization

One chicken (Gallus gallus domesticus) was immunized with recombinant human EGFR (extracellular domain containing C-terminal hexahistidine-tag, produced, and purified in-house) as described by Grzeschik and colleagues at Davids Biotechnologie (Regensburg, Germany) [25]. Immunization was performed using 150 µg of antigen combined with AddaVax (InvivoGen) adjuvant. After initial administration, the chicken received boosts after 2, 4, 5, and 8 weeks. After 9 weeks, the animal was sacrificed and splenic RNA was isolated. All experimental procedures and animal care were in accordance with local animal welfare protection laws and regulations.

Moreover, two approximately five-year-old llamas (*Lama glama*) were immunized with recombinant human EGFR at preclinics GmbH (Potsdam, Germany). All experimental procedures and animal care were in accordance with local animal welfare protection laws and regulations. In brief, for each immunization 300 µg of EGFR diluted in a volume of 1 ml PBS were emulsified with either 1 ml Complete Freund's Adjuvant (first immunization) or Incomplete Freund's Adjuvant (subsequent immunizations). Injections were administered subcutaneously at three sites. A total of four immunizations were performed over the course of 56 days (day 0, 28, 42, and 56). On day 60, blood (100 ml) was collected and total RNA was extracted. After the study, camelids remained alive. All animals in this study were obtained from the respective service provider.

Plasmids

All plasmids were designed in-house and synthesized at GeneArt (Thermo Fisher Scientific). The plasmid pHAL14 served as template for the Golden Gate Cloning-compatible cloning approach [20]. All destination plasmids were designed to contain an ampicillin resistance cassette, whereas the respective entry plasmids comprised a kanamycin resistance gene.

Library Construction

Following RNA extraction, cDNA was synthesized using 50 µl RNA extract, 10 µl random hexamer primers (50 ng/µl), 10 µl 50 µM dNTPs, 30 µl H_2O, 40 µl 25 mM $MgCl_2$, 20 µl 10 × RT-buffer, 20 µL 0.1 M DTT, 10 µl RNase OUT,

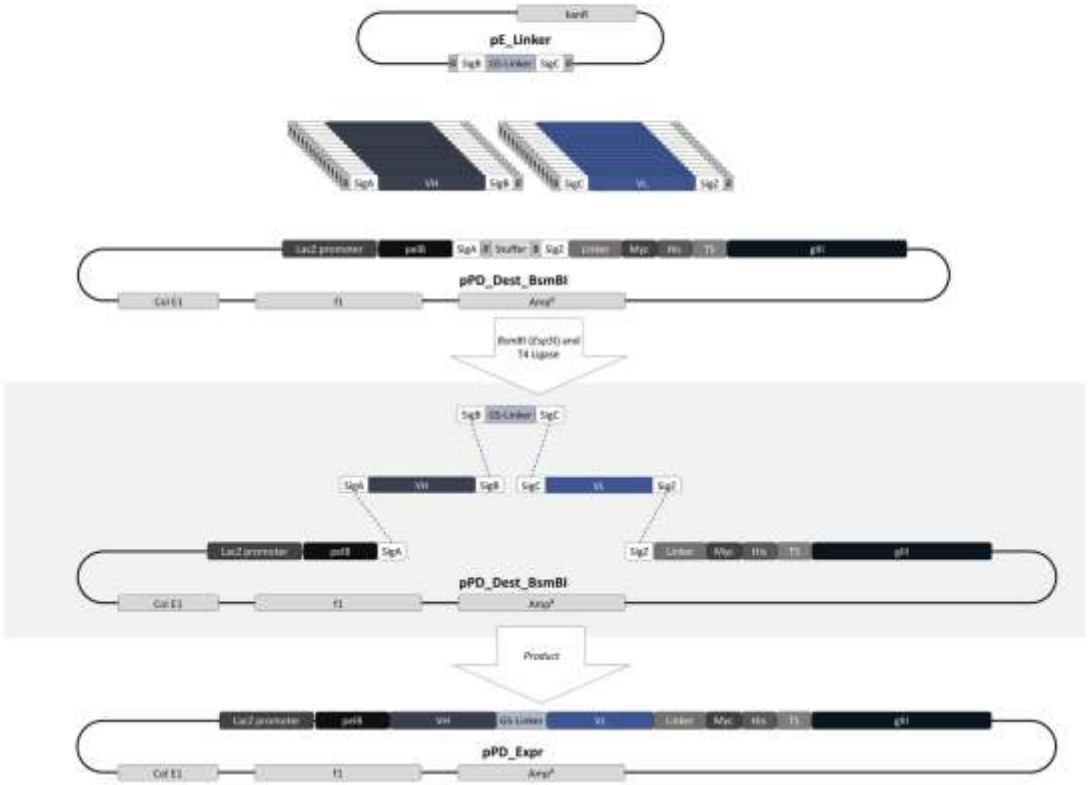

Fig. 1 Schematic overview of the one-step generation process of phage display plasmids for the construction of scFv antibody libraries. The destination plasmid (pPD_Dest_BsmBI) as well as the PCR-amplified VH and VL repertoires contain or are flanked by BsmBI recognition sites in opposite orientations (B: CGTCTCN, *B*: NGAG ACG). Complementary overhangs i.e., signature sequences (SigX) after Esp3I digestion enable the defined one-pot assembly of the four-component system during ligation resulting in the final display plasmid (pPD_Expr). ColE1: origin of replication. f1: origin of replication. Amp^R: Ampicillin resistance gene, pelB: leader sequence. Linker: amino acids AAAGS, Myc: c-Myc epitope EQKLISEEDL, His: hexahistidine-tag, TS: trypsin site KDIR, gIII: gene encoding for phage protein pIII. Note that an amber stop codon is introduced between the hexahistidine-tag and the trypsin site

and 10 µl SuperScript III reverse transcriptase in a volume of 200 µl (SuperScript III First-Strand Kit, Thermo Fisher Scientific). Reaction conditions were as follows: 5 min at 25 °C, 60 min at 50 °C followed by 5 min at 85 °C. 1 µl RNase was added followed by incubation for 20 min at 37 °C.

For the generation of chicken scFv phage display libraries, heavy and light chain antibody variable regions were amplified from cDNA in PCR reactions using germline specific primers annealing either to chicken heavy or light chain variable region framework 1 (Chicken_BsmBI_VH_up, Chicken_BsmBI_VL_up) and to the chicken framework 4 (Chicken_BsmBI_VH_lo, Chicken_BsmBI_VL_lo). Primer sequences are given in Table S1. The reaction was carried out with 1 µl cDNA, the corresponding primer pair for VH or VL amplification (each 1 µl à 10 pmol), and Q5 High-Fidelity 2 × Master Mix (NEB) in a volume of 50 µl using the following parameters: 30 s at 98 °C, 30 cycles of 30 s at 98 °C, 20 s at 60 °C, and 30 s at 72 °C, followed by a final elongation for 2 min at 72 °C. After PCR purification using Wizard® SV Gel and PCR Clean-up System (Promega) according to the manufacturer's instructions, amplified VH and VL regions were subjected to GGC employing 1 µg of destination plasmid pPD_Dest_BsmBI, 1.4 µg entry plasmid including the linker sequence pE_Linker, each 160 ng of VH and VL PCR product together with 400 units Esp3I, 1000 units T4 DNA ligase, and 10 µl T4 Ligase buffer (all NEB) in a final volume of 100 µl (Fig. 1). The reaction mixture was incubated for 40 cycles of 1 min at 37 °C and 1 min at 16 °C followed by a final digestion step for 10 min at 55 °C. Following heat inactivation for 20 min at 80 °C, an additional restriction step with 5 µl HindIII (NEB) was performed to digest residual destination plasmid. After

purification of the Golden Gate Cloning reaction by Wizard® SV Gel and PCR Clean-up System (Promega), 30 µl ligation product was mixed with 50 µl of ER2738 electrocompetent *E. coli* cells (Lucigen) on ice. Electroporation was carried out in prechilled 2 mm cuvettes (Genepulser Xcell™) using a MicroPulser electroporator (BioRad) with 2.5 kV. Immediately after pulsing, electroporated cells were diluted in 920 µl SOC medium (Lucigen) with subsequent incubation at 37 °C at 400 rpm for 1 h. The transformation was then plated out on 245 × 245 mm Petri dishes (Thermo Scientific) with 2xYT-GA agar (1.6% (w/v) tryptone, 1% (w/v) yeast extract, 0.5% (w/v) NaCl, 1.5% (w/v) agar–agar, 100 nM glucose, 100 µg/ml ampicillin) and incubated overnight at 37 °C. For evaluating the transformation rate, 10^{-6} and 10^{-8} dilutions were prepared for each transformation reaction which were analogously plated out and incubated on small Petri dishes (Greiner). The GGC rate was determined either by colony PCR using primers pHAL30_14_fw and pHAL30_14_rev in RedTaq Mix 1.1x (VWR) to check for the correct insert length or by sequencing (Tab. S1). After overnight incubation, transformants were harvested in 25 mL 2xYT medium. 200 µl glycerol (Roth) was added to 800 µl aliquots of bacteria solution which were subsequently stored at − 80 °C.

For amplification of llama VHH, germline specific primers annealing to VHH framework 1 (VHH_SapI_up) and to the hinge region (short hinge: VHH_SapI_sh_lo, long hinge: VHH_SapI_lh_lo) was performed as described above (Tab. S1). Subsequently, for GGC 500 ng of purified PCR product was incubated with 1 µg destination plasmid pPD_Dest_SapI with 200 units SapI, 1000 units T4 DNA Ligase, and 10 µl 10 × T4 Ligase Buffer (all NEB) using the following reaction parameters: 40 cycles of 1 min at 37 °C and 1 min at 16 °C followed by a final digestion step for 10 min at 65 °C. Plasmid transformation and titration was performed analogously to chicken scFv library construction.

In general, we utilized three different *E. coli* strains for phage display library construction and selections. For library generation, we used ER2738 cells due to very high transformation rates. Because of fast growth rates that allow for performing one round of panning per day, TG1 cells were employed for selections. Finally, XL1 MRF's were used for final infection and plasmid rescue due to adequate plasmid quality after plasmid preparation.

Phage Display Library Packaging

Packaging of each antibody immune library was performed separately by inoculation of the library glycerol stock in 100 ml 2xYT-GA medium (2xTY medium supplemented with 100 µg/ml ampicillin and 100 mM glucose) with a starting OD of ~ 0.1. The cultures were incubated at 37 °C with 200 rpm until reaching an OD of ~ 0.5. Then, 5 ml bacteria culture (~ 2.5×10^9 cfu) were infected with 5×10^{10} M13K07 helper phage (NEB) followed by first 30 min incubation at 37 °C without shaking followed by 30 min incubation at 37 °C at 200 rpm. After centrifugation for 10 min at 3220×*g* at 4 °C, the infected cells were resuspended in 30 ml 2xYT-medium supplemented with 100 µg/ml ampicillin and 50 µg/ml kanamycin. Phages were produced by incubation at 30 °C at 200 rpm overnight. The next day, the cultures were centrifuged for 15 min at 3220×*g* at 4 °C and the phage containing supernatant was precipitated with 1/5 volume of 20% PEG/2.5 M NaCl solution for 1 h on ice. After centrifugation at 10,000 g for 1 h at 4 °C, the phage pellet was resuspended in 5 ml phage dilution buffer (10 mM Tris, 20 mM NaCl, 2 mM EDTA, pH 7.5). Residual cell debris was removed by further centrifugation at 16,000 g at 4 °C for 15 min and filtrated. After additional precipitation with 1 ml 20% PEG/2.5 M NaCl solution, centrifugation for 45 min at 16,000×*g* at 4 °C, resuspension in 500 µl phage dilution buffer, and final centrifugation for 1 min at 13,000×*g*, the phage eluate was stored at 4 °C. Phages were titrated by incubating 10 µl of phage eluate serial dilution (10^{-2} to 10^{-8}) with 1 µl trypsin (Sigma) and 990 µl PBS pH 7.4 for 15 min at 37 °C and adding 10 µl of trypsinated phage reaction to 50 µl ER2738 cells (Lucigen). Cells were plated on 2xYT-GA agar plates overnight at 37 °C and cfu was counted and the number of infecting phage particles was calculated. Display of antibody fragments on phage was evaluated by 4–12% Bis–Tris-SDS-PAGE (Thermo Fisher) and Western Blot which was developed with mouse anti-pIII antibody (1:1000; MobiTec) and peroxidase conjugated goat anti-mouse antibody (1:1000; Jackson Immuno Research, Fig. S2). For each library, 10^9 of library phage (pfu) were analyzed along with three concentrations of M13K07 helper phage control (10^7, 10^8 ,and 10^9 pfu, NEB).

Phage Display Selection

In panning round one, approx. 1×10^{11} antibody fragment displaying phages for each library were separately diluted in 2% panning block (2% (w/v) milk powder, 2% (w/v) BSA, 0.05% Tween-20 in PBS pH 7.4), pre-incubated for 1 h in a 96-well microtiter plate well, blocked, and coated with an unrelated protein for negative selection at room temperature (RT). Subsequently, the supernatant was transferred to a well with 250 ng immobilized human EGFR-His (in-house production) for 2 h at RT. Non-bound phages were removed by washing 10-time with PBST (300 µl PBS with 0.05% Tween 20). Target-specific antibody fragment displaying phages were trypsinized for 30 min at 37 °C (10 µg/ml trypsin in 150 µl, Sigma) and were used for infection of 1 ml TG1 cells with OD 0.5 for 30 min without shaking followed by 30 min at 550 rpm at 37 °C. For the output titration, 1 µl of infected TG1 cells was diluted after the first 30 min in 1 ml PBS and

1/10 was plated on 2xYT-GA plates and incubated overnight at 37 °C. To the remaining infected TG1 cells, 3.5 ml 2xYT-GA medium was added for further 30 min incubation. For phage packaging, the TG1 cells were additionally infected with 1×10^{10} M13K07 helper phage (NEB) by 30 min incubation without shaking and 30 min at 550 rpm and 37 °C. After centrifugation at 3220×*g* for 10 min, the pellet was resuspended in 5 ml 2xYT-AK medium and incubated overnight with 550 rpm at 30 °C. The next day, bacteria were pelleted by centrifugation at 3220×*g* for 10 min and phage containing supernatant was either stored at 4 °C or used for the subsequent panning rounds. For panning round two and three, the antigen concentration of negative selection target and human EGFR protein was decreased to 100 ng and 50 ng, respectively, and for higher stringency, the number of washing steps was increased to 20-times and 30-times, respectively. For both round two and three, 100 µl phage supernatant from the respective previous round was mixed with 50 µl 2% panning block as input. After the third panning round, trypsinized phages were used to infect 1 ml XL1 MRF' supercompetent cells (Stratagene) for 30 min at 37 °C without shaking. Bacteria were pelleted at 3200 g for 10 min, resuspended in 250 µl 2xYT medium, and plated on 2xYT-A agar plates. The next day, bacteria were harvested from plates in 25 mL 2xYT medium. Bacterial stocks containing 20% (v/v) glycerol were prepared as described above and stored at − 80 °C.

Antibody Production and Screening in Microtiter Plates

Single bacteria clones carrying antibody fragment phagemids were picked from 2xYT-GA agar plates after selection and used for inoculation of 96-well polypropylene MTPs (Greiner) filled with 2xYT-GA medium. After incubation overnight at 37 °C and 700 rpm with 70% humidity, 10 µl of this pre-culture was transferred to 190 µl fresh phosphate-buffered 2xYT-A medium in a new MTP. After 2 h further incubation, 100 µM isopropyl-beta-D-thiogalacto pyranoside (IPTG) and 50 mM sucrose were added followed by incubation at 30 °C at 800 rpm overnight. Bacteria were pelleted by centrifugation for 10 min at 3220×*g* at 4 °C, supernatants were transferred to 384-well MTPs (Greiner) and diluted 1:1 with 2% BSA-PBS.

For the antigen ELISA, 50 ng positive or negative target protein were immobilized on 384-well MTPs (MaxiSorp, Nunc) in PBS pH 7.4 overnight at 4 °C. The next day, wells were washed three times with 100 µl PBST and blocked with 2% BSA-PBST for 1 h at room temperature (RT). After three times of washing with PBST, the expressed antibody fragments were added for an additional 1 h at RT. Antibody fragments bound to the antigen were detected with mouse anti-c-myc antibody followed by goat-anti-mouse IgG secondary antibody conjugated to peroxidase (Jackson Immuno Research). The colorimetric reaction was performed with the substrate TMB (3,3',5,5'-tetramethylbenzidne) which was stopped with 1 N sulfuric acid after 2 min. Absorbance was measured with a Paradigm™ MTP reader (Beckman Coulter). A clone was declared as hit when absorbance at 450 nm for EGFR-coated well exceeded 1.5, whereas the ELISA signal for the negative control well was lower than 0.8.

Expression and Purification of Isolated Library Candidates

Isolated VHHs were reformatted into pTT5 plasmid as human Fc-fusions. Isolated chicken scFv regions were reformatted as scFv-Fc antibodies (human) [26]. For antibody production, Expi293 cells were transiently transfected with expression vectors (pTT5) according to the manufacturer's instructions (Thermo Fisher Scientific). Supernatants were harvested by centrifugation five days post transfection and purified via MabSelect antibody purification chromatography resin (GE Healthcare). Finally, buffer was exchanged to PBS, pH 6.8, over 24 h at 4 °C using Pur-A-Lyzer™ Maxi 3500 Dialysis Kit (Sigma Aldrich/Merck KGaA) followed by a sterile filtration step employing Ultrafree®-CL GV 0.22 µm Centrifugal Devices (Merck Millipore).

Bio-layer Interferometry (BLI)

The Octet RED96 system was employed to perform binding kinetic measurements (ForteBio, Pall Life Science). All steps were performed at 30 °C and 1000 rpm agitation. Camelid and chicken-derived antibodies were loaded on anti-human Fc biosensors (AHC) at 5 µg/ml in PBS for 3 min. Subsequently, tips were transferred to kinetics buffer (KB; PBS, 0.1% (v/v) Tween-20 and 1% (w/v) BSA) for 60 s. Association to recombinant human EGFR (concentration range 100–6.25 nM) was measured for 300 s in KB followed by dissociation for 300 s in KB. For each antibody-derivative, a negative control was measured using KB and an unrelated antigen at 100 nM in KB instead of EGFR. Moreover, species cross-reactive binding was assessed at a single concentration of 100 nM recombinant mouse EGFR (ECD, produced in-house). Data fitting and analysis was performed with ForteBio data analysis software 8.0 using a 1:1 binding model after Savitzky–Golay filtering.

Results

Analysis of Type IIs Restriction Sites in Chicken and Camelid Antibody Repertoires

In order to identify suitable type IIs restriction enzymes for Golden Gate Cloning of chicken and camelid antibody

repertoires following immunization, we retrieved IGHV, IgHJ, IgLV, and IgLJ datasets from the IMGT database [27]. Moreover, approximately 100 randomly chosen sequences of PCR-amplified VH and VL genes (*Gallus gallus domesticus*) as well as amplified VHH genes (*Lama glama*) were analyzed in this respect. To this end, we only focused on commonly used type IIs enzyme BsaI as well as on SapI and BsmBI. The two latter enzymes have been proven to be useful for cloning of antibody repertoires [24]. As presented in Table 1, for BsaI, which is one of the most commonly utilized enzymes for GGC-based approaches, a high frequency of restriction sites in chicken IgLV sets was found. This finding was also confirmed for the PCR-amplified VL repertoire. Similarly, BsaI recognition sites were also found frequently in *Lama glama* IgHV sets as well as PCR-amplified VHH genes. Consequently, this enzyme was excluded for further investigations. On the other hand, chicken as well as llama antibody genes exhibited only very few recognition sites for BsmBI (or Esp3I) and SapI. In case of BsmBI, a restriction site was identified in chicken and camelid IgHJ sets. This has also been reported for human, murine, and rabbit IgHJ genes [24]. Likewise, due to its location near the end of the gene, this site can be readily removed during primer design. Due to a lower presence of BsmBI recognition sites in chicken IgHV sets, this enzyme was selected for cloning of chicken scFv libraries, while SapI was chosen for the construction of VHH single domain antibody libraries.

Design of Phage Display Library Components

For the generation of scFv libraries, we designed a four-component system comprising a destination plasmid, the amplified variable region repertoire of the heavy chain, the amplified variable region repertoire of the light chain as well as an entry module for the incorporation of a linker of choice (Fig. 1). The destination plasmid was pHAL14-derived [20] and major elements were the LacZ promoter, the pelB leader followed by a stuffer sequence (containing a HindIII restriction site), and the short linker, as well as a myc-tag, a hexahistidine-tag, a trypsin-site, and phage coat protein gene III. Between the his-tag and the trypsin-cleavage site, we incorporated an amber stop codon. Moreover, the stuffer sequence contained BsmBI recognition sites for seamless cloning of ScFv entities. Resulting overhangs, i.e., signature sequences were part of the pelB leader (SigA) or part of the short linker (SigZ). Besides, the plasmid contained an ampicillin resistance gene cassette as well as the ColE1 and the f1 origins of replication. The entry plasmid contained an 18 amino acid scFv linker, flanked by BsmBI recognition sites. Signature sequences were part of the linker sequence (SigB, SigC). Moreover, this plasmid contained the ColE1 ori for propagation as well as a kanamycin resistance gene. Amplified VH and VL genes were flanked by BsmBI recognition sites as well as corresponding signature sequences (SigA and SigB for VH, SigC and SigZ for VL). Primer sequences for specific chicken antibody variable domain amplification as well as signature sequences can be found in the supplementary material section (Tab. S1, Tab. S2).

For VHH library construction, we designed a two-component system comprising a destination plasmid as well as the amplified VHH repertoire module (Fig. S1). The destination plasmid was designed in a very similar way to the scFv destination module, except for an exchange of the BsmBI recognition sites for SapI recognition sites. Consequently, the amplified VHH repertoire was flanked by SapI sites as well as corresponding signature sequences (SigA, SigZ).

Table 1 Frequency of pre-selected type IIs recognition sites in chicken and llama gene repertoires

		BsaI (%)	BsmBI (%)	SapI (%)
Chicken sets				
Gallus gallus domesticus[a]	IMGT IGH-V	4.90	0	1.60
	IMGT IGH-J	0.00	0[b]	0
	PCR-amplified VH repertoire	0	1.40[b]	1.40
	IMGT IGL-V	41.20	0	1.90
	IMGT IGL-J	0	0	0
	PCR-amplified VL repertoire	71.20	0	0
Camelid sets				
Lama glama[a]	IGH-V3	37.50	12.50	12.50
	for germline genes VHH1-5 [31]	20	0	0
	IgH-J	0	0[b]	0
	PCR-amplified VHH repertoire	51.20	7.10[b]	0

[a]In genes and pseudogenes

[b]After silent mutagenesis of conserved *BsmBI* site at 3′end of IgH-J segment

Library Construction, Selection, and Characterization of EGFR-Specific Chicken-Derived Scfv Fragments

It's been known for quite some time, that chicken antibodies can be readily obtained by combining animal immunization with display technologies [28, 29]. To demonstrate that the designed GGC-based approach for library generation allows for the facile isolation of antigen-specific antibodies following avian immunization, we constructed a scFv library of a recombinant human EGFR (extracellular domain)-immunized chicken. To this end, after cDNA synthesis, the heavy chain variable region repertoire as well as the light chain variable region repertoire was amplified using a single PCR step, respectively. Subsequently, both PCR products served as entry modules, together with the entry module comprising the scFv linker and the destination plasmid in a Golden Gate Cloning reaction, yielding the final display vector (Fig. 1, pPD_Expr). Due to its optimal temperature of activity at 37 °C, we decided to utilize the enzyme Esp3I, which is an isoschizomer of BsmBI instead of the latter enzyme that has a temperature optimum of 55 °C. To enhance the efficacy of the reaction i.e., insert rate, a final restriction step with HindIII was performed in order to digest residual destination plasmid. After clean-up, the resulting product was transformed into ER2738 *E. coli* cells in a single electroporation reaction, yielding a small library with a calculated size of 4×10^6 independent clones (Table 2). Library analysis via colony PCR of 48 clones revealed an GGC rate of 92%. Moreover, sequencing of approximately 100 single clones revealed a high correctness of 84% (data not shown). Successful display was verified by Western Blot (Fig. S2). Subsequently, the library was subjected for panning against EGFR. After three rounds of phage display panning with decreasing antigen concentrations (250, 100, 50 ng/well; Tab. S3) and increasing washing cycles, 192 clones were sent out for sequencing (Fig. S3 and Fig. S4), ultimately resulting in 41 unique VHs and 55 unique VLs. To get a more comprehensive view of the diversity of the library output, a clustering strategy was applied in which clones with less than three amino acid exchanges within CDR-H3 belong to the same family. Moreover, at least three sequences must fulfil this criterion to be considered as cluster. This resulted in the identification of eight sequence clusters.

To add another layer of quality assessment of the library output, we also screened 188 selected library candidates for EGFR binding via ELISA after microtiter expression in *E. coli* (Fig. 2a, Fig. S5) yielding in a hit rate of approximately 50%.

In order to demonstrate, that the isolated chicken-derived entities also bind EGFR when expressed in mammalian expression systems, based on sequence analysis, eight clones were reformatted as scFv-Fc fragments and produced in Expi293 cells (Fig. 3). After purification via Protein A, binding kinetics to recombinant human EGFR were investigated via BLI (Table 3, Fig. S6). All reformatted and expressed scFv fusion protein showed binding against EGFR in the single digit to double digit nanomolar range. Moreover, species cross-reactivity against the murine counterpart, which shows approximately 90% sequence identity to the human protein, was assessed at 100 nM mouse EGFR (ECD). This revealed that six out of eight clones were also able to bind to recombinant murine EGFR in a comparable manner, demonstrating that those molecules might be beneficial as tools in pre-clinical models.

Library Construction, Selection, and Characterization of EGFR-Specific Camelid-Derived VHH Single Domain Antibodies

Similar to the generation of the scFv immune library, we aimed at constructing camelid-derived VHH single domain antibody libraries following llama immunization. To this end, we used PBMC-derived cDNA from two EGFR-immunized *Lama glama* as starting material. The forward primer was designed to specifically anneal in framework 1, whereas reverse primers were designed to anneal in the hinge region. Since camelids produce different VHH isotypes comprising short hinge regions and a long hinge regions [30, 31], we designed two different oligonucleotides, respectively (Tab. S1). For each immunized animal, two sub-libraries were constructed, yielding a total number of four VHH phage

Table 2 Analysis of constructed EGFR scFv and VHH libraries

Library	Misc	Library size (per electroporation reaction)	GGC rate (%)	Phage titer (total)
Chicken ScFv	–	4×10^6	92	3.5×10^{12}
Llama 1 VHH	Short hinge	1×10^6	83	4.0×10^{12}
	Long hinge	5×10^6	96	4.5×10^{12}
Llama 2 VHH	Short hinge	4×10^6	83	3.0×10^{12}
	Long hinge	5×10^6	75	3.5×10^{12}

Library sizes as calculated by serial dilution plating are given per electroporation reaction. GGC rates were determined by colony PCR. Phage titer was assessed by serial dilution plating

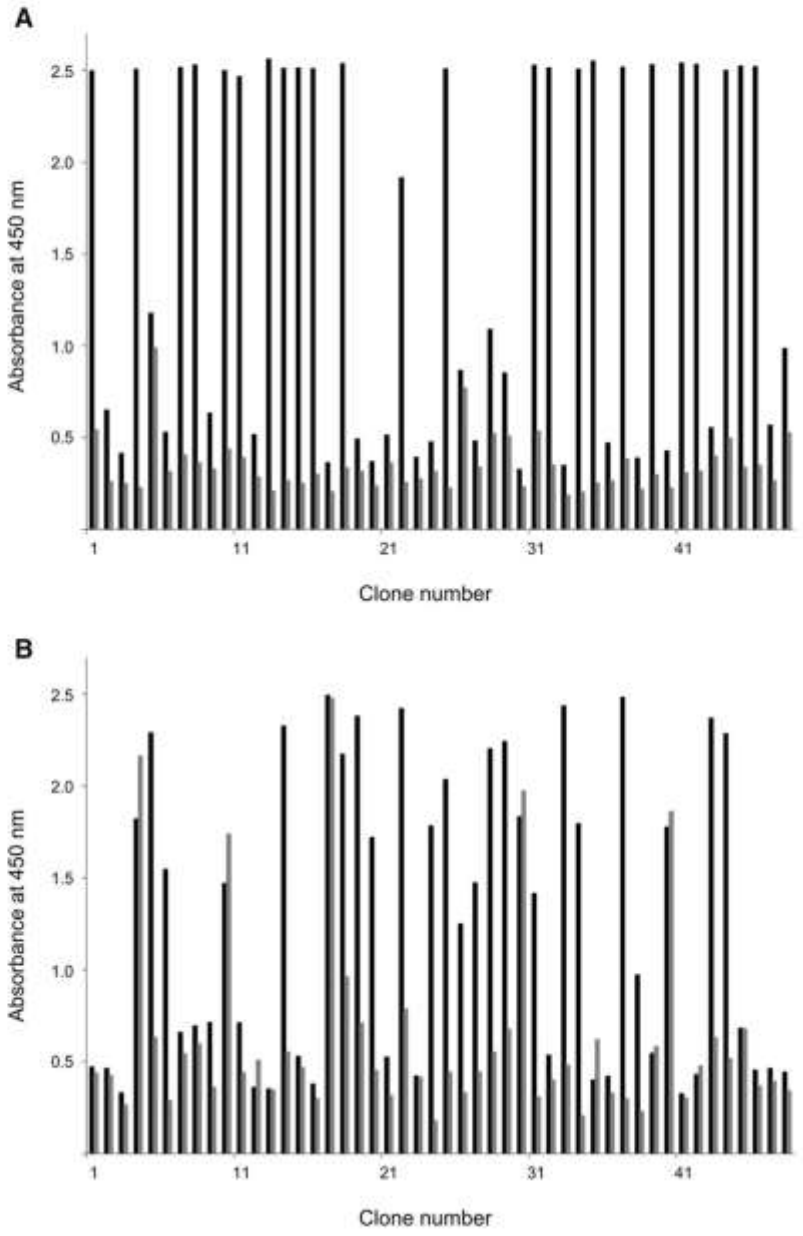

Fig. 2 ELISA screening after microtiter production of selected library candidates in *E. coli*. **a** Screening outcome of EGFR-immunized avian scFv antibody library after three rounds of selection. **b** Screening outcome of EGFR-immunized llama VHH single domain antibody library after three rounds of panning. A representative block of 48 consecutive clones as assessed by ELISA is shown. Black: ELISA signal against EGFR, gray: Absorbance at 450 nm against unrelated negative control antigen

display immune libraries. Consequently, four GGC reactions were performed in total using the respective PCR product as entry module and the destination plasmid (Fig. S1). For each library, only one electroporation reaction was performed into ER2738 cells, yielding library sizes in the range of 1 to 5×10^6. GGC rates as determined by colony PCR were in the range of 75% to 96% (Table 2). All constructed libraries showed display on the surface of phage particles, as demonstrated by Western Blot (Fig. S2). Subsequently, the different VHH libraries were selected against plate-immobilized EGFR in parallel. After three rounds of library panning using step-wise reduced antigen concentrations (Tab. S3), a

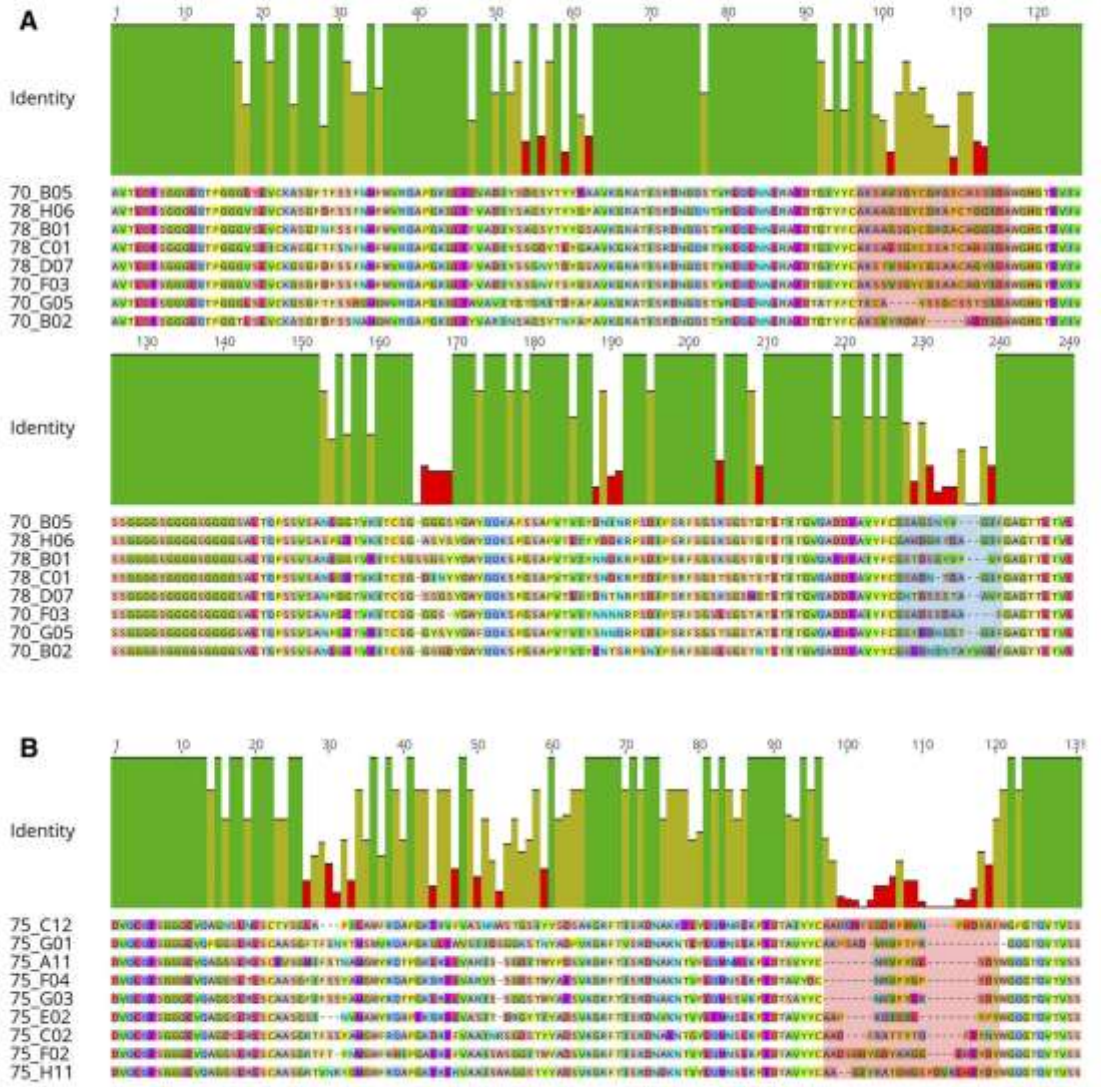

Fig. 3 Multiple sequence alignment of chicken-derived scFv clones (**a**) and llama-derived VHH single domain antibodies (**b**) chosen for expression as Fc-fusion proteins after phage display panning. CDR-H3 is shaded in red, CDR-L3 shown in blue. Alignment was created using MUSCLE Alignment tool within Geneious Prime software (www.geneious.com)

total number of 192 clones (i.e., 48 clones per sub-library) were sent out for sequencing revealing 69 unique sequences (Fig. S7). Moreover, a total number of 752 clones were screened for EGFR binding in an ELISA screening after MTP production, resulting in a hit rate of approximately 20% (Fig. 2b, Fig. S8). Nine clones were reformatted into a VHH-Fc fusion and expressed in Expi293 cells. After purification via protein A, binding kinetics were obtained using BLI (Table 3, Fig. S6). This revealed binding of six VHH-Fc fusion proteins against recombinant human EGFR with a broad spectrum of affinities, ranging from high-affinity binding (picomolar) to moderate binding in the triple digit nanomolar range. Moreover, three clones also showed species cross-reactive binding against recombinant mouse EGFR similar to the human counterpart.

Table 3 Binding kinetics of selected and recombinantly expressed scFv-Fc and VHH-Fc fragments against rhEGFR as assessed by BLI

Name	Format	KD (M)	k_{on} (1/Ms)	k_{off} (1/s)	Cross-reactivity (murine EGFR)
70_B02	scFv Fc-fusion	7.91E−09	4.85E+05	3.84E−03	No
70_B05	scFv Fc-fusion	2.86E−08	1.20E+05	3.45E−03	Yes
70_F03	scFv Fc-fusion	3.66E−08	4.45E+04	1.63E−03	Yes
70_G05	scFv Fc-fusion	3.08E−09	9.71E+04	2.99E−04	No
78_B01	scFv Fc-fusion	1.90E−08	1.26E+05	2.39E−03	Yes
78_C01	scFv Fc-fusion	1.35E−08	1.85E+05	2.50E−03	Yes
78_D07	scFv Fc-fusion	6.62E−08	6.86E+04	4.54E−03	Yes
78_H06	scFv Fc-fusion	4.43E−09	9.44E+04	4.18E−04	Yes
75_H11	VHH Fc-fusion	1.27E−07	3.16E+04	4.03E−03	No
75_G03	VHH Fc-fusion	4.91E−10	2.20E+05	1.08E−04	Yes
75_G01	VHH Fc-fusion	–	–	–	No
75_F04	VHH Fc-fusion	5.11E−09	1.97E+05	1.00E−03	Yes
75_F02	VHH Fc-fusion	–	–	–	No
75_E02	VHH Fc-fusion	–	–	–	No
75_C12	VHH Fc-fusion	1.11E−08	3.50E+05	3.90E−03	No
75_C02	VHH Fc-fusion	2.40E−08	1.23E+05	2.95E−03	No
75_A11	VHH Fc-fusion	1.46E−09	2.36E+05	3.45E−04	Yes

Cross-reactive binding against rmEGFR at 100 nM is also indicated

Discussion

Phage display is the most frequently used platform technology for antibody hit discovery and has delivered several therapeutic entities that have been granted marketing approval [13]. It was demonstrated that therapeutic entities can be successfully generated from synthetic or naïve as well as from immunized repertoires [32-36]. Canonical antibodies i.e., antibodies comprising heavy as well as light chain diversities, are typically displayed either as Fab- or scFv fragments on the surface of phage particles [15, 16]. Either way, the construction of such libraries is typically tedious, involving multiple consecutive steps [16, 20]. Our group has recently demonstrated that the construction of antibody Fab libraries for Yeast Surface Display can be significantly simplified by employing a one-step, one-pot type IIs restriction enzyme-based process referred to as Golden Gate Cloning [21, 22]. Likewise, it was shown by Nelson and Valadon that GGC also enables the facile generation of Fab antibody libraries for phage display [24]. Moreover, the authors elegantly analyzed the occurrence of type IIs restriction sites in human, mouse as well as rabbit antibody gene repertoires. In this present work, we set out to adapt a similar strategy for the construction of scFv antibody libraries as well as camelid single domain antibody libraries for phage display. To this end, we first analyzed the frequency of three different type II restriction sites in chicken and llama antibody repertoires. Essentially, we focused on BsaI as one as the most commonly used enzyme for GGC approaches as well as on BsmBI and SapI, since those enzymes were found to be suitable for the construction of human, mouse, and rabbit antibody libraries [24]. Essentially, this revealed optimal enzymes for the construction of chicken scFv as well as camelid VHH single domain libraries. We demonstrate that the GGC approach enables the generation of libraries in the range of 5×10^6 unique clones per electroporation reaction and that the constructed libraries exhibited high functionalities i.e., insert rates. Consequently, libraries with diversities in the range of 10^8 clones can be readily constructed in a convenient way which should be sufficient to adequately sample immune repertoires following immunization. However, for the generation of naïve or synthetic libraries, one typically aims for diversities in the range of 10^{10}–10^{11} in order to be generally applicable [37]. In this respect, a lot of optimization would be required. Nonetheless, even with the constructed proof-of-concept libraries we were able to select for a diverse panel of antigen-binding antibodies from both, the EGFR-immunized avian scFv as well as from the EGFR-immunized camelid VHH libraries. Recombinantly expressed entities showed a broad spectrum of different affinities against EGFR in the single to double digit nanomolar range for chicken-derived scFv-Fc proteins and triple digit picomolar to triple digit nanomolar range for camelid-derived VHH-Fc fusions.

Conclusion

Besides being the most successfully applied platform technology for the generation of therapeutic antibodies, the construction of phage display library remains challenging and cumbersome. Recently, a significantly simplified process

of library construction was presented by Nelson and Valadon [24]. In their work, the authors describe the generation of phage display Fab libraries using a type IIs restriction enzyme-based process. Herein, we adopted a similar strategy for the establishment of scFv and single domain antibody libraries. We demonstrate that libraries with adequate qualities can be readily cloned using this one-step approach enabling the rapid isolation of antigen-specific antibodies from immunized animals.

Acknowledgements We are grateful to Prof. Harald Kolmar for providing RNA and cDNA from EGFR-immunized chicken.

Author contributions SZ, CS and LP designed the experiments. LP, CB, EC, BV, LT, SB and SK performed in silico analysis and experiments. JK, AF and MH gave scientific advice and guidance on overall strategy. CS, LP and SZ wrote the manuscript.

Compliance with Ethical Standards

Conflict of interests All authors are either affiliated with Merck Healthcare KGaA or Yumab GmbH.

References

1. Kaplon, H., & Reichert, J. M. (2019). Antibodies to watch in 2019. *mAbs, 11*(2), 219–238.
2. Köhler, G., & Milstein, C. (1975). Continuous cultures of fused cells secreting antibody of predefined specificity. *Nature, 256*(5517), 495–497.
3. Brüggemann, M., et al. (2015). Human antibody production in transgenic animals. *Archivum Immunologiae et Therapiae Experimentalis, 63*(2), 101–108.
4. Ching, K. H., et al. (2018). Chickens with humanized immunoglobulin genes generate antibodies with high affinity and broad epitope coverage to conserved targets. *mAbs, 10*(1), 71–80.
5. Harris, K. E., et al. (2018). Sequence-based discovery demonstrates that fixed light chain human transgenic rats produce a diverse repertoire of antigen-specific antibodies. *Frontiers in Immunology, 9*, 889.
6. Jakobovits, A. (1995). Production of fully human antibodies by transgenic mice. *Current Opinion in Biotechnology, 6*(5), 561–566.
7. Lonberg, N. (2005). Human antibodies from transgenic animals. *Nature Biotechnology, 23*(9), 1117–1125.
8. Mondon, P. (2008). Human antibody libraries: A race to engineer and explore a larger diversity. *Frontiers in Bioscience, 13*(13), 1117.
9. Frenzel, A., et al. (2017). Designing human antibodies by phage display. *Transfusion Medicine and Hemotherapy, 44*(5), 312–318.
10. Lipovsek, D., & Plückthun, A. (2004). In-vitro protein evolution by ribosome display and mRNA display. *Journal of Immunological Methods, 290*(1–2), 51–67.
11. Doerner, A., Rhiel, L., Zielonka, S., & Kolmar, H. (2014). Therapeutic antibody engineering by high efficiency cell screening. *FEBS Letters, 588*(2), 278–287.
12. Bradbury, A. R. M., Sidhu, S., Dübel, S., & McCafferty, J. (2011). Beyond natural antibodies: The power of in vitro display technologies. *Nature Biotechnology, 29*(3), 245–254.
13. Frenzel, A., Schirrmann, T., & Hust, M. (2016). Phage display-derived human antibodies in clinical development and therapy. *Mabs, 8*(7), 1177–1194.
14. Breitling, F., Dübel, S., Seehaus, T., Klewinghaus, I., & Little, M. (1991). A surface expression vector for antibody screening. *Gene, 104*(2), 147–153.
15. Hust, M., et al. (2011). A human scFv antibody generation pipeline for proteome research. *Journal of Biotechnology, 152*(4), 159–170.
16. de Haard, H. J., et al. (1999). A large non-immunized human Fab fragment phage library that permits rapid isolation and kinetic analysis of high affinity antibodies. *Journal of Biological Chemistry, 274*(26), 18218–18230.
17. Vincke, C., Gutiérrez, C., Wernery, U., Devoogdt, N., Hassanzadeh-Ghassabeh, G., & Muyldermans, S. (2012). Generation of single domain antibody fragments derived from camelids and generation of manifold constructs. In P. Chames (Ed.), *Antibody engineering* (Vol. 907, pp. 145–176). Totowa, NJ: Humana Press.
18. Könning, D., et al. (2017). Camelid and shark single domain antibodies: Structural features and therapeutic potential. *Current Opinion in Structural Biology, 45*, 10–16.
19. Ubah, O. C., Barelle, C. J., Buschhaus, M. J., & Porter, A. J. (2016). Phage display derived IgNAR V region binding domains for therapeutic development. *Current Pharmaceutical Design, 22*(43), 6519–6526.
20. Kügler, J., et al. (2015). Generation and analysis of the improved human HAL9/10 antibody phage display libraries. *BMC Biotechnology, 15*(1), 10.
21. Roth, L., et al. (2019). Facile generation of antibody heavy and light chain diversities for yeast surface display by Golden Gate Cloning. *Biological Chemistry, 400*(3), 383–393.
22. Rosowski, S., et al. (2018). A novel one-step approach for the construction of yeast surface display Fab antibody libraries. *Microbial Cell Factories, 17*(1), 3.
23. Krah, S., et al. (2018). A streamlined approach for the construction of large yeast surface display Fab antibody libraries. In D. Nevoltris & P. Chames (Eds.), *Antibody engineering* (Vol. 1827, pp. 145–161). New York: Springer.
24. Nelson, R. S., & Valadon, P. (2017). A universal phage display system for the seamless construction of Fab libraries. *Journal of Immunological Methods, 450*, 41–49.
25. Grzeschik, J., et al. (2019). Yeast surface display in combination with fluorescence-activated cell sorting enables the rapid isolation of antibody fragments derived from immunized chickens. *Biotechnology Journal, 14*(4), 1800466.
26. Jäger, V., et al. (2013). High level transient production of recombinant antibodies and antibody fusion proteins in HEK293 cells. *BMC Biotechnology, 13*, 52.
27. Lefranc, M.-P., et al. (2015). IMGT®, the international ImMunoGeneTics information system® 25 years on. *Nucleic Acids Research, 43*(D1), D413–D422.
28. Tsurushita, N., et al. (2004). Humanization of a chicken anti-IL-12 monoclonal antibody. *Journal of Immunological Methods, 295*(1–2), 9–19.
29. Nishibori, N., Horiuchi, H., Furusawa, S., & Matsuda, H. (2006). Humanization of chicken monoclonal antibody using phage-display system. *Molecular Immunology, 43*(6), 634–642.
30. Conrath, K., Wernery, U., Muyldermans, S., & Nguyen, V. (2003). Emergence and evolution of functional heavy-chain antibodies in Camelidae. *Developmental & Comparative Immunology, 27*(2), 87–103.
31. De Genst, E., Saerens, D., Muyldermans, S., & Conrath, K. (2006). Antibody repertoire development in camelids. *Developmental & Comparative Immunology, 30*(1–2), 187–198.

32. Dübel, S., Stoevesandt, O., Taussig, M. J., & Hust, M. (2010). Generating recombinant antibodies to the complete human proteome. *Trends in Biotechnology, 28*(7), 333–339.
33. Hoet, R. M., et al. (2005). Generation of high-affinity human antibodies by combining donor-derived and synthetic complementarity-determining-region diversity. *Nature Biotechnology, 23*(3), 344–348.
34. Griffiths, A. D., et al. (1994). Isolation of high affinity human antibodies directly from large synthetic repertoires. *EMBO Journal, 13*(14), 3245–3260.
35. Knappik, A., et al. (2000). Fully synthetic human combinatorial antibody libraries (HuCAL) based on modular consensus frameworks and CDRs randomized with trinucleotides. *Journal of Molecular Biology, 296*(1), 57–86.
36. Rasetti-Escargueil, C., et al. (2015). Development of human-like scFv-Fc antibodies neutralizing Botulinum toxin serotype B. *mAbs, 7*(6), 1161–1177.
37. Almagro, J. C., Pedraza-Escalona, M., Arrieta, H. I., & Pérez-Tapia, S. M. (2019). Phage display libraries for antibody therapeutic discovery and development. *Antibodies, 8*(3), 44.

6.3 Biophysical and biochemical characterization of a VHH-based IgG-like bi- and trispecific antibody platform

Authors

Lukas Pekar, Michael Busch, Bernhard Valldorf, Steffen C. Hinz, Lars Toleikis, Simon Krah, Stefan Zielonka

Bibliographic information

mAbs

Volume 12, Issue 1, Article 1812210, September 2020

DOI: https://doi.org/10.1080/19420862.2020.1812210

Contributions by Lukas Pekar

- Designed experiments together with S. Zielonka
- Conducted all antibody expression and purification as well as melting point measurements
- Conducted all BLI experiments
- Conducted all flow cytometric measurements
- Conducted all tumor cell killing assays
- Wrote manuscript together with S. Zielonka
- Prepared tables and figures together with S. Zielonka
- Prepared supplementary section

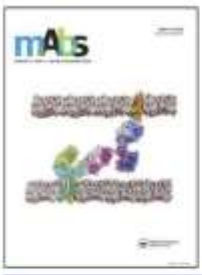

mAbs

ISSN: (Print) (Online) Journal homepage: https://www.tandfonline.com/loi/kmab20

Biophysical and biochemical characterization of a VHH-based IgG-like bi- and trispecific antibody platform

Lukas Pekar , Michael Busch , Bernhard Valldorf , Steffen C. Hinz , Lars Toleikis , Simon Krah & Stefan Zielonka

To cite this article: Lukas Pekar , Michael Busch , Bernhard Valldorf , Steffen C. Hinz , Lars Toleikis , Simon Krah & Stefan Zielonka (2020) Biophysical and biochemical characterization of a VHH-based IgG-like bi- and trispecific antibody platform, mAbs, 12:1, 1812210, DOI: 10.1080/19420862.2020.1812210

To link to this article: https://doi.org/10.1080/19420862.2020.1812210

MABS
2020, VOL. 12, NO. 1, e1812210 (12 pages)
https://doi.org/10.1080/19420862.2020.1812210

Taylor & Francis
Taylor & Francis Group

REPORT

OPEN ACCESS

Biophysical and biochemical characterization of a VHH-based IgG-like bi- and trispecific antibody platform

Lukas Pekar[a], Michael Busch[b], Bernhard Valldorf[c], Steffen C. Hinz[a], Lars Toleikis[d], Simon Krah[d], and Stefan Zielonka[d]

[a]Institute for Organic Chemistry and Biochemistry, Technische Universität Darmstadt, Darmstadt, Germany; [b]Discovery Pharmacology, Merck KGaA, Darmstadt, Germany; [c]Chemical and Pharmaceutical Development, Merck KGaA, Darmstadt, Germany; [d]Protein Engineering and Antibody Technologies, Merck KGaA, Darmstadt, Germany

ABSTRACT

Here, we report the characterization of a VHH-derived IgG-like bi- and trispecific antibody platform that essentially relies on the replacement of the VH and VL regions of a conventional antibody by two independently functioning VHH domains. Consequently, a VHH is engrafted onto constant region CH1 while the other VHH-based paratope is engrafted on the constant region of the light chain, Cκ or Cλ, resulting in a tetravalent bispecific IgG-like molecule. Combined with a heavy chain heterodimerization technique, this platform allows facile engineering of bi- and trispecific antibodies with flexible valencies. We demonstrate the general applicability of this generic platform approach and elaborate on the limitations of specific formats.

ARTICLE HISTORY
Received 11 February 2020
Revised 30 July 2020
Accepted 15 August 2020

KEYWORDS
Antibody engineering; bispecific antibody; camelid; IgG-like; nanobody; single-domain antibody; trispecific antibody; VHH

Introduction

During the past decades, monoclonal antibodies emerged as promising treatment options for various diseases. Today, more than 80 entities have been granted marketing approval and over 570 antibody-based therapeutics are currently being evaluated in clinical trials.[1,2] From a structural perspective, conventional antibodies are large and complex hetero-tetrameric proteins composed of two identical heavy chains as well as two identical light chains, and are monospecific by nature. Consequently, they can only target one antigen. However, diseases are typically complex and originate from multiple different factors or mediators.[3,4] In order to address diseases more adequately, substantial efforts have been made to engineer antibodies for bispecificity, and a plethora of different formats with different layers of complexity are known today.[5,6]

In addition to conventional antibodies, sharks and camelids produce antibodies that are composed of heavy chains only. The paratopes of those isotypes consist of a single variable domain that solely facilitate antigen binding and that are referred to as variable domains of New Antigen Receptor (vNARs, in sharks) or variable domains of the heavy chain of a heavy chain only antibody (VHHs, in camelids).[7,8] Due to their small size, which might be beneficial for tissue penetration[9] as well as their ease of generation[10–12] good stability and simple architecture, which allows multiple reformatting options, single-domain antibodies evolved as promising alternatives to conventional antibodies.[13] While the therapeutic engineering of shark-derived single-domain antibodies is still at a preclinical stage, numerous VHH-derived molecules have progressed into clinical development.[14] Moreover, one VHH-based therapeutic, caplacizumab was approved for the treatment of patients with acquired thrombotic thrombocytopenic purpura by the US Food and Drug Administration (FDA) in 2019.[15]

The general modularity of VHHs enables unprecedented possibilities for the construction of bi- and multispecific antibodies. Consequently, a multitude of VHH-based formats with different valencies as well as specificities have been described in the literature, including multispecific tandem arrangements in a 'beads-on-string' manner, VHH-Fc fusions and VHH-antibody fusions.[16,17] In 2013, Baty and colleagues described a bispecific VHH-based format that uses the constant domains Cκ and CH1 of IgG as natural dimerization domains.[18] In this regard, the authors replaced the variable domain of the heavy chain as well as the variable domain of the light chain by two VHHs, targeting carcinoembryonic antigen and FcγRIIIa, respectively. This resulted in an antigen-binding fragment (Fab)-like bispecific molecule eliciting potent tumor lysis by natural killer (NK) cells. More recently, the authors extended the applicability of this format by targeting human epidermal growth factor receptor 2 (HER2)[19] and mesothelin.[20]

In this study, we set out to investigate whether this Fab-derived bispecific building block can be used to generate a generic IgG-like platform that allows for facile reformatting in bi- and trispecific VHH-based antibodies with flexible valencies (Figure 1(a)). By genetically fusing this Fab-derived bispecific VHH module on an IgG1 Fc backbone, bivalent (for each antigen) bispecific IgG-like antibodies can be obtained (Figure 1(b)). Combining this building block with a heavy chain heterodimerization technique allows facile reformatting into a monovalent bispecific IgG-like entity (Figure 1(c)). To this end, the strand-exchanged engineered domain (SEED)

CONTACT Simon Krah Simon.Krah@merckgroup.com; Stefan Zielonka Stefan.Zielonka@merckgroup.com Protein Engineering and Antibody Technologies, Merck KGaA, Darmstadt D-64293, Germany

Supplemental data for this article can be accessed on the publisher's website.

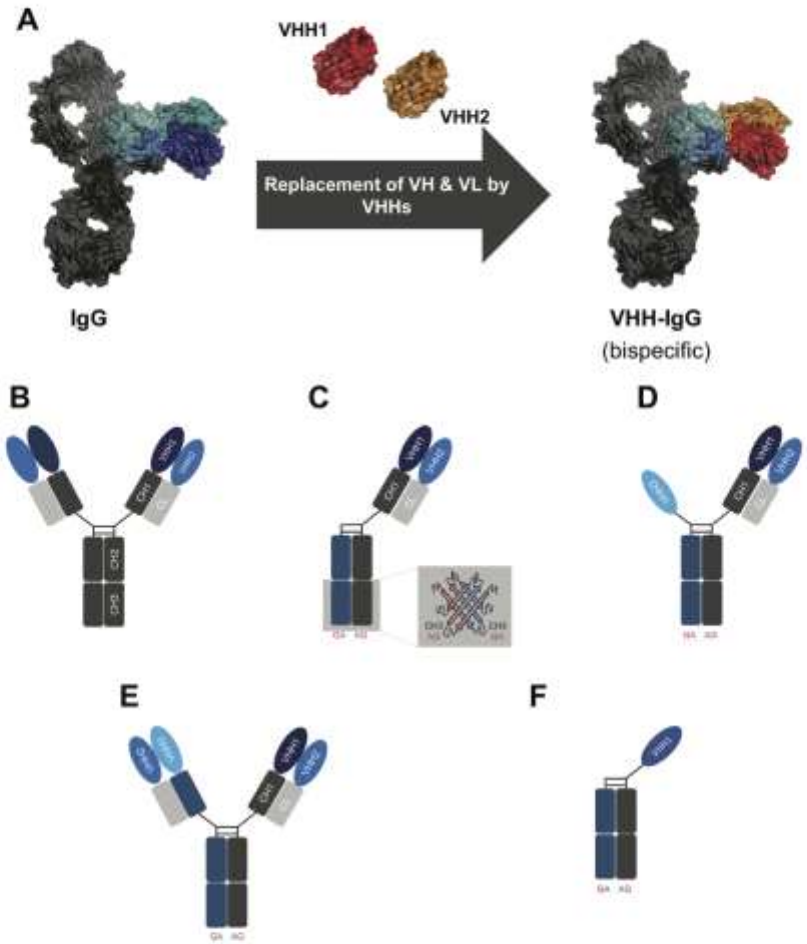

Figure 1. Schematic representation of the overall strategy for the generation of VHH-based IgG-like multispecific antibodies. (a) Model depicting the approach to replace domains VH and VL of a conventional IgG by two independently functioning VHHs for the generation of a bispecific entity. The model is based on pdb:5dk3[21] and was generated using PyMOL v0.99. (b) Bivalent bispecific VHH-based IgG-like antibody employing an IgG backbone. (c) Utilization of the strand-exchanged engineered domains (SEED) technology enables the generation of monovalent bispecific moieties. (d) Monovalent trispecific VHH-based SEEDbodies can be generated by grafting a third VHH onto the hinge region of the SEED GA chain. (e) Trispecific VHH-based SEEDbody comprising bivalency of the light chain-engrafted VHH. (f) Schematic depiction of a one-armed VHH-derived control molecule.

technology was applied.[22] This method is based on beta-strand exchanges of IgG and IgA CH3 domains, yielding preferentially heterodimers without impairing Fc-mediated effector functions. This also enables the generation of trispecific moieties with different valencies (Figure 1(d,e)). By characterizing this platform with respect to biophysical and biochemical properties, we show the benefits as well as limitations of the herein described in different formats. Moreover, when substantial paratope-dependent effects (i.e., steric hindrance) arise, we demonstrate that this can be counteracted by simply placing a 10 amino acid flexible linker between the respective VHH domain and the constant domain region of the light chain. Ultimately, we conclude that most of the different formats of the herein presented platform approach seem to be adequate to expand the 'playground' of multispecific VHH-based antibody engineering.

Results

Design of different formats

Within this study, we aimed at developing and characterizing a generic platform approach for the facile generation of IgG-like bi- and trispecific VHH-derived antibodies. Essentially, the platform is based on the replacement of the variable domains of a human antibody by two independent VHH-based paratopes (Figure 1(a)). Consequently, one VHH is grafted onto domain CH1 of IgG1, whereas the second VHH is grafted either on domain Cκ or Cλ. In order to get a profound understanding of this platform approach, i.e., of the respective formats (Figure 1(b,e)), we decided to use four different VHHs. One VHH was directed against HER2 (sequence derived from WO2016016021). Two paratopes were directed against epidermal growth factor receptor (EGFR), wherein clone 9G8 was

described by Ferguson and coworkers[23] and clone 722C03 was derived from an internal yeast surface display campaign.[24] Finally, an NKG2D-targeting VHH sequence was obtained from WO2017081190. Sequences of the respective VHHs can be found in supplementary Figure S1A. Design examples of VHH engraftments on constant antibody regions CH1, Cκ, or Cλ are shown in supplementary Figure S1B.

In regard to the different formats, we wanted to include at least some flexibility regarding specificities (bi- and trispecific versions) as well as valencies for a cognate epitope (mono- and bivalent). When the VHH-engrafted Fab is expressed on an IgG backbone for instance (Figure 1(b)), this results in a bispecific IgG-looking molecule, that is tetravalent by design (and bivalent for each antigen). By simply using a heavy chain heterodimerization technique, i.e., SEED technology (Figure 1(c)), one can express one-armed versions of the VHH-based bispecific. This enables bivalency and accordingly monovalent targeting of each epitope. Consequently, this also allows for a very thorough characterization of the platform with respect to functional properties, e.g., simultaneous binding on the protein and cellular level as well as investigations on paratope-dependent effects, i.e., steric hindrance. This monovalent bispecific format (i.e., monovalent for the respective target) can easily be extended into a trispecific format that is monovalent for each antigen by simply placing a third VHH-derived paratope onto the hinge region of the second heavy chain (Figure 1(d)). Finally, by placing two VHH-engrafted Fabs on each heavy chain, the platform also allows trispecific targeting in which the paratope grafted onto the constant region of the light chain is bivalent (Figure 1(e)).

Expression and characterization of monovalent bispecific IgG-like VHH-based antibodies

To gain a thorough understanding of the functionality of each engrafted paratope in this platform approach, we first focused on the generation of monovalent IgG-like VHH-based bispecific antibodies (Figure 1(c)). For heavy chain heterodimerization, the SEED technology was applied, which is based on beta-strand exchanges of IgG and IgA CH3 domains, resulting in two non-identical heavy chains referred to as AG chain and GA chain. For the SEED GA chain, it is known that homodimers might form, clearly representing a misassembled side product that might affect the analysis of the respective construct in manifold ways, e.g., kinetic measurements and size exclusion profiles. In order to obviate this, the RF mutation was introduced, preventing binding of GA:GA homodimers to protein A.[25] Consequently, only AG-GA heterodimers are purified, since AG-AG species typically do not assemble. In this particular monovalent bispecific format, the VHH-based heavy chain of the Fab was expressed on the AG chain, while the GA chain solely comprised the hinge region (one-armed IgG-like VHH-SEED). To allow for direct comparisons to the parental VHHs, i.e., VHHs not engrafted into this bispecific construct, each camelid-derived variable domain was also expressed as one-armed SEED control (Figure 1(f)). To get a more comprehensive view on this format, we produced all four different VHHs in the bispecific monovalent IgG-like scaffold and tried different orientations as well as lambda and kappa backbones for grafting the second paratope onto the constant region of the light chain. The expression of all monovalent bispecific IgG-like VHH-based molecules resulted in fairly equal expression yields compared to one-armed control molecules (Table 1). To be more precise, expression yields as determined after protein A purification were in the triple-digit milligram per liter scale, indicating good expression profiles of all the molecules scrutinized in this particular format. Moreover, thermal stabilities of individual bispecific constructs were very similar to the implemented VHH displaying the lower aggregation onset temperature. Aggregation properties were also in general quite similar to the control molecules as well. Except for one molecule (Table1, monovalent bispecific entry MoBi12) size exclusion chromatography (SEC) profiles were above 90% target peak. Hence, the results clearly indicate the favorable biophysical properties of the herein described monovalent bispecific IgG-like VHH-based antibody format.

Table 1. Biophysical and biochemical properties of one-armed control molecules and monovalent bispecific series of engineered molecules. Format designs are indicated as well as expression yields post protein A purification, T_{onset} and size exclusion chromatography target monomer peaks. Affinities as determined by biolayer interferometry are also given.

Name	Format (Figure 1)	Paratope 1 (AG chain)	Paratope 2 (Light chain)	KD (M) Paratope 1	KD (M) Paratope 2	Tonset (°C)	SEC (%)	Expression yield (mg/L)
Ctrl1	F	EGFR (9G8)	-	1.36E-09	-	58.4	95	200
Ctrl2	F	NKG2D	-	1.09E-08	-	58.7	97	250
Ctrl3	F	HER2	-	7.32E-09	-	44.5	97	80
Ctrl4	F	EGFR (722C03)	-	2.20E-09	-	57.6	98	350
MoBi1	C (Kappa)	EGFR (9G8)	NKG2D	1.80E-09	5.98E-09	56.9	96	220
MoBi2	C (Lambda)	EGFR (9G8)	NKG2D	1.54E-09	6.18E-09	55.0	96	220
MoBi3	C (Kappa)	NKG2D	EGFR (9G8)	4.13E-09	1.59E-09	56.2	95	190
MoBi4	C (Lambda)	NKG2D	EGFR (9G8)	4.37E-09	1.47E-09	55.9	94	190
MoBi5	C (Kappa)	NKG2D	EGFR (722C03)	1.19E-08	2.83E-09	60.1	93	230
MoBi6	C (Lambda)	NKG2D	EGFR (722C03)	9.87E-09	2.60E-09	59.9	95	180
MoBi7	C (Kappa)	EGFR (9G8)	HER2	6.98E-10	9.75E-09	47.2	93	130
MoBi8	C (Lambda)	EGFR (9G8)	HER2	1.42E-09	8.11E-09	45.1	90	100
MoBi9	C (Kappa)	EGFR (722C03)	HER2	2.59E-09	1.37E-08	48.3	92	220
MoBi10	C (Lambda)	EGFR (722C03)	HER2	2.49E-09	1.28E-08	47.1	94	190
MoBi11	C (Kappa)	NKG2D	HER2	1.44E-08	1.03E-08	50.3	92	150
MoBi12	C (Lambda)	NKG2D	HER2	1.65E-08	6.56E-09	48.9	86	100
MoBi13	C (Kappa + 10aa linker)	EGFR (9G8)	HER2	1.26E-09	1.12E-08	45.4	94	210
MoBi14	C (Kappa + 10 aa linker)	EGFR (722C03)	HER2	2.51E-09	1.24E-08	47.3	92	170

Next, we aimed at characterizing the biochemical properties. To this end, affinities were determined *via* biolayer interferometry (Table 1). For all different VHH-derived paratopes and all the different orientations as well as kappa and lambda backbones, affinities of the bispecific molecules were similar to the parental molecules. However, as shown in Fig. S2, the total interference pattern shift in the association step of all analyzed monovalent bispecifics was slightly diminished compared to the parental clones. Still, association and dissociation rates were nearly identical, indicating no substantial loss of affinities (Tab. S1). To analyze this in more detail in a cellular context, we focused on molecule MoBi8 (Table 1), which consists of EGFR-specific VHH 9G8 engrafted on the AG chain as well as a HER2-specific VHH fused to the constant region of the lambda chain. As shown in Figure 2, both paratopes can independently engage in the cellular binding of target-positive cell lines in a concentration-dependent manner similar to the respective monospecific control molecules (Ctrl1 and Ctrl3), supporting the notion that the functionality of each VHH is not compromised significantly in this bispecific architecture. Importantly, no binding was observed against the antigen-negative control cell line.

In addition, all bispecific one-armed IgG-like VHH-SEEDs showed simultaneous binding to their antigens on the protein level (Fig. S3). Interestingly, as depicted in Figure 3(a), when grafted onto the kappa constant region, the HER2-specific VHH (Table 1, entry MoBi7) showed compromised HER2-binding compared to the lambda counterpart (Table 1, entry MoBi8), when EGFR-specific VHH clone 9G8 that was fused to the AG heavy chain already bound its antigen, clearly demonstrating paratope-dependent positioning effects in the kappa context. Surprisingly, this phenomenon was neither observed to a significant extent when EGFR-specific clone 722C03 was grafted onto the AG chain nor when the VHH directed against NKG2D was used for the AG chain (Figure 3(b,c)). NKG2D (extra-cellular domain (ECD)) with a molecular weight of 18.4 kDa is a much smaller protein compared to EGFR (ECD) with 71.4 kDa. Consequently, it is tempting to speculate that steric

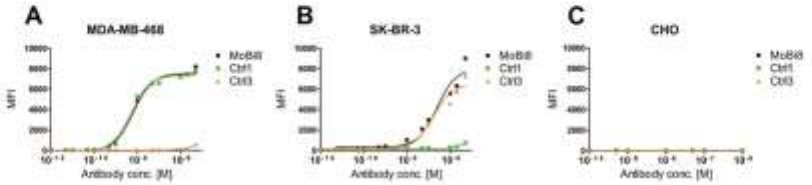

Figure 2. Cellular binding of monovalent bispecific antibody MoBi8 (black) and monospecific control molecules Ctrl1 (green) and Ctrl3 (orange) to EGFR-positive MDA-MB-468 (a) and HER2-positive SK-BR-3 cells (b) as well as to EGFR/HER2-negative CHO cells (c). 1 × 10^5 target cells were incubated with the respective antibody in varying concentrations.

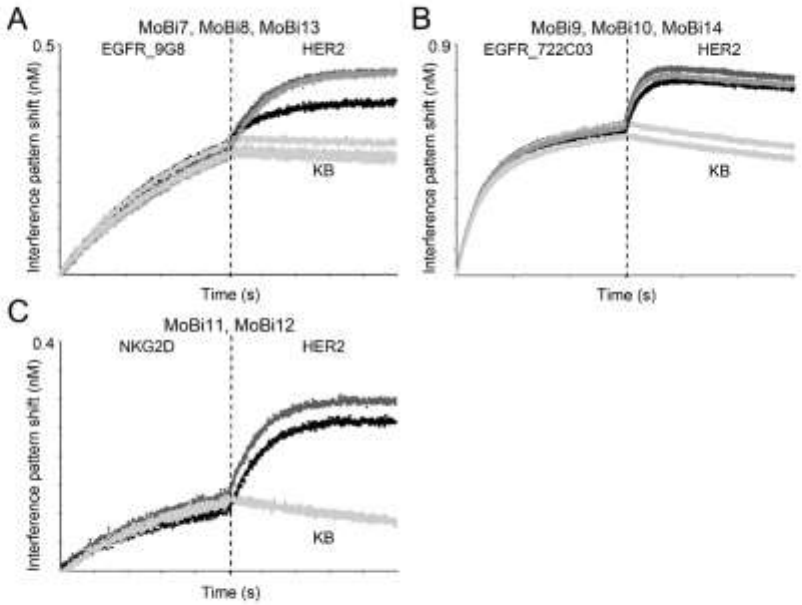

Figure 3. Biolayer interferometry analysis to assess simultaneous binding of one-armed monovalent bispecific molecules. The association of the respective antigen (50 nM) was measured, followed by a second association step using HER2 (50 nM). (a) Association of one armed monovalent bispecific entities MoBi7 (CLκ, black), MoBi8 (CLλ, dark gray) and MoBi13 (CLκ +10 aa linker, gray) against EGFR and HER2 (or kinetics buffer (KB) as control, light gray). (b) Simultaneous binding of one armed monovalent bispecific molecules MoBi9 (CLκ, black), MoBi10 (CLλ, dark gray) and MoBi14 (CLκ +10 aa linker, gray) against EGFR and HER2 (or KB, light gray). (c) Binding of one armed monovalent bispecific moieties MoBi11 (CLκ, black) and MoBi12 (CLλ, dark gray) against NKG2D and HER2 (or KB, light gray).

hindrance might be the cause for impeded simultaneous binding. In terms of the strikingly different binding behavior of the HER2 paratope in the EGFR context, it is worth noting that both EGFR-specific VHHs address different non-overlapping epitopes (Fig. S4). Therefore, we assume that 9G8 binds an epitope of EGFR in a way that EGFR negatively impacts the accessibility of HER2 to the kappa-engrafted entity. In order to address this more meticulously, we simply placed a 10 amino acid linker between the HER2-specific paratope and the kappa constant region (Fig. S1B, Table 1, entry MoBi13). This restored the binding capacity of the HER2-VHH, clearly corroborating that steric hindrance is the main reason for the positioning effects (Figure 3(a)). We also determined the affinities of all three monovalent bispecifics against HER2, when the inner (AG chain) EGFR-directed VHH 9G8 bound its antigen in saturation (Figure 4). When grafted onto the lambda chain, the overall affinities for HER2 were quite similar, irrespective of the EGFR-specific paratope engaged in antigen-binding or not. Still, even in the lambda context, the total interference pattern shift during association decreased somewhat, indicating also a moderate decline in binding capacity. However, when grafted onto the kappa light chain, not only the total interference pattern shift dropped substantially but also the overall affinities were compromised by a factor of approximately 10 for HER2-binding. This effect could be counteracted in both regards by placing a 10 amino acid linker between the HER2-paratope and the kappa constant region. Interestingly, when the VHH orientation in this format was inverted, i.e., when the HER2-specific paratope was grafted onto the AG chain and EGFR-specific VHH 9G8 was placed onto the light chain, this effect was also observed (Fig. S5), corroborating this paratope-specific positioning effect.

In certain disease settings, a therapeutic (bispecific) antibody must be able to bind to its antigen multiple times throughout its half-life. To investigate whether the architecture of this format permits periodic binding, consecutive association and dissociation cycles were performed for one exemplarily chosen molecule (MoBi8) on the Octet Red system (Figure 5). The bispecific entity showed periodic binding to EGFR as well as HER2 comparable to the mono-specific controls. Moreover, consecutive association and dissociation against both antigens in an alternating manner was also observed, clearly demonstrating the ability to bind multiple times in a bispecific mode of action.

Furthermore, we set out to investigate if this format also enables simultaneous binding on a cellular level. To this end, the EGFR-positive cell line MDA-MB-468 was labeled with CellTracker™ Deep Red Dye whereas HER2-positive SK-BR-3 cells were labeled with CellTrace™ CFSE. Of note, HER2-positive cell line SK-BR-3 is also slightly EGFR-positive. However, since only one EGFR-paratope was engrafted into this monovalent bispecific format, the entity can either bind one cell type or the other, not both. If a bispecific molecule is able to bind both antigens simultaneously, this will result in antibody-mediated clustering of both cells. Consequently, this can be analyzed by fluorescence-activated cell sorting since cell clustering appears as a double-positive event. As shown in Figure 6, EGFR- and HER2-targeting monovalent bispecific IgG-like VHH-based SEED MoBi8 bound simultaneously to both cell types because clustering was observed in a concentration-dependent manner, whereas no significant increase in double-positive events was detected for EGFR- or HER2-specific one-armed monospecific control molecules (Fig. S6). Importantly, monovalent bispecific IgG-like VHH-based SEED molecules either targeting HER2 and NKG2D or EGFR and NKG2D did not enable the clustering of both cell types, giving clear evidence that the architecture of this platform approach affords the benefit of simultaneous binding also in a cellular context.

Similar to Baty and coworkers,[18-20] we set out to demonstrate whether this format bears the potential to be used for effector cell redirection. To this end, a tumor cell killing assay was performed using all four different EGFR (9G8) and NKG2D-specific variants of the MoBi series using peripheral blood mononuclear cell (PBMC)-isolated NK cells as effector cell population (Fig. S7). All EGFR- and NKG2D-targeting monovalent bispecific entities elicited the killing of EGFR-overexpressing A431 cells in a dose-dependent manner,

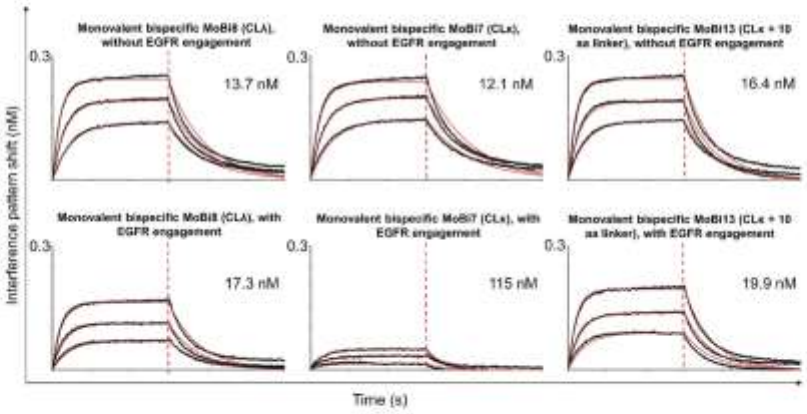

Figure 4. Kinetic measurements of monovalent bispecific VHH-derived IgG-like SEEDbodies MoBi7, MoBi8 and MoBi13 against HER2 in the presence or absence of EGFR binding of the heavy chain-engrafted VHH 9G8 in saturation. After loading and sensor rinsing, a first association step was performed using EGFR in saturating conditions or kinetics buffer (KB). Afterward, kinetics where analyzed against HER2 in the presence or absence of EGFR.

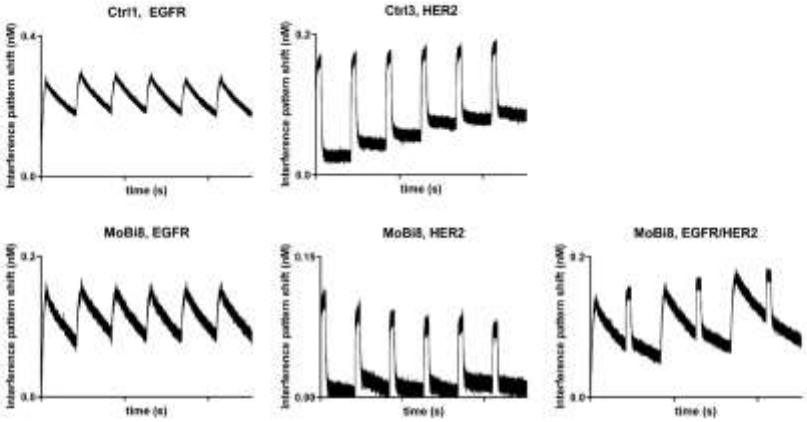

Figure 5. Periodic binding of mono-specific controls Ctrl1 (EGFR) and Ctrl3 (HER2) as well as bispecific MoBi8 (EGFR/HER2) antibody to their corresponding antigens at a concentration of 50 nM. Consecutive association (300 s) and dissociation (30 min) cycles were performed six times in total.

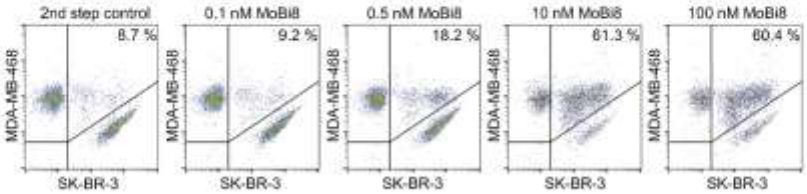

Figure 6. Simultaneous cellular binding analysis of monovalent bispecific antibody MoBi8. Binding to EGFR-positive cell line MDA-MB-468 and HER2-positive cell line SK-BR-3 was assessed by flow cytometric analysis. Of note, MDA MB 468 was labeled with CellTracker™ Deep Red Dye and HER2-positive SK-BR-3 cells were labeled with CellTrace™ CFSE to allow for double-positive fluorescence gating.

whereas no significant tumor cell lysis was observed for unrelated control molecules.

Expression and characterization of bivalent bispecific IgG-like VHH-based antibodies

Bivalent targeting of two different disease mediators might be beneficial for specific therapeutic applications such as cytokine trapping. From a conceptional perspective, the herein characterized monovalent bispecific format can be readily extended into a bivalent counterpart by exchanging the SEED technology for an IgG1 backbone (Figure 1(b)). To get a glimpse of the biochemical and biophysical properties of this format, we expressed nine different bivalent bispecific IgG-like VHH-based antibodies, essentially using all four different paratopes. Moreover, the kappa as well as the lambda constant regions were taken into consideration for light-chain engraftments. Interestingly, expression yields after protein A chromatography indicated in general good production profiles (Table 2). Some of the molecules, however, were prone to aggregation or showed low molecular weight species as determined by analytical SEC (Fig. S8). In direct comparison to the monovalent counterparts, it is noteworthy that tendencies for aggregation or mis-assembly of the molecule (as indicated by small molecular weight species) were significantly aggravated. In this respect, for one molecule (BiBi4), the target peak declined to only 72%, meaning that substantial efforts in downstream processing would be required in order to consider such a molecule for further development. On the other hand, two molecules exhibited quite decent SEC profiles (BiBi1 and BiBi6). Since some of the molecules with

Table 2. Biophysical and biochemical properties of bivalent bispecific series of engineered VHH-based IgG-like antibodies. Format designs are indicated as well as expression yields post protein A purification and size exclusion chromatography target monomer peaks. Affinities as determined by biolayer interferometry are also given.

Name	Format (Figure 1)	Paratope 1 (AG chain)	Paratope 2 (Light chain)	KD (M) Paratope 1	KD (M) Paratope 2	SEC (%)	Expression yield (mg/L)
BiBi1	B (Kappa)	EGFR (9G8)	HER2	9.27E-10	1.11E-08	95	190
BiBi2	B (Lambda)	EGFR (9G8)	HER2	1.56E-09	7.11E-09	85	130
BiBi3	B (Kappa)	NKG2D	HER2	5.92E-09	7.44E-09	88	250
BiBi4	B (Lambda)	NKG2D	HER2	7.87E-09	5.01E-09	72	160
BiBi5	B (Kappa)	NKG2D	EGFR (9G8)	4.73E-09	9.82E-10	79	160
BiBi6	B (Lambda)	NKG2D	EGFR (9G8)	4.33E-09	1.27E-09	91	200
BiBi7	B (Kappa)	NKG2D	EGFR (722C03)	7.75E-09	2.79E-09	77	180
BiBi8	B (Lambda)	NKG2D	EGFR (722C03)	4.37E-09	1.47E-09	81	150
BiBi9	B (Kappa + 10 aa linker)	EGFR (9G8)	HER2	1.79E-09	1.73E-08	73	150

exceptionally good as well as bad aggregation properties were grafted onto the kappa and lambda backbone, it is tempting to speculate that this observation is more related to the paratopes themselves and the individual orientation of the VHHs in the overall architecture. In terms of biochemical properties, all analyzed molecules retained their affinities as compared to the monospecific control molecules (Table 1, Ctrl1-4; Table 2). Moreover, all bivalent bispecifics were able to engage in simultaneous binding (Fig. S3). As expected, when EGFR-specific VHH 9G8 was placed onto the heavy chain and the HER2-specific VHH was engrafted onto the kappa constant chain (BiBi1), simultaneous binding was again compromised (Fig. S9). Similar to the monovalent counterpart, this decline in binding capacity could be partially compensated by employing a 10 amino acid linker (BiBi9).

Expression and characterization of trispecific IgG-like VHH-based SEEDbodies

By simply placing a third VHH-derived moiety on top of the hinge region of the GA chain of the IgG-like VHH-based SEEDbody, we also set out to characterize this platform approach with respect to trispecific targeting (Figure 1(d), Table 3, MoTri series of molecules). In this regard, we wanted to directly compare this monovalent trispecific format with another format enabling trispecificity, in which the light-chain-based VHH is bivalent (Figure 1(e), Table 3, BiTri entries). To this end, SEED molecules were produced, where on each chain of the SEEDbody (AG and GA) a different VHH was engrafted on domain CH1. Simultaneous expression of a VHH engrafted onto the constant region of the light chain results in the pairing of both heavy chain-derived paratopes with the light chain-embedded paratope.

The strictly monovalent trispecific SEEDbodies displayed rather beneficial biophysical properties. Expression yields were constantly in the triple-digit mg per liter scale, and SEC profiles (Fig. S8) were reasonably acceptable, even when compared to the bivalent bispecific format (Table 2, BiBi series of molecules). This was to our surprise, since the sophisticated architecture of this asymmetric trispecific format seems to be fairly complex, at least in direct comparison to the bivalent bispecific approach, where not even a heavy chain heterodimerization technique is needed. However, this is in stark contrast to the bivalent trispecific format (Table 3, BiTri series of entries). While expression yields were still reasonable, the SEC profiles, i.e., the target peaks, declined significantly, to only little more than 50% for some of the scrutinized molecules, clearly demonstrating strongly compromised biophysical properties. Noteworthy, these detrimental attributes are not only related to aggregation propensities but also due to significant amounts of low molecular weight species, clearly indicating mis-assembled molecules (Fig. S8).

Similar to the design of the bivalent bispecific format (BiBi series), the expression of entities of the bivalent trispecific series (BiTri) result in a symmetric overall architecture of the respective molecules. On the contrary, molecules of the MoBi and MoTri series that in general display more adequate biophysical properties, i.e., target monomer peaks in SEC, are asymmetric by design. Consequently, this suggests that an asymmetric molecule design of the herein presented 'plug-and-play' approach generally results in fairly favorable biophysical attributes.

With respect to biochemical properties, as anticipated, no significant decline of affinities was detected for each embedded VHH against the respective antigen. Likewise, all molecules analyzed engaged in trispecific simultaneous binding against each antigen, as exemplarily shown for molecules MoTri 2 and BiTri4 (Figure 7, Fig. S3).

Discussion

Bi- and multispecific antibodies have recently emerged as promising molecules for disease treatment.[5,6] In this respect, bi- and multispecific entities opened up new avenues to address the complex biology of several diseases more appropriately compared to monospecific antibodies.[26-30] Accordingly, an unparalleled repertoire of different antibody formats was developed, each with its own characteristics, beneficial attributes, and limitations, as elegantly reviewed elsewhere.[5,6] In this context, VHH-derived constructs afford the benefit of multiple reformatting options.[16,17] Moreover, antigen-specific single-domain antibodies from camelids can be readily obtained by combining animal immunization with antibody display systems enabling genotype-phenotype coupling.[10,11] However, for therapeutic use in patients, it must be noted that the foreign nature of camelid-derived VHHs bears the

Table 3. Biophysical and biochemical properties of trispecific VHH-derived SEEDbodies. Format designs are indicated as well as expression yields post protein A purification and size exclusion chromatography target monomer peaks. Affinities as determined by biolayer interferometry are also given.

Name	Format (Figure 1)	Paratope 1 (AG chain)	Paratope 2 (Light chain)	Paratope 3 (GA chain)	KD (M) Paratope 1	KD (M) Paratope 2	KD (M) Paratope 3	SEC (%)	Expression yield (mg/L)
MoTri1	D (Kappa)	EGFR (9G8)	HER2	NKG2D	2.59E-09	9.53E-09	1.31E-08	84	220
MoTri2	D (Lambda)	EGFR (9G8)	HER2	NKG2D	2.72E-09	4.85E-09	1.16E-08	83	220
MoTri3	D (Kappa)	NKG2D	HER2	EGFR (9G8)	7.91E-09	2.22E-09	1.43E-09	88	260
MoTri4	D (Lambda)	NKG2D	HER2	EGFR (9G8)	8.11E-09	4.09E-09	1.96E-09	80	170
MoTri5	D (Kappa)	HER2	EGFR (722C03)	NKG2D	1.35E-08	1.44E-09	1.14E-08	92	150
MoTri6	D (Lambda)	HER2	EGFR (722C03)	NKG2D	1.23E-08	1.65E-09	8.05E-09	89	160
MoTri7	D (Kappa + 10 aa linker)	EGFR (9G8)	HER2	NKG2D	2.82E-09	1.64E-09	1.06E-08	85	240
BiTri1	E (Kappa)	EGFR (9G8)	HER2	NKG2D	1.07E-09	1.09E-08	9.94E-09	65	140
BiTri2	E (Lambda)	EGFR (9G8)	HER2	NKG2D	1.74E-09	9.90E-09	9.00E-09	51	80
BiTri3	E (Kappa)	EGFR (722C03)	HER2	NKG2D	1.37E-09	1.20E-08	1.37E-08	85	200
BiTri4	E (Lambda)	EGFR (722C03)	HER2	NKG2D	1.63E-09	9.92E-09	7.95E-09	84	180
BiTri5	E (Kappa + 10 aa linker))	EGFR (9G8)	HER2	NKG2D	1.48E-09	5.42E-09	9.23E-09	55	100

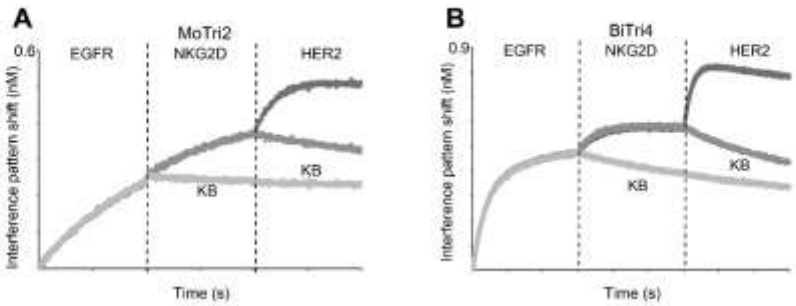

Figure 7. Simultaneous trispecific antigen binding of (a) monovalent trispecific VHH-derived IgG-like antibody MoTri2 and (b) bivalent trispecific entity BiTri4 against 50 nM EGFR followed by 50 nM NKG2D and 50 nM HER2. For each association step a control in KB is shown.

risk of immunogenicity. In this respect, Vincke et *al.* described a general strategy for humanization.[31] Currently, multiple VHH-derived entities are being investigated in clinical trials, and bivalent single-domain caplacizumab (Cablivi®) has been approved for the treatment of patients with acquired thrombotic thrombocytopenic purpura by the FDA.[14,15] To the best of our knowledge, most if not all of these molecules were humanized. This gives clear evidence that the risk of substantial immunogenicity can be circumvented by humanization.

Within this work, we aimed at characterizing a VHH-based platform for facile construction of different IgG-like bi- and multispecific antibody constructs that differ significantly among themselves with respect to their biophysical characteristics as well as biochemical properties. Essentially, the main building block in this platform approach was described some time ago by Baty and coworkers.[18] We set out to investigate to what extent this approach can be broadened for the generation of bi- and trispecific moieties comprising flexible valencies without fundamentally compromising essential intrinsic attributes, for instance aggregation behavior or binding capacities.

In regard to biophysical properties, it is remarkable that expression yields, as determined after protein A purification of most of the bi- and trispecific molecules, were fairly high compared to other technologies reported.[32-34] Most importantly, yields were quite similar to the parental molecules, i.e., controls. This was also true for aggregation onset temperatures, indicating in general adequate stabilities of VHHs when engrafted into the Fab-based architecture. With respect to aggregate formation and potential mis-assembly of molecules, substantial differences were determined for the different herein described formats. In general, asymmetric formats, i.e., monovalent IgG-like VHH-based bispecific antibodies as well as strictly monovalent trispecific SEEDbodies, displayed rather favorable aggregation propensities while symmetric formats tended to be more prone to malfunction. In this context, SEC profiles for bivalent bispecific VHH-based IgG-like antibodies indicated still acceptable target monomer formation. For the bivalent (for the light chain) trispecific format (BiTri series of molecules), however, aggregate formation and mis-assembled molecules (low molecular weight species) were fundamentally worsened clearly disqualifying this format for further consideration.

It is important to note that for all the different VHHs that were embedded into the Fab scaffold, overall affinities were quite similar to the control molecules. The interference pattern shift, however, was slightly decreased in every instance, indeed indicating impeded binding capacities to a minor extent for engrafted paratopes. Yet, this effect appears to be almost neglectable, since cellular binding did not seem to be impaired substantially. From a functional aspect, we were able to demonstrate that both Fab-engrafted single-domain paratopes can engage in simultaneous binding in a cellular context. This is especially vital for several therapeutic concepts that involve targeting of different cell types at the same time, such as effector cell redirection.[35-37] Similar to Baty and coworkers,[18] we were able to show that the overall architecture of this platform clearly allows for effector cell recruitment enabling tumor cell killing.

Furthermore, we report that for one VHH analyzed (HER2) in this platform approach, engraftment onto the kappa chain causes a substantial loss of affinity when the other embedded VHH (EGFR, clone 9G8) already engages in antigen binding. Positioning effects have also been described for other bispecific platform technologies, for instance, DVD-Igs or TriFabs and others,[34,38-40] typically resulting in compromised binding affinities. Surprisingly, the individual binding affinity of the engrafted paratope against the respective antigen was not impaired substantially. Accordingly, this positioning effect does not diminish the binding capacity of the individual paratope per se, but only in the context of simultaneous binding. We were also able to show that a 10 amino acid linker between the impacted VHH and the kappa chain reversed this effect. In addition, this affinity sink in simultaneous binding was not observed in the lambda context. Stanfield and colleagues were able to demonstrate that Fabs comprising lambda chains tend to have hypervariable elbow angles, i.e., angles between the variable regions and the constant domains.[41] On average, these elbow bends are significantly wider than those of kappa chain Fabs. Presumably, this is due to a glycine insertion at the switch region between the variable domain of the light chain and the constant region that appears to increase the flexibility of the Fab. This increased flexibility might be the main reason why this positioning effect was not detected for VHH engrafted onto the lambda light chain. Thus, this gives clear evidence that positioning effects can be circumvented either by simple linker design or by replacing the kappa chain for a lambda chain.

Ultimately, the herein presented VHH-based IgG-like bi- and trispecific antibody platform appears to have the versatility to combine up to three preexisting VHHs in one multispecific molecule. We demonstrated that the different described formats, except for molecules of the BiTri series seem to comprise acceptable properties and that early-stage 'developability' is feasible. Essentially, this 'plug-and-play' platform affords the benefit to tailor multispecific entities with respect to their biophysical and biochemical properties.

Materials and methods

Antibody expression and purification

All constructs were designed in-house and synthesized by GeneArt (Thermo Fisher Scientific). In general, all antibody-like constructs and SEED molecules were cloned into pTT5 plasmid backbone (GeneArt/Thermo Fisher Scientific). For SEEDbody expression, the RF mutation was introduced to prevent the formation of undesired GA:GA chain homodimers.[25] Expi293 cells were transiently transfected with expression vectors according to the manufacturer's recommendations (Thermo Fisher Scientific). Five days post transfection, the antibody-containing supernatants were harvested by centrifugation and purified via MabSelect antibody purification chromatography resin (GE Healthcare). A final dialysis step using Pur-A-LyzerTM Maxi 3500 Dialysis Kit (Sigma Aldrich/Merck KGaA) was performed at 4°C for 24 h to ensure sample formulation in phosphate-buffered saline (PBS) pH 6.8, followed by an additional protein concentration step via Amicon Ultra-4 Centrifugal Filters (EMD Millipore), if necessary. UV-Vis spectrophotometric measurement (Nanodrop ND-1000, Peqlab) was used to determine protein concentrations. Additionally, the expressed antibodies were analyzed in duplicates by differential scanning fluorometry on Prometheus NT.48 (Nanotemper Technologies) to evaluate the stability of expressed molecules. When measuring the thermal stability of proteins, multiple values like T_{onset}, T_{m1} and T_{agg} can be reported. The lowest temperature at which the protein starts to unfold is defined as the T_{onset} while T_{m1} is the melting point at which 50% of the thermally least stable domain is unfolded. Multiple unfolding events of protein domains can overlap, and therefore T_{m1} can vary more between similar constructs than T_{onset}. Thus, we chose T_{onset} as a discriminator to compare the thermal stability of multiple protein variants. Furthermore, aggregate formation was analyzed by analytical SEC of 10 µg protein per sample, using a TSKgel SuperSW3000 column (4.6 × 300 mm, Tosoh Bioscience LLC) in an Agilent HPLC system with a flow rate of 0.35 ml/min.

Biolayer Interferometry

Simultaneous binding, periodic binding, epitope binning, as well as kinetic measurements were performed on the Octet RED96 system (ForteBio, Pall Life Science) at 25°C and 1000 rpm agitation. For kinetic analysis, the antibody-like molecules to be analyzed were loaded on anti-human-FC (AHC) Biosensors at 5 µg/mL in PBS for 3 min. Afterward, tips were transferred to kinetics buffer (KB; PBS, 0.1% Tween-20 and 1% bovine serum albumin, BSA) for 60 s for sensor rinsing. Association to the corresponding antigen human EGFR (in-house), human NKG2D (Sino Biological, Cat: 10575-H07B) and human HER2 (Sino Biological, Cat: 10004-H08H) in varying concentrations ranging from 12.5 nM to 50 nM in KB was measured for 300 s followed by dissociation in KB for 300 s. In each experiment, one negative control was included where the association was monitored against an unrelated antigen (50 nM in KB). Moreover, one reference value was included with the association in KB instead of the antigen. Resulting data were fitted and analyzed with ForteBio data analysis software 8.0 using a 1:1 binding model after Savitzky-Golay filtering.

To demonstrate simultaneous antigen binding, respective antibody-like molecules were captured to the surface of anti-human IgG Fc (AHC) biosensors for 3 min at a concentration of 5 µg/ml and sensor rinsing was conducted in KB for 60 s. Afterward, sensors were transferred to first antigen solution (50 nM in KB) and incubated for 100 s to 300 s, followed by an association in second antigen solution for 100 s to 300 s (50 nM in KB) and consecutively, when applicable, in antigen three for 100 s to 300 s (50 nM in KB).

Furthermore, for the kinetic measurements with EGFR bound in saturation or without prior EGFR binding the antibody was loaded on anti-Penta His biosensors for 180 s, followed by 60 s of sensor rinsing in KB. Afterward, 500 nM EGFR was used to saturate the binding capacity of the antibody for 300 s. Accordingly, KB was used instead of EGFR for the measurements without EGFR binding in saturation. Afterward, the association was determined against HER2 (300 s) using varying concentrations from 0 to 50 nM. To avoid a dissociation of EGFR in this step, 50 nM EGFR was used for every HER2 concentration tested. For the following dissociation step (300 s), EGFR was also used at 50 nM to assess dissociation against HER2 only.

For the assessment of periodic antigen-binding antibodies were loaded on Anti-human-Fc (AHC) biosensors at 1 µg/mL for 3 min. After 60 s of sensor rinsing in KB association was analyzed at a concentration of 50 nM for 300 s followed by a dissociation step in KB for 30 min. The association and dissociation steps were consecutively repeated for six times in total.

Epitope binning analysis was performed by loading EGFR (ECD) via its histidine-tag on anti-Penta His (HIS1K) biosensors at 3 µg/mL in PBS for 3 min. After a step of sensor rinsing in KB for 60 s association to the respective EGFR-specific molecule (at 100 nM) was performed (Table 1, Ctrl1 or Ctrl4), followed by either dissociation in KB or by another association step with the second EGFR-derived VHH (at 100 nM). One negative control was measured in parallel, where the sensor was not loaded with antigen to check for unspecific association of the antibodies to the biosensor. Moreover, one reference value using buffer instead of antibody association was measured as 'association baseline.'

Flow cytometry

Flow cytometric analyses were conducted on the Guava® easyCyte 12HT device (Merck Millipore) using guavaSoft 3.2 Software. For each experiment, 5000 events/well were measured.

To determine cellular binding properties of the expressed antibodies, EGFR-positive MDA-MB-468, HER2-positive SK-BR-3, and EGFR/HER2 negative CHO cells were used. For staining assays, 1×10^5 cells per well were seeded. After two consecutive washing steps with PBS+1% BSA, cells were incubated for 1 h on ice with antibodies in varying concentrations. Afterward, two additional washing steps with PBS+1% BSA were performed, followed by staining with a detection antibody at 4°C for another 1 h. Cell binding was identified with Alexa Fluor® 488 AffiniPure $F(ab')_2$ Fragment Goat Anti-Human IgG, Fcγ fragment specific antibody (Jackson ImmunoResearch, Cat: 109–546-008) for EGFR- and HER2-positive cells lines, respectively, as well as Alexa Fluor® 488 AffiniPure Fab Fragment Goat Anti-Human IgG (H + L) antibody (Jackson ImmunoResearch, Cat: 109–547-003) for the negative CHO cells. After two washing steps with PBS+1% BSA, dead cells were stained via 20 µg/ml propidium iodide (Invitrogen) addition in a total volume of 200 µl/well. Additionally, a negative control without antibody treatment as well as a control using the detection antibody only and a control using in-house produced cetuximab (Erbitux®) or trastuzumab (Herceptin®) as positive reaction, was conducted in each experiment for each cell line (not shown).

For the investigation of simultaneous cellular binding, EGFR-positive MDA-MB-468 cells were stained prior to the assay with CellTracker™ Deep Red Dye (ThermoFisher). To this end, the cells were harvested and washed once in PBS before staining 1×10^6 cells/ml with the reagent (1:1000 in PBS) for 15 min at 37°C in the dark. Following incubation, the cells were washed once with respective complete medium and finally washed once with PBS+1% BSA. This staining procedure was performed accordingly for HER2-positive SK-BR-3 cells, except using CellTrace™ CFSE Cell Proliferation Kit as dye (1:100'000 in PBS). For both cell lines, 1×10^5 cells each were combined and inserted per well. As controls, wells containing just one cell line were used, allowing for gating the single-cell populations. After a washing step with PBS+1% BSA, cells were incubated for 1 h on ice with the antibodies in varying concentrations ranging from 0.1 nM to 1 µM. Finally, two more washing steps with PBS+1% BSA were conducted and the cells were resuspended in 200 µl volume for flow cytometric measurements. By applying a rectangular gate, the single-cell populations were discriminated from the simultaneously bound cells forming duplets and showing a positive signal for both fluorescence dyes.

Tumor cell killing assay

PBMCs cells were isolated from whole blood samples of healthy human donors by density gradient centrifugation with consecutive NK cell isolation using EasySep™ Human NK Cell Isolation Kit (Stemcell Technologies). Effector cells were adjusted to 0.625×10^6 vc/ml after overnight incubation in complete medium containing 100 U/ml recombinant human interleukin-2 (R&D systems). A431 target cells were prepared in parallel by staining with CellTracker™ Deep Red Dye (ThermoFisher) according to the manufacturer's instructions. For the assay, 20 µl target cells (resulting in 2'500 c/well) were seeded in 384-well clear bottom microtiter plate (Greiner Bio-One) and incubated for 3 h. Afterward, 5 µl of the bispecific antibodies were added with varying concentrations ranging from 10^{-7} M to 10^{-12} M followed by the addition of 20 µl NK cell suspension, resulting in an effector cell to target cell (E:T) ratio of 5:1. Finally, SYTOX™ Green Dead Cell Stain (Invitrogen) was added to the assay.

NK cells cultivated with A431 cells in the absence of antibodies as well as A431 cultivated with antibodies without adding NK cells as well as A431 cells with the highest antibody concentration without NK cells were used as controls. To assess maximum tumor cell lysis, staurosporine was dispensed to A431 cells as another control with a final concentration of 30 µM. For the incubation (24 h) and on-line imaging of the assay an Incucyte® Live Cell Analysis System (Sartorius) was used. Overlay (green and red fluorescence) signals per well allowed for analysis of dead target cells only.

Acknowledgments

The authors kindly thank Laura Unmuth, Dirk Müller-Pompalla, Alexander Müller, Stephan Keller, Sigrid Auth, Marion Wetter, Pia Stroh, Stefan Becker, Janina Klemm and Kerstin Hallstein for experimental support.

Disclosure of potential conflicts of interest

BV, MB, LT, SK and SZ are employees of Merck Healthcare KGaA. Besides, the authors declare no conflict of interest.

Abbreviations

CH1	constant domain 1 of the heavy chain;
Cκ	constant kappa region of the light chain
Cλ	constant lambda region of the light chain
EGFR	epidermal growth factor receptor
Fab	antigen-binding fragment
HER2	human epidermal growth factor receptor 2
NK cell	natural killer cell
NKG2D	natural killer group 2 member D
PBMC	peripheral blood mononuclear cell
PBS	phosphate-buffered saline
SEC	size exclusion chromatography
SEED	strand-exchanged engineered domain
VH	variable domain of the heavy chain
VHH	variable domain of the heavy chain of a heavy chain only antibody
VL	variable domain of the light chain
vNAR	variable domain of New Antigen Receptor

References

1. Kaplon H, Reichert JM. Antibodies to watch in 2019. mAbs. 2019 Feb;11(2):219–38. doi:10.1080/19420862.2018.1556465.
2. Kaplon H, Muralidharan M, Schneider Z, Reichert JM. Antibodies to watch in 2020. mAbs. 2020 Jan;12(1):1703531. doi:10.1080/19420862.2019.1703531.
3. Krah S, Kolmar H, Becker S, Zielonka S. Engineering IgG-like bispecific antibodies—an overview. Antibodies. 2018 Aug;7(3):28. doi:10.3390/antib7030028.

4. Wu C, Ying H, Grinnell C, Bryant S, Miller R, Clabbers A, Bose S, McCarthy D, Zhu -R-R, Santora L, et al. Simultaneous targeting of multiple disease mediators by a dual-variable-domain immunoglobulin. Nat Biotechnol. 2007 Nov;25(11):1290–97. doi:10.1038/nbt1345.
5. Labrijn AF, Janmaat ML, Reichert JM, Parren PWHI. Bispecific antibodies: a mechanistic review of the pipeline. Nat Rev Drug Discov. 2019 Aug;18(8):585–608.
6. Brinkmann U, Kontermann RE. The making of bispecific antibodies. mAbs. 2017 Feb;9(2):182–212. doi:10.1080/19420862.2016.1268307.
7. Könning D, Zielonka S, Grzeschik J, Empting M, Valldorf B, Krah S, Schröter C, Sellmann C, Hock B, Kolmar H, et al. Camelid and shark single domain antibodies: structural features and therapeutic potential. Curr Opin Struct Biol. 2017 Aug;45:10–16. doi:10.1016/j.sbi.2016.10.019.
8. Zielonka S, Empting M, Grzeschik J, Könning D, Barelle CJ, Kolmar H. Structural insights and biomedical potential of IgNAR scaffolds from sharks. mAbs. 2015 Jan;7(1):15–25. doi:10.4161/19420862.2015.989032.
9. Li Z, Krippendorff B-F, Sharma S, Walz AC, Lavé T, Shah DK. Influence of molecular size on tissue distribution of antibody fragments. MAbs. 2016;8(1):113–19. doi:10.1080/19420862.2015.1111497.
10. Sellmann C, Pekar L, Bauer C, Ciesielski E, Krah S, Becker S, Toleikis L, Kügler J, Frenzel A, Valldorf B, et al. A one-step process for the construction of phage display scFv and VHH libraries. Mol Biotechnol. 2020 Jan;62(4):228–39. doi:10.1007/s12033-020-00236-0.
11. Uchański T, Zögg T, Yin J, Yuan D, Wohlkönig A, Fischer B, Rosenbaum DM, Kobilka BK, Pardon E, Steyaert J, et al. An improved yeast surface display platform for the screening of nanobody immune libraries. Sci Rep. 2019 Dec;9(1). doi:10.1038/s41598-018-37212-3.
12. Pardon E, Laeremans T, Triest S, Rasmussen SGF, Wohlkönig A, Ruf A, Muyldermans S, Hol WGJ, Kobilka BK, Steyaert J, et al. A general protocol for the generation of Nanobodies for structural biology. Nat Protoc. 2014 Mar;9(3):674–93. doi:10.1038/nprot.2014.039.
13. Krah S, Schröter C, Zielonka S, Empting M, Valldorf B, Kolmar H. Single-domain antibodies for biomedical applications. Immunopharmacol Immunotoxicol. 2016;38(1):21–28. doi:10.3109/08923973.2015.1102934.
14. Jovčevska I, Muyldermans S. The therapeutic potential of nanobodies. BioDrugs. 2020 Feb;34(1):11–26. doi: 10.1007/s40259-019-00392-z
15. Duggan S. Caplacizumab: first Global Approval. Drugs. 2018 Oct;78(15):1639–42. doi:10.1007/s40265-018-0989-0.
16. Bannas P, Hambach J, Koch-Nolte F. Nanobodies and nanobody-based human heavy chain antibodies as antitumor therapeutics. Front Immunol. 2017 Nov;8. doi:10.3389/fimmu.2017.01603.
17. Chanier T, Chames P. Nanobody engineering: toward next generation immunotherapies and immunoimaging of cancer. Antibodies. 2019 Jan;8(1):13. doi:10.3390/antib8010013.
18. Rozan C, Cornillon A, Petiard C, Chartier M, Behar G, Boix C, Kerfelec B, Robert B, Pelegrin A, Chames P, et al. Single-domain antibody-based and linker-free bispecific antibodies targeting Fc RIII induce potent antitumor activity without recruiting regulatory T cells. Mol Cancer Ther. 2013 Aug;12(8):1481–91. doi:10.1158/1535-7163.MCT-12-1012.
19. Turini M, Chames P, Bruhns P, Baty D, Kerfelec B. A FcγRIII-engaging bispecific antibody expands the range of HER2-expressing breast tumors eligible to antibody therapy. Oncotarget. 2014 Jul;5(14):5304–19. doi:10.18632/oncotarget.2093.
20. Del Bano J, Florès-Florès R, Josselin E, Goubard A, Ganier L, Castellano R, Chames P, Baty D, Kerfelec B. A bispecific antibody-based approach for targeting mesothelin in triple negative breast cancer. Front Immunol. 2019 Jul;10. doi:10.3389/fimmu.2019.01593.
21. Scapin G, Yang X, Prosise WW, McCoy M, Reichert P, Johnston JM, Kashi RS, Strickland C. Structure of full-length human anti-PD1 therapeutic IgG4 antibody pembrolizumab. Nat Struct Mol Biol. 2015 Dec;22(12):953–58. doi:10.1038/nsmb.3129.
22. Davis JH, Aperlo C, Li Y, Kurosawa E, Lan Y, Lo K-M, Huston JS. SEEDbodies: fusion proteins based on strand-exchange engineered domain (SEED) CH3 heterodimers in an Fc analogue platform for asymmetric binders or immunofusions and bispecific antibodies†. Protein Eng Des Sel. 2010 Apr;23(4):195–202. doi:10.1093/protein/gzp094.
23. Schmitz KR, Bagchi A, Roovers RC, van Bergen En Henegouwen PMP, Ferguson KM. Structural evaluation of EGFR inhibition mechanisms for nanobodies/VHH domains. Structure. 2013 Jul;21(7):1214–24. doi:10.1016/j.str.2013.05.008.
24. Roth L, Krah S, Klemm J, Günther R, Toleikis L, Busch M, Becker S, Zielonka S. Isolation of antigen-specific VHH single-domain antibodies by combining animal immunization with yeast surface display. Methods Mol Biol. 2020;2070:173–89.
25. Tustian AD, Endicott C, Adams B, Mattila J, Bak H. Development of purification processes for fully human bispecific antibodies based upon modification of protein A binding avidity. mAbs. 2016 May;8(4):828–38. doi:10.1080/19420862.2016.1160192.
26. Dheilly E, Moine V, Broyer L, Salgado-Pires S, Johnson Z, Papaioannou A, Cons L, Calloud S, Majocchi S, Nelson R. Selective Blockade of the Ubiquitous Checkpoint Receptor CD47 Is Enabled by Dual-Targeting Bispecific Antibodies. Mole Ther. 2017 Feb;25(2):523–33. doi:10.1016/j.ymthe.2016.11.006.
27. Rothe A, Sasse S, Topp MS, Eichenauer DA, Hummel H, Reiners KS, Dietlein M, Kuhnert G, Kessler J, Buerkle C, et al. A phase 1 study of the bispecific anti-CD30/CD16A antibody construct AFM13 in patients with relapsed or refractory Hodgkin lymphoma. Blood. 2015 Jun;125(26):4024–31. doi:10.1182/blood-2014-12-614636.
28. Sun LL, Ellerman D, Mathieu M, Hristopoulos M, Chen X, Li Y, Yan X, Clark R, Reyes A, Stefanich E, et al. Anti-CD20/CD3 T cell–dependent bispecific antibody for the treatment of B cell malignancies. Sci Transl Med. 2015 May;7(287):287ra70–287ra70. doi:10.1126/scitranslmed.aaa4802.
29. Yu YJ, Atwal JK, Zhang Y, Tong RK, Wildsmith KR, Tan C, Bien-Ly N, Hersom M, Maloney JA, Meilandt WJ, et al. Therapeutic bispecific antibodies cross the blood-brain barrier in nonhuman primates. Sci Transl Med. 2014 Nov;6(261):261ra154–261ra154. doi:10.1126/scitranslmed.3009835.
30. Khan SN, Sok D, Tran K, Movsesyan A, Dubrovskaya V, Burton DR, Wyatt RT. Targeting the HIV-1 spike and coreceptor with Bi- and trispecific antibodies for single-component broad inhibition of entry. J Virol. 2018 Jul;92(18). doi:10.1128/JVI.00384-18
31. Vincke C, Loris R, Saerens D, Martinez-Rodriguez S, Muyldermans S, Conrath K. General strategy to humanize a camelid single-domain antibody and identification of a universal humanized nanobody scaffold. J Biol Chem. 2009 Jan;284(5):3273–84. doi:10.1074/jbc.M806889200.
32. Scheuer W, Thomas M, Hanke P, Sam J, Osl F, Weininger D, Baehner M, Seeber S, Kettenberger H, Schanzer J. Anti-tumoral, anti-angiogenic and anti-metastatic efficacy of a tetravalent bispecific antibody (TAvi6) targeting VEGF-A and angiopoietin-2. mAbs. 2016 Apr;8(3):562–73. doi:10.1080/19420862.2016.1147640.
33. Croasdale R, Wartha K, Schanzer JM, Kuenkele K-P, Ries C, Mayer K, Gassner C, Wagner M, Dimoudis N, Herter S, et al. Development of tetravalent IgG1 dual targeting IGF-1R–EGFR antibodies with potent tumor inhibition. Arch Biochem Biophys. 2012 Oct;526(2):206–18. doi:10.1016/j.abb.2012.03.016.
34. Wu C, Ying H, Bose S, Miller R, Medina L, Santora L, Ghayur T. Molecular construction and optimization of anti-human IL-1α/β dual variable domain immunoglobulin (DVD-Ig ^{TM}) molecules. mAbs. 2009 Aug;1(4):339–47. doi:10.4161/mabs.1.4.8755.
35. Gauthier L, Morel A, Anceriz N, Rossi B, Blanchard-Alvarez A, Grondin G, Trichard S, Cesari C, Sapet M, Bosco F. Multifunctional natural killer cell engagers targeting NKp46 trigger

protective tumor immunity. Cell. 2019 Jun;177(7):1701–1713.e16. doi:10.1016/j.cell.2019.04.041.
36. Peipp M, Derer S, Lohse S, Staudinger M, Klausz K, Valerius T, Gramatzki M, Kellner C. HER2-specific immunoligands engaging NKp30 or NKp80 trigger NK-cell-mediated lysis of tumor cells and enhance antibody-dependent cell-mediated cytotoxicity. Oncotarget. 2015 Oct;6(31):32075–88. doi:10.18632/oncotarget.5135.
37. Satta A, Mezzanzanica D, Turatti F, Canevari S, Figini M. Redirection of T-cell effector functions for cancer therapy: bispecific antibodies and chimeric antigen receptors. Future Oncol. 2013 Apr;9(4):527–39. doi:10.2217/fon.12.203.
38. DiGiammarino EL, Harlan JE, Walter KA, Ladror US, Edalji RP, Hutchins CW, Lake MR, Greischar AJ, Liu J, Ghayur T. Ligand association rates to the inner-variable-domain of a dual-variable-domain immunoglobulin are significantly impacted by linker design. mAbs. 2011 Sep;3(5):487–94. doi:10.4161/mabs.3.5.16326.
39. Mayer K, Baumann A-L, Grote M, Seeber S, Kettenberger H, Breuer S, Killian T, Schäfer W, Brinkmann U. TriFabs—trivalent IgG-shaped bispecific antibody derivatives: design, generation, characterization and application for targeted payload delivery. Int J Mol Sci. 2015 Nov;16(11):27497–507. doi:10.3390/ijms161126037.
40. Metz S, Panke C, Haas AK, Schanzer J, Lau W, Croasdale R, Hoffmann E, Schneider B, Auer J, Gassner C. Bispecific antibody derivatives with restricted binding functionalities that are activated by proteolytic processing. Protein Eng Des Sel. 2012 Oct;25(10):571–80. doi:10.1093/protein/gzs064.
41. Stanfield RL, Zemla A, Wilson IA, Rupp B. Antibody elbow angles are influenced by their light chain class. J Mol Biol. 2006 Apr;357(5):1566–74. doi:10.1016/j.jmb.2006.01.023.

6.4 Affinity maturation of B7-H6 translates into enhanced NK cell-mediated tumor cell lysis and improved proinflammatory cytokine release of bispecific immunoligands via NKp30 engagement

Authors

Lukas Pekar1, Katja Klausz1, Michael Busch, Bernhard Valldorf, Harald Kolmar, Daniela Wesch, Hans-Heinrich Oberg, Steffen Krohn, Ammelie Boje, Carina-Lynn Gehlert, Lars Toleikis, Simon Krah, Tushar Gupta, Brian Rabinovich, Stefan Zielonka and Matthias Peipp

1 These authors contributed equally to this work

Bibliographic information

Submitted for publication in August 2020. Shown manuscript herein represents a submitted author manuscript.

Contributions by Lukas Pekar

- Coordinated the project together with K. Klausz, S. Zielonka and M. Peipp
- Designed experiments together with K. Klausz, S. Zielonka and M. Peipp
- Generated yeast surface display library
- Conducted library sorting
- Conducted all protein expressions and purifications as well as molecules characterization regarding biophysical properties
- Conducted all BLI experiments
- Wrote the manuscript together with K. Klausz, B. Rabinovich, S. Zielonka and K. Klausz
- Conducted all NK cell activation and cytokine release assays
- Prepared tables and figures together with K. Klausz, S. Zielonka and M. Peipp
- Prepared supplementary section together with K. Klausz

Affinity maturation of B7-H6 translates into enhanced NK cell-mediated tumor cell lysis and improved proinflammatory cytokine release of bispecific immunoligands via NKp30 engagement

Lukas Pekar[*¶1], Katja Klausz[†1], Michael Busch[¶], Bernhard Valldorf[#], Harald Kolmar[‡], Daniela Wesch[§], Hans-Heinrich Oberg[§], Steffen Krohn[†], Ammelie Svea Boje[†], Carina Lynn Gehlert[†], Lars Toleikis[*], Simon Krah[*], Tushar Gupta[||], Brian Rabinovich[||], Stefan Zielonka[*2] and Matthias Peipp[†2]

[*]Protein Engineering and Antibody Technologies, Merck KGaA, Frankfurter Straße 250, D-64293 Darmstadt, Germany

[†]Division of Stem Cell Transplantation and Immunotherapy, Department of Medicine II, University Hospital Schleswig-Holstein and Christian-Albrechts-University Kiel, Rosalind-Franklin-Straße 12, D-24105 Kiel, Germany

[¶]Discovery Pharmacology, Merck KGaA, Frankfurter Straße 250, D-64293 Darmstadt, Germany

[#]Chemical and Pharmaceutical Development, Merck KGaA, Frankfurter Straße 250, D-64293 Darmstadt, Germany

[‡]Institute for Organic Chemistry and Biochemistry, Technische Universität Darmstadt, Alarich-Weiss-Straße 4, D-64287 Darmstadt, Germany

[§]Institute of Immunology, University Hospital Schleswig-Holstein and Christian-Albrechts-University Kiel, Michaelisstrasse 5, Bldg. U30, D-24105 Kiel, Germany

[||]Department of Immuno-oncology, EMD Serono Research & Development Institute Inc., 45A Middlesex Turnpike, MA-01821 Billerica, USA

[1]These authors contributed equally to this work.

[2]To whom correspondence should be addressed:

Matthias Peipp, Division of Stem Cell Transplantation and Immunotherapy, Department of Medicine II, University Hospital Schleswig-Holstein and Christian-Albrechts-University Kiel, Rosalind-Franklin-Straße 12, D-24105 Kiel, Germany, E-mail: m.peipp@med2.uni-kiel.de.de

Stefan Zielonka, Protein Engineering and Antibody Technologies, Merck Healthcare KGaA, Frankfurter Straße 250, D-64293 Darmstadt, Germany, E-mail: Stefan.Zielonka@merckgroup.com

Running title (max. 60 characters!)

Tumor lysis by affinity matured B7-H6-based NK cell engagers

Keywords

ADCC, Affinity maturation; Antibody engineering; B7-H6; Bispecific antibody; Immunoligand; NKp30; NK cell engager; Protein engineering

Grant support

This work was supported by research funding by the German Cancer Aid (Mildred-Scheel-Professorship-Program) to MP.

Abstract

Activating Natural Killer (NK) cell receptors represent promising target structures to elicit potent anti-tumor immune responses. Here, novel immunoligands were generated that bridge the activating NK cell receptor NKp30 on NK cells with epidermal growth factor receptor (EGFR) on tumor cells in a bispecific IgG-like format based on affinity-optimized versions of B7-H6 and the Fab arm derived from Cetuximab. To enhance NKp30 binding, the solitary *N*-terminal IgV domain of B7-H6 (ΔB7-H6) was affinity matured by an evolutionary library approach combined with yeast surface display. Biochemical and functional characterization of 36 of these novel ΔB7-H6-derived NK cell engagers revealed an up to 45-fold enhanced affinity for NKp30 and significantly improved NK cell-mediated, EGFR-dependent killing of tumor cells compared to the NK cell engager based on the wild-type ΔB7-H6 domain. In this regard, potencies (EC_{50} killing) of the best immunoligands were substantially improved by up to 87-fold. Moreover, release of interferon-γ (IFN-γ) and tumor necrosis factor-α (TNF-α) was significantly increased. Importantly, equipment of the ΔB7-H6-based NK cell engagers with a human IgG1 Fc part competent in Fc receptor binding resulted in an almost 10-fold superior killing of EGFR-overexpressing tumor cells compared to molecules either triggering FcγRIIIa or NKp30. Additionally, INF-γ and TNF-α release was increased compared to molecules solely triggering FcγRIIIa including the clinically approved antibody Cetuximab. Thus, incorporating affinity-matured ligands for NK cell activating receptors might represent an effective strategy for the generation of potent novel therapeutic agents with unique effector functions in cancer immunotherapy.

Key points

- B7-H6 was affinity matured by yeast surface display
- NK cell engagers harboring optimized B7-H6 have improved cytotoxic capacities
- NK cell engagers based on improved B7-H6 display a differentiated cytokine profile

Introduction

Natural killer (NK) cells are innate lymphocytes that recognize discontinuity and danger in multiple tissue compartments by integrating positive and negative signals (1). The negative signals are generally mediated by the interaction between self MHC-I on tissues and either Killer-Immunoglobulin-like Receptor (KIR) family members or Natural Killer Group 2A (NKG2A) (2). Positive signals are transduced via the interaction of an array of NK activation receptors including the Natural Cytotoxicity Receptors (NCRs; NKp30, NKp46, NKp44), NKG2D and DNAM-1 as well as costimulatory molecules including 4-1BB and their ligands (3–5). For the NCRs and NKG2D, many of the ligands are 'danger signals' that are upregulated on stressed and diseased tissues including viral infected cells and tumor cells (6-8). Another mechanism by which NK cells are activated is the bridging of the low affinity activating FcγRIIIa (CD16a) on NK cells with cells opsonized with IgG antibodies or bispecific antibodies (9, 10). Unlike the NCRs and NKG2D, signaling through FcγRIIIa is often more robust in resting NK cells but is modulated by multiple variables including functionally distinct polymorphic variants of FcγRIIIa as well as competition for binding with circulating IgG (11-15). Ultimately, the balance of activation and inhibitory signal determines whether an NK cell will become activated. As such, NK cells have an endogenous capacity to differentiate between healthy and diseased tissues (16, 17).

Recently, several early clinical trials employing the adoptive transfer of wild-type or genetically modified (e.g. CAR) NK cells either alone or in combination with antibodies as a therapeutic modality for cancer have been initiated with encouraging early results for hematological malignancies (18–21). Although adoptive cell therapy with *ex vivo* activated NK cells represents a promising approach (22) the logistic complexity has also driven the development of NK cell-directed antibody-based approaches to cancer immunotherapy such as bispecific or trifunctional entities that form a bridge between an activation receptor on NK cells and a tumor

associated antigen (TAA) on the tumor cell, referred to as NK cell engager or immunoligand (11, 23, 24). Bispecific antibodies targeting a TAA (e.g. CD20) and NKp46 (25), NKG2D (26) and NKp30 (27, 28) either via an antibody moiety or a recombinant form of the ectodomain of a ligand (e.g. ULBP2) (29) have demonstrated potent target-dependent cytotoxicity and cytokine release *in vitro*.

NKp30 is an activation receptor expressed on the majority of NK cells (30). Its cell bound ligand, B7-H6 is upregulated on tumor cells and absent on most normal cells (7). The other less well characterized ligand is HLA-B-associated transcript 3 (BAT3)/Bcl2-associated athanogene 6 (BAG6), which is expressed in the nucleus and can be transported to the plasma membrane or released in exosomes (31, 32). Importantly, decreased NKp30 expression has been correlated with reduced survival in AML (33) and a lower number of NK cells expressing NKp30 were found in patients with gastric or breast cancer compared to healthy donors (34), (35). Together, these data suggest that the NKp30 receptor axis may play an important role in tumor surveillance of different tumor entities. Therefore, potent strategies modulating the NKp30 axis may represent promising approaches to promote antitumor NK cell responses.

In this work, we designed human EGFR x NKp30 NK cell engagers (i.e. immunoligands) to trigger NKp30-mediated tumor cell elimination using bispecific antibody-like fusion proteins containing a humanized Fab variant derived from Cetuximab and a panel of affinity-optimized variants of the *N*-terminal Ig-like V-type domain of B7-H6 (ΔB7-H6) engineered by yeast surface display. The bispecific NK cell engagers harboring affinity-matured variants facilitated substantially increased NK cell-mediated killing of tumor cells of up to 87-fold compared to molecules harboring the wild-type ΔB7-H6 domain. Importantly, target-dependent cytokine release of TNF-α and IFN-γ was also fundamentally elevated. Intriguingly, this proinflammatory cytokine release was also significantly increased compared to therapeutic antibody Cetuximab. Furthermore, we demonstrated that expression of ΔB7-H6-based

immunoligands in an effector competent human IgG1 backbone further enhanced killing of EGFR-overexpressing tumor cells by one order of magnitude compared to molecules either triggering FcγRIIIa or NKp30 alone. Taken together, our data suggests that an EGFR x NKp30 NK cell engager based on affinity engineered variants of B7-H6 can elicit potent NK cell-mediated lysis with a differentiated profile of released cytokines that could be envisioned to result in targeted inflammation of tumors.

Materials and Methods

Yeast surface display and affinity maturation of ΔB7-H6 variants

Saccharomyces cerevisiae strain EBY100 (*MATa URA3-52 trp1 leu2Δ1 his3Δ200 pep4::HIS3 prb1Δ1.6R can1 GAL (pIU211:URA3)*) (Thermo Fisher Scientific) was used for yeast surface display. Initially, cells were cultivated in YPD medium composed of 20 g/L peptone, 20 g/L dextrose and 10 g/L yeast extract supplemented with 10 ml/L penicillin-streptomycin (Gibco). Homologous recombination in yeast (gap repair cloning) was utilized for generation of the ΔB7-H6 library. Eight residues of the *N*-terminal IgV domain of B7-H6 at the binding interface of B7-H6 and NKp30 (pdb: 4ZSO) were randomized via TRIM technology at GeneArt (Thermo Fisher Scientific). As described previously, sequences were cloned in a pYD-derived backbone as destination vector (pDest) in frame with Aga2p *C*-terminally carrying an HA epitope to enable yeast cell surface presentation and detection of full-length molecules (36). Cells harboring library plasmids were cultivated at 30°C and 120 rpm in minimal SD-base medium with dropout mix composed of all essential amino acids except from tryptophan to maintain selection pressure according to the manufacturer's instructions (Clontech), supplemented with 5.4 g/L Na_2HPO_4 and 8.6 g/L $NaH_2PO_4 \times H_2O$. ΔB7-H6 expression for library sorting was achieved by culture of 10^7 cells/ml for 48 h at 20°C in SG medium with dropout mix wherein glucose was replaced by galactose (Clontech) and 10% (w/v) polyethylene glycol 8000 (PEG 8000). NKp30 binding of yeast surface expressed ΔB7-H6 was monitored by indirect immunofluorescence using his-tagged NKp30 (Abcam) in combination with Penta-His Alexa Fluor 647 antibody (Qiagen, diluted 1:20). Simultaneously, ΔB7-H6 surface expression was detected by an anti-HA-PE antibody (Abcam, diluted 1:20). Detection and sorting of yeast candidates was done on a SH800S cell sorter (Sony) using a 70 µm sorting chip in three successive rounds. For the first sorting round 10^8 yeast cells were incubated with 1 µM NKp30 followed by a second round with 100 nM NKp30 and a third round with 50 nM NKp30.

Incubation was performed for 1 h on ice prior washing with PBS and sorting. For the second and third sorting round, cells were incubated for 30 min in 3 ml and 30 ml PBS, respectively, to increase sorting stringencies.

Expression and purification of NK cell engagers

Unique ΔB7-H6 sequences were fused to SEED AG chain and cloned into pTT5 (either in house or at GeneArt/Thermo Fisher Scientific) to allow full-length bispecific SEED production by combination with humanized Cetuximab (hu225) Fab on the SEED GA chain. Molecules were either produced in an effector silenced backbone by introduction of amino acid exchanges L234A, L235A, P329G (SEED_PGLALA) or in an effector competent IgG1 backbone (SEED). To this end, Expi293 cells were transiently transfected with respective expression vectors according to manufacturer's instructions (Thermo Fisher Scientific). Antibody containing supernatants were harvested and purified via MabSelect antibody purification chromatography resin (GE Healthcare). NK cell engagers were dialyzed overnight against PBS pH 6.8 using Pur-A-Lyzer™ Maxi 3500 Dialysis Kit (Sigma Aldrich). Protein concentrations were determined by UV-Vis spectrophotometric measurement (Nanodrop ND-1000, Peqlab) and thermal stabilities were evaluated by differential scanning fluorimetry on a Prometheus NT.48 (Nanotemper Technologies). To assess purity and aggregations, proteins were analyzed by analytical size exclusion chromatography with a TSKgel SuperSW3000 column (4.6×300 mm, Tosoh Bioscience LLC) in an Agilent HPLC system with a flow rate of 0.35 ml/min.

Biolayer interferometry (BLI)

Kinetic measurements were performed on Octet RED96 system (ForteBio, Pall Life Science) at 25°C and 1000 rpm. Immunoligands (5 µg/ml in PBS) were loaded on anti-human Fc biosensors for 5 min followed by 60 s rinsing the sensor with kinetics buffer (KB; PBS + 0.1 %

Tween-20 + 1% BSA). Afterwards, association to human NKp30 (Abcam) in varying concentrations (15.6-1000 nM) was measured for 60 s followed by dissociation measurement for 180 s in KB. An irrelevant antigen was measured as negative control in each experiment. Data was fitted and analyzed with ForteBio data analysis software 8.0 using a 1:1 binding model after Savitzky-Golay filtering.

Cell culture

EGFR-expressing epidermoid carcinoma cell line A431 and non-small cell lung carcinoma cell line A549 were obtained from DSMZ and cultured in RPMI 1640 Glutamax-I or Dulbecco's Modified Eagle's medium supplemented with 10% FCS, 100 U/ml penicillin and 100 mg/ml streptomycin (R10+ and D10+), respectively (all components from Thermo Fisher Scientific). Human Expi293 cells for production of immunoligands were cultivated in suspension with complete Expi293 expression medium (Thermo Fisher Scientific).

Tumor cell killings assays

Experiments were approved by the Ethics Committee of the Christian-Albrechts-University of Kiel (Kiel, Germany) and in accordance with Merck internal guidelines and with the Declaration of Helsinki. Preparation of PBMCs from healthy donors was performed as previously described after receiving written informed consent (37). NK cells were isolated by negative selection using NK cell isolation kit (Miltenyi Biotech) and maintained overnight at a density of $2x10^6$ cells/ml in R10+ medium. Cytotoxicity was analyzed in standard 4 h ^{51}Cr release assays performed in 96-well microtiter plates in a total volume of 200 µl as described previously (37). Human PBMCs or purified NK cells were used as effector cells at effector-to-target cell (E:T) ratios of 80:1 and 10:1, respectively. NK cell engagers or Cetuximab were applied at concentrations indicated. For blocking experiments, cells were pre-incubated for 15 min with 50 µg/ml of either anti-NKp30 mouse IgG2A antibody (mouse IgG2A isotype

control antibody was used as a control in these experiments; both R&D Systems) to block NKp30 binding on NK cells or oa_hu225-SEED-PGLALA to block EGFR binding on tumor cells before the respective NK cell engagers were added. Percent lysis was calculated as follows from counts per minute (cpm): % lysis = (experimental cpm-basal cpm)/(maximal cpm-basal cpm)x100 and normalized (0 % = % lysis of oa_hu225-SEED-PGLALA control molecule, 100 % = % lysis of Cetuximab at saturating concentration) to allow for direct comparison of affinity-matured ΔB7-H6-derived molecules between individual donors. Inhibited lysis was calculated as follows: 100 % - (% $lysis_{blocked}$*100)/% lysis).

Cytokine release assay

For cytokine release assays, NK cells were isolated with EasySep™ Human NK Cell Isolation Kit (Stemcell Technologies) and incubated overnight in AIM V medium containing 100 U/ml recombinant human interleukin-2 (R&D Systems). 2.500 A431 cells were seeded in 384-well microtiter plates (Greiner Bio-One) and incubated for 3 h. Immunoligands were added to a final concentration of 85 nM followed by addition of NK cells at an E:T ratio of 5:1. After 24 h, supernatants were analyzed using human IFN-γ or TNF-α HTRF kit (Cisbio) according to manufacturer's instructions. Plates were measured with PHERAstar FSX (BMG Labtech) and data were analyzed by MARS software (v.3.32, BMG) enabling a 4-parameter logistic (4PL 1/y) model fitting of the standard curve.

NK cell activation assay

20.000 A431 cells/well were seeded in 96-well V-bottom microtiter plates (Thermo Fisher Scientific) and incubated for 3 h prior addition of 100.000 NK cells/well (E:T ratio of 5:1), which were treated with 100 U/ml recombinant human interleukin-2 overnight. Immunoligands were added at a final concentration of 85 nM followed by 24 h incubation at 37°C. Cells were washed two times with PBS + 1 % BSA prior incubation with LIVE/DEAD™ Fixable Near-IR

Dead Cell Stain (Thermo Fisher Scientific), anti-human CD56-PE (Miltenyi Biotec) and anti-human CD69-APC (Abcam) for 1 h on ice. After washing, cells were measured via flow cytometry with Intellicyt® iQue® Screener Plus (Sartorius). For compensation of fluorochromes antibody capturing analysis beads (OneComp eBeads™ Compensation Beads, Thermo Fisher Scientific) were employed according to the manufacturer's instructions. The gating strategy is shown in supplementary figure 1 (**Fig. S1**).

Data processing and statistical analysis

Graphical and statistical analyses were performed with GraphPad Prism 8 software. *P*-values were calculated employing repeated measures ANOVA and the Bonferroni or Tukey post-test as recommended, or the student's *t*-test when appropriate. $p \leq 0.05$ were regarded as statistically significant.

Results

Extracellular IgV domain of B7-H6 is sufficient to engage NK cells for tumor cell lysis

In previous studies, it was shown that B7-H6 scFv fusion proteins trigger NK cell-mediated lysis of tumor cells (28, 38). Since the NKp30 binding site is located in the IgV domain of B7-H6, we hypothesized that this isolated domain alone is sufficient to trigger NK cell activation and tumor cell killing. To address this question, the *N*-terminal Ig-like V-type domain (Asp25-Ala144) of the extracellular region of B7-H6 (termed ΔB7-H6) was used to design a novel EGFR-targeting NKp30 NK cell engager (**Fig. 1A, B**). To completely abolish Fc-mediated immune effector functions, the LALA-PG amino acid exchanges (L234A, L235A, P329G) were introduced (39). Kinetic studies of this ΔB7-H6_wt-SEED-PGLALA molecule revealed functional binding to NKp30 (**Fig. 1C**), in accordance with previously published work (40, 41). Most importantly, significant lysis of EGFR-expressing A431 tumor cells was triggered by this novel immunoligand (**Fig. 1D**), demonstrating that the isolated ΔB7-H6 domain is sufficient to promote NK cell-mediated lysis of target cells. However, the extent of tumor cell lysis with the monovalent EGFR binding NK cell engager ΔB7-H6_wt-SEED-PGLALA (EC_{50} = 244.8 pM) was significantly reduced compared to a similarly designed one-armed (oa) EGFR-targeting molecule (oa_hu225-SEED) lacking the NKp30 binding domain but harboring an active IgG1 Fc region triggering FcγRIIIa, one of the strongest known trigger molecules expressed on NK cells (EC_{50} = 27.8 pM).

Affinity maturation of the B7-H6 IgV domain by yeast display

In order to improve the cytotoxic activity of the novel ΔB7-H6-based NK cell engager, we designed a focused combinatorial mutant library of ΔB7-H6 for yeast surface display using trinucleotide mutagenesis technology with the aim of enhancing affinity of ΔB7-H6 for NKp30. ΔB7-H6 was displayed successfully and showed specific binding to recombinant NKp30

(**Fig. S2**). Based on the co-crystal structure of B7-H6 and NKp30 eight residues of B7-H6 (Ser60, Gly62, Phe82, Gly83, Val125, Thr127, Leu129 and Lys130) at the contact interface with NKp30 were chosen for library design (**Fig. 2A**). Randomization of these residues was designed in a semi-rational way such that only amino acids that were thought to be potentially beneficial for binding affinity were taken into account. As shown in **Fig. 2B**, the synthesized library matched fairly well with the initial design showing only little bias. The resulting library (comprising approximately $1x10^7$ unique clones) was sorted by fluorescence-activated cell sorting (FACS) against recombinant NKp30 to isolate variants with significantly enhanced affinities (**Fig. 2C**). To this end, a two-dimensional labeling strategy was employed to simultaneously detect full-length ΔB7-H6 and binding to NKp30. Due to the low affinity interaction of B7-H6 and NKp30, that was reported to be in the μM range (40), an NKp30 protein concentration of 1 μM was utilized in the first selection round and subsequently reduced to 100 nM and 50 nM, respectively (**Fig. 2C**). Library output after three rounds of selection was analyzed for NKp30 binding in direct comparison with the wild-type ΔB7-H6 and revealed improved NKp30 binding of the vast majority of affinity-matured ΔB7-H6 clones (**Fig. S2C, D**). After sequencing of approximately 200 clones from sorting round two and three, we were able to identify 47 unique clones (**Tab. SI**). Interestingly, none of those comprised mutations at positions Thr127 or Lys130. Consequently, it is tempting to speculate that these two residues are essential for B7-H6 binding to NKp30 or for structural integrity of the molecule.

Generation and characterization of affinity-matured ΔB7-H6 NK cell engagers

All 47 unique affinity-matured ΔB7-H6 clones were reformatted as Fc-silenced SEEDbodies with monovalent EGFR binding by using the humanized Fab arm of Cetuximab (hu225) as shown already for the wild-type ΔB7-H6 NK cell engager (**Fig. 1B**). As summarized in **Table SI**, besides two variants that showed either very low expression (S2#8) or no productivity

at all (S2#9), expression yields of all variants after protein A chromatography were in the double to triple digit milligram per liter scale. This is generally acceptable for transient expression of bifunctional antibody-like fusion proteins. Moreover, melting temperatures of all variants were quite similar to the denaturation point of the SEEDbody comprising ΔB7-H6 wild-type domain (**Table SI**), giving clear evidence that no substantial loss in stability was observed by introducing mutations into ΔB7-H6. Most importantly, the vast majority of the affinity-matured variants showed significantly enhanced affinities for NKp30 of up to 45.1-fold (S3#18) compared to the wild-type ΔB7-H6 NK cell engager (**Table I, Fig. S2E**). In general, improved off-rates contributed substantially more to the overall affinity maturation than modulations of on-rates of the ΔB7-H6 SEED PGLALA immunoligands. Interestingly, variant S3#13 that did not bind NKp30, was the only clone isolated that contained a mutation of Gly62 (Gly62Ile). This observation suggests that in addition to Thr127 or Lys130, Gly62 may also be indispensable for ΔB7-H6 binding to NKp30. For subsequent functional evaluation of the affinity-matured ΔB7-H6-derived NK cell engagers, we focused on immunoligands showing at least 85 % monomers (i.e. a maximum of 15 % aggregates) as determined by size exclusion chromatography. Accordingly, 36 affinity-matured ΔB7-H6 NK cell engagers were selected for functional experiments (**Table I**).

Affinity-matured ΔB7-H6 immunoligands elicit strongly enhanced NK cell-mediated cytotoxicity against EGFR-expressing tumor cells

As an initial screening, the 36 remaining ΔB7-H6, EGFR-targeting NK cell engagers were tested for their capacity to mediate tumor cell killing using PBMCs (containing 5-20 % NK cells) from healthy donors as effector cells and the EGFR-positive tumor cell line A431 as target cells in chromium release assays. To allow comparison and ranking of the 36 molecules, data sets derived from different effector cell donors, who usually show varying donor-

dependent maximal lytic activity, were normalized. An internal positive control was set to 100 % and oa_hu225-SEED-PGLALA-mediated lysis to 0 % since this molecule is functionally inactive and reflects the tumor cell lysis induced by the NK cells alone (**Fig. 1D**). In these experiments shown in **Figure S3**, the Fc effector silenced wild-type ΔB7-H6 NK cell engager ΔB7-H6_wt SEED-PGLALA triggered significant tumor cell lysis (EC_{50} = 1.1 nM). Of note, all 36 ΔB7-H6 affinity-matured SEED-PGLALA molecules mediated higher maximum tumor cell lysis and achieved enhanced potency of up to 187-fold (S3#25) compared to the wild-type ΔB7-H6 immunoligand (**Fig. S3**). Among them, 11 constructs bound to NKp30 with affinity improvements of more than 10-fold (KD < 40 nM) and five variants comprised enhanced affinities between 5-fold and 10-fold, whereas the majority of clones comprised optimized affinities of less than 5-fold (KD > 120 nM; **Table I, Fig. S3**). Six of the 11 NK cell engagers constructed with the high-affinity ΔB7-H6 clones (KD < 40 nM), i.e. S3#14, S3#15, S3#16, S3#18, S3#24 and S3#29, induced NK cell-mediated killing of tumor cells with EC_{50} values ranging from 10.6-71.1 pM, representing a 16-fold to 106-fold increase compared to the wild-type ΔB7-H6 NK cell engager (**Fig. S3**). Of the NK cell engagers using ΔB7-H6 clones with optimized affinities for NKp30 between 5-fold and 10-fold, S3#25 and S3#31 were the most potent, displaying NKp30 affinity enhancements of 6.3-fold and 9.4-fold, respectively. These molecules induced NK cell-mediated killing of tumor cells with half-maximal killing activity of 6 pM (S3#25) and 25.1 pM (S3#31). From the variants comprising optimized NKp30 affinities of less than 5-fold, clone S3#27 (KD = 83 nM) elicited significant tumor cell lysis (EC_{50} = 27.6 pM) with 41-fold improved potency compared to wild-type ΔB7-H6 and was also selected for further characterization.

Next, the potency of the nine most active candidates from the initial screening (i.e. S3#14, S3#15, S3#16, S3#18, S3#24, S3#25, S3#27, S3#29, S3#31) was further compared via chromium release assays using A431 and A549 cells with PBMCs from 3 different donors

(**Fig. 3A**). As observed for A431 cells, the nine candidates also mediated substantially improved maximum killing and significantly enhanced potency in tumor cell lysis compared to the NK cell engager harboring wild-type ΔB7-H6 against tumor cell line A549 expressing significantly lower EGFR levels compared to A431 cells (**Fig. 3A**). While wild-type ΔB7-H6 NK cell engager ΔB7-H6_wt SEED-PGLALA showed significant, but limited activity ($EC_{50\ A431}$ = 1.8 nM), the most active affinity-optimized NK cell engager S3#15 demonstrated improved potency at low pM concentrations with PBMCs of 3 different donors (EC_{50} = 29.9 pM). Extent of lysis of A549 cells achieved by the most effective affinity-matured ΔB7-H6 NK cell engager S3#24 (EC_{50} = 108.3 pM), is about 3.6-times higher compared to A431 cells (**Table II**). This might most likely reflect the impact of the lower EGFR expression level on A549 target cells, a well-known parameter affecting effector cell killing. To further characterize the four most potent NK cell engagers S3#15, S3#18, S3#24 and S3#25, we performed killings assays with purified, non-stimulated NK cells (**Fig. 3B**). Using A431 cells, the four ΔB7-H6 affinity-maturated NK cell engagers mediated tumor cell killing in the single digit picomolar range, representing an increase in potency of up to 87-fold (S3#15) compared to the NK cell engager harboring the wild-type ΔB7-H6 domain (**Table II**). Even for A549 target cells, potencies of all four leading hits were still in the picomolar range. Notably, efficacy of wild-type ΔB7-H6 NK cell engager was not substantially different from the negative control in NK cell ADCC with A549 cells (**Fig. 3A, B**). Finally, EGFR-specific and NKp30-mediated killing by the four leading NK cell engagers was further verified by either blocking EGFR on cell surface of A431 cells or by pre-incubation of NK cells with an excess of an anti-human NKp30 antibody. As shown in **Figure 3C**, lysis of A431 tumor cells was significantly inhibited for all four NK cell engagers under both conditions demonstrating the specificity and prerequisite of bispecific engagement of these novel B7-H6 affinity-matured immunoligands (**Fig. 3C**).

ΔB7-H6 affinity-maturated NK cell engagers exhibit a distinct NK cell activation profile

Next, we set out to scrutinize activation of NK cells in the presence of tumor cells overexpressing EGFR (A431) and the four leading immunoligands via analyzing CD69 upregulation as early NK cell activation marker. As expected, negative control (i.e. oa_hu225-SEED-PGLALA) mediated neglectable NK cell activation, whereas the NK cell engager harboring wild-type ΔB7-H6 elicited CD69 expression on approximately 17 % of NK cells on average (**Fig. 4A**). Compared to the wild-type ΔB7-H6 immunoligand, the four most potent affinity-optimized ΔB7-H6 immunoligands activated nearly twice as many NK cells ranging from 30.7 % to 33.8 % CD69-positive NK cells (**Fig. 4A**). In addition, all four leading NK cell engagers promoted significantly increased NK cell production of proinflammatory cytokines IFN-γ and TNF-α in a target-dependent manner (**Fig. 4B, C**). In comparison to the wild-type ΔB7-H6 molecule, which induced release of 141 pg/ml IFN-γ and 37 pg/ml TNF-α, S3#15, S3#18, S3#24 and S3#25 induced release of 615-824 pg/ml IFN-γ and 152-214 pg/ml TNF-α on average (**Fig. 4B, C**). Thus, affinity-engineered NK cell engagers induced up to 5.8-fold increased levels of IFN-γ and TNF-α compared to the wild-type ΔB7-H6 immunoligand. These findings are in line with the substantially enhanced killing potencies and efficacies of the affinity-engineered ΔB7-H6 NK cell engagers observed before.

ΔB7-H6 affinity-maturated NK cell engagers elucidate improved killing by concomitant engagement of FcγRIIIa

Finally, we tested the NK cell engager ΔB7-H6 S3#18, which has the highest binding affinity for NKp30 (KD = 9 nM), in the background of an Fc region capable of FcγRIIIa binding (SEEDbody lacking the L234A, L235A, P329G amino acid exchanges) to analyze whether tumor cell lysis can be further enhanced by concomitant NKp30 and FcγRIIIa activation of NK cells. The oa_hu225-SEED molecule harboring an Fc domain capable of FcR binding, but

lacking a ΔB7-H6 domain, was as potent as the affinity-matured Fc-silenced ΔB7-H6 S3#18 SEED-PGLALA molecule, which solely activates NKp30 (**Fig. 5A**). Intriguingly, incorporation of a functional Fc in the NK cell engager S3#18 (i.e. ΔB7-H6 S3#18-SEED) significantly improved half-maximal killing by 9.2-fold (**Fig. 5A**). Furthermore, as shown in **Figure 5B**, half-maximal killing achieved with ΔB7-H6 S3#18-SEED was in the range or even slightly exceeded the cytotoxic activity of the clinically applied antibody Cetuximab. These data give clear evidence that activating NK cells via NKp30 with an high affinity-engineered B7-H6-derived NK cell engager is as effective as activating NK cells via FcγRIIIa, and that the combination of NKp30 and FcγRIIIa activation of NK cells in one molecule can further potentiate the lysis of EGFR-expressing tumor cells.

Finally, we compared the capacity to trigger IFN-γ and TNF-α by the molecule engaging both NKp30 and FcγRIIIa with constructs engaging either NKp30 or FcγRIIIa and with the clinically approved antibody Cetuximab (**Fig. 5C, D**). Interestingly, the capacity to trigger cytokine release was maintained in the molecule engaging both activating receptors compared to the molecule solely engaging NKp30, with a trend towards higher TNF-α release induced by the molecule with an effector competent IgG1 backbone. Of note, compared to the therapeutic antibody Cetuximab the release of IFN-γ and TNF-α was substantially elevated, irrespective of the utilized Fc. Moreover, activation of NK cells was comparable to Cetuximab (**Fig. 5E**) Ultimately, our data demonstrate that the herein engineered NK cell engagers are capable in triggering NK cell-mediated lysis similarly effective as the clinically approved antibody Cetuximab, but in addition triggers significant IFN-γ and TNF-α release to potentially modulate anti-tumor immune responses.

Discussion

To efficiently trigger anti-tumor NK cell responses using activating NK cell engagers, the solitary *N*-terminal IgV domain of B7-H6 (ΔB7-H6) was affinity maturated by a rational design and screening approach. Engineered molecules with increased NKp30 binding activity resulted in significantly improved NK cell-mediated lysis of tumor cells and enhanced secretion of proinflammatory cytokines INF-γ and TNF-α. Coligation of NKp30 and FcγRIIIa on NK cells further enhanced their cytotoxic activity by almost 10-fold compared to molecules engaging either receptor alone. Furthermore, the most potent novel NK cell engager was similarly effective in triggering NK cell-mediated lysis of EGFR-expressing tumor cells as the clinically approved antibody Cetuximab, but additionally promoted considerably higher release of proinflammatory cytokines. These findings suggest that the novel NK cell activating molecules may represent attractive agents to elicit strong NK cell-mediated antitumor responses.

NK cell-based therapeutic interventions represent promising approaches to improve cancer therapy by initiating a multifaceted immune response (1, 42). Since NK cell activation is tightly regulated by integrating signals of a large set of activating and inhibitory receptors (16, 17), potential therapeutic options have been proposed by either blocking inhibitory NK cell checkpoints such as NKG2A (43) or by enhancing stimulatory signals such as NKG2D, NKp30, NKp46 or the FcγRIIIa (23, 25, 26, 29). Since tumor cells evade NK cell recognition by down-modulation or shedding of the natural ligands of activating NK cell receptors such as MICA/B or B7-H6 (44–48), restoring NK cell recognition by enhancing surface density of activating ligands may represent a promising approach for cancer therapy. In previous studies this has been realized by fusing the natural ligands for activating NK cell receptors to scFvs or full antibodies (27–29, 38). Here, we designed novel IgG-based bispecific, multifunctional fusion proteins using the SEED technology (49) and an engineered minimal NKp30 binding domain derived from B7-H6. Since these molecules display IgG-like properties in terms of stability and

harbor an IgG Fc domain allowing FcRn binding, such molecules may show favorable characteristics compared to previously described B7-H6-based immunoligands when applied *in vivo* (50). We were able to demonstrate that the IgV domain of B7-H6 is sufficient to trigger NK cell activation. Affinity maturation of the ΔB7-H6 domain by exchanging key residues at the B7-H6/NKp30 contact interface using a combinatorial library approach resulted in significantly enhanced tumor cell lysis by NK cells. This data clearly demonstrates that similar to the Fc/FcγRIIIa system, which could be potently modulated by Fc-engineering, high affinity receptor engagement of NKp30 results in fundamentally improved cytotoxic response. Interestingly, also variants displaying only a moderate affinity improvement resulted in significantly increased lytic activity, which is in line with other bispecific effector cell engagers and engineered Fc domains, for which it has been demonstrated that maximal affinity enhancement may not necessarily result in improved cytolytic activity (37, 51–53). Since the observed cytolytic activity of our novel molecules does not directly correlate with binding affinity of the receptor-ligand interaction, the mechanisms of enhanced recognition might be more complex. From our experiments it could not be excluded that engineering the ΔB7-H6 domain may e.g. impact protein flexibility which in turn may have a strong impact on receptor clustering or activating synapse formation. Intriguingly, one of the best affinity-engineered ΔB7-H6 candidates triggered NK cell-mediated lysis of tumor cells via activation of NKp30 similarly effective as molecules activating FcγRIIIa, one of the most potent known trigger molecule on NK cells that moreover is expressed at significantly higher levels compared to NKp30 (70.000 *vs* 1.000 specific antigen binding sites (27)). Additionally, concomitant activation of FcγRIIIa and NKp30 by incorporating an effector competent IgG1 Fc backbone resulted in an almost 10-fold improved lytic capacity. This is in line with previous findings that combining monoclonal antibodies with B7-H6-based immunoligands demonstrate improved cytolytic activity (28). Moreover, Gauthier and co-workers were able to demonstrate that

simultaneous triggering of NKp46 and FcγRIIIa substantially enhances efficiencies of multifunctional antibodies (25). The precise underlying mechanism is not fully understood, since NKp30 and FcγRIIIa signal via the same adaptor chains (CD3ζ, common γ-chain; (54)). Beyond, engagement of NKp30 via improved B7-H6-based engagers clearly differ from exclusive FcγRIIIa engagers in their capacity to trigger the production of pro-inflammatory cytokines. NKp30 engagers demonstrated up to 5-fold increased production of TNF-α and INF-γ compared to molecules solely triggering FcγRIIIa. This feature was also observed with molecules allowing concomitant NKp30 and FcγRIIIa engagement, indicating that FcγRIIIa triggering has no inhibitory effect in NKp30-mediated cytokine release. Whether this is due to distinct signaling events triggered by the two receptor systems or by activating distinct NK cell subsets must be further investigated.

Cao and colleagues demonstrated that different therapeutic treatments such as 5-FU, cisplatin, radiation and cytokine therapy with TNF-α resulted in the upregulation of B7-H6, rendering tumor cells more sensitive to NK cell-mediated killing in a NKp30-dependent fashion (55). The optimized ΔB7-H6-based agents may therefore significantly increase levels of surface-exposed B7-H6 by two different mechanisms. While obviously "artificial" decoration of tumor cells using bispecific EGFR-directed ΔB7-H6 fusion proteins results in higher surface density of ΔB7-H6, the affinity enhanced variants also significantly triggered TNF-α release by NK cells, which might in turn, as described by Cao and colleagues, lead to upregulation of endogenous B7-H6 on tumor cells in close vicinity. This might be especially interesting in situations in which the target antigen addressed by antibody-based approaches is inhomogeneously expressed, since this mechanism might sensitize tumor cells sensitive to NK cell lysis also in an antigen-independent way.

Besides TNF-α production, by triggering NKp30 the herein described immunoligands also promoted INF-γ release in a strictly targeted fashion and to a significantly larger extent than

molecules such as Cetuximab exclusively activating NK cells via FcγRIIIa. Considering the pleiotropic effects of IFN-γ (56–59) on several different immune cell subsets present in the tumor microenvironment, this may have major consequences when applied *in vivo*, especially in the treatment of solid tumors. While IFN-γ signaling has been demonstrated to promote tumor elimination by inhibiting suppressive immune cells, such as regulatory T cells (60), myeloid-derived suppressor cells (61) and tumor-associated macrophages (TAMs), IFN-γ is also critical for NK, NKT and T cell trafficking into tumors through chemokine induction (62, 63). In addition, IFN-γ activates antigen-presenting cells and cytotoxic T lymphocytes. Hence, the NK cell engagers described in this work might be able to turn *cold* tumors *hot* and may therefore represent also interesting candidates in combination with other immunomodulatory agents, such as immune checkpoint inhibitors (64, 65).

In conclusion, the herein engineered novel B7-H6-based NK cell engagers combine a unique set of effector functions to directly eliminate tumor cells by triggering NK cell cytotoxicity and eliciting a multifaceted immune reaction by promoting release of proinflammatory cytokines and therefore represent an interesting new class of immunomodulatory agents.

Acknowledgements

We kindly thank Britta von Below and Anja Muskulus for excellent technical assistance. Moreover, we are grateful to Kerstin Hallstein, Laura Unmuth, Stephan Keller, Alexander Müller, Sigrid Auth, Pia Stroh, Marion Wetter, Thomas Rysiok, Janina Klemm, Stefan Becker and Dirk Müller-Pompalla for experimental support. This work is dedicated to Prof. Stefan Hüttenhain on the occasion of his retirement.

References

1. Chiossone, L., P.-Y. Dumas, M. Vienne, and E. Vivier. 2018. Natural killer cells and other innate lymphoid cells in cancer. *Nature Reviews Immunology* 18: 671–688.
2. Vivier, E., E. Tomasello, M. Baratin, T. Walzer, and S. Ugolini. 2008. Functions of natural killer cells. *Nat. Immunol.* 9: 503–510.
3. Carlsten, M., and M. Järås. 2019. Natural Killer Cells in Myeloid Malignancies: Immune Surveillance, NK Cell Dysfunction, and Pharmacological Opportunities to Bolster the Endogenous NK Cells. *Frontiers in Immunology* 10.
4. Barrow, A. D., C. J. Martin, and M. Colonna. 2019. The Natural Cytotoxicity Receptors in Health and Disease. *Frontiers in Immunology* 10.
5. Moretta, L. 2001. Human natural killer cell function and receptors. *Current Opinion in Pharmacology* 1: 387–391.
6. Kruse, P. H., J. Matta, S. Ugolini, and E. Vivier. 2014. Natural cytotoxicity receptors and their ligands. *Immunology & Cell Biology* 92: 221–229.
7. Brandt, C. S., M. Baratin, E. C. Yi, J. Kennedy, Z. Gao, B. Fox, B. Haldeman, C. D. Ostrander, T. Kaifu, C. Chabannon, A. Moretta, R. West, W. Xu, E. Vivier, and S. D. Levin. 2009. The B7 family member B7-H6 is a tumor cell ligand for the activating natural killer cell receptor NKp30 in humans. *The Journal of Experimental Medicine* 206: 1495–1503.
8. Spear, P., M.-R. Wu, M.-L. Sentman, and C. L. Sentman. 2013. NKG2D ligands as therapeutic targets. *Cancer Immun.* 13: 8.
9. Seidel, U. J. E., P. Schlegel, and P. Lang. 2013. Natural Killer Cell Mediated Antibody-Dependent Cellular Cytotoxicity in Tumor Immunotherapy with Therapeutic Antibodies. *Frontiers in Immunology* 4.
10. Schubert, I., C. Kellner, C. Stein, M. Kügler, M. Schwenkert, D. Saul, B. Stockmeyer, C. Berens, F. S. Oduncu, A. Mackensen, and G. H. Fey. 2012. A recombinant triplebody with specificity for CD19 and HLA-DR mediates preferential binding to antigen double-positive cells by dual-targeting. *mAbs* 4: 45–56.
11. Koch, J., and M. Tesar. 2017. Recombinant Antibodies to Arm Cytotoxic Lymphocytes in Cancer Immunotherapy. *Transfusion Medicine and Hemotherapy* 44: 337–350.
12. Weng, W.-K., and R. Levy. 2003. Two Immunoglobulin G Fragment C Receptor Polymorphisms Independently Predict Response to Rituximab in Patients With Follicular Lymphoma. *Journal of Clinical Oncology* 21: 3940–3947.
13. Musolino, A., N. Naldi, B. Bortesi, D. Pezzuolo, M. Capelletti, G. Missale, D. Laccabue, A. Zerbini, R. Camisa, G. Bisagni, T. M. Neri, and A. Ardizzoni. 2008. Immunoglobulin G Fragment C Receptor Polymorphisms and Clinical Efficacy of Trastuzumab-Based Therapy in Patients With HER-2/ *neu* –Positive Metastatic Breast Cancer. *Journal of Clinical Oncology* 26: 1789–1796.
14. Bibeau, F., E. Lopez-Crapez, F. Di Fiore, S. Thezenas, M. Ychou, F. Blanchard, A. Lamy, F. Penault-Llorca, T. Frébourg, P. Michel, J.-C. Sabourin, and F. Boissière-Michot. 2009. Impact of FcγRIIa-FcγRIIIa Polymorphisms and *KRAS* Mutations on the Clinical Outcome of Patients With Metastatic Colorectal Cancer Treated With Cetuximab Plus Irinotecan. *Journal of Clinical Oncology* 27: 1122–1129.
15. Preithner, S., S. Elm, S. Lippold, M. Locher, A. Wolf, A. J. da Silva, P. A. Baeuerle, and N. S. Prang. 2006. High concentrations of therapeutic IgG1 antibodies are needed to compensate for inhibition of antibody-dependent cellular cytotoxicity by excess endogenous immunoglobulin G. *Molecular Immunology* 43: 1183–1193.
16. Morvan, M. G., and L. L. Lanier. 2016. NK cells and cancer: you can teach innate cells new tricks. *Nature Reviews Cancer* 16: 7–19.
17. Shimasaki, N., A. Jain, and D. Campana. 2020. NK cells for cancer immunotherapy. *Nature Reviews Drug Discovery* 19: 200–218.

18. Rezvani, K. 2019. Adoptive cell therapy using engineered natural killer cells. *Bone Marrow Transplantation* 54: 785–788.
19. Liu, E., D. Marin, P. Banerjee, H. A. Macapinlac, P. Thompson, R. Basar, L. Nassif Kerbauy, B. Overman, P. Thall, M. Kaplan, V. Nandivada, I. Kaur, A. Nunez Cortes, K. Cao, M. Daher, C. Hosing, E. N. Cohen, P. Kebriaei, R. Mehta, S. Neelapu, Y. Nieto, M. Wang, W. Wierda, M. Keating, R. Champlin, E. J. Shpall, and K. Rezvani. 2020. Use of CAR-Transduced Natural Killer Cells in CD19-Positive Lymphoid Tumors. *New England Journal of Medicine* 382: 545–553.
20. Björklund, A. T., M. Carlsten, E. Sohlberg, L. L. Liu, T. Clancy, M. Karimi, S. Cooley, J. S. Miller, M. Klimkowska, M. Schaffer, E. Watz, K. Wikström, P. Blomberg, B. E. Wahlin, M. Palma, L. Hansson, P. Ljungman, E. Hellström-Lindberg, H.-G. Ljunggren, and K.-J. Malmberg. 2018. Complete Remission with Reduction of High-Risk Clones following Haploidentical NK-Cell Therapy against MDS and AML. *Clinical Cancer Research* 24: 1834–1844.
21. Tanaka, J., and J. S. Miller. 2020. Recent progress in and challenges in cellular therapy using NK cells for hematological malignancies. *Blood Reviews* 100678.
22. Granzin, M., J. Wagner, U. Köhl, A. Cerwenka, V. Huppert, and E. Ullrich. 2017. Shaping of Natural Killer Cell Antitumor Activity by Ex Vivo Cultivation. *Frontiers in Immunology* 8.
23. Ellwanger, K., U. Reusch, I. Fucek, S. Wingert, T. Ross, T. Müller, U. Schniegler-Mattox, T. Haneke, E. Rajkovic, J. Koch, M. Treder, and M. Tesar. 2019. Redirected optimized cell killing (ROCK®): A highly versatile multispecific fit-for-purpose antibody platform for engaging innate immunity. *mAbs* 11: 899–918.
24. Felices, M., T. R. Lenvik, B. Kodal, A. J. Lenvik, P. Hinderlie, L. E. Bendzick, D. K. Schirm, M. F. Kaminski, R. T. McElmurry, M. A. Geller, C. E. Eckfeldt, D. A. Vallera, and J. S. Miller. 2020. Potent Cytolytic Activity and Specific IL15 Delivery in a 2nd Generation Trispecific Killer Engager. *Cancer Immunology Research* 8: 1139-1149
25. Gauthier, L., A. Morel, N. Anceriz, B. Rossi, A. Blanchard-Alvarez, G. Grondin, S. Trichard, C. Cesari, M. Sapet, F. Bosco, H. Rispaud-Blanc, F. Guillot, S. Cornen, A. Roussel, B. Amigues, G. Habif, F. Caraguel, S. Arrufat, R. Remark, F. Romagné, Y. Morel, E. Narni-Mancinelli, and E. Vivier. 2019. Multifunctional Natural Killer Cell Engagers Targeting NKp46 Trigger Protective Tumor Immunity. *Cell* 177: 1701-1713.e16.
26. Chan, W. K., S. Kang, Y. Youssef, E. N. Glankler, E. R. Barrett, A. M. Carter, E. H. Ahmed, A. Prasad, L. Chen, J. Zhang, D. M. Benson, M. A. Caligiuri, and J. Yu. 2018. A CS1-NKG2D Bispecific Antibody Collectively Activates Cytolytic Immune Cells against Multiple Myeloma. *Cancer Immunology Research* 6: 776–787.
27. Peipp, M., S. Derer, S. Lohse, M. Staudinger, K. Klausz, T. Valerius, M. Gramatzki, and C. Kellner. 2015. HER2-specific immunoligands engaging NKp30 or NKp80 trigger NK-cell-mediated lysis of tumor cells and enhance antibody-dependent cell-mediated cytotoxicity. *Oncotarget* 6: 32075-32088
28. Kellner, C., A. Günther, A. Humpe, R. Repp, K. Klausz, S. Derer, T. Valerius, M. Ritgen, M. Brüggemann, J. G. van de Winkel, P. W. Parren, M. Kneba, M. Gramatzki, and M. Peipp. 2016. Enhancing natural killer cell-mediated lysis of lymphoma cells by combining therapeutic antibodies with CD20-specific immunoligands engaging NKG2D or NKp30. *OncoImmunology* 5: e1058459.
29. von Strandmann, E. P., H. P. Hansen, K. S. Reiners, R. Schnell, P. Borchmann, S. Merkert, V. R. Simhadri, A. Draube, M. Reiser, I. Purr, M. Hallek, and A. Engert. 2006. A novel bispecific protein (ULBP2-BB4) targeting the NKG2D receptor on natural killer (NK) cells and CD138 activates NK cells and has potent antitumor activity against human multiple myeloma in vitro and in vivo. *Blood* 107: 1955–1962.

30. Pende, D., S. Parolini, A. Pessino, S. Sivori, R. Augugliaro, L. Morelli, E. Marcenaro, L. Accame, A. Malaspina, R. Biassoni, C. Bottino, L. Moretta, and A. Moretta. 1999. Identification and Molecular Characterization of Nkp30, a Novel Triggering Receptor Involved in Natural Cytotoxicity Mediated by Human Natural Killer Cells. *Journal of Experimental Medicine* 190: 1505–1516.
31. Pogge von Strandmann, E., V. R. Simhadri, B. von Tresckow, S. Sasse, K. S. Reiners, H. P. Hansen, A. Rothe, B. Böll, V. L. Simhadri, P. Borchmann, P. J. McKinnon, M. Hallek, and A. Engert. 2007. Human Leukocyte Antigen-B-Associated Transcript 3 Is Released from Tumor Cells and Engages the NKp30 Receptor on Natural Killer Cells. *Immunity* 27: 965–974.
32. Simhadri, V. R., K. S. Reiners, H. P. Hansen, D. Topolar, V. L. Simhadri, K. Nohroudi, T. A. Kufer, A. Engert, and E. Pogge von Strandmann. 2008. Dendritic Cells Release HLA-B-Associated Transcript-3 Positive Exosomes to Regulate Natural Killer Function. *PLoS ONE* 3: e3377.
33. Fauriat, C., S. Just-Landi, F. Mallet, C. Arnoulet, D. Sainty, D. Olive, and R. T. Costello. 2007. Deficient expression of NCR in NK cells from acute myeloid leukemia: evolution during leukemia treatment and impact of leukemia cells in NCRdull phenotype induction. *Blood* 109: 323–330.
34. Han, B., F. Mao, Y. Zhao, Y. Lv, Y. Teng, M. Duan, W. Chen, P. Cheng, T. Wang, Z. Liang, J. Zhang, Y. Liu, G. Guo, Q. Zou, Y. Zhuang, and L. Peng. 2018. Altered NKp30, NKp46, NKG2D, and DNAM-1 Expression on Circulating NK Cells Is Associated with Tumor Progression in Human Gastric Cancer. *Journal of Immunology Research* 2018: 1–9.
35. Nieto-Velázquez, N. G., Y. D. Torres-Ramos, J. L. Muñoz-Sánchez, L. Espinosa-Godoy, S. Gómez-Cortés, J. Moreno, and M. A. Moreno-Eutimio. 2016. Altered Expression of Natural Cytotoxicity Receptors and NKG2D on Peripheral Blood NK Cell Subsets in Breast Cancer Patients. *Translational Oncology* 9: 384–391.
36. Roth, L., S. Krah, J. Klemm, R. Günther, L. Toleikis, M. Busch, S. Becker, and S. Zielonka. 2020. Isolation of Antigen-Specific VHH Single-Domain Antibodies by Combining Animal Immunization with Yeast Surface Display. *Methods Mol. Biol.* 2070: 173–189.
37. Repp, R., C. Kellner, A. Muskulus, M. Staudinger, S. Mohseni Nodehi, P. Glorius, D. Akramiene, M. Dechant, G. H. Fey, P. H. C. van Berkel, J. G. J. van de Winkel, P. W. H. I. Parren, T. Valerius, M. Gramatzki, and M. Peipp. 2011. Combined Fc-protein- and Fc-glyco-engineering of scFv-Fc fusion proteins synergistically enhances CD16a binding but does not further enhance NK-cell mediated ADCC. *Journal of Immunological Methods* 373: 67–78.
38. Kellner, C., T. Maurer, D. Hallack, R. Repp, J. G. J. van de Winkel, P. W. H. I. Parren, T. Valerius, A. Humpe, M. Gramatzki, and M. Peipp. 2012. Mimicking an Induced Self Phenotype by Coating Lymphomas with the NKp30 Ligand B7-H6 Promotes NK Cell Cytotoxicity. *The Journal of Immunology* 189: 5037–5046.
39. Schlothauer, T., S. Herter, C. F. Koller, S. Grau-Richards, V. Steinhart, C. Spick, M. Kubbies, C. Klein, P. Umaña, and E. Mössner. 2016. Novel human IgG1 and IgG4 Fc-engineered antibodies with completely abolished immune effector functions. *Protein Engineering Design and Selection* 29: 457–466.
40. Li, Y., Q. Wang, and R. A. Mariuzza. 2011. Structure of the human activating natural cytotoxicity receptor NKp30 bound to its tumor cell ligand B7-H6. *The Journal of Experimental Medicine* 208: 703–714.
41. Joyce, M. G., P. Tran, M. A. Zhuravleva, J. Jaw, M. Colonna, and P. D. Sun. 2011. Crystal structure of human natural cytotoxicity receptor NKp30 and identification of its ligand binding site. *Proceedings of the National Academy of Sciences* 108: 6223–6228.
42. Huntington, N. D., J. Cursons, and J. Rautela. 2020. The cancer–natural killer cell immunity cycle. *Nature Reviews Cancer* 20: 437–454.

43. van Hall, T., P. André, A. Horowitz, D. F. Ruan, L. Borst, R. Zerbib, E. Narni-Mancinelli, S. H. van der Burg, and E. Vivier. 2019. Monalizumab: inhibiting the novel immune checkpoint NKG2A. *Journal for ImmunoTherapy of Cancer* 7.
44. Reiners, K. S., D. Topolar, A. Henke, V. R. Simhadri, J. Kessler, M. Sauer, M. Bessler, H. P. Hansen, S. Tawadros, M. Herling, M. Krönke, M. Hallek, and E. Pogge von Strandmann. 2013. Soluble ligands for NK cell receptors promote evasion of chronic lymphocytic leukemia cells from NK cell anti-tumor activity. *Blood* 121: 3658–3665.
45. Wang, W., H. Guo, J. Geng, X. Zheng, H. Wei, R. Sun, and Z. Tian. 2014. Tumor-released Galectin-3, a Soluble Inhibitory Ligand of Human NKp30, Plays an Important Role in Tumor Escape from NK Cell Attack. *Journal of Biological Chemistry* 289: 33311–33319.
46. Schlecker, E., N. Fiegler, A. Arnold, P. Altevogt, S. Rose-John, G. Moldenhauer, A. Sucker, A. Paschen, E. P. von Strandmann, S. Textor, and A. Cerwenka. 2014. Metalloprotease-Mediated Tumor Cell Shedding of B7-H6, the Ligand of the Natural Killer Cell-Activating Receptor NKp30. *Cancer Research* 74: 3429–3440.
47. Chitadze, G., M. Lettau, J. Bhat, D. Wesch, A. Steinle, D. Fürst, J. Mytilineos, H. Kalthoff, O. Janssen, H.-H. Oberg, and D. Kabelitz. 2013. Shedding of endogenous MHC class I-related chain molecules A and B from different human tumor entities: Heterogeneous involvement of the "a disintegrin and metalloproteases" 10 and 17: Heterogeneity of MICA/B shedding. *International Journal of Cancer* 133: 1557–1566.
48. Salih, H. R., H.-G. Rammensee, and A. Steinle. 2002. Cutting Edge: Down-Regulation of MICA on Human Tumors by Proteolytic Shedding. *The Journal of Immunology* 169: 4098–4102.
49. Davis, J. H., C. Aperlo, Y. Li, E. Kurosawa, Y. Lan, K.-M. Lo, and J. S. Huston. 2010. SEEDbodies: fusion proteins based on strand-exchange engineered domain (SEED) CH3 heterodimers in an Fc analogue platform for asymmetric binders or immunofusions and bispecific antibodies. *Protein Engineering, Design and Selection* 23: 195–202.
50. Pyzik, M., T. Rath, W. I. Lencer, K. Baker, and R. S. Blumberg. 2015. FcRn: The Architect Behind the Immune and Nonimmune Functions of IgG and Albumin. *The Journal of Immunology* 194: 4595–4603.
51. Bortoletto, N., E. Scotet, Y. Myamoto, U. D'Oro, and A. Lanzavecchia. 2002. Optimizing anti-CD3 affinity for effective T cell targeting against tumor cells. *European Journal of Immunology* 32: 3102–3107.
52. Staflin, K., C. L. Zuch de Zafra, L. K. Schutt, V. Clark, F. Zhong, M. Hristopoulos, R. Clark, J. Li, M. Mathieu, X. Chen, J. Johnston, J. Low, R. Ybarra, D. Slaga, J. Yang, M. Ovacik, N. O. Dybdal, K. Totpal, M. R. Junttila, D. Ellerman, G. Lee, M. S. Dennis, R. Prell, and T. T. Junttila. 2020. Target arm affinities determine preclinical efficacy and safety of anti-HER2/CD3 bispecific antibody. *JCI Insight* 5.
53. Ellerman, D. 2019. Bispecific T-cell engagers: Towards understanding variables influencing the in vitro potency and tumor selectivity and their modulation to enhance their efficacy and safety. *Methods* 154: 102–117.
54. Vivier, E., D. H. Raulet, A. Moretta, M. A. Caligiuri, L. Zitvogel, L. L. Lanier, W. M. Yokoyama, and S. Ugolini. 2011. Innate or Adaptive Immunity? The Example of Natural Killer Cells. *Science* 331: 44–49.
55. Cao, G., J. Wang, X. Zheng, H. Wei, Z. Tian, and R. Sun. 2015. Tumor Therapeutics Work as Stress Inducers to Enhance Tumor Sensitivity to Natural Killer (NK) Cell Cytolysis by Up-regulating NKp30 Ligand B7-H6. *Journal of Biological Chemistry* 290: 29964–29973.
56. Burke, J. D., and H. A. Young. 2019. IFN-γ: A cytokine at the right time, is in the right place. *Seminars in Immunology* 43: 101280.
57. Alspach, E., D. M. Lussier, and R. D. Schreiber. 2019. Interferon γ and Its Important Roles in Promoting and Inhibiting Spontaneous and Therapeutic Cancer Immunity. *Cold Spring Harbor Perspectives in Biology* 11: a028480.

58. Ivashkiv, L. B. 2018. IFNγ: signalling, epigenetics and roles in immunity, metabolism, disease and cancer immunotherapy. *Nature Reviews Immunology* 18: 545–558.
59. Castro, F., A. P. Cardoso, R. M. Gonçalves, K. Serre, and M. J. Oliveira. 2018. Interferon-Gamma at the Crossroads of Tumor Immune Surveillance or Evasion. *Frontiers in Immunology* 9.
60. Overacre-Delgoffe, A. E., M. Chikina, R. E. Dadey, H. Yano, E. A. Brunazzi, G. Shayan, W. Horne, J. M. Moskovitz, J. K. Kolls, C. Sander, Y. Shuai, D. P. Normolle, J. M. Kirkwood, R. L. Ferris, G. M. Delgoffe, T. C. Bruno, C. J. Workman, and D. A. A. Vignali. 2017. Interferon-γ Drives T reg Fragility to Promote Anti-tumor Immunity. *Cell* 169: 1130-1141
61. Medina-Echeverz, J., L. A. Haile, F. Zhao, J. Gamrekelashvili, C. Ma, J.-Y. Métais, C. E. Dunbar, V. Kapoor, M. P. Manns, F. Korangy, and T. F. Greten. 2014. IFN-γ regulates survival and function of tumor-induced CD11b $^{+}$ Gr-1 ^{high} myeloid derived suppressor cells by modulating the anti-apoptotic molecule Bcl2a1: Immunomodulation. *European Journal of Immunology* 44: 2457–2467.
62. Groom, J. R., and A. D. Luster. 2011. CXCR3 ligands: redundant, collaborative and antagonistic functions. *Immunology & Cell Biology* 89: 207–215.
63. Melero, I., A. Rouzaut, G. T. Motz, and G. Coukos. 2014. T-Cell and NK-Cell Infiltration into Solid Tumors: A Key Limiting Factor for Efficacious Cancer Immunotherapy. *Cancer Discovery* 4: 522–526.
64. Sharma, P., and J. P. Allison. 2020. Dissecting the mechanisms of immune checkpoint therapy. *Nature Reviews Immunology* 20: 75–76.
65. Sharma, P., and J. P. Allison. 2015. The future of immune checkpoint therapy. *Science* 348: 56–61.

Table I: Biochemical characterization of immunoligands based on affinity-optimized ΔB7-H6 variants.

Identifier	KD (M)	x-fold KD improve-ment*	Kon (1/Ms)	Koff (1/s)	x-fold Koff improve-ment*	Mutations
ΔB7-H6_wt	4.09E-07	-	4.12E+05	1.68E-01	-	-
ΔB7-H6_S3#1	3.91E-08	10.5	7.54E+05	2.95E-02	5.7	S60T, F82W, L129Y
ΔB7-H6_S3#3	1.04E-07	3.9	1.05E+06	1.09E-01	1.5	S60H, V125F, L129Y
ΔB7-H6_S3#5	2.25E-08	18.2	7.99E+05	1.80E-02	9.3	S60V, F82W, L129Y
ΔB7-H6_S3#6	3.31E-08	12.4	7.37E+05	2.44E-02	6.9	S60H, F82W, L129Y
ΔB7-H6_S3#7	1.10E-07	3.7	4.78E+05	5.25E-02	3.2	S60H, F82Y, L129Y
ΔB7-H6_S3#8	8.07E-08	5.1	5.64E+05	4.55E-02	3.7	S60H, F82W, V125I
ΔB7-H6_S3#9	5.78E-08	7.1	9.70E+05	5.60E-02	3.0	S60H, L129Y
ΔB7-H6_S3#10	1.45E-07	2.8	6.89E+05	9.98E-02	1.7	F82Y, V125F, L129Y
ΔB7-H6_S3#11	3.91E-08	10.5	1.11E+06	4.32E-02	3.9	S60L, F82W, V125I, L129F
ΔB7-H6_S3#12	1.29E-07	3.2	6.71E+05	8.65E-02	1.9	S60E, L129Y
ΔB7-H6_S3#14	3.45E-08	11.9	9.33E+05	3.22E-02	5.2	S60T, F82Y, L129Y
ΔB7-H6_S3#15	1.24E-08	33.0	8.17E+05	1.01E-02	16.6	S60I, F82W, L129Y
ΔB7-H6_S3#16	2.87E-08	14.3	1.01E+06	2.89E-02	5.8	S60L, F82Y, L129Y
ΔB7-H6_S3#17	5.91E-08	6.9	9.69E+05	5.73E-02	2.9	F82Y, V125F
ΔB7-H6_S3#18	9.06E-09	45.1	1.50E+06	1.36E-02	12.4	S60Y, F82W, L129Y
ΔB7-H6_S3#19	1.46E-07	2.8	6.73E+05	9.81E-02	1.7	S60Q, F82W, L129Y
ΔB7-H6_S3#21	1.79E-08	22.8	1.18E+06	2.11E-02	8.0	S60L, F82W, L129Y
ΔB7-H6_S3#22	9.52E-08	4.3	4.63E+05	4.41E-02	3.8	S60E, F82W, L129Y
ΔB7-H6_S3#23	1.10E-07	3.7	4.79E+05	5.25E-02	3.2	S60E, F82Y, L129Y
ΔB7-H6_S3#24	1.49E-08	27.5	7.02E+05	1.04E-02	16.1	S60I, F82Y, L129Y
ΔB7-H6_S3#25	6.52E-08	6.3	7.45E+05	4.86E-02	3.5	S60W, F82Y, L129Y
ΔB7-H6_S3#26	1.13E-07	3.6	4.09E+05	4.64E-02	3.6	S60T, F82W, G83D, L129Y
ΔB7-H6_S3#27	8.30E-08	4.9	6.69E+05	5.56E-02	3.0	S60T, F82W, V125I, L129Y
ΔB7-H6_S3#28	4.43E-07	0.9	3.06E+05	1.36E-01	1.2	S60H, F82W
ΔB7-H6_S3#29	2.48E-08	16.5	7.05E+05	1.75E-02	9.6	S60V, F82W, V125I, L129Y
ΔB7-H6_S3#30	1.25E-07	3.3	6.22E+05	7.76E-02	2.2	S60E, F82W, V125I
ΔB7-H6_S3#31	4.36E-08	9.4	6.16E+05	2.69E-02	6.3	S60I, F82Y
ΔB7-H6_S2#1	2.05E-07	2.0	3.80E+05	7.80E-02	2.2	F82Y, L129Y
ΔB7-H6_S2#2	2.17E-07	1.9	3.40E+05	7.37E-02	2.3	F82W, L129Y
ΔB7-H6_S2#3	1.94E-07	2.1	5.46E+05	1.06E-01	1.6	S60T, F82W
ΔB7-H6_S2#7	1.91E-07	2.1	5.04E+05	9.64E-02	1.7	F82Y, V125I, L129Y
ΔB7-H6_S2#10	1.87E-07	2.2	5.97E+05	1.11E-01	1.5	S60L, F82W
ΔB7-H6_S2#11	2.34E-07	1.7	4.91E+05	1.15E-01	1.5	S60T, F82W
ΔB7-H6_S2#13	2.05E-07	2.0	4.10E+05	8.42E-02	2.0	F82W, L129Y
ΔB7-H6_S2#14	2.17E-07	1.9	5.70E+05	1.24E-01	1.4	S60T, L129Y
ΔB7-H6_S2#15	3.50E-07	1.2	4.01E+05	1.40E-01	1.2	S60E, F82Y

X-fold improvement values represent the improvement factor of respective overall affinities and off-rates against NKp30 compared to the ΔB7-H6 wild-type NK cell engager. Expression yields were determined post protein A purification. SEC indicates target monomer peaks as determined by analytical size exclusion chromatography. Mutations describes the incorporated amino acid exchanges of the variants compared to the ΔB7-H6 wild-type NK cell engager. All molecules were expressed as Fc immune effector silenced variants harboring the LALA-PG amino acid exchanges.

Table II: Potencies of selected EGFR-targeting, affinity-matured ΔB7-H6 immunoligands.

molecule	A431 EC_{50} with PBMC (pM)	A549 EC_{50} with PBMC (pM)	A431 EC_{50} with NK cells (pM)	A549 EC_{50} with NK cells (pM)
oa_hu225	no lysis	no lysis	no lysis	no lysis
B7-H6_wt	1839	n.a.	244.8	n.a.
B7-H6_S3#14	150.1	556.5	n.d.	n.d.
B7-H6_S3#15	**29.9**	**133.2**	**2.80**	**31.31**
B7-H6_S3#16	87.3	205.8	n.d.	n.d.
B7-H6_S3#18	**51.1**	**132.0**	**4.31**	**42.47**
B7-H6_S3#24	**39.7**	**108.3**	**3.55**	**35.19**
B7-H6_S3#25	**37.8**	**134.9**	**4.25**	**34.62**
B7-H6_S3#27	60.2	355.6	n.d.	n.d.
B7-H6_S3#29	33.6	172.3	n.d.	n.d.
B7-H6_S3#31	34.8	223.8	n.d.	n.d.

Bold = leading 4 immunoligands; underlined = best molecule in respective category; n.d. = not determined; n.a. = not applicable due to insignificant killing. All molecules were produced as Fc immune effector silenced variants harboring the LALA-PG amino acid exchanges.

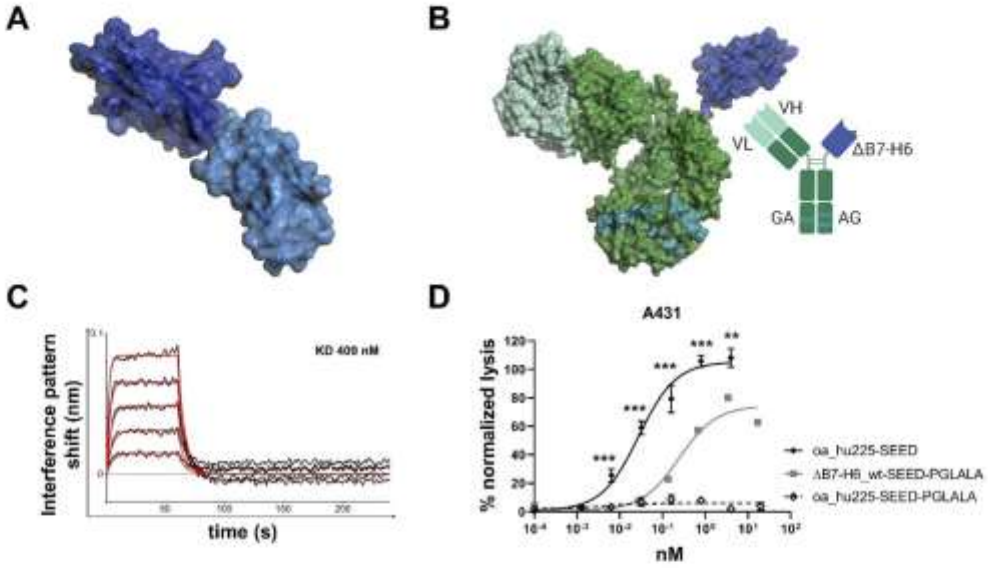

Figure 1: **B7-H6 IgV domain is sufficient to elicit NK cell-mediated tumor cell lysis. (A)** Structure of the extracellular domain of B7-H6 with *N*-terminal IgV domain colored in dark blue and IgC part depicted in light blue. Model based on pdb entry: 3pv7 and was generated with PyMOL v0.99. **(B)** Structural model (left) and scheme (right) of generated immunoligands for NK cell redirection consisting of the B7-H6 IgV domain (ΔB7-H6; dark blue) and the humanized Fab of Cetuximab (hu225) in an effector-silenced IgG1 SEED backbone comprising amino acid exchanges L234A, L235A, P329G. VH and VL colored in greencyan, antibody backbone in green, SEED GA and AG in CH3 domains indicated by deepteal coloring. Model based on pdb entries: 5dk3 and 3pv7 and constructed using PyMOL v0.99. Scheme generated with biorender (www.biorender.com). **(C)** BLI analysis of wild-type (wt) ΔB7-H6 immunoligand binding to NKp30. **(D)** Killing property of ΔB7H6_wt-SEED-PGLALA (■) was compared to one-armed (oa)_hu225-SEED activating FcγRIIIa (◆) and Fc silenced oa_hu225-SEED-PGLALA lacking the B7-H6 IgV domain (◇) as a control molecule in standard 4 h ^{51}Cr release experiments using freshly isolated human NK cells of healthy donors and A431 tumor cells in an effector-to-target cell (E:T) ratio of 10:1. Normalized percent tumor cell lysis of 3 independent experiments with different donors is shown as mean ± SEM. *** $p < 0.001$; ** $p < 0.01$ of oa_hu225-SEED vs. ΔB7-H6-SEED-PGLALA.

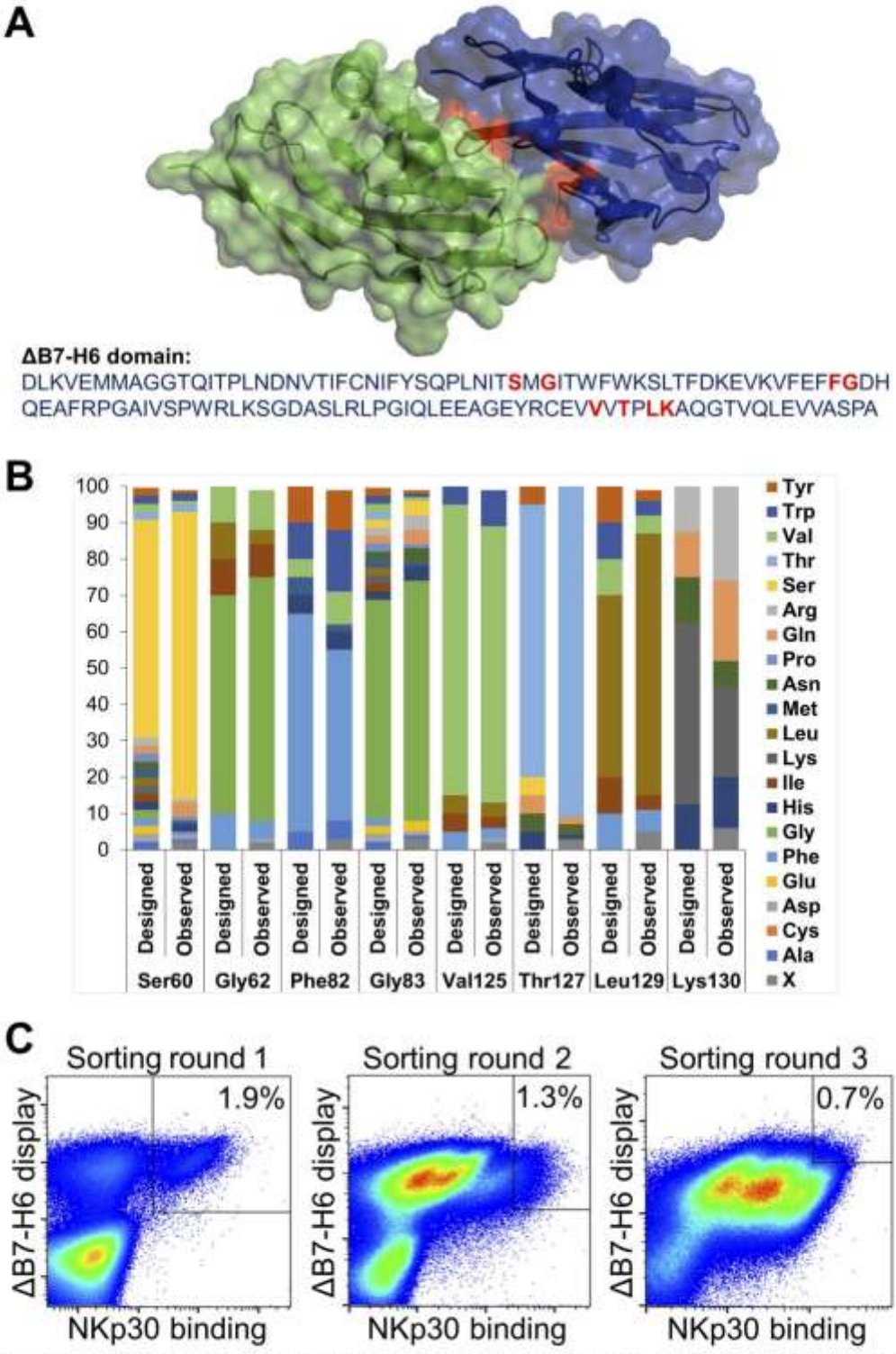

Figure 2: **Affinity maturation of ΔB7-H6 by yeast surface display. (A)** Co-crystal structure of ΔB7-H6 (blue) with NKp30 extracellular domain (green). Residues of ΔB7-H6 at the

interface with NKp30 and considered for focused randomization are colored in red. This illustration is based on pdb entry: 4ZSO and was generated using PyMOL v0.99. **(B)** Designated and observed amino acid distribution for specified positions of ΔB7-H6 as determined by sequencing of 96 clones. X, ambiguous. **(C)** FACS selection for the enrichment of affinity-improved variants of ΔB7-H6 by yeast surface display. A two-dimensional staining strategy for correctly displayed library candidates simultaneously binding to NKp30 was employed. 1 µM, 100 nM and 50 nM NKp30 were used for sorting round one, two and three, respectively, to enrich high affinity binders.

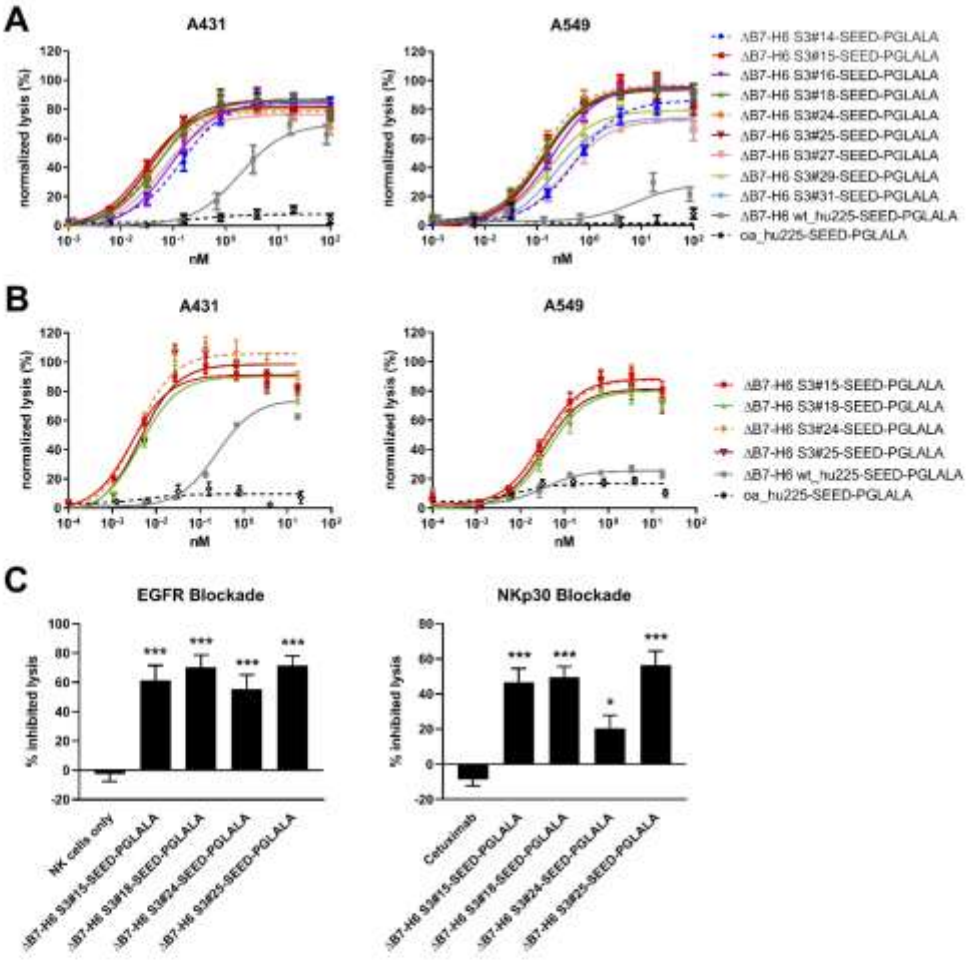

Figure 3: Cytotoxic activity of affinity-optimized ΔB7-H6-based NK cell engager. Standard 4h ^{51}Cr release assays were performed with A431 cells expressing high EGFR levels (left) and A549 cells expressing low EGFR levels (right) using human PBMCs at an E:T ratio of 80:1 **(A)** or purified NK cells at an E:T ratio of 10:1 **(B)** to analyze dose-dependent killing of the leading ΔB7-H6 SEED-PGLALA NK cell engager. The affinity-matured ΔB7-H6 variants were compared to wild-type ΔB7-H6 wt_hu225-SEED-PGLALA (grey) and a control molecule

lacking ΔB7-H6, but still binding one-armed (oa) to EGFR via the humanized Cetuximab Fab-fragment (oa_hu225-SEED-PGLALA; dotted black line). To allow comparison of the results, data of each experiment were normalized. Graphs show normalized means ± SEM of three experiments performed with PBMCs or NK cell from different donors. **(C)** Specificity of A431 lysis mediated by the leading 4 NK cell engagers (applied at 0.6 nM) was verified by either blocking EGFR binding by pre-incubation of A431 cells with 50 µg/ml of the Fc-silenced oa_hu225-SEED-PGLALA (left graph) or NKp30 binding by pre-incubation of NK cells with 50 µg/ml anti-NKp30 antibody (right graph). Graphs show percentage of inhibited lysis as means ± SEM of 4 individual experiments. *** $p < 0.001$; * $p < 0.05$ compared to NK cells only (left graph) or Cetuximab (right graph).

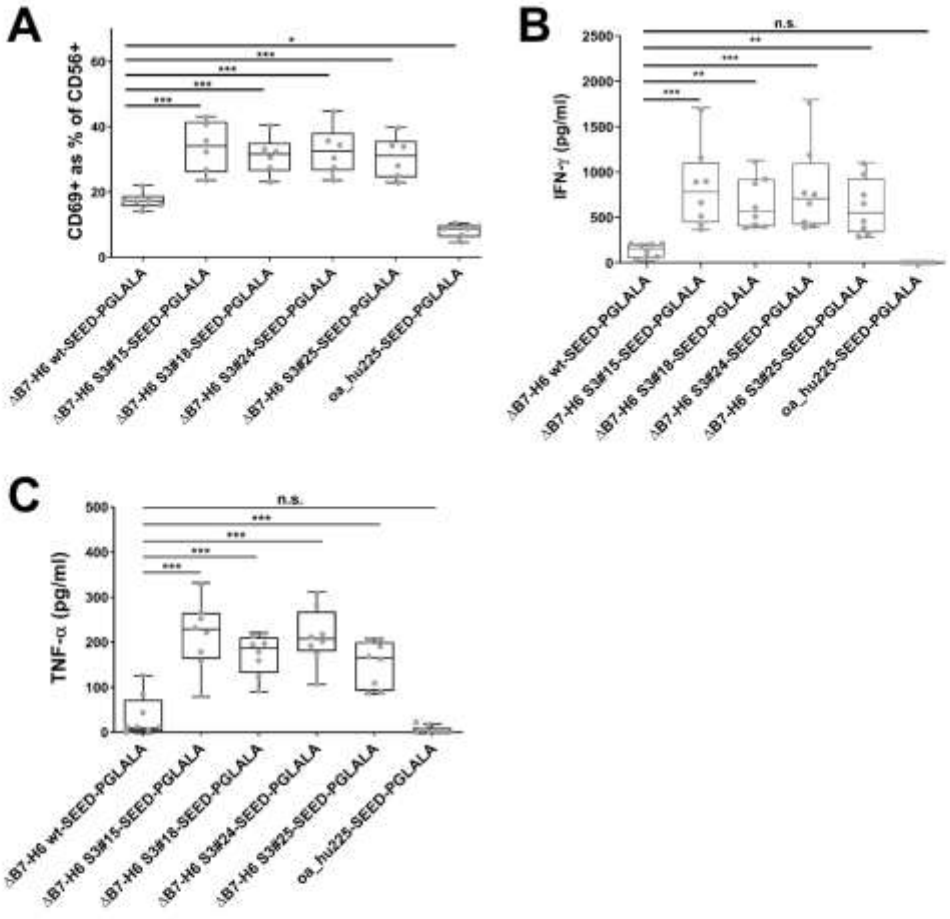

Figure 4: NK cell activation, IFN-γ and TNF-α release of the four leading ΔB7-H6 SEED-PGLALA immunoligands. Human purified NK cells were co-cultured for 24 h with A431 cells at an E:T ratio of 5:1 prior analyses of NK cell activation **(A)**, IFN-γ **(B)** and TNF-α **(C)** release. Affinity-matured ΔB7-H6 NK cell engagers and oa_hu225-SEED-PGLALA were compared to wild-type ΔB7-H6_wt-SEED-PGLALA (all at 85 nM). Percentage of CD69-positive NK cells was determined by double staining of viable NK cells with CD56-PE and

CD69-APC using flow cytometric analyses. Human cytokine HTRF kits were utilized for the quantification of IFN-γ and TNF-α release of NK cells. Graphs show box and whiskers plots as superimposition with dot plots of six **(A)** and eight **(B, C)** individual experiments, respectively. *** $p < 0.001$; ** $p < 0.01$, * $p < 0.05$, n.s. not significant compared to ΔB7-H6_wt-SEED-PGLALA.

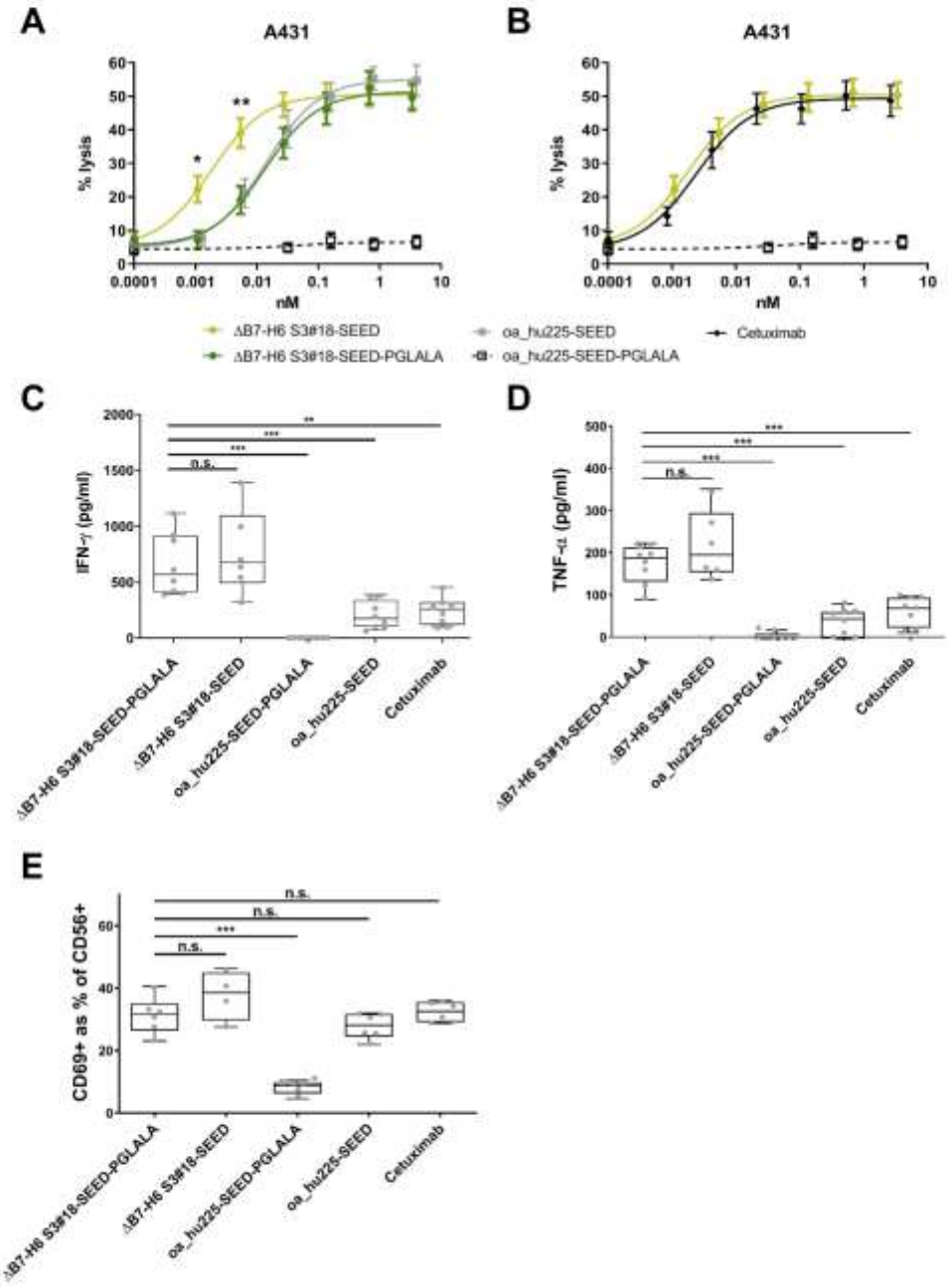

Fig. 5: Synergistic cytotoxic activity by concomitant NKp30 and FcγRIIIa engagement of ΔB7-H6-based immunoligands with functional IgG1 Fc. The highest affinity variant for NKp30 binding, S3#18, was tested in 4h ^{51}Cr release assays with A431 cells and purified NK cells at an E:T ratio of 10:1 to compare dose-dependent killing of **(A)** the Fc-silenced ΔB7-H6 S3#18-SEED-PGLALA (dark green), oa_hu225-SEED (grey) lacking ΔB7-H6 and ΔB7-H6 S3#18-SEED with a functional Fc (light green) or **(B)** Cetuximab (black) and ΔB7-H6 S3#18 SEED both carrying a functional Fc. Fc-silenced oa_hu225-SEED-PGLALA (dotted black line) lacking also ΔB7-H6 and thus NKp30 activation was used as control. Graph shows percentage of lysis as means ± SEM of 7 independent experiments. Cytokine release of IFN-γ **(C)** and TNF-α **(D)** as well as NK cell activation **(E)** for effector silenced and effector competent ΔB7-H6 S3#18-SEED molecules as well as effector silenced and effector competent oa_hu225-SEED and Cetuximab (all at 85 nM). Cytokine release was analyzed after 24 h incubation of purified NK cells with A431 cells at an E:T ratio of 5:1 with human cytokine HTRF kits. Percentage of CD69-positive NK cells was determined by double staining of viable NK cells with CD56-PE and CD69-APC using flow cytometry. Human cytokine HTRF kits were utilized for the quantification of IFN-γ and TNF-α release of NK cells. Profiles show box and whiskers plots as superimpositions with dot plots of eight independent experiments. *** $p < 0.001$; ** $p < 0.01$, * $p < 0.05$, n.s. not significant compared to the ΔB7-H6 S3#18-SEED-PGLALA.

6.5 Antibody Display Systems

Antibodies are promising tools for biomedical applications. With respect to functionality, scientists nowadays have a plethora of options to tailor-make therapeutic antibodies with prescribed properties. Besides Hybridoma technology, which is still state-of-the-art for antibody hit discovery but that also has intrinsic limitations regarding throughput, several other promising methodologies emerged. All of these have in common that they couple the phenotype i.e. the binding properties of an antibody to its genotype, the genetic information that encodes for that particular moiety. In this chapter, the reader will learn about the most commonly applied technologies for antibody hit discovery.

Authors

Janina Klemm*, **Lukas Pekar***, Simon Krah and Stefan Zielonka

*both authors contributed equally

Bibliographic information

Accepted for publication in the textbook Rüker & Wozniak-Knopp (eds)

Introduction to Antibody Engineering (publication planned Q3/2020)

DOI: 10.1007/978-3-030-54630-4

Contributions by Lukas Pekar

- Wrote the introduction together with J. Klemm and S. Zielonka
- Conduction of the literature research
- Wrote the section: *E. coli* Display
- Modified the other sections

Antibody Display Systems

4

Janina Klemm, Lukas Pekar, Simon Krah, und Stefan Zielonka

Contents

What You Will Learn in This Chapter

Antibodies are promising tools for biomedical applications. With respect to functionality, scientists nowadays have a plethora of options to tailor-make therapeutic antibodies with prescribed properties. Besides hybridoma technology, which is still state of the art for antibody hit discovery but that also has intrinsic limitations regarding throughput, several other promising methodologies emerged. All of these have in common that they couple the phenotype, i.e., the binding properties of an antibody to its genotype, the

Authors "Janina Klemm" and "Lukas Pekar" contributed equally.

J. Klemm · L. Pekar · S. Krah · S. Zielonka (✉)
Protein Engineering and Antibody Technologies, Merck Healthcare KGaA, Darmstadt, Germany
e-mail: stefan.zielonka@merckgroup.com

F. Rüker, G. Wozniak-Knopp (eds.), *Introduction to Antibody Engineering*, Learning Materials in Biosciences,
https://doi.org/10.1007/978-3-030-54630-4_4

genetic information that encodes for that particular moiety. In this chapter, the reader will learn about the most commonly applied technologies for antibody hit discovery.

Keywords

Antibody hit discovery · B-cell cloning · cDNA display · *E. coli* display · Genotype phenotype coupling · Mammalian display · Phage display · Ribosome display · Yeast surface display

4.1 Introduction

Antibodies are multifunctional components of the immune system. They facilitate numerous cellular and humoral reactions to a plethora of different antigens. Protein-based therapeutics, such as monoclonal antibodies (mAbs), have proven to be successful treatment options for patients in various indications, e.g., in cancer. Since 1986 over 80 mAb therapeutics have been granted marketing approval either in the USA or the EU [1]. In this respect, one of the most successful moieties referred to as adalimumab (Humira) was approved for arthritis therapy. Adalimumab is a human IgG1 with specificity for human tumor necrosis factor α (TNFα) and was developed by Abbott and Cambridge Antibody Technology [2]. While human antibody repertoires yield a large source for human mAbs, the search for appropriate antibodies with prescribed properties during preclinical phase remains laborious and challenging.

In general, two approaches are predominant for antibody discovery: animal immunization and surface display methodologies. Since display systems can overcome the limitations of animal immunizations due to a possible immune tolerance, different systems, based on the in vitro selection from naïve, immunized or synthetic repertoires [3], were developed over the last 30 years. Those in vitro selection platforms mimic the in vivo process in B-cell lymphocytes: the generation of genotypic diversity, the coupling of genotype to phenotype, application of selective pressure, and the amplification of desired candidates. The first description of an in vitro display technology for the selection of antibodies, namely, phage display [4], has been published in the 1990s. Since then, many antibodies have been selected or optimized with the use of display methods. To this date, several display systems were developed, where the polypeptide library is presented at the outside of the cell wall or membrane, allowing for interaction of the library candidates with the antigen. With respect to prokaryotic display systems as well as display on lower eukaryotes, typically antibody derivatives are displayed as fragments such as single chain Fv (scFv) or fragment antigen binding (Fab) since full length display of immunoglobulin G (IgG) is rather difficult.

In vitro display systems can be divided into cellular and acellular approaches. Cellular approaches, for example, yeast display, require the polypeptide libraries to be cloned and expressed from cells, whereas in acellular approaches, for example, cDNA display, expression and display is accomplished without the need for transformation or transfection. Cell-

based systems rely on the multi-copy presentation of recombinant peptide libraries linked to their coding sequence on the cell surface in functional form. Repetitions of the screening and selection process with libraries of mutants enable the isolation of variants that are improved in terms of specificity and affinity. Affinities of identified antibodies in the picomolar range [5] are frequently obtained using display technologies. In contrast to the commonly applied hybridoma-technique for the generation of mAbs [6], these in vitro methods, based on microbial systems, have the possibility to automate the selection and screening process, affording the benefit of identifying a multitude of different antibody leads against a given therapeutic target. High-throughput screening allows for the selection of clones presenting an antibody variant with the desired affinity, specificity, and stability. Besides selecting antibodies against protein epitopes, display technologies also allow screening for binders recognizing chemical modifications, small molecules, toxins, and pathogens [7]. In this chapter the reader will learn about the function, applications, advantages, and limitations of the following display systems: phage, yeast, *E. coli*, mammalian, cDNA, and ribosomal display, as well as B-cell cloning.

4.2 Phage Display

Antibody phage display was the first developed and still is the most widely applied in vitro selection technology and has enabled the generation of the first fully human therapeutic antibody [2]. This platform technology has proven to be a robust and versatile methodology for the discovery of human antibodies and allows scientist to access and the rich and diverse human antibody repertoire in vitro. Phage display is based on the work of George P. Smith on filamentous *E. coli* phage M13, where Smith fused peptides to phage envelope proteins. The fusion of gene fragments of oligopeptides to the minor coat protein III gene led to genotype-phenotype coupling and consequently enabled affinity purification of the peptide and its corresponding gene (Fig. 4.1) [8]. This groundbreaking work, together with advanced applications of phage display for antibody engineering as developed by Sir Gregory P. Winter, was awarded with the Nobel Prize in Chemistry in 2018 [9]. Nowadays different phage display systems are available, most of them based on antibody::pIII fusion proteins. In this respect, integration of the antibody::pIII encoding gene into the phage genome [10] was not as successful as the commonly used phagemid system [11]. The latter has a useful and very flexible mode of action: the separation of the antibody::pIII fusion from phage protein expression, as well as phage replication. Consequently, antibody expression is uncoupled from phage propagation by keeping the genes encoding the antibody::pIII fusion proteins on a separate plasmid (called "phagemid"). This phagemid contains a phage morphogenetic signal for packing the vector into the assembled phage particles enabling coupling of the genotype (the antibody::pIII fusion) to its phenotype (antibody expression on the phage particle). However, for the production of antibody phage particles helper phage is needed [4, 11].

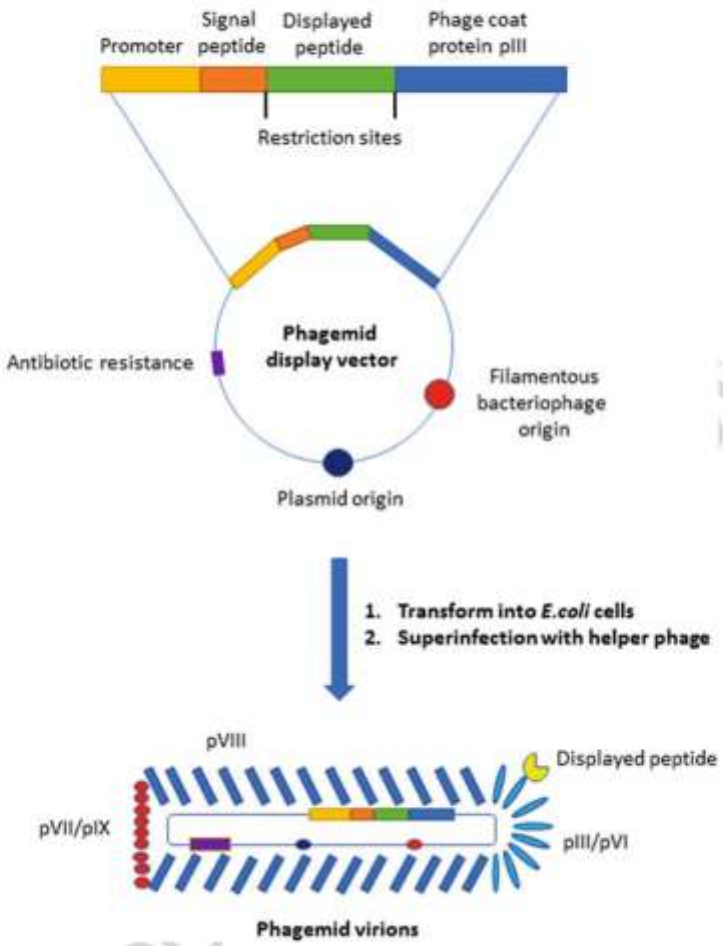

Fig. 4.1 Phage display using phagemid vectors. Typically, phagemids contain a plasmid origin of replication, a filamentous bacteriophage origin, as well as an antibiotic resistance gene for plasmid selection in *E. coli*. The library candidate is expressed as fusion protein with a phage coat protein such as pIII. A promoter enables construct expression and a signal peptide is added N-terminally. The phagemid vector is incorporated into infective phage by superinfection of phagemid bearing *E. coli* cells with helper phage. Modified from [14]

Inspired by the work on peptide phage display of G.P. Smith antibody phage display was developed independently in Heidelberg by Breitling and Dübel [11], in Cambridge by McCafferty et al. [10], and in California by Barbas et al. [4] Due to limitations of the *E. coli* folding machinery, only antibody fragments like scFv, Fab, the variable heavy domain of camels (VHH), or humans (dAb) are commonly used formats for antibody phage display [12]. The production of full-length IgG in *E. coli* remains challenging [13].

Essential sources for antibody discovery by phage display are antibody libraries, which can be divided into immune and universal libraries. Immune libraries are built from B-cells of immunized donors via vaccination or from patients suffering from disease. Furthermore, immune libraries can be built from samples of immunized animals, especially transgenic animals harboring the human antibody variable gene repertoire enable the selection of human antibodies without the need for a human donor. In medical research, immune libraries are used to generate an antibody against one target antigen, e.g., of an infectious pathogen [15]. Those libraries have the advantage that their V-genes contain hypermutations and are usually affinity maturated. The term universal or "single-pot" libraries include naïve, semi-synthetic, and synthetic libraries. In theory, they are designed to isolate antibody fragments binding to virtually every possible antigen [16]. Naïve libraries are generated from rearranged V genes of B-cells of non-immunized donors. Semi-synthetic libraries are constructed from unrearranged V genes of germline cells or from one antibody framework in which one or several complementary determining regions (CDR), most frequently CDR-H3, are randomized [17]. Fully synthetic libraries are typically made of human frameworks with randomized CDR cassettes [18].

The first step of phage display is antibody library construction, meaning cloning of the desired antibody repertoire into the phagemid in *E. coli*. Subsequently, this *E. coli* library is infected with helper phage, providing all the necessary viral components that enable single-stranded DNA replication and packaging of the phagemid DNA into phage particles. Integration of antibody genes in phage particles leads to bacteriophages displaying the encoded antibody molecule on their outside. Consequently, the phage particle can be considered as kind of a nanoparticle displaying a distinct antibody fragment on its outside while carrying its corresponding genetic information on the inside (Fig. 4.2). The next important step to obtain a specific antibody with phage display is the "panning" process, referring to the gold washer's tool. Therefore, a mix of billions of different bacteriophages, all displaying another antibody on their surface (in theory), is tested against one immobilized antigen molecule. The antigen can be immobilized on nitrocellulose [19], magnetic beads [20], column matrices [11], plastic surfaces like polystyrene tubes [21] or 96 well microtiter plates [4]. During this incubation step, physical (e.g., temperature), chemical (e.g., pH), and biological (e.g., competitor) parameters can be controlled. These settings enable the selection of antibodies, which can bind the antigen under these defined conditions. Due to washing steps with flexible applied stringencies, only those bacteriophages, displaying an antibody with required specificities and affinities, still bind the antigen while the others are removed by washing. After this step of enrichment, the bound and therewith desired bacteriophages can be eluted (e.g., by trypsination or pH shift) and are used to infect new *E. coli* cells enabling propagation of phagemids harboring enriched library candidates. Afterwards, those phagemid-containing *E. coli* cells are again infected with helper phage to produce new antibody phage particles (enriched for variants specific to the antigen), which can be used for further panning rounds. Normally two or three panning rounds, rarely up to six, are necessary to select antigen-binding antibody fragments. For the identification of individual binders, an antigen-binding ELISA analysis

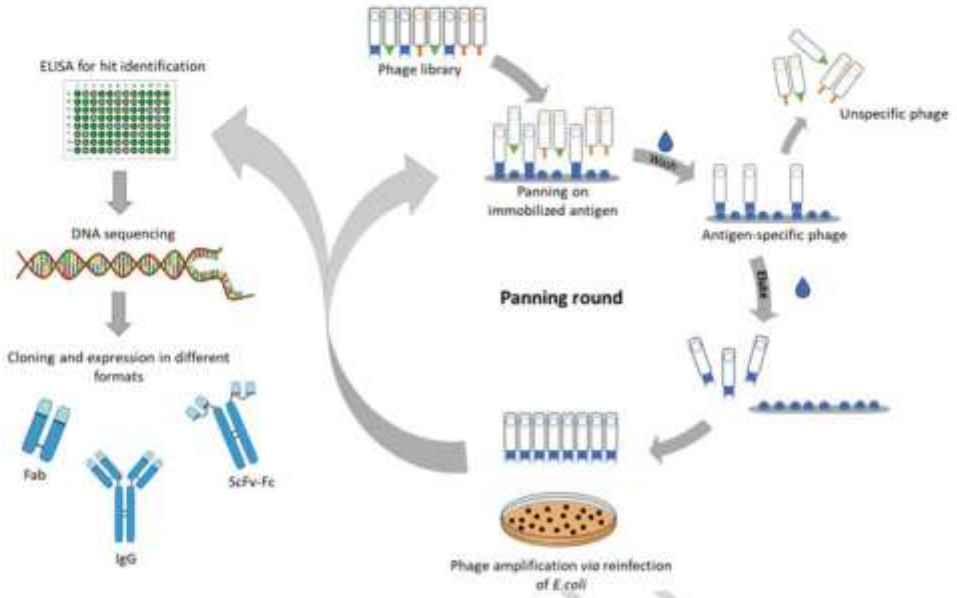

Fig. 4.2 Schematic representation of antibody phage display selection, screening, and reformatting/production. Phage library is selected for target binding, unspecific phages are removed by applying washing steps, and antigen-specific phage are eluted and amplified via reinfection of *E. coli* cells. Usually, after 2–6 panning rounds monoclonal binders are identified by ELISA, DNA-sequencing is performed and after subcloning different antibody formats can be produced. Modified from [23]

is commonly used. At this point it is possible to readout the genetic information through sequencing. Further biochemically characterizations can be performed. The panning process can also be performed in a high-throughput manner with automated screenings [22].

Initial identification of antibody candidates is often followed by an optimization step to improve affinity, stability, production yield, or other properties. Affinity maturation is an in vitro technique to evolve high-affinity ligands from polypeptide libraries. The term originates from immunology, where during a natural antibody response to an antigen, the overall affinity of circulating antibodies to the specific antigen improves. In the course of natural affinity maturation, the antibody genes of responding B-cell lymphocytes get hypermutated. Translated to antibody phage display, this means that due to gradually increasing selection stringency (e.g., decreasing antigen concentrations) only high-affinity antibodies "survive." This principle was first demonstrated by a graduate student named Jinan Yu from the lab of George P. Smith who used an affinity maturation technique to overcome the leanness of random peptides in her starting library. She introduced random mutations into the DNA inserts during the amplification step of each round of selection. At the same time, she gradually increased stringency, similar to the decline of antigen concentrations during natural affinity maturation [24]. The successful outcome of an affinity maturation campaign is a so-called "dark horse" peptide: a peptide with higher

affinity to the antigen compared to all the other clones, which have evolved from the initial peptide ancestor [25]. Another commonly used strategy is the so called light-chain-shuffling, which combines the heavy chains of a panned subset of antibodies with the whole light-chain repertoire of a naïve or synthetic library [26]. This newly generated library is then re-screened under modified conditions to obtain antibodies with improved properties.

Today the typical task of antibody research facilities is to generate antibodies to many different antigens in a high-throughput manner requiring minimal effort. To compete here, automation and miniaturization are essential. With the use of deep-screening, nowadays, one can typically analyze more than 20,000 individual clones, often resulting in more than 100 different binders. A huge improvement of efficiency was the development of hyperphage, a helper phage significantly enhancing antibody display efficiency [27]. This very elegant approach developed by Stefan Dübel and co-workers has been nicely described elsewhere [27].

At present, multiple phage display-derived mAbs are in clinical or preclinical stages of development, with several antibodies that have been granted marketing access either in the USA or the EU. The most successful phage display-derived mAbs are described in the following paragraph.

Adalimumab (marketed as Humira) was the first phage display-derived monoclonal antibody approved for therapy. It is used as a TNF-inhibiting anti-inflammatory drug and is approved by the FDA for treatment of rheumatoid arthritis, juvenile idiopathic arthritis, psoriatic arthritis, ankylosing spondylitis, Crohn's disease, ulcerative colitis, and plaque psoriasis [28–30]. In 2011 the phage display-derived antibody Belimumab, which inhibits B-cell-activating factor, was approved by the FDA. It is used for treatment of autoimmune diseases, mainly systemic lupus erythematosus [31]. Ranibizumab, FDA approved in 2006, is an antibody against VEGF-A and neutralizes its activity. The antibody was affinity matured by phage display and is used for treatment of wet age-related macular edema [32]. Another human mAb, generated with the use of phage display, was FDA approved in the year 2012: Raxibacumab, an antibody binding to the protective antigen (PA83) of *Bacillus anthracis*. Nowadays Raxibacumab is used for treatment of inhalational anthrax raised from *B. anthracis* in combination with antibacterial drugs [33]. In addition to the four herein described phage display-derived mAbs, two more (Necitumumab and Ramucirumab) entities were approved by the US authorities as of May 2016, and a plethora of antibodies is currently undergoing clinical evaluation, clearly demonstrating the versatility of phage display for antibody selection in terms of disease therapy [23].

4.3 Yeast Surface Display

The in vitro selection of human antibody fragment libraries displayed on yeast surfaces represents a well-established technology capable of generating target-specific mAbs. The most commonly used species in this strategy is *Saccharomyces cerevisiae*. This eukaryotic

organism normally uses its cell wall surface agglutinins as adhesion proteins for instance during mating events [34]. Yeast surface display (YSD) is based on the genetic fusion of an antibody fragment to such cell wall proteins, e.g., to Aga2p, as developed by Boder and Wittrup in 1997 [35, 36]. In this well-established system employing mating-related proteins Aga1p and Aga2p, the Aga2p subunit, to which the protein of interest is fused, is covalently linked to the yeast cell wall via two disulfide bonds to Aga1p [37]. The subunit Aga1p contains the glycosylphosphatidylinositol (GPI) anchor and consequently is responsible for cell wall anchoring, whereas Aga2p acts as interaction module with Aga1p [38] (Fig. 4.3).

The first step to construct yeast antibody display libraries relies in the cloning of the immunoglobulin gene pool into the yeast display plasmid [39–42] as fusion to the gene encoding for Aga2p. Using this platform technology libraries in the range of 10^7 to 10^9, unique variants can readily be obtained [37, 43]. In the most established system developed by Boder and Wittrup, the expression of both Aga1p (integrated into the yeast genome) and the mAb-Aga2p fusion construct (expressed from the display plasmid) is under the control of the galactose-inducible GAL1 promoter. The presence of galactose as carbon source (instead of glucose) enables the yeast cells to display the antibody fragment fused to Aga2p subunit on their surface [43, 44]. ScFv is the most commonly used antibody format in yeast display; however Fabs [45], whole IgG1s, and camelid antibodies [46] can be displayed as well [44].

It's been known quite well that YSD enables the obtain antigen-specific antibodies [47]. Isolation of antibody clones from yeast libraries can be performed using magnetic-assisted cell sorting (MACS) and fluorescence-activated cell sorting (FACS) [43]. MACS steps are typically used to remove nonbinding mAb fragments to reduce the number of cells for subsequent FACS selection, since throughput is the limiting factor for the latter. These MACS separations are comparable with the phage panning process and can reduce the nonreactive background by approximately 100 times [44]. After MACS-based depletion, the antigen-enriched population of yeast cells is screened by FACS in order to isolate antigen-specific library candidates (Fig. 4.4). The antigen concentration during FACS screening is often kept at tenfold excess above the desired dissociation constant (K_D) of individual clones to allow the majority of the displayed mAb fragments to bind the target at equilibrium. Implementation of epitope tags, for instance, a hemagglutinin (HA) tag or a c-myc epitope at the termini of the respective library candidate allow for immunofluorescent detection of full-length proteins that are displayed on the surface of the yeast cell. This is advantageous since it allows for getting rid of frame-shifted library candidates or candidates containing stop codons. Both malfunctioned versions of library candidates typically have a tendency for aggregation as well as unspecific binding which would result in false-positive events. The screened yeast cells are labeled for the simultaneous detection of antibody fragment expression, i.e., display on the cell surface (using, e.g., the c-myc tag) and antigen binding (using a fluorescence label on the target). During the first FACS selection round, typically the complete double-positive population is collected in order to enrich the complete antigen-specific diversity. In subsequent FACS rounds, the selection

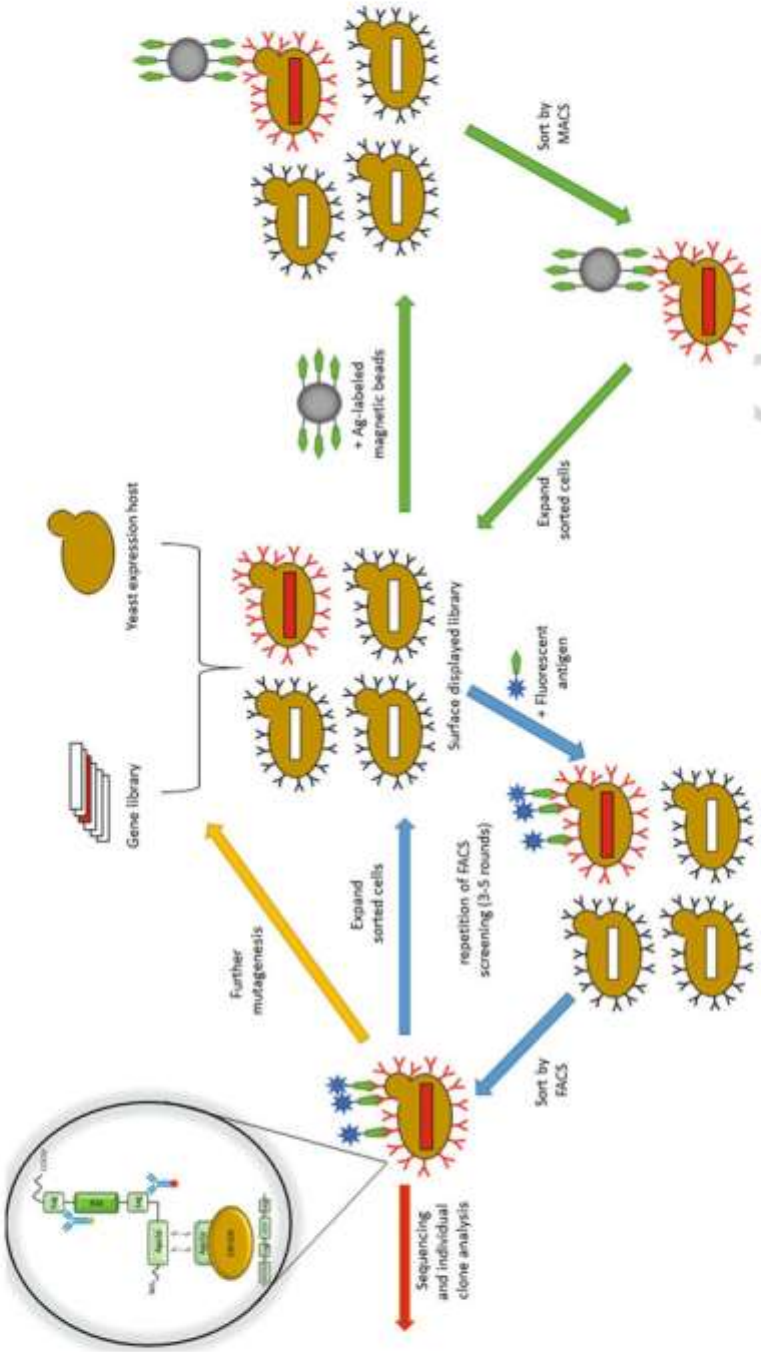

Fig. 4.3 Schematic representation of yeast display and yeast display library selection. In yeast display, the protein of interest (POI) is expressed as fusion protein with Aga2p, which upon secretion forms a covalent linkage with Aga1p that is situated on the cell surface. Tags can be included for the detection of full-length display and the POI can be fused N- or C-terminally to Aga2p. GOI, gene of interest. After library construction, the yeast display library can be either selected by MACS using antigen-coated magnetic beads or by FACS using fluorescently-labeled antigen. After a particular selection round, enriched cells are expanded and subsequently utilized for further rounds of selection. Typically, after 3–5 FACS-based selections, individual plasmids are analyzed by sequencing. Moreover, antigen-enriched cells can be further modified by mutagenesis. Modified from [44, 48]

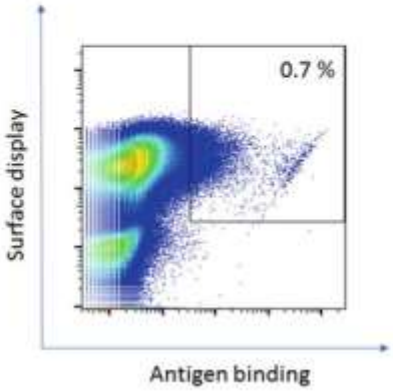

Fig. 4.4 Exemplary blot showing first round of selection of a single domain antibody library constructed from immunized camelids against a given target. The Y-axis indicates full-length surface display by antibody-mediated fluorescence labeling of a tag that has been included in plasmid design and the X-axis represents antigen binding (using a fluorescently labeled antigen). By applying a sorting gate, the double-positive population can be sorted

gate can then be adjusted to increase sorting stringency [43]. Typically, after three to five rounds of these FACS selections, the plasmid DNA of the enriched antigen binding population is collected and sent out for sequencing to obtain the genetic information for the respective paratopes. These can further be subcloned into appropriate plasmids enabling antibody expression in mammalian cells.

When comparing yeast and phage antibody library technologies, both advantages and disadvantages exist. A big advantage of yeast display is the precise control over selection parameters during FACS screening [47]. This ability to prescribe binding criteria during the FACS process represents an advantage over phage display platforms, where variant discrimination is dependent on washing steps rather than real-time kinetic observations [44]. Moreover, due to the utilization of a eukaryotic expression host with proper quality control machineries, proteins are believed to be more properly folded compared to phage display, where a prokaryotic expression host is employed [44]. However, compared to phage display, there are also some obvious drawbacks. Total library sizes using yeast libraries tend to be significantly lower (several orders of magnitude) than typical phage display library sizes. The reason therefore relies in lower transformation efficiencies observed in yeast cells. While yeast libraries with up to 10^{10} total clones can be constructed with a reasonable effort, phage libraries with more than 10^{11} variants can readily be obtained [43, 49]. Another potential disadvantage of YSD is the high number of antibody copies displayed per cell (ranges between 10^4 and 10^5 copies per cell), leading to a selection based on antibody avidity, rather than affinity (at least in theory. However, this is not true by all means, as shown in the next paragraph). Modern selection strategies make use of both yeast and phage display in combinatorial approaches. The two-system strategy takes advantage of the strengths of both technologies: the large library size and affinity-

based selections of phage display and the well-controlled isolation of variants from yeast display [50].

A conventional application of YSD is affinity maturation of antibody fragments. Wittrup and co-workers were able to demonstrate the effectiveness of YSD in protein affinity maturation with their studies on an anti-fluorescein scFv in 1997 [36]. Flow cytometry allows for the detection as well as quantification of the fluorescence signal from each yeast cell [36]. This feature allows for precise affinity measurements and rapid enrichment of high-affinity populations within mutant libraries [36, 51]. These mutant libraries are often screened with a limiting concentration of soluble antigen to select mutants having higher affinities. In this way Boder et al. developed an antibody with affinity among the highest reported so far (K_D = 48 fM) [51]. Chao et al. gave a detailed methodical protocol for affinity engineering by YSD [43]. They described the use of random mutagenesis through error-prone PCR, enabling the control of mutation frequencies by varying the number of PCR cycles [43]. Other methodologies of generating diversity, such as DNA shuffling [52], are also compatible with YSD. Besides affinity maturation of antibodies, the feasibility of this approach has been extended to T-cell receptors [53, 54]. Moreover, YSD can also be used for epitope mapping of antibodies [55].

A more recent application of YSD are cell-based selections. Shusta et al. showed that yeast cells displaying high-affinity single-chain T-cell receptors (scTCRs) can build a cell-cell complex with an antigen presenting cell (APC) [56]. These results give clear evidence that the YSD can be used to screen yeast polypeptide libraries against cell surface ligands. Indeed, several reports show that such cell-based selection can be effectively performed. In this respect Wang et al. identified 34 unique antibodies binding and in some cases internalizing into rat brain endothelial cells [57]. Cell-based selections enable the identification of antibodies against complex membrane proteins, avoiding the requirement for sophisticated and difficult membrane protein expression and purification.

As of January 2020, one yeast display-derived mAb was approved by the Chinese authorities. This antibody, referred to as Sintilimab, is a fully human therapeutic entity blocking the interaction of PD-1 to PD-L1 and PD-L2 [58].

4.4 Mammalian Display

Phage display and yeast display enable the isolation of antigen-specific antibodies with desired functionalities. However, essential intrinsic properties that qualify an antibody to become a potential therapeutic such as high-level expression in mammalian cells, aggregation behavior, or accurate glycosylation (that might impact immunogenicity) can only insufficiently be controlled using microbial display technologies. To address these characteristics more adequately, mammalian-based selection systems have been developed. In this section, we aim at giving the reader an overview of some of the key principles of this selection strategy.

Mammalian cell display systems can be broadly categorized into methods employing transient protein candidate expression and those taking advantage of stable cell lines. Transient expression is a very effective way for short-term expression of proteins. Yet, it results in loss of overall DNA within the course of a few days and consequently to inefficient mid-term and long-term expression. Typically, such transient expression systems are utilized for a single round of selection followed by plasmid rescue. In contrast to this, stable integration would result in constant mid-term (and long-term) expression of library candidates. Nevertheless, stable integration is a relatively rare event and such systems are commonly used the construction of rather small libraries. Selection from large libraries using stably integrated gene expression used to be extremely inefficient [59]. With the event of modern technologies of genetic engineering and gene editing, however, huge progress has been in this respect during the last years.

Higuchi and colleagues were one of the first groups developing methods for mammalian antibody display (Fig. 4.5). They constructed a novel screening system, which allows to obtain variable region (V) genes of antigen-specific antibodies using mammalian cells as an expression host. To this end, they displayed an antibody library on the surface of COS cells by utilization of a plasmid allowing for expression of membrane-bound antibodies. In more detail, the first step was library generation, which was prepared from peripheral blood lymphocytes of a human donor vaccinated against hepatitis B surface antigen (HBsAg). mRNA extraction and cDNA synthesis were performed, followed by gene amplification of antibody variable regions via PCR and cloning into a display vector. Afterwards COS7 cells were transiently transfected. Membrane-anchoring was achieved by *in frame* genetic fusion of the antibody variant to the transmembrane domain of human thrombomodulin. The generated combinatorial library had a size of approximately 5×10^6 independent clones. In order to select for antigen-specific antibodies, the COS library was stained with biotin-labeled antigen and sorted by flow cytometry. Afterwards, plasmids were extracted from antigen-enriched cells followed by re-amplification in *E. coli* and repetition of the whole process for three rounds. Overall, this led to a 450-fold enrichment of V genes coding for HBsAg-specific antibodies. Finally, variable region genes were isolated and inserted into an expression allowing for soluble antibody expression, resulting ultimately into the isolation of four unique clones specific for HBsAg [60].

In recent years, several different technologies for mammalian display emerged. In 2009 Ho and Pastan showed that human embryonic kidney cells (HEK293T) can be used for surface display of scFvs and affinity maturation of those [61]. Moreover, Zhou et al. described the presentation of full-length antibodies on the surface of CHO cells by applying the Flp-In technology (Invitrogen). In this approach, recombinase-mediated chromosomal (stable) DNA integration was used to generate library diversity, and antibodies with significantly improved neutralizing activity and affinities could be isolated [62].

Retrocyte display, a technique where the natural expression apparatus of B-cells is exploited for retroviral B lymphocyte display, was developed in 2014 [63]. Here, libraries in the range of 10^9 clones were generated by step-wise transduction of immortalized pre-B-cells with retroviral particles carrying light chain and heavy chain diversities, respectively.

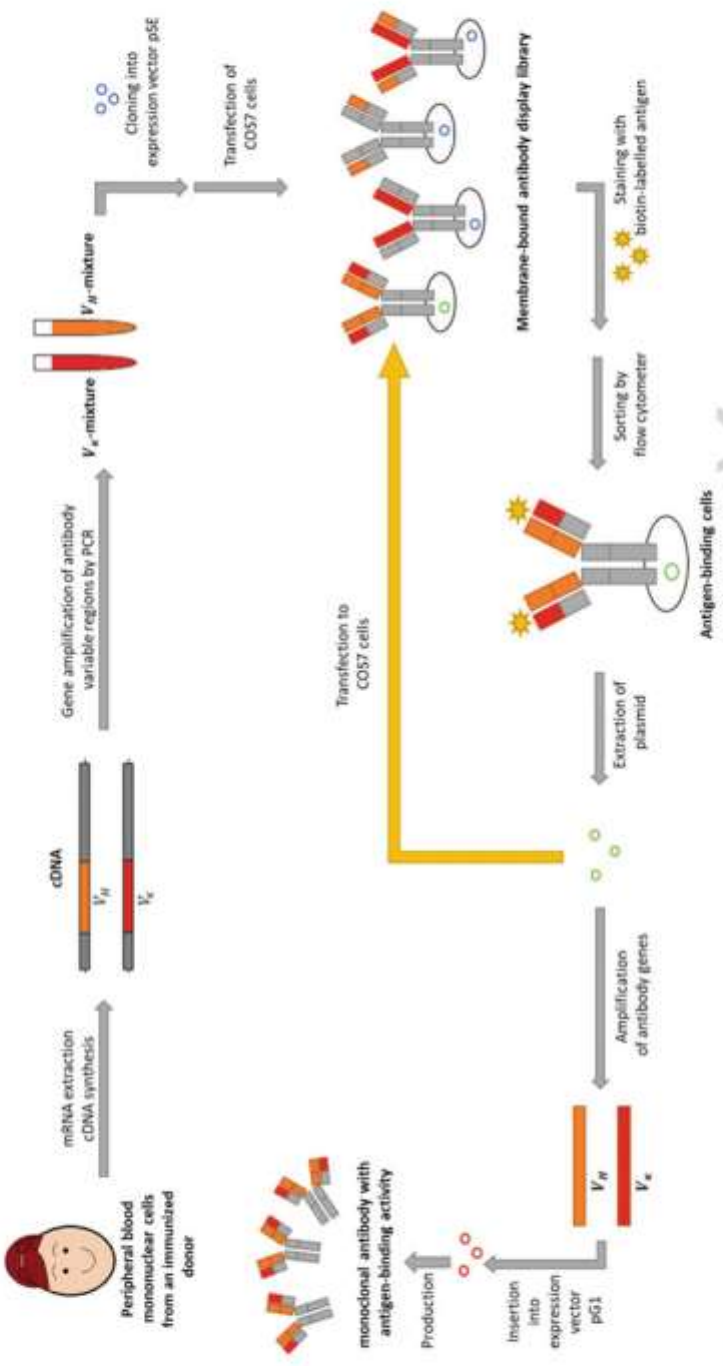

Fig. 4.5 Scheme of the preparation of a cell display library and the selection of antigen-specific antibody V genes by FACS. Messenger RNA was extracted from peripheral blood mononuclear cells of an immunized human donor. Antibody V genes were obtained from mRNA by RT-PCR and inserted into expression vector pSE. A cell display library was prepared by transfecting COS7 cells with the resultant plasmids. The library was stained with biotin-conjugated antigen followed by PE-conjugated streptavidin, and then positively stained cells were sorted by flow cytometry. Plasmids containing antigen-specific antibody V genes were recovered from the collected cells, and this enrichment process was repeated several times. Antigen-specific antibody V genes were isolated from the finally obtained plasmids and inserted into expression vector pG1 to produce monoclonal antibodies with antigen-binding activity. Modified from [60]

Besides remarkable library sizes for mammalian display, this technology is supposed to have the advantage of enhanced antibody display efficacy. This is due to the utilization of naturally antibody producing B-lineage cells with the presence of all necessary co-factors that ensure proper protein folding, antibody heavy-light chain assembly, glycosylation, and disulfide bridge formation. Besides, Beerli and co-workers described a mammalian display system relying on a Sindbis virus expression system [64]. Another technology employing viral components for mammalian display is referred to as vaccinia virus display. This virus infects most mammalian cell lines, leading to expression of recombinant genes with mammalian quality control and post-translational modification [65]. In this approach, mammalian cells were co-transduced with an antibody heavy chain library and an additional light chain library. Interestingly, the heavy chain was produced as a fusion with a vaccinia virus membrane protein. Consequently, the full-length antibody was not only expressed on the surface of the infected cell but also on the surface of the virus particle shed from the cell. Similar to phage display, this allows for "panning" of huge diversities and enrichment of antigen-specific clones. Subsequently, infected mammalian cells can be sorted by FACS enabling precise control over selection. Besides viral transduction in the context of mammalian display, libraries can also be generated using non-viral transposition technology [66].

Another fascinating system of mammalian display was described by Bowers et al. [67]. Essentially, this method makes use of the enzyme named activation-induced cytidine deaminase (AID) that is responsible for the initiation of the natural affinity maturation process in B-cells, which is referred to as somatic hypermutation [67]. In a first step, low affinity antibodies were selected against a given target and assessed for functionality. Subsequently, genes for antigen-positive antibodies were co-transfected with AID into HEK293 cells allowing for simultaneous display and affinity maturation. Ultimately, this enabled the isolation of high-affinity antibodies. Another approach focusing on a natural diversification mechanism of antibody repertoires was presented in 2005 by Ohta and co-workers [68]. Here, the authors utilized a chicken B-cell line for antibody diversification. In chickens, antibody diversity is generated in a process called gene conversion, a kind of homologous recombination. By treating the chicken B-cell line with a histone deacetylase inhibitor, the gene conversion frequency increased massively, resulting in a diversity at the immunoglobulin locus sufficient for the selection of antigen-specific antibodies. Other approaches employ CRISPR/Cas9 or TALE nucleases as tools for library construction as well as for homology-directed mutagenesis [69, 70].

In addition to the selection and affinity maturation of antigen-specific antibodies, mammalian display systems can also be utilized for the selection of functional, e.g., agonistic or antagonistic antibodies. In 2012 Lerner et al. published a new lentiviral screening method that allowed for the selection for erythropoietin agonistic antibodies. The authors first enriched antibodies specific to EpoR via phage display, followed by lentiviral library preparation. Afterwards, reporter cells were transduced with the pre-enriched lentiviral library and the phenotype, i.e., function of the antibodies was monitored

[71]. The authors further demonstrated the applicability of their studies by appropriate reporter cell engineering and by optimizing the autocrine selection system itself [72].

4.5 *E. coli* Display

Besides the often cumbersome application of eukaryotic systems, the use of prokaryotic *Escherichia coli* cells for the cell surface display of heterologous peptides offers a facile and rapid alternative. The availability of numerous genetic tools, mutant strains, and the high transformation efficiencies of *E. coli* makes it an attractive host for screening large peptide libraries. Microbial cell-surface display has many potential applications, e.g., live vaccine development, peptide library screening, antibody production in animals, bioconversion using whole cell biocatalysts, biosensor development, and bioadsorption [73]. To this end, the protein of interest to be presented, referred to as passenger protein, can be fused by N-terminal, C-terminal, or sandwich fusion to the surface anchor, the so-called carrier protein. The utilized fusion arrangement, as well as the characteristics of the carrier protein, passenger protein, and the host cell strain, affects the efficiency of surface display regarding immobilization yield, stability, specific activity, and post-translational modification of the fusion protein [73].

Unfortunately, there is no microbial equivalent of the glycosylphosphatidylinositol (GPI) anchor found in eukaryotic cells for facile display of heterologous proteins in prokaryotic cells. Thus, the carrier protein must be adjusted for each passenger protein as well as for each individual application to enable adequate transport through the inner membrane. Moreover, the carrier protein should be insusceptible for protease degradation, anchor the passenger protein reliable to the membrane, and utilize the fusion or insertion of foreign peptide sequences and therefore their proper orientation and surface presentation [73, 74].

Based on those requirements and the complex cell envelope of gram negative bacteria such as *E. coli*, most carrier proteins developed to date are based on the outer membrane proteins (Fig. 4.6), supporting the accessibility of the passenger protein [74]. These proteins comprise a plethora of different molecules, e.g., bacterial fimbriae, S-layer proteins, ice nucleation protein (INP) [75–78], protein peptidoglycan-associated lipoprotein (PAL) [79], members of the immunoglobulin A (IgA) protease family [80], *Shigella* outer membrane autotransporter protein (IcsA/VirG), and many others more (Fig. 4.6).

Combining the appropriate fusion profile with a suitable carrier protein is therefore essential for microbial surface display.

Jose et al. demonstrated, for example, the surface presentation of *Vibrio cholerae* toxin B subunit (CtxB) as a heterologous passenger via N-terminal fusion to the β domain of IgA protease which mediates the translocation due autotransporter function [80]. Another example for the N-terminal fusion arrangement was the display of alkaline phosphatase (PhoA) and maltose-binding protein (MalE) by the group of Sasakawa [81] via *Shigella* VirG protein, which is important for the deposition of filamentous actin.

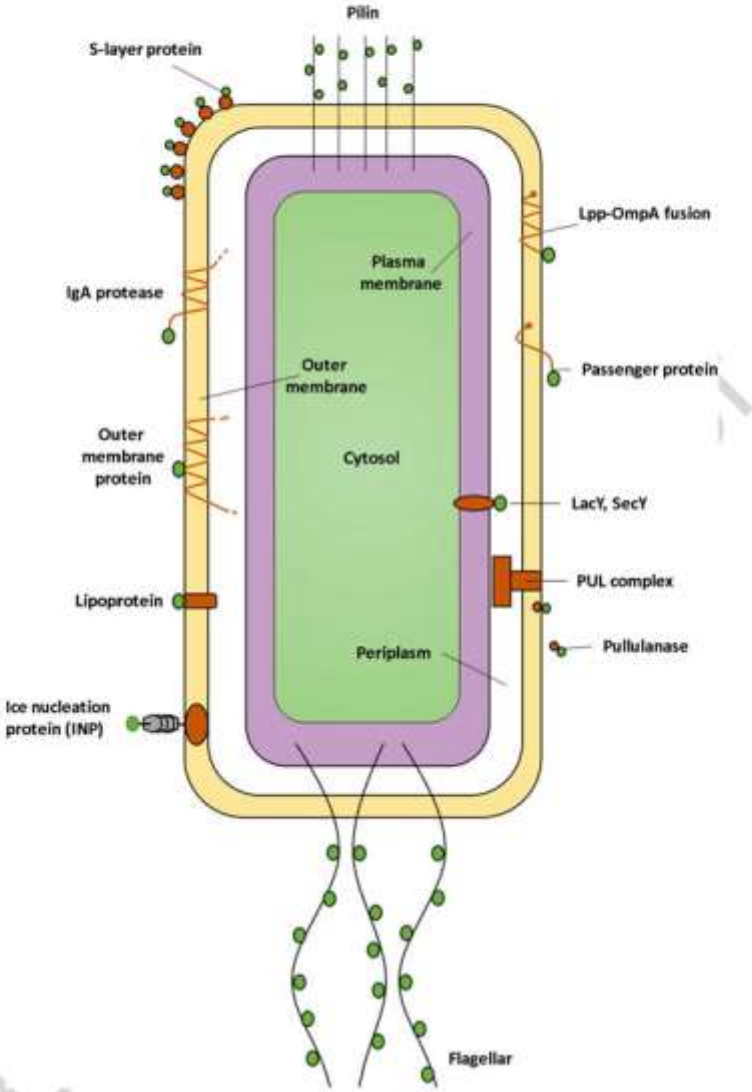

Fig. 4.6 Different surface display systems developed in Gram-negative bacteria; Modified from [73]

In contrast to that, the Lpp-OmpA-hybrid carrier system is an example for a mechanism constructed with the C-terminal fusion method. It takes advantage of the signal sequence and the first N-terminal residues of the mature *E. coli* lipoprotein and residues of the E. *coli* outer membrane protein A (OmpA). Lpp is responsible for the adequate translocalization of the fusion protein in the periplasm, whereas OmpA is necessary for crossing the outer membrane [82–85].

Despite N-terminal and C-terminal fusion, sandwich arrangement is a suitable strategy for the surface display of peptides on Gram-negative bacteria using whole structure proteins. The lack of anchoring regions does not allow for the truncation of these outer membrane proteins (OMPs), subunit proteins of extracellular extensions, and S-layer proteins (Fig. 4.6). For example, OmpC forms a transmembrane β-barrel structure spanning the outer membrane and allowing its external loops to be used as fusion sites, as shown in 1999 by Zhaohui Xu and Sang Yup Lee [74]. More recently, Bessette et al. developed a system based on a surface-exposed loop of *E. coli* OmpA allowing rapid isolation of high-affinity protein-binding peptides. Using sequential MACS and FACS analysis, proteins with high binding affinities (K_D in the low nanomolar range) for a variety of distinct antigens (e.g., streptavidin and HIV-1 GP120) could be isolated straightforward [86].

One of the major drawbacks of the microbial display system was the difficulty in presenting complex structures such as antibodies.

In 2008 Georgiou and colleagues addressed this issue by bacterial periplasmic display of so-called E-clonal mAbs [87]. Therefore, antibody heavy and light chains were secreted into the periplasm of *E. coli,* where they were properly folded and assembled into aglycosylated IgGs. The antibody immobilization on the inner membrane facing the periplasm was mediated by a chrimeric NlpA-ZZ fusion protein. Permeabilization of the outer membrane resulted in spheroplast clones that could be screened via FACS for specific antigen binding.

Another approach of microbial antibody display was published in 2015 by Wang and colleagues. They were able to present the neutralizing single-chain antibody VRC01 against HIV-1 infection on *E. coli* cells and showed that the engineered bacterial cells could capture HIV-1 particles and inhibit HIV-1 infection in cell culture [88]. Furthermore, in 2016 the group of Fernández isolated human fibrinogen nanobodies (VHHs) using *E. coli* display by fusing an immune library of VHH domains to the β-domain of intimin [89, 90].

As mentioned before, bacterial display systems are interesting for the development of recombinant bacterial vaccines. They consist of an avirulent bacterial or viral carrier expressing foreign passenger antigens. Bacteria, e.g., *E. coli*, are attractive candidates as carriers, because they are often strongly immunogenic and capable of colonizing host tissues. Another advantage of bacterial vaccines is their ability to express various foreign antigens in different forms (e.g., soluble, membrane bound, secreted). Moreover, surface-exposed antigens may facilitate the recognition by the immune system with bacterial lipopolysaccharides (LPS) acting as immune-adjuvants due to their immunogenicity [91]. This approach was already used in 1987 by Charbit et al. to display foreign epitopes of hepatitis B virus surface antigen on *E. coli*. Intravenous injections into rabbits and mice resulted in high titer specific antibody responses indicating a decent immune response [92]. In addition, Agterberg and colleagues immunized guinea pigs with partially purified outer membrane pore protein E (PhoE) carrying inserted epitopes from foot-and-mouth disease virus, which yielded substantial titers of neutralizing antibodies, protecting the guinea pigs completely against challenge with the virus [93].

4.6 Ribosome Display

A representative of the next generation of display technologies is ribosome display, which may overcome some limitations of cell-based display strategies by using a cell-free expression system.

One limitation of conventional cellular systems is the host's transformation efficiency, which can limit the overall number of library variants.

During ribosome display, genotype phenotype coupling is mediated by the formation of ternary antibody-ribosome-mRNA (ARM) complexes in cell extracts, without the requirement of transformation steps. The absence of a stop-codon on the mRNA leads to a stalling of the ribosome at the end of translation. The release of the polypeptide chain cannot be triggered by release factors that normally take the place of the tRNA at that position.

Thereby the individual protein of interest (e.g., an antibody fragment) is connected to its corresponding mRNA, which enables the simultaneous isolation of the functional protein and its encoding mRNA (genotype-phenotype coupling). ARM complexes are stabilized by high concentrations of magnesium ions and low temperature for several days [94]. Selection steps are performed through affinity capture with a specific ligand, e.g., bound on magnetic beads. Afterwards the mRNA is recovered as DNA by reverse transcription (RT)-PCR. Successive screening rounds allow the isolation of high-affinity antibodies. Both prokaryotic and eukaryotic ribosome display systems have been developed (Fig. 4.7) [95, 96].

The biggest advantage of ribosome display over phage display and cell surface display systems is the possibility to generate and screen larger libraries. As uncloned PCR fragments are utilized as source of diversity, libraries with 10^{12-14} members can easily be produced [97]. Restrictions are the number of functional ribosomes as well as the presence of different mRNA molecules in the reaction.

In addition, uncloned PCR fragments can be easily used to introduce new diversity during selection [98, 99]. For example, non-proofreading polymerases [100], error-prone PCR, DNase I shuffling [101, 102] and amplification of templates by PCR in the presence of dNTP-analogs such as 8-oxo-guanosine or dPTP [103] are convenient methods for diversification of the repertoire. This capability of continuously diversifying DNA followed by selection against an antigen provides an optimal system for in vitro antibody maturation and directed evolution of binding proteins [104, 105].

At last, ribosome display is also suited to display proteins that are difficult or impossible to express by cell-based systems, since cell-free systems tolerate also toxic, proteolytically sensitive, or unstable proteins.

In the following, the different types of ribosome display systems (*E. coli* S30 system, eukaryotic systems, and wheat germ system) will be described. In the first publication of ribosome display, the *E. coli* S30 system was utilized for peptide selection (Fig. 4.7). The so-called polysome display generates polysome complexes (stalled Ribosome/mRNA complexes) with chloramphenicol [106]. The isolation of polysome complexes displaying interacting peptide epitopes was performed by capture with an immobilized antibody on

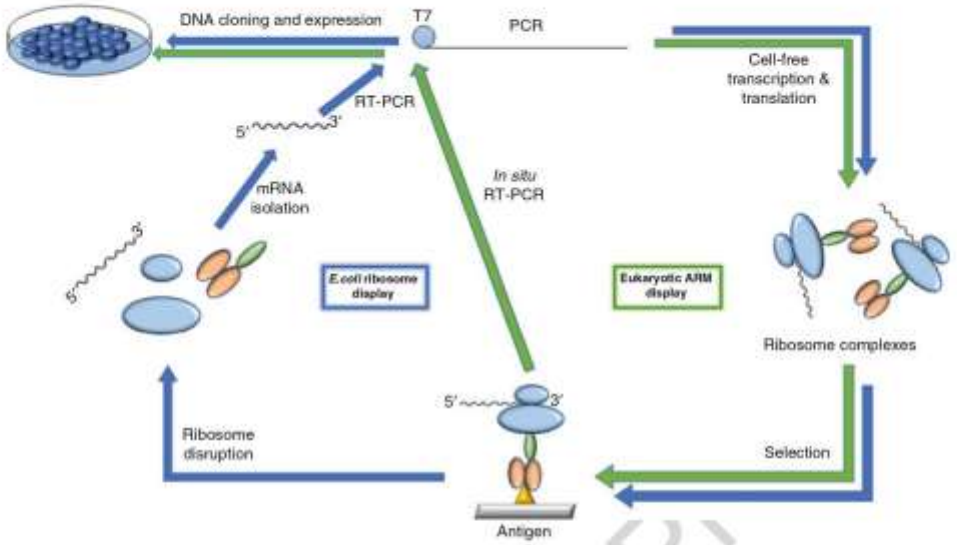

Fig. 4.7 Ribosome display cycles. *E. coli* ribosome display cycle (left side in blue) and eukaryotic ARM display cycle (right side in green). RT: reverse transcription, T7: T7 promoter, ARM: antibody-ribosome-mRNA. Modified from [95]

microtiter wells. The dissociation of the complexes was accomplished by EDTA to release the bound mRNA. Afterwards DNA recovery was performed by RT-PCR. To display single-chain antibody fragments, the system was later modified by Hanes and colleagues. They generated ARM complexes through deletion of the 3′ terminal stop codon from DNA [107]. In 2004, Sawata et al. further refined the *E. coli* S30 system by introducing a protein-mRNA interaction to generate even more stable ribosome complexes, leading to an improved selection efficiency [108].

In the meantime, a eukaryotic ribosome display system was developed for selection of single-chain antibody fragments. The coupled rabbit reticulocyte lysate system was initially termed "ARM display" (Fig. 4.7) [109]. This system also utilized the deletion of the stop codon from the DNA to generate eukaryotic ribosome complexes. A novel recovery procedure was developed, in which RT-PCR was performed directly on the ribosome complexes without the dissociation step used in former systems. For this, in situ RT-PCR primers were designed, which hybridize slightly upstream of the mRNA 3′ end, thereby preventing binding to the ribosome-covered region [109]. In situ RT-PCR facilitates automation of the entire ribosome display process.

The procedure was later modified by inclusion of oxidized/reduced glutathione and Qβ RNA-dependent RNA polymerase for improvement of protein folding and introduction of mutations [110].

Kanamori and colleagues developed a highly controllable ribosome display using the PURE (Protein synthesis Using Recombinant Elements) system in the year 2014. Herein,

ARM complexes are highly stable, and the selected mRNA can easily be recovered, because of very low nuclease activity combined with reconstitution of components such as ribosome and translation factors [111]. In 2002, a wheat germ cell-free protein synthesis system has also been developed for ribosome display of folded proteins [112].

There are some key factors affecting ribosome display, which are mentioned below. Constructs for ribosome display require a promoter such as T7 and a translation initiation sequence (Shine-Dalgarno for *E. coli* S30 system or Kozak sequence for eukaryotic systems). Furthermore, a linker of at least 23–30 amino acids in length is required at the proteins C-terminus. This generates a spacer between the ribosome and the displayed protein and abolishes steric hindrance [96]. In addition, a sequence for the hybridization of primers in RT-PCR recovery stage, as well as the incorporation of sequences containing stem-loop structures at both ends of the DNA to stabilize mRNA against degradation, is required [106]. The choice of a cell-free system may affect the formation of ribosome complexes either as monoribosome or polysome complexes, which can carry more than one ribosome translating a single mRNA molecule and can lead to avidity effects. Rabbit reticulocyte lysate can produce mainly monoribosome complexes, whereas *E. coli* S30 usually generates polysomes [95, 106]. Furthermore, cell-free systems can be divided into coupled (simpler and more efficient) and uncoupled systems. In a coupled system, transcription of the DNA template is immediately followed by translation. An uncoupled system translates mRNA, which is generated either by in vitro transcription or isolated from native sources. It allows the optimization of the transcription and translation step separately.

Ribosome display systems have been successfully applied for in vitro antibody selection, evolution, and humanization. Repeated rounds of mutation and selection led to the isolation of antibody variants with improved affinity, specificity, and stability [94, 96, 98, 113]. In 2006, Groves and colleagues could show that ribosome display is suited for affinity maturation of phage display-derived antibody populations. In addition, they compared the output of phage and ribosome display which were able to demonstrate that higher affinity antibodies were isolated using ribosome display [114]. AU4

4.7 cDNA Display

After the development of ribosome display [107] (described above) and mRNA display [115], in which the protein of interest is linked to its coding mRNA via a puromycin-linker (Pu-linker), the cDNA display technology was developed utilizing a similar strategy (Fig. 4.8). cDNA display is a powerful in vitro display technology in which complementary DNA is fused to its coding peptide or protein via a covalent puromycin linkage [116]. The technology is used to explore functional peptides and proteins from huge libraries by in vitro selection. In contrast to mRNA display, where a puromycin molecule is covalently linked to the mRNA via a DNA spacer, in cDNA display, the DNA is directly fused to the C-terminus of the peptide or protein via puromycin. This makes cDNA display more stable

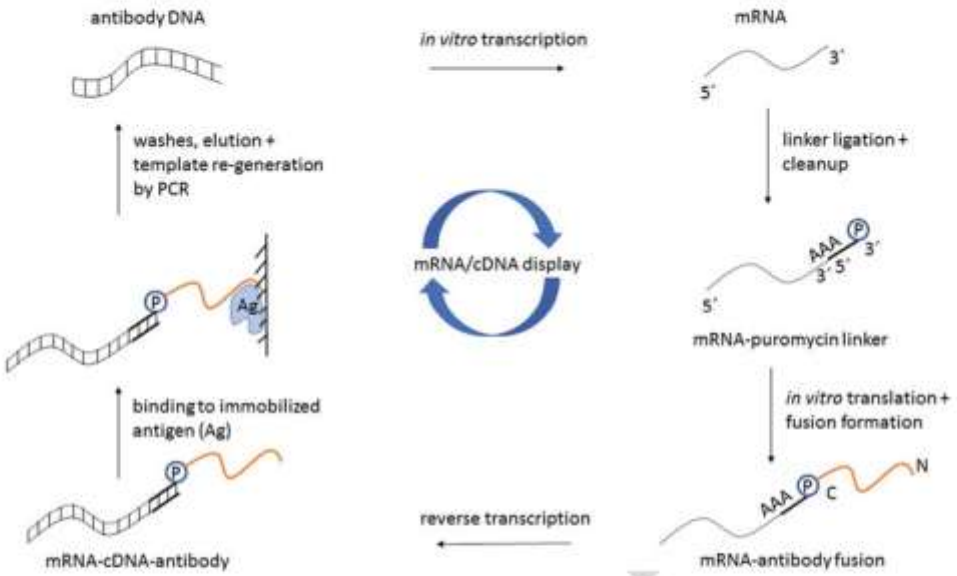

Fig. 4.8 Schematic for mRNA/cDNA display of antibodies. Antibody-encoding DNA is in vitro transcribed to mRNA and ligated to a 3′ puromycin (P) containing DNA linker. Following in vitro translation and fusion formation, reverse transcription is performed to synthesize cDNA. mRNA-cDNA-antibody complexes are exposed to the antigen (Ag) of interest, which is immobilized on a solid-phase affinity matrix. Following washes and elution, PCR is performed to retrieve antibody-encoding amplicons. N/C: N- and C-termini of displayed antibody. Modified from [118]

compared to other in vitro selection methods. Besides others, cDNA display was used for selection of peptide-based affinity reagents against cell surface proteins. For example, peptides binding to G protein-coupled receptors (GPCRs) could be selected, using cells with high GPCR expression [117].

cDNA display was further refined during the last years, especially the Pu-linker technology. Mochizuki, Ueno, and colleagues could improve the preparation efficiency of the cDNA display complex by developing additional Pu-linkers [119, 120] and modifying the preparation protocol [121]. These modifications make cDNA display more practical. The novel Pu-linker, developed by the same group., contains 3-cyanovinylcarbazole nucleoside (cnvK) and is called the cnvK-Pu-linker. cnvK is an ultrafast photo-cross-linker using UV irradiation to connect hybridized oligonucleotides, which enables ultrafast cross-linking without the use of an enzymatic ligation reaction [122]. Furthermore, cDNA display can be used as screening method for functional disulfide-rich peptides by solid-phase synthesis, promoting protein folding. Yamaguchi and colleagues could select novel peptides against the interleukin-6 receptor, containing multiple disulfide bonds [116].

4.8 B-Cell Cloning

Similar to hybridoma technology, single B-cell technologies retain the natural heavy and light chain pairing of immunized B-cells. However, in contrast to hybridoma that has the disadvantage of low fusion efficacies resulting in inadequate diversity sampling and the potential loss of rare but specific antibodies, an efficient mining of the immunized B-cell population is enabled by single cell B-cell cloning [123, 124]. Generally, this platform technology comprises of several consecutive steps, i.e., detection of (antigen-specific) B-cells within a population of different cells (e.g., splenocytes, lymphocytes, or PBMCs), amplification of the variable regions of the heavy chain and the light chain from selected single B-cells, cloning into expression vectors, antibody production, and characterization (Fig. 4.9). Single B-cell isolation can either be performed randomly (i.e., without selecting for antigen specificity) or in an antigen-selective manner. Techniques for the isolation of B cells in randomly comprise but are not limited to cell picking by micromanipulation [125], laser capture microdissection, [126] and FACS [127, 128]. Alternatively, single B-cell isolation in an antigen-selective manner has been described with the use of antigen-coated magnetic beads [129], fluorochrome-labeled antigens via multi-parameter FACS [130], the hemolytic plaque assay, [131] and a fluorescent foci method [132]. One of the most commonly applied techniques for the isolation of antigen-specific B-cells is fluorescence-activated cell sorting. Here, a multi-parameter labeling strategy is typically employed: On the one hand, fluorescently labeled antibodies against surface markers of B-cells (such as CD19) are utilized to gate for the specific B-cell population within the tissue sample. On the other hand, a fluorescently labeled antigen allows for the isolation of antigen-positive B cells. Single B-cell technologies have been elegantly reviewed by Rashidian and Lloyd [133].

Tiller et al. developed a highly efficient strategy to generate monoclonal antibodies from human B-cells at different stages of development based on surface marker expression [128]. Antibodies targeting different surface markers of B-cells and labeled with different fluorescence dyes allowed to discriminate between subpopulations of B-cells at different stages of development. A nested RT-PCR approach on sorted B-cells allowed for the amplification of heavy chain as well as light chain variable regions, followed by cloning into appropriate expression plasmids, antibody production, and characterization.

Starkie and co-workers described an efficient strategy for the isolation of antigen-specific antibodies from immunized mice [123]. Here, B-cells from the spleen were first enriched by MACS using anti-mouse CD45R microbeads. Afterwards, a multi-parameter staining strategy involving fluorescently labeled antibodies targeting different mouse isotypes such as IgG, IgM, and IgD as well as antibodies targeting different surface markers of desired (B-cell) and undesired (e.g., T-cell) populations enabled the isolation of antigen-specific class-switched IgG-positive memory B-cells.

In 2017, Carbonetti et al. described an efficient mAb discovery platform that combines single B-cell selection as well as B-cell cultivation [135]. Initially, after immunization of mice, spleens were harvested, homogenized to single cell suspension, and MACS was

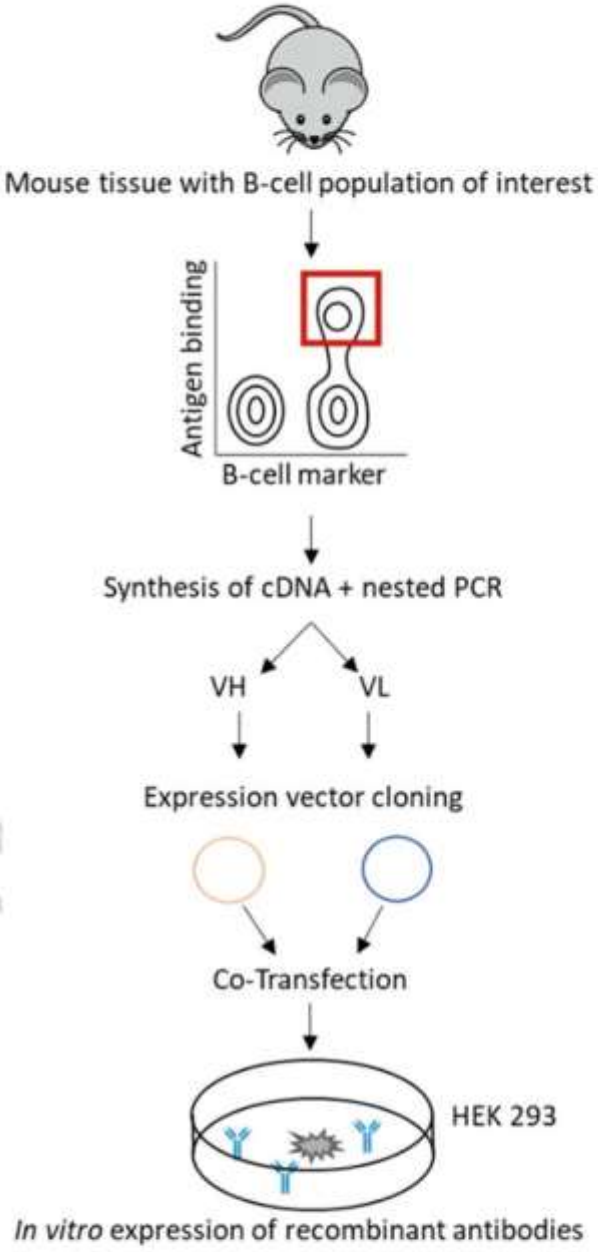

Fig. 4.9 Schematic representation of the B-cell cloning technology from immunized mice. Single B-cells isolated from mouse tissues are sorted by FACS. After reverse transcription, VH and VL genes are amplified from sorted single B-cell cDNA in independent PCRs. Subsequently, variable regions are cloned into expression vectors comprising constant antibody regions. For production of monoclonal antibodies, expression vectors can be con-transfected into mammalian cells such as HEK 293. Modified from [134]

employed for the enrichment of B-cell populations. A multi-parameter labeling strategy was further applied for FACS-based sorting of antigen-positive cells. Subsequently, isolated B-cells were co-cultured with CD40L-positive feeder cells as well as supportive cytokines for the induction of proliferation and mAb production. Antibody-containing

supernatants were then assessed with respect to reactivity. Afterwards, positive cells were harvested for RNA isolation, variable gene amplification, cloning, and antibody expression.

Besides the selection of antigen-specific B-cells using different methodologies with varying levels of complexities [136–140], also methods for the selection of mAbs from plasma cells have been described. Plasma cells are differentiated B-cells that secrete antibodies (in fact, they are responsible for producing immunoglobulins in the blood circulation). However, plasma cells normally do not express the antibody moiety on their surface, a fact that makes the isolation of antigen-specific plasma cells rather complicated. In this respect, Lightwood and co-workers described a method referred to as fluorescent foci method [141]. This fluorescence-based system was performed on microscope slides with the use of a micromanipulator device for isolation of antigen-specific IgG secreting cells. Here, IgG-secreting cells were mixed with a solid phase antigen as well as with a FITC-labeled anti-Fcγ-specific antibody and plated as a monolayer on glass slides. Antigen-specific plasma cells secreting the desired antibody were visualized through the formation of a FITC-based halo surrounding the cell. This is because the secreted specific antibodies bind the antigen in the direct surrounding of the antigen-specific plasma cell, allowing for labeling with the Fcγ-targeting detection moiety.

Recent progress in microfluidic systems enabled new strategies in single-cell technology with significant advantages in terms of phenotypic screenings for antibodies with desired properties (e.g., total assay volumes in a small range allowing to obtain detectable concentrations of secreted antibodies from single cells). Nowadays, reactions can be compartmentalized in droplets surrounded by oil or air. The droplets typically shaped in a very uniform size (typically between 10 and 200 μm in diameter) contain all assay reagents needed as well as a single cell to be characterized. In this way thousands of individual compartments can be generated per second. The generated droplets can be sorted according to fluorescence signals in an automated fashion via fluorescence-activated droplet sorting (FADS), enabling phenotypic screening of hundreds of samples per second. The technology overcomes the need for any slow mechanical equipment such as micromanipulators. Furthermore, the approach should also be applicable to non-immortalized primary B-cells, because no cell proliferation is required. In addition to the phenotypic screens, next-generation sequencing (NGS)-based approaches can be exploited to gather information about antibody binding. Those approaches are called "Ig-seq" [142]. DeKosky and colleagues developed an entirely emulsion-based technology, where single B-cells were encapsulated in water-in-oil droplets. The technology allowed the sequencing of repertoires of more than 2×10^6 B-cells in a single experiment [143]. In the near to mid-term future, microfluidics might ultimately allow to screen B-cells from humans to generate highly specific therapeutics. Screenings will become more efficient by the use of highly advanced devices for single cell manipulation, which can be rapidly automated and remotely controlled. In this respect, several services and devices from different companies are available [124, 144, 145].

4.9 Take Home Message

- Antibody display systems enable the identification of antibodies with prescribed properties from huge repertoires.
- The key feature that facilitates the selection of a favored library candidate relies in coupling the phenotype (i.e., the antibody protein) to its genotype (i.e., the DNA encoding for the entity).
- The most frequently used technology is phage display that enabled the generation or isolation of multiple marketed antibody derivatives.
- Yeast surface display emerged as another platform technology that has proven to be successful for antibody hit discovery and engineering.
- In recent years several different mammalian display systems were developed that make use of higher eukaryotic quality control machineries.
- B-cell cloning can be considered as the most natural form of genotype phenotype coupling utilizing the native protein production and secretion apparatus of antibody producing cells.

References

1. Kaplon H, Reichert JM. Antibodies to watch in 2019. MAbs. 2019;11:219–38.
2. Rau R. Adalimumab (a fully human anti-tumour necrosis factor α monoclonal antibody) in the treatment of active rheumatoid arthritis: the initial results of five trials. Ann Rheum Dis. 2002;61:70–3.
3. Hoogenboom HR. Selecting and screening recombinant antibody libraries. Nat Biotechnol. 2005;23:1105–16.
4. Barbas CF, Kang AS, Lerner RA, Benkovic SJ. Assembly of combinatorial antibody libraries on phage surfaces: the gene III site. Proc Natl Acad Sci U S A. 1991;88:7978–82.
5. Yang WP, et al. CDR walking mutagenesis for the affinity maturation of a potent human anti-HIV-1 antibody into the picomolar range. J Mol Biol. 1995;254:392–403.
6. Köhler G, Milstein C. Continuous cultures of fused cells secreting antibody of predefined specificity. Nature. 1975;256:495.
7. Bradbury ARM, Sidhu S, Mccafferty J, Alamos L. Beyond natural antibodies: the power of in vitro display technologies. Nat Biotechnol. 2011;29:245–54.
8. Smith GP. Filamentous fusion phage: novel expression vectors that display cloned antigens on the virion surface. Science. 1985;228:1315–7.
9. Arnold FH and Smith GP. Nobel prize in chemistry: 2018 press release. 50005 (2018).
10. McCafferty J, Griffiths AD, Winter G, Chiswell DJ. Phage antibodies: filamentous phage displaying antibody variable domains. Nature. 1990;348:552–4.
11. Breitling F, Dübel S, Seehaus T, Klewinghaus I, Little M. A surface expression vector for antibody screening. Gene. 1991;104:147–53.
12. Hust M, Dübel S. Phage display vectors for the in vitro generation of human antibody fragments. In: Burns R, editor. Immunochemical protocols: Humana Press; 2005. p. 71–96. https://doi.org/10.1385/1-59259-873-0:071.
13. Mazor Y, Van Blarcom T, Mabry R, Iverson BL, Georgiou G. Isolation of engineered, full-length antibodies from libraries expressed in *Escherichia coli*. Nat Biotechnol. 2007;25:563–5.

14. Naqid I. Investigation of antibody-based immune recognition of infections with *Salmonella enterica* serovars Typhimurium and Enteritidis. (2017).
15. Clackson T, Hoogenboom HR, Griffiths AD, Winter G. Making antibody fragments using phage display libraries. Lett to Nat. 1991;352
16. Hust M, Dübel S. Mating antibody phage display with proteomics. Trends Biotechnol. 2004;22:8–14.
17. Pini A, et al. Design and use of a phage display library. J Biol Chem. 1998;273:21769–76.
18. Knappik A, et al. Fully synthetic human combinatorial antibody libraries (HuCAL) based on modular consensus frameworks and CDRs randomized with trinucleotides. J Mol Biol. 2000;296:57–86.
19. Hawlisch H, et al. Site-specific anti-c3a receptor single-chain antibodies selected by differential panning on cellulose sheets. Anal Biochem. 2001;293:142–5.
20. Moghaddam A, et al. Identification of scFv antibody fragments that specifically recognise the heroin metabolite 6-monoacetylmorphine but not morphine. J Immunol Methods. 2003;280:139–55.
21. Hust M, Maiss E, Jacobsen HJ, Reinard T. The production of a genus-specific recombinant antibody (scFv) using a recombinant potyvirus protease. J Virol Methods. 2002;106:225–33.
22. Buckler DR, Park A, Viswanathan M, Hoet RM, Ladner RC. Screening isolates from antibody phage-display libraries. Drug Discov Today. 2008;13:318–24.
23. Frenzel A, Schirrmann T, Hust M. Phage display-derived human antibodies in clinical development and therapy. MAbs. 2016;8:1177–94.
24. Yu J, Smith GP. Affinity maturation of phage-displayed peptide ligands. In: Methods in enzymology, vol. 267: Academic Press; 1996. p. 3–27.
25. Smith GP. Phage display: simple evolution in a Petri dish (Nobel lecture). Angew Chemie Int Ed. 2019;58:14428–37.
26. Kang AS, Jones TM, Burton DR. Antibody redesign by chain shuffling from random combinatorial immunoglobulin libraries. Proc Natl Acad Sci U S A. 1991;88:11120–3.
27. Rondot S, Koch J, Breitling F, Dübel S. A helper phage to improve single-chain antibody presentation in phage display. Nat Biotechnol. 2001;19:75–8.
28. Kaymakcalan Z, et al. Comparisons of affinities, avidities, and complement activation of adalimumab, infliximab, and etanercept in binding to soluble and membrane tumor necrosis factor. Clin Immunol. 2009;131:308–16.
29. Schirrmann T, Meyer T, Schütte M, Frenzel A, Hust M. Phage display for the generation of antibodies for proteome research, diagnostics and therapy. Molecules. 2011;16:412–26.
30. Nelson AL, Dhimolea E, Reichert JM. Development trends for human monoclonal antibody therapeutics. Nat Rev Drug Discov. 2010;9:767–74.
31. Baker KP, et al. Generation and characterization of LymphoStat-B, a human monoclonal antibody that antagonizes the bioactivities of B lymphocyte stimulator. Arthritis Rheum. 2003;48:3253–65.
32. Steinbrook R. Treatment of macular degeneration. October 1409–1412 (2006).
33. Mazumdar S. Raxibacumab. MAbs. 2009;1:531–8.
34. Lipkel PN, Kurjan J. Agglutination. Jpn J Med Mycol. 2016;57:125.
35. Cherf GM, Cochran JR. Applications of yeast surface display for protein engineering. Methods Mol Biol. 2015:155–75.
36. Boder ET, Wittrup KD. Yeast surface display for screening combinatorial polypeptide libraries. Nat Biotechnol. 1997;15:553–7.
37. Gera N, Hussain M, Rao BM. Protein selection using yeast surface display. Methods. 2013;60:15–26.

38. Huang G, Zhang M, Erdman SE. Posttranslational modifications required for cell surface localization and function of the fungal adhesin Aga1p. Eukaryot Cell. 2003;2:1099–114.
39. Weaver-Feldhaus JM, et al. Yeast mating for combinatorial Fab library generation and surface display. FEBS Lett. 2004;564:24–34.
40. Krah S, et al. Generation of human bispecific common light chain antibodies by combining animal immunization and yeast display. Protein Eng Des Sel. 2017;30:291–301.
41. Engler C, Kandzia R, Marillonnet S. A one pot, one step, precision cloning method with high throughput capability. PLoS One. 2008;3:e3647.
42. Rosowski S, et al. A novel one-step approach for the construction of yeast surface display Fab antibody libraries. Microb Cell Factories. 2018;17:3.
43. Chao G, et al. Isolating and engineering human antibodies using yeast surface display. Nat Protoc. 2006;1:755–68.
44. Boder ET, Raeeszadeh-Sarmazdeh M, Price JV. Engineering antibodies by yeast display. Arch Biochem Biophys. 2012;526:99–106.
45. Schröter C, et al. Selection of antibodies with tailored properties by application of high-throughput multiparameter fluorescence-activated cell sorting of yeast-displayed immune libraries. Mol Biotechnol. 2018;60:727–35.
46. Roth L, et al. Isolation of antigen-specific VHH single-domain antibodies by combining animal immunization with yeast surface display. Methods Mol Biol. 2019:173–89.
47. Sheehan J, Marasco WA. Phage display and yeast display. Microbiol Spectr. 2015;3:1–12.
48. Doerner A, Rhiel L, Zielonka S, Kolmar H. Therapeutic antibody engineering by high efficiency cell screening. FEBS Lett. 2014;588:278–87.
49. Benatuil L, Perez JM, Belk J, Hsieh CM. An improved yeast transformation method for the generation of very large human antibody libraries. Protein Eng Des Sel. 2010;23:155–9.
50. Ferrara F, et al. Using phage and yeast display to select hundreds of monoclonal antibodies: application to antigen 85, a tuberculosis biomarker. PLoS One. 2012;7:e49535.
51. Boder ET, Midelfort KS, Wittrup KD. Directed evolution of antibody fragments with monovalent femtomolar antigen-binding affinity. Proc Natl Acad Sci U S A. 2000;97:10701–5.
52. Swers JS. Shuffled antibody libraries created by in vivo homologous recombination and yeast surface display. Nucleic Acids Res. 2004;32:36.
53. Holler PD, et al. In vitro evolution of a T cell receptor with high affinity for peptide/MHC. Proc Natl Acad Sci U S A. 2000;97:5387–92.
54. Weber KS, Donermeyer DL, Allen PM, Kranz DM. Class II-restricted T cell receptor engineered in vitro for higher affinity retains peptide specificity and function. Proc Natl Acad Sci U S A. 2005;102:19033–8.
55. Chao G, Cochran JR, Dane Wittrup K. Fine epitope mapping of anti-epidermal growth factor receptor antibodies through random mutagenesis and yeast surface display. J Mol Biol. 2004;342:539–50.
56. Shusta EV, Holler PD, Kieke MC, Kranz DM, Wittrup KD. Directed evolution of a stable scaffold for T-cell receptor engineering. Nat Biotechnol. 2000;18:754–9.
57. Wang X, Cho Y, Shusta E. Mining a yeast library for brain endothelial cell-binding antibodies. Nat Methods. 2007;135:612. https://doi.org/10.1038/jid.2014.371.
58. Zhang S, et al. Preclinical characterization of Sintilimab, a fully human anti-PD-1 therapeutic monoclonal antibody for cancer. Antib Ther. 2018;1:65–73.
59. Bowers PM, et al. Mammalian cell display for the discovery and optimization of antibody therapeutics. Methods. 2014;65:44–56.
60. Higuchi K, et al. Cell display library for gene cloning of variable regions of human antibodies to hepatitis B surface antigen. J Immunol Methods. 1997;202:193–204.

61. Ho M, Pastan I. Mammalian cell display for antibody engineering. In: Dimitrov AS, editor. Therapeutic antibodies: methods and protocols: Humana Press; 2009. p. 337–52. https://doi.org/10.1007/978-1-59745-554-1_18.
62. Zhou C, Jacobsen FW, Cai L, Chen Q, Shen WD. Development of a novel mammalian cell surface antibody display platform. MAbs. 2010;2:508–18.
63. Breous-Nystrom E, et al. Retrocyte Display® technology: generation and screening of a high diversity cellular antibody library. Methods. 2014;65:57–67.
64. Beerli RR, et al. Isolation of human monoclonal antibodies by mammalian cell display. Proc Natl Acad Sci U S A. 2008;105:14336–41.
65. Smith ES, Zauderer M. Antibody library display on a mammalian virus vector: combining the advantages of both phage and yeast display into one technology. Curr Drug Discov Technol. 2014;11:48.
66. Waldmeier L, et al. Transpo-mAb display: transposition-mediated B cell display and functional screening of full-length IgG antibody libraries. MAbs. 2016;8:726–40.
67. Bowers PM, et al. Coupling mammalian cell surface display with somatic hypermutation for the discovery and maturation of human antibodies. Proc Natl Acad Sci U S A. 2011;108:20455–60.
68. Seo H, et al. Rapid generation of specific antibodies by enhanced homologous recombination. Nat Biotechnol. 2005;23:731–5.
69. Mason DM, et al. High-throughput antibody engineering in mammalian cells by CRISPR/Cas9-mediated homology-directed mutagenesis. Nucleic Acids Res. 2018;46:7436–49.
70. Parthiban K, et al. A comprehensive search of functional sequence space using large mammalian display libraries created by gene editing. MAbs. 2019;11:884–98.
71. Zhang H, Wilson IA, Lerner RA. Selection of antibodies that regulate phenotype from intracellular combinatorial antibody libraries. Proc Natl Acad Sci U S A. 2012;109:15728–33.
72. Xie J, Zhang H, Yea K, Lerner RA. Autocrine signaling based selection of combinatorial antibodies that transdifferentiate human stem cells. Proc Natl Acad Sci U S A. 2013;110:8099–104.
73. Lee SY, Choi JH, Xu Z. Microbial cell-surface display. Trends Biotechnol. 2003;21:45–52.
74. Xu Z, Lee SY. Display of polyhistidine peptides on the *Escherichia coli* cell surface by using outer membrane protein C as an anchoring motif. Appl Environ Microbiol. 1999;65:5142–7.
75. Chang H, Sheu S, Lo S. Expression of foreign antigens on the surface of *Escherichia coli* by fusion to the outer membrane protein traT. J Biomed Sci. 1999:64–70.
76. Chang HH, Lo SJ. Modification with a phosphorylation tag of PKA in the TraT-based display vector of *Escherichia coli*. J Biotechnol. 2000;78:115–22.
77. Lee JS, Shin KS, Pan JG, Kim CJ. Surface-displayed viral antigens on Salmonella carrier vaccine. Nat Biotechnol. 2000;18:645–8.
78. Jung H, Lebeault J, Pan J. Surface display of Zymomonas mobilis levansucrase by using the ice-nucleation protein of Pseudomonas syringae. Nat Biotechnol. 1998;66:1124. https://doi.org/10.1271/nogeikagaku1924.66.1124.
79. Dhillon JK, Drew PD, Porter AJR. Bacterial surface display of an anti-pollutant antibody fragment. Lett Appl Microbiol. 1999;28:350–4.
80. Jose J, Krämer J, Klauser T, Pohlner J, Meyer TF. Absence of periplasmic DsbA oxidoreductase facilitates export of cysteine-containing passenger proteins to the *Escherichia coli* cell surface via the Iga(β) autotransporter pathway. Gene. 1996;178:107–10.
81. Suzuki T, Lett MC, Sasakawa C. Extracellular transport of VirG protein in Shigella. J Biol Chem. 1995;270:30874–80.
82. Chen W, Bae W, Mehra R, Mulchandani A. Enhanced bioaccumulation of heavy metals by bacterial cells with surface-displayed synthetic phytochelatins. ACS Symp Ser. 2002;806:411–8.

83. Francisco JA, Earhart CF, Georgiou G. Transport and anchoring of β-lactamase to the external surface of *Escherichia coli*. Proc Natl Acad Sci U S A. 1992;89:2713–7.
84. Francisco JA, Campbell R, Iverson BL, Georgiou G. Production and fluorescence-activated cell sorting of *Escherichia coli* expressing a functional antibody fragment on the external surface. Proc Natl Acad Sci U S A. 1993;90:10444–8.
85. Stathopoulos C, Georgiou G, Earhart CF. Characterization of *Escherichia coli* expressing an Lpp'OmpA(46-159)-PhoA fusion protein localized in the outer membrane. Appl Microbiol Biotechnol. 1996;45:112.
86. Bessette PH, Rice JJ, Daugherty PS. Rapid isolation of high-affinity protein binding peptides using bacterial display. Protein Eng Des Sel. 2004;17:731–9.
87. Mazor Y, Van Blarcom T, Iverson BL, Georgiou G. E-clonal antibodies: selection of full-length igg antibodies using bacterial periplasmic display. Nat Protoc. 2008;3:1766–77.
88. Wang L-X, et al. *Escherichia coli* surface display of single-chain antibody VRC01 against HIV-1 infection. Virology. 2015;475:179. https://doi.org/10.1016/j.cortex.2009.08.003.Predictive.
89. Salema V, López-Guajardo A, Gutierrez C, Mencía M, Fernández LÁ. Characterization of nanobodies binding human fibrinogen selected by *E. coli* display. J Biotechnol. 2016;234:58–65.
90. Salema V, Fernández LÁ. *Escherichia coli* surface display for the selection of nanobodies. Microb Biotechnol. 2017;10:1468–84.
91. Georgiou G, et al. Display of heterologous proteins on the surface of microorganisms: from the screening of combinatorial libraries to live recombinant vaccines. Nat Biotechnol. 1997;15:29–34.
92. Charbit A, et al. Presentation of two epitopes of the preS2 region of hepatitis B virus on live recombinant bacteria. J Immunol. 1987;139:1658–64.
93. Agterberg M, Adriaanse H, Barteling S, van Maanen K, Tommassen J. Protection of Guinea-pigs against foot-and-mouth disease virus by immunization with a PhoE-FMDV hybrid protein. Vaccine. 1990;8:438–40.
94. Schaffitzel C, Hanes J, Jermutus L, Plückthun A. Ribosome display: an in vitro method for selection and evolution of antibodies from libraries. J Immunol Methods. 1999;231:119–35.
95. He M, Khan F. Ribosome display: next-generation display technologies for production of antibodies in vitro. Expert Rev Proteomics. 2005;2:421–30.
96. He M, Taussig MJ. Ribosome display: cell-free protein display technology. Br Funct Genomic Proteomic. 2002;1:204.
97. Lamla T, Erdmann VA. Searching sequence space for high-affinity binding peptides using ribosome display. J Mol Biol. 2003;329:381–8.
98. Plückthun A, Schaffitzel C, Hanes J, Jermutus L. In vitro selection and evolution of proteins. In: Evolutionary protein design, vol. 55: Academic Press; 2001. p. 367–403.
99. Jermutus L, Honegger A, Schwesinger F, Hanes J, Plückthun A. Tailoring in vitro evolution for protein affinity or stability. Proc Natl Acad Sci U S A. 2001;3:29. https://doi.org/10.2116/analsci.3.29.
100. Hanes J, Jermutus L, Weber-Bornhauser S, Bosshard HR, Plückthun A. Ribosome display efficiently selects and evolves high-affinity antibodies in vitro from immune libraries. Proc Natl Acad Sci U S A. 1998;95:14130–5.
101. Cadwell RC, Joyce GF. Randomization of genes by PCR mutagenesis. Genome Res. 1992;2:28–33.
102. Stemmer W. Rapid evolution of a protein in vitro by DNA shuffling. Nature. 1994;370:389.
103. Zaccolo M, Williams DM, Brown DM, Gherardi E. An approach to random mutagenesis of DNA using mixtures of triphosphate derivatives of nucleoside analogues. J Mol Biol. 1996;255:589–603.

104. Zahnd C, Amstutz P, Plückthun A. Ribosome display: selecting and evolving proteins in vitro that specifically bind to a target. Nat Methods. 2007;4:269–79.
105. Yan X, Xu Z. Ribosome-display technology: applications for directed evolution of functional proteins. Drug Discov Today. 2006;11:911–6.
106. Mattheakis LC, Bhatt RR, Dower WJ. An in vitro polysome display system for identifying ligands from very large peptide libraries. Proc Natl Acad Sci U S A. 1994;91:9022–6.
107. Hanes J, Plückthun A. In vitro selection and evolution of functional proteins by using ribosome display. Proc Natl Acad Sci U S A. 1997;94:4937–42.
108. Sawata SY, Suyama E, Taira K. A system based on specific protein-RNA interactions for analysis of target protein-protein interactions in vitro: successful selection of membrane-bound Bak-Bcl-xL proteins in vitro. Protein Eng Des Sel. 2004;17:501–8.
109. He M, Taussig MJ. Antibody-ribosome-mRNA (ARM) complexes as efficient selection particles for in vitro display and evolution of antibody combining sites. Nucleic Acids Res. 1997;25:5132–4.
110. Forster AC, Cornish VW, Blacklow SC. Pure translation display. Anal Biochem. 2004;333:358–64.
111. Kanamori T, Fujino Y, Ueda T. PURE ribosome display and its application in antibody technology. Biochim Biophys Acta - Proteins Proteomics. 2014;1844:1925–32.
112. Takahashi F, et al. Ribosome display for selection of active dihydrofolate reductase mutants using immobilized methotrexate on agarose beads. FEBS Lett. 2002;514:106–10.
113. Lipovsek D, Plückthun A. In-vitro protein evolution by ribosome display and mRNA display. J Immunol Methods. 2004;290:51–67.
114. Groves MA, Nickson AA. Affinity maturation of phage display antibody populations using ribosome display. Methods Mol Biol. 2012;805:163–90.
115. Nemoto N, Miyamoto-Sato E, Husimi Y, Yanagawa H. In vitro virus: bonding of mRNA bearing puromycin at the 3′-terminal end to the C-terminal end of its encoded protein on the ribosome in vitro. FEBS Lett. 1997;414:405–8.
116. Yamaguchi J, et al. cDNA display: a novel screening method for functional disulfide-rich peptides by solid-phase synthesis and stabilization of mRNA-protein fusions. Nucleic Acids Res. 2009;37:e108.
117. Ueno S, et al. In vitro selection of a peptide antagonist of growth hormone secretagogue receptor using cDNA display. Proc Natl Acad Sci U S A. 2012;109:11121–6.
118. Doshi R, et al. In vitro nanobody discovery for integral membrane protein targets. Sci Rep. 2014;4
119. Mochizuki Y, et al. One-pot preparation of mRNA/cDNA display by a novel and versatile Puromycin-linker DNA. ACS Comb Sci. 2011;13:478–85.
120. Ueno S, Kimura S, Ichiki T, Nemoto N. Improvement of a puromycin-linker to extend the selection target varieties in cDNA display method. J Biotechnol. 2012;162:299–302.
121. Mochizuki Y, Kumachi S, Nishigaki K, Nemoto N. Increasing the library size in cDNA display by optimizing purification procedures. Biol Proced Online. 2013;15:1–5.
122. Mochizuki Y, Suzuki T, Fujimoto K, Nemoto N. A versatile puromycin-linker using cnvK for high-throughput in vitro selection by cDNA display. J Biotechnol. 2015;212:174–80.
123. Starkie DEO, Compson JE, Rapecki S, Lightwood DJ. Generation of recombinant monoclonal antibodies from immunised mice and rabbits via flow cytometry and sorting of antigen-specific IgG+ memory B cells. PLoS One. 2016;11:1–26.
124. Fitzgerald V, Leonard P. Single cell screening approaches for antibody discovery. Methods. 2017;116:34–42.
125. Küppers R, Zhao M, Hansmann ML, Rajewsky K. Tracing B cell development in human germinal centres by molecular analysis of single cells picked from histological sections. EMBO J. 1993;12:4955–67.

126. Obiakor H, et al. A comparison of hydraulic and laser capture microdissection methods for collection of single B cells, PCR, and sequencing of antibody VDJ. Anal Biochem. 2002;306:55–62.
127. Smith K, et al. Rapid generation of fully human monoclonal antibodies specific to a vaccinating antigen. Nat Protocol. 2009;4:372–84.
128. Tiller T, et al. Efficient generation of monoclonal antibodies from single human B cells by single cell RT-PCR and expression vector cloning. J Immunol Methods. 2008;329:112–24.
129. Lagerkvist A, Furebring C, Borrebaeck C. Single, antigen-specific B cells used to generate Fab fragments using CD40-mediated amplification or direct PCR cloning. BioTechniques. 1995:862–9.
130. Battye FL, Light A, Tarlinton DM. Single cell sorting and cloning. J Immunol Methods. 2000;243:25–32.
131. Leslie KB, Babcook JS, Qlsen OA, Salmon RA, Schrader JW. The single lymphocyte antibody method (SLAM): a novel strategy for generating monoclonal antibodies form single, isolated lymphocytes producing antibodies of defined specificities. FASEB J. 1996;10:7843–8.
132. Tickle S, et al. High-throughput screening for high affinity antibodies. J Lab Autom. 2009;14:303–7.
133. Rashidian J, Lloyd J. Single B cell cloning and production of rabbit monoclonal antibodies. Methods Mol Biol. 2020;2070:423–41.
134. Tiller T, Busse CE, Wardemann H. Cloning and expression of murine Ig genes from single B cells. J Immunol Methods. 2009;350:183–93.
135. Carbonetti S, et al. A method for the isolation and characterization of functional murine monoclonal antibodies by single B cell cloning. J Immunol Methods. 2017;176:139. https://doi.org/10.1016/j.physbeh.2017.03.040.
136. Di Niro R, et al. Rapid generation of rotavirus-specific human monoclonal antibodies from small-intestinal mucosa. J Immunol. 2010;185:5377–83.
137. Ouisse LH, et al. Antigen-specific single B cell sorting and expression-cloning from immunoglobulin humanized rats: a rapid and versatile method for the generation of high affinity and discriminative human monoclonal antibodies. BMC Biotechnol. 2017;17:3.
138. Wrammert J, et al. Rapid cloning of high-affinity human monoclonal antibodies against influenza virus. Nature. 2008;453:667–71.
139. Scheid JF, et al. Broad diversity of neutralizing antibodies isolated from memory B cells in HIV-infected individuals. Nature. 2009;458:636–40.
140. Mietzner B, et al. Autoreactive IgG memory antibodies in patients with systemic lupus erythematosus arise from nonreactive and polyreactive precursors. Proc Natl Acad Sci. 2008;105:1–6.
141. Clargo AM, et al. The rapid generation of recombinant functional monoclonal antibodies from individual, antigen-specific bone marrow-derived plasma cells isolated using a novel fluorescence-based method. MAbs. 2014;6:143–59.
142. Seah YFS, Hu H, Merten CA. Microfluidic single-cell technology in immunology and antibody screening. Mol Asp Med. 2018;59:47–61.
143. DeKosky BJ, et al. In-depth determination and analysis of the human paired heavy- and light-chain antibody repertoire. Nat Med. 2015;21:86–91.
144. Eyer K, et al. Single-cell deep phenotyping of IgG-secreting cells for high-resolution immune monitoring. Nat Biotechnol. 2017;35:977–82.
145. Winters A, et al. Rapid single B cell antibody discovery using nanopens and structured light. MAbs. 2019;11:1025–35.

6.6 Isolation of antigen-specific VHH single domain antibodies by combining animal immunization with yeast surface display

Authors

Lukas Roth, Simon Krah, Ralf Guenther, Lars Toleikis, Michael Busch, Stefan Becker and Stefan Zielonka

Bibliographic information

In *Zielonka S., Krah S. (eds) Genotype Phenotype Coupling* as part of

Methods in Molecular Biology

Volume 2070, Pages 173-189, © 2020

DOI: https://doi.org/10.1007/978-1-4939-9853-1_10

Contributions by Lukas Pekar

- Conduction of the experiments
- Wrote the introduction together with S. Krah and S. Zielonka
- Wrote the materials section
- Wrote the methods section
- Wrote the notes section
- Prepared the tables and figures

Chapter 10

Isolation of Antigen-Specific VHH Single-Domain Antibodies by Combining Animal Immunization with Yeast Surface Display

Lukas Roth, Simon Krah, Janina Klemm, Ralf Günther, Lars Toleikis, Michael Busch, Stefan Becker, and Stefan Zielonka

Abstract

In addition to conventional hetero-tetrameric antibodies, the adaptive immune repertoire of camelids comprises the so-called heavy chain-only antibodies devoid of light chains. Consequently, antigen binding is mediated solely by the variable domain of the heavy chain, referred to as VHH. In recent years, these single-domain moieties emerged as promising tools for biotechnological and biomedical applications. In this chapter, we describe the generation of VHH antibody yeast surface display libraries from immunized Alpacas and Lamas as well as the facile isolation of antigen-specific molecules in a convenient fluorescence-activated cell sorting (FACS)-based selection process.

Key words Yeast surface display, Antibody engineering, Protein engineering, Camelid antibodies, Single-domain antibodies, VHH (variable domain of the heavy chain of heavy chain-only antibodies)

1 Introduction

From a structural aspect, conventional antibodies are homodimers of heavy- and light-chain heterodimers (Fig. 1). The antigen binding site, i.e., paratope is formed by the variable domain of the heavy chain and the variable domain of the light chain. In addition to this, it's been known for quite some time that camelids and sharks produce heavy chain-only antibodies (HcAbs) [1, 2]. Such molecules are homodimeric by nature since they are composed of two heavy chains and lack light chain counterparts. Moreover, with respect to camelid-derived heavy chain-only antibodies the first constant domain CH1 that typically interacts with the constant region of the light chain is absent in these moieties (Fig. 1). Interestingly, HcAbs specifically recognize an antigen with only one variable domain, referred to as variable domain of the heavy chain of heavy chain-only antibodies (VHH) for camelid-derived

Stefan Zielonka and Simon Krah (eds.), *Genotype Phenotype Coupling: Methods and Protocols*, Methods in Molecular Biology, vol. 2070, https://doi.org/10.1007/978-1-4939-9853-1_10,

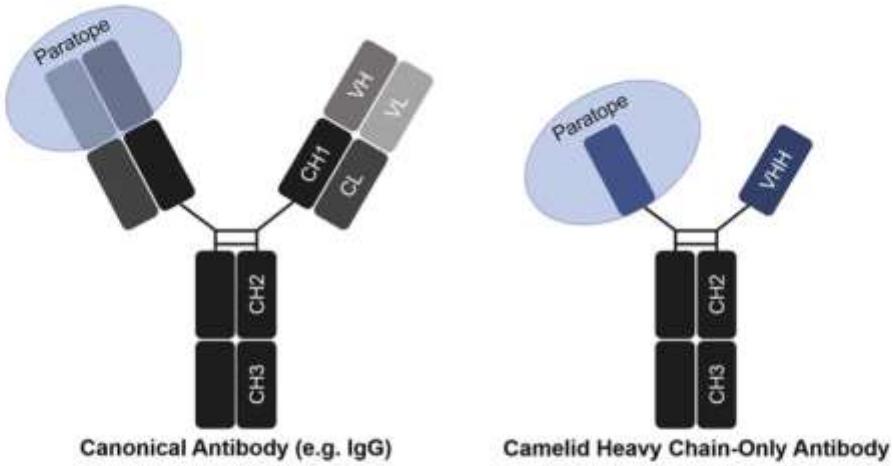

Fig. 1 Structural illustration of conventional hetero-tetrameric antibodies (left) and camelid-derived heavy chain-only antibodies

molecules [3]. This VHH domain displays several attributes making it interesting for biomedical and biotechnological applications. In this respect, complementarity determining region 3 (CDR3) is typically elongated compared to conventional antibodies [4]. This protruding loop enables engagement of epitopes that are typically not antigenic to canonical antibodies, i.e., cryptic or recessed epitopes such as catalytic clefts [5–7]. Besides, also the hypervariable region, corresponding to CDR1, is extended by four residues at the N-terminal end and is likely involved in antigen binding [3]. Moreover, camelid VHH domains are generally highly water soluble. This is due to replacements of large and hydrophobic residues by small and hydrophilic amino acids in framework region-2 that normally builds the interaction surface with the variable domain of the light chain [8, 9]. Furthermore, the surface-exposed loop of CDR3 is often connected with CDR1 or CDR2 via an additional disulfide bond [4, 10]. However, also CDR3 intraloop disulfides have been described for VHHs [11]. Camelid VHH domains share a high sequence similarity with human VH domains [3]. Notwithstanding, to reduce the potential for immunogenicity, a general strategy for humanization has been presented by Vincke and colleagues [12].

Due to their simple architecture, camelid VHH domains afford the benefit of flexible reformatting options, including bi- and multispecific constructs opening new avenues for targeting diseases [13–16]. Consequently, a plethora of different strategies have been described for the generation of antigen-specific VHH fragments, including naïve, semi-synthetic, synthetic, and immunized library approaches [17–22], and several VHH-derived molecules are currently investigated in clinical trials [4, 10, 23].

Although the vast majority of engineered VHH domains were obtained using phage display as platform technology [20, 24], it has been shown that such antigen-specific single-domain antibodies can readily be isolated using yeast surface display (YSD) [25]. Pioneered by Boder and Wittrup in 1997 [26], this genotype-phenotype coupling technology relies on the expression of the protein of interest as fusion with Aga2p mating adhesion receptor of *Saccharomyces cerevisiae*. Surface display is enabled through covalent linkage of Aga2p to Aga1p that is anchored to the cell wall. One of the major benefits of YSD is the utilization of a eukaryotic expression system comprising unfolded protein response for the degradation of misfolded or aggregated proteins [27]. Moreover, its compatibility with fluorescence-activated cell sorting (FACS) enables online and real-time analysis of individual library candidates [28].

In this chapter, we provide protocols for facile VHH library construction following Alpaca and Lama immunization as well as for the isolation of antigen-specific molecules using a FACS-based selection strategy. To this end, VHH genes are amplified from PBMC-derived cDNA in a one-step PCR and introduced into a yeast surface display vector in a homologous recombination-based process referred to as gap repair cloning. By application of a two-dimensional sorting strategy for the detection of full-length surface display as well as antigen binding, we show that target-specific VHHs can readily be obtained within two rounds of FACS selections.

2 Materials

2.1 Strains

1. *Saccharomyces cerevisiae* strain EBY100 (MATa) (URA3-52 trp1 leu2Δ1 his3Δ200 pep4::HIS3 prb1Δ1.6R can1 GAL) (pIU211:URA3).
2. *E. coli* strain Top10 (F-*mcr*A Δ(*mrr-hsd*RMS-*mcr*BC) Φ80*lacZ*ΔM15 Δ*lac*X74 *rec*A1 *ara*D139 Δ(*ara leu*) 7697 *gal*U *gal*K *rps*L (StrR) *end*A1 *nup*G).

2.2 Plasmids

Substantial features of display plasmid are schematically shown in Fig. 2. A pYD-derived backbone is used as destination vector (pDest) containing essential features, i.e., tryptophan auxotrophic marker for selection in EBY100, ampicillin resistance marker (AmpR) for selection in *E. coli*, GAL1 promoter and replication origins in *S. cerevisiae* (ARS4/CEN6) and *E. coli* (ColE1), and terminator sequences (not shown). The coding VHH region is genetically fused *in frame* to Aga2p by replacement of stuffer sequence after pDest digestion with *Bsa*I and gap repair cloning. Therefore, the VHH gene is flanked by homologous overhangs to

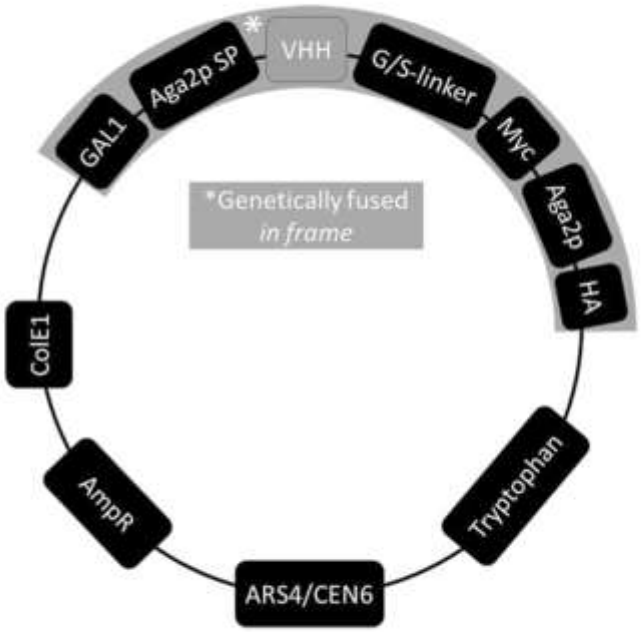

Fig. 2 Schematic illustration of generated yeast surface display plasmid. Main genetic components of the system are shown. GAL1, GAL1 promoter; Aga2 SP, Aga2 signal peptide; VHH, camelid variable domain of the heavy chain of heavy chain-only antibodies; G/S-linker, glycine-serine linker; Myc, Myc epitope; Aga2p, Aga2p cell adhesion molecule; HA, HA-tag; tryptophan, tryptophan auxotrophic marker; ARS4/CEN6, replication origin for yeast; AmpR, ampicillin resistance marker; ColE1, replication origin for *E. coli*. Illustrated features from GAL1 to HA were genetically fused in frame on the used plasmid

G/S linker as well as Aga2p signal sequence (*see* **Note 1**) facilitating homologous recombination (Fig. 3). A HA-tag is linked to Aga2p allowing for the detection of VHH surface expression.

2.3 Media

1. YPD media: Dissolve 20 g D(+)-glucose, 20 g peptone, and 10 g yeast extract in 1 l deionized H_2O. Sterilize by autoclaving. Add 10 ml of Penicillin–Streptomycin (10,000 units/ml) and remove any particles by sterile filtration using a 0.22 μm bottle top filter.
2. SD-Trp media: Dissolve 26.7 g minimal SD-Base (Clontech) in deionized H_2O and adjust volume to 890 ml. Sterilize by autoclaving. Dissolve 8.56 g $NaH_2PO_4 \times H_2O$, 5.4 g Na_2HPO_4, and 0.74 g Dropout-mix -Trp (Clontech) in deionized H_2O and adjust the volume to 100 ml. Sterilize by autoclaving. Combine both solutions, add 10 ml of Penicillin–Streptomycin (Gibco, 10,000 units/ml), and remove any particles by sterile filtration using a 0.22 μm bottle top filter.

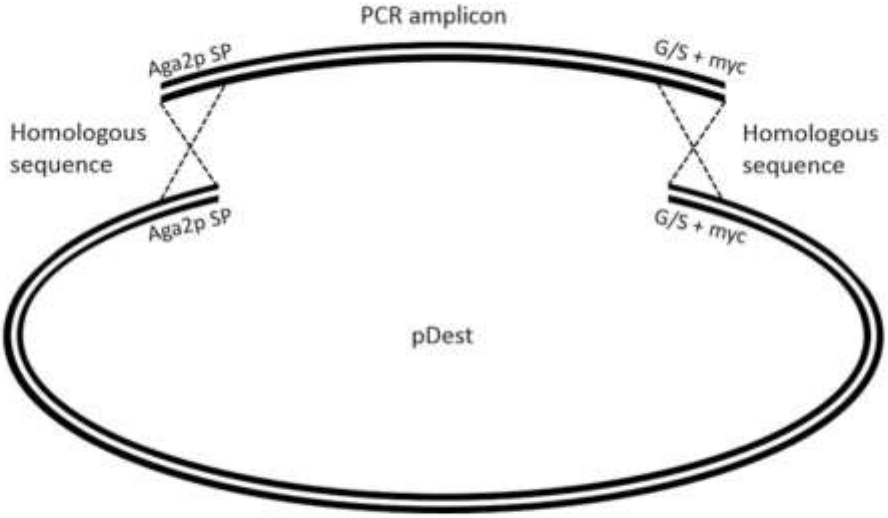

Fig. 3 Gap repair cloning scheme for generation of yeast surface display antibody libraries by homologous recombination. Restriction enzyme digested destination plasmid (pDest) and PCR amplicons with homologous overhangs are shown. Homologous regions are embedded in Aga2p signal peptide sequence and G/S-linker with joined myc-tag, respectively, facilitating homologous recombination to generate the final display plasmid

3. SD-Trp plates: Dissolve 23.35 g of minimal SD-Agar Base (Clontech) in deionized H_2O and adjust volume to 445 ml. Sterilize by autoclaving. Dissolve 4.28 g of $NaH_2PO_4 \times H_2O$, 2.7 g of Na_2HPO_4, and 0.37 g Dropout-mix -Trp in deionized H_2O and adjust the volume to 50 ml. Sterilize by autoclaving. Combine both solutions, add 10 ml of Penicillin–Streptomycin (Gibco, 10,000 units/ml), and prepare plates.
4. SG -Trp media: Dissolve 37 g of minimal SD-Base + Gal/Raf in deionized H_2O and adjust volume to 490 ml. Dissolve 8.56 g of $NaH_2PO_4 \times H_2O$, 5.4 g of Na_2HPO_4, and 0.74 g Dropout-mix -Trp in deionized H_2O and adjust the volume to 100 ml. Dissolve 110 g of PEG8000 in deionized H_2O and adjust the volume to 400 ml. Sterilize by autoclaving and combine all three solutions. Add 10 ml of Penicillin–Streptomycin (10,000 units/ml) and remove any particles by sterile filtration using a 0.22 μm bottle top filter.
5. SD Low -Trp medium: Dissolve 5 g dextrose, 6.7 g yeast nitrogen base (w/o amino acids) in deionized H_2O, and adjust volume to 890 ml. Sterilize by autoclaving. Dissolve 8.56 g $NaH_2PO_4 \times H_2O$, 5.4 g Na_2HPO_4 and 0.74 g Dropout-mix -Trp in deionized H_2O and adjust the volume to 100 ml. Sterilize by autoclaving. Combine both solutions, add 10 ml of Penicillin–Streptomycin (10,000 units/ml), and remove any particles by sterile filtration using a 0.22 μm bottle top filter.

6. Yeast library freezing solution: Dissolve 2 g of glycerol and 0.67 g of yeast nitrogen base in a volume of 100 ml deionized H_2O. Sterile filter the solution.
7. LB Amp media: Dissolve 10 g NaCl, 10 g peptone, and 5 g yeast extract in 1 l deionized water. Sterilize by autoclaving. Once the medium has chilled (to approximately 50 °C), add 1 ml of sterile filtered ampicillin solution (100 mg/ml in deionized H_2O).
8. LB Amp plates: Dissolve 10 g NaCl, 10 g peptone, 5 g yeast extract, and 15 g agar to a volume of 1 l in deionized water. Sterilize by autoclaving. When medium has chilled (to approximately 50 °C), add 1 ml of sterile filtrated ampicillin solution (100 mg/ml in deionized H_2O) and prepare plates.

2.4 Peripheral Blood Mononuclear Cell (PBMC) Isolation by Density Gradient Centrifugation

1. PBMC prep buffer: Dulbecco's phosphate-buffered saline (DPBS), 2% (v/v) fetal bovine serum (FBS).
2. Biocoll separation solution.

2.5 Total RNA Isolation from PBMCs

1. Qiashredder (Qiagen).
2. RNeasy Mini Kit (Qiagen).
3. Ethanol 70%.
4. RNase-free water.

2.6 cDNA Synthesis

1. Superscript III First-Strand Kit (Invitrogen).
2. RNase-free water.

2.7 Gene-Specific Amplification of VHH Regions

1. Q5 High-Fidelity 2× Master Mix (New England Biolabs).
2. Nuclease-free water.
3. Primer sequences for VHH gap repair cloning are given in Table 1.
4. Wizard SV gel and PCR Clean-Up System (Promega).

Table 1
Oligonucleotide primers used in this study (overhang sequences are shown in italic)

Name	Sequence (5′–3′)
VHH_fwd	*CGCTGTTTTTCAATATTTTCTGTTATTGCTAGCGTTTTAGCAGGTG*ATGTGCAGC TGCAGGAGTCTGGRGGAGG
VHH1_rev	*CAATTTTTGTTCAGAACCACCACCACCAGAACCACCACCACCGCT*GGGGTC TTCGCTGTGGTGCG
VHH2_rev	*CAATTTTTGTTCAGAACCACCACCACCAGAACCACCACCACCT*GGTTGTGG TTTTGGTGTCTTGGG

2.8 Destination Vector (pDest) Digestion

1. *Bsa*I High-Fidelity (20,000 units/ml, New England Biolabs).
2. Cut Smart Buffer 10× (New England Biolabs).
3. Nuclease-free water.
4. Wizard SV gel and PCR Clean-Up System.
5. pDest according to Subheading 2.2.

2.9 Library Transformation into S. cerevisiae Strain EBY100

1. *Bsa*I digested pDest according to Subheading 3.5.
2. VHH PCR inserts according to Subheading 3.4.
3. Electroporation buffer: 1 M Sorbitol, 1 mM $CaCl_2 \times 2H_2O$ (autoclaved).
4. LiAc buffer: 100 mM LiAc, 10 mM DTT (sterile filtered).
5. 1 M Sorbitol (autoclaved).

2.10 Yeast Surface Display and Selections Using Fluorescence-Activated Cell Sorting (FACS)

1. Dulbecco's phosphate-buffered saline (DPBS).
2. Penta-His Alexa Fluor 647 Conjugate antibody (Qiagen).
3. Anti-HA tag antibody (FITC) (abcam).
4. Target protein, his-tagged.

2.11 Equipment

1. Cryogenic vials.
2. Freezing container.
3. 0.22 μm Steriflip and Steritop filtration units.
4. Shaking flasks (150 ml–3 l volume).
5. Electroporator Gene Pulser Xcell™ (Bio-Rad).
6. 0.2 cm Electroporation Cuvettes (Bio-Rad).
7. MasterPure Yeast DNA Purification Kit (Lucigen).
8. Shaking incubator (20 °C, 30 °C, and 37 °C).
9. Flow cytometry device (i.e., cell sorter).
10. Thermocycler.
11. Device and reagents for agarose gel electrophoresis.
12. Benchtop centrifuge.
13. 9 cm Petri dishes.
14. Cell density meter.
15. BioSpec Nano or equivalent instrumentation.
16. SepMate tubes.

3 Methods

In this section, we describe the construction of large yeast surface display antibody VHH libraries following Lama or Alpaca immunization. In this particular example, two Alpacas (*Vicugna pacos*) and

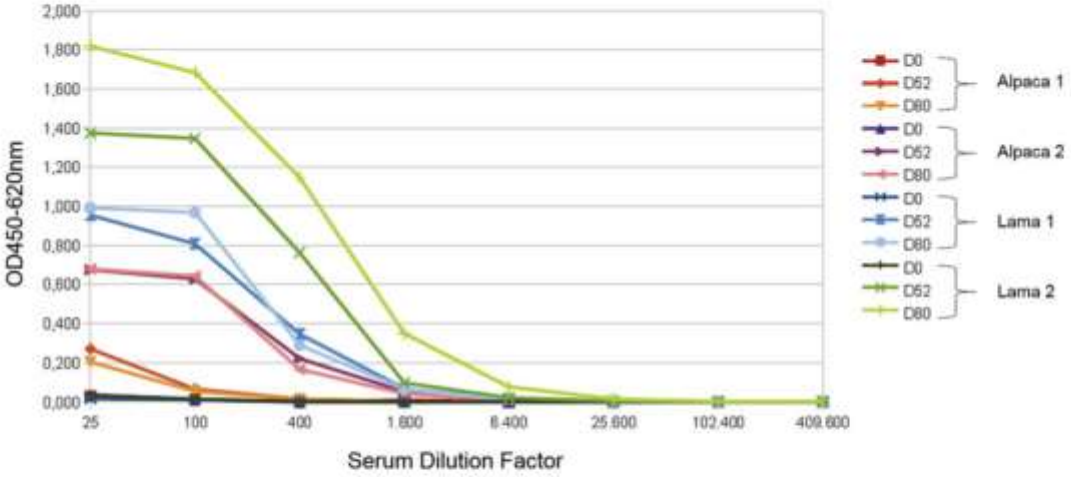

Fig. 4 Example of immune response of two Alpacas and two Lamas after immunization with a protein antigen. Immunizations were performed at Preclinics GmbH and antibody titers were determined by serum ELISA

two Lamas (*Lama glama*) were immunized at Preclinics GmbH (http://www.preclinics.com/) with a protein antigen. During the immunization procedure, Preclinics GmbH assessed the antigen-specific immune response in a serum ELISA, as exemplarily shown in Fig. 4. Afterwards, total RNA was isolated from 100 ml PBMCs followed by cDNA synthesis which was subsequently used for gene-specific amplification. In order to allow for a broader applicability of this herein described protocol, we also include methods for the generation of cDNA starting from whole blood. Gene-specific oligonucleotide sequences for the amplification of camelid VHH repertoires can also be found elsewhere [16, 24]. However, all protocols, components, concentrations and volumes given below can be used without any modification for the introduction of VHH diversities into yeast surface display libraries. Additionally, in Subheading 3.10, we also present a labeling strategy for the detection of surface display and antigen binding using fluorescence-activated cell sorting.

3.1 PBMC Isolation by Density Gradient Centrifugation

1. Dilute blood samples with an equal volume of PBMC prep buffer.
2. Fill SepMate tubes with 16 ml Biocoll Separation Solution.
3. Transfer approx. 30 ml diluted blood carefully into the SepMate tubes. Avoid subsidence of the blood under the separating disc.
4. Centrifuge for 20 min at 1200 × *g* and room temperature with medium acceleration and deceleration profile.

5. Remove blood plasma phase by pipetting. Please note that the PBMC fraction is located directly below and should not be affected by pipetting.
6. If PMC cells are aggregated at SepMate inner surface, remove them mechanically by scraping.
7. Decant residual blood plasma and PBMC into clean tube (ensure that no erythrocytes are transferred) and add 50 ml PBMC prep buffer.
8. Centrifuge for 8 min at 300 × *g* and room temperature with maximum acceleration and medium deceleration profile. Discard supernatant.
9. Wash cells twice by resuspending in 50 ml volume with PBMC prep buffer and repeat centrifugation as in **step 8**, respectively.
10. Resuspend cells in defined volume of PBMC prep buffer and count PBMC number.

3.2 Total RNA Isolation from PBMCs

1. Pellet 1 × 10^7 cells by centrifugation for 2 min at room temperature and 1200 × *g* (microfuge).
2. Lyse cells by resuspending in 600 µl of RLT and subsequent vortexing or pipetting.
3. Add the lysate into Qiashredder column in a 2 ml collection tube and centrifuge for 2 min at maximum speed and room temperature.
4. Remove the Qiashredder column and determine the volume of homogenized lysate before adding same amount of 70% ethanol.
5. Transfer the sample into RNeasy spin column in a 2 ml collection tube and centrifuge for 60 s at 8000 × *g* and room temperature. Discard flow-through. If sample volume exceeds 700 µl, centrifuge aliquots stepwise.
6. Add 700 µl of RW1 buffer into RNeasy spin column. Centrifuge for 60 s at 8000 × *g* and room temperature. Discard flow-through.
7. Wash the sample twice by adding 500 µl of RPE buffer and successive centrifugation for 60 s at maximum speed and room temperature, respectively.
8. Transfer RNeasy spin column containing bound RNA into a clean collection tube and add 50 µl of RNase-free water.
9. Incubate for 15 min at room temperature.
10. Eluate RNA by centrifugation for 60 s at maximum speed and room temperature. To increase RNA yield load flow-through again onto RNeasy, spin column and repeat the latter centrifugation step.

3.3 cDNA Synthesis

1. Prepare a RNA and primer mix by adding 5 µl RNA solution from RNA isolation as template, 1 µl random hexamer primers (50 ng/µl) as well as 1 µl of 10 mM dNTP mix. Add 10 µl with RNase-free water.
2. Place the mix in thermocycler at 65 °C for 5 min, followed by 60 s incubation on ice.
3. Prepare reverse transcriptase Master Mix by combining 2 µl RT buffer, 4 µl 25 mM $MgCl_2$, 2 µl 100 µM DTT as well as 1 µl RNaseOut (40 U/µl), and 1 µl SuperScript III RT (200 U/µl).
4. Add an equal volume of reverse transcriptase Master Mix to the RNA and primer mix.
5. Incubate the reaction solution in a thermocycler with 12 min at 25 °C followed by 52 min at 50 °C and as final step 5 min at 85 °C.
6. Add 20 µl of RNase H solution and incubate at 37 °C for 20 min.

3.4 Amplification of Lama and Alpaca HcAbs Variable Domains (VHHs)

1. Place PCR tube on ice and add 25 µl Q5 high fidelity 2× Master Mix. Add 1 µl (100 ng/µl) of DNA encoding for alpaca VHH region as template as well as 2.5 µl corresponding forward primer and 2.5 µl reverse primer (out of a 10 µM stock, primer sequences are listed in Table. 1) and 19 µl nuclease-free water. Alpaca VHHs can be amplified using primer combination VHH_fwd and VHH1_rev. Lama VHH regions can be amplified using the VHH_fwd and both reverse oligonucleotides (*see* **Note 2**).
2. Carry out PCR using the following parameters: Initial denaturation at 98 °C for 30 s. 30 cycles of 10 s denaturation at 98 °C, 30 s primer annealing at 57 °C, and 30 s elongation at 72 °C, followed by final step at 72 °C for 2 min.
3. Analyze PCR products by 1–2% (w/v) agarose gel electrophoresis. Amplified VHH region genes should give a distinct band at approx. 500 bp. Purify PCR products using Wizard® SV Gel and PCR Clean-Up System according to the manufacturer's instruction (*see* **Note 3**). Determine DNA concentration via BioSpec Nano or equivalent instrumentation. PCR products might be stored at −20 °C.

3.5 Destination Vector (pDest) Digestion

1. Place PCR tube on ice and add 40 µg of pDest (1 mg/ml), 8 µl Cut Smart 10×. Buffer as well as 2 µl *Bsa*I-HF (20000 U/ml) in a final volume of 80 µl (add nuclease-free water in order to achieve this volume).
2. Carry out reaction at room temperature overnight.
3. Analyze digestion product by 1–2% (w/v) agarose gel electrophoresis. Successful digestion should give a distinct band at

approx. 6000 bp. Purify digestion reaction using Wizard® SV Gel and PCR Clean-Up System according to the manufacturer's instruction.

3.6 Yeast Transformation for Library Establishment

In the following section, we describe library construction steps as modified version of the improved *S. cerevisiae* yeast transformation protocol of Benatuil and colleagues [29]. Therefore, it is herein only presented in brief. In this protocol all centrifugation steps to pellet yeast cells are performed at 4000 × *g* for 3 min.

1. Incubate EBY100 overnight to stationary phase in YPD media at 120 rpm and 30 °C.
2. Inoculate 500 ml fresh YPD media with the overnight culture to an OD_{600} of about 0.3.
3. Incubate cells at 30 °C and 120 rpm until OD_{600} reaches about 1.6–1.9.
4. Centrifuge cells and remove supernatant.
5. Wash cells twice by resuspension in 250 ml ice-cold water followed by a wash step using 250 ml ice-cold electroporation buffer.
6. Resuspend cells in 100 ml LiAc-buffer and incubate for 30 min at 30 °C and 120 rpm.
7. Centrifuge cells and wash afterwards once with 250 ml ice-cold electroporation buffer.
8. Resuspend cell pellet in electroporation buffer to a final volume of approx. 5 ml. This results in ten electroporation reactions with approx. 400 µl electro-competent EBY100 each.
9. Add 4 µg digested pDest and 12 µg VHH PCR product to 400 µl electro-competent cells per reaction.
10. Transfer cell-DNA mix to ice-cold electroporation cuvette (0.2 cm). Electroporate at 2500 V. Time constant should range from 3.0 to 4.5 ms. Transfer cells from each electroporation reaction into 8–10 ml of a mixture of YPD and 1 M sorbitol (1:1 ratio). Incubate for 1 h at 30 °C and 120 rpm.
11. Centrifuge cells and resuspend cell pellet in 10 ml SD-Trp media to calculate library size by dilution plating (*see* **Note 4**, SD-Trp agar plates; estimate number of transformants after 72 h).
12. Decant cells in 1 l in SD-Trp media and incubate for 2 days at 30 °C and 120 rpm.
13. Transfer library to SD Low -Trp medium. To this end, transfer at least a tenfold excess of cells as calculated by dilution plating. Inoculate at an OD_{600} of ~1.0. An absorbance value of 1 at 600 nm corresponds to approximately 1×10^7 cells per ml.

14. Incubate for two more days at 30 °C and 120 rpm.
15. The final library is henceforth prepared for long-term storage (*see* Subheading 3.8) or screening via FACS. To evaluate the quality of the final library, the authors recommend sending out at least 100 clones for sequencing (*see* **Note 5**).

3.7 Sequencing of Display Vector from Yeast Cells

1. Pick clones (e.g., from serial dilution) and inoculate approximately 10 ml SD-Trp medium in a baffled flask followed by incubation for 48 h at 30 °C and 120 rpm. Subsequently, isolate display plasmid using the MasterPure Yeast DNA Purification Kit following the manufacturer's protocol.
2. Transform 50 µl electro-competent *E. coli* Top10 cells with 5 µl isolated plasmid.
3. After incubation for approximately 60 min in LB medium without antibiotics, plate cells on LB Amp agar plates and incubate overnight at 37 °C. Afterwards pick single colonies and inoculate 700 µl LB Amp media in a Masterblock microplate. Incubate overnight at 37 °C and 700 rpm.
4. Mix 60 µl of *E. coli* Top10 culture with 40 µl glycerol solution (50% v/v) in an appropriate microplate. Deep-freeze at −80 °C until sending out for sequencing.

3.8 Yeast Library Cryopreservation for Long-Term Storage

1. Harvest cells from a freshly grown SD-Trp culture by centrifugation.
2. Inoculate SD Low -Trp medium with cells to an OD_{600} of 1 and cultivate for 48–72 h at 30 °C and 120 rpm. Library diversity should be oversampled by at least the factor of ten.
3. Harvest cells by centrifugation and remove supernatant.
4. Wash cells once with DPBS. Afterwards pellet cells by centrifugation, decant, and discard supernatant.
5. Resuspend cells in yeast library freezing solution with final cell concentrations of approximately 1×10^{10} cells/ml and transfer suspensions into cryogenic vials.
6. Freeze vials at −80 °C.

3.9 Induction of VHH Expression for Antibody Surface Display

1. Thaw an aliquot of the frozen library at room temperature and resuspend cells in SD-Trp.
2. The total number of cells in the starting culture should exceed the calculated library diversity at least ten times.
3. Incubate overnight at 30 °C and 120 rpm.
4. Harvest at least the number of cells corresponding to a tenfold excess of the library diversity by centrifugation and resuspend cells in SG -Trp medium to an initiate OD_{600} of 1. Cultivate cells for at least 24 h at 20 °C and 120 rpm for expression of VHHs.

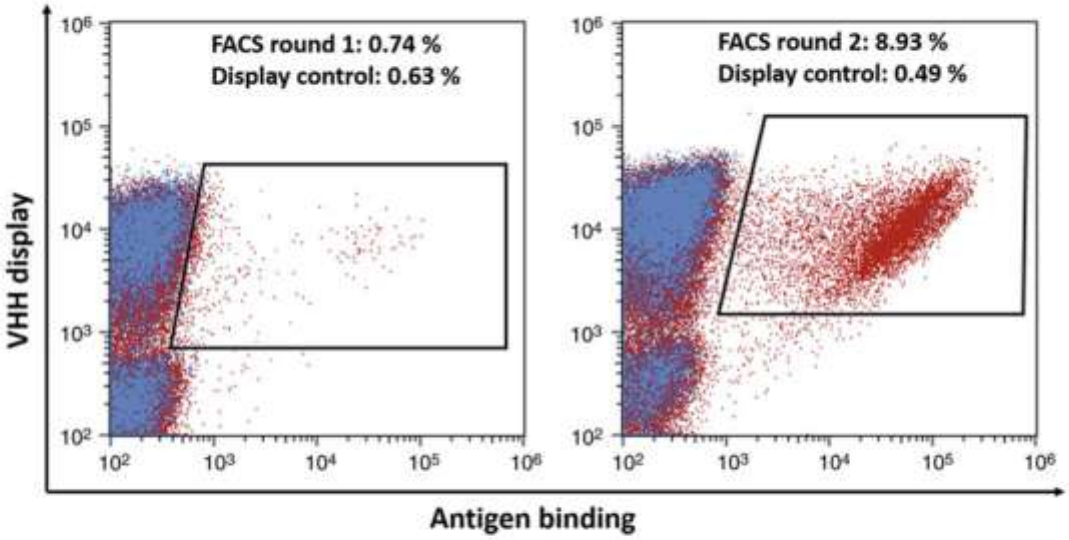

Fig. 5 Detection of VHH display and antigen binding of yeast surface display library candidates using FACS. Overlays of VHH display control (blue) and antigen binding yeast cells (red). Blue: yeast cells labeled with Penta-His Alexa Fluor 647 Conjugate antibody and anti-HA tag antibody (FITC) only. Red: staining for VHH surface display (same detection antibodies as for display control) as well as for antigen binding. Left: FACS sorting round 1. Right: FACS sorting round 2. Sorting gates are shown as well as percentage of cells in sorting gate

3.10 Detection of Yeast Surface Display and Antigen Binding by Fluorescence-Activated Cell Sorting (FACS)

In the following chapter, we describe a labeling strategy to detect surface expression of VHH molecules via binding of a fluorescently labeled anti-HA tag antibody (FITC) as well as antigen binding via his-tag staining (Penta-His Alexa Fluor 647 Conjugate antibody). An equivalent staining procedure can be carried out for library sorting (*see* **Notes 6** and 7). Please note that the fluorophores should be shielded from light and labeling steps are performed on ice. For all FACS sorting rounds as well as for flow cytometric analysis, we recommend staining an antibody display control (without antigen) in order to be able to adjust sorting gates accordingly (Fig. 5). Furthermore, a positive control, i.e., a single clone displaying a target-positive VHH should be used to ensure functional integrity of labeling reagents as well as target proteins. It is also possible to carry out positive control staining with different antibody formats. Consequently, staining reagents need to be adapted accordingly (e.g., detection of Fab fragment presentation via staining of the constant domain of the light chain).

3.10.1 Antibody Display Control

1. Pellet approximately 2×10^7 cells by centrifugation and remove supernatant. Wash cells two times with DPBS and resuspend cells in 40 µl DPBS. Incubate on ice for about 30 min.

2. Wash cells twice with DPBS and resuspend in 40 µl DPBS containing Penta-His Alexa Fluor 647 Conjugate antibody (diluted 1:20) and anti-HA tag antibody (FITC) (diluted 1:20), followed by incubation on ice for 30 min.
3. Wash cells again two times and resuspend the cell pellet finally in 600 µl DPBS. Keep on ice protected from light until FACS analysis.

3.10.2 Library Staining

The following section describes staining protocol of antibody displaying yeast cells regarding VHH surface expression as well as target binding. Essentially the same protocol can be used to label positive controls and libraries in general. Scale up for sorting purposes (*see* **Note 6**).

1. Pellet 2×10^7 yeast cells by centrifugation and remove supernatant. Wash cells twice with DPBS and resuspend in 40 µl DPBS containing antigen with a concentration of 1 µM (*see* **Note 8**). Incubate cells on ice for 30 min.
2. Wash cells two times and resuspend in 40 µl DPBS containing Penta-His Alexa Fluor 647 Conjugate antibody (diluted 1:20) and anti-HA tag antibody (FITC) (diluted 1:20), followed by incubation on ice for 30 min (*see* **Note 9**).
3. Wash cells again two times and resuspend the cell pellet finally in 600 µl DPBS. Keep on ice protected from light until FACS analysis.

3.10.3 Further Proceeding with Cells After FACS Sorting

This section describes briefly the treatment of the sorted cells after FACS analysis for further cytometric analysis rounds and cell storage.

1. Transfer sorted cells collected in sorter tube containing 500 µl DPBS into corresponding volume of SD media (approximately 20 ml media per 1×10^6 cells). Incubate at 30 °C and 120 rpm for 2 days.
2. Count cell number and induce VHH expression (*see* **Note 6**) by media exchange, as described in Subheading 3.9.
3. Deep-freeze remaining cells according to Subheading 3.8 for long-term storage.

4 Notes

1. In general, overhang sequences were part of constant components of the display system. The *N-terminal* overhang comprised nucleotides that were identical with those of a part of the Aga2p signal peptide, whereas *C-terminal* overhang was homologous to the glycine-serine linker fused to the myc-tag.

The herein described pDest allowed for N-terminal presentation of VHH moieties (i.e., free N-terminus of VHH and C-terminus fused to Aga2p). C-terminal display of VHHs is also a valid strategy for surface expression as already described by our group for the display of shark-derived single-domain antibodies [29–31].

2. Reverse primers were designed to anneal in the hinge region of camelid-derived IgG2b and IgG3b isotypes. Another alternative is the utilization of oligonucleotides annealing in framework region 4 of the VHH domain.
3. By using the primer sets shown in Table 1, one co-amplifies also the VH as well as CH1 region of conventional IgG antibodies. This results in an unwanted product with a size of approximately 800–900 bp on the agarose gel. We typically do not gel-excise the VHH-specific band since this would require a second-step re-amplification and a potential bias. Still, this crude mixture delivers nearly exclusively VHH domains after library establishment.
4. One transformation electroporation reaction usually yields in approximately 1×10^7 to 5×10^7 unique EBY100 clones. Scale up gap repair cloning and electroporation reactions by parallelization to obtain a sufficient library size. This is especially required for the construction of libraries from non-immunized animals.
5. For quality maintenance we recommend sequencing of the constructed library. Thus, the sequencing primer should be designed with respect to VHH region coverage in a single run. To this end, oligonucleotides should anneal approximately 60 bp upstream of the variable region.
6. In general, labeling steps are performed with 2×10^7 cells in a volume of 40 µl. For library sorting purposes, scale up in order to be able to sample a sufficient number of clones. By increasing the numbers of cells, volumes and amounts of labeling reagents should be increased proportionally. We recommend oversampling the generated diversity by at least the factor of ten. However, when large libraries are being generated, the limiting factor is throughput by FACS. For the first round of FACS, a maximum number of cells should be sorted. For subsequent sorting rounds, we typically oversample the number of isolated cells from the previous round by the factor of ten.
7. A variety of labeling reagents are commercially available. Thus, different combinations of fluorescent dyes and detection reagents are possible. For fluorophore selection, please note that no overlapping of excitation and emission spectra occur. Otherwise, appropriate compensation needs to be applied on the FACS device. Guidance should be given by the respective manufacturer.

8. To enhance stringency, the antigen concentration can be reduced significantly. However, we recommend starting sorting at an antigen concentration of 1 μM for initial rounds and to successively reduce the concentration as soon as cells are enriched for an antigen-binding population.
9. When working with non-immunized antibody repertoires, different secondary detection reagents should be alternated to avoid enrichment of off-target binders.

Acknowledgments

We like to thank Preclinics GmbH for collaborating on this project.

References

1. Hamers-Casterman C, Atarhouch T, Muyldermans S et al (1993) Naturally occurring antibodies devoid of light chains. Nature 363:446–448
2. Zielonka S, Empting M, Grzeschik J et al (2015) Structural insights and biomedical potential of IgNAR scaffolds from sharks. MAbs 7:15–25
3. Arezumand R, Alibakhshi A, Ranjbari J et al (2017) Nanobodies as novel agents for targeting angiogenesis in solid cancers. Front Immunol 8:1746
4. Könning D, Zielonka S, Grzeschik J et al (2017) Camelid and shark single domain antibodies: structural features and therapeutic potential. Curr Opin Struct Biol 45:10–16
5. Wesolowski J, Alzogaray V, Reyelt J et al (2009) Single domain antibodies: promising experimental and therapeutic tools in infection and immunity. Med Microbiol Immunol 198:157–174
6. Jähnichen S, Blanchetot C, Maussang D et al (2010) CXCR4 nanobodies (VHH-based single variable domains) potently inhibit chemotaxis and HIV-1 replication and mobilize stem cells. Proc Natl Acad Sci U S A 107:20565–20570
7. Maussang D, Mujić-Delić A, Descamps FJ et al (2013) Llama-derived single variable domains (nanobodies) directed against chemokine receptor CXCR7 reduce head and neck cancer cell growth *in vivo*. J Biol Chem 288:29562–29572
8. Nguyen VK, Hamers R, Wyns L et al (2000) Camel heavy-chain antibodies: diverse germline VHH and specific mechanisms enlarge the antigen-binding repertoire. EMBO J 19:921–930
9. Muyldermans S, Smider VV (2016) Distinct antibody species: structural differences creating therapeutic opportunities. Curr Opin Immunol 40:7–13
10. Krah S, Schröter C, Zielonka S et al (2016) Single-domain antibodies for biomedical applications. Immunopharmacol Immunotoxicol 38:21–28
11. Conrath KE, Wernery U, Muyldermans S et al (2003) Emergence and evolution of functional heavy-chain antibodies in Camelidae. Dev Comp Immunol 27:87–103
12. Vincke C, Loris R, Saerens D et al (2009) General strategy to humanize a camelid single-domain antibody and identification of a universal humanized nanobody scaffold. J Biol Chem 284:3273–3284
13. Tijink BM, Laeremans T, Budde M et al (2008) Improved tumor targeting of anti-epidermal growth factor receptor Nanobodies through albumin binding: taking advantage of modular Nanobody technology. Mol Cancer Ther 7:2288–2297
14. Helma J, Cardoso MC, Muyldermans S et al (2015) Nanobodies and recombinant binders in cell biology. J Cell Biol 209:633–644
15. Alvarez-Cienfuegos A, Nuñez-Prado N, Compte M et al (2016) Intramolecular trimerization, a novel strategy for making multispecific antibodies with controlled orientation of the antigen binding domains. Sci Rep 6:28643
16. Desmyter A, Spinelli S, Boutton C et al (2017) Neutralization of human interleukin 23 by multivalent nanobodies explained by the structure of cytokine–nanobody complex. Front Immunol 8:884

17. Goldman E, Liu J, Bernstein R et al (2009) Ricin detection using phage displayed single domain antibodies. Sensors 9:542–555
18. Yan J, Li G, Hu Y et al (2014) Construction of a synthetic phage-displayed Nanobody library with CDR3 regions randomized by trinucleotide cassettes for diagnostic applications. J Transl Med 12:343
19. Bencurova E, Pulzova L, Flachbartova Z et al (2015) A rapid and simple pipeline for synthesis of mRNA–ribosome–V_HH complexes used in single-domain antibody ribosome display. Mol BioSyst 11:1515–1524
20. Romao E, Morales-Yanez F, Hu Y et al (2016) Identification of useful nanobodies by phage display of immune single domain libraries derived from camelid heavy chain antibodies. Curr Pharm Des 22:6500–6518
21. Cavallari M (2017) Rapid and direct VHH and target identification by staphylococcal surface display libraries. Int J Mol Sci 18:1507
22. Eden T, Menzel S, Wesolowski J et al (2018) A cDNA immunization strategy to generate nanobodies against membrane proteins in native conformation. Front Immunol 8:1989
23. Wu Y, Jiang S, Ying T (2017) Single-domain antibodies as therapeutics against human viral diseases. Front Immunol 8:1802
24. Pardon E, Laeremans T, Triest S et al (2014) A general protocol for the generation of Nanobodies for structural biology. Nat Protoc 9:674–693
25. McMahon C, Baier AS, Pascolutti R et al (2018) Yeast surface display platform for rapid discovery of conformationally selective nanobodies. Nat Struct Mol Biol 25:289–296
26. Boder ET, Wittrup KD (1997) Yeast surface display for screening combinatorial polypeptide libraries. Nat Biotechnol 15:553–557
27. Lu Z-J (2012) Frontier of therapeutic antibody discovery: The challenges and how to face them. World J Biol Chem 3:187
28. Doerner A, Rhiel L, Zielonka S et al (2014) Therapeutic antibody engineering by high efficiency cell screening. FEBS Lett 588:278–287
29. Zielonka S, Weber N, Becker S et al (2014) Shark Attack: high affinity binding proteins derived from shark vNAR domains by stepwise in vitro affinity maturation. J Biotechnol 191:236–245
30. Zielonka S, Empting M, Könning D et al (2015) The shark strikes twice: hypervariable loop 2 of shark IgNAR antibody variable domains and its potential to function as an autonomous paratope. Mar Biotechnol (NY) 17:386–392
31. Grzeschik J, Könning D, Hinz SC et al (2018) Generation of semi-synthetic shark IgNAR single-domain antibody libraries. Methods Mol Biol 1701:147–167

7 Supporting information

7.1 Facile generation of antibody heavy and light chain diversities for yeast surface display by Golden Gate Cloning

Supplementary Information: Facile generation of antibody heavy and light chain diversities for yeast surface display by Golden Gate Cloning

Lukas Roth[1+], Julius Grzeschik[1+], Steffen C. Hinz[1], Stefan Becker[2], Lars Toleikis[2], Michael Busch[3], Harald Kolmar[1], Simon Krah[2]* and Stefan Zielonka[2]*

[1]Institute for Organic Chemistry and Biochemistry, Technische Universität Darmstadt, Alarich-Weiss-Strasse 4, D-64287 Darmstadt, Germany

[2]Protein Engineering and Antibody Technologies, Merck KGaA, Frankfurter Strasse 250, D-64293 Darmstadt, Germany

[3]Discovery Pharmacology, Merck KGaA, Frankfurter Strasse 250, D-64293 Darmstadt, Germany

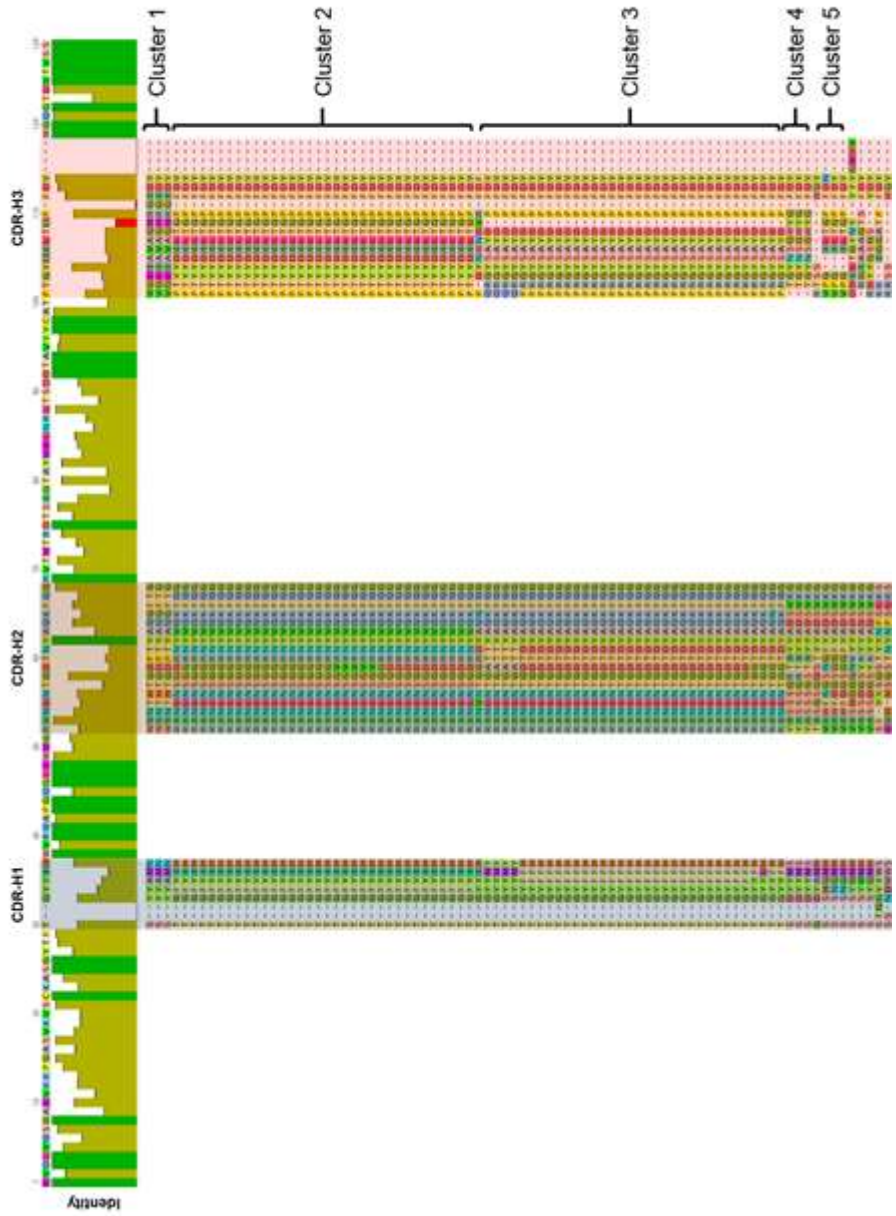

Supplementary Figure 1: Multiple sequence alignment of domain VH for GGC-derived library after enrichment against CEACAM6. CDR-H1, CDR-H2 and CDR-H3 are highlighted as well as clones falling into distinct sequence clusters. Alignment was performed using Geneious Alignment, Cost Matrix (1.0/0.0), Gap open penalty: 12, Gap extension penalty 3 and Refinement iterations 1 using Geneious 10.0.5 software (www.geneious.com).

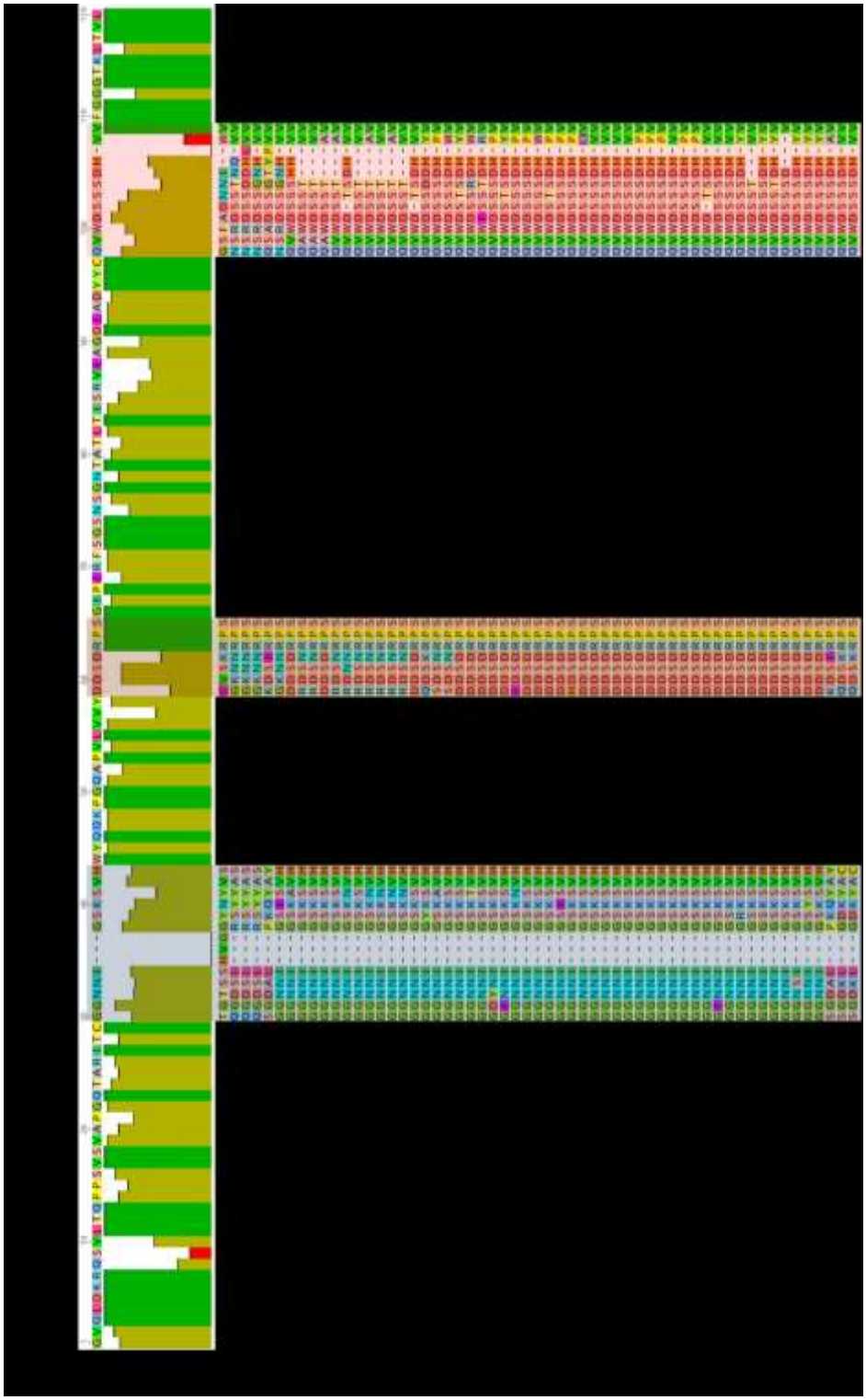

Supplementary Figure 2: Multiple sequence alignment of VLλ for GGC-derived library after enrichment against CEACAM6. CDR-L1, CDR-L2 and CDR-L3 are highlighted. Alignment was performed using Geneious Alignment, Cost Matrix (1.0/0.0), Gap open penalty: 12, Gap extension penalty 3 and Refinement iterations 1 using Geneious 10.0.5 software (www.geneious.com).

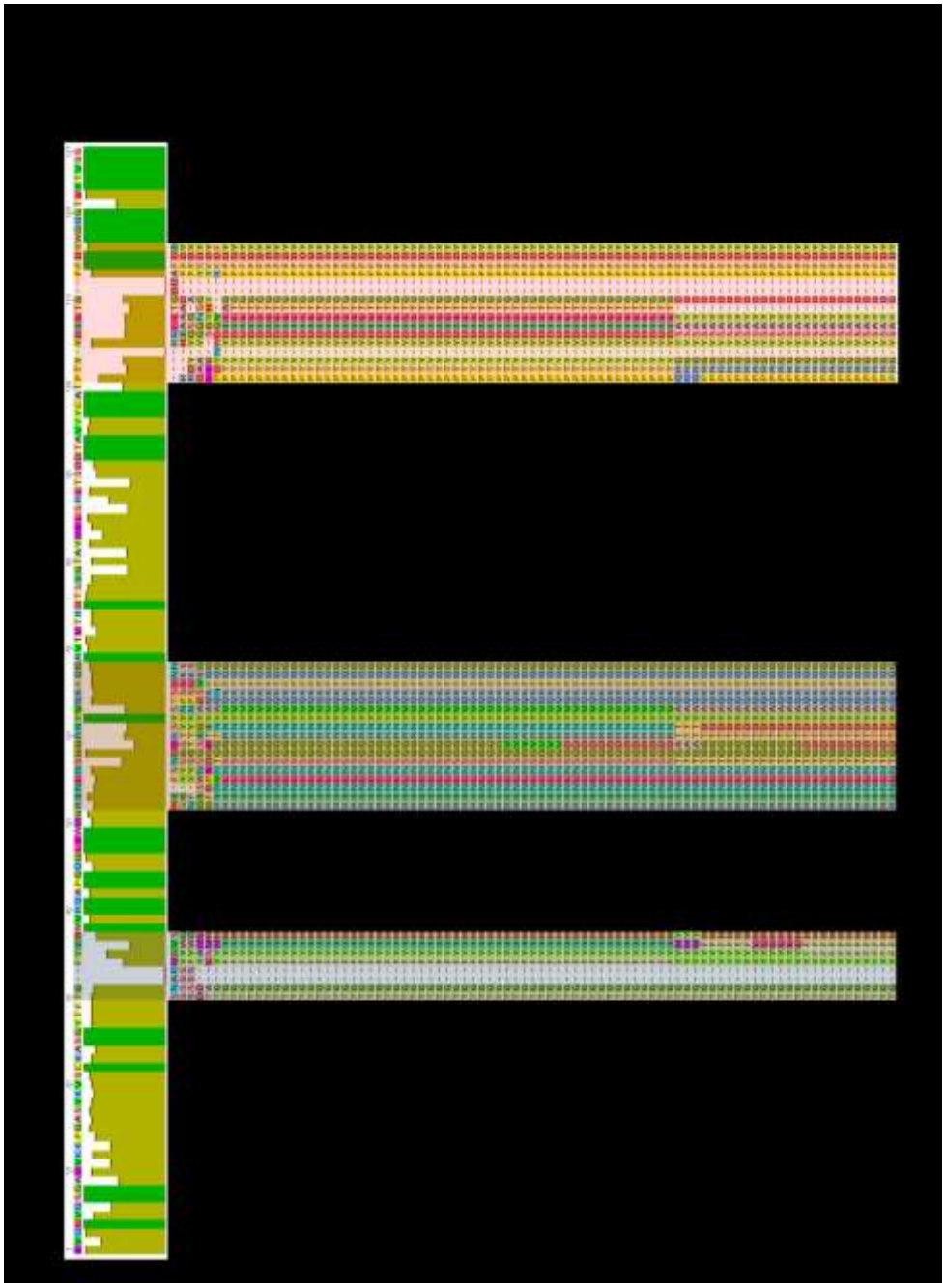

Supplementary Figure 3: Multiple sequence alignment of domain VH for YM-derived library after enrichment against CEACAM6. CDR-H1, CDR-H2 and CDR-H3 are highlighted as well as clones falling into distinct sequence clusters. Alignment was performed using Geneious Alignment, Cost Matrix (1.0/0.0), Gap open penalty: 12, Gap extension penalty 3 and Refinement iterations 1 using Geneious 10.0.5 software (www.geneious.com).

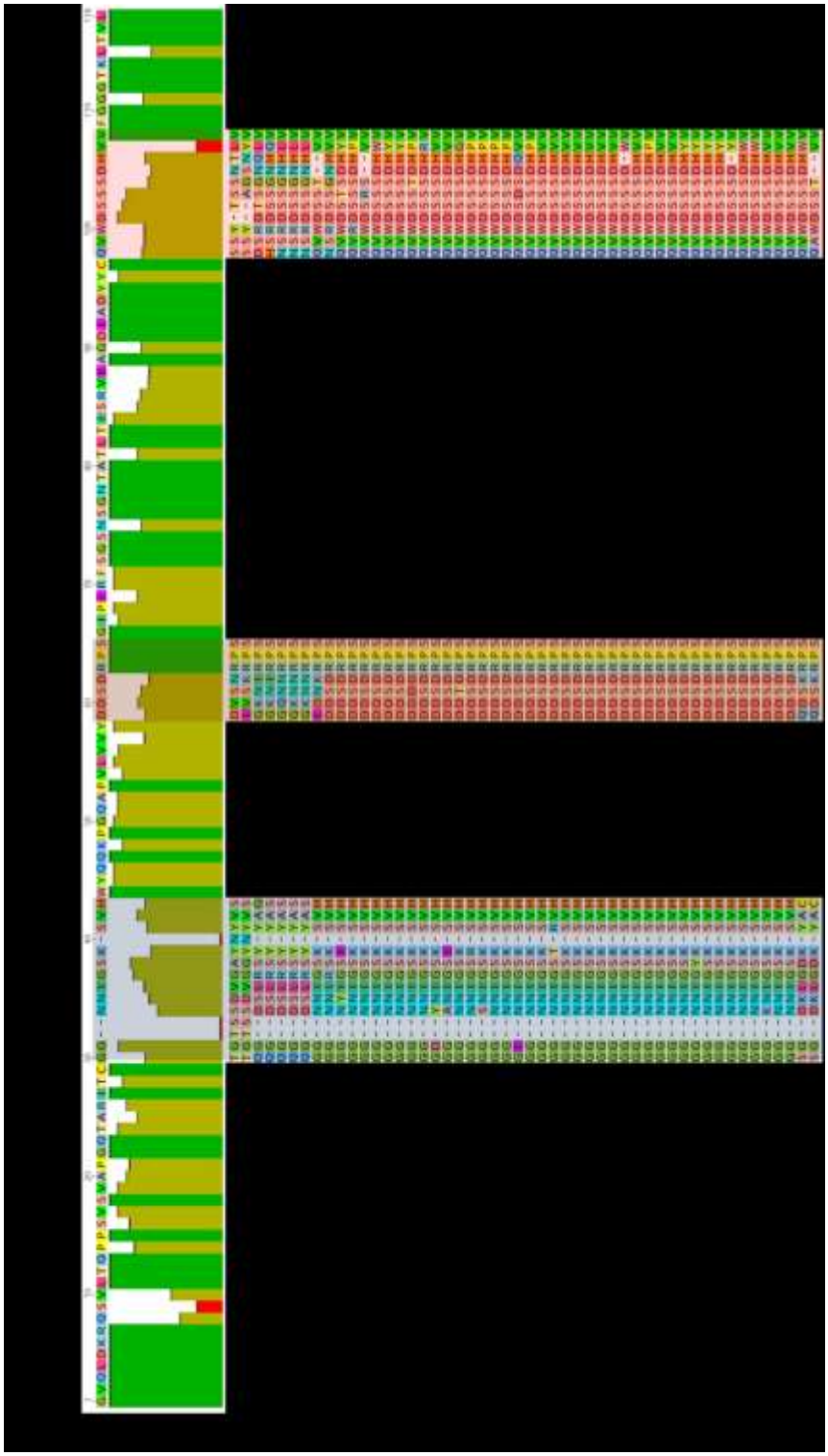

Supplementary Figure 4: Multiple sequence alignment of VLλ for YM-derived library after enrichment against CEACAM6. CDR-L1, CDR-L2 and CDR-L3 are highlighted. Alignment was performed using Geneious Alignment, Cost Matrix (1.0/0.0), Gap open penalty: 12, Gap extension penalty 3 and Refinement iterations 1 using Geneious 10.0.5 software (www.geneious.com).

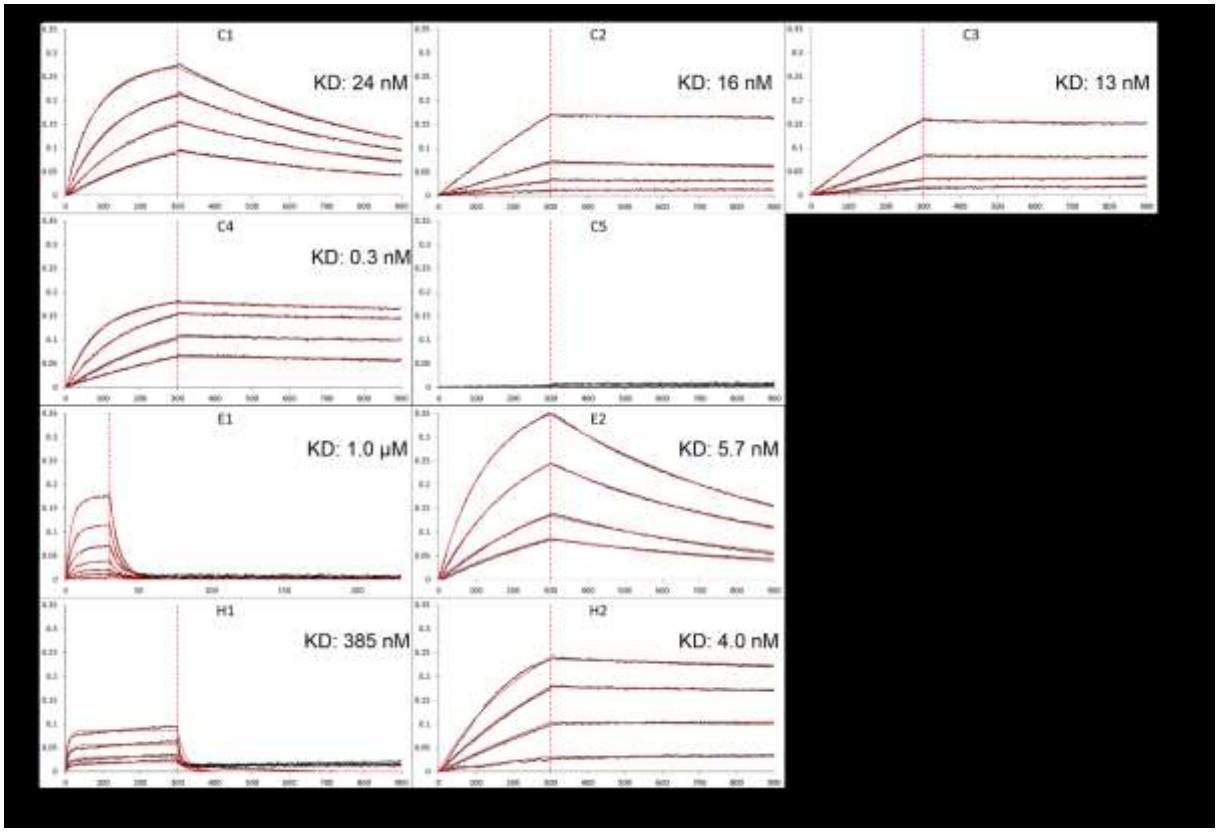

Supplementary Figure 5: Binding kinetics of human IgG variants (C1 – C5) and chimeric chicken/human IgG moieties (E1, E2, H1, H2) as determined by Bio-Layer Interferometry and an Octet® RED96 system. C1-C5: Cluster representatives selected against CEACAM6, E1, E2: Variants obtained from EGFR library, H1, H3: Molecules derived from hCG library sorting. Fitting (red lines) of binding curves (colored lines) was calculated using a 1:1 binding model and Savitzky-Golay filtering.

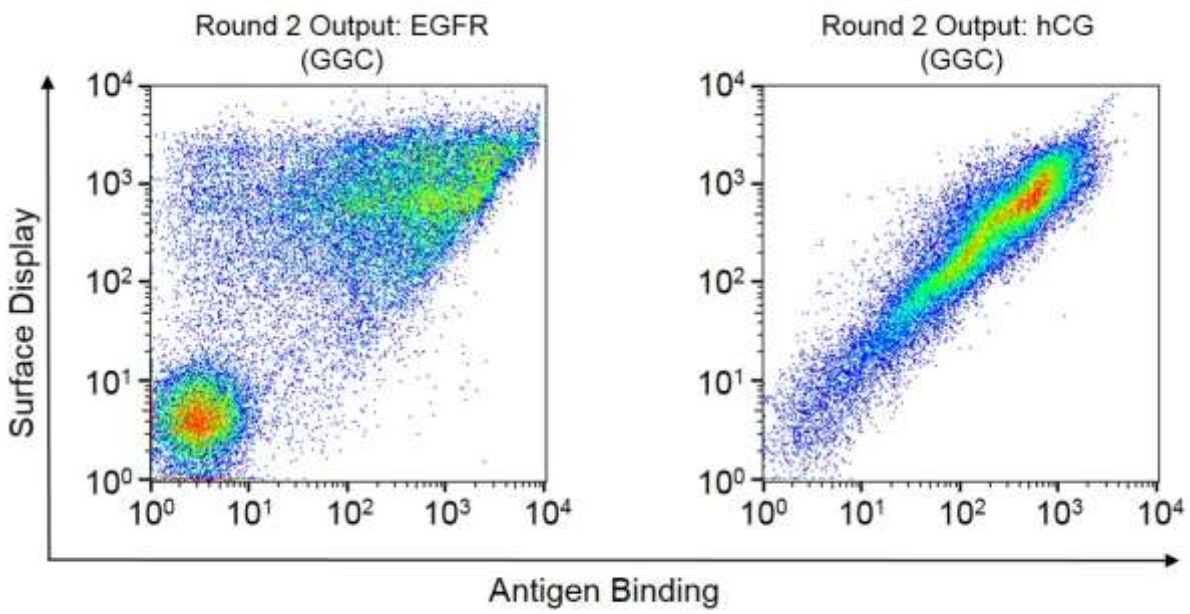

Supplementary Figure 6: Screening output of chimeric chicken/human YSD Fab immune libraries. Cells were stained after two rounds of sorting for antigen binding and Fab surface expression.

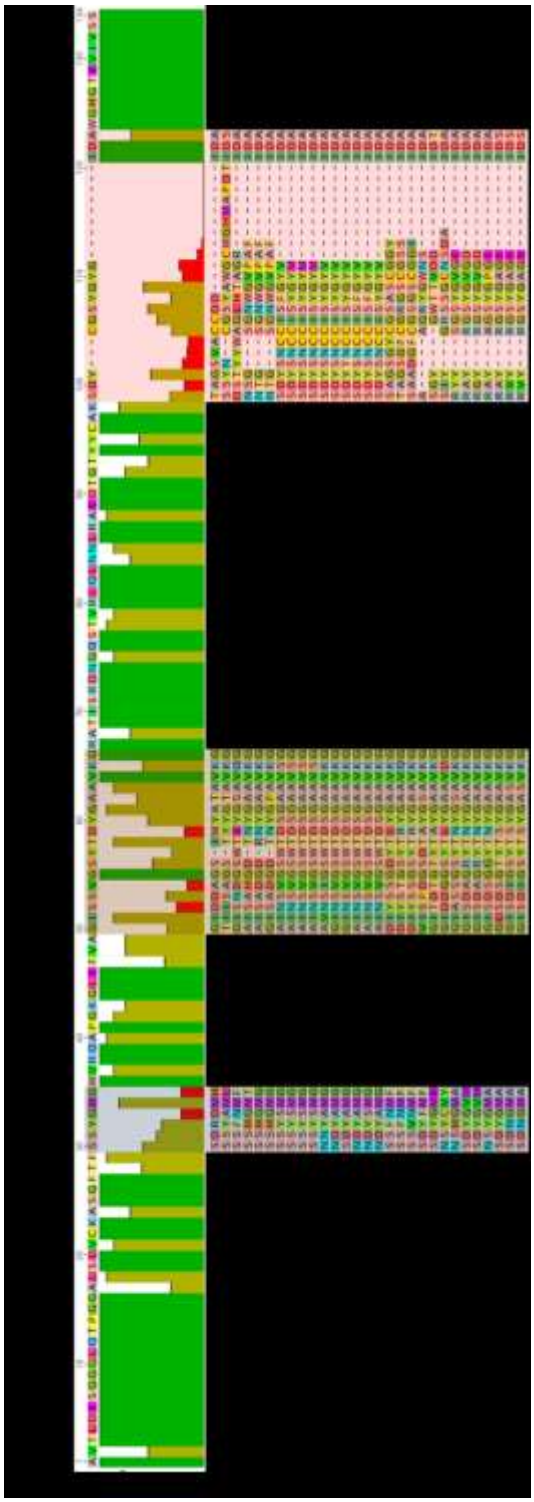

Supplementary Figure 7: Multiple sequence alignment of domain VH for GGC-derived chimeric chicken/human Fab library after enrichment against EGFR. CDR-H1, CDR-H2 and CDR-H3 are highlighted. Alignment was performed using Geneious Alignment, Cost Matrix (1.0/0.0), Gap open penalty: 12, Gap extension penalty 3 and Refinement iterations 1 using Geneious 10.0.5 software (www.geneious.com).

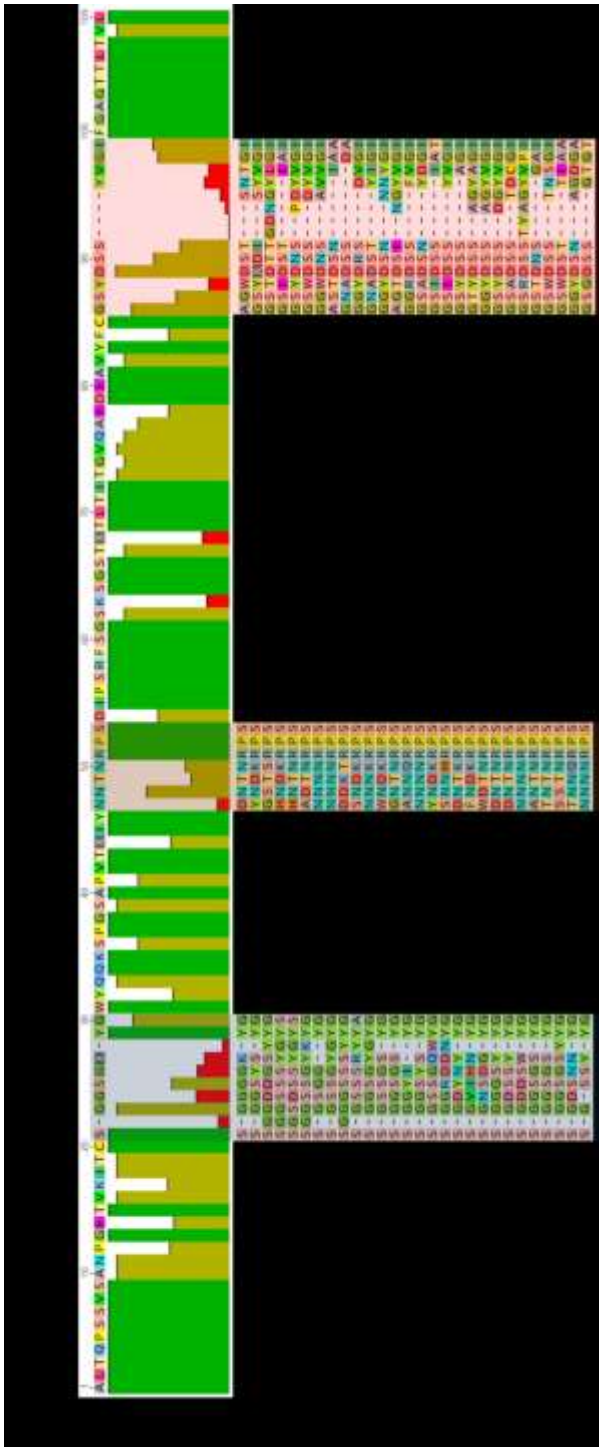

Supplementary Figure 8: Multiple sequence alignment of VL for GGC-derived chimeric chicken/human Fab library after enrichment against EGFR. CDR-L1, CDR-L2 and CDR-L3 are highlighted. Alignment was performed using Geneious Alignment, Cost Matrix (1.0/0.0), Gap open penalty: 12, Gap extension penalty 3 and Refinement iterations 1 using Geneious 10.0.5 software (www.geneious.com).

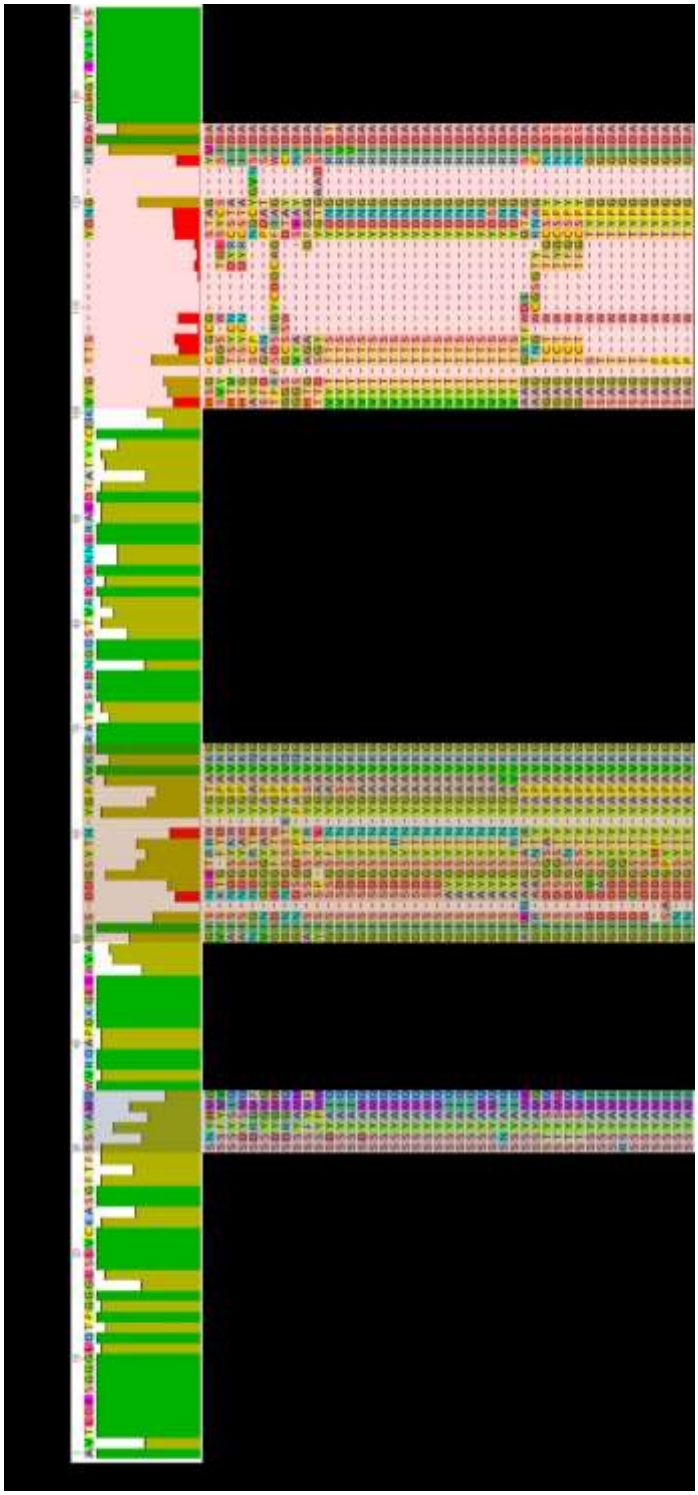

Supplementary Figure 9: Multiple sequence alignment of domain VH for GGC-derived chimeric chicken/human Fab library after enrichment against hCG. CDR-H1, CDR-H2 and CDR-H3 are highlighted. Alignment was performed using Geneious Alignment, Cost Matrix (1.0/0.0), Gap open penalty: 12, Gap extension penalty 3 and Refinement iterations 1 using Geneious 10.0.5 software (www.geneious.com).

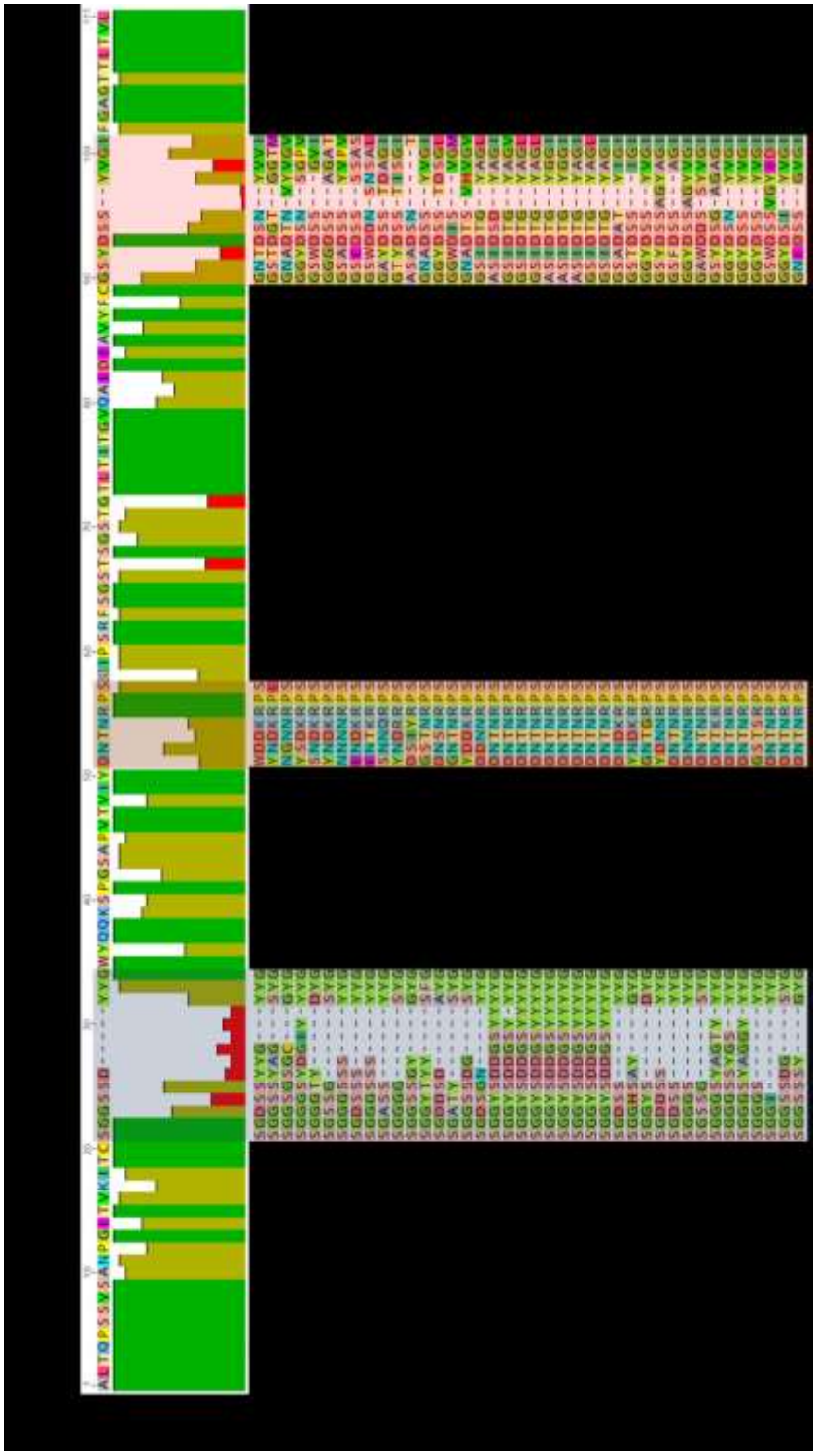

Supplementary Figure 10: Multiple sequence alignment of VL for GGC-derived chimeric chicken/human Fab library after enrichment against hCG. CDR-L1, CDR-L2 and CDR-L3 are highlighted. Alignment was performed using Geneious Alignment, Cost Matrix (1.0/0.0), Gap open penalty: 12, Gap extension penalty 3 and Refinement iterations 1 using Geneious 10.0.5 software (www.geneious.com).

Supplementary Table 1: Comparison of the functionality of VH and VL clones in YSD libraries constructed by GGC or the YM approach.

Library	Functionality [%]	
	VH repertoire	VLλ repertoire
Golden Gate Cloning (GGC)	90.4	78.8
Conventional (YM)	92.1	73.2

Supplementary Table 2: Oligonucleotide primers used in this study.

Name	Sequence (5′–3′)
1GGC_VH_up	GCGCGCGCGGTCTCTAGGTGAGGTBCAGCTGGTGCAGTCTGG
2GGC_VH_up	GCGCGCGCGGTCTCTAGGTGARRTSCAGCTGGTRCARTCTGG
3GGC_VH_up	GCGCGCGCGGTCTCTAGGTGAGRTCACCTTGAAGGAGTCTGG
4GGC_VH_up	GCGCGCGCGGTCTCTAGGTGARGTGCAGCTGGTGGAGTCTGG
5GGC_VH_up	GCGCGCGCGGTCTCTAGGTGAGGTGCAGCTGKTGGAGWCYSG
6GGC_VH_up	GCGCGCGCGGTCTCTAGGTGAGGTGCARCTGCAGGAGTCGGG
7GGC_VH_up	GCGCGCGCGGTCTCTAGGTGAGSTGCAGCTRCAGSAGTSSGG
8GGC_VH_up	GCGCGCGCGGTCTCTAGGTGARGTGCAGCTGGTGCAGTCTGG
9GGC_VH_up	GCGCGCGCGGTCTCTAGGTGAGGTACAGCTGCAGCAGTCAGG
1GGC_VH_lo	GCGCGCTGGTCTCTTAGTAGAAGCTGARGAGACRGTGACC
1GGC_VL_up	GCGCGCTGGTCTCTAAGCGACAGTCTGTGCTGACTCAGCCACC
2GGC_VL_up	GCGCGCTGGTCTCTAAGCGACAGTCTGTGYTGACGCAGCCGCC
3GGC_VL_up	GCGCGCTGGTCTCTAAGCGACAGTCTGCCCTGACTCAGCCT
4GGC_VL_up	GCGCGCTGGTCTCTAAGCGATCCTATGWGCTGACWCAGCCACC
5GGC_VL_up	GCGCGCTGGTCTCTAAGCGATCTTCTGAGCTGACTCAGGACCC
6GGC_VL_up	GCGCGCTGGTCTCTAAGCGACTGCCTGTGCTGACTCAGCCC
7GGC_VL_up	GCGCGCTGGTCTCTAAGCGACAGCYTGTGCTGACTCAATCRYC
8GGC_VL_up	GCGCGCTGGTCTCTAAGCGACAGSCTGTGCTGACTCAGCC
9GGC_VL_up	GCGCGCTGGTCTCTAAGCGAAATTTTATGCTGACTCAGCCCCA
10GGC_VL_up	GCGCGCTGGTCTCTAAGCGACAGRCTGTGGTGACYCAGGAGCC
11GGC_VL_up	GCGCGCTGGTCTCTAAGCGACAGSCWGKGCTGACTCAGCCACC
1GGC_VL_lo	GCGCGCGGTCTCTGTCCTAGGACGGTSASCTTG
1YM_VH_up	TGTTTTTCAATATTTTCTGTTATTGCTAGCGTTTTAGCAGGGGAG GTBCAGCTGGTGCAGTCTGG

2YM_VH_up	TGTTTTTCAATATTTTCTGTTATTGCTAGCGTTTTAGCAGGGGAR RTSCAGCTGGTRCARTCTGG
3YM_VH_up	TGTTTTTCAATATTTTCTGTTATTGCTAGCGTTTTAGCAGGGGAG RTCACCTTGAAGGAGTCTGG
4YM_VH_up	TGTTTTTCAATATTTTCTGTTATTGCTAGCGTTTTAGCAGGGGAR GTGCAGCTGGTGGAGTCTGG
5YM_VH_up	TGTTTTTCAATATTTTCTGTTATTGCTAGCGTTTTAGCAGGGGAG GTGCAGCTGKTGGAGWCYSG
6YM_VH_up	TGTTTTTCAATATTTTCTGTTATTGCTAGCGTTTTAGCAGGGGAG GTGCARCTGCAGGAGTCGGG
7YM_VH_up	TGTTTTTCAATATTTTCTGTTATTGCTAGCGTTTTAGCAGGGGAG STGCAGCTRCAGSAGTSSGG
8YM_VH_up	TGTTTTTCAATATTTTCTGTTATTGCTAGCGTTTTAGCAGGGGAR GTGCAGCTGGTGCAGTCTGG
9YM_VH_up	TGTTTTTCAATATTTTCTGTTATTGCTAGCGTTTTAGCAGGGGAG GTACAGCTGCAGCAGTCAGG
1YM_VH_lo	GGAGGAGGGTGCCAGGGGGAAGACCGATGGGCCCTTGGTACTA GCTGARGAGACRGTGACC
1YM_VL_up	GCCAGCATTGCTGCTAAAGAAGAAGGGGTACAACTCGATAAAA GACAGTCTGTGCTGACTCAGCCACC
2YM_VL_up	GCCAGCATTGCTGCTAAAGAAGAAGGGGTACAACTCGATAAAA GACAGTCTGTGYTGACGCAGCCGCC
3YM_VL_up	GCCAGCATTGCTGCTAAAGAAGAAGGGGTACAACTCGATAAAA GACAGTCTGCCCTGACTCAGCCT
4YM_VL_up	GCCAGCATTGCTGCTAAAGAAGAAGGGGTACAACTCGATAAAA GATCCTATGWGCTGACWCAGCCACC
5YM_VL_up	GCCAGCATTGCTGCTAAAGAAGAAGGGGTACAACTCGATAAAA GATCTTCTGAGCTGACTCAGGACCC
6YM_VL_up	GCCAGCATTGCTGCTAAAGAAGAAGGGGTACAACTCGATAAAA GACTGCCTGTGCTGACTCAGCCC
7YM_VL_up	GCCAGCATTGCTGCTAAAGAAGAAGGGGTACAACTCGATAAAA GACAGCYTGTGCTGACTCAATCRYC
8YM_VL_up	GCCAGCATTGCTGCTAAAGAAGAAGGGGTACAACTCGATAAAA GACAGSCTGTGCTGACTCAGCC
9YM_VL_up	GCCAGCATTGCTGCTAAAGAAGAAGGGGTACAACTCGATAAAA GAAATTTTATGCTGACTCAGCCCCA
10YM_VL_up	GCCAGCATTGCTGCTAAAGAAGAAGGGGTACAACTCGATAAAA GACAGRCTGTGGTGACYCAGGAGCC
11YM_VL_up	GCCAGCATTGCTGCTAAAGAAGAAGGGGTACAACTCGATAAAA GACAGSCWGKGCTGACTCAGCCACC
1YM_VL_lo	GGATGGCGGGAACAGAGTGACCGAAGGGGCGGCCTTCGGCTGA CCTAGGACGGTSASCTTG
1chic_chim_VH_up	GCGCGCGCGGTCTCTAGGTGCCGTGACGTTGGACGAG
2chic_chim_VH_up	GCGCGCGCGGTCTCTAGGTGCCCTGACGTTGGACGAG
1chic_chim_VH_lo	GCGCGCTGGTCTCTTAGTAGAAGCGGAGGAGACGATGACTTCG GT
1chic_chim_VL_up	GCGCGCTGGTCTCTAAGCGAGCGCTGACTCAGCCGTCCTCG
1chic_chim_VL_lo	GCGCGCGGTCTCTGTCCTAGGACGGTCAGGGTTGTCCC

7.2 A One-Step Process for the Construction of Phage Display scFv and VHH Libraries

Supplementary Information: A one-step process for the construction of Phage Display scFv and VHH libraries

Carolin Sellmann[1*], Lukas Pekar[1*], Christina Bauer[1], Elke Ciesielski[1], Simon Krah[1], Stefan Becker[1], Lars Toleikis[1], Jonas Kügler[2], André Frenzel[2], Bernhard Valldorf[3], Michael Hust[2,4] and Stefan Zielonka[1+]

[1]Protein Engineering and Antibody Technologies, Merck Healthcare KGaA, Frankfurter Strasse 250, D-64293 Darmstadt, Germany

[2]YUMAB GmbH, Inhoffenstraße 7, D-38124 Braunschweig, Germany

[3]Chemical and Pharmaceutical Development, Merck Healthcare KGaA, Frankfurter Strasse 250, D-64293 Darmstadt, Germany

[4]Technische Universität Braunschweig, Institut für Biochemie, Biotechnologie und Bioinformatik, Spielmannstr. 7, D-38106, Braunschweig, Germany

[*]These authors contributed equally to this work

[+] To whom correspondence should be addressed: Stefan Zielonka, Protein Engineering and Antibody Technologies, Merck KGaA, Frankfurter Strasse 250, D-64293 Darmstadt, Germany, E-mail: Stefan.Zielonka@merckgroup.com

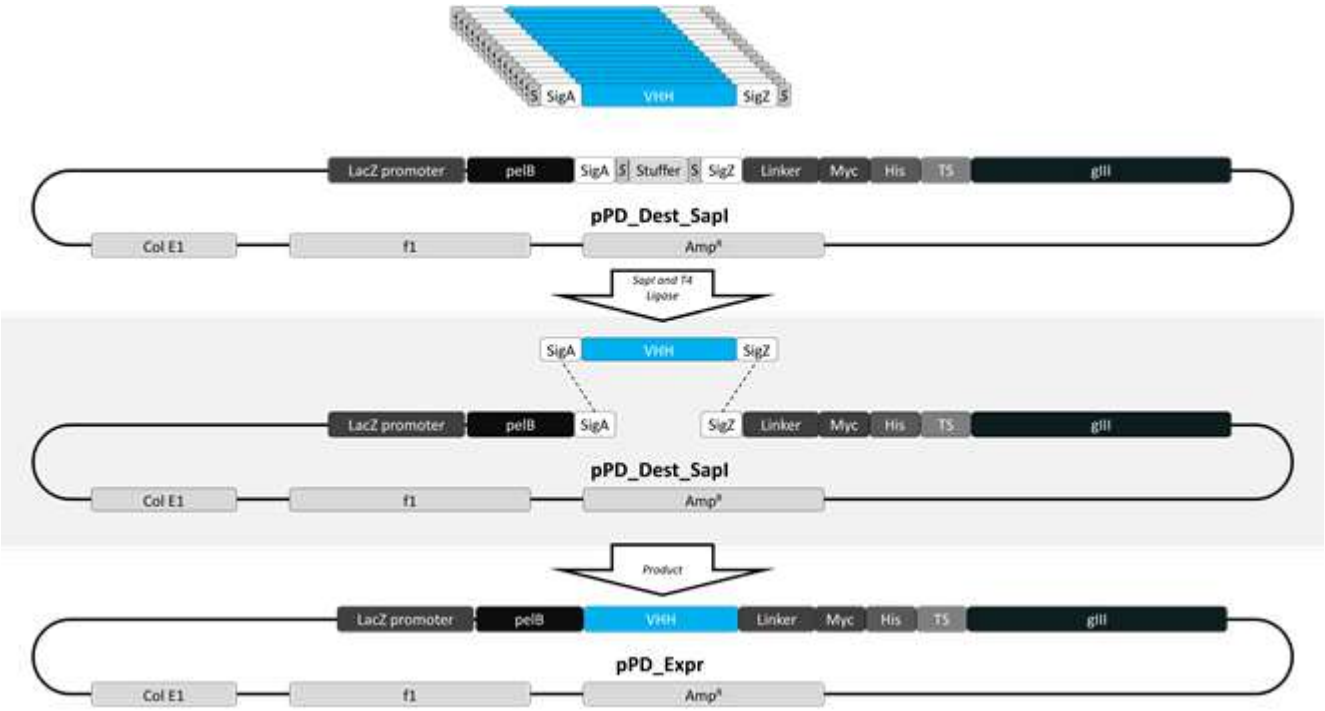

Figure S1: Schematic overview of the one-step generation process of phage display plasmids for the construction of VHH-derived single domain antibody libraries. The destination plasmid (pPD_Dest_SapI) as well as the PCR-amplified VHH repertoire contains or is flanked by SapI recognition sites in opposite orientations (S: GCTCTTCN, *S*: NGAAGAGC). Complimentary overhangs i.e. signature sequences (SigX) after SapI digestion enable the defined one-pot assembly during ligation resulting in the final display plasmid (pPD_Expr). ColE1: origin of replication. f1: origin of replication. Amp^R: Ampicillin resistance gene, pelB: leader sequence. Linker: amino acids AAAGS, Myc: c-Myc epitope EQKLISEEDL, His: hexahistidine tag, TS: trypsin site KDIR, gIII. gene encoding for phage protein pIII. Note that an amber stop codon is introduced between the hexahistidine tag and the trypsin site.

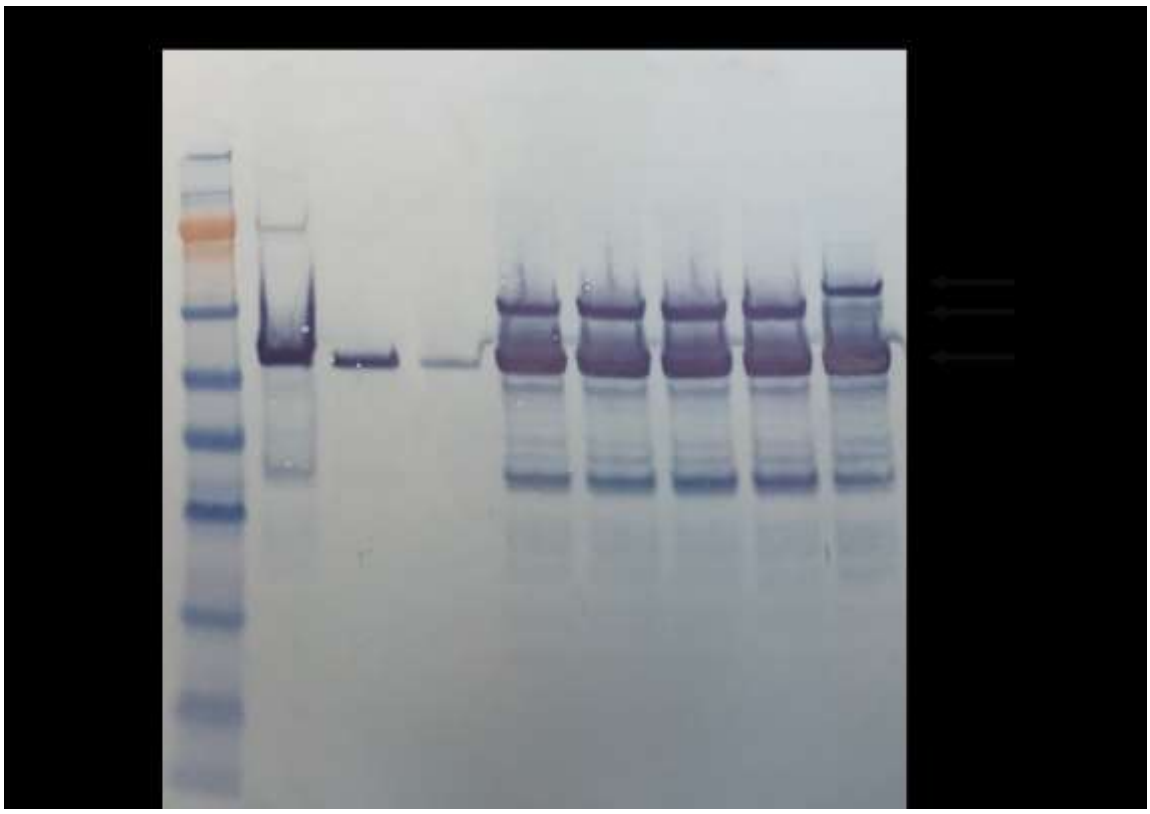

Figure S2: Western Blot analysis of different camelid-derived single domain VHH libraries as displayed on the surface of phage particles. M: marker; H1, H2, H3: Helper phage (10^9, 10^8, 10^7 phage particles loaded on the gel; L1.1: Llama 1 VHH sub-library short hinge; L1.2: Llama 1 VHH sub-library long hinge; L2.1: Llama 2 VHH sub-library short hinge; L2.2: Llama 2 VHH sub-library long hinge; C: Chicken-derived ScFv library. For each library, 10^9 phage particles (pfu) were loaded on the gel. Bands corresponding to pIII, VHH:pIII fusion and ScFv:pIII fusion are indicated by arrows. Western Blot was developed with mouse anti-pIII antibody (MobiTec) and peroxidase conjugated goat anti-moise antibody (Jackson Immuno Research).

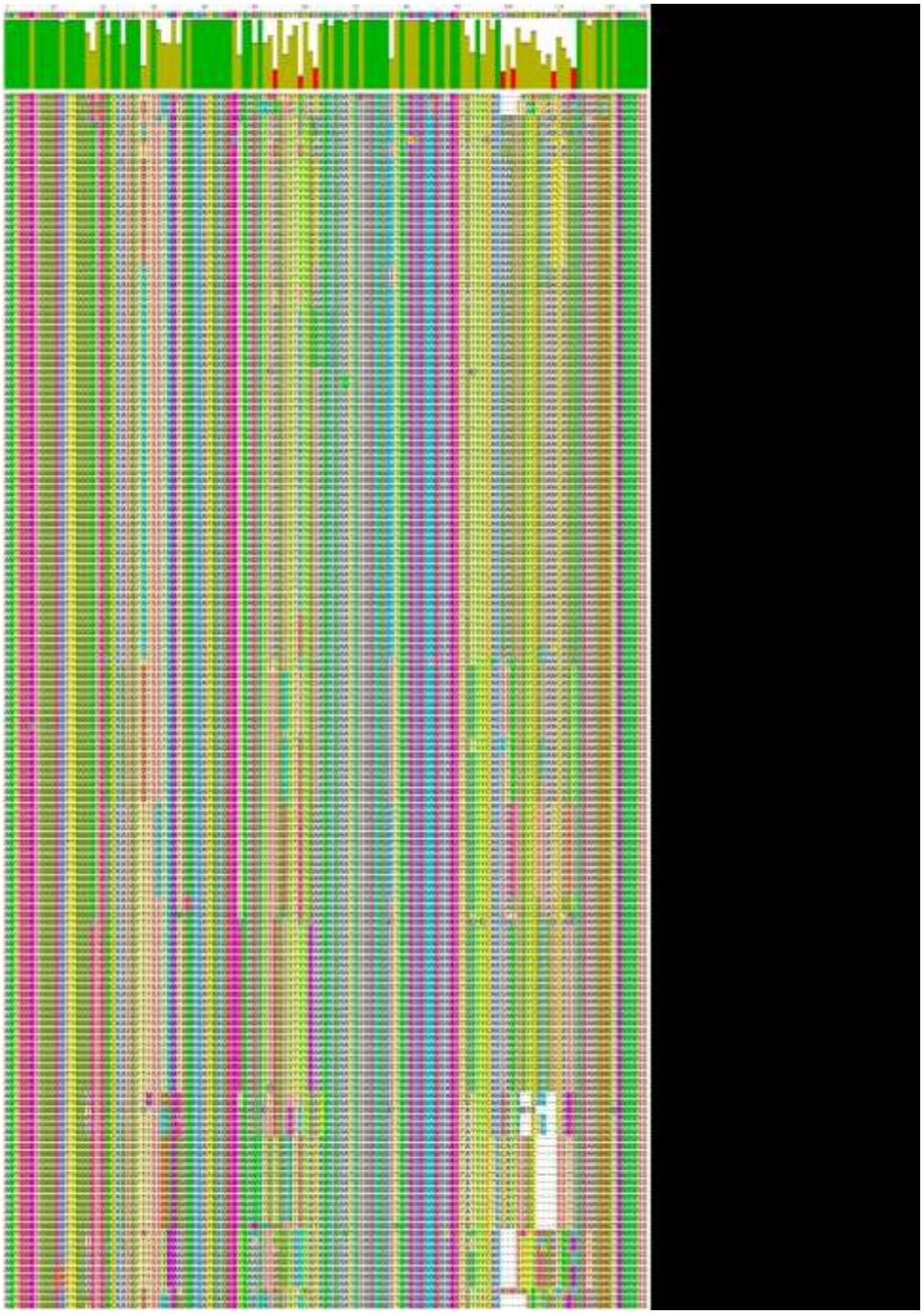

Figure S3: Multiple sequence alignment of VH after panning the EGFR-immunized chicken scFv library via Phage Display. Clusters are indicated. For calculation of unique clones, sequences containing ambiguities (X) where not taken into account. Sequences containing stop-codons or frame-shifts were excluded from analysis. Alignment was created using MUSCLE Alignment tool within Geneious Prime software (www.geneious.com).

Figure S4: Multiple sequence alignment of VL after panning the EGFR-immunized chicken scFv library via Phage Display. For calculation of unique clones, sequences containing ambiguities (X) where not taken into account. Sequences containing stop-codons or frame-shifts were excluded from analysis. Alignment was created using MUSCLE Alignment tool within Geneious Prime software (www.geneious.com).

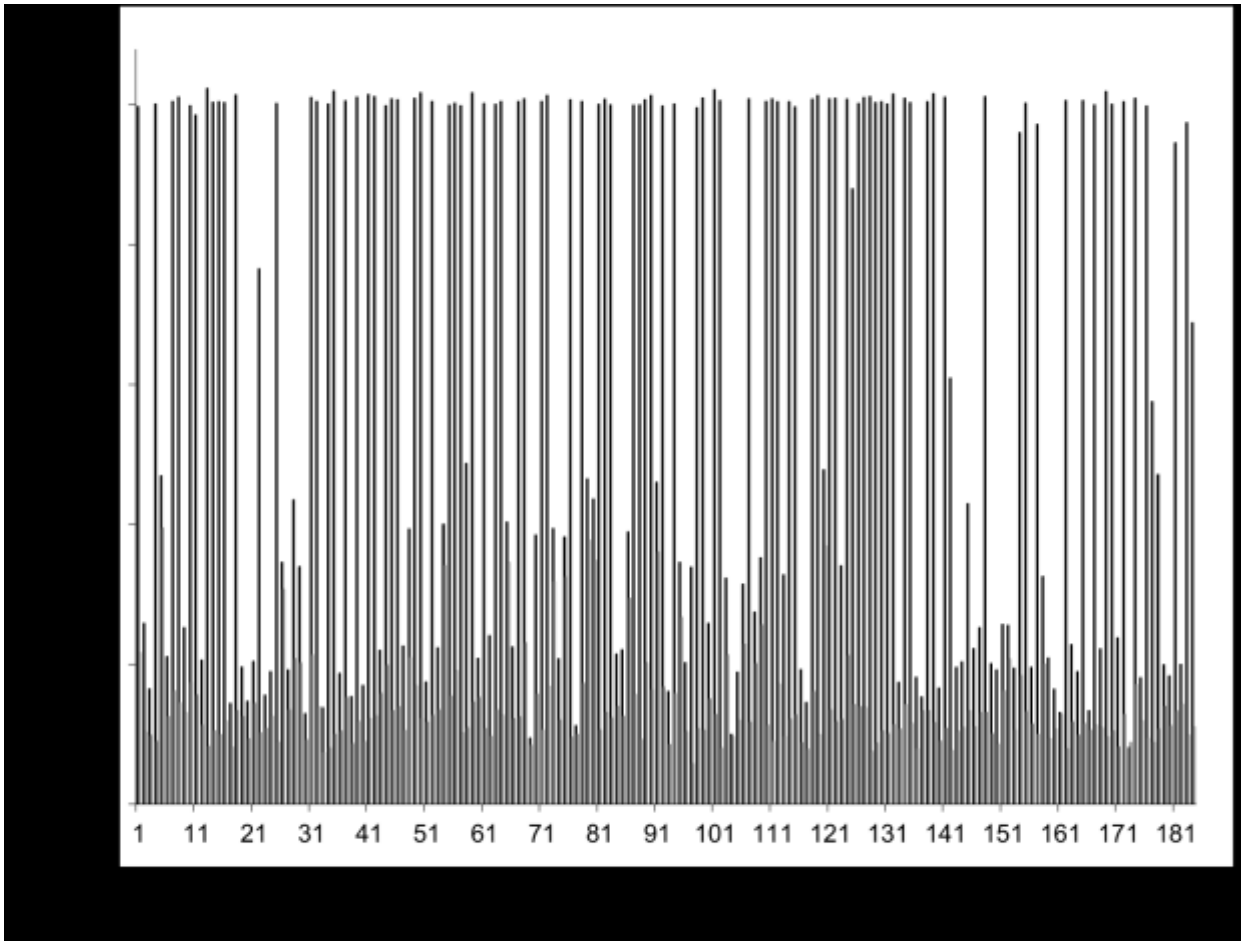

Figure S5: ELISA screening after microtiter production of selected chicken scFv library candidates in *E. coli*. Black: ELISA signal against EGFR, grey: Absorbance at 450 nm against unrelated negative control antigen.

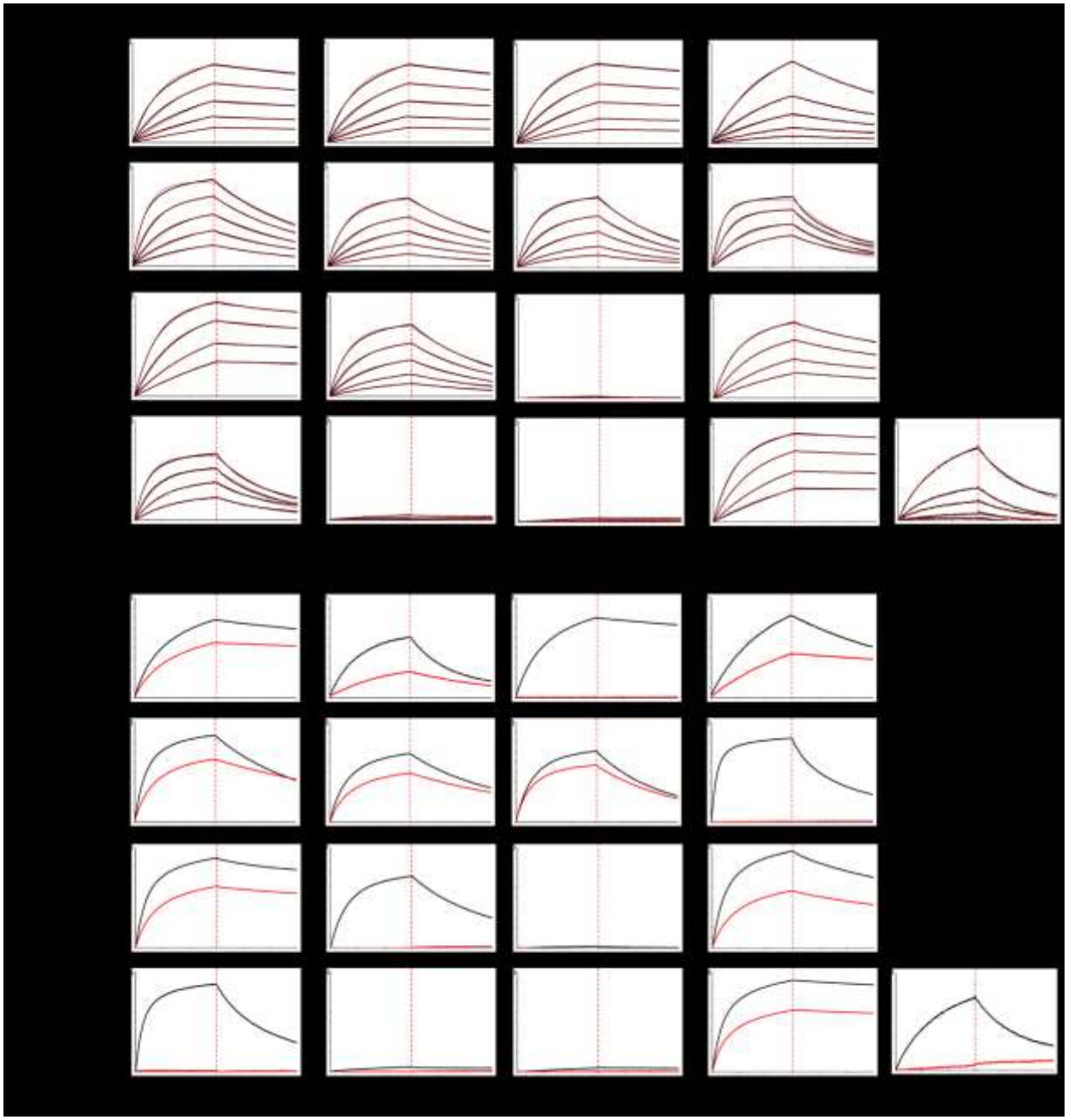

Figure S6: (A) Binding kinetics of phage display-derived anti-EGFR scFvs (78_H06-70_B02) and VHHs (75_A11-75_H11) as determined via BLI. Antibody binders were loaded onto AHC tips. Association was measured against soluble human EGFR (ECD, concentration range: 100 nM – 6.25 nM)). (B) Species-crossreactive binding against recombinant human EGFR (ECD, black) and recombinant mouse EGFR (ECD, red) for given antibody derivatives. Antibodies were captured onto AHC tips. Binding was measured at a concentration of 100 nM antigen.

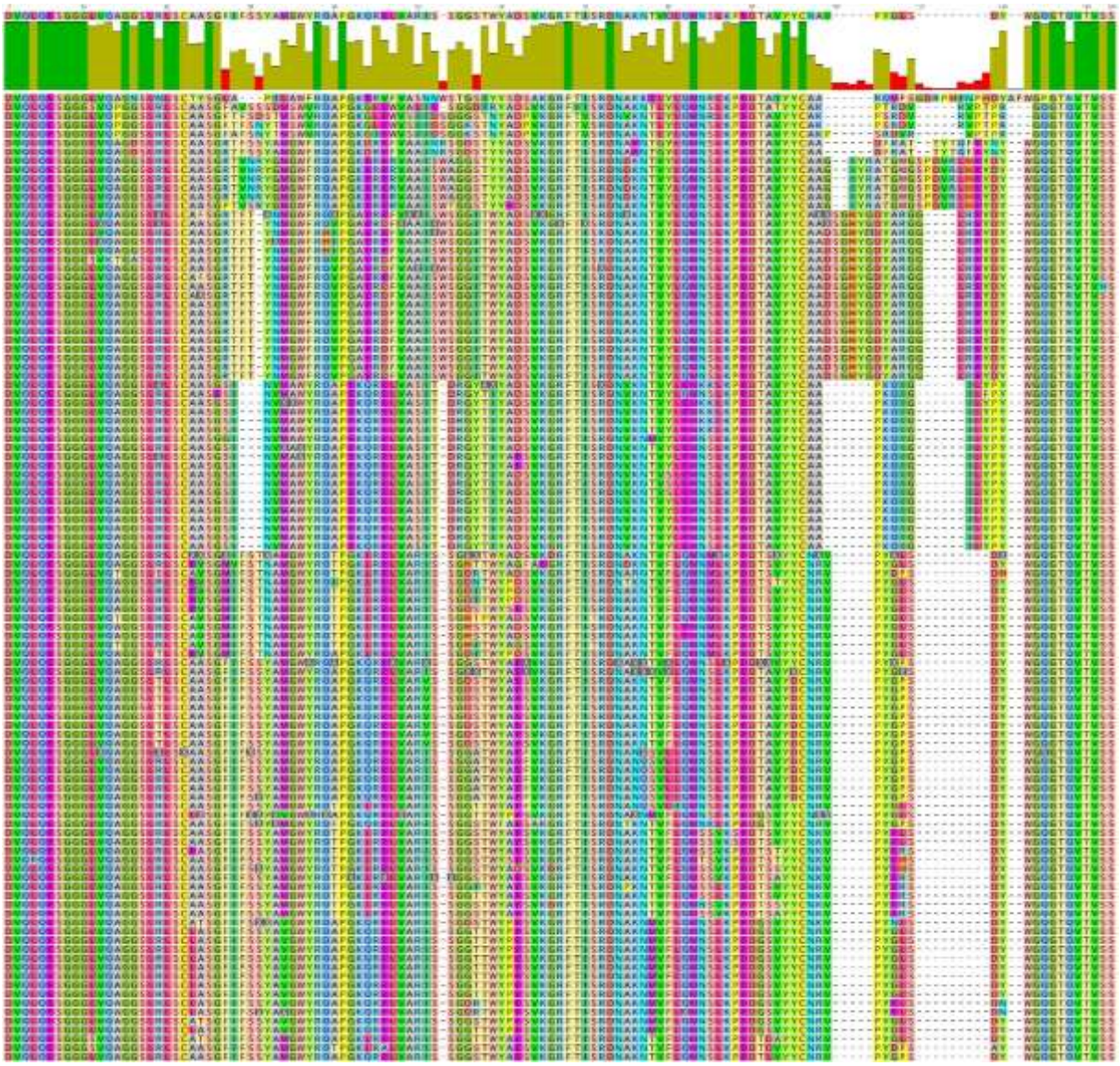

Figure S7: Multiple sequence alignment of VHH after panning the EGFR-immunized Llama-derived VHH libraries via Phage Display. For calculation of unique clones, sequences containing ambiguities (X) where not taken into account. Sequences containing stop-codons or frame-shifts were excluded from analysis. Alignment was created using MUSCLE Alignment tool within Geneious Prime software (www.geneious.com).

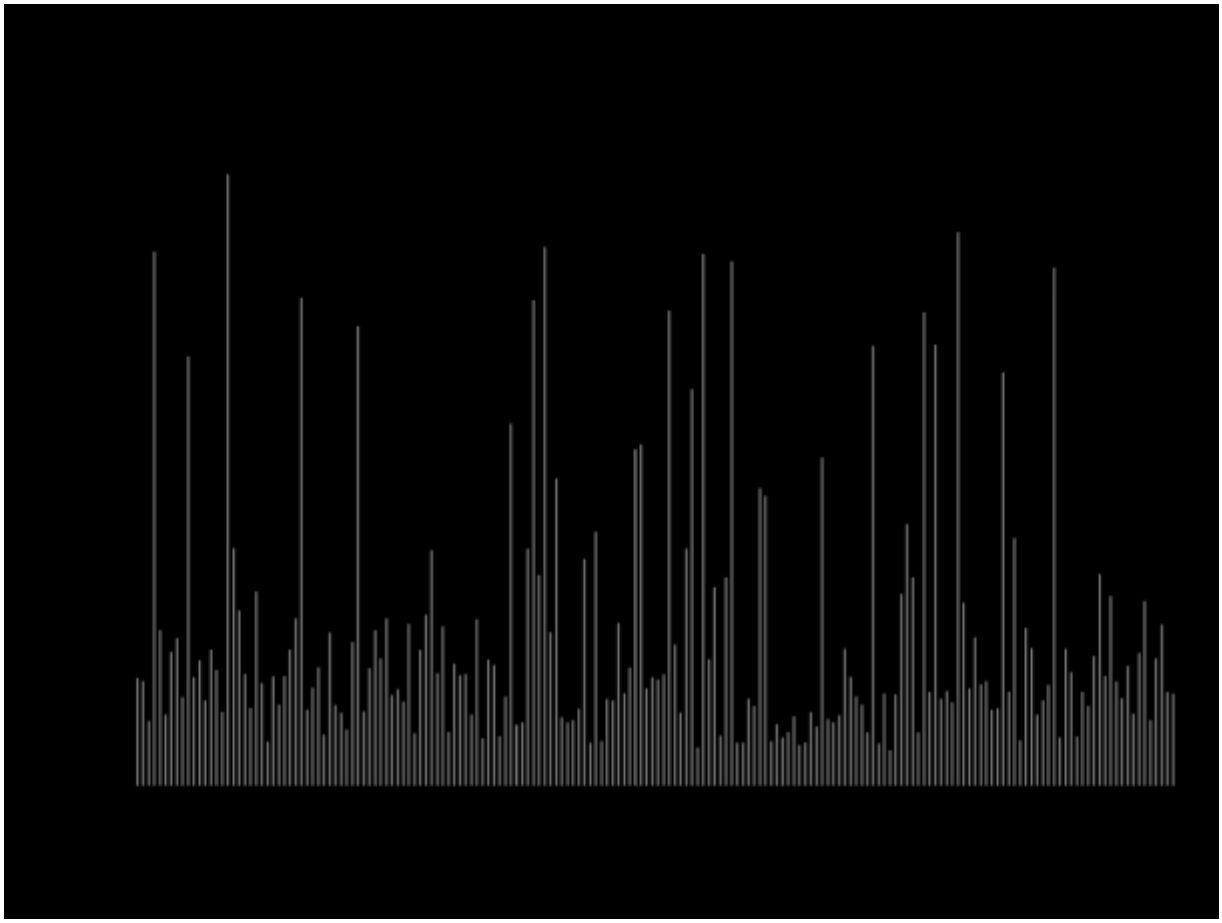

Figure S8: ELISA screening after microtiter production of selected camelid VHH library candidates in *E. coli*. A representative block of 188 consecutive clones as assessed by ELISA is shown. Black: ELISA signal against EGFR, grey: Absorbance at 450 nm against unrelated negative control antigen.

Table S1: Oligonucleotide primers used in this study. TypeIIs restriction sites are shown in italic, resulting overhangs i.e. signature sequences are underlined.

Name	Sequence (5′–3′)
Chicken_BsmBI_VH_up	TAGCTA***CGTCTC***TCCATGGCTGCCGTGACGTTGGACGAG
Chicken_BsmBI_VH_lo	TAGCTA***CGTCTC***TCACCGGAACTGACGATGACTTCGGT
Chicken_BsmBI_VL_up	TAGCTA***CGTCTC***TCGGTGCGCTGACTCAGCCGTCCTCG
Chicken_BsmBI_VL_lo	TAGCTA***CGTCTC***TCCGCTAGGACGGTCAGGGTTGTCCC
VHH_SapI_up	TAGCTA**GCTCTTC**TATGGCTGATGTGCAGCTGCAGGAGT CTGGGGGAGG
VHH_SapI_sh_lo	TAGCTA**GCTCTTC**TCGCGGGGTCTTCGCTGTGGTGCG
VHH_SapI_lh_lo	TAGCTA**GCTCTTC**TCGCTGGTTGTGGTTTTGGTGTCTTGG G
pHAL30_14_fw	TATGTTGTGTGGAATTGTGAGC
pHAL30_14_rev	GCTCTGATATCTTTGGATCCC

Table S2: Signature sequences

Name	Sequence (5′–3′)
BsmBI (ScFv Display)	
SigA	CCAT
SigB	GGTG
SigC	CGGT
SigZ	GCGG
SapI (VHH Display)	
SigA	ATG
SigZ	GCG

Table S3: Output titers during Phage Display panning.

Library	Primer/Germline	Round 1 [cfu]	Round 2 [cfu]	Round 3 [cfu]
Chicken scFv	-	1×10^6	0.7×10^6	1×10^4
Llama 1 VHH	Short hinge	4×10^6	5×10^6	3×10^4
	Long hinge	10×10^6	8×10^6	2×10^5
Llama 2 VHH	Short hinge	4×10^5	7×10^6	3×10^5
	Long hinge	2×10^6	5×10^5	3×10^5

7.3 Biophysical and biochemical characterization of a VHH-based IgG-like bi- and trispecific antibody platform

Supplementary Information: Biophysical and biochemical characterization of a VHH-based IgG-like bi- and trispecific antibody platform

Lukas Pekar[1], Michael Busch[2], Bernhard Valldorf[3], Steffen C. Hinz[1], Lars Toleikis[4], Simon Krah[4], Stefan Zielonka[4+]

[1]Institute for Organic Chemistry and Biochemistry, Technische Universität Darmstadt, Alarich-Weiss-Strasse 4, D-64287 Darmstadt, Germany

[2]Discovery Pharmacology, Merck KGaA, Frankfurter Strasse 250, D-64293 Darmstadt, Germany

[3]Chemical and Pharmaceutical Development, Merck KGaA, Frankfurter Straße 250, D-64293 Darmstadt, Germany

[4]Protein Engineering and Antibody Technologies, Merck KGaA, Frankfurter Strasse 250, D-64293 Darmstadt, Germany

[+] To whom correspondence should be addressed:

Stefan Zielonka, Protein Engineering and Antibody Technologies, Merck KGaA, Frankfurter Strasse 250, D-64293 Darmstadt, Germany, E-mail: Stefan.Zielonka@merckgroup.com

A

>Her2_2Rb17c (WO2016016021)
QVQLQESGGGLVQPGGSLRLSCAASGFIFSNDAMTWVRQAPGKGLQWVSSINWSGTHTNYADSVKGRFTISRDNAKRTLY
LQMNSLKDQDTALYYCVTGYGVTKTPTGQGTQVTVSS
>EGFR_722C03 (internal yeast surface display campaign)
DVQLQESGGGLVQAGGSLRLSCAASGFIFSSYAMGWYRQAPGKLRELVARISSGGSTWYSESVKGRFTISRDNAKNTVFL
QMNKLKPEDGVVYYCNRVPYGPSDYWGQGTQVTVSS
>EGFR_9G8 (PDB 4KRP)
EVQLVESGGGLVQAGGSLRLSCAASGRTFSSYAMGWFRQAPGKEREFVVAINWSSGSTYYADSVKGRFTISRDNAKNTMY
LQMNSLKPEDTAVYYCAAGYQINSGNYNFKDYEYDYWGQGTQVTVSS
>NKG2D_ET1F08 (WO2017081190)
QVQLVQSGGGLVQAGGSLRLSCAASGLTISNYAMAWFRQAPGKEREFVALINWSGNKYYADSVKGRFTIARDNAKNTVDL
QMNSLKPEDTAVYYCAARFHSYAASTYYSASTYKFWGQGTQVTVSS

B

> EGFR_9G8 grafted on CH1
EVQLVESGGGLVQAGGSLRLSCAASGRTFSSYAMGWFRQAPGKEREFVVAINWSSGSTYYADSVKGRFTISRDNAKNTMY
LQMNSLKPEDTAVYYCAAGYQINSGNYNFKDYEYDYWGQGTQVTVSSASTKGPSVFPLAPSSKSTSGGTAALGCLVKDYF
PEPVTVSWNSGALTSGVHTFPAVLQSSGLYSLSSVVTVPSSSLGTQTYICNVNHKPSNTKVDKKVEPKSC
> Her2_2Rb17c grafted on Cλ
QVQLQESGGGLVQPGGSLRLSCAASGFIFSNDAMTWVRQAPGKGLQWVSSINWSGTHTNYADSVKGRFTISRDNAKRTLY
LQMNSLKDQDTALYYCVTGYGVTKTPTGQGTQVTVSSGQPKAAPSVTLFPPSSEELQANKATLVCLISDFYPGAVTVAWK
ADSSPVKAGVETTTPSKQSNNKYAASSYLSLTPEQWKSHKSYSCQVTHEGSTVEKTVAPTECS
> Her2_2Rb17c grafted on Cκ
QVQLQESGGGLVQPGGSLRLSCAASGFIFSNDAMTWVRQAPGKGLQWVSSINWSGTHTNYADSVKGRFTISRDNAKRTLY
LQMNSLKDQDTALYYCVTGYGVTKTPTGQGTQVTVSSRTVAAPSVFIFPPSDEQLKSGTASVVCLLNNFYPREAKVQWKV
DNALQSGNSQESVTEQDSKDSTYSLSSTLTLSKADYEKHKVYACEVTHQGLSSPVTKSFNRGEC
> Her2_2Rb17c grafted on Cκ with 10 amino acid linker between VHH and Cκ
QVQLQESGGGLVQPGGSLRLSCAASGFIFSNDAMTWVRQAPGKGLQWVSSINWSGTHTNYADSVKGRFTISRDNAKRTLY
LQMNSLKDQDTALYYCVTGYGVTKTPTGQGTQVTVSSGGSGGSGSGSRTVAAPSVFIFPPSDEQLKSGTASVVCLLNNFY
PREAKVQWKVDNALQSGNSQESVTEQDSKDSTYSLSSTLTLSKADYEKHKVYACEVTHQGLSSPVTKSFNRGEC

Fig. S1: (A) Amino acid sequences of VHHs used in this study. HER2-specific VHH_2Rb17c sequence was obtained from WO2016016021, EGFR_722C03 was generated by combining camelid immunization and yeast surface display, EGFR_9G8 was derived from PDB:KRP and NKG2D_ET1F08 from WO2017081190. (B) Design examples of VHHs as grafted on constant regions of human antibodies (IgG1).

Table S1: Binding affinities (KD) and corresponding on-rates (Kon) and off-rates (Koff) for each paratope of the antibody molecules tested in this study. Every KD value was determined individually via biolayer interferometry analysis.

Name	Format (Fig. 1)	Paratope 1 (AG chain)	Paratope 2 (Light chain)	Paratope 3 (GA chain)	KD (M) Paratope 1	Kon (1/Ms) Paratope 1	Koff (1/s) Paratope 1	KD (M) Paratope 2	Kon (1/Ms) Paratope 2	Koff (1/s) Paratope 2	KD (M) Paratope 3	Kon (1/Ms) Paratope 3	Koff (1/s) Paratope 3
Ctrl1	F	EGFR (9G8)	-	-	1.36E-09	2.01E+05	2.72E-04	-	-	-	-	-	-
Ctrl2	F	NKG2D	-	-	7.32E-09	9.45E+05	6.92E-03	-	-	-	-	-	-
Ctrl3	F	HER2	-	-	1.09E-08	2.08E+05	2.26E-03	-	-	-	-	-	-
Ctrl4	F	EGFR (722C03)	-	-	2.20E-09	3.05E+05	6.71E-04	-	-	-	-	-	-
MoBi1	C (Kappa)	EGFR (9G8)	NKG2D	-	1.80E-09	1.56E+05	2.81E-04	5.98E-09	2.88E+05	1.72E-03	-	-	-
MoBi2	C (Lambda)	EGFR (9G8)	NKG2D	-	1.54E-09	1.84E+05	2.84E-04	6.18E-09	2.36E+05	1.46E-03	-	-	-
MoBi3	C (Kappa)	NKG2D	EGFR (9G8)	-	4.13E-09	2.75E+05	1.13E-03	1.59E-09	1.75E+05	2.78E-04	-	-	-
MoBi4	C (Lambda)	NKG2D	EGFR (9G8)	-	4.37E-09	2.71E+05	1.18E-03	1.47E-09	1.75E+05	2.58E-04	-	-	-
MoBi5	C (Kappa)	NKG2D	EGFR (722C03)	-	1.19E-08	2.09E+05	2.48E-03	2.83E-09	3.43E+05	9.69E-04	-	-	-
MoBi6	C (Lambda)	NKG2D	EGFR (722C03)	-	9.87E-09	2.44E+05	2.41E-03	2.60E-09	2.78E+05	7.23E-04	-	-	-
MoBi7	C (Kappa)	EGFR (9G8)	HER2	-	6.98E-10	2.13E+05	1.48E-04	9.75E-09	8.87E+05	8.65E-03	-	-	-
MoBi8	C (Lambda)	EGFR (9G8)	HER2	-	1.42E-09	2.29E+05	3.26E-04	8.11E-09	1.14E+06	9.24E-03	-	-	-
MoBi9	C (Kappa)	EGFR (722C03)	HER2	-	2.59E-09	2.99E+05	7.73E-04	1.37E-08	6.46E+05	8.85E-03	-	-	-
MoBi10	C (Lambda)	EGFR (722C03)	HER2	-	2.49E-09	3.09E+05	7.67E-04	1.28E-08	7.17E+05	9.17E-03	-	-	-
MoBi11	C (Kappa)	NKG2D	HER2	-	1.44E-08	1.72E+05	2.48E-03	1.03E-08	9.22E+05	9.51E-03	-	-	-
MoBi12	C (Lambda)	NKG2D	HER2	-	1.65E-08	1.82E+05	3.00E-03	6.56E-09	1.12E+06	7.37E-03	-	-	-
MoBi13	C (Kappa + 10 aa linker)	EGFR (9G8)	HER2	-	1.26E-09	2.33E+05	2.94E-04	1.12E-08	8.90E+05	9.93E-03	-	-	-
MoBi14	C (Kappa + 10 aa linker)	EGFR (722C03)	HER2	-	2.51E-09	3.13E+05	7.86E-04	1.24E-08	7.22E+05	8.94E-03	-	-	-
BiBi1	B (Kappa)	EGFR (9G8)	HER2	-	9.27E-10	1.98E+05	1.83E-04	1.11E-08	8.55E+05	9.46E-03	-	-	-
BiBi2	B (Lambda)	EGFR (9G8)	HER2	-	1.56E-09	1.85E+05	2.90E-04	7.11E-09	1.08E+06	7.71E-03	-	-	-
BiBi3	B (Kappa)	NKG2D	HER2	-	5.92E-09	2.05E+05	1.22E-03	7.44E-09	8.70E+05	6.47E-03	-	-	-

BiBi4	B (Lambda)	NKG2D	HER2	-	7.87E-09	2.41E+05	1.90E-03	5.01E-09	1.33E+06	6.68E-03	-	-	-
BiBi5	B (Kappa)	NKG2D	EGFR (9G8)	-	4.73E-09	2.16E+05	1.02E-03	9.82E-10	2.06E+05	2.03E-04	-	-	-
BiBi6	B (Lambda)	NKG2D	EGFR (9G8)	-	4.33E-09	2.28E+05	9.86E-04	1.27E-09	1.95E+05	2.48E-04	-	-	-
BiBi7	B (Kappa)	NKG2D	EGFR (722C03)	-	7.75E-09	2.01E+05	1.56E-03	2.79E-09	3.04E+05	8.49E-04	-	-	-
BiBi8	B (Lambda)	NKG2D	EGFR (722C03)	-	6.08E-09	2.08E+05	1.27E-03	2.91E-09	2.95E+05	8.59E-04	-	-	-
BiBi9	B (Kappa + 10 aa linker)	EGFR (9G8)	HER2	-	1.79E-09	1.63E+05	2.92E-04	1.73E-08	7.03E+05	1.22E-02	-	-	-
MoTri1	D (Kappa)	EGFR (9G8)	HER2	NKG2D	2.59E-09	1.34E+05	3.47E-04	9.53E-09	1.13E+06	1.08E-02	1.31E-08	2.15E+05	2.82E-03
MoTri2	D (Lambda)	EGFR (9G8)	HER2	NKG2D	2.72E-09	1.33E+05	3.62E-04	4.85E-09	1.70E+06	8.26E-03	1.16E-08	2.26E+05	2.61E-03
MoTri3	D (Kappa)	NKG2D	HER2	EGFR (9G8)	7.91E-09	3.14E+05	2.48E-03	2.22E-09	2.45E+06	5.43E-03	1.43E-09	1.68E+05	2.40E-04
MoTri4	D (Lambda)	NKG2D	HER2	EGFR (9G8)	8.11E-09	2.66E+05	2.16E-03	4.09E-09	1.86E+06	7.60E-03	1.96E-09	1.92E+05	3.76E-04
MoTri5	D (Kappa)	HER2	EGFR (722C03)	NKG2D	1.35E-08	6.43E+05	8.69E-03	1.44E-09	3.09E+05	4.45E-04	1.14E-08	2.17E+05	2.48E-03
MoTri6	D (Lambda)	HER2	EGFR (722C03)	NKG2D	1.23E-08	7.14E+05	8.79E-03	1.65E-09	2.98E+05	4.92E-04	8.05E-09	2.78E+05	2.24E-03
MoTri7	D (Kappa + 10 aa linker)	EGFR (9G8)	HER2	NKG2D	2.82E-09	1.40E+05	3.93E-04	1.64E-09	3.89E+06	6.40E-03	1.06E-08	2.61E+05	2.77E-03
BiTri1	E (Kappa)	EGFR (9G8)	HER2	NKG2D	1.07E-09	2.26E+05	2.40E-04	1.09E-08	8.22E+05	8.98E-03	9.94E-09	2.26E+05	2.25E-03
BiTri2	E (Lambda)	EGFR (9G8)	HER2	NKG2D	1.74E-09	1.73E+05	3.02E-04	9.90E-09	1.09E+06	1.08E-02	9.00E-09	2.84E+05	2.56E-03
BiTri3	E (Kappa)	EGFR (722C03)	HER2	NKG2D	1.37E-09	3.35E+05	4.57E-04	1.20E-08	6.36E+05	7.62E-03	1.37E-08	1.99E+05	2.71E-03
BiTri4	E (Lambda)	EGFR (722C03)	HER2	NKG2D	1.63E-09	3.27E+05	5.31E-04	9.92E-09	6.98E+05	6.92E-03	7.95E-09	2.97E+05	2.36E-03
BiTri5	E (Kappa + 10 aa linker)	EGFR (9G8)	HER2	NKG2D	1.48E-09	2.16E+05	3.19E-04	5.42E-09	1.86E+06	1.01E-02	9.23E-09	2.55E+05	2.35E-03

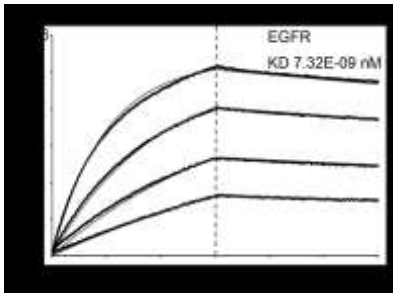
EGFR
KD 7.32E-09 nM

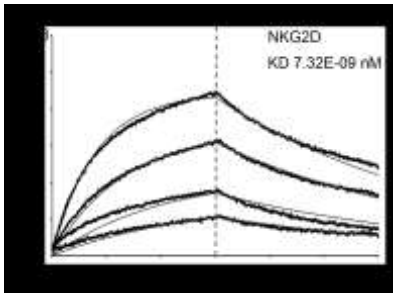
NKG2D
KD 7.32E-09 nM

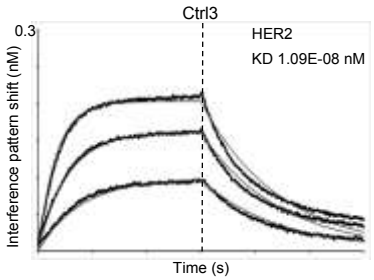
Ctrl3
0.3
HER2
KD 1.09E-08 nM
Interference pattern shift (nM)
Time (s)

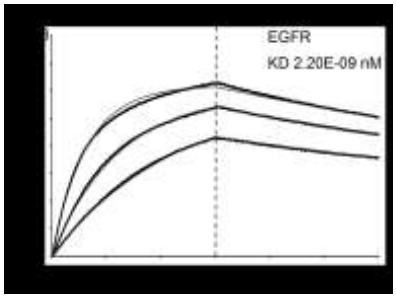
EGFR
KD 2.20E-09 nM

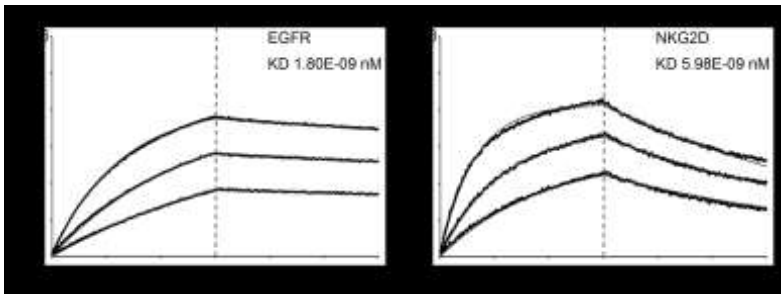
EGFR
KD 1.80E-09 nM
NKG2D
KD 5.98E-09 nM

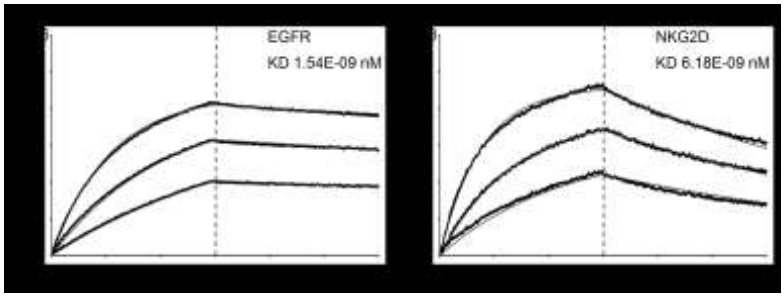
EGFR
KD 1.54E-09 nM
NKG2D
KD 6.18E-09 nM

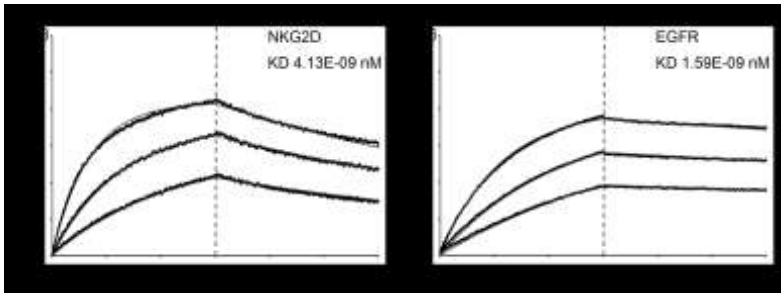
NKG2D
KD 4.13E-09 nM
EGFR
KD 1.59E-09 nM

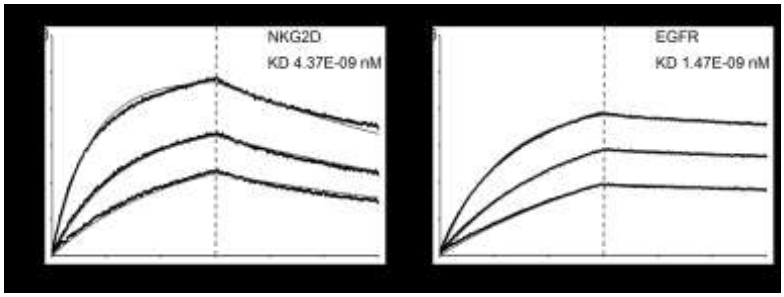
NKG2D
KD 4.37E-09 nM
EGFR
KD 1.47E-09 nM

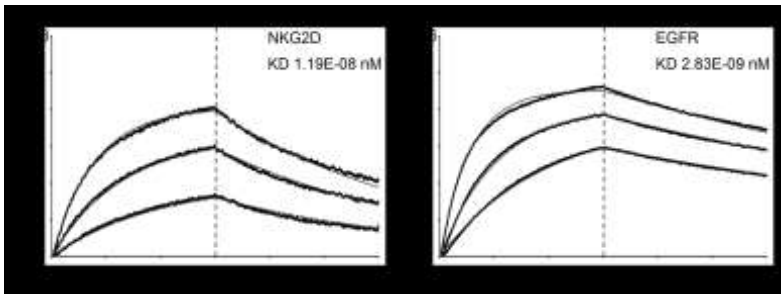
NKG2D
KD 1.19E-08 nM
EGFR
KD 2.83E-09 nM

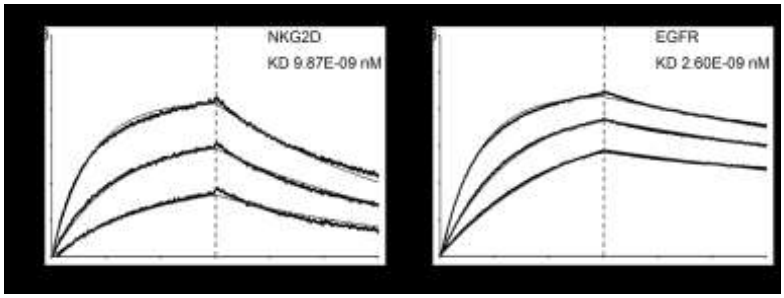
NKG2D
KD 9.87E-09 nM
EGFR
KD 2.60E-09 nM

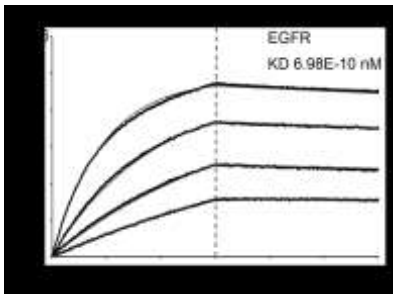
EGFR
KD 6.98E-10 nM

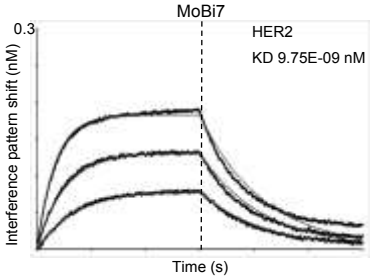
MoBi7
0.3
HER2
KD 9.75E-09 nM
Interference pattern shift (nM)
Time (s)

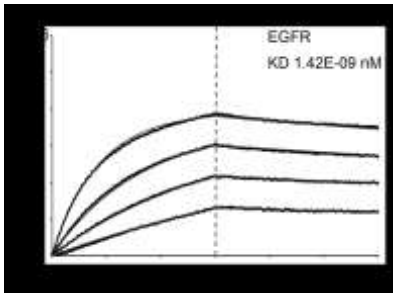
EGFR
KD 1.42E-09 nM

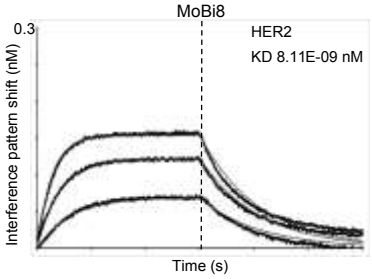
MoBi8
0.3
HER2
KD 8.11E-09 nM
Interference pattern shift (nM)
Time (s)

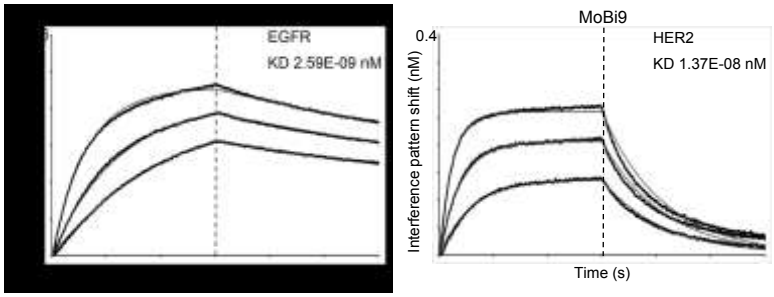
EGFR
KD 2.59E-09 nM
MoBi9
HER2
KD 1.37E-08 nM
0.4
Interference pattern shift (nM)
Time (s)

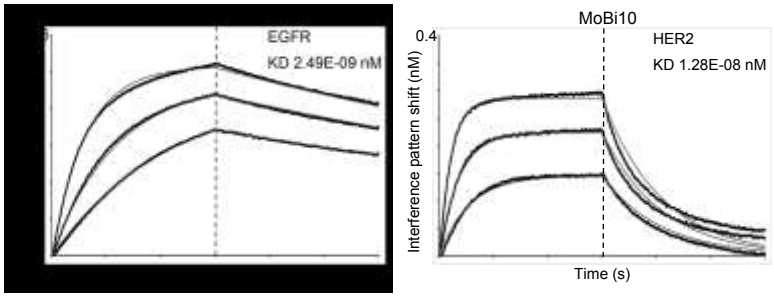
EGFR
KD 2.49E-09 nM
MoBi10
HER2
KD 1.28E-08 nM
0.4
Interference pattern shift (nM)
Time (s)

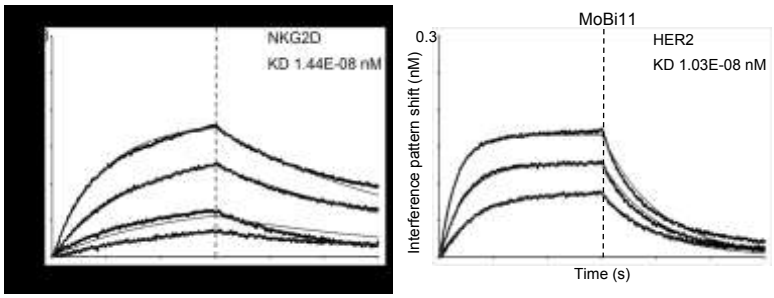
NKG2D
KD 1.44E-08 nM
MoBi11
HER2
KD 1.03E-08 nM
0.3
Interference pattern shift (nM)
Time (s)

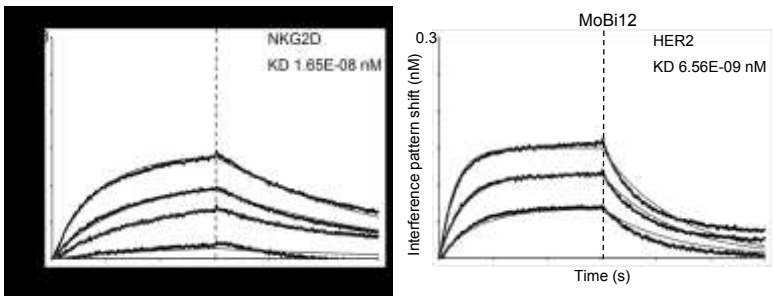
NKG2D
KD 1.65E-08 nM
MoBi12
HER2
KD 6.56E-09 nM
0.3
Interference pattern shift (nM)
Time (s)

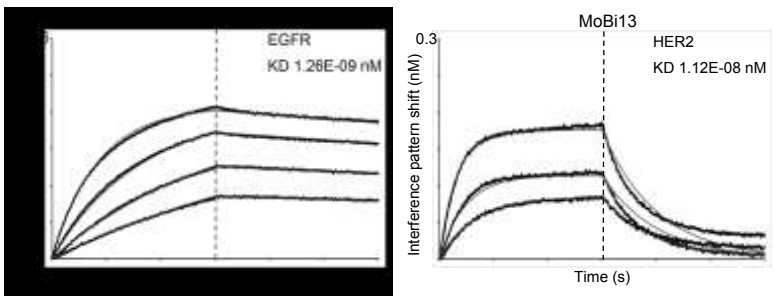
EGFR
KD 1.26E-09 nM
MoBi13
HER2
KD 1.12E-08 nM
0.3
Interference pattern shift (nM)
Time (s)

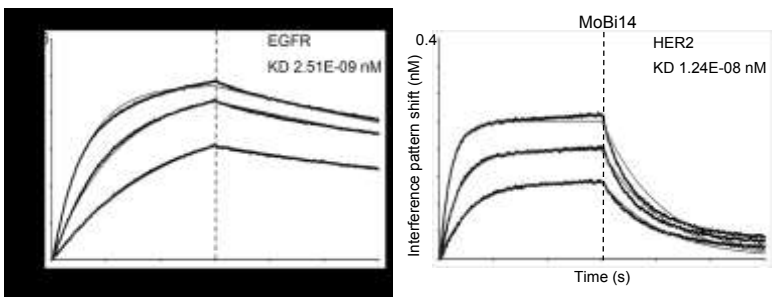
EGFR
KD 2.51E-09 nM
MoBi14
HER2
KD 1.24E-08 nM
0.4
Interference pattern shift (nM)
Time (s)

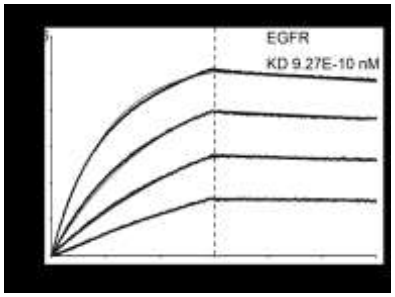
EGFR
KD 9.27E-10 nM

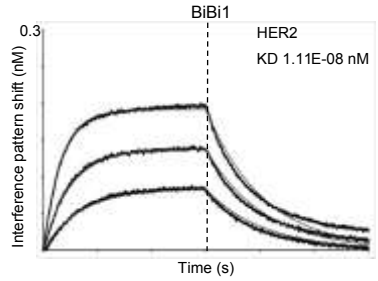
BiBi1
HER2
KD 1.11E-08 nM
0.3
Interference pattern shift (nM)
Time (s)

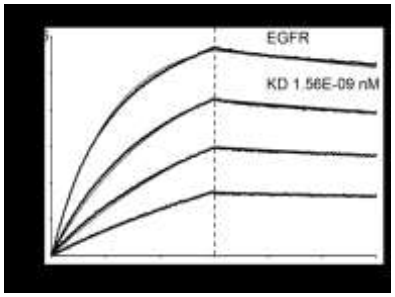
EGFR
KD 1.56E-09 nM

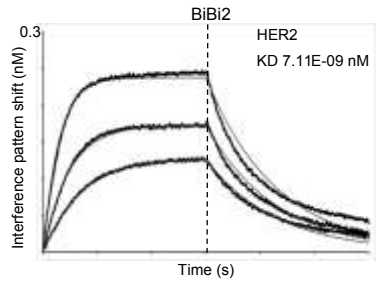
BiBi2
HER2
KD 7.11E-09 nM
0.3
Interference pattern shift (nM)
Time (s)

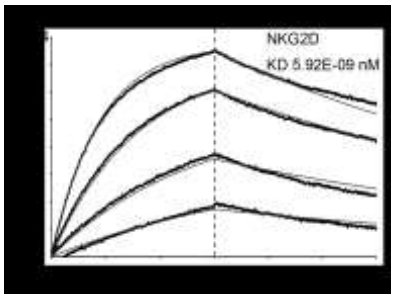
NKG2D
KD 5.92E-09 nM

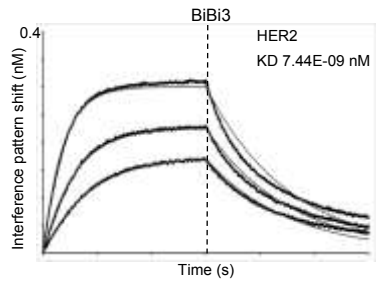
BiBi3
HER2
KD 7.44E-09 nM
0.4
Interference pattern shift (nM)
Time (s)

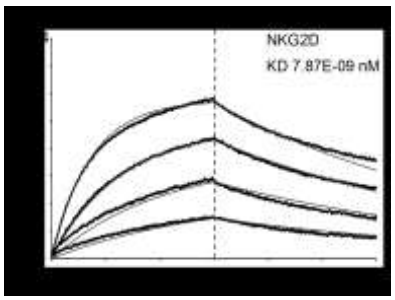
NKG2D
KD 7.87E-09 nM

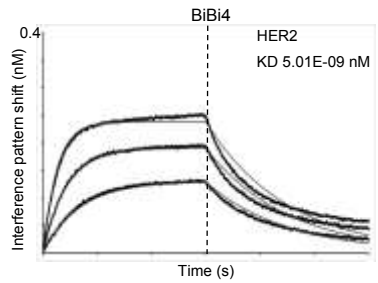
BiBi4
HER2
KD 5.01E-09 nM
0.4
Interference pattern shift (nM)
Time (s)

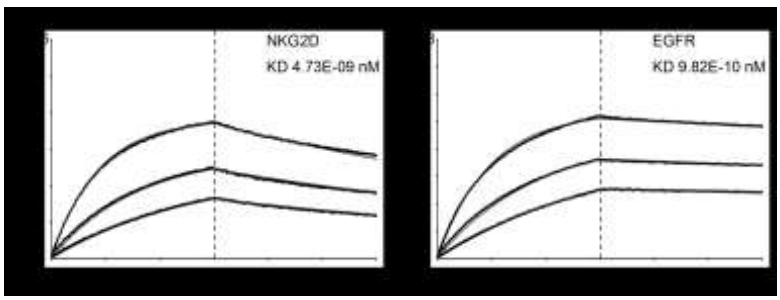
NKG2D
KD 4.73E-09 nM
EGFR
KD 9.82E-10 nM

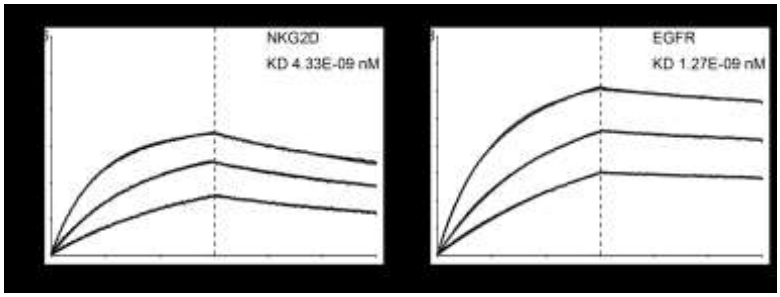
NKG2D
KD 4.33E-09 nM
EGFR
KD 1.27E-09 nM

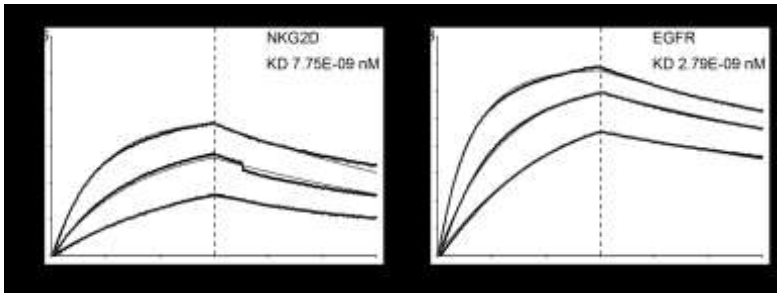
NKG2D
KD 7.75E-09 nM
EGFR
KD 2.79E-09 nM

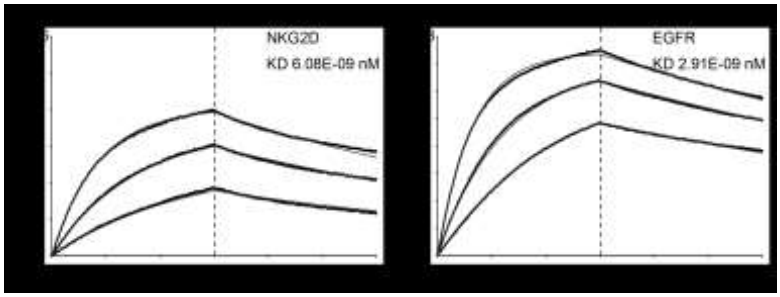
NKG2D
KD 6.08E-09 nM
EGFR
KD 2.91E-09 nM

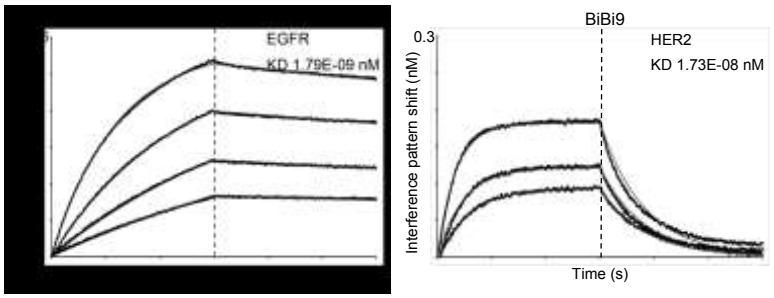
EGFR
KD 1.79E-09 nM
BiBi9
0.3
HER2
KD 1.73E-08 nM
Interference pattern shift (nM)
Time (s)

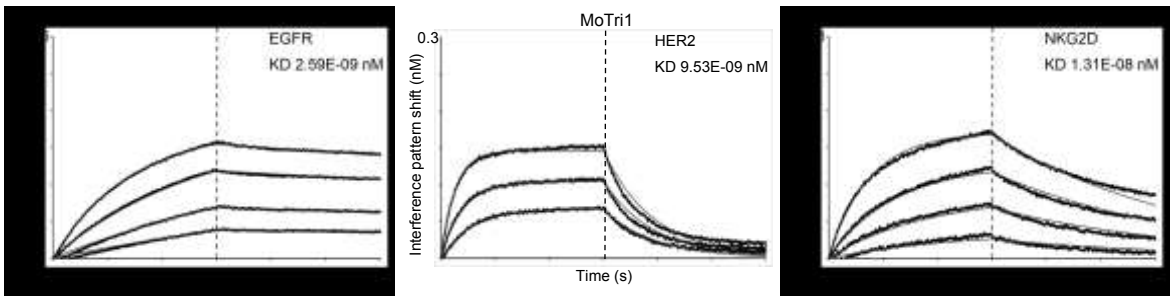
EGFR
KD 2.59E-09 nM
MoTri1
0.3
HER2
KD 9.53E-09 nM
Interference pattern shift (nM)
Time (s)
NKG2D
KD 1.31E-08 nM

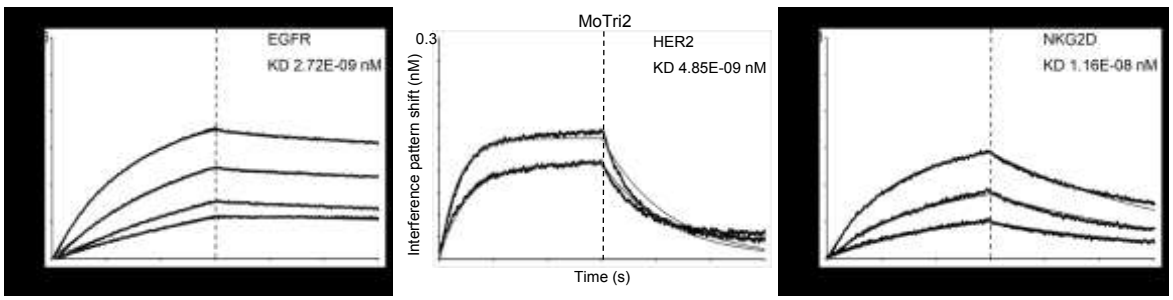
EGFR
KD 2.72E-09 nM
MoTri2
0.3
HER2
KD 4.85E-09 nM
Interference pattern shift (nM)
Time (s)
NKG2D
KD 1.16E-08 nM

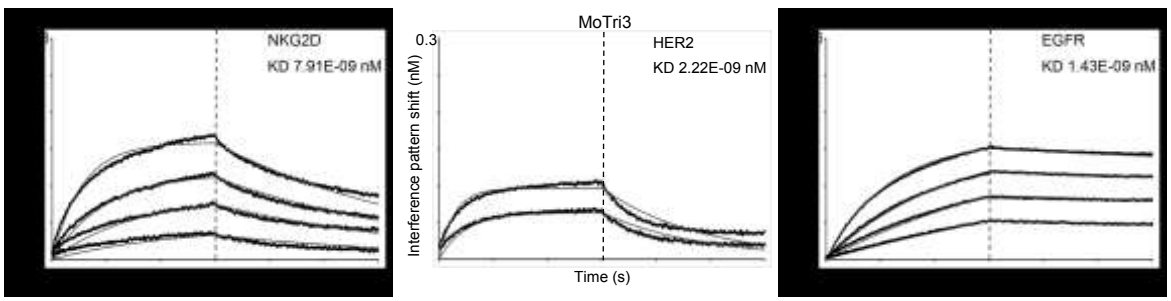
NKG2D
KD 7.91E-09 nM
MoTri3
0.3
HER2
KD 2.22E-09 nM
Interference pattern shift (nM)
Time (s)
EGFR
KD 1.43E-09 nM

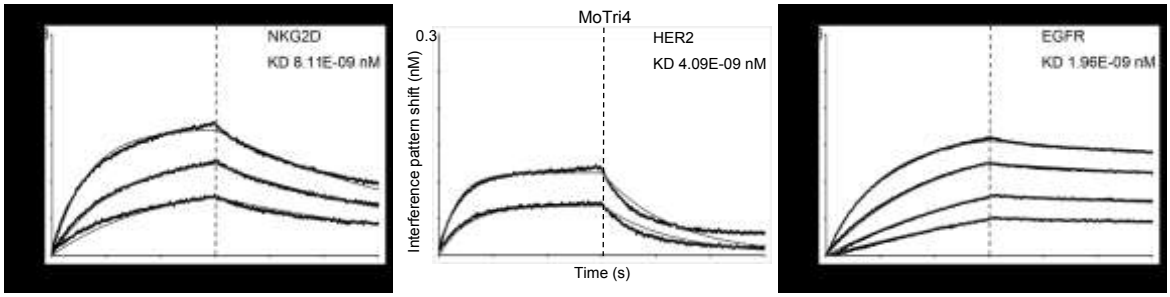
NKG2D
KD 8.11E-09 nM
MoTri4
0.3
HER2
KD 4.09E-09 nM
Interference pattern shift (nM)
Time (s)
EGFR
KD 1.96E-09 nM

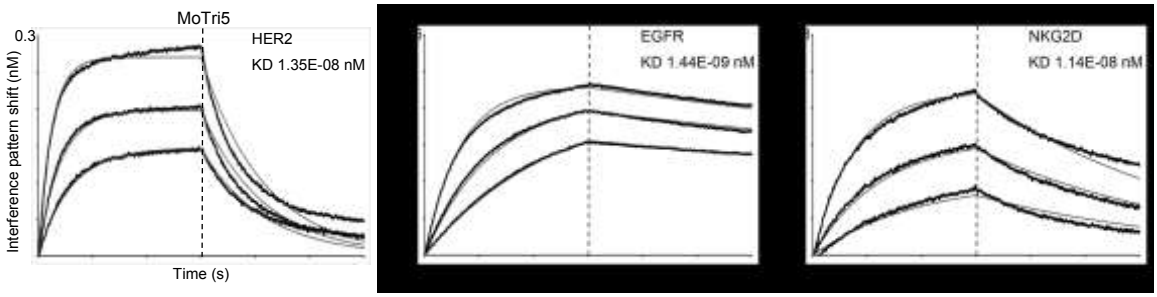
MoTri5
0.3
HER2
KD 1.35E-08 nM
Interference pattern shift (nM)
Time (s)
EGFR
KD 1.44E-09 nM
NKG2D
KD 1.14E-08 nM

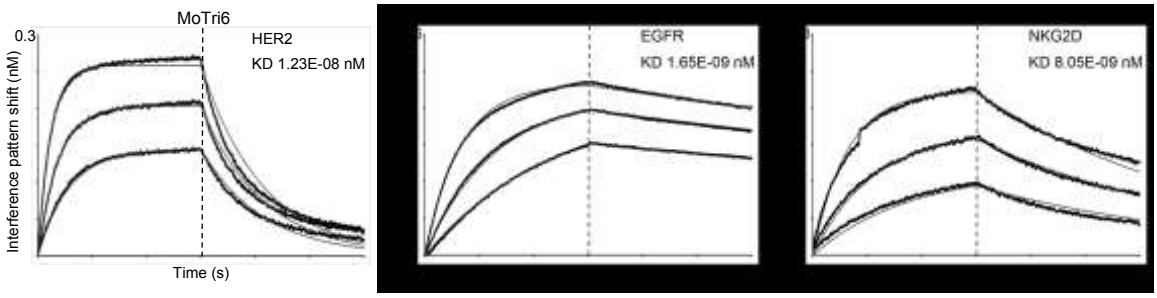
MoTri6
0.3
HER2
KD 1.23E-08 nM
Interference pattern shift (nM)
Time (s)
EGFR
KD 1.65E-09 nM
NKG2D
KD 8.05E-09 nM

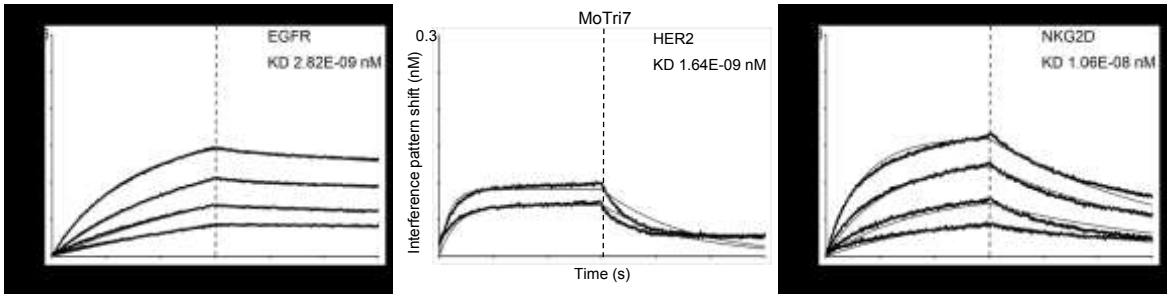
EGFR
KD 2.82E-09 nM
MoTri7
0.3
HER2
KD 1.64E-09 nM
Interference pattern shift (nM)
Time (s)
NKG2D
KD 1.06E-08 nM

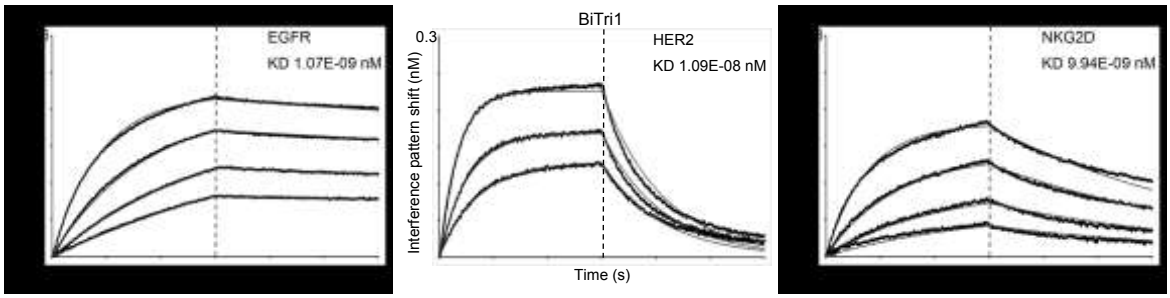
EGFR
KD 1.07E-09 nM
BiTri1
0.3
HER2
KD 1.09E-08 nM
Interference pattern shift (nM)
Time (s)
NKG2D
KD 9.94E-09 nM

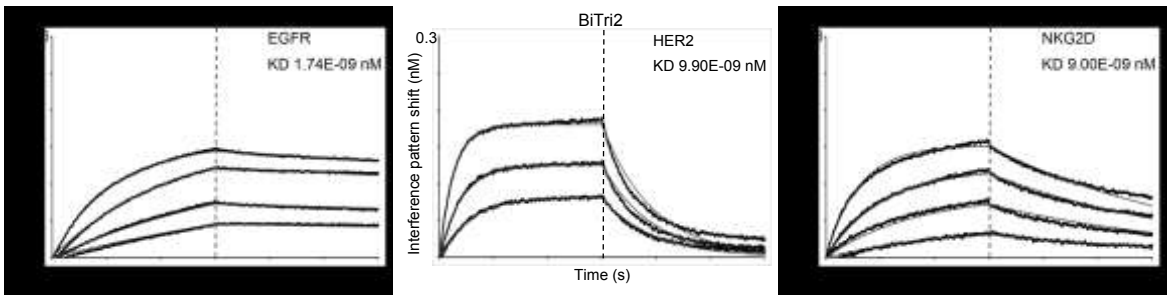
EGFR
KD 1.74E-09 nM
BiTri2
0.3
HER2
KD 9.90E-09 nM
Interference pattern shift (nM)
Time (s)
NKG2D
KD 9.00E-09 nM

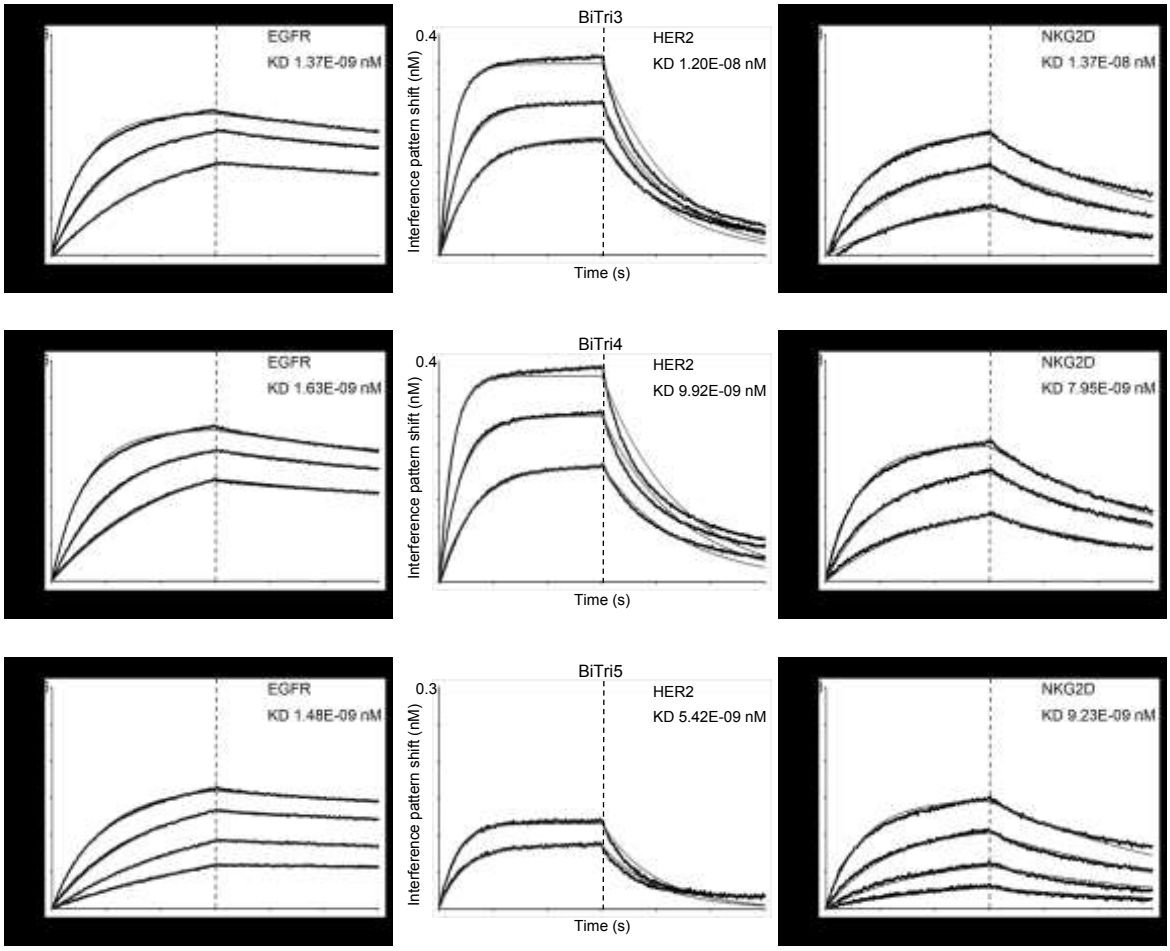

Fig. S2: Biolayer interferometry analysis for affinity determination of antibody molecules used in this study. One armed monovalent monospecific, one armed monovalent bispecific, bivalent bispecific, monovalent trispecific and bivalent trispecific molecules were characterized. Antigen binding was conducted for each antibody paratope separately with the respective antigen (EGFR, NKG2D and Her2) for 300 s, followed by a dissociation step in kinetics buffer for another 300 s.

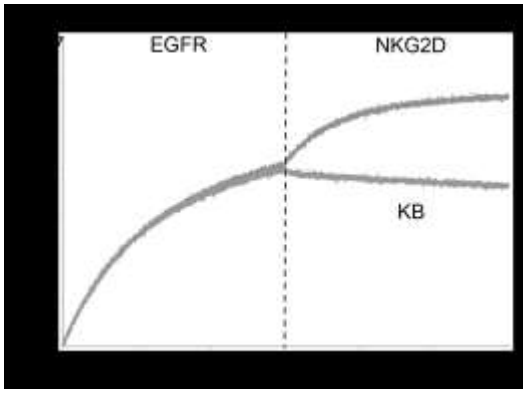
EGFR
NKG2D
KB

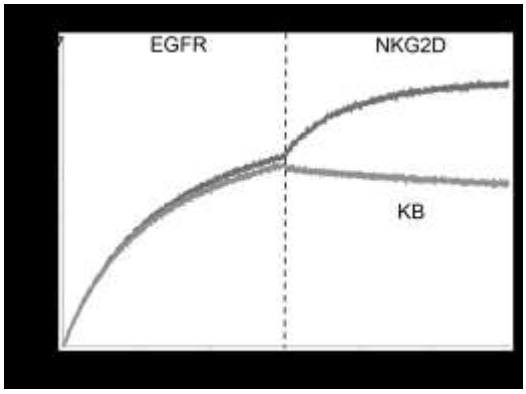
EGFR
NKG2D
KB

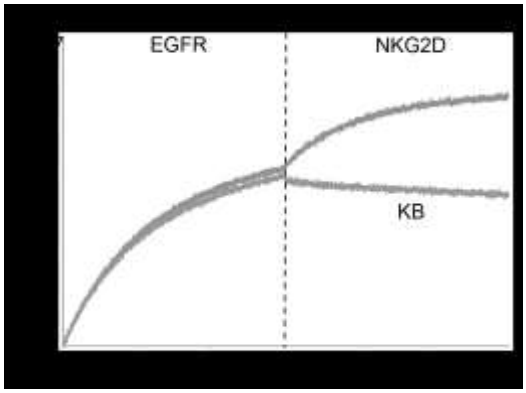
EGFR
NKG2D
KB

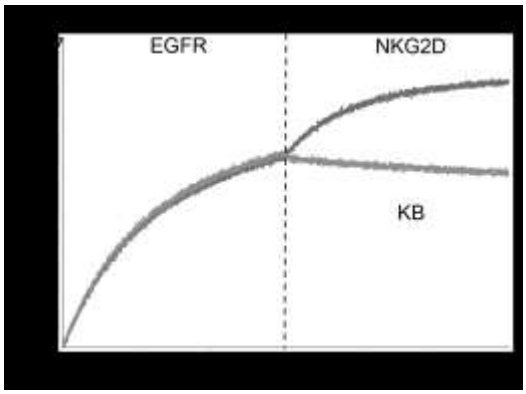
EGFR
NKG2D
KB

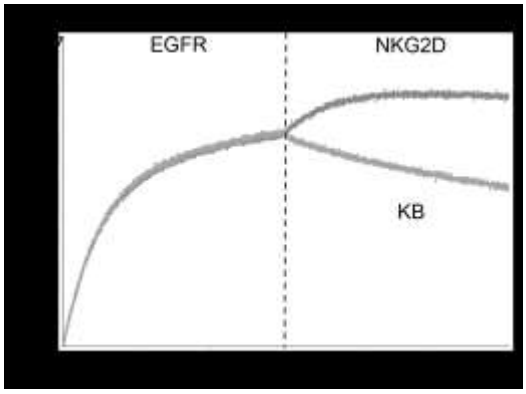
EGFR
NKG2D
KB

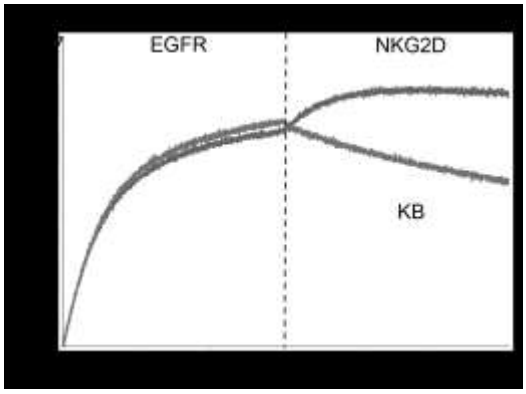
EGFR
NKG2D
KB

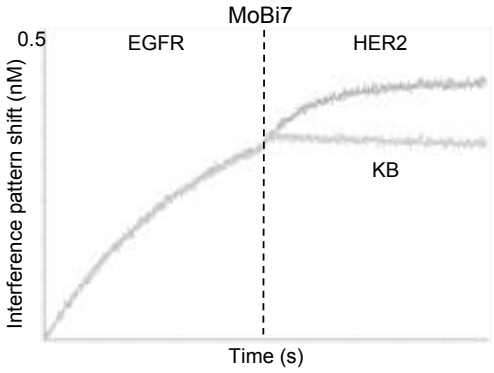
MoBi7
0.5
EGFR
HER2
KB
Interference pattern shift (nM)
Time (s)

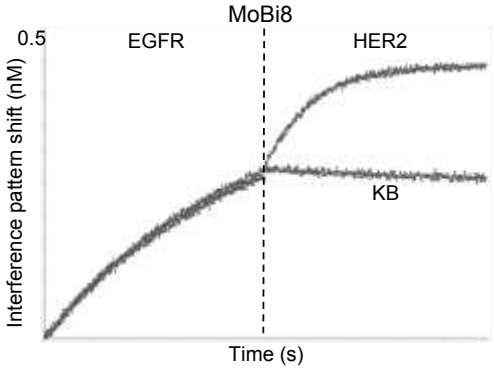
MoBi8
0.5
EGFR
HER2
KB
Interference pattern shift (nM)
Time (s)

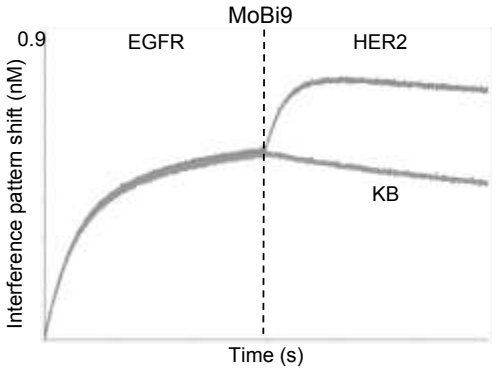
MoBi9
0.9
EGFR
HER2
KB
Interference pattern shift (nM)
Time (s)

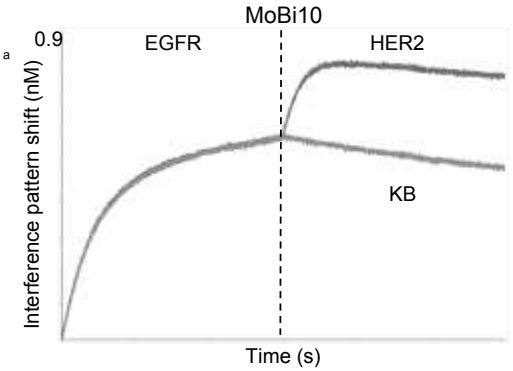
MoBi10
0.9
EGFR
HER2
KB
Interference pattern shift (nM)
Time (s)

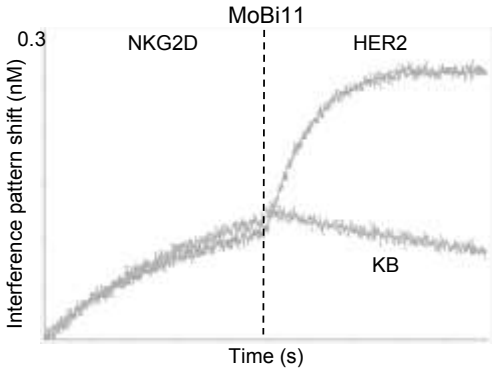
MoBi11
0.3
NKG2D
HER2
KB
Interference pattern shift (nM)
Time (s)

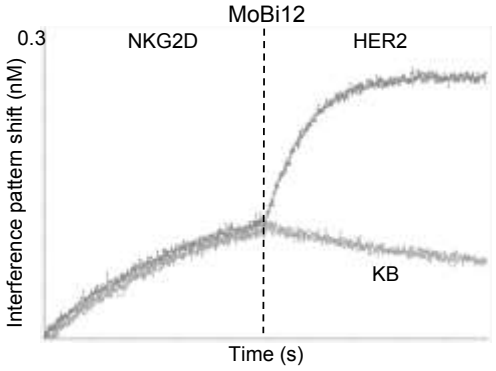
MoBi12
0.3
NKG2D
HER2
KB
Interference pattern shift (nM)
Time (s)

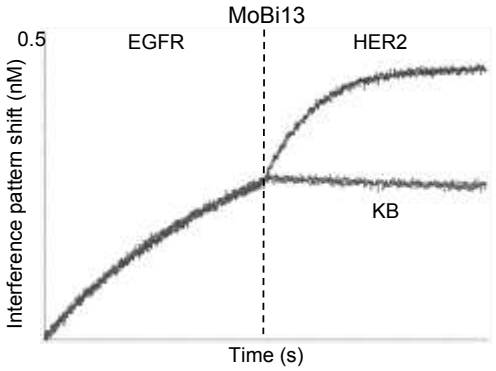
MoBi13
0.5
EGFR
HER2
KB
Interference pattern shift (nM)
Time (s)

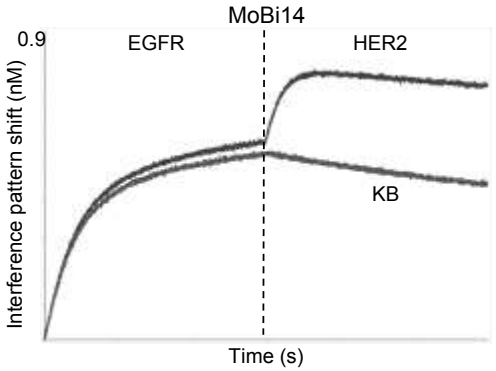
MoBi14
0.9
EGFR
HER2
KB
Interference pattern shift (nM)
Time (s)

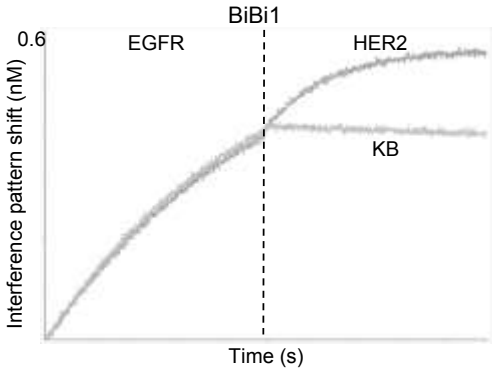
BiBi1
0.6
EGFR
HER2
KB
Interference pattern shift (nM)
Time (s)

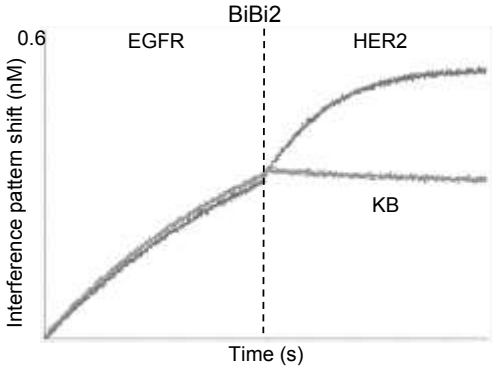
BiBi2
0.6
EGFR
HER2
KB
Interference pattern shift (nM)
Time (s)

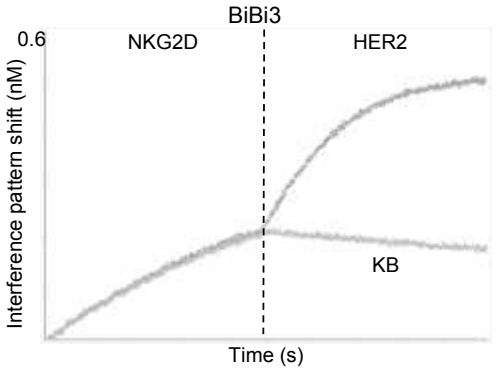
BiBi3
0.6
NKG2D
HER2
Interference pattern shift (nM)
KB
Time (s)

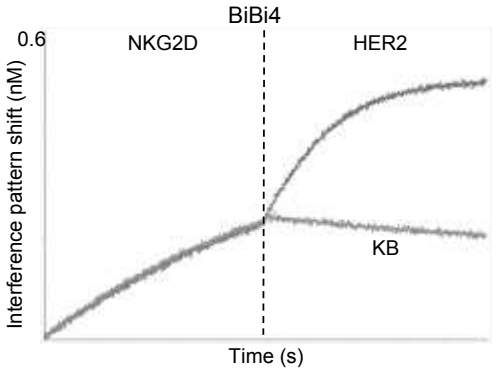
BiBi4
0.6
NKG2D
HER2
Interference pattern shift (nM)
KB
Time (s)

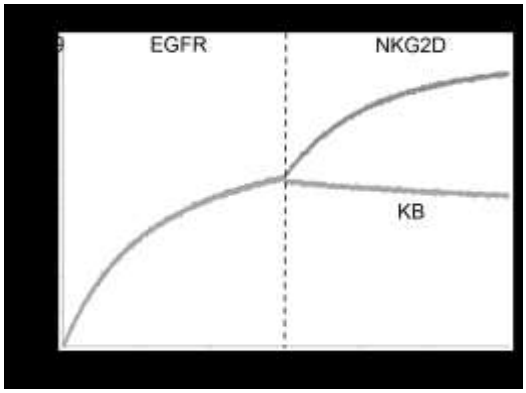
EGFR
NKG2D
KB

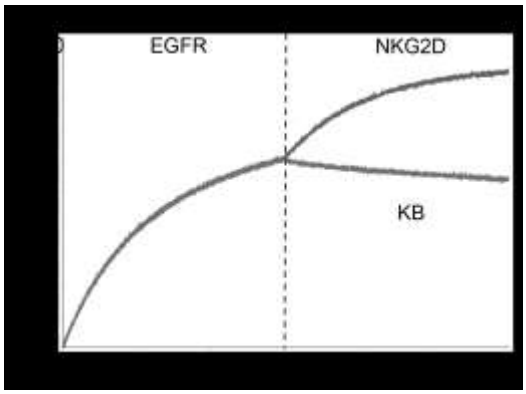
EGFR
NKG2D
KB

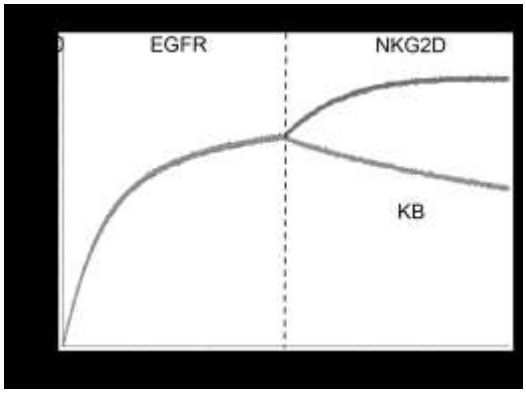
EGFR
NKG2D
KB

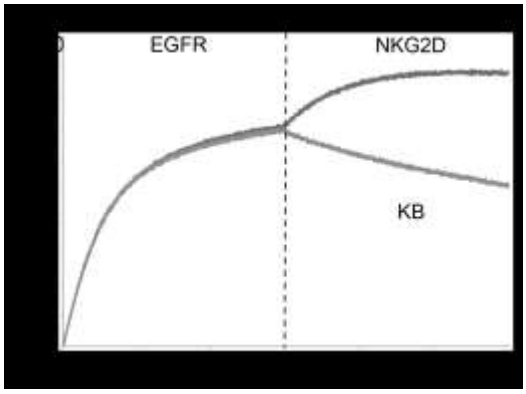
EGFR
NKG2D
KB

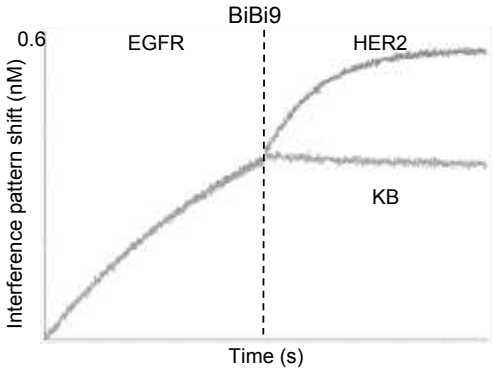
BiBi9
0.6
EGFR
HER2
KB
Interference pattern shift (nM)
Time (s)

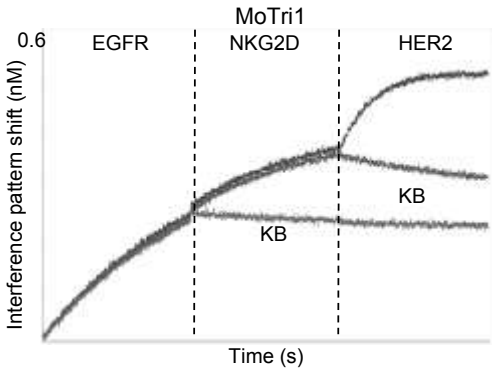
MoTri1
0.6
EGFR
NKG2D
HER2
KB
KB
Interference pattern shift (nM)
Time (s)

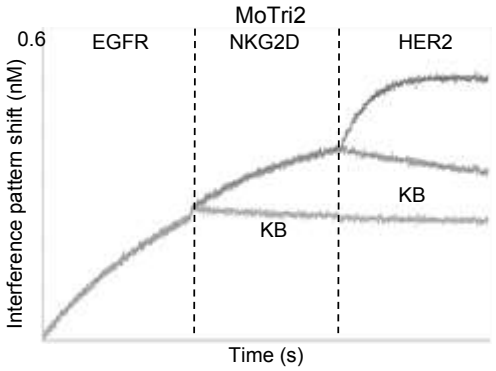
MoTri2
0.6
EGFR
NKG2D
HER2
Interference pattern shift (nM)
KB
KB
Time (s)

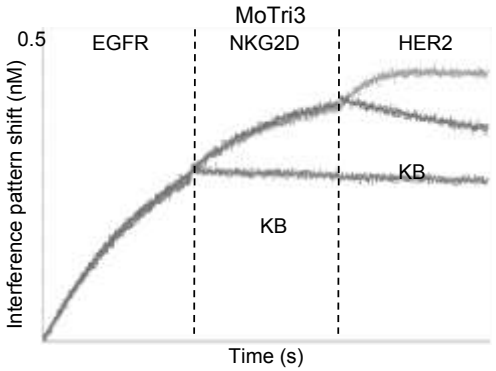
MoTri3
0.5
EGFR
NKG2D
HER2
Interference pattern shift (nM)
KB
KB
Time (s)

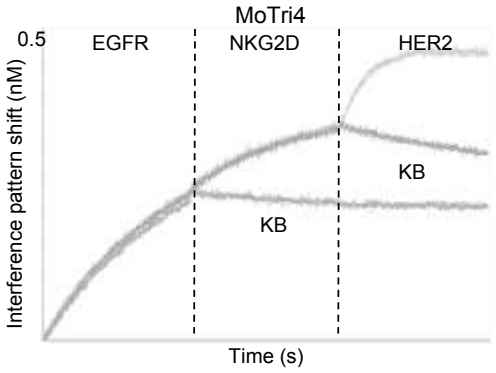
MoTri4
0.5
EGFR
NKG2D
HER2
Interference pattern shift (nM)
KB
KB
Time (s)

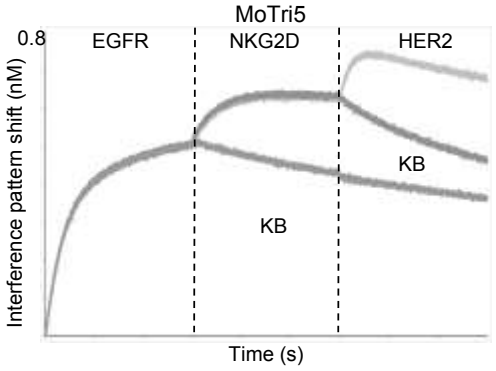
MoTri5
0.8
EGFR
NKG2D
HER2
Interference pattern shift (nM)
KB
KB
Time (s)

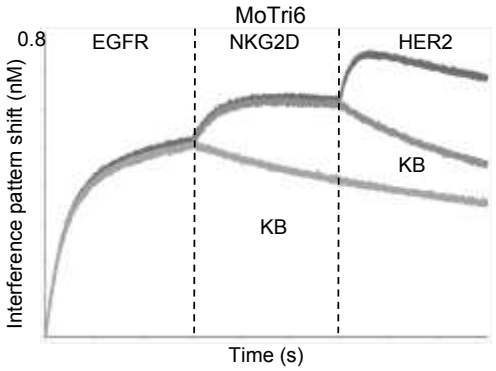
MoTri6
0.8
EGFR
NKG2D
HER2
KB
KB
Interference pattern shift (nM)
Time (s)

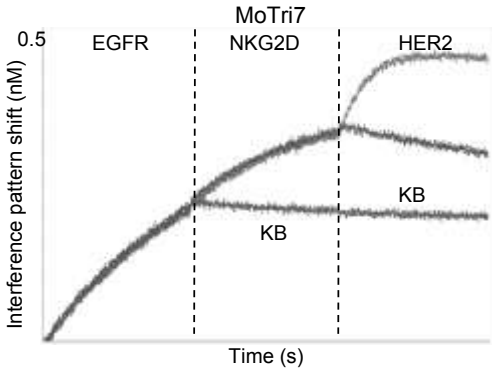
MoTri7
0.5
EGFR
NKG2D
HER2
KB
KB
Interference pattern shift (nM)
Time (s)

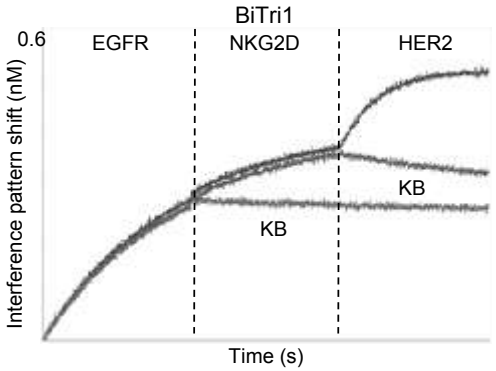
BiTri1
0.6
EGFR
NKG2D
HER2
KB
KB
Interference pattern shift (nM)
Time (s)

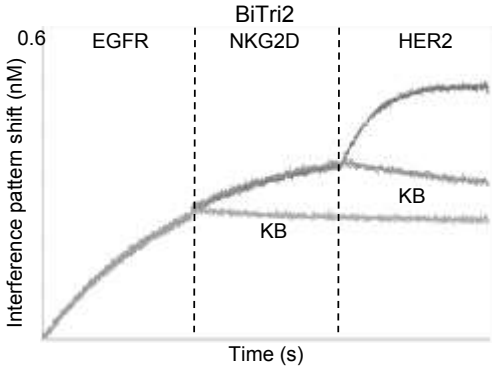
BiTri2
0.6
EGFR
NKG2D
HER2
KB
KB
Interference pattern shift (nM)
Time (s)

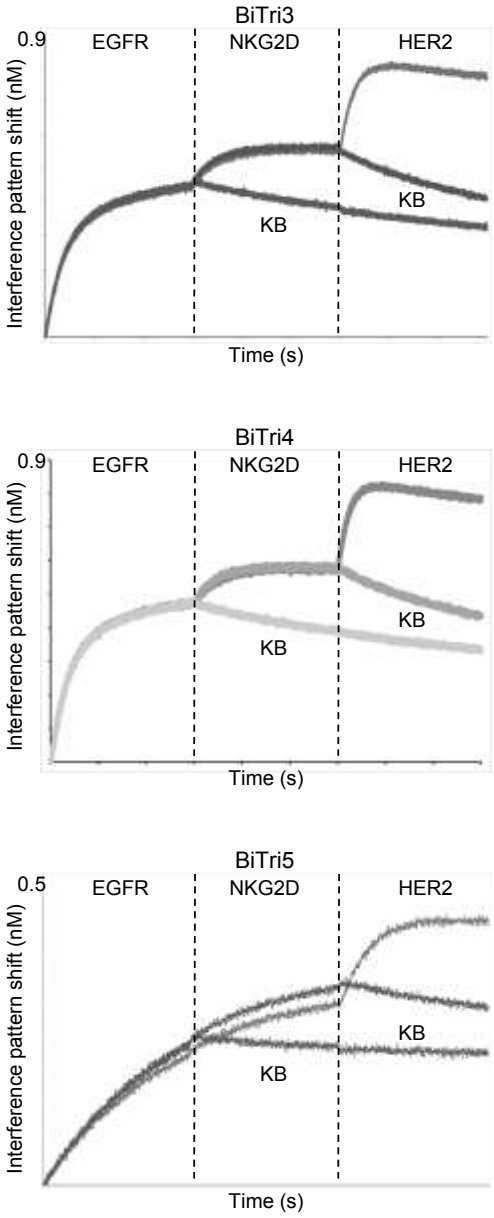

Fig. S3: Simultaneous binding of the antibody molecules used in this study via biolayer interferometry analysis. One armed monovalent bispecific, bivalent bispecific, monovalent trispecific and bivalent trispecific molecules were characterized. Consecutive binding against each antigen (EGFR, NKG2D and HER2) was measured at a concentration of 50 nM. Control measurements with kinetics buffer were conducted in parallel for each association step.

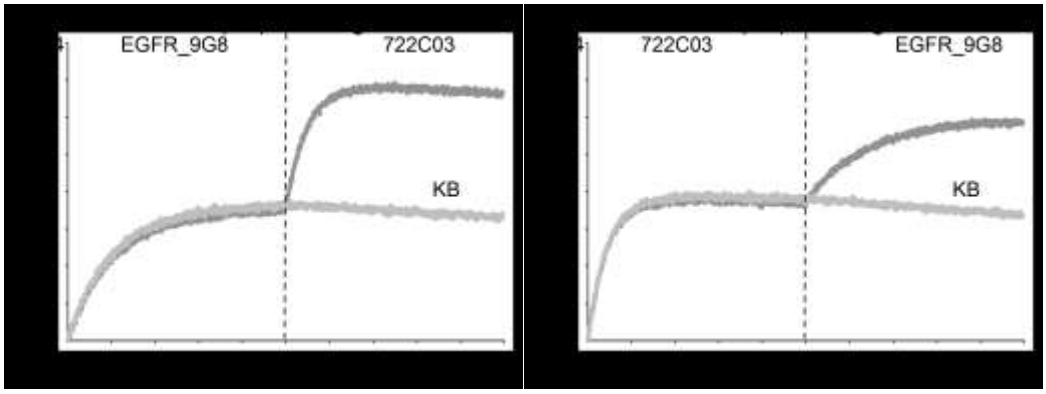

Fig. S4: Epitope binning experiments performed using Biolayer Interferometry. EGFR was captured via its histidine-tag on anti-Penta His (HIS1K) biosensors. Consecutive binding of one-armed control molecules (Ctrl1:9G8 and Ctrl4:722C03) is shown in both orientations.

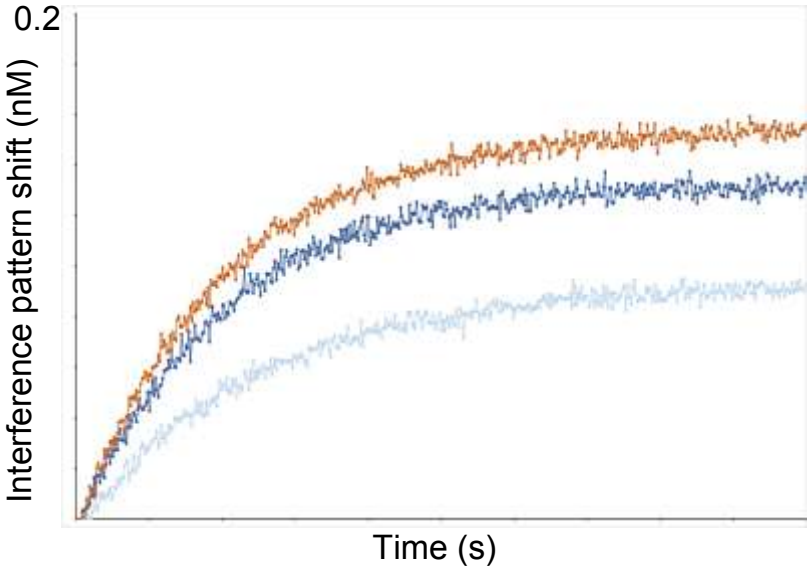

Fig. S5: Biolayer interferometry analysis to assess simultaneous binding capacities of one armed monovalent bispecific molecules comprising HER2-specific VHH grafted onto the SEED AG chain and EGFR-specific VHH 9G8 grafted onto light chain constant regions. Association of EGFR (50 nM) was measured (not shown), followed by a second association step of HER2 (50 nM). Brown: HER2-targeting VHH engrafted onto CH1 of the SEED AG chain and VHH 9G8 grafted onto CLλ. Light blue: HER2-specific paratope placed on AG chain (CH1) and 9G8 grafted onto CLκ. Dark blue: HER2-targeting single domain entity grafted onto the SEED AG chain (CH1) and 9G8 engrafted onto CLκ with ten amino acid flexible linker in between.

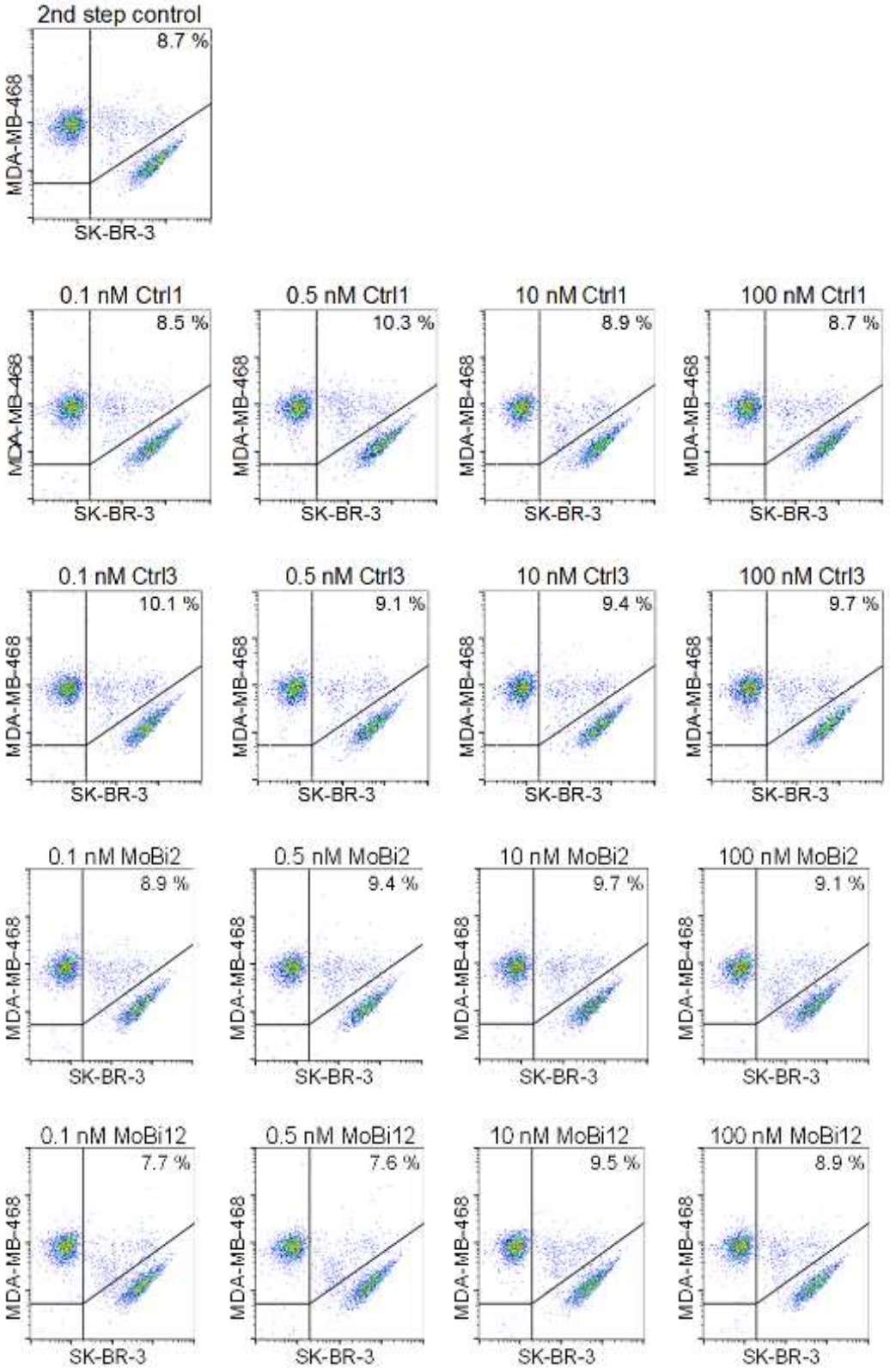

Fig. S6: Simultaneous cellular binding analysis of monovalent monospecific antibody Ctrl1 and Ctrl3, as well as monovalent bispecific antibody MoBi2 and MoBi12. Binding to EGFR-positive cell line MDA-MB-468 and Her2-positive cell line SK-BR-3 was assessed by flow cytometric analysis. Of note, MDA MB 468 was labelled with CellTracker™ Deep Red Dye and HER2-positive SK-BR-3 cells were labelled with CellTrace™ CFSE to allow for double positive fluorescence gating.

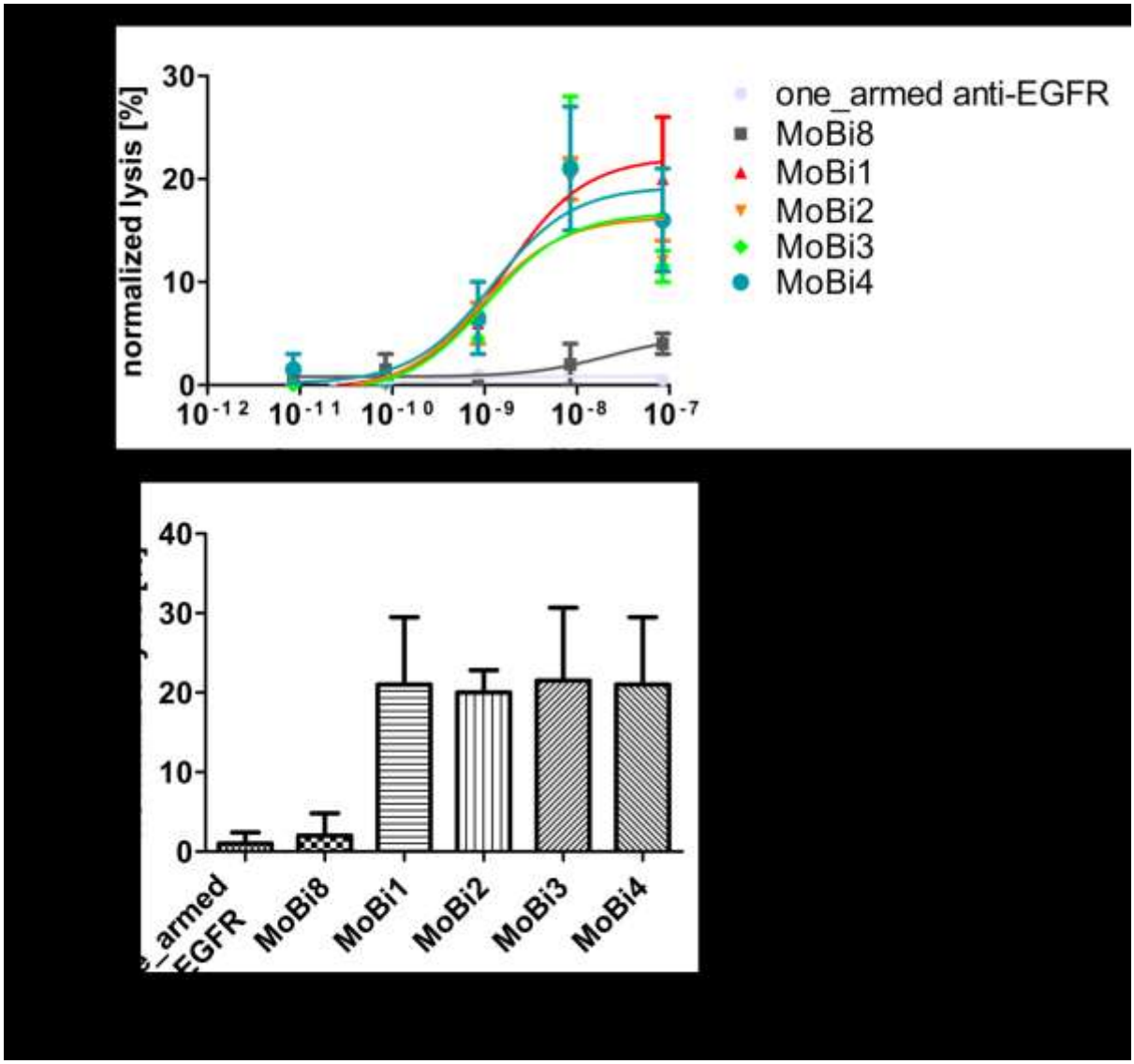

Fig. S7: NK cell-mediated tumor cell killing of EGFR-overexpressing cell line A431 using monovalent bispecific constructs and control molecules. All molecules used in this study were effector silenced (L234A, L235A, P329G). (A) Dose-response curve of one armed anti-EGFR (bright grey) and MoBi8 (EGFR AG:HER2 CLλ, dark grey) used as controls as well as EGFR and NKG2D engrafted molecules MoBi1 (EGFR AG:NKG2D CLκ, red), MoBi2 (EGFR AG:NKG2D CLλ, orange) MoBi3 (NKG2D AG:EGFR CLκ, green) and MoBi4 (NKG2D AG:EGFR CLλ, blue). (B) A431 tumor cell lysis mediated by bispecific NK cell redirection at a concentration of 10 nM. Cell lysis was normalized to staurosporine-mediated killing.

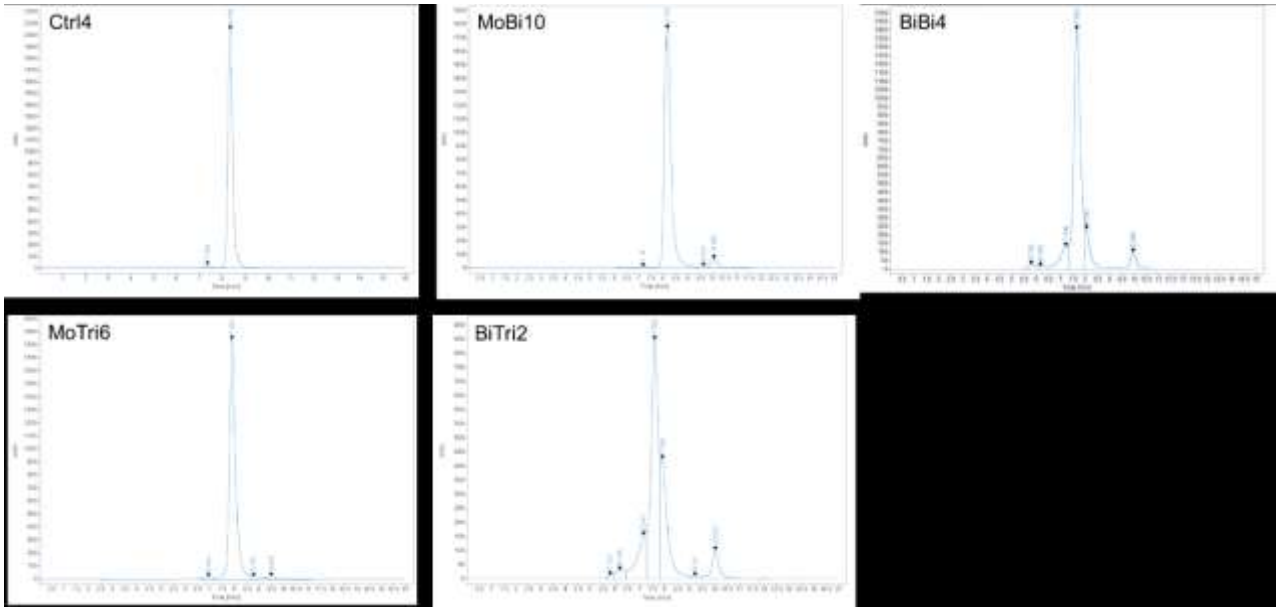

Fig. S8: Representative size exclusion chromatography profiles for selected control molecule Ctrl4, monovalent bispecific molecule MoBi10, bivalent bispecific VHH-derived IgG-like antibody BiBi4, monovalent trispecific entity MoTri6 and bivalent trispecific VHH-based IgG-like SEEDbody BiTri2.

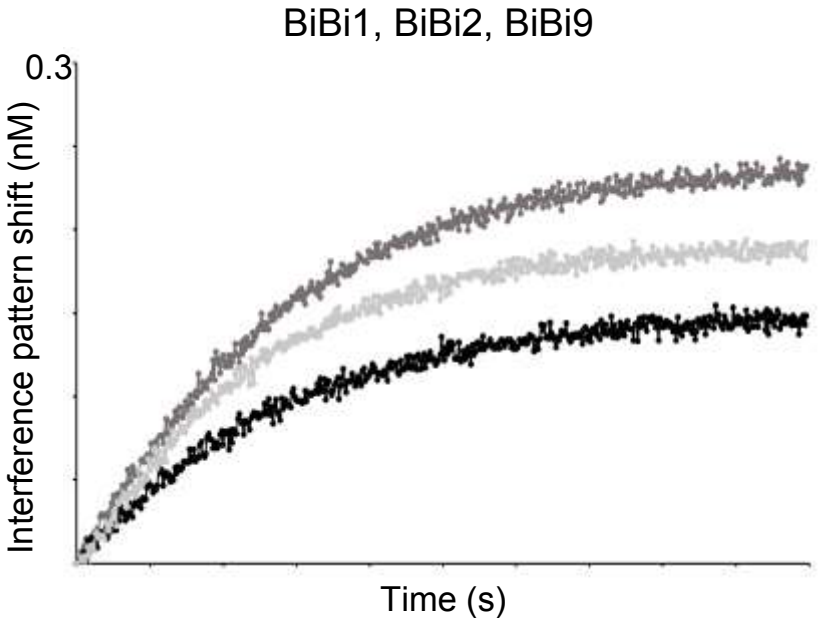

Fig. S9: Biolayer interferometry analysis to assess binding of bivalent bispecific molecules to HER2 after association against EGFR. First association was performed against EGFR at a concentration of 50 nM (not shown), followed by a second association step with HER2 at 50 nM. Association against HER2 shown for bivalent bispecific BiBi7 (CLκ, black), BiBi2 (CLλ, dark grey) and BiBi9 (CLκ +10 aa linker, grey).

7.4 Affinity maturation of B7-H6 translates into enhanced NK cell-mediated tumor cell lysis and improved proinflammatory cytokine release of bispecific immunoligands via NKp30 engagement

Supplementary Material

Affinity maturation of B7-H6 translates into enhanced NK cell-mediated tumor cell lysis and improved proinflammatory cytokine release of bispecific immunoligands via NKp30 engagement

Lukas Pekar[*¶1], Katja Klausz†[1], Michael Busch¶, Bernhard Valldorf[#], Harald Kolmar[‡], Daniela Wesch[§], Hans-Heinrich Oberg[§], Steffen Krohn†, Ammelie Svea Boje†, Carina Lynn Gehlert†, Lars Toleikis[*], Simon Krah[*], Tushar Gupta[||], Brian Rabinovich[||], Stefan Zielonka[*2] and Matthias Peipp†[2]

[*]Protein Engineering and Antibody Technologies, Merck KGaA, Frankfurter Straße 250, D-64293 Darmstadt, Germany

†Division of Stem Cell Transplantation and Immunotherapy, Department of Medicine II, University Hospital Schleswig-Holstein and Christian-Albrechts-University Kiel, Rosalind-Franklin-Straße 12, D-24105 Kiel, Germany

¶Discovery Pharmacology, Merck KGaA, Frankfurter Straße 250, D-64293 Darmstadt, Germany

[#]Chemical and Pharmaceutical Development, Merck KGaA, Frankfurter Straße 250, D-64293 Darmstadt, Germany

[‡]Institute for Organic Chemistry and Biochemistry, Technische Universität Darmstadt, Alarich-Weiss-Straße 4, D-64287 Darmstadt, Germany

[§]Institute of Immunology, University Hospital Schleswig-Holstein and Christian-Albrechts-University Kiel, Michaelisstrasse 5, Bldg. U30, D-24105 Kiel, Germany

[||]Department of Immuno-oncology, EMD Serono Research & Development Institute Inc., 45A Middlesex Turnpike, MA-01821 Billerica, USA

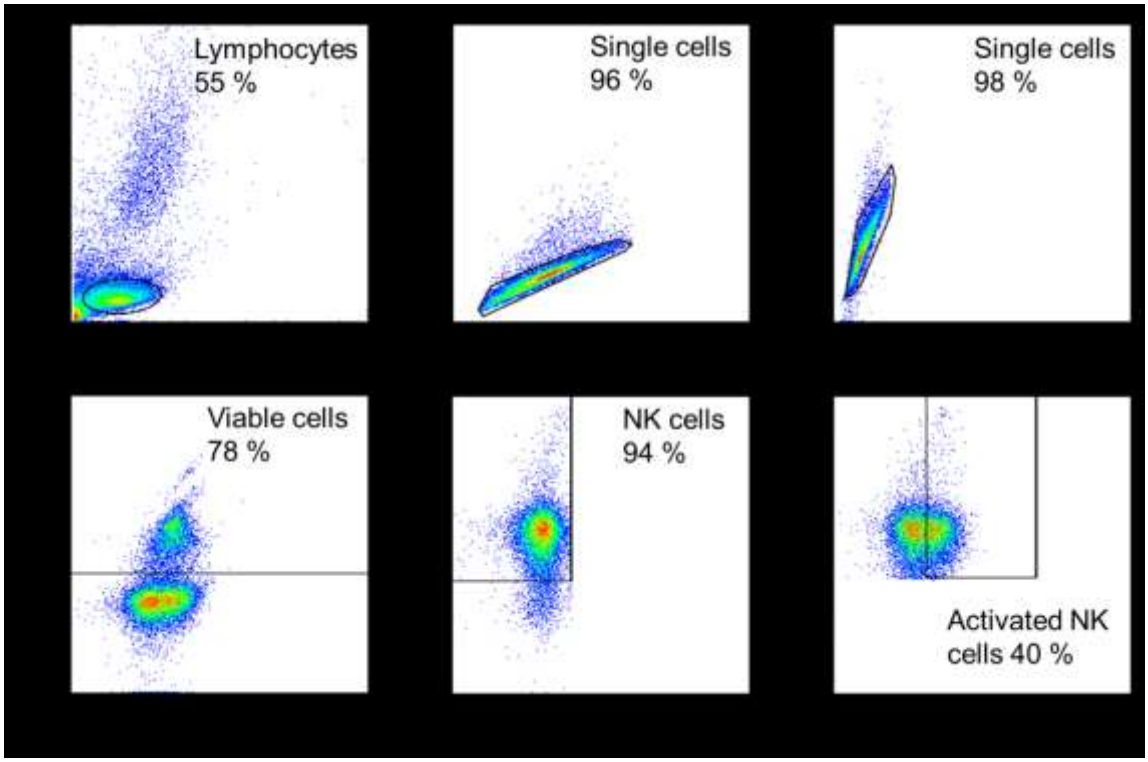

Fig. S1: Analysis of human NK cell activation by flow cytometry. Purified NK cells were incubated with A431 target cells (E:T = 5:1) for 24 hours at 37°C, stained with LIVE/DEAD™ Fixable Near-IR Dead Cell Stain and fluorochrome-conjugated anti-CD56 and anti-CD69 antibodies. FACS plots exemplarily demonstrate the gating strategy. Upper row: Side scatter (SSC) vs. forward scatter (FCS) for identification of single NK cells. Near IR and CD56 staining versus an unrelated channel was used for the identification of living $CD56^+$ NK cells (lower row, left and middle plot) followed by gating on activated $CD56^+$ $CD69^+$ NK cells (lower row, right plot).

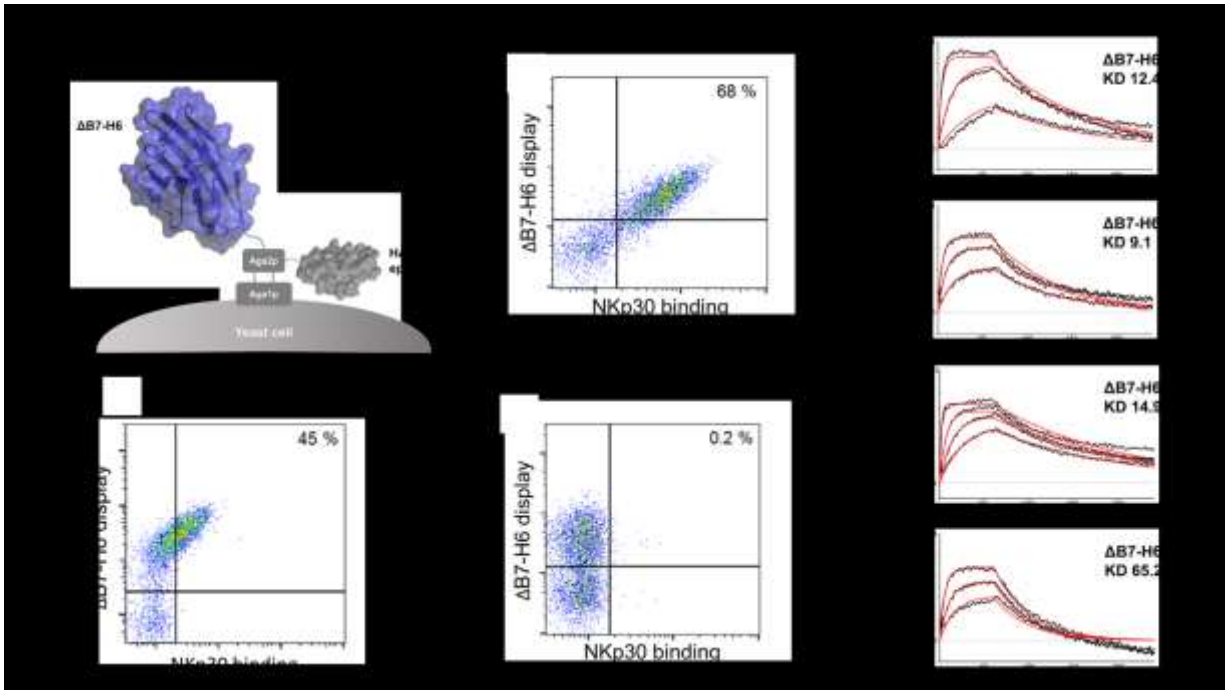

Fig. S2: Yeast surface display of ΔB7-H6 binding to NKp30 and analysis of the enrichment of affinity-enhanced ΔB7-H6 variants. **(A)** Schematic representation of ΔB7-H6 display by yeast surface display. For surface display, wildtype ΔB7-H6 as well as library candidates were expressed as fusion protein with Aga2p. A *C*-terminal HA tag was included for the detection of full-length ΔB7-H6 candidates. Simultaneous detection of ΔB7-H6 display and NKp30 binding at a concentration of 1 µM **(B)**, as well as library output of sorting round 3 **(C)** and wild-type ΔB7-H6 **(D)** stained with 50 nM NKp30. 10^7 yeast cells per sample were incubated simultaneously with pre-mixed anti-HA-PE, Penta-His Alexa Fluor 647 antibody and histidine-tagged human NKp30 solution for flow cytometric analysis. **(E)** BLI analysis of four leading affinity-optimized ΔB7-H6 immunoligand variants binding to NKp30.

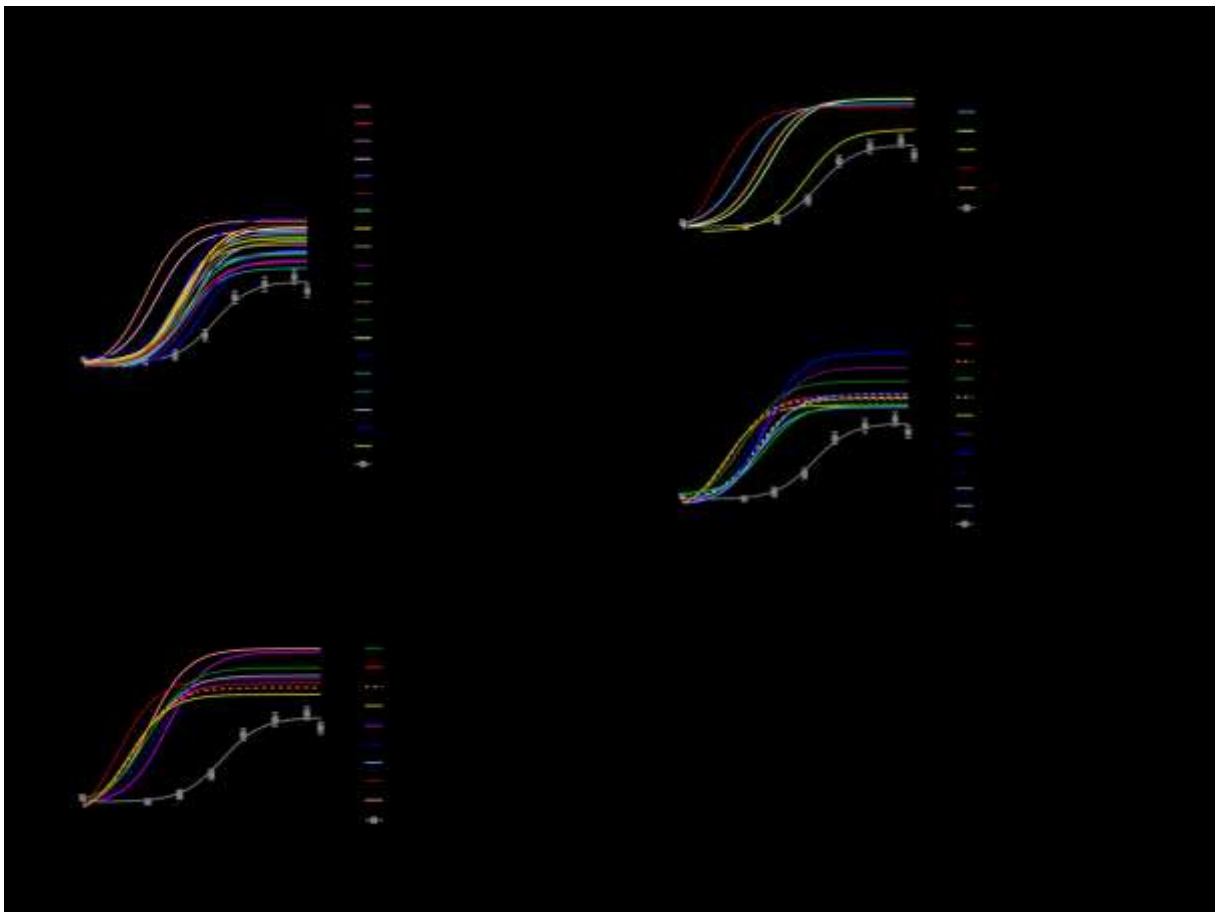

Fig. S3: **EGFR-targeting, affinity-optimized ΔB7-H6 immunoligands exert potent killing of tumor cell line A431**. Standard 4 h ^{51}Cr release assays were performed with human PBMCs and A431 cells at an E:T ratio of 80:1 to analyze concentration-dependent killing mediated by the 36 monovalent EGFR-targeting, affinity-matured ΔB7-H6 SEED-PGLALA NK cell engagers. ΔB7-H6 variants were compared to wild-type ΔB7-H6 NK cell engager (ΔB7H6 wt_hu225-SEED-PGLALA; grey line with grey squares) and a control molecule lacking ΔB7-H6, but still binding one-armed (oa) to EGFR via the humanized Cetuximab Fab (oa_hu225-SEED-PGLALA; dotted black line). To allow comparison of the results obtained from different donor PBMCs, data of each experiment were normalized using Cetuximab induced lysis at saturating concentration as 100 % and oa_hu225-SEED-PGLALA induced lysis as 0 %. B7-H6 variants are grouped in graphs according to their KD values with candidates having less than 5-fold improved NKp30 binding shown on the upper left, variants with 5- to 10-fold improved binding shown on the upper right and variants with more than 10-fold improved NKp30 binding shown on the lower right. Selected ΔB7-H6 candidates are in bold and the leading 9 candidates are summarized in the graph on the lower right. Data shown in all graphs represent normalized means ± SEM of individual experiments with different donors.

Table SI: Biochemical and biophysical characterization of immunoligands based on affinity-optimized ΔB7-H6 variants.

Identifier	KD (M)	Kon (1/Ms)	Koff (1/s)	Tm (°C)	SEC (%)	Expression yield (mg/L)
ΔB7-H6_wt	4.09E-07	4.12E+05	1.68E-01	64	92	136
ΔB7-H6_S3#1	3.91E-08	7.54E+05	2.95E-02	63	95	111
ΔB7-H6_S3#2	1.17E-08	1.04E+06	1.22E-02	63	75	57
ΔB7-H6_S3#3	1.04E-07	1.05E+06	1.09E-01	63	93	82
ΔB7-H6_S3#4	2.39E-08	6.21E+05	1.49E-02	63	81	23
ΔB7-H6_S3#5	2.25E-08	7.99E+05	1.80E-02	63	89	27
ΔB7-H6_S3#6	3.31E-08	7.37E+05	2.44E-02	63	96	39
ΔB7-H6_S3#7	1.10E-07	4.78E+05	5.25E-02	63	96	43
ΔB7-H6_S3#8	8.07E-08	5.64E+05	4.55E-02	63	86	27
ΔB7-H6_S3#9	5.78E-08	9.70E+05	5.60E-02	63	96	41
ΔB7-H6_S3#10	1.45E-07	6.89E+05	9.98E-02	63	91	34
ΔB7-H6_S3#11	3.91E-08	1.11E+06	4.32E-02	63	89	19
ΔB7-H6_S3#12	1.29E-07	6.71E+05	8.65E-02	63	95	51
ΔB7-H6_S3#13	Non binding	-	-	64	94	23
ΔB7-H6_S3#14	3.45E-08	9.33E+05	3.22E-02	64	96	42
ΔB7-H6_S3#15	1.24E-08	8.17E+05	1.01E-02	64	90	23
ΔB7-H6_S3#16	2.87E-08	1.01E+06	2.89E-02	63	93	32
ΔB7-H6_S3#17	5.91E-08	9.69E+05	5.73E-02	63	88	23
ΔB7-H6_S3#18	9.06E-09	1.50E+06	1.36E-02	63	88	20
ΔB7-H6_S3#19	1.46E-07	6.73E+05	9.81E-02	63	96	40
ΔB7-H6_S3#20	6.16E-08	1.04E+06	6.42E-02	63	81	25
ΔB7-H6_S3#21	1.79E-08	1.18E+06	2.11E-02	63	91	33
ΔB7-H6_S3#22	9.52E-08	4.63E+05	4.41E-02	63	96	43
ΔB7-H6_S3#23	1.10E-07	4.79E+05	5.25E-02	63	95	40
ΔB7-H6_S3#24	1.49E-08	7.02E+05	1.04E-02	64	92	26
ΔB7-H6_S3#25	6.52E-08	7.45E+05	4.86E-02	63	98	16
ΔB7-H6_S3#26	1.13E-07	4.09E+05	4.64E-02	64	93	24
ΔB7-H6_S3#27	8.30E-08	6.69E+05	5.56E-02	64	97	31
ΔB7-H6_S3#28	4.43E-07	3.06E+05	1.36E-01	63	89	42
ΔB7-H6_S3#29	2.48E-08	7.05E+05	1.75E-02	63	88	25
ΔB7-H6_S3#30	1.25E-07	6.22E+05	7.76E-02	63	90	47
ΔB7-H6_S3#31	4.36E-08	6.16E+05	2.69E-02	64	86	28
ΔB7-H6_S3#32	1.88E-07	4.09E+05	7.66E-02	63	83	32

ΔB7-H6_S2#1	2.05E-07	3.80E+05	7.80E-02	63	95	54
ΔB7-H6_S2#2	2.17E-07	3.40E+05	7.37E-02	64	93	47
ΔB7-H6_S2#3	1.94E-07	5.46E+05	1.06E-01	63	91	45
ΔB7-H6_S2#4	1.47E-07	8.30E+05	1.22E-01	64	69	22
ΔB7-H6_S2#5	2.53E-07	5.85E+05	1.48E-01	63	76	28
ΔB7-H6_S2#6	2.85E-07	1.32E+06	3.76E-01	63	57	29
ΔB7-H6_S2#7	1.91E-07	5.04E+05	9.64E-02	64	95	49
ΔB7-H6_S2#8	Non binding	-	-	64	17	9
ΔB7-H6_S2#9	-	-	-	-	-	No expression yield obtained
ΔB7-H6_S2#10	1.87E-07	5.97E+05	1.11E-01	63	90	40
ΔB7-H6_S2#11	2.34E-07	4.91E+05	1.15E-01	63	88	41
ΔB7-H6_S2#12	2.91E-07	5.56E+05	1.62E-01	63	73	27
ΔB7-H6_S2#13	2.05E-07	4.10E+05	8.42E-02	63	96	49
ΔB7-H6_S2#14	2.17E-07	5.70E+05	1.24E-01	63	95	44
ΔB7-H6_S2#15	3.50E-07	4.01E+05	1.40E-01	63	94	52

Expression yields were determined post protein A purification. SEC indicates target monomer peaks as determined by analytical size exclusion chromatography. Grey colored variants were not applied for cellular assays due to their biophysical properties.

7.5 Antibody Display Systems

SPRINGER NATURE

Springer Nature Switzerland AG
Gewerbestrasse 11
6330 Cham, Switzerland

T +41 41 7473600
F +41 41 7473601
www.springernature.com

Silvia Herold
Editor Biomedicine
T +43 1 3302415-316
F +43 1 3302426-65
silvia.herold@springer.at

Springer Nature, Gewerbestrasse 11, 6330 Cham, Switzerland

Dr. Stefan Zielonka
Protein Engineering and Antibody Technologies
Merck Healthcare KGaA
Frankfurter Strasse 250
64293 Darmstadt, Germany

April 6th, 2020

Letter of Acceptance

Dear Authors,

I'm pleased to confirm that your chapter **Display Systems and Libraries of Antibodies (phage, yeast, ribosome, mammalian)**, authored by Janina Klemm, Lukas Pekar, Simon Krah and Stefan Zielonka, was accepted for publication in the textbook *Rüker & Wozniak-Knopp (eds), Introduction to Antibody Engineering*. The book is currently in preparation; its publication is planned for Q3 2020.

With best wishes,
Silvia Herold

Dr. Silvia Herold
Editor
Editorial Biomedicine

Springer Nature
Prinz Eugen-Straße 8-10, 1040 Vienna, Austria
T +43 (0) 1 / 330 24 15-316
F +43 (0) 1 / 330 24 26-65
silvia.herold@springer.at
www.springernature.com

8 Appendix

8.1 Yeast Surface Display in Combination with Fluorescence-activated Cell Sorting Enables the Rapid Isolation of Antibody Fragments Derived from Immunized Chickens

Authors

Julius Grzeschik, Desislava Yanakieva, **Lukas Roth**, Simon Krah, Steffen C. Hinz, Adrian Elter, Tina Zollmann, Gerhard Schwall, Stefan Zielonka, and Harald Kolmar

Bibliographic information

Biotechnology Journal

Volume 14, Issue 4, April 2019

DOI: https://doi.org/10.1002/biot.201800466

RESEARCH ARTICLE

Monoclonal Antibodies

Biotechnology Journal

www.biotechnology-journal.com

Yeast Surface Display in Combination with Fluorescence-activated Cell Sorting Enables the Rapid Isolation of Antibody Fragments Derived from Immunized Chickens

*Julius Grzeschik, Desislava Yanakieva, Lukas Roth, Simon Krah, Steffen C. Hinz, Adrian Elter, Tina Zollmann, Gerhard Schwall, Stefan Zielonka, and Harald Kolmar**

Dedicated to Professor Hans Günter Gassen on the occasion of his 80th birthday.

Yeast surface display emerged as a viable tool for the generation of human and murine monoclonal antibodies. This platform technology enables the careful definition of selection conditions, the potential for high-throughput screening, as well as the isolation of antibodies recognizing predefined epitopes. In this study, the applicability of yeast surface display in combination with fluorescence-activated cell sorting (FACS) for the isolation of antigen-specific chicken-derived antibodies is demonstrated. To this end, yeast-displayed recombinant antibody libraries from splenic mRNA of chickens immunized with epidermal growth factor receptor (EGFR) and human chorionic gonadotropin (hCG) were constructed as single chain variable fragments (scFv) by overlap extension polymerase chain reaction. A large number of antigen binding scFvs were readily isolated in a convenient screening process. Target-specific scFv-Fc molecules were produced as soluble proteins and more extensively characterized by confirming specificity, thermostability and high affinity. Essentially, we demonstrated the biotechnological applicability of binders directed against both antigens via specific cellular binding for EGFR and in the context of a lateral flow test by utilizing hCG-binding scFvs as capturing antibodies for pregnancy detection. Altogether, the described strategy using yeast surface display expands the repertoire of display methods for the isolation of antibodies resulting from chicken immunization campaigns.

1. Introduction

Antibodies and antibody-based formats (Fab, scFv) have become some of the most successfully and frequently used biomolecules both for biotechnological and biomedical purposes. As of March 2017, more than 58 antibodies were clinically available for treatment of various diseases and monoclonal antibodies (mAbs) represented 25% of the biopharmaceutical market, which on its side took about 25% of the global pharmaceutical market.[1] The huge success of antibodies is based on their function as versatile ligands which target various antigens with high-affinity and selectivity. This makes them suitable for therapeutic applications like treatment of cancer, inflammatory, and autoimmune diseases, as well as for analytical and diagnostical purposes such as various formats of immunoassays: Western Blot,[2] enzyme-linked immunosorbent assay (ELISA),[3] and lateral flow tests.[4]

Antibody discovery can be performed using immunized animals, followed by surface display screening techniques, e.g., phage display,[5] yeast surface display,[6] ribosomal display,[7–9] mammalian display.[8,10] While originally immunized mice have been primarily used as a source of immunoglobulin (Ig) repertoires, today also other animals such as camelids, sharks, and chickens have been chosen as hosts for the generation of target-specific variable domains.[11] These animals bring the advantages of distinct antibody formats (e.g., heavy-chain-only antibodies from camelids and cartilaginous fish[12]) and a potentially high immunogenicity of a particular antigen due to the phylogenetic distance from humans, which makes them useful for the generation of antibodies recognizing conserved epitopes on mammalian molecules.[13] Moreover, the peculiar Ig gene diversification mechanism in chickens that is based on somatic gene conversion events allows the facile generation of antibody libraries by using single primer pairs for the heavy and light chain, respectively, enabling one-step PCR amplification of the variable domain gene repertoire.[14–18]

J. Grzeschik, D. Yanakieva, S. C. Hinz, A. Elter, Prof. H. Kolmar
Institute for Organic Chemistry and Biochemistry
Technische Universität Darmstadt
Alarich-Weiss-Strasse 4, D-64287 Darmstadt, Germany
E-mail: kolmar@biochemie-tud.de

L. Roth, Dr. S. Krah, Dr. S. Zielonka
Protein Engineering and Antibody Technologies
Merck KGaA
Frankfurter Strasse 250, D-64293 Darmstadt, Germany

Dr. T. Zollmann, Dr. G. Schwall
Science Relations
Merck KGaA
Frankfurter Strasse 250, D-64293 Darmstadt, Germany

J. Grzeschik, D. Yanakieva, S. C. Hinz, A. Elter, Prof. H. Kolmar, Dr. T. Zollmann, Dr. G. Schwall
Merck Lab @ Technische Universität Darmstadt
Alarich-Weiss-Strasse 8, D-64287 Darmstadt, Germany

DOI: 10.1002/biot.201800466

While chicken V-gene sequences are theoretically uniform and humanizable,[19,20] chicken CDR3 repertoire differs significantly from those of human and mouse. CDR3 loops of chickens tend to be longer and have much higher cysteine content, which suggests the presence of noncanonical disulfides, leading to increased CDR stability and complexity.[21]

To date, multiple chicken-derived single-chain variable fragments (scFvs) against various targets have been successfully generated and characterized using phage display technology.[13,22–24] In this process, the variable domains of the heavy and light chains are amplified from the chicken immunoglobulin repertoire and randomly connected via short polypeptide linker sequences, resulting in a high-diversity gene library of scFvs with antigen-binding properties.[22,25] In order to identify high affinity antigen binders, scFvs are genetically fused to the coat protein of filamentous bacteriophage and displayed on the surface of the phage particles.[26,27] Selection of antigen-specific binders from phage libraries is performed through a multi-step in vitro panning procedure, consisting of binding to the immobilized antigen, washing, elution, and enrichment of phages in *Escherichia coli*, repeated in multiple cycles.[28]

Alternatively, yeast surface display can be employed as a platform for the screening and isolation of antibody fragments. This strategy combines the benefits of online and real-time analysis of the library candidates by fluorescent-activated cell sorting (FACS)[29] with the advantages of an eukaryotic expression apparatus and unfolded protein response for degradation of misfolded or aggregated proteins.[30,31] For the generation of yeast cell libraries, the protein of interest is genetically fused to a cell wall-anchored protein. Most commonly used is the a-agglutinin-system, where the antibody DNA sequence is fused to the gene of a-agglutinin II subunit (Aga2p).[6] Upon expression in the yeast cell, the fusion protein is secreted and forms two disulfide bonds with the a-agglutinin I subunit (Aga1p), anchored through its C-terminal glycosylphosphatidyl-inositol (GPI) attachment signal to the cell wall (**Figure 1**). High-throughput selection of high affinity binders can be performed by multiple rounds of FACS, leading to an enrichment of target binding cells.[4]

We reasoned that microbial display in combination with controlled screening by FACS sorting with online monitoring of binding capabilities might facilitate isolation of affine, stable and specific binders of chicken-derived antibodies via accurate setting of screening conditions and monitoring of binding capabilities of each clone at a given target concentration in solution. To this end we immunized two specimens with epidermal growth factor receptor (EGFR) and human chorionic gonadotropin (hCG), respectively, both of pharmaceutical or diagnostic relevance.

EGFR is a transmembrane receptor tyrosine kinase, stimulated by growth factors (transforming growth factor (TGF)-α and EGF), involved in the regulation of cellular differentiation and proliferation.[32] It is overexpressed on many tumor cells and thus has emerged as a promising target for cancer therapy.[33] Anti-EGFR antibodies cetuximab (Erbitux) and panitumumab (Vectibux) build up to date the foundation of metastatic colorectal cancer treatment.[34]

HCG is a glycoprotein hormone, synthesized by the syncytiotrophoblast cells of the placenta.[35] Also referred to as "pregnancy hormone", it can be detected as early as six days after conception,[36] thus being used as the earliest indication of pregnancy. The generation of specific monoclonal antibodies against the beta subunit of hCG has enabled simple and very sensitive detection of the hormone in the urine, leading to development of multiple pregnancy tests well suited as well as for the public as for healthcare professionals.[37]

In this study we report to our knowledge the first application of yeast surface display in combination with FACS for facile and efficient generation of high affinity chicken-derived binders against model target proteins EGFR and hCG with therapeutic or diagnostic relevance. Both, anti-EGFR and anti-hCG binders show high affinities in the single-digit nanomolar range determined via Bio-Layer Interferometry. The functionality of the generated chicken-derived antibody formats was proven with the aid of immunofluorescent staining experiments (EGFR) and lateral flow tests (hCG) showing comparable results to the commercial available constructs.

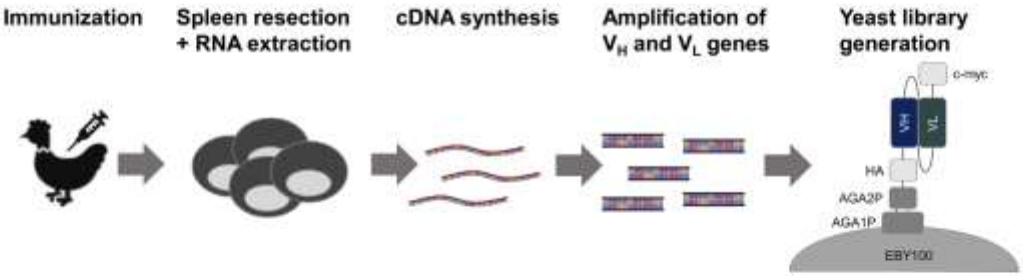

Figure 1. Workflow for the generation of chicken-derived antibody fragments from immune evolved repertoires. Chickens were immunized separately with two different antigens, EGFR and hCG. Spleen cells were isolated followed by extraction of total RNA and cDNA-synthesis. Afterwards cDNA was used as template for the amplification of variable regions. Resulting scFv molecules were presented on the yeast surface as Aga2p fusions with a N-terminal HA-tag as well as C-terminal cMyc-tag for the detection of antibody surface expression.

2. Experimental Section

2.1. Chicken Immunization

Two different antigen cocktails were used for chicken immunization: One chicken (*Gallus gallus domesticus*) was immunized with human EGFR (extracellular domain, produced and purified in house) and another specimen with a cocktail of EGFR and hCG (BBI Solutions P111-0). The whole immunization process was performed at Davids Biotechnologie (Regensburg, Germany). Briefly, two pathogen-free adult laying hens were immunized by injecting intramuscularly 150 µg of the respective antigens using AddaVax (InvivoGen) as vaccine adjuvant. After initial injection, the birds received boosters after 2, 4, 5, and 8 weeks. Immune response to the target antigens was determined after 5 weeks by monitoring their antigen-specific titer[38] using ELISA. Experimental procedures and animal care were in accordance with EU animal welfare protection laws and regulations. After 9 weeks both animals were sacrificed followed by isolation of total splenic RNA using TriFast reagent (VWR).[39]

2.2. Yeast Strains, Media, and Reagents

For yeast surface display the *Saccharomyces cerevisiae* strain EBY100 was utilized.[6] YPD medium was prepared using 20 g L^{-1} dextrose, 20 g L^{-1} tryptone, and 10 g L^{-1} yeast extract. SD-CAA medium was composed of 8.6 g L^{-1} $NaH_2PO_4 \times H_2O$, 5.4 g L^{-1} Na_2HPO_4, 1.7 g L^{-1} yeast nitrogen base without amino acids, 5 g L^{-1} ammonium sulphate, 5 g L^{-1} Bacto Casamino Acids, and 20 g L^{-1} dextrose. SG-CAA medium was prepared identically except for the substitution of dextrose sugar with galactose. Phosphate-buffered saline (PBS) contained 8.1 g L^{-1} NaCl, 1.13 g L^{-1} Na_2HPO_4, 0.75 g L^{-1} KCl, and 0.27 g L^{-1} KH_2PO_4.

2.3. Yeast Library Construction

After RNA extraction, cDNA-synthesis was performed using 50 µl RNA extract, 10 µl random hexamer primers (50 ng µl^{-1}), 10 µl 50 µM dNTPs, 30 µl H_2O, 40 µl 25 mM $MgCl_2$, 20 µl 10× RT-buffer, 20 µL 0.1 M DTT, 10 µl RNase OUT, and 10 µl SuperScript III reverse transcriptase (all components from SuperScript III First-Strand Kit, Thermo Fisher Scientific). The mixture was incubated for 5 min at 25 °C followed by incubation for 60 min at 50 °C and a subsequent inactivation step at 85 °C for 5 min. Afterwards, 1 µl RNAaseH was added and the solution was incubated for 20 min at 37 °C. The synthesized cDNA was stored at −20 °C. Variable antibody regions were amplified from cDNA in two separate PCR reactions using *Taq* Polymerase (NEB) in a reaction volume of 100 µl. For each animal and chain 6 different reactions were prepared using 3 µl cDNA. Amplification of V_H genes was performed using the primer pair VH_gr_up/VH_SOE_lo, for V_L genes with VL_SOE_up/VL_gr_lo, respectively. Primer sequences are listed in Table S1, Supporting Information. For all reactions the following conditions were set: 95 °C for 30 s, 30 cycles of 20 s at 95 °C, 30 s at 55 °C, and 30 s at 68 °C, followed by 68 °C for 5 min. PCR products were purified via Wizard SV Gel and PCR Clean-up System (Promega). Assembly of scFv constructs including $(Gly_4Ser)_3$ linker sequences and overlaps up- and downstream of the *Nhe*I and *Bam*HI restriction sites of the pCT-plasmid[6] was performed *via* fusion PCR under the following conditions: 200 ng of each V_H and V_L domains were amplified using *Taq* polymerase for 15 cycles without addition of primers with an elongation time of 50 s. Subsequently, 15 PCR cycles were performed after addition of the primer pair VH_gr_up/VL_gr_lo. The pCT vector used for gap repair cloning and surface presentation of scFv variants was digested with *Nhe*I and *Bam*HI and purified *via* Wizard SV Gel and PCR Clean-up System. Library generation in *S. cerevisiae* EBY100 cells was performed according to Benatuil and colleagues.[40]

For large-scale yeast library generation 4 µg of digested pCT plasmid was mixed with 12 µg of insert DNA for each electroporation reaction. In total, 14 transformation reactions per library were performed. Yeast cells were transferred to SD-CAA medium and incubated overnight at 30 °C and 180 rpm. Determination of library sizes was performed via analysis of serial dilution platings after 3 days.

2.4. Yeast Library Screening

Induction of gene expression and surface presentation was performed by inoculation of SG-CAA medium to a cell density of 1×10^7 cells ml^{-1} followed by incubation at 30 °C and 180 rpm for 24 h. Prior to labeling the libraries for sorting, cells were washed two times with BPBS (PBS + 0.1 % bovine serum albumin (BSA)). Antigen staining was performed either by employing biotinylated hCG using EZ-Link Sulfo-NHS-LC-Biotin (Thermo Fisher Scientific), Penta-His Alexa Fluor 647 Conjugate antibody (Qiagen) for his-tagged EGFR or anti-Human IgG Fc-PE conjugate (Affymetrix eBioscience) for Fc-tagged EGFR (R&D Systems). Labeling steps were performed for 30 min with 1×10^7 cells per 20 µl on ice. After incubation with the target protein cells were washed two times with BPBS followed by staining for surface presentation using anti-cMyc antibody (produced in-house; undiluted) or anti-c-myc-Biotin antibody (Miltenyi Biotec; 1:50 diluted). Final staining steps were performed using an anti-mouse IgG antibody APC conjugate (Affymetrix eBioscience, diluted 1:50), Penta-His Alexa Fluor 647 Conjugate antibody (diluted 1:20), Streptavidin conjugated to APC or PE (Affymetrix eBioscience; diluted 1:75) or anti-Human IgG Fc PE conjugate (diluted 1:75). After washing with BPBS library cells were prepared for flow cytometry sorting. Library screening was performed on a BD Influx cell sorter following the instructions of the manufacturer and analyzed via BD FACS Sortware v1.0. Sorted cells were subsequently transferred to SD-CAA medium for further incubation at 30 °C for 2 days. The second screening round was performed with at least a 10-fold excess of cells collected in the previous round to ensure coverage of the enriched populations. Plasmid DNA from antigen-binding populations was isolated *via* Zymoprep Yeast Plasmid Miniprep (Zymo Research) and transformed into Top 10 competent *E. coli* cells for plasmid rescue and sent out for sequencing with pCT_seq_lo and pCT_seq_up oligonucleotides. Mapping of hCG epitopes by flow cytometry was

performed after induction of cells resulting from R2.1 using an anti hCG beta antibody (Fitzgerald; monoclonal; 10-C25D; diluted 1:200) or biotinylated human TSH (R&D systems).

2.5. Expression of Selected scFv-Fc Variants

Reformatting of the identified scFv variants was performed by genetic fusion to human IgG1 Fc region encoded in the mammalian expression vector pEXPR-IBA42. After introducing flanking *Nhe*I and *Apa*I sites for ligation into the linearized plasmid, constructs were sequenced followed by transient transfection of Expi293F™ cells using polyethylenimine (Polysciences) following the instructions of the manufacturer (Thermo Fisher Scientific). After 5 days culture supernatants were harvested, sterile-filtered (0.22 µm Filtropur S 0.2, Sarstedt) and purified using HiTrap Protein A HP columns (GE Healthcare) in combination with an ÄKTA purification system (GE Healthcare). Buffer exchange was carried out via dialysis against PBS using a membrane with a MWCO ≈14 kDa. Aggregate formation was analyzed by analytical size exclusion chromatography. Therefore, a TSKgel SuperSW3000 column (4.6 × 300 mm, Tosoh Bioscience LLC) and an Agilent HPLC system was used.

2.6. Binding Kinetics

Binding kinetic measurements were performed on Octet RED96 system (FortéBio) at 30 °C and 1000 rpm agitation in 200 µl. For EGFR binders scFv-Fc molecules were loaded on anti-human Fc biosensors (AHC) at 3 µg ml^{-1} in kinetics buffer (KB; PBS, 0.1% Tween 20 and 1% BSA) for 90 s. For analysis of hCG binders biotinylated hCG was loaded on SAX tips at 1.5 µg ml^{-1} for 120 s. Afterwards, tips were transferred to KB for 60 s for sensor rinsing. Subsequently, association of varying concentrations from 100 nM to 3.125 nM of EGFR or hCG-binding scFv-Fc was measured for 300 s followed by dissociation for 300 s in KB. In each experiment, a negative control was implemented by incubating the captured scFv with unrelated antigen or incubating tips loaded with unrelated antigen with soluble scFv-Fc for analysis of anti-hCG moieties. Data fitting and analysis was carried out with FortéBio data analysis software 9.1 using a 1:1 Langmuir binding model after subtraction of control curve after Savitzky–Golay filtering.

2.7. Thermal Shift Assay

Experiments were performed in triplicates on a BioRad96CFX RT-PCR detection system with 0.5 °C/30 s to 99 °C. T_m values were collected from melting curves using the corresponding BioRad analysis software. All reactions were performed in PBS, pH 7.4 in presence of 0.1 mg ml^{-1} protein and SYPRO Orange (diluted 1:800, Sigma–Aldrich).

2.8. Lateral Flow Test

Anti-hCG chicken scFv fragments were tested for application in a classical lateral flow test setup using Hi-Flow™ Plus HF120 nitrocellulose membranes (HF12002XSS, Merck) and a mouse anti-hCG 40 nm gold conjugate (BA.HCG40, BBI Solutions). As positive control an anti-beta hCG monoclonal capture antibody (01041131C, BBI Solutions) was used.

Test line solutions containing 0.25 mg ml^{-1} anti-hCG specific capture antibody domains in 10 mM MES (pH 6.5) and control line solution containing 0.25 mg/ml goat anti-mouse capture antibody (M8890, Merck) in 10 mM MES (pH 6.5) were striped 4-times onto membranes using a Kinematic Matrix 1600 Reagent Dispensing Module (bed speed: 6 cm s^{-1}, pump: 1 µl cm^{-1}) to yield 0.5 µg capture protein per strip. Membranes were dried 2 h at 37 °C.

Anti-hCG gold conjugates (OD 2) in 5% (w/v) trehalose were applied onto glass fiber conjugate pads (GFDX203000, Merck) and dried o/n at RT.

Membranes and conjugate pads were assembled with cellulose sample pads (CFSP223000, Merck; treated with 10 mM Tris-HCl pH 8.2, 1% (w/v) Tween 20, 0.75% (w/v) BSA), and absorbent pads (CFSP223000, Merck) into a classical lateral flow test setup.

Chicken scFv functionality in lateral flow tests was analyzed by either hCG positive (200–400 mIU mL^{-1}) or negative human urine (Biochemical Diagnostics Inc.) or a hCG concentration series spiked in synthetic urine (S-020, Cerilliant).

2.9. Cellular Binding

Human cancer cell lines MDA-MB-468 and MCF-7 Cells were obtained from the American Type Culture Collection and maintained according to standard culture conditions (37 °C, 5 % CO2, 95 % humidity) using recommended media formulations. Both cell lines were maintained in RPMI-1640 (Life Technologies) supplemented with 10% FBS, 2 mM L-glutamine and 1 mM sodium pyruvate (both Life Technologies).

Prior to analysis of cellular binding both cell lines were trypsinized from the culture flask and then spun down. Cells were washed three times with 1% BPBS followed by incubation with the respective scFv-Fc constructs (100 µl; 100 nM scFv-Fc in 1% BPBS) for 1 h. Consequently, cells were washed and incubated with the fluorescently labeled secondary antibody (10 µg mL^{-1}; Alexa Fluor 488-conjugated AffiniPure goat anti-human IgG, Fcγ fragment specific (Jackson Immuno Research)) for 1 h, washed again and stained with propidium-iodide (1:200 dilution in 1% BPBS). Finally, cells were analyzed using a Guava EasyCyte HT flow cytometer device (EMD Millipore).

3. Results

3.1. Chicken Immunization and Yeast Library Generation

In order to test the suitability of yeast surface display in combination with FACS for the selection of chicken-derived antibodies resulting from animal immunization, two immunization campaigns utilizing the antigens EGFR and hCG were started. Serum IgY titer analysis of both specimens after 35 d indicated a positive immune response against both antigens

(Figure S1, Supporting Information). cDNA was prepared utilizing total RNA from spleen tissues via reverse transcription.

V_L and V_H genes were amplified separately by PCR using synthesized cDNA as template as well as primer sequences already reported for the generation of phage display libraries from chicken antibody repertoires.[43–44] Afterwards, the amplicons coding for V_L and V_H domains were randomly connected via a flexible $(Gly_4Ser)_3$ linker using fusion PCR resulting in the combinatorial scFv gene repertoire. For both animals, individual scFv yeast libraries were generated by a homologous recombination-based process referred to as yeast gap repair cloning (Figure 1). This resulted in two libraries with calculated library sizes of approximately 5×10^8 (EGFR) and 4×10^8 (EGFR/hCG) unique clones, respectively. Analysis of cMyc tag labeling intensity after induction of library cells with galactose revealed a surface presentation of >50 % of yeast cells for both libraries (Figure S2, Supporting Information).

3.2. Yeast Library Screening

The libraries were screened separately by FACS for binders of recombinant human EGFR and human hCG protein. Target binding was identified by indirect antigen fluorescence staining according to section 2.4. scFv surface display levels were analyzed simultaneously by cMyc tag labeling. Furthermore, negative controls in absence of antigen were performed to confirm only antigen positive cell populations being considered in the gating strategy. As shown in **Figure 2** we were able to enrich for antigen-positive populations within two consecutive screening rounds by employing 1 µM or 500 nM antigen, for EGFR and hCG, respectively. Moreover, no binding against secondary detection reagents was observed. Both sorts were repeated with decreased concentrations of 1 nM for EGFR and 5 nM for hCG, respectively to enable the isolation of high-affinity scFvs. FACS analysis after library sorting showed for both campaigns nearly exclusively antigen binding populations (Figure S3, Supporting Information).

In addition to enriching of antigen-binding populations, yeast surface display also allows for facile epitope analysis of enriched library candidates.[45] Related to this, hCG is a heterodimeric protein comprising a generic alpha subunit present in many hormones as well as a hCG-specific beta subunit. In order to estimate the fraction of hCG-specific variants targeting the beta subunit, the antigen enriched population after sorting round II was analyzed for binding to TSH (Thyroid-stimulating hormone) that shares the same alpha subunit with hCG. This indicated a relative amount of approximately 40% of cells displaying scFvs most likely binding the hCG-specific beta subunit (Figure S4, Supporting Information).

To evaluate potential sequence patterns and to confirm the presence of a sufficient diversity after library sorting, plasmid DNA from both enriched libraries was sent out for sequencing. With respect to EGFR binders unique amino acid sequences were identified in 70 out of 71 analyzed clones for heavy chain genes and 73 out of 73 clones for the light chains (Figure S5, Supporting Information). Akin to this, sequencing of hCG binders resulted in 74 out of 78 unique clones for heavy chain variants and 66 out of 74 unique variants for light chain genes, respectively. However, in both sequencing approaches the enrichment of several distinct heavy chain CDR3 sequences allowed for the assignment into different clustered sequence patterns that have been accumulated in the sorting process. Furthermore, the sequence analysis revealed the presence of several clones bearing noncanonical disulfide patterns in the V_H domain, which can be divided into: Type 1, containing two cysteines in the heavy chain CDR3 loop, type 2 with no incorporated cysteine residues and type 3, containing one cysteine in the CDR1 plus one cysteine in the CDR3.

3.3. Generation of scFv-Fc Variants and Characterization

From both enriched populations three clones were chosen for reformatting based on their CDR3 sequence abundance and expressed as scFv-Fc fusion proteins in Expi293F cells, termed E1-E3 for EGFR binders and H1-H3 for hCG binders. After production and purification using Protein A columns, the proteins were assessed by SDS-PAGE, indicating bands with the expected molecular weight of approximately 52.5 kDa as well as a high purity (Figure S6, Supporting Information). Thermal stabilities were determined by differential scanning fluorimetry

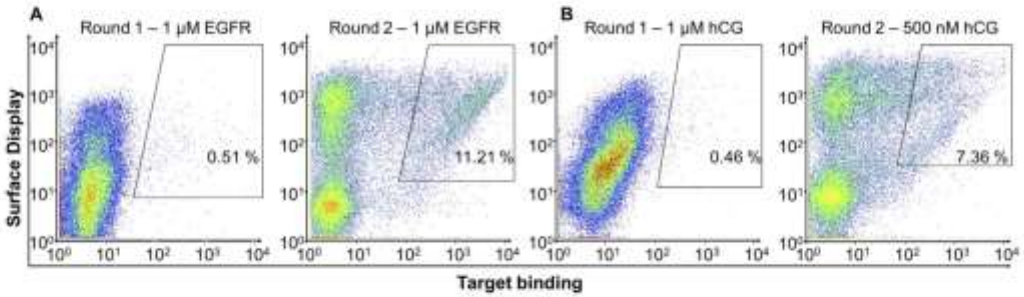

Figure 2. Chicken-derived scFv library screening against EGFR (A) and hCG (B). Sorting gates, percentages of cells in the respective gate and target concentrations are shown. Yeast cells were labeled for simultaneous detection of full-length scFv expression using cMyc-tag staining as well as for antigen-binding. In each round cells in the sorting gate were isolated, grown and induced for the second round of selection. After the second screening round clones of the enriched binding populations were sequenced.

Table 1. Kinetic parameters of chicken-derived scFv-Fc determined using bio-layer interferometry.

scFv-Fc variant	K_D [nM]	k_{on} [$M^{-1} s^{-1}$]	k_{dis} [s^{-1}]
H1	1.2 ± 0.01	$1.8 \times 10^6 \pm 1.5 \times 10^6$	$2 \times 10^{-3} \pm 1.2 \times 10^{-5}$
H2	4.2 ± 0.05	$5 \times 10^5 \pm 7.3 \times 10^3$	$1.2 \times 10^{-3} \pm 1.9 \times 10^{-5}$
H3	6.8 ± 0.1	$4.2 \times 10^5 \pm 6.2 \times 10^3$	$2.6 \times 10^{-3} \pm 2 \times 10^{-5}$
E1	6.8 ± 0.04	$3.4 \times 10^5 \pm 1.6 \times 10^3$	$2.3 \times 10^{-4} \pm 6 \times 10^{-6}$
E2	28 ± 0.25	$3 \times 10^5 \pm 2.4 \times 10^3$	$8.7 \times 10^{-3} \pm 2.1 \times 10^{-5}$
E3	43 ± 1.3	$2.4 \times 10^5 \pm 7.5 \times 10^3$	$1 \times 10^{-2} \pm 5.9 \times 10^{-5}$

(Figure S7, Supporting Information), revealing melting temperatures in the range of 53–59 °C, which is in accordance with stabilities reported for murine scFv constructs.[41]

Furthermore protein purity was analyzed by size-exclusion chromatography (Figure S8, Supporting Information). For the six generated scFv-Fcs 0.5–15.5% aggregates were determined. Additionally binding kinetics of binders resulting from both immunization campaigns were measured using Bio-Layer Interferometry (BLI). This revealed binding affinities ranging from low single-digit nanomolar to double-digit nanomolar apparent binding constants (**Table 1**/Figure S9, Supporting Information). Finally, within this study we aimed to demonstrate the applicability of chicken antibodies selected via yeast surface display for biotechnological applications. To this end, the behavior of the generated hCG binders was analyzed in lateral flow tests (LFT) for detection of small quantities of hCG as it is used in commercially available pregnancy tests (**Figure 3**A). Two chicken-derived scFv-Fc molecules showing the highest affinity in the BLI analysis were used as capturing antibodies in combination with a commercially available anti-hCG gold conjugate. In both cases, using pregnancy-positive urine as sample, this resulted in clearly visible test lines on the LFT, whereas the application of pregnancy-negative urine led to no visible test band. Further investigations were made to evaluate the limit of detection of the LFTs utilizing the chicken-derived scFvs as capturing antibodies (Figure 3B). This resulted for both binders in a detection limit at concentrations comparable with the LFT performed using the pair of commercially available anti hCG antibodies. To confirm the applicability of the selected EGFR-binding scFv molecules for biotechnological purposes, the selective binding of scFv molecules to EGFR overexpressing cells was analyzed (Figure 3C and D). This resulted for all tested constructs at 100 nM in a highly specific cell-binding to EGFR-positive MDA-MB-468 cells while testing EGFR-negative MCF-7 cells showed no binding.

4. Discussion

Our study confirms the suitability of chickens as immunization hosts for antibody discovery as well as that of chicken-based

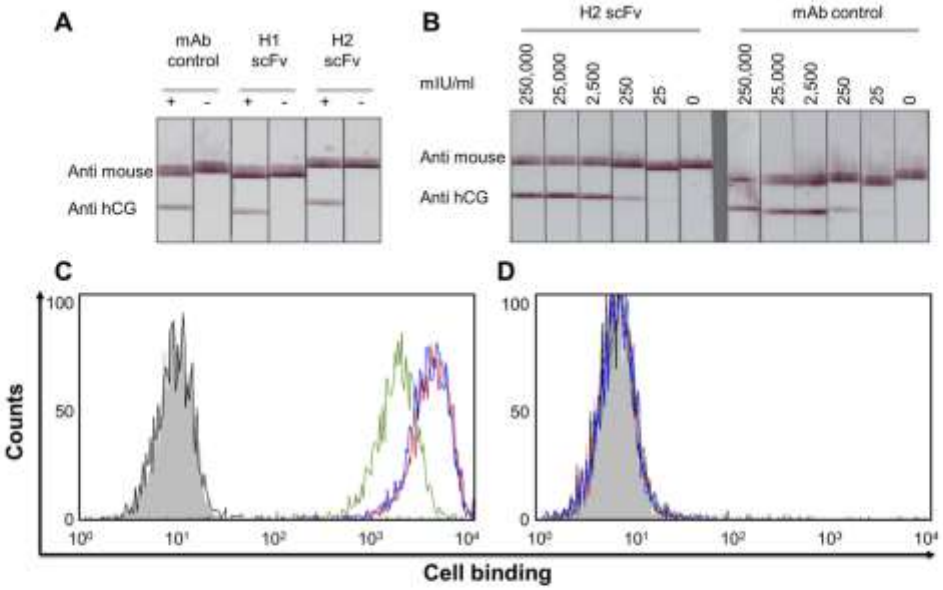

Figure 3. Biotechnological applications of generated scFv-Fc constructs. hCG-binding variants H1 and H2 were used as capturing antibodies in combination with anti-hCG gold conjugate in lateral flow tests using pregnancy-positive (200–400 mIU ml^{-1}) as well as negative urine as sample (A). Limit of detection for scFv-Fc H2 was evaluated using varying concentrations of hCG (B). For EGFR-binding scFv-Fc variants binding to EGFR-positive MDA-MB-468 (C) and EGFR-negative MCF-7 (D) cell lines was determined by flow cytometry. 10^5 cells were incubated with 100 nM of scFv-Fc variants followed by incubation with an Alexa Fluor 488-conjugated anti-human IgG-antibody. Grey: unstained; black: only secondary antibody; blue: scFv E1; red: scFv E2; green: scFv E3.

antibody formats for generation of antibody fragments displaying high affinity and selectivity. In addition to being low-maintenance animals with relatively low care costs, chickens are evolutionary very distinct to mammalians, which presumably resulted in high and rapid immunogenic respond to the human target proteins EGFR and hCG. Furthermore, the complete chicken antibody repertoire could be covered to a high degree using two single primer pairs for the heavy and light chains, respectively. This enabled facile yeast library construction, while ensuring high library diversity. Moreover, for the generation of the scFv fragments, the amplified V_H and V_L genes were randomly combined, which on its side increased the library diversity tremendously and could have led to the generation of variants with increased affinities.[46]

Using FACS, we achieved enrichment of nearly exclusively antigen binding populations in only two screening rounds. Sequence analysis of the isolated binders revealed on one hand clustering of similar CDR3 regions, while on the other hand the clones showed still high sequence diversity. Thus, it is tempting to speculate that extended sequencing of more single clones would lead to identification of even more unique binders. Additionally, the presence of non-canonical cysteines was observed in the analyzed sequences. This is in accordance with the literature[21] and demonstrates that chicken antibodies are characterized with disulfide bond-constrained CDR3s, presumably as a strategy for additional structural diversification as compensation for the otherwise restricted germline V-gene repertoire.

Heterologous expression of selected scFvs as Fc fusion proteins in a mammalian Expi293F™ system was successful and after purification protein yields of 20–100 mg per liter cell culture were obtained. The melting temperatures of the constructs lies in the expected range of 53–59 °C.[41] If required, further increase of the thermal stability may be achieved by reformatting the scFvs as conventional full-length antibodies.

Ultimately, we demonstrate that in addition to the well-established phage display technology,[13] also yeast surface display in combination with FACS could be successfully implemented for the generation and selection of chicken-derived scFvs against mammalian target proteins. One advantage of the herein presented screening strategy lies in the online control of the binding properties of the enriched candidates, which also enables epitope binning. This is especially beneficial for applications like sandwich immunoassays (e.g., ELISA and LFT), where a pair of two antibodies, binding different epitopes on the same target protein, is required.[4] We were able to demonstrate the favorable feature of this system in case of hCG, where a contra-screen with TSH was performed. In this way it was possible to identify selective binders against the beta subunit of hCG. The biotechnological applicability of the generated chicken-derived EGFR and hCG binders was proven in functional tests based on immunofluorescent staining and lateral flow assays, respectively. The selected anti-EGFR scFvs showed selective cellular binding to EGFR-overexpressing MDA MB 468 cells. Furthermore, no unspecific binding of the EGFR binders to MCF-7 cells was observed, indicating sufficient specificity of the generated constructs. At the same time, utilizing the hCG binders in a standard LFT revealed comparable functionality and selectivity compared to antibodies used in commercial pregnancy tests.

In conclusion, we have demonstrated that yeast surface display in combination with FACS represents a suitable platform for facile generation of selective and functional chicken-derived scFv molecules. scFvs represent a very convenient antibody format due to their small size and their ability to be produced in prokaryotic expression systems.[47] However, compared with Fab fragments, they are less stable and more prone to aggregation[48,49] and thus generally tend to bind with lower affinities than Fabs.[50] Nevertheless, our screening strategy at low antigen concentration of 1 nM resulted in high-affinity binders with excellent aggregation properties when formatted as Fc fusion proteins. It will be interesting to see, whether further screening of the enriched population of binders by one or more rounds using more stringent conditions using scFv or Fab yeast libraries would deliver binders with sub-nanomolar affinity, albeit most likely at the cost of clonal diversity.

Abbreviations

Aga1p, a agglutinin I subunit; Aga2p, a-agglutinin II subunit; BLI, Bio-Layer Interferometry; BSA, bovine serum albumin; EGFR, epidermal growth factor receptor; ELISA, enzyme-linked immunosorbent assay; Fab, antigen-binding fragment; FACS, fluorescence-activated cell sorting; GPI, glycosylphosphatidyl-inositol; hCG, human chorionic gonadotropin; Ig, immunoglobulin; KB, kinetics buffer; LFT, lateral flow test; mAb, monoclonal antibodies; PBS, phosphate-buffered saline; PCR, polymerase chain reaction; scFv, single chain variable fragment.

Acknowledgements

Julius Grzeschik and Desislava Yanakieva contributed equally to this work. This work was supported by the Merck Lab @ Technische Universität Darmstadt and by the Department of Protein Engineering and Antibody Technologies at Merck KGaA, Darmstadt. We would like to thank to the departments of Biomonitoring R&D and OEM Diagnostics R&D at Merck KGaA for material and technical support on lateral flow test development.

Conflict of Interest

The authors declare no financial or commercial conflict of interest.

Keywords

chicken antibody, EGFR, hCG, scFv, yeast surface display

Received: July 31, 2018
Revised: October 11, 2018
Published online:

[1] J. Chung, *Exp. Mol. Med.* **2017**, *49*, e304.
[2] W. N. Burnette, *Anal. Biochem.* **1981**, *112*, 195.
[3] E. Engvall, P. Perlmann, *Immunochemistry* **1971**, *8*, 871.
[4] G. A. Posthuma-Trumpie, J. Korf, A. van Amerongen, *Anal. Bioanal. Chem.* **2009**, *393*, 569.
[5] J. McCafferty, A. D. Griffiths, G. Winter, D. J. Chiswell, *Nature* **1990**, *348*, 552.
[6] E. T. Boder, K. D. Wittrup, *Nat. Biotechnol.* **1997**, *15*, 553.

[7] J. Hanes, A. Plückthun, *Proc. Natl. Acad. Sci. USA* **1997**, *94*, 4937.
[8] Y. Akamatsu, K. Pakabunto, Z. Xu, Y. Zhang, N. Tsurushita, *J. Immunol. Methods* **2007**, *327*, 40.
[9] M. He, M. Taussig, *Biochem. Soc. Trans.* **2007**, *35*, 962.
[10] M. Ho, I. Pastan, *Therapeutic Antibodies: Methods and Protocols*. (Ed: A. S. Dimitrov), Humana Press, New York, USA **2009**, p. 337.
[11] W. R Strohl, *Curr. Drug Discov. Technol.* **2014**, *11*, 3.
[12] S. Zielonka, N. Weber, S. Becker, A. Doerner, A. Christmann, C. Christmann, C. Uth, J. Fritz, E. Schäfer, B. Steinmann, *J. Biotechnol.* **2014**, *191*, 236.
[13] E. L. Davies, J. S. Smith, C. R. Birkett, J. M. Manser, D. V. Anderson-Dear, J. R. Young, *J. Immunol. Methods* **1995**, *186*, 125.
[14] W. T. McCormack, L. W. Tjoelker, C. B. Thompson, *Prog. Nucleic Acid Res. Mol. Biol.* **1993**, *45*, 27.
[15] C.-A. Reynaud, V. Anquez, H. Grimal, J.-C. Weill, *Cell* **1987**, *48*, 379.
[16] C.-A. Reynaud, A. Dahan, V. Anquez, J.-C. Weill, *Cell* **1989**, *59*, 171.
[17] C. A. Reynaud, V. Anquez, J. C. Weill, *Eur. J. Immunol.* **1991**, *21*, 2661.
[18] C. B. Thompson, P. E. Neiman, *Cell* **1987**, *48*, 369.
[19] N. Tsurushita, M. Park, K. Pakabunto, K. Ong, A. Avdalovic, H. Fu, A. Jia, M. Vásquez, S. Kumar, *J. Immunol. Methods* **2004**, *295*, 9.
[20] N. Nishibori, H. Horiuchi, S. Furusawa, H. Matsuda, *Mol. Immunol.* **2006**, *43*, 634.
[21] L. Wu, K. Oficjalska, M. Lambert, B. J. Fennell, A. Darmanin-Sheehan, D. N. Shúilleabháin, B. Autin, E. Cummins, L. Tchistiakova, L. Bloom, *J. Immunol.* **2011**, 1102466.
[22] H. I. Yamanaka, T. Inoue, O. Ikeda-Tanaka, *J. Immunol.* **1996**, *157*, 1156.
[23] J. Li, Y. Xu, X. Wang, Y. Li, L. Wang, X. Li, *Int. Immunopharmacol.* **2016**, *35*, 149.
[24] Z.-Q. Hu, H.-P. Li, J.-B. Zhang, T. Huang, J.-L. Liu, S. Xue, A.-B. Wu, Y.-C. Liao, *Anal. Chim. Acta* **2013**, *764*, 84.
[25] J. S. Huston, D. Levinson, M. Mudgett-Hunter, M.-S. Tai, J. Novotný, M. N. Margolies, R. J. Ridge, R. E. Bruccoleri, E. Haber, R. Crea, *Proc. Natl. Acad. Sci. USA* **1988**, *85*, 5879.
[26] G. P. Smith, *Science* **1985**, *228*, 1315.
[27] G. Winter, A. D. Griffiths, R. E. Hawkins, H. R. Hoogenboom, *Annu. Rev. Immunol.* **1994**, *12*, 433.
[28] J. W. Kehoe, B. K. Kay, *Chem. Rev.* **2005**, *105*, 4056.
[29] A. Doerner, L. Rhiel, S. Zielonka, H. Kolmar, *FEBS Lett.* **2014**, *588*, 278.
[30] A. A. Welihinda, R. J. Kaufman, *J. Biol. Chem.* **1996**, *271*, 18181.
[31] Z.-J. Lu, S.-J. Deng, D.-G. Huang, Y. He, M. Lei, L. Zhou, P. Jin, *World J. Biol. Chem.* **2012**, *3*, 187.
[32] J. Baselga, *Eur. J. Cancer* **2001**, *37*, 16.
[33] S. M. Huang, P. M. Harari, *Invest. New Drugs* **1999**, *17*, 259.
[34] S. Kasper, H. Reis, S. Ziegler, S. Nothdurft, A. Mueller, M. Goetz, M. Wiesweg, J. Phasue, S. Ting, S. Wieczorek, A. Even, K. Worm, M. Pogorzelski, S. Breitenbuecher, J. Meiler, A. Paul, T. Trarbach, K. W. Schmid, F. Breitenbuecher, M. Schuler, *Oncotarget* **2017**, *8*, 45898.
[35] M. Mochizuki, *Nihon Sanka Fujinka Gakkai Zasshi* **1992**, *44*, 918.
[36] G. D. Braunstein, J. Rasor, H. Danzer, D. Adler, M. E. Wade, *Am. J. Obstet. Gynecol.* **1976**, *126*, 678.
[37] T. Chard, *Hum. Reprod.* **1992**, *7*, 701.
[38] H. Sunwoo, T. Nakano, W. Dixon, J. Sim, *Poult. Sci.* **1996**, *75*, 342.
[39] J. Andris-Widhopf, P. Steinberger, R. Fuller, C. Rader, *Phage display: A laboratory manual*, (Eds: C. F. Barbas, D. R. Burton, J. K. Scott, S. Fraser). CSHL Press, Cold Spring Harbor, NY, USA **2001**, Ch. 9.
[40] L. Benatuil, J. M. Perez, J. Belk, C.-M. Hsieh, *Protein Eng. Des. Sel.* **2010**, *23*, 155.
[41] F. Unverdorben, F. Richter, M. Hutt, O. Seifert, P. Malinge, N. Fischer, R. E. Kontermann, *MAbs* **2016**, *8*, 120.
[42] W. J. Finlay, L. Bloom, O. Cunningham, *Methods Mol. Biol.* **2011**, *681*, 383.
[43] J. Fehrsen, S. Wemmer, W. van Wyngaardt, *Phage Display: Methods and Protocols*. (Eds: M. Hust, T. S. Lim), Springer New York, New York, NY **2018**, p. 189.
[44] W. van Wyngaardt, T. Malatji, C. Mashau, J. Fehrsen, F. Jordaan, D. Miltiadou, D. H. du Plessis, *BMC Biotechnol.* **2004**, *4*, 6.
[45] R. W. Siegel, J. R. Coleman, K. D. Miller, M. J. Feldhaus, *J. Immunol. Methods* **2004**, *286*, 141.
[46] G. Rojas, A. Talavera, Y. Munoz, E. Rengifo, U. Krengel, J. Ångström, J. Gavilondo, E. Moreno, *J. Immunol. Methods* **2004**, *293*, 71.
[47] D. Han, J. Wu, Y. Han, M. Wei, S. Han, R. Lin, Z. Sun, F. Yang, D. Jiao, P. Xie, *Oncotarget* **2016**, *7*, 59471.
[48] J. F. Rippmann, M. Klein, C. Hoischen, B. Brocks, W. J. Rettig, J. Gumpert, K. Pfizenmaier, R. Mattes, D. Moosmayer, *Appl. Environ. Microbiol.* **1998**, *64*, 4862.
[49] J. Marks, H. Hoogenboom, A. Griffiths, G. Winter, *J. Biol. Chem.* **1992**, *267*, 16007.
[50] L. M. Walker, D. R. Bowley, D. R. Burton, *J. Mol. Biol.* **2009**, *389*, 365.

8.2 Antibody Display Technologies – Selecting the cream of the crop

Antibody display technologies enable the successful isolation of antigen-specific antibodies with therapeutic potential. The key feature that facilitates the selection of an antibody with prescribed properties is the coupling of the protein variant to its genetic information and is referred to as genotype phenotype coupling. There are several different platform technologies based on prokaryotic organisms as well as strategies employing higher eukaryotes. Among those, phage display is the most established system with more than a dozen of therapeutic antibodies approved for therapy that have been discovered or engineered using this approach. In recent years several other technologies gained a certain level of maturity, most strikingly mammalian display. In this review, we delineate the most important selection systems with respect to antibody generation with an emphasis on recent developments.

Authors

Bernhard Valldorf*, Steffen C. Hinz*, Giulio Russo, **Lukas Pekar***, Laura Mohr, Janina Klemm, Achim Doerner, Simon Krah, Michael Hust and Stefan Zielonka

* These authors contributed equally to this work

Bibliographic information

Submitted for publication in August 2020. Shown manuscript herein represents a submitted author manuscript.

Antibody Display Technologies – Selecting the cream of the crop

Bernhard Valldorf[1*], Steffen C. Hinz[2*], Giulio Russo[3,4], Lukas Pekar[5*], Laura Mohr[6], Janina Klemm[2], Achim Doerner[5], Simon Krah[5], Michael Hust[4] and Stefan Zielonka[5+]

[1]Chemical and Pharmaceutical Development, Merck KGaA, Frankfurter Strasse 250, D-64293 Darmstadt, Germany

[2]Institute for Organic Chemistry and Biochemistry, Technische Universität Darmstadt, Alarich-Weiss-Strasse 4, D-64287 Darmstadt, Germany

[3]Abcalis GmbH, Inhoffenstrasse 7, D-38124 Braunschweig, Germany

[4]Institut für Biochemie, Biotechnologie und Bioinformatik, Technische Universität Braunschweig, Spielmannstrasse 7, D-38106, Braunschweig, Germany

[5]Protein Engineering and Antibody Technologies, Merck KGaA, Frankfurter Strasse 250, D-64293 Darmstadt, Germany

[6]Institute of Cell Biology and Neuroscience and Buchmann Institute for Molecular Life Sciences, University of Frankfurt, Max-von-Laue-Strasse 13, D-60438 Frankfurt am Main, Germany

[+]**Correspondence:**

Protein Engineering and Antibody Technologies, Merck KGaA, Frankfurter Strasse 250, D-64293 Darmstadt, Germany

Stefan.Zielonka@merckgroup.com

*These authors contributed equally to this work

Keywords: Antibody display, antibody engineering, bacterial display, B cell selection, genotype phenotype coupling, mammalian display, microfluidics, phage display, protein engineering, ribosome display, yeast surface display

Abstract

Antibody display technologies enable the successful isolation of antigen-specific antibodies with therapeutic potential. The key feature that facilitates the selection of an antibody with prescribed properties is the coupling of the protein variant to its genetic information and is referred to as genotype phenotype coupling. There are several different platform technologies based on prokaryotic organisms as well as strategies employing higher eukaryotes. Among those, phage display is the most established system with more than a dozen of therapeutic antibodies approved for therapy that have been discovered or engineered using this approach. In recent years several other technologies gained a certain level of maturity, most strikingly mammalian display. In this review, we delineate the most important selection systems with respect to antibody generation with an emphasis on recent developments.

1. Introduction

Monoclonal antibodies (mAbs) have proven to be remarkably versatile therapeutics for disease treatment including cancer and inflammatory disorders [1–3]. This is exemplified by the fact that as of November 2019, around 80 mAbs have been granted marketing approval either in the US or the EU and 79 antibody-derived modalities were investigated in late stage clinical trials [4]. Also, from a commercial perspective, antibody-based therapeutics are tremendously successful. In 2018, the global mAbs market was valued approximately 115 billion US dollars and is expected to grow to about 300 billion US dollars until 2025 [5]. Moreover, the majority of top ten drugs by global sales are antibody

47 (Ab) therapeutics with Humira (Adalimumab) still being the most profitable entity [6]. As such, antibody-
48 based therapeutics are one of the main drivers of revenues of the pharmaceutical market.
49 Antigen-specific mAbs can be obtained by immunization combined with hybridoma technology, which
50 was pioneered in the 1970s by Köhler and Milstein and still remains state-of-the-art in Ab hit discovery
51 [7]. Alternatively, Ab display systems such as phage display or yeast surface display enable the isolation
52 of molecules with prescribed properties essentially resulting in several mAb therapeutics approved by
53 healthcare authorities [5,8–10]. Herein, the key feature enabling the isolation of a desired candidate relies
54 on the linkage of the protein of interest (POI) (i.e. the phenotype) to its genetic information (i.e. the
55 genotype). Hence, this principle of genotype phenotype coupling allows for 'barcoding' of up to several
56 billion different protein variants of which binders can be selected via high-throughput identification in
57 an iterative process. Several different display technologies are available today, comprising for instance
58 ribosomal display, mammalian display, phage display or yeast surface display, with phage display
59 being the most established one [11]. In this review, we describe main Ab display systems without raising
60 the claim of giving a full comprehensive picture. We aim at summarizing core principles of different
61 platform technologies with an emphasis on recent developments and trends.
62
63 **2. Antibody formats utilized for Display**
64 Humans produce five different isotypes of immunoglobulins (Igs) referred to as IgG, IgM, IgA, IgD
65 and IgE. Among those, IgG, which can be further divided into four different subclasses, is the most
66 prevalent isotype in the serum [12]. Importantly, IgG is also the most relevant class in terms of therapeutic
67 applications [13]. The Y-shaped IgG is a complex heterotetrameric protein composed of two identical
68 heavy chains (HCs) as well as two identical light chains (LCs) with a molecular weight of
69 approximately 150 kDa (**Fig. 1**). Each light chain, either assigned to the κ- or λ-type, forms a
70 heterodimer with a heavy chain and two of those resulting heterodimers, which are linked via disulfide
71 bonds (LC-HC as well as HC-HC), represent the intact Ig. Within the molecule, each light chain is

72 generally composed of a *N*-terminal variable domain (VL) as well as a constant domain (either CLκ or
73 CLλ), whereas each of the heavy chains of an IgG1 consists of a *N*-terminal variable domain (VH)
74 followed by three constant regions (CH1-CH3). From a functional perspective, this isotype has two
75 identical fragments responsible for antigen binding (fragment antigen binding, Fab) and the fragment
76 crystallizable (Fc part) that mediates effector functions as well as long serum half-life via binding to
77 several distinct Fc receptors and complement proteins [14,15].
78 Each Fab fragment is a heterodimer consisting of the VH-CH1 region of the heavy chain and the entire
79 light chain (VL-CLκ or λ). Within the Fab region domain, VH and VL harbor the antigen binding site,
80 i.e. the paratope. This paratope is composed of three hypervariable loops of the variable domain of the
81 heavy chain and light chain, respectively. These hypervariable loops are referred to as complementarity
82 determining regions (CDRs) and offer extraordinary variability with respect to loop length as well as
83 amino acid composition (most strikingly in CDR-H3). Overall, those CDRs mediate highly specific
84 antigen binding. Since Abs contain two identical Fab arms, antigen binding is bivalent and
85 monospecific by nature. Simultaneous bivalent binding of two identical targets is enabled by the hinge
86 region, which connects both Fab arms as wells as the Fc part and mediates sufficient flexibility [16]. Due
87 to their complex nature, display of full-length IgGs is usually difficult to achieve using prokaryotic
88 display systems or technologies engaging lower eukaryotes (of note, full IgGs can readily be displayed
89 using mammalian systems). Consequently, Ab fragments are typically utilized for those platform
90 technologies. Those include Fab fragments [17] as well as single chain variable fragments (scFvs) [18].
91 ScFvs only consist of the VH and the VL domains connected by a flexible linker **(Fig. 1)**. In addition
92 to this, camelids and sharks produce heavy chain only Abs, where antigen binding is mediated by a
93 single variable domain [19–21]. These single domain antibody (sdAb) repertoires can also be efficiently
94 accessed employing genotype phenotype coupling [22–24]. Moreover, the display of bispecific entities as
95 well as engineered Ab scaffolds has been described in literature [25,26].
96

3. Sources of Antibody Diversity

Different sources of diversity can be harnessed for the construction of Ab libraries. In principle, libraries can be divided into immune libraries and libraries of universal use. Immune libraries are typically constructed from tissues or blood samples of immunized animals [27–31]. With the advent of transgenic animals harboring the (partial) human Ig variable region gene repertoire [32–38], fully human Abs can be obtained nowadays by the combination of immunization with an Ab display platform of choice [39]. Moreover, those libraries can be generated based on humans that either have received vaccination or from patients who have suffered from a disease [40–45]. These kinds of libraries are heavily biased towards a given target, since the Ab repertoire has already been pre-selected *in vivo*. Hence, they typically contain high-affinity variants. However, their applicability is usually limited to single use only.

On the contrary, universal libraries can be considered as 'one-stop-shops' for the isolation of antigen-specific Abs against virtually every target. Accordingly, these types of libraries are of general use. Universal libraries can be sub-divided into naïve, synthetic and semi-synthetic approaches [46]. Naïve libraries make use of rearranged Ig V genes from non-immunized donors and, as consequence, typically access the IgM repertoire [17,47–49]. One of the hallmarks of such libraries relies on their combinatorial nature, i.e. during library construction heavy and light chains are randomly combined. While much efforts were made recently to keep the natural heavy and light chain pairing for immune libraries [50,51], this random i.e. unnatural pairing is generally considered to be advantageous in case of universal libraries [52]. Many therapeutic antigens are self-molecules, but during B cell maturation autoreactive Abs expressed on the B cell surface (i.e. B cell receptors) are usually eliminated. Generally, it is considered that owing to the random combinatorial assembly of heavy and light chains, this immunological tolerance can be circumvented (at least partially), enabling the generation of Abs targeting self-antigens. Synthetic strategies are intended to maximize the functionality of libraries, e.g. by focusing on developable scaffolds, by obviating the introduction of sequence liabilities or by precise

122 control of loop length and amino acid composition using state-of-the-art methods of molecular biology
123 [46,53–58]. Semi-synthetic approaches typically combine natural and synthetic Ab sequences or sequence
124 parts [8]. Regarding this, one extravagant examples was described by Hoet and colleagues, who
125 combined light chains from autoimmune patients with the human IGHV3-23 framework harboring
126 autoimmune patient-derived CDR-H3 as well as synthetic CDR-H1 and CDR-H2 regions [59]. Beyond,
127 libraries can also be constructed for a specific intended purpose, i.e. for humanization of candidates or
128 for affinity maturation [60–64].
129
130 **4. Phage display**
131 The most successfully applied platform technology in the context of Ab discovery is phage display
132 (PD). As of today, 14 marketed therapeutic Abs were identified or engineered using this Nobel prize-
133 awarded approach[65] (**Table 1**), and a multitude of PD derived molecules are currently investigated in
134 clinical trials [8]. PD has its origins in 1985, when George P. Smith was able to display and affinity purify
135 short peptides (genetically) fused to the pIII minor coat protein of M13 filamentous phage [66]. With
136 respect to Ab discovery, it was independently shown by three groups in the early 1990s that PD can be
137 exploited for the *in vitro* selection of Ab fragments: the working groups around McCafferty and
138 Chiswell in Cambridge [67], Barbas in La Jolla [68] as well as Breitling and Dübel in Heidelberg [69]. In
139 general, the Ab candidate fused to pIII can be integrated into the phage genome [67]. However, due to its
140 enhanced flexibility, nowadays, the phagemid system is used much more frequently [69]. Here,
141 expression of the antibody::pIII fusion is uncoupled from phage replication and phage protein
142 production. For single-stranded DNA replication and packaging into phage particles, a morphogenic
143 signal is added. Assembly of functional phage particles is then facilitated by helper phage providing
144 all crucial components for M13 phage packaging. This also allows for utilization of specialized helper
145 phage, e.g. Hyperphage, enabling multicopy display and consequently avidity-based selections [70,71].
146 Eventually, incorporation of the antibody::pIII fusion into the phage coat results in display on the phage

147 surface, while the corresponding genetic material resides within the phage particle (**Fig. 2**). Albeit
148 display of full-length Igs has been described [72], usually Ab fragments such as scFvs [18], Fabs [59] or single
149 domain entities [22] are employed for PD, owing to a more robust and reliable processing by the bacterial
150 expression host *Escherichia coli* (*E. coli)*. One of the main advantages of PD compared to most other
151 platform technologies described in this review is the ease of library generation comprising huge
152 diversities. In this respect, libraries with more than 10^{11} clones have been constructed [73,74]. Hence,
153 highly specific and high-affinity variants in the low nanomolar to sub-nanomolar range can be readily
154 obtained not only from immune libraries [22,30,75], but also from universal approaches, as elegantly
155 reviewed by Almagro and co-workers [46]. Ab library generation can be conducted in several ways, for
156 instance by sequential cloning of the light and heavy chain repertoire [47], *via* splicing by overlap
157 extension PCR [76,77] or utilizing type IIs restriction enzymes for simultaneous introduction of heavy and
158 light chain diversities [22,78]. Once constructed, library candidates with desired characteristics such as
159 affinity, selectivity or stability can be selected in a process referred to as panning (**Fig. 2**), inspired by
160 the process of gold mining. To this end, the library of Ab-displaying phage is incubated with the
161 respective antigen. On the one hand, antigens can be immobilized to a solid surface e.g. to
162 nitrocellulose [79], magnetic beads [80], column matrixes [81], polystyrene tubes [82] or microtiter plates [83,84]
163 with high protein binding capacities. On the other hand, panning can alternatively be performed in
164 solution using biotinylated antigens followed by 'pull-down' employing streptavidin-coated beads [85].
165 Moreover, selections can be carried out on primary cell lines or utilizing recombinant cells expressing
166 the target of choice, clearly demonstrating the vast flexibility of PD. By applying stringent washing
167 steps, the excess of target-unspecific phages can be removed and subsequently, antigen-bound phage
168 are eluted (e.g. enzymatically [22,47] or by pH-shift [66,86]) and used for re-infection and re-amplification
169 of *E. coli*. Since phagemid-harboring *E. coli* cells only express the antibody::pIII fusion, helper phage
170 infection is again needed for the production of functional phage particles. This iterative procedure is
171 typically repeated for several rounds in order to highly enrich for antigen specific clones followed by

soluble mAb production and screening for specific binding either by ELISA [84], immunoblot [82] or flow cytometry [87]. The ability to produce soluble Ab fragments simultaneously to the expression of the pIII fusion derives from the presence of an amber stop codon placed in frame between the Ab gene and the pIII gene in combination with the utilization of an amber-suppressor strain of *E. coli*. Afterwards, the genetic information of positive hits is retrieved by sequencing. Moreover, sorting stringencies can be increased by implementing different depletion strategies [88,89]. Due to its high versatility, PD has been applied in manifold ways for Ab discovery and engineering. In this respect, this technology commonly is the method of choice for the de novo generation of candidates from universal library approaches and consequently a plethora of universal libraries is known today, as described elsewhere [46,47,53,54,58,59,73,90]. Moreover, typical other applications of PD are Ab humanization [60,91,92] as well as affinity maturation of Abs. Affinity optimization of library candidates by phage display can be executed in many ways, for instance using different mutagenesis strategies [62,93]. Another prominent approach is referred to as light chain shuffling [94,95]. Here, the heavy chain of a pre-selected binder (or heavy chains from a panel of binders) is paired with the light chain repertoire of a universal library (e.g. naïve) and re-selected under enhanced stringencies in order to obtain affinity-matured hits [96]. A very elegant PD strategy relies in guided selection [97]. Here, usually a rodent Ab is employed as template and each of its variable domains (e.g. the VH domain) is paired with the complementary human antibody variable domain repertoire (e.g. the human VL repertoire), respectively, and selected against the original target. Subsequently, both enriched human VH and VL repertoires are combined and further panned in order to isolate antigen-specific binders. Ultimately, this strategy leads to the identification of human Abs having similar properties as the parental non-human clone. Guided selection has been used in combination with PD for the generation of Adalimumab [8]. Moreover, PD has proven to be versatile for a more extravagant engineering of 'next-generation' mAb entities such as common light chain bispecifics[98], common heavy chain bispecifics (also known as κλ-bodies)[99] or Abs comprising pH-dependent binding properties [100,101].

5. Yeast surface display

In addition to PD, another platform technology that successfully demonstrated to be suitable for the generation of therapeutic Abs is yeast surface display (YSD). YSD enabled the generation of the PD-1 blocking Ab molecule Sintilimab, which has gained marketing approval in China for the treatment of refractory classical Hodgkin's lymphoma (**Table 1**) [102–104]. This technology was pioneered in 1997 by Boder and Wittrup and relies on the genetic fusion of the library candidate to a microbial cell surface protein [105]. Albeit several different anchor proteins have been evaluated for displaying proteins on the surface of *Saccharomyces cerevisiae* [106–108], the most commonly and successfully applied system is composed of the a-agglutinin complex subunits Aga1p and Aga2p (**Fig. 3**). Here, the POI can be fused *N*-terminally or *C*-terminally to Aga2p, clearly enabling flexibility with respect to the optimal orientation that might be needed for a particular protein [105,109]. Typically, the resulting plasmid-encoded fusion protein is produced under the control of the galactose-inducible GAL1/10 promoter system, whereas Aga1p, which is also controlled by a galactose-inducible promoter, is integrated into the yeast genome. Upon expression, Aga2p forms two disulfide bonds with Aga1p [110]. Hence, covalent tethering of the POI is facilitated on the yeast surface, usually resulting in the display of 10^4-10^5 copies of the library candidate [105]. Although full-length Ig display has been achieved for YSD [111–113], Ab fragments, for instance scFvs and Fabs, are most commonly exploited in the context of Ab engineering *via* YSD [105,114,115,115–118]. Moreover, sdAbs [24,119] as well as scaffold proteins are frequently engineered using this platform approach [120]. YSD libraries can be constructed in manifold ways, e.g. by conventional cloning [121], in a homologous recombination-based process referred to as gap repair cloning [122] or by Golden Gate Cloning involving type IIs restriction enzymes [123,124].

One of the main benefits of YSD is its compatibility with fluorescence activated cell sorting (FACS), enabling online and real-time analysis of library candidates and consequently precise control over selection on a quantitative basis [11]. In this regard, a two-dimensionally sorting strategy can be implemented using fluorescently labeled antigens as well as immunofluorescence staining to gate for

222 clones with structural integrity (i.e. clones without frame shifts or stop codons). This can be
223 accomplished by either employing epitope tags or by using fluorescently labeled detection reagents
224 directed against constant components of the protein to be displayed, such as reagents targeting the
225 constant region of the light chain in the case of Fab display (**Fig. 3**) [39,105]. Alternatively, reporter
226 systems have been described which couple functional protein display to a fluorescence reporter read-
227 out [125,126] This allows for fine discrimination of clones based on binding affinities or kinetics.
228 Moreover, due to the presence of more sophisticated quality control machineries for proper protein
229 folding, it is believed that YSD enables the engineering of more complex molecules compared to
230 technologies involving prokaryotes [11,127,128]. After library sorting, enriched cell populations are
231 expanded, followed by subsequent FACS-based selection rounds. Finally, the genetic information is
232 obtained by sequencing. Additionally, enriched clones can directly be characterized in terms of binding
233 functionality or affinity *via* flow cytometry without the need for subcloning. In direct comparison to
234 PD, the main bottleneck of YSD is confined library sizes. While libraries in the range of 10^9 clones
235 can be readily constructed for YSD [123,129,130], libraries for PD are able to outperform this by several
236 orders of magnitude [46]. Nevertheless, it was shown that YSD also allows for the isolation of antigen-
237 specific Abs from universal libraries [119,131,132]. Moreover, the daily throughput of FACS is limited to
238 the range of approximately 10^9 cells, which, however, can be increased for huge libraries by a pre-
239 enrichment using magnetic-activated cell sorting. One of the main applications of YSD in Ab
240 engineering is affinity maturation [105,117,133]. Similar to PD, this can be achieved utilizing different
241 randomization strategies, such as CDR-targeted mutagenesis [119,134] or light chain shuffling [129].
242 Additionally, it has been shown that YSD allows for facile isolation of high-affinity candidates after
243 animal immunization [28,29,39,114]. Related to this, Johnson and colleagues demonstrated that the
244 construction of natively paired Ab libraries (i.e. libraries retaining the original pairing of the heavy and
245 the light chain from a distinct B cell) yield proteins with higher sensitivities and specificities after
246 immunization than libraries with random paired chains [50]. Consequently, sophisticated techniques have

247 been established aiming at the maintenance of this natural heavy and light chain pairing [50,51].
248 Additionally, YSD can be employed for mAb humanization. Like PD, YSD has proven to be versatile
249 for the engineering of next-generation Abs such as pH-dependent mAbs [135–139], common chain entities
250 [123,140], anti-idiotypic entities [141] or antigen-binding Fc parts [26]. A very elegant approach for the isolation
251 of mAbs exhibiting excellent developability properties originating from YSD libraries has been
252 published by Krauland and colleagues [142]. During Ab selection, the authors implemented a depletion
253 step, i.e. a negative selection by employing a polyspecificity reagent, in order to enrich for clones with
254 significantly reduced polyspecific binding. In another work, published by Lerner and colleagues, it was
255 demonstrated that also complex antigens such as G protein-coupled receptors can be targeted by YSD
256 in a FACS-based biopanning approach [143]. In addition, yeast display can be utilized to scrutinize PD
257 selection outputs in a high-throughput manner [144].
258
259 **6. Ribosome display**
260 Besides cellular display technologies or approaches involving filamentous phage, cell-free *in vitro*
261 methods were developed with ribosome display (RD) being the most established cell-free platform
262 technology. Herein, compared to cellular display systems, the number of library-members is not limited
263 by the transformation efficiency of the host. This allows for the generation and screening of larger
264 diversities in the range of 10^{12}-10^{15} variants [145,146]. RD mediates genotype phenotype coupling by
265 fusing the library candidate to its corresponding mRNA, which is reverse-transcribed to DNA after
266 selection, PCR-amplified and sequenced (**Fig. 4**) [147]. Technically, the mRNA lacks the information of
267 the terminal stop codon at the end of the sequence encoding for the POI. During translation, the
268 ribosome is stalled at that position on the mRNA, because release-factors cannot enter the A-position
269 of the ribosome, which further impedes the release of the respective polypeptide chain. This results in
270 the formation of mRNA-ribosome-polypeptide complexes. Similar to PD, selections can be carried out
271 by using antigen coupled magnetic beads or antigen-coating on microtiter plates. The isolation of high

affinity binders can be promoted by applying stringencies, such as a reduced antigen-concentration and an increased washing intensity during subsequent selection rounds. A limiting factor of RD is the accessibility of functional ribosomes per library reaction, which can reduce the library-size on the protein level [145,148].

Historically, Mattheakis and colleagues demonstrated the isolation of peptides binding a mAb with high affinity by using the display on polysomes in 1994 [149]. Hanes and Plückthun described RD in 1997 for the first time in the context of Ab selections and were able to 10^8-fold enrich a complete disulfide containing protein (i.e. an anti-hemagglutinin scFv) out of a mixture with another scFv, specific to β-Lactam [150]. For *in vitro* translation, both groups utilized *E. coli* cell extracts. In the same year, generation of antibody-ribosome-mRNA (ARM) complexes using eukaryotic cell extracts was described. To this end, single chain VH/κ fragments (i.e. a fusion of VH to a complete κ-light chain) specific to progesterone were selected by application of antigen-coupled magnetic beads enabling a 10^4-10^5 enrichment in a single cycle [151]. In another approach, the yeast transcription factor GCN4 was utilized for the generation of a murine immune library, which was subsequently used for RD selection, enabling the isolation of a scFv binding the antigen with a double digit picomolar affinity [152]. This scFv exhibited a 65-fold higher affinity than its "presumed" progenitor with only one amino acid substitution in CDR-L1. Plückthun and colleagues hypothesized that the incorporation of this mutation occured during the RD process itself and not during *in vivo* Ab maturation. Therefore, the use of RD for molecule selection may overcome tedious optimization steps, as features like the maturation of Ab affinity might be inherent in the RD process.

Today, RD has been extensively studied, especially for Ab affinity maturation [153–155]. Library candidates from immune and PD repertoires have been affinity optimized with improvements of more than 1000-fold [156]. Moreover, RD has been applied to generate high-affinity Abs from a synthetic library (HuCAL) [157]. Unlike cellular display approaches RD allows the simple incorporation of additional diversity also throughout the screening process, by applying gene-shuffling or error-prone

297 PCR amplification. In this regard, selected scFvs against insulin accumulated mutations introduced by
298 Ab amplification with a low fidelity DNA-polymerase, resulting in 40-fold improved binding affinities
299 compared to their progenitors, originally present in HuCAL [157].
300 Besides RD, mRNA-display or cDNA-display represent complementary technologies, fusing mRNA
301 to puromycin, which is an analogue of a tyrosyl-tRNA and mimics tyrosine and adenosine with part of
302 its structure. Essentially, the amide bond in the puromycin molecule is not hydrolysable and resulting
303 in a physical linkage between the mRNA and its protein at the end of translation [158]. As mRNA is
304 unstable, a puromycin linker DNA is used as a primer for reverse transcription in cDNA-display,
305 forming mRNA-cDNA hybrids [159].
306
307 **7. Mammalian surface display**
308 Unlike PD or yeast YSD, where mainly one specific methodology dominates the display field, many
309 different systems of mammalian surface display have been developed in parallel. With the advent of
310 sophisticated tools of gene editing and genetic engineering, e.g. CRISPR/Cas9 or transposon
311 technologies, tremendous progress has been made within recent years. This section aims at briefly
312 giving an overview about some of the main techniques and recent trends.
313 Mammalian Ab display offers some distinct advantages compared to other selection techniques
314 described in this review due to the use of cells not only suitable for screening but also for the production
315 of the desired proteins. The mammalian expression and secretory apparatus is particularly favorable
316 for the production of properly folded full-length Ig molecules with human glycosylation patterns and
317 other post-translational modifications. The vast majority of marketed Ab therapeutics is produced in
318 mammalian cells [160,161]. Hence, a mammalian platform technology for Ab selection enables processing
319 of library candidates similar to the final production cell line. Furthermore, this also facilitates a
320 thorough selection for high-level expression besides the binding functionality by FACS. Thereby
321 greater insights into the detailed characteristics of the respective library candidate can be obtained.

322 Mammalian cell surface display of Abs is typically enabled by the genetic fusion of the *C*-terminus of
323 the heavy chain constant region to a transmembrane domain e.g. of the murine H-2Kk protein or the
324 human platelet-derived growth factor (PDGF) receptor (**Fig. 5**) [162,163]. While transient transfection has
325 traditionally been used for library construction in mammalian cells [164], the field rapidly shifted to stable
326 library generation due to a much more robust genotype phenotype coupling [163]. Since transiently
327 transfected cells generally produce the Ab only for a certain time period, the introduced plasmid DNA
328 must typically be rescued after one round of selection, clearly impeding throughput and convenience
329 in handling [164,165]. This is in stark contrast to stable library generation, where, in theory, infinite rounds
330 of selection can be carried out without plasmid loss [163,165–168].
331 In addition to surface display, simultaneous secretion can be achieved, for instance, by inclusion of
332 LoxP sites flanking the sequence which encodes for the membrane anchoring protein domain, yielding
333 cryptic splice donor sites. The alternatively spliced product lacks the transmembrane domain and is
334 directly secreted into the medium, which enables further biophysical characterization of Abs expressed
335 by selected cells [162,163]. As example, Waldmeister and colleagues used the supernatants from sorted
336 clones for affinity determination but also checked their suitability as antibody-drug conjugates in a
337 secondary ADC cell killing assay [167]. In a recent publication, Aebischer-Gumy and colleagues turned
338 this concept upside-down resulting in a proportion of the secreted protein as displayed molecule on the
339 cell surface by alternative splicing using the chicken cardiac troponin intron 4 between the coding
340 sequence of the HC and the transmembrane domain[169]. Due to the small size (0.5 kbs) of the chicken
341 cardiac troponin intron 4, it can easily be used in plasmids for Ab display compared to the natural
342 intron of the Ig gene (5 kbs), which has been used with transposable vectors [167,169]. The technology
343 called SPLICELECT™ claims that the level of cell surface display can be correlated with expression
344 titers and product quality attributes. In addition, the intron sequence can be modified in a nature either
345 favoring display or mAb secretion, clearly enabling a certain degree of flexibility. Beyond, alternative
346 strategies for simultaneous display and secretion have been described by utilization of, i.e. by a leaky

347 translation termination signal between the HC of the Ab and a transmembrane domain [170], by non-
348 sense codons [171] or by amber suppression [172].
349 One of the biggest challenges in mammalian display is the construction of large libraries comparable
350 to those in bacteria or yeast. Depending on the strategy chosen for stable cell library generation,
351 multiple or single copies of Ig genes can be integrated into the genome either randomly or in a site-
352 specifically manner. Standard transfection, viral transduction or transposon technologies for library
353 generation can yield clones with multiple DNA integrations encoding for different Ab genes [166–168]. Of
354 note, polyclonal display negatively impacts genotype phenotype coupling, and consequently the
355 isolation of the genetic information of a favored library candidate. Besides, due to the presence of
356 different Ab chains, mispaired heavy and light chains are displayed and the enrichment of specific
357 clones can be hampered substantially. To obviate this, the DNA utilized for transfection or viral
358 particles can be titrated carefully, thereby enabling an average of one transfected cell displaying only
359 one protein variant[166–168].
360 In general, irrespective of titration in order to obtain pseudo-monoclonal display, large libraries can be
361 generated by random introduction of Ab genes into cells using viral transduction or transposon
362 technology [166–168,173]. The Transpo-mAb display platform e.g. applies DNA transposition to generate
363 mammalian cell libraries with a potential complexity of 10^9 by simple transfection [167]. Libraries of
364 more than 10^9 clones have also been generated by B cell transduction with retroviral particles carrying
365 light chain and heavy chain diversities, respectively, as described by Breous-Nystrom in 2014 [168].
366 However, one of the main downsides of random Ab gene insertion is the variation in the expression
367 level, which strongly depends on the transcriptional activity at the integration site.
368 In recent years, mammalian display made significant advances due to the application of progressive
369 genetic engineering tools, i.e., CRISPR/Cas9 or TALE nucleases. Genetic engineering can be used to
370 efficiently create libraries of up to 10^7 clones with strictly monoclonal display as well as gene insertion
371 at a pre-defined integration site [163]. In this respect, the group of McCafferty was able to create a

functional chain-shuffled library of 1.8 x 10^6 clones using a population of VH genes pre-selected against PD-L1 combined with a repertoire of light chains. Novel high-affinity IgGs specific for PD-L1 could be selected from this mammalian Ab display library [163]. In a different set-up Cas9-driven homology-directed repair (HDR) has been used to generate site-directed mutagenesis antibody libraries with about 10^5 variants [174]. Herein, variations were introduced utilizing single-stranded oligonucleotides as the donor template at individual complementarity determining regions of a pre-integrated Ab gene in a modified hybridoma cell line, referred to as plug-and-(dis)play hybridomas [174,175]. The group was able to increase Cas9-mediated integration efficiency by more than 15-fold in the hybridoma cell line by improving an HDR plasmid donor setup that applies in situ linearization [176]. Furthermore, this allowed for the efficient integration of complete VL and VH chain cassette libraries into the genome of the hybridoma cells. Interestingly, in another publication, the group combined mammalian library screening with machine learning. To this end, they trained a neural network by screening and deep-sequencing fractions of rational site-directed mutagenesis libraries based on the therapeutic entity Trastuzumab. By using this approach, antigen-binding could accurately be predicted based on Ab sequences from an in silico library of ~10^8 variants, which was confirmed by the expression and characterization of 30 mAbs [177]. In future, this strategy could guide the rational design of mammalian Ab display libraries and help to overcome the remaining challenge of sampling the huge theoretical sequence space.

Another benefit of mammalian cell display relies on the possibility to directly implement somatic hypermutation (SHM) *in vitro*. Naturally, SHM is mediated by the enzyme activation-induced cytidine deaminase (AID) and is an essential process for optimizing Ab affinity [178]. In 2013, Bowers and colleagues have used SHM directed by AID to affinity mature and isolate antibodies [162]. In a first step, cells displaying Abs with a rather low antigen affinity were selected and their functionality was tested. In a second step, those variants were affinity optimized by *in vitro* SHM mediated by AID expression. This procedure enabled the evolution of functional high-affinity binders. In 2020, this technology has

been further improved by Luo and colleagues through reengineering of the AID enzyme, optimizing the Ab sequence and the AID gene transfection procedure [179]. Besides selection, affinity maturation and production of antigen-specific Igs, mammalian display also allows to directly transduce reporter cells with an Ab library and, thereby, to directly screen for agonistic or antagonistic molecules as shown by Lerner and colleagues [173]. In this work, EpoR specific binders were enriched via PD and selected genes were switched afterwards into lentiviruses for the transduction of reporter cells. These reporter cells were infected with one to four different lentiviruses resulting in an expression of the Abs inside the cell as well as a secretion of the molecules. A subsequent phenotypic screening enabled the selection of heterodimeric bispecific agonistic molecules. The same group was able to confirm this concept in another publication by selecting an agonistic Ab specific for the granulocyte colony-stimulating factor receptor (G-CSFR) inducing human CD34+ stem cells to form neural progenitor cells [180].

8. Bacterial display

Bacteria have been utilized for surface display in order to combine fast growth rates as well as easy and cost-efficient handling with real-time multiparameter fluorescence analysis for cell sorting. Similar to mammalian display, a variety of different technologies, each employing unique setups, have been reported of which some will be discussed in the following.

Francisco and colleagues, e.g., utilized the translocation properties of the major lipoprotein (lpp) of *E. coli* in combination with the outer membrane protein A (ompA) mediating the anchorage of the antibody on the outer membrane to achieve surface presentation [181]. Subsequently, this system was used to affinity mature an anti-digoxin scFv, which resulted in the isolation of a binder with sub-nanomolar affinity [182]. Additional approaches employ alternative bacterial proteins either for display

420 on the outer membrane, such as peptidoglycan associated lipoprotein (PAL) [183,184], β-domains of EhaA
421 and intimin [185], or for the display on the inner membrane.
422 In 2004, the anchored periplasmic expression technology (APEx) was published [186]. Here, in contrast
423 to the lpp-ompA setup, the Ab fragment is either fused to lipoprotein NlpA (*N*-terminal setup) or to
424 M13 phage gene 3 minor coat protein (g3p) (*C*-terminal setup) and displayed on the inner membrane.
425 Another approach is the MAD-TRAP system, described by Karlsson and colleagues, which utilizes the
426 twin-arginine translocation (tat) pathway to achieve inner membrane display of scFv molecules [187].
427 Due to the location of the displayed Ab fragment, the outer membrane and cell wall need to be
428 permeabilized or removed with EDTA and lysozyme in order to achieve accessibility for antigen and
429 staining reagents.
430 The more sophisticated display of full-length Abs was achieved by Mazor and colleagues expanding
431 the APEx system. To this end, the protein A-derived Ab-binding ZZ-domain was fused downstream of
432 NlpA and displayed on the inner membrane of *E. coli* [188]. Additional expression of the light as well as
433 the heavy chains and subsequent secretion into the periplasm allowed for capturing the full-length Igs
434 via the ZZ-domain. In contrast to the display of immobilized Ab fragments, the periplasmic expression
435 with cytometric screening (PECS) technology exploits periplasmic expression of Abs, which are
436 retained by the outer membrane [189]. Further, the antibody-antigen complex is detected by antigen-
437 fluorophore conjugates which are limited to around 10 kDa owing to same permeability limitations
438 retaining the Ab in the periplasm. More recently, Lombana and colleagues employed a lpp knock out
439 *E coli* strain for non-immobilized full-length IgG display [190]. Due to the lpp gene deletion and
440 supplementation with EDTA, the loss of outer membrane integrity allowed for antigens and
441 immunostaining agents of up to 100 kDa to enter into the periplasm.
442 Besides surface display employing gram-negative bacteria, several approaches emerged relying on
443 gram-positive bacteria such as *Staphylococcus xylosus, Staphylococcus aureus* or *Staphylococcus*
444 *carnosus*. In these approaches, Ab fragments are either anchored by the cell surface attachment regions

445 of protein A (XM domain) directly on the cell wall [191,192] or by endogenous sortase mediated attachment
446 to peptidoglycan [193]. The capabilities of the gram-positive bacterial display method were demonstrated
447 by e.g. Fleetwood and colleagues, who screened a VHH immune library against GFP and isolated
448 several high affinity variants [194]. However, low transformation efficiencies for gram-positive bacteria
449 still seems to limit their broad applicability in Ab discovery. Additionally, non-human-like post-
450 translational modifications are drawbacks still existing for the different bacterial display platforms.
451
452 **9. B cell selection**
453 Albeit not being considered an engineered platform technology *per se*, the most natural kind of
454 genotype phenotype coupling is provided by the B cell itself. Besides displaying an Ab variant on its
455 surface in form of a B cell receptor, the B cell carries the corresponding genetic information inside the
456 cell as mRNA. Hence, it is tempting to directly utilize B cells and their Ig repertoire (e.g. after
457 immunization) for Ab discovery. This also affords the benefit to preserve the natural heavy and light
458 chain pairing of a particular B cell, which is advantageous since random reassembly during library
459 generation may cause a loss of specificity and affinity [50] or even evoke self-reactive molecules (which
460 is wanted for universal libraries as discussed above but may be considered as detrimental for immune
461 approaches) [195]. In contrast to hybridoma technology, selecting B cells directly obviates the need for
462 cell fusion with tumor cell lines which is typically a tedious and inefficient procedure and might also
463 result in polyclonal Ab variants [196]. Moreover, with hybridoma one is kind of restricted to certain
464 species, while exploiting B cells for selection enables mining of (in theory) every species imaginable.
465 In general, single B cell Ab selection is a consecutive multi-step process. At first, (antigen-specific)
466 single B cells must be detected within a population of different cells. After detection and isolation, the
467 genetic information encoding for the Ab variable genes have to be obtained by molecular biology
468 techniques, e.g. RT-PCR, and subcloned into adequate expression vectors. Finally, the identified
469 variant can be produced and characterized in more detail. Single cell B cell isolation can either be

performed in a random fashion, i.e. without selecting for the binding functionality, or in an antigen-selective manner which obviously is the more sophisticated and promising approach for hit discovery. To this end, several different techniques have been described [197] utilizing e.g. antigen-coated magnetic beads [196,197] or fluorochrome-labeled antigens via multi-parameter FACS[200]. In this regard, one of the most commonly applied methodologies for the isolation of antigen-specific B cells is fluorescence-activated cell sorting. Here, a multi-parameter labeling strategy can easily be employed. For instance, fluorescently labeled Abs against surface markers of B cells (such as CD19) can be utilized to gate for the specific B cell population within a tissue sample. Application of fluorochrome-labeled antigen further enables the isolation of antigen-positive B cells. In addition to this, the involvement of next generation sequencing (NGS) for high-throughput sequencing of Ig genes in single B cell approaches allows for gathering detailed information about the diversities and dynamics of B lymphocyte populations in individuals [201,202].

To this date, several human mAbs addressing different diseases have been developed based on single B cell selection, of which several are currently under clinical evaluation [203–207].

Complementary to B cell selection and other *in vitro* display methodologies described herein, certain hit discovery campaigns demand screening of secreted molecules directly from mAb producing cells. Recent years have seen unparalleled development of microfluidic applications for Ab discovery, both in academic and pharmaceutical research [208 209 210]. Microfluidics can support native chain paired library generation [211 212] as well as direct screening of Ig secreting cells such as plasma cells obtained by rodent immunization [213] or plasmablasts from human peripheral blood [214 215]. Abs secreted from single cells are interrogated after compartmentalization in droplets or nanostructures, such as nanopens or nanowells, mostly by fluorescence-based methods allowing real-time and high-throughput sorting. Methodologies range from selection for binding on recombinant target or cells to internalization or functional screening utilizing reporter gene target cells, as exemplified by recent work from Gérard and co-workers [213]. While broad diversities of neutralizing Abs against infectious diseases such as HIV,

Ebola or COVID-19 have been identified from convalescent individuals [215 216 217], microfluidics can also yield tool [218] as well as therapeutic molecules targeting cancer or immunological diseases [219 220]. Several companies offer customizable microfluidic chips and Ab screening campaigns [208,216,221] and stand-alone devices are commercially available [218,222], further driving development and diversification of microfluidic methodologies for therapeutic Ab discovery.

10. Conclusion

Display technologies enable the selection and engineering of Abs with therapeutic relevance. The fact that - to the best of our knowledge - 15 mAb-derived entities have been granted marketing approval either by US, European or Chinese healthcare authorities (**Table 1**), of which ten molecules reached market access within the last five years [8], is clearly corroborating the major impact those platform technologies have, with respect to drug discovery. Among all therapeutics obtained by Ab display, PD is evidently the most successfully applied approach with 14 therapeutic molecules, either identified or engineered using this technology. Notwithstanding, meanwhile several mAb-derived entities obtained from other display techniques are under clinical investigation, culminating in the approval of Sintilimab in China [9,102]. Essentially, each display technology comes with its own benefits and downsides. For instance, YSD allows for a very precise control over selection due to the possibility of FACS-based real-time and on-line analysis of library candidates [11]. However, library sizes are appreciably restricted compared to PD or RD [46,129,130,145]. In recent years, mammalian display emerged as promising platform technology for Ab engineering. At least, this can be partially explained by the advent of sophisticated genetic engineering tools such as Nobel-prize awarded CRISPR/Cas9 or transposase-based systems allowing for stable generation of libraries with adequate sizes as well as mono-copy insertions at a pre-defined integration site [223]. In this respect, a plethora of different technologies have been described [163,167,169,175,176]. Ultimately, mammalian display aims at ensuring translatable features for a potential therapeutic candidate after reformatting (i.e. biophysical properties or expression yields), since the Ab

production and processing apparatus of the library host is quite similar to the final production cell line. However, slow growth rates of mammalian cells can obviously be considered as one significant limitation compared to prokaryotic display systems or platform technologies based on lower eukaryotes. Beyond display technologies, microfluidic systems were developed that have proven to support mAb discovery from Ig secreting cells, such as plasmablasts or plasma cells [213,215]. In addition to select exclusively for binding, those devices also enable the implementation of functional screenings. As such, microfluidics has the capability to enrich the toolbox for Ab hit discovery. This also holds true for NGS which can be combined with literally every platform technology imaginable [224–228]. Additionally, NGS can be used as platform technology for Ab hit discovery on its own [229,230]. Eventually, it will be interesting to see how all these different approaches contribute to the global drug discovery engine within the near future.

Conflict of Interest

GS is affiliated with Abcalis GmbH. MH is affiliated with Yumab GmbH. BV, SK, AD and SZ are employees of Merck KGaA. Besides, the authors declare that the work was conducted in the absence of any commercial or financial relationships that could be construed as a potential conflict of interest.

Author Contributions

All authors contributed to this work by writing at least one section.

Funding

This work was partially funded by EU project ATAC (Horizon2020 number: 101003650).

Acknowledgments

This work is dedicated to Harald Kolmar on the occasion of his 60th birthday.

Abbreviations

Ab	antibody
AID	activation-induced cytidine deaminase
APEx	anchored periplasmic expression technology
CDR	complementarity determining region
CH	constant domain of the heavy chain
CL	constant domain of the light chain
E. coli	Escherichia coli
Fab	fragment antigen binding
FACS	fluorescence activated cell sorting
Fc	fragment cristallizable
HC	heavy chain
HDR	homology-directed repair
HuCAL	human combinatorial antibody libraries
Ig	immunoglobulin
kb	kilobase
kDa	kilodalton
LC	light chain
lpp	lipoprotein
mAb	monoclonal antibody
NGS	next generation sequencing
ompA	outer membrane protein A
PD	phage display
POI	protein of interest
RD	ribosomal display

570	scFv	single chain variable fragment
571	sdAb	single domain antibody
572	SHM	somatic hypermutation
573	VH	variable domain of the heavy chain
574	VL	variable domain of the light chain
575	YSD	Yeast surface display
576		
577		
578		
579		
580		
581		
582		
583		
584		
585		
586		
587		
588		
589		
590		
591		
592		
593		
594		

References

1. Yasunaga, M. Antibody therapeutics and immunoregulation in cancer and autoimmune disease. *Seminars in Cancer Biology* **64**, 1–12 (2020).
2. Scott, A. M., Wolchok, J. D. & Old, L. J. Antibody therapy of cancer. *Nature Reviews Cancer* **12**, 278–287 (2012).
3. Chan, A. C. & Carter, P. J. Therapeutic antibodies for autoimmunity and inflammation. *Nature Reviews Immunology* **10**, 301–316 (2010).
4. Kaplon, H., Muralidharan, M., Schneider, Z. & Reichert, J. M. Antibodies to watch in 2020. *mAbs* **12**, 1703531 (2020).
5. Lu, R.-M. *et al.* Development of therapeutic antibodies for the treatment of diseases. *Journal of Biomedical Science* **27**, (2020).
6. Urquhart, L. Top companies and drugs by sales in 2019. *Nature Reviews Drug Discovery* **19**, 228–228 (2020).
7. KöHler, G. & Milstein, C. Continuous cultures of fused cells secreting antibody of predefined specificity. *Nature* **256**, 495–497 (1975).
8. Frenzel, A., Schirrmann, T. & Hust, M. Phage display-derived human antibodies in clinical development and therapy. *mAbs* **8**, 1177–1194 (2016).
9. Deng, M. The approval of sintilimab for classical Hodgkin's lymphoma: views and perspectives of anti-PD-1/PD-L1 antibodies in China. *Antibody Therapeutics* **2**, 54–55 (2019).
10. Bradbury, A. R. M., Sidhu, S., Dübel, S. & McCafferty, J. Beyond natural antibodies: the power of in vitro display technologies. *Nature Biotechnology* **29**, 245–254 (2011).
11. Doerner, A., Rhiel, L., Zielonka, S. & Kolmar, H. Therapeutic antibody engineering by high efficiency cell screening. *FEBS Letters* **588**, 278–287 (2014).
12. Schroeder, H. W. & Cavacini, L. Structure and function of immunoglobulins. *Journal of Allergy and Clinical Immunology* **125**, S41–S52 (2010).
13. Grilo, A. L. & Mantalaris, A. The Increasingly Human and Profitable Monoclonal Antibody Market. *Trends in Biotechnology* **37**, 9–16 (2019).
14. van Erp, E. A., Luytjes, W., Ferwerda, G. & van Kasteren, P. B. Fc-Mediated Antibody Effector Functions During Respiratory Syncytial Virus Infection and Disease. *Frontiers in Immunology* **10**, (2019).
15. Lu, L. L., Suscovich, T. J., Fortune, S. M. & Alter, G. Beyond binding: antibody effector functions in infectious diseases. *Nature Reviews Immunology* **18**, 46–61 (2018).
16. Thouvenin, E. *et al.* Bivalent binding of a neutralising antibody to a calicivirus involves the torsional flexibility of the antibody hinge. *Journal of Molecular Biology* **270**, 238–246 (1997).
17. de Haard, H. J. *et al.* A large non-immunized human Fab fragment phage library that permits rapid isolation and kinetic analysis of high affinity antibodies. *J. Biol. Chem.* **274**, 18218–18230 (1999).
18. Vaughan, T. J. *et al.* Human Antibodies with Sub-nanomolar Affinities Isolated from a Large Non-immunized Phage Display Library. *Nature Biotechnology* **14**, 309–314 (1996).
19. Zielonka, S. *et al.* Structural insights and biomedical potential of IgNAR scaffolds from sharks. *mAbs* **7**, 15–25 (2015).
20. Könning, D. *et al.* Camelid and shark single domain antibodies: structural features and therapeutic potential. *Current Opinion in Structural Biology* **45**, 10–16 (2017).

21. Jovčevska, I. & Muyldermans, S. The Therapeutic Potential of Nanobodies. *BioDrugs* (2019) doi:10.1007/s40259-019-00392-z.

22. Sellmann, C. *et al.* A One-Step Process for the Construction of Phage Display scFv and VHH Libraries. *Molecular Biotechnology* (2020) doi:10.1007/s12033-020-00236-0.

23. Roth, L. *et al.* Isolation of Antigen-Specific VHH Single-Domain Antibodies by Combining Animal Immunization with Yeast Surface Display. *Methods Mol. Biol.* **2070**, 173–189 (2020).

24. Uchański, T. *et al.* An improved yeast surface display platform for the screening of nanobody immune libraries. *Scientific Reports* **9**, (2019).

25. Fagète, S. *et al.* Dual display: phage selection driven by co-engagement of two targets by two different antibody fragments. *Protein Engineering, Design and Selection* **30**, 575–582 (2017).

26. Wozniak-Knopp, G. *et al.* Introducing antigen-binding sites in structural loops of immunoglobulin constant domains: Fc fragments with engineered HER2/neu-binding sites and antibody properties. *Protein Engineering, Design and Selection* **23**, 289–297 (2010).

27. Clackson, T., Hoogenboom, H. R., Griffiths, A. D. & Winter, G. Making antibody fragments using phage display libraries. *Nature* **352**, 624–628 (1991).

28. Grzeschik, J. *et al.* Yeast Surface Display in Combination with Fluorescence-activated Cell Sorting Enables the Rapid Isolation of Antibody Fragments Derived from Immunized Chickens. *Biotechnology Journal* **14**, 1800466 (2019).

29. Wang, B. *et al.* Discovery of high affinity anti-ricin antibodies by B cell receptor sequencing and by yeast display of combinatorial V_H:V_L libraries from immunized animals. *mAbs* **8**, 1035–1044 (2016).

30. Rasetti-Escargueil, C. *et al.* Development of human-like scFv-Fc antibodies neutralizing Botulinum toxin serotype B. *MAbs* **7**, 1161–1177 (2015).

31. Rossant, C. J. *et al.* Phage display and hybridoma generation of antibodies to human CXCR2 yields antibodies with distinct mechanisms and epitopes. *mAbs* **6**, 1425–1438 (2014).

32. Brüggemann, M. *et al.* Human Antibody Production in Transgenic Animals. *Archivum Immunologiae et Therapiae Experimentalis* **63**, 101–108 (2015).

33. Osborn, M. J. *et al.* High-Affinity IgG Antibodies Develop Naturally in Ig-Knockout Rats Carrying Germline Human IgH/Igκ/Igλ Loci Bearing the Rat C_H Region. *The Journal of Immunology* **190**, 1481–1490 (2013).

34. Murphy, A. J. *et al.* Mice with megabase humanization of their immunoglobulin genes generate antibodies as efficiently as normal mice. *Proceedings of the National Academy of Sciences* **111**, 5153–5158 (2014).

35. Ching, K. H. *et al.* Chickens with humanized immunoglobulin genes generate antibodies with high affinity and broad epitope coverage to conserved targets. *mAbs* **10**, 71–80 (2018).

36. Lonberg, N. Human antibodies from transgenic animals. *Nature Biotechnology* **23**, 1117–1125 (2005).

37. Lonberg, N. *et al.* Antigen-specific human antibodies from mice comprising four distinct genetic modifications. *Nature* **368**, 856–859 (1994).

38. Green, L. L. *et al.* Antigen–specific human monoclonal antibodies from mice engineered with human Ig heavy and light chain YACs. *Nature Genetics* **7**, 13–21 (1994).

39. Schröter, C. *et al.* Selection of Antibodies with Tailored Properties by Application of High-Throughput Multiparameter Fluorescence-Activated Cell Sorting of Yeast-Displayed Immune Libraries. *Molecular Biotechnology* **60**, 727–735 (2018).

40. Trott, M. *et al.* Functional Characterization of Two scFv-Fc Antibodies from an HIV Controller Selected on Soluble HIV-1 Env Complexes: A Neutralizing V3- and a Trimer-Specific gp41 Antibody. *PLoS ONE* **9**, e97478 (2014).

41. Duan, T., Ferguson, M., Yuan, L., Xu, F. & Li, G. Human Monoclonal Fab Antibodies Against West Nile Virus and its Neutralizing Activity Analyzed in Vitro and in Vivo. *Journal of Antivirals & Antiretrovirals* **01**, 036–042 (2009).

42. Duan, J. *et al.* A human SARS-CoV neutralizing antibody against epitope on S2 protein. *Biochemical and Biophysical Research Communications* **333**, 186–193 (2005).

43. Cai, X. & Garen, A. Anti-melanoma antibodies from melanoma patients immunized with genetically modified autologous tumor cells: selection of specific antibodies from single-chain Fv fusion phage libraries. *Proceedings of the National Academy of Sciences* **92**, 6537–6541 (1995).

44. Coomber, D. W., Hawkins, N. J., Clark, M. A. & Ward, R. L. Generation of anti-p53 Fab fragments from individuals with colorectal cancer using phage display. *J. Immunol.* **163**, 2276–2283 (1999).

45. Wenzel, E. V. *et al.* Human antibodies neutralizing diphtheria toxin in vitro and in vivo. *Sci Rep* **10**, 571 (2020).

46. Almagro, J. C., Pedraza-Escalona, M., Arrieta, H. I. & Pérez-Tapia, S. M. Phage Display Libraries for Antibody Therapeutic Discovery and Development. *Antibodies* **8**, 44 (2019).

47. Kügler, J. *et al.* Generation and analysis of the improved human HAL9/10 antibody phage display libraries. *BMC Biotechnology* **15**, 10 (2015).

48. Schofield, D. J. *et al.* Application of phage display to high throughput antibody generation and characterization. *Genome Biology* **8**, R254 (2007).

49. Omar, N. *et al.* Generation and selection of naïve Fab library for parasitic antigen: Anti- *Bm* SXP antibodies for lymphatic filariasis. *Biotechnology and Applied Biochemistry* **65**, 346–354 (2018).

50. Adler, A. S. *et al.* A natively paired antibody library yields drug leads with higher sensitivity and specificity than a randomly paired antibody library. *mAbs* **10**, 431–443 (2018).

51. Wang, B. *et al.* Functional interrogation and mining of natively paired human VH:VL antibody repertoires. *Nature Biotechnology* **36**, 152–155 (2018).

52. Lerner, R. A. Combinatorial antibody libraries: new advances, new immunological insights. *Nature Reviews Immunology* **16**, 498–508 (2016).

53. Prassler, J. *et al.* HuCAL PLATINUM, a Synthetic Fab Library Optimized for Sequence Diversity and Superior Performance in Mammalian Expression Systems. *Journal of Molecular Biology* **413**, 261–278 (2011).

54. Weber, M. *et al.* A Highly Functional Synthetic Phage Display Library Containing over 40 Billion Human Antibody Clones. *PLoS ONE* **9**, e100000 (2014).

55. Chen, G. & Sidhu, S. S. Design and Generation of Synthetic Antibody Libraries for Phage Display. in *Monoclonal Antibodies* (eds. Ossipow, V. & Fischer, N.) vol. 1131 113–131 (Humana Press, 2014).

686 56. Nilvebrant, J. & Sidhu, S. S. Construction of Synthetic Antibody Phage-Display Libraries. in *Phage Display* (eds. Hust, M. & Lim, T. S.) vol. 1701 45–60 (Springer New York, 2018).

688 57. Fellouse, F. A. *et al.* High-throughput Generation of Synthetic Antibodies from Highly Functional Minimalist Phage-displayed Libraries. *Journal of Molecular Biology* **373**, 924–940 (2007).

690 58. Knappik, A. *et al.* Fully synthetic human combinatorial antibody libraries (HuCAL) based on modular consensus frameworks and CDRs randomized with trinucleotides. *J. Mol. Biol.* **296**, 57–86 (2000).

692 59. Hoet, R. M. *et al.* Generation of high-affinity human antibodies by combining donor-derived and synthetic complementarity-determining-region diversity. *Nat. Biotechnol.* **23**, 344–348 (2005).

694 60. Rader, C., Cheresh, D. A. & Barbas, C. F. A phage display approach for rapid antibody humanization: Designed combinatorial V gene libraries. *Proceedings of the National Academy of Sciences* **95**, 8910–8915 (1998).

696 61. Hu, D. *et al.* Effective Optimization of Antibody Affinity by Phage Display Integrated with High-Throughput DNA Synthesis and Sequencing Technologies. *PLOS ONE* **10**, e0129125 (2015).

698 62. Tiller, K. E. *et al.* Facile Affinity Maturation of Antibody Variable Domains Using Natural Diversity Mutagenesis. *Frontiers in Immunology* **8**, (2017).

700 63. Lou, J. *et al.* Affinity maturation of human botulinum neurotoxin antibodies by light chain shuffling via yeast mating. *Protein Engineering Design and Selection* **23**, 311–319 (2010).

702 64. Lai, J. Y., Loh, Q., Choong, Y. S. & Lim, T. S. Cassette hybridization for vector assembly application in antibody chain shuffling. *BioTechniques* **65**, 269–274 (2018).

704 65. Smith, G. P. Phage Display: Simple Evolution in a Petri Dish (Nobel Lecture). *Angewandte Chemie International Edition* **58**, 14428–14437 (2019).

706 66. Smith, G. Filamentous fusion phage: novel expression vectors that display cloned antigens on the virion surface. *Science* **228**, 1315–1317 (1985).

707 67. McCafferty, J., Griffiths, A. D., Winter, G. & Chiswell, D. J. Phage antibodies: filamentous phage displaying antibody variable domains. *Nature* **348**, 552–554 (1990).

709 68. Barbas, C. F., Kang, A. S., Lerner, R. A. & Benkovic, S. J. Assembly of combinatorial antibody libraries on phage surfaces: the gene III site. *Proceedings of the National Academy of Sciences* **88**, 7978–7982 (1991).

711 69. Breitling, F., Dübel, S., Seehaus, T., Klewinghaus, I. & Little, M. A surface expression vector for antibody screening. *Gene* **104**, 147–153 (1991).

712 70. Rondot, S., Koch, J., Breitling, F. & Dübel, S. A helper phage to improve single-chain antibody presentation in phage display. *Nature Biotechnology* **19**, 75–78 (2001).

714 71. Soltes, G. *et al.* On the influence of vector design on antibody phage display. *J Biotechnol* **127**, 626–637 (2007).

715 72. Mazor, Y., Van Blarcom, T., Carroll, S. & Georgiou, G. Selection of full-length IgGs by tandem display on filamentous phage particles and Escherichia coli fluorescence-activated cell sorting screening: Selection of IgG by tandem phage panning-FACS. *FEBS Journal* **277**, 2291–2303 (2010).

73. Schwimmer, L. J. *et al.* Discovery of diverse and functional antibodies from large human repertoire antibody libraries. *Journal of Immunological Methods* **391**, 60–71 (2013).

74. Tiller, T. *et al.* A fully synthetic human Fab antibody library based on fixed VH/VL framework pairings with favorable biophysical properties. *mAbs* **5**, 445–470 (2013).

75. Miethe, S. *et al.* Development of neutralizing scFv-Fc against botulinum neurotoxin A light chain from a macaque immune library. *mAbs* **6**, 446–459 (2014).

76. De Jaeger, G. *et al.* Use of phage display for isolation and characterization of single-chain variable fragments against dihydroflavonol 4-reductase from *Petunia hybrida*. *FEBS Letters* **403**, 116–122 (1997).

77. Davies, E. L. *et al.* Selection of specific phage-display antibodies using libraries derived from chicken immunoglobulin genes. *Journal of Immunological Methods* **186**, 125–135 (1995).

78. Nelson, R. S. & Valadon, P. A universal phage display system for the seamless construction of Fab libraries. *Journal of Immunological Methods* **450**, 41–49 (2017).

79. Hawlisch, H. *et al.* Site-specific anti-C3a receptor single-chain antibodies selected by differential panning on cellulose sheets. *Anal. Biochem.* **293**, 142–145 (2001).

80. Moghaddam, A. *et al.* Identification of scFv antibody fragments that specifically recognise the heroin metabolite 6-monoacetylmorphine but not morphine. *J. Immunol. Methods* **280**, 139–155 (2003).

81. Breitling, F., Dübel, S., Seehaus, T., Klewinghaus, I. & Little, M. A surface expression vector for antibody screening. *Gene* **104**, 147–153 (1991).

82. Hust, M., Maiss, E., Jacobsen, H.-J. & Reinard, T. The production of a genus-specific recombinant antibody (scFv) using a recombinant potyvirus protease. *J. Virol. Methods* **106**, 225–233 (2002).

83. Barbas, C. F., Kang, A. S., Lerner, R. A. & Benkovic, S. J. Assembly of combinatorial antibody libraries on phage surfaces: the gene III site. *Proc. Natl. Acad. Sci. U.S.A.* **88**, 7978–7982 (1991).

84. Russo, G. *et al.* Parallelized Antibody Selection in Microtiter Plates. *Methods Mol. Biol.* **1701**, 273–284 (2018).

85. Wenzel, E. V. *et al.* Antibody Phage Display: Antibody Selection in Solution Using Biotinylated Antigens. *Methods Mol. Biol.* **2070**, 143–155 (2020).

86. Harrison, J. L., Williams, S. C., Winter, G. & Nissim, A. [5] Screening of phage antibody libraries. in *Methods in Enzymology* vol. 267 83–109 (Elsevier, 1996).

87. Ayriss, J., Woods, T., Bradbury, A. & Pavlik, P. High-throughput screening of single-chain antibodies using multiplexed flow cytometry. *J. Proteome Res.* **6**, 1072–1082 (2007).

88. Even-Desrumeaux, K. & Chames, P. Phage Display and Selections on Cells. in *Antibody Engineering* (ed. Chames, P.) vol. 907 225–235 (Humana Press, 2012).

89. Droste, P. *et al.* Structural differences of amyloid-β fibrils revealed by antibodies from phage display. *BMC Biotechnology* **15**, (2015).

90. Generation, Diversity Determination, and Application to Antibody Selection of a Human Naïve Fab Library. *Molecules and Cells* (2017) doi:10.14348/molcells.2017.0106.

91. Baca, M., Presta, L. G., O'Connor, S. J. & Wells, J. A. Antibody Humanization Using Monovalent Phage Display. *Journal of Biological Chemistry* **272**, 10678–10684 (1997).

92. Nishibori, N., Horiuchi, H., Furusawa, S. & Matsuda, H. Humanization of chicken monoclonal antibody using phage-display system. *Molecular Immunology* **43**, 634–642 (2006).

93. Gram, H. *et al.* In vitro selection and affinity maturation of antibodies from a naive combinatorial immunoglobulin library. *Proceedings of the National Academy of Sciences* **89**, 3576–3580 (1992).

94. Kang, A. S., Jones, T. M. & Burton, D. R. Antibody redesign by chain shuffling from random combinatorial immunoglobulin libraries. *Proceedings of the National Academy of Sciences* **88**, 11120–11123 (1991).

95. Osbourn, J. K. *et al.* Generation of a panel of related human scFv antibodies with high affinities for human CEA. *Immunotechnology* **2**, 181–196 (1996).

96. Frenzel, A. *et al.* Designing Human Antibodies by Phage Display. *Transfusion Medicine and Hemotherapy* **44**, 312–318 (2017).

97. Osbourn, J., Groves, M. & Vaughan, T. From rodent reagents to human therapeutics using antibody guided selection. *Methods* **36**, 61–68 (2005).

98. Merchant, A. M. *et al.* An efficient route to human bispecific IgG. *Nature Biotechnology* **16**, 677–681 (1998).

99. Fischer, N. *et al.* Exploiting light chains for the scalable generation and platform purification of native human bispecific IgG. *Nature Communications* **6**, (2015).

100. Boenvin, P. *et al.* *De novo* isolation of antibodies with pH-dependent binding properties. *mAbs* **7**, 294–302 (2015).

101. Murtaugh, M. L., Fanning, S. W., Sharma, T. M., Terry, A. M. & Horn, J. R. A combinatorial histidine scanning library approach to engineer highly pH-dependent protein switches: Engineering pH-Sensitive Protein Switches. *Protein Science* **20**, 1619–1631 (2011).

102. Hoy, S. M. Sintilimab: First Global Approval. *Drugs* **79**, 341–346 (2019).

103. Zhang, S. *et al.* Preclinical characterization of Sintilimab, a fully human anti-PD-1 therapeutic monoclonal antibody for cancer. *Antibody Therapeutics* **1**, 45–53 (2018).

104. Wang, J. *et al.* Durable blockade of PD-1 signaling links preclinical efficacy of sintilimab to its clinical benefit. *mAbs* **11**, 1443–1451 (2019).

105. Boder, E. T. & Wittrup, K. D. Yeast surface display for screening combinatorial polypeptide libraries. *Nature Biotechnology* **15**, 553–557 (1997).

106. N., S. *et al.* Long anchor using Flo1 protein enhances reactivity of cell surface-displayed glucoamylase to polymer substrates. *Applied Microbiology and Biotechnology* **60**, 469–474 (2002).

107. Ueda, M. & Tanaka, A. Genetic immobilization of proteins on the yeast cell surface. *Biotechnology Advances* **18**, 121–140 (2000).

108. Kondo, A. & Ueda, M. Yeast cell-surface display?applications of molecular display. *Applied Microbiology and Biotechnology* **64**, 28–40 (2004).

109. Wang, Z., Mathias, A., Stavrou, S. & Neville, D. M. A new yeast display vector permitting free scFv amino termini can augment ligand binding affinities. *Protein Engineering, Design and Selection* **18**, 337–343 (2005).

780 110. Pepper, L. R., Cho, Y. K., Boder, E. T. & Shusta, E. V. A decade of yeast surface display technology: where are we now? *Comb. Chem. High*
781 *Throughput Screen.* **11**, 127–134 (2008).

782 111. Rhiel, L. *et al.* REAL-Select: Full-Length Antibody Display and Library Screening by Surface Capture on Yeast Cells. *PLoS ONE* **9**, e114887
783 (2014).

784 112. Rouha, H. *et al.* Five birds, one stone: Neutralization of α-hemolysin and 4 bi-component leukocidins of *Staphylococcus aureus* with a single
785 human monoclonal antibody. *mAbs* **7**, 243–254 (2015).

786 113. Rakestraw, J. A., Aird, D., Aha, P. M., Baynes, B. M. & Lipovsek, D. Secretion-and-capture cell-surface display for selection of target-binding
787 proteins. *Protein Engineering Design and Selection* **24**, 525–530 (2011).

788 114. Roth, L. *et al.* Facile generation of antibody heavy and light chain diversities for yeast surface display by Golden Gate Cloning. *Biological*
789 *Chemistry* **400**, 383–393 (2019).

790 115. Sivelle, C. *et al.* Fab is the most efficient format to express functional antibodies by yeast surface display. *mAbs* **10**, 720–729 (2018).

791 116. Chao, G. *et al.* Isolating and engineering human antibodies using yeast surface display. *Nature Protocols* **1**, 755–768 (2006).

792 117. van den Beucken, T. *et al.* Affinity maturation of Fab antibody fragments by fluorescent-activated cell sorting of yeast-displayed libraries. *FEBS*
793 *Letters* **546**, 288–294 (2003).

794 118. Weaver-Feldhaus, J. M. *et al.* Yeast mating for combinatorial Fab library generation and surface display. *FEBS Letters* **564**, 24–34 (2004).

795 119. Zielonka, S. *et al.* Shark Attack: High affinity binding proteins derived from shark vNAR domains by stepwise in vitro affinity maturation.
796 *Journal of Biotechnology* **191**, 236–245 (2014).

797 120. Könning, D. & Kolmar, H. Beyond antibody engineering: directed evolution of alternative binding scaffolds and enzymes using yeast surface
798 display. *Microbial Cell Factories* **17**, (2018).

799 121. Graff, C. P., Chester, K., Begent, R. & Wittrup, K. D. Directed evolution of an anti-carcinoembryonic antigen scFv with a 4-day monovalent
800 dissociation half-time at 37 C. *Protein Engineering Design and Selection* **17**, 293–304 (2004).

801 122. Swers, J. S. Shuffled antibody libraries created by in vivo homologous recombination and yeast surface display. *Nucleic Acids Research* **32**, 36e –
802 36 (2004).

803 123. Rosowski, S. *et al.* A novel one-step approach for the construction of yeast surface display Fab antibody libraries. *Microbial Cell Factories* **17**,
804 (2018).

805 124. Krah, S. *et al.* A Streamlined Approach for the Construction of Large Yeast Surface Display Fab Antibody Libraries. in *Antibody Engineering*
806 (eds. Nevoltris, D. & Chames, P.) vol. 1827 145–161 (Springer New York, 2018).

807 125. Grzeschik, J. *et al.* A simplified procedure for antibody engineering by yeast surface display: Coupling display levels and target binding by
808 ribosomal skipping. *Biotechnology Journal* **12**, 1600454 (2017).

809 126. Lim, S., Glasgow, J. E., Filsinger Interrante, M., Storm, E. M. & Cochran, J. R. Dual display of proteins on the yeast cell surface simplifies
810 quantification of binding interactions and enzymatic bioconjugation reactions. *Biotechnology Journal* **12**, 1600696 (2017).

127. Boder, E. T., Raeeszadeh-Sarmazdeh, M. & Price, J. V. Engineering antibodies by yeast display. *Archives of Biochemistry and Biophysics* **526**, 99–106 (2012).

128. Bowley, D. R., Labrijn, A. F., Zwick, M. B. & Burton, D. R. Antigen selection from an HIV-1 immune antibody library displayed on yeast yields many novel antibodies compared to selection from the same library displayed on phage. *Protein Engineering, Design and Selection* **20**, 81–90 (2007).

129. Blaise, L. *et al.* Construction and diversification of yeast cell surface displayed libraries by yeast mating: application to the affinity maturation of Fab antibody fragments. *Gene* **342**, 211–218 (2004).

130. Benatuil, L., Perez, J. M., Belk, J. & Hsieh, C.-M. An improved yeast transformation method for the generation of very large human antibody libraries. *Protein Engineering, Design and Selection* **23**, 155–159 (2010).

131. Feldhaus, M. J. *et al.* Flow-cytometric isolation of human antibodies from a nonimmune Saccharomyces cerevisiae surface display library. *Nature Biotechnology* **21**, 163–170 (2003).

132. Puri, V., Streaker, E., Prabakaran, P., Zhu, Z. & Dimitrov, D. S. Highly efficient selection of epitope specific antibody through competitive yeast display library sorting. *mAbs* **5**, 533–539 (2013).

133. Tillotson, B. J., Lajoie, J. M. & Shusta, E. V. Yeast Display-Based Antibody Affinity Maturation Using Detergent-Solubilized Cell Lysates. in *Yeast Surface Display* (ed. Liu, B.) vol. 1319 65–78 (Springer New York, 2015).

134. Yang, Z. *et al.* Affinity maturation of an TpoR targeting antibody in full-length IgG form for enhanced agonist activity. *Protein Engineering, Design and Selection* **31**, 233–241 (2018).

135. Schröter, C. *et al.* A generic approach to engineer antibody pH-switches using combinatorial histidine scanning libraries and yeast display. *mAbs* **7**, 138–151 (2015).

136. Könning, D. *et al.* Isolation of a pH-Sensitive IgNAR Variable Domain from a Yeast-Displayed, Histidine-Doped Master Library. *Marine Biotechnology* **18**, 161–167 (2016).

137. Hinz, S. C. *et al.* A Generic Procedure for the Isolation of pH- and Magnesium-Responsive Chicken scFvs for Downstream Purification of Human Antibodies. *Frontiers in Bioengineering and Biotechnology* **8**, (2020).

138. Bogen, J. P. *et al.* Dual Function pH Responsive Bispecific Antibodies for Tumor Targeting and Antigen Depletion in Plasma. *Frontiers in Immunology* **10**, (2019).

139. Tillotson, B. J., Goulatis, L. I., Parenti, I., Duxbury, E. & Shusta, E. V. Engineering an Anti-Transferrin Receptor ScFv for pH-Sensitive Binding Leads to Increased Intracellular Accumulation. *PLOS ONE* **10**, e0145820 (2015).

140. Krah, S. *et al.* Generation of human bispecific common light chain antibodies by combining animal immunization and yeast display. *Protein Eng. Des. Sel.* **30**, 291–301 (2017).

141. Könning, D. *et al.* Semi-synthetic vNAR libraries screened against therapeutic antibodies primarily deliver anti-idiotypic binders. *Scientific Reports* **7**, (2017).

142. Xu, Y. *et al.* Addressing polyspecificity of antibodies selected from an in vitro yeast presentation system: a FACS-based, high-throughput selection and analytical tool. *Protein Engineering Design and Selection* **26**, 663–670 (2013).

143. Yang, Z. *et al.* A cell–cell interaction format for selection of high-affinity antibodies to membrane proteins. *Proceedings of the National Academy of Sciences* **116**, 14971–14978 (2019).

144. Ferrara, F. *et al.* Using Phage and Yeast Display to Select Hundreds of Monoclonal Antibodies: Application to Antigen 85, a Tuberculosis Biomarker. *PLoS ONE* **7**, e49535 (2012).

145. Plückthun, A. Ribosome Display: A Perspective. in *Ribosome Display and Related Technologies* (eds. Douthwaite, J. A. & Jackson, R. H.) vol. 805 3–28 (Springer New York, 2012).

146. Lipovsek, D. & Plückthun, A. In-vitro protein evolution by ribosome display and mRNA display. *Journal of Immunological Methods* **290**, 51–67 (2004).

147. Yan, X. & Xu, Z. Ribosome-display technology: applications for directed evolution of functional proteins. *Drug Discovery Today* **11**, 911–916 (2006).

148. Kunamneni, A., Ogaugwu, C., Bradfute, S. & Durvasula, R. Ribosome Display Technology: Applications in Disease Diagnosis and Control. *Antibodies* **9**, 28 (2020).

149. Mattheakis, L. C., Bhatt, R. R. & Dower, W. J. An in vitro polysome display system for identifying ligands from very large peptide libraries. *Proceedings of the National Academy of Sciences* **91**, 9022–9026 (1994).

150. Hanes, J. & Pluckthun, A. In vitro selection and evolution of functional proteins by using ribosome display. *Proceedings of the National Academy of Sciences* **94**, 4937–4942 (1997).

151. He, M. Antibody-ribosome-mRNA (ARM) complexes as efficient selection particles for in vitro display and evolution of antibody combining sites. *Nucleic Acids Research* **25**, 5132–5134 (1997).

152. Hanes, J., Jermutus, L., Weber-Bornhauser, S., Bosshard, H. R. & Pluckthun, A. Ribosome display efficiently selects and evolves high-affinity antibodies in vitro from immune libraries. *Proceedings of the National Academy of Sciences* **95**, 14130–14135 (1998).

153. Levin, A. M. & Weiss, G. A. Optimizing the affinity and specificity of proteins with molecular display. *Mol. BioSyst.* **2**, 49–57 (2006).

154. Jermutus, L. Tailoring in vitro evolution for protein affinity or stability. *Proceedings of the National Academy of Sciences* **98**, 75–80 (2001).

155. Dreier, B. & Plückthun, A. Rapid Selection of High-Affinity Binders Using Ribosome Display. in *Ribosome Display and Related Technologies* (eds. Douthwaite, J. A. & Jackson, R. H.) vol. 805 261–286 (Springer New York, 2012).

156. Groves, M. A. & Osbourn, J. K. Applications of ribosome display to antibody drug discovery. *Expert Opinion on Biological Therapy* **5**, 125–135 (2005).

157. Hanes, J., Schaffitzel, C., Knappik, A. & Plückthun, A. Picomolar affinity antibodies from a fully synthetic naive library selected and evolved by ribosome display. *Nature Biotechnology* **18**, 1287–1292 (2000).

158. Josephson, K., Ricardo, A. & Szostak, J. W. mRNA display: from basic principles to macrocycle drug discovery. *Drug Discovery Today* **19**, 388–399 (2014).

159. Yamaguchi, J. *et al.* cDNA display: a novel screening method for functional disulfide-rich peptides by solid-phase synthesis and stabilization of mRNA-protein fusions. *Nucleic Acids Research* **37**, e108–e108 (2009).

160. Wurm, F. M. Production of recombinant protein therapeutics in cultivated mammalian cells. *Nature Biotechnology* **22**, 1393–1398 (2004).

161. Birch, J. R. & Racher, A. J. Antibody production. *Advanced Drug Delivery Reviews* **58**, 671–685 (2006).

162. Bowers, P. M. *et al.* Mammalian cell display for the discovery and optimization of antibody therapeutics. *Methods* **65**, 44–56 (2014).

163. Parthiban, K. *et al.* A comprehensive search of functional sequence space using large mammalian display libraries created by gene editing. *mAbs* **11**, 884–898 (2019).

164. Higuchi, K. *et al.* Cell display library for gene cloning of variable regions of human antibodies to hepatitis B surface antigen. *Journal of Immunological Methods* **202**, 193–204 (1997).

165. Ho, M. & Pastan, I. Mammalian Cell Display for Antibody Engineering. in *Therapeutic Antibodies* (ed. Dimitrov, A. S.) vol. 525 337–352 (Humana Press, 2009).

166. Beerli, R. R. *et al.* Isolation of human monoclonal antibodies by mammalian cell display. *Proceedings of the National Academy of Sciences* **105**, 14336–14341 (2008).

167. Waldmeier, L. *et al.* Transpo-mAb display: Transposition-mediated B cell display and functional screening of full-length IgG antibody libraries. *mAbs* **8**, 726–740 (2016).

168. Breous-Nystrom, E. *et al.* Retrocyte Display® technology: Generation and screening of a high diversity cellular antibody library. *Methods* **65**, 57–67 (2014).

169. Aebischer-Gumy, C. *et al.* SPLICELECT™: an adaptable cell surface display technology based on alternative splicing allowing the qualitative and quantitative prediction of secreted product at a single-cell level. *mAbs* **12**, 1709333 (2020).

170. Lang, S. *et al.* Surface display vectors for selective detection and isolation of high level antibody producing cells: Surface Display Vectors for Cell Line Development. *Biotechnology and Bioengineering* **113**, 2386–2393 (2016).

171. Bouquin, T., Rasmussen, P. B., Bertilsson, P.-A. & Okkels, J. S. Regulated readthrough: A new method for the alternative tagging and targeting of recombinant proteins. *Journal of Biotechnology* **125**, 516–528 (2006).

172. Chakrabarti, L. *et al.* Amber Suppression Coupled with Inducible Surface Display Identifies Cells with High Recombinant Protein Productivity. *Biotechnology and Bioengineering* (2018) doi:10.1002/bit.26892.

173. Zhang, H., Wilson, I. A. & Lerner, R. A. Selection of antibodies that regulate phenotype from intracellular combinatorial antibody libraries. *Proceedings of the National Academy of Sciences* **109**, 15728–15733 (2012).

174. Mason, D. M. *et al.* High-throughput antibody engineering in mammalian cells by CRISPR/Cas9-mediated homology-directed mutagenesis. *Nucleic Acids Research* **46**, 7436–7449 (2018).

175. Pogson, M., Parola, C., Kelton, W. J., Heuberger, P. & Reddy, S. T. Immunogenomic engineering of a plug-and-(dis)play hybridoma platform. *Nature Communications* **7**, (2016).

176. Parola, C. *et al.* Antibody discovery and engineering by enhanced CRISPR-Cas9 integration of variable gene cassette libraries in mammalian cells. *mAbs* **11**, 1367–1380 (2019).

177. Mason, D. M. *et al.* Deep learning enables therapeutic antibody optimization in mammalian cells by deciphering high-dimensional protein sequence space. *bioRxiv* 617860 (2019) doi:10.1101/617860.

178. Di Noia, J. M. & Neuberger, M. S. Molecular Mechanisms of Antibody Somatic Hypermutation. *Annual Review of Biochemistry* **76**, 1–22 (2007).

179. Luo, R. *et al.* High efficiency CHO cell display-based antibody maturation. *Scientific Reports* **10**, (2020).

180. Xie, J., Zhang, H., Yea, K. & Lerner, R. A. Autocrine signaling based selection of combinatorial antibodies that transdifferentiate human stem cells. *Proceedings of the National Academy of Sciences* **110**, 8099–8104 (2013).

181. Francisco, J. A., Campbell, R., Iverson, B. L. & Georgiou, G. Production and fluorescence-activated cell sorting of Escherichia coli expressing a functional antibody fragment on the external surface. *PNAS* **90**, 10444–10448 (1993).

182. Daugherty, P. S., Chen, G., Olsen, M. J., Iverson, B. L. & Georgiou, G. Antibody affinity maturation using bacterial surface display. *Protein Eng Des Sel* **11**, 825–832 (1998).

183. Dhillon, J. K., Drew, P. D. & Porter, A. J. Bacterial surface display of an anti-pollutant antibody fragment. *Lett. Appl. Microbiol.* **28**, 350–354 (1999).

184. Fuchs, P., Breitling, F., Dübel, S., Seehaus, T. & Little, M. Targeting Recombinant Antibodies to the Surface of Escherichia coli : Fusion to a Peptidoglycan Associated Lipoprotein. *Bio/Technology* **9**, 1369–1372 (1991).

185. Veiga, E., de Lorenzo, V. & Fernández, L. A. Structural tolerance of bacterial autotransporters for folded passenger protein domains. *Mol. Microbiol.* **52**, 1069–1080 (2004).

186. Harvey, B. R. *et al.* Anchored periplasmic expression, a versatile technology for the isolation of high-affinity antibodies from Escherichia coli-expressed libraries. *PNAS* **101**, 9193–9198 (2004).

187. Karlsson, A. J. *et al.* Engineering Antibody Fitness and Function Using Membrane-Anchored Display of Correctly Folded Proteins. *Journal of Molecular Biology* **416**, 94–107 (2012).

188. Mazor, Y., Van Blarcom, T., Mabry, R., Iverson, B. L. & Georgiou, G. Isolation of engineered, full-length antibodies from libraries expressed in Escherichia coli. *Nat. Biotechnol.* **25**, 563–565 (2007).

189. Chen, G. *et al.* Isolation of high-affinity ligand-binding proteins by periplasmic expression with cytometric screening (PECS). *Nat Biotechnol* **19**, 537–542 (2001).

190. Lombana, T. N., Dillon, M., Bevers Iii, J. & Spiess, C. Optimizing antibody expression by using the naturally occurring framework diversity in a live bacterial antibody display system. *Scientific Reports* **5**, 17488 (2015).

191. Gunneriusson, E., Samuelson, P., Uhlen, M., Nygren, P. A. & Stähl, S. Surface display of a functional single-chain Fv antibody on staphylococci. *J Bacteriol* **178**, 1341–1346 (1996).

192. Hu, F. J. *et al.* Combination of phage and Gram-positive bacterial display of human antibody repertoires enables isolation of functional high affinity binders. *New Biotechnology* **45**, 80–88 (2018).

193. Cavallari, M. Rapid and Direct VHH and Target Identification by Staphylococcal Surface Display Libraries. *International Journal of Molecular Sciences* **18**, 1507 (2017).

194. Fleetwood, F. *et al.* Surface display of a single-domain antibody library on Gram-positive bacteria. *Cell. Mol. Life Sci.* **70**, 1081–1093 (2013).

195. Moon, S. A. *et al.* Antibodies against non-immunizing antigens derived from a large immune scFv library. *Molecules and Cells* **31**, 509–513 (2011).

196. Bradbury, A. R. M. *et al.* When monoclonal antibodies are not monospecific: Hybridomas frequently express additional functional variable regions. *mAbs* **10**, 539–546 (2018).

197. Gross, A. *et al.* Technologies for Single-Cell Isolation. *International Journal of Molecular Sciences* **16**, 16897–16919 (2015).

198. Lagerkvist, A., Furebring, C. & Borrebaeck, C. Single, antigen-specific B cells used to generate Fab fragments using CD40-mediated amplification or direct PCR cloning. *Biotechniques*. (1995).

199. Lundkvist, A., Horling, J., Athlin, L., Rosen, A. & Niklasson, B. Neutralizing human monoclonal antibodies against Puumala virus, causative agent of nephropathia epidemica: a novel method using antigen-coated magnetic beads for specific B cell isolation. *Journal of General Virology* **74**, 1303–1310 (1993).

200. Malkiel, S. *et al.* Checkpoints for Autoreactive B Cells in the Peripheral Blood of Lupus Patients Assessed by Flow Cytometry: AUTOREACTIVE B CELL CHECKPOINTS ASSESSED BY FLOW CYTOMETRY. *Arthritis & Rheumatology* **68**, 2210–2220 (2016).

201. Goldstein, L. D. *et al.* Massively parallel single-cell B-cell receptor sequencing enables rapid discovery of diverse antigen-reactive antibodies. *Communications Biology* **2**, (2019).

202. Singh, M. *et al.* High-throughput targeted long-read single cell sequencing reveals the clonal and transcriptional landscape of lymphocytes. *Nature Communications* **10**, (2019).

203. Yang, L. *et al.* COVID-19 antibody therapeutics tracker: a global online database of antibody therapeutics for the prevention and treatment of COVID-19. *Antibody Therapeutics* **3**, 204–211 (2020).

204. Cox, K. S. *et al.* Rapid isolation of dengue-neutralizing antibodies from single cell-sorted human antigen-specific memory B-cell cultures. *mAbs* **8**, 129–140 (2016).

205. Bailey, M. J. *et al.* Human antibodies targeting Zika virus NS1 provide protection against disease in a mouse model. *Nature Communications* **9**, (2018).

206. Morris, L. *et al.* Isolation of a Human Anti-HIV gp41 Membrane Proximal Region Neutralizing Antibody by Antigen-Specific Single B Cell Sorting. *PLoS ONE* **6**, e23532 (2011).

207. Fu, Y. *et al.* A broadly neutralizing anti-influenza antibody reveals ongoing capacity of haemagglutinin-specific memory B cells to evolve. *Nature Communications* **7**, (2016).

208. Nachiket Shembekar, C. A. M. Shembekar Merten et al., 2018 Cell Reports_Single-Cell Droplet Microfluidic Screening for Antibodies Specifically Binding to Target Cells.pdf. *Cell Reports* **22**, 2206–2215 (2018).

209. Fitzgerald, V. & Leonard, P. Single cell screening approaches for antibody discovery. *Methods* **116**, 34–42 (2017).

969 210. Seah, Y. F. S., Hu, H. & Merten, C. A. Microfluidic single-cell technology in immunology and antibody screening. *Molecular Aspects of*
970 *Medicine* **59**, 47–61 (2018).

971 211. Rajan, S. *et al.* Recombinant human B cell repertoires enable screening for rare, specific, and natively paired antibodies. *Communications Biology*
972 **1**, 1–8 (2018).

973 212. Tanno, H. *et al.* A facile technology for the high-throughput sequencing of the paired VH:VL and TCRβ:TCRα repertoires. *Science Advances* **6**,
974 (2020).

975 213. Gérard, A. *et al.* High-throughput single-cell activity-based screening and sequencing of antibodies using droplet microfluidics. *Nature*
976 *Biotechnology* **38**, 715–721 (2020).

977 214. Rogers, T. F. *et al.* animal model. *Science* **963**, 956–963 (2020).

978 215. Renn, A., Fu, Y., Hu, X., Hall, M. D. & Simeonov, A. Fruitful Neutralizing Antibody Pipeline Brings Hope To Defeat SARS-Cov-2. *Trends in*
979 *Pharmacological Sciences* 1–15 (2020) doi:10.1016/j.tips.2020.07.004.

980 216. Wippold, J. A. *et al.* PRESCIENT: platform for the rapid evaluation of antibody success using integrated microfluidics enabled technology. *Lab*
981 *on a Chip* **20**, 1628–1638 (2020).

982 217. Wang, B. *et al.* Functional interrogation and mining of natively paired human v H:V L antibody repertoires. *Nature Biotechnology* **36**, 152–155
983 (2018).

984 218. Winters, A. *et al.* Rapid single B cell antibody discovery using nanopens and structured light. *mAbs* **11**, 1025–1035 (2019).

985 219. Bounab, Y. *et al.* Dynamic single-cell phenotyping of immune cells using the microfluidic platform DropMap. *Nature Protocols* (2020)
986 doi:10.1038/s41596-020-0354-0.

987 220. Asensio, M. A. *et al.* Antibody repertoire analysis of mouse immunization protocols using microfluidics and molecular genomics. *mAbs* **11**, 870–
988 883 (2019).

989 221. Gérard, A. *et al.* Screening and Sequencing of Antibodies Using Droplet Microfluidics. *Nature Biotechnology* **38**, (2020).

990 222. Josephides, D. *et al.* Cyto-Mine: An Integrated, Picodroplet System for High-Throughput Single-Cell Analysis, Sorting, Dispensing, and
991 Monoclonality Assurance. *SLAS Technology* (2020) doi:10.1177/2472630319892571.

992 223. Ledford, H. & Callaway, E. Pioneers of revolutionary CRISPR gene editing win chemistry Nobel. *Nature* **586**, 346–347 (2020).

993 224. Rouet, R., Jackson, K. J. L., Langley, D. B. & Christ, D. Next-Generation Sequencing of Antibody Display Repertoires. *Frontiers in Immunology*
994 **9**, (2018).

995 225. Yang, W. *et al.* Next-generation sequencing enables the discovery of more diverse positive clones from a phage-displayed antibody library.
996 *Experimental & Molecular Medicine* **49**, e308–e308 (2017).

997 226. Barreto, K. *et al.* Next-generation sequencing-guided identification and reconstruction of antibody CDR combinations from phage selection
998 outputs. *Nucleic Acids Research* **47**, e50–e50 (2019).

999 227. D'Angelo, S. *et al.* From deep sequencing to actual clones. *Protein Engineering Design and Selection* **27**, 301–307 (2014).

228. Ferrara, F. *et al.* Exploiting next-generation sequencing in antibody selections – a simple PCR method to recover binders. *mAbs* **12**, 1701792 (2020).

229. Saggy, I. *et al.* Antibody isolation from immunized animals: comparison of phage display and antibody discovery via V gene repertoire mining. *Protein Engineering Design and Selection* **25**, 539–549 (2012).

230. Valdés-Alemán, J. *et al.* Hybridization-based antibody cDNA recovery for the production of recombinant antibodies identified by repertoire sequencing. *mAbs* **6**, 493–501 (2014).

231. Scapin, G. *et al.* Structure of full-length human anti-PD1 therapeutic IgG4 antibody pembrolizumab. *Nature Structural & Molecular Biology* **22**, 953–958 (2015).

1011 **Table 1: Antibodies granted marketing approval discovered or engineered using phage display or yeast surface display.**

	Name	Trade name	Company	Display Technology	Approach	Target	Approval	Indication(s)
1	Adalimumab	Humira	Abbott (Abbvie)	phage display	humanization by guided selections	TNF-α	2002 (USA), 2003 (EU)	rheumatoide arthritis, psoriasis, Morbus Bechterew, Morbus Crohn
2	Ranibizumab	Lucentis	Novartis, Genentech/Roche	phage display	humanization, affinity maturation	VEGF-A	2006 (USA), 2007 (EU)	wet macular degeneration
3	Belimumab (LymphoStat-B)	Benlysta	CAT, human Genome Sciences, GlaxoSmithKline (GSK)	phage display	initial selection	B-lymphocyte stimulator (BLyS, BAFF)	2011 (USA, EU)	systemic lupus erythematosus (SLE)
4	Raxibacumab	ABThrax	human Genome Sciences/CAT, GSK	phage display	initial selection	B. anthracis PA	2012 (USA)	anthrax
5	Ramucirumab	Cyramza	Imclone(Dyax)/ Lilly	phage display	initial selection	VEGFR2	2014 (USA, EU)	stomach cancer, non-small-cell lung carcinoma (NSCLC)
6	Necitumumab	Portrazza	Eli Lilly	phage display	initial selection	EGFR	2015 (USA, EU)	NSLCC
7	Ixekizumab	Taltz	Eli Lilly	phage display	humanization	IL-17a	2016 (USA, EU)	psoriasis
8	Atezolizumab	Tencentriq	Roche/Genentech	phage display	initial selection	PD-L1, immunmodul.	2016 (USA), 2017 (EU)	bladder cancer
9	Avelumab	Bavencio	Merck KGaA/EMD	phage display	initial selection	PD-L1	2017 (EU, USA)	Merkel-cell carcinoma
10	Guselkumab	Tremfya	Morphosys	phage display	initial selection	IL-23	2017 (EU, USA)	psoriasis
11	Lanadelumab	Takhzyro	Dyax/Shire	phage display	initial selection	Plasma Kallikrein	2018 (USA, EU)	hereditary angioedema
12	Caplacizumab	Cablivi	Ablynx	phage display	initial Nanobody selection	von Willebrandt Faktor	2018 (USA), 2019 (EU)	thrombotic thrombocytopenic purpura
13	Moxetumomab pasudotox	Lumoxiti	Medimmune/AstraZeneca	phage display	murine scFv, affinity maturation	CD22	2018 (USA)	hairy cell leukemia
14	Emapalumab	Gamifant	Novimmune	phage display	initial selection	INF-Gamma	2018 (USA)	hemophagocytic lymphohistiocytosis (HLH)
15	Sintilimab	Tyvyt	Innovent Biologics / Eli Lilly	yeast surface display	initial selection	PD-1	2018 (China)	Hodgkin lymphoma

1012

1013 **Figures**

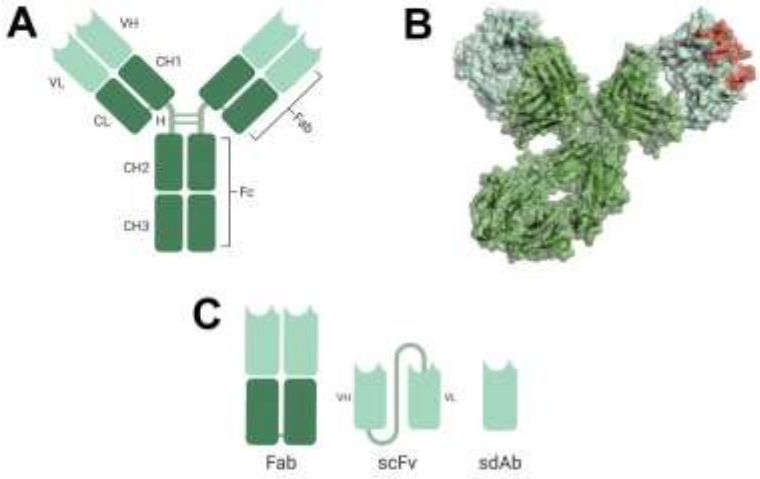

1014

1015 **Fig. 1:** Antibody formats used in different display technologies. (A) Schematic structure of an IgG antibody. VH, variable domain of the heavy
1016 chain; VL, variable domain of the light chain; CL, constant domain of the light chain; CH1-CH3, constant regions of the heavy chain; H, hinge
1017 region; Fab, fragment antigen binding, Fc, fragment crystallizable. (B) Model structure of an IgG based on pdb entry: 5dk3 [231] generated using
1018 PyMOL v0.99. Variable domains colored in light green, constant regions in dark green and CDRs of one paratope are highlighted in red. (C)
1019 Schematic depiction of fragments used for display. ScFv, single chain fragment variable; sdAb, single domain antibody. Schemes depicted in
1020 (A) and (C) generated with biorender (www.biorender.com).

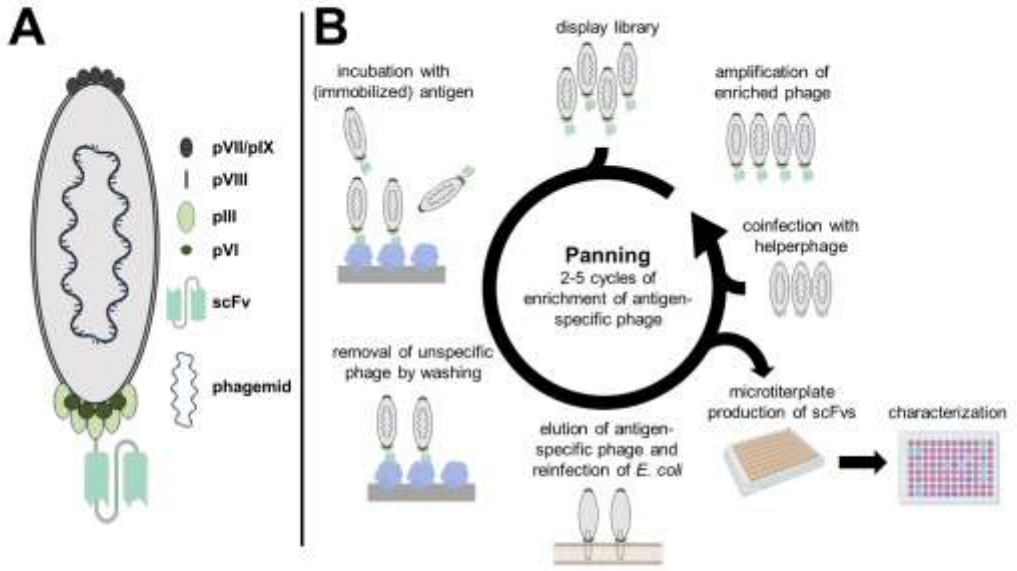

1021

1022 **Fig. 2:** Schematic representation of scFv-displaying phage (A) and phage display procedure (B). Main components of antibody-displaying
1023 phage are shown (A). pIII, phage protein III; pVI, phage protein VI; pVII, phage protein VII; pVIII, phage protein VIII; pIX, phage protein
1024 IX. (B) Overview of phage display panning. After library construction, antibody displaying phage are incubated with a particular antigen (here
1025 shown with surface immobilized antigen). Subsequently, unspecific phage are removed by washing followed by elution of antigen-specific
1026 phage *via* enzymatic treatment or pH-shift. Afterwards, antigen-enriched phage are exploited for infection of *E. coli* for propagation.
1027 Coinfection with helperphage enables production and amplification of enriched phage. This procedure is commonly repeated for 2-5 cycles.
1028 Finally, after reinfection, scFvs can be produced in microtiterplates and utilized for characterization. Components created using biorender
1029 (www.biorender.com).

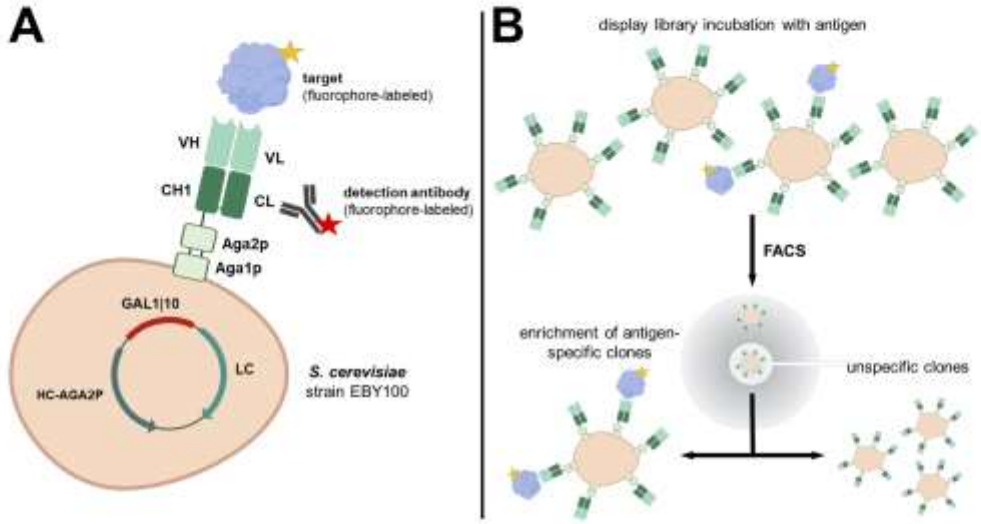

1030

1031 **Fig. 3:** Overview of yeast surface display. (A) Schematic illustration of yeast surface display based on *S. cerevisiae* strain EBY100. In this
1032 representation, expression of the heavy and the light chain for antibody Fab display is enabled by employing a one plasmid system under the
1033 control of galactose-inducible promoters. Surface display is achieved by genetically fusing the *C*-terminus of the CH1 domain to Aga2p, which
1034 upon secretion forms a covalent linkage with Aga1p. Of note, chromosomally integrated Aga1p is not shown. Utilization of fluorophore-
1035 labeled detection reagents (in this scheme directed against domain CL) as well as fluorescently labeled antigen allows FACS-based gating for
1036 functional surface expression simultaneous to antigen binding. (B) Process of library selection *via* FACS. After library generation, Fab-
1037 displaying yeast cells are incubated with the fluorophore-labeled antigen (labeling with detection reagents not shown). Hence, cells displaying
1038 an antigen-specific antibody fragment can be detected as fluorescence-positive event and sorted. Depending on the type of library, 2-5 rounds
1039 of selection can be carried out before the genetic information is obtained by sequencing. Scheme generated with biorender
1040 (www.biorender.com).

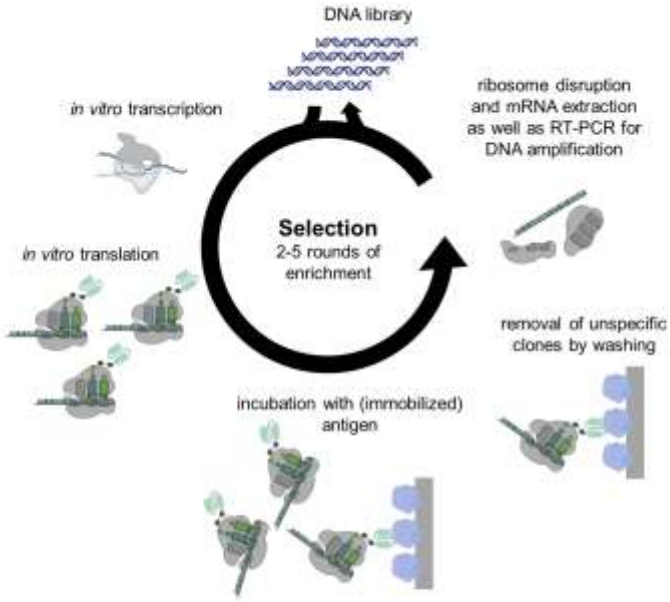

Fig. 4: Principle of Ribosome display**.** The amplified DNA library consists of (5' to 3') a promotor, the ribosomal binding site, the gene of interest and no stop codon. DNA is transcribed *in vitro* to RNA followed by *in vitro* translation with cell extracts (prokaryotic or eukaryotic). At the end of translation, mRNA-ribosome complexes are formed that are incubated with immobilized antigen. After successive washing steps, non-binding complexes are removed, and *in situ* RT-PCR followed by PCR-amplification is applied to recover DNA of antigen binding variants. This DNA output can either be exploited for post selection characterization or another ribosome display cycle. Figure created with biorender (www.biorender.com).

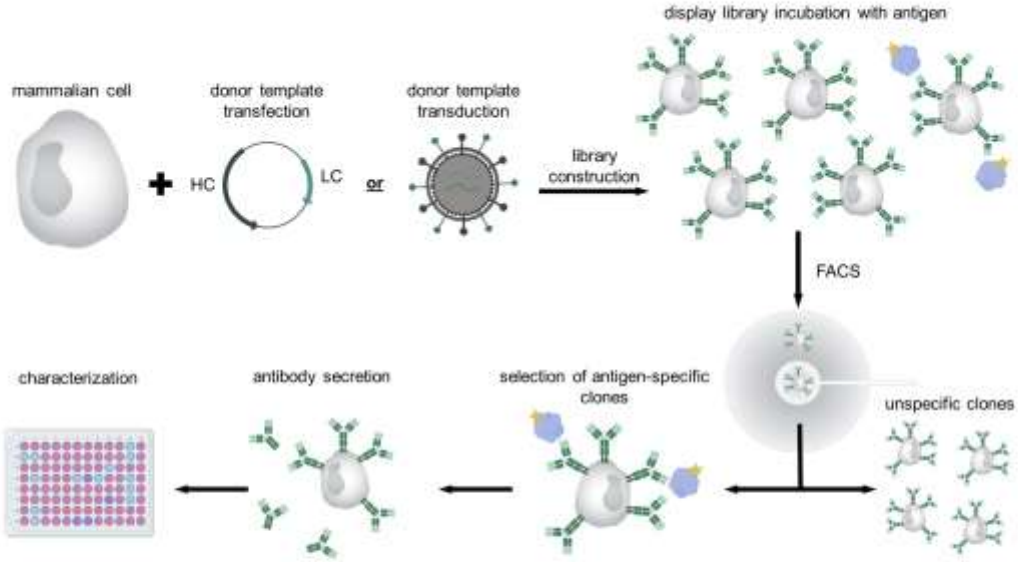

Fig. 5: Schematic representation of mammalian surface display. Antibody libraries can be generated by transfection of mammalian cells with plasmids encoding for antibody diversities. In this respect, the use of modern genetic engineering tools ensures mono-copy integrations into a predefined site and hence, monoclonal display. Moreover, libraries can also be constructed via transduction or transposase-mediated integration. Library sorting by FACS is similar to yeast surface display i.e. via incubation with fluorophore-labeled antigen and detection reagents (not shown). In several mammalian systems, owing to simultaneous display and secretion, library cells can be exploited directly for antibody production and characterization after several rounds of FACS-based enrichment. Partially generated with biorender (www.biorender.com).

Danksagung

Zuerst möchte ich mich ganz herzlich bei meinem Prüfungskomitee bedanken. Im Speziellen bei Prof. Dr. Harald Kolmar für die Möglichkeit der Promotion in seiner Arbeitsgruppe und der akademischen Betreuung meiner Doktorarbeit. Bei Prof. Dr. Siegfried Neumann für die Übernahme des Koreferats und bei Prof. Dr. Matthias Peipp, sowie Prof. Dr. Johannes Kabisch für ihre Funktion als Fachprüfer.

In diesem Rahmen auch nochmal Danke an Matthias Peipp und Katja Klausz vom Universitätsklinikum Schleswig-Holstein für die hervorragende Projektunterstützung und -zusammenarbeit, die erfreulicherweise schon während dieser Arbeit die ersten Früchte getragen hat.

Dr. Michael Busch danke ich herzlich für die Merck seitige Betreuung im Bereich DiscoPharm bzw. Molecular Pharmacology. Danke für deinen Einsatz, deine Anregungen und Denkanstöße, deine Gesprächsbereitschaft und deine unermüdlich positive Art.

Dr. Stefan Zielonka danke ich herzlich für die Merck seitige Betreuung im Bereich PEAT. Danke für deine schier endlos vielen Ideen für interessante und innovative Projekte, deine mitreißende Art diese Ideen auch zu verkaufen und die Projekte anzugehen. Danke für deine Engagement und teilweise auch die gutgemeinten Schubser in die richtige Richtung.

Dr. Simon Krah danke ich herzlich für die Unterstützung bei Projekten, die meist doch aufmunternd gemeinten Worte und das offene Ohr für Fragen und Probleme. Danke auch an seine tollkühne Crew im Hefe Labor Filmriss und Dennis für Kost und Logis und sonst auch einfach danke für alles. Dieser Dank geht genauso auch an Rambo, Almuth und Kevin. Danke für die genauso treue Unterstützung beim alltäglichen Merck-Leben.

Dr. Lars Toleikis und Dr. Mirek Jurzak danke ich herzlich für die Möglichkeit dieser Promotion. Ihr habt es mir ermöglicht, eine spannende Arbeit gestalten und Einblicke in die Welt von PEAT und DiscoPharm erhalten zu können.

Vielen Dank auch an die Arbeitsgruppe Kolmar, die immer mit Rat und Tat zu Seite standen und auch an alle Merck Doktoranden und PostDocs: Tim, Janis, Janina, Martina, Jäger, Marie, Desi, Marcel, Lubda, Greg für eure Unterstützung.

Weiterer Dank geht an das Team von Cellular Pharmacology bei Merck, das ich bei euch viele zielführende Versuche machen durfte und sowohl Unterstützung durch Praktisches, als auch in inhaltlicher Art und Weise bekommen habe. Ein großes Danke hier besonders an Jennifer Loehr für die Unterstützung zum Aufstellen des NK Cell Killing Assays.

Danke sagen möchte ich auch bei Sigrid, Stefan, Alex Jenni und Amanda für die analytische Unterstützung dieser Arbeit und an die „Expressionistas“ Pia und Marion für ihre Hilfestellung, sowie bei Marion, Oli und Elli.

Und zu guter Letzt danke ich meiner Familie und meinen Freunden. Meiner Frau Lisa, meinen Sohn Jakob, meiner Tochter Charlotte und meinem Hund Toni für die Bestärkung, Ablenkung und Erdung zu Hause. Ihr steht immer hinter mir und seid immer für mich da! Genauso wie auch meine Eltern Ingrid und Thomas, meine Schwester Judith und meine Oma Hildegard, die mich in meiner Ausbildung seit Beginn an unterstützt haben.

Danke auch an all die anderen, die mich hierbei begleitet und mir zur Seite gestanden haben. Auch wenn ich euch nicht namentlich erwähnt habe, sage ich doch Danke.

Curriculum Vitae

Persönliche Daten

Name	Lukas Pekar (geb. Roth)
Geburtsdatum	28.06.1990
Geburtsort	Flörsheim am Main
Staatsangehörigkeit	deutsch
Familienstand	verheiratet

Ausbildung und wissenschaftlicher Werdegang

2017 – Heute	Technische Universität Darmstadt/Merck KGaA Wissenschaftlicher Mitarbeiter in der Arbeitsgruppe von Prof. Dr. Harald Kolmar am Clemens-Schöpf Institut für Organische und Biochemie an der TU Darmstadt im Rahmen eines Doktorandenverhältnisses in Kooperation mit den Abteilungen „Molecular Pharmacology“ (MolPharm) und „Protein Engineering and Antibody Technologies“ (PEAT) von Merck KGaA
2016 – 2017	Merck KGaA Angestelltenverhältnis als Clinical Engineer in der Abteilung MolPharm der Firma Merck KGaA
2015 – 2016	Merck KGaA Praktikum mit anschließender Masterarbeit in der Abteilung Protein & Cell Sciences Abschluss: Master of Engineering
2013 – 2015	University of Applied Sciences Rhein-Main/ Merck KGaA Masterstudiengang „Bio- und Umweltverfahrenstechnik“ (Abschlussnote 1,1) und wiederholte Werksstudententätigkeiten in der Abteilung MolPharm der Firma Merck KGaA
2013	Merck KGaA Praktikum mit anschließender Bachelorarbeit in der Abteilung MolPharm (mit Auszeichnungen des VDI und ISPE) Abschluss: Bachelor of Engineering
2010 – 2013	University of Applied Sciences Frankfurt Bachelorstudiengang „Bioverfahrenstechnik“ (Abschlussnote 1,3)

Darmstadt, 26.10.2020

(Ort, Datum) (Unterschrift Lukas Pekar)

Erklärung gemäß §8(1) Promotionsordnung

Hiermit erkläre ich, dass ich die vorgelegte Dissertation selbstständig und nur mit den mir zulässigen Hilfsmitteln angefertigt habe. Die Dissertation wurde in der vorgelegten Form oder einer ähnlichen Fassung zu keinem früheren Zeitpunkt an einer in- oder ausländischen Hochschule eingereicht.

Die schriftliche Version stimmt zudem mit der elektronischen Version überein. Die identische elektronische Version für die Durchführung des Promotionsverfahrens liegt vor.

Außerdem erkläre ich, noch keinen Promotionsversuch unternommen zu haben.

Darmstadt, 26.10.2020 

(Ort, Datum) (Unterschrift Lukas Pekar)

Erklärung gemäß §9 Promotionsordnung

Hiermit versichere ich, dass ich die vorliegende Dissertation selbstständig angefertigt und keine anderen als die angegebenen Quellen und Hilfsmittel verwendet habe. Alle wörtlichen und paraphrasierten Zitate wurden angemessen kenntlich gemacht. Die Dissertation wurde in der vorgelegten oder einer ähnlichen Fassung zu keinem früheren Zeitpunkt an einer in- oder ausländischen Hochschule eingereicht.

Darmstadt, 26.10.2020 

(Ort, Datum) (Unterschrift Lukas Pekar)

Erklärung zur Begutachtung der Veröffentlichungen

Prof. Dr. Harald Kolmar

Referent*in

Prof. Dr. Siegfried Neumann

Koreferent*in

Weder Referent (Prof. Dr. Harald Kolmar) noch Koreferent (Prof. Dr. Siegfried Neumann) der vorliegenden kumulativen Doktorarbeit waren an der Begutachtung nachstehender Veröffentlichungen beteiligt:

[1] Roth L, Grzeschik J, Hinz SC, et al. Facile generation of antibody heavy and light chain diversities for yeast surface display by Golden Gate Cloning. Biol Chem. 2019;400(3):383-393. doi:10.1515/hsz-2018-0347

[2] Sellmann, C, Pekar, L, Bauer, C. et al. A One-Step Process for the Construction of Phage Display scFv and VHH Libraries. Mol Biotechnol 62, 228–239 (2020). https://doi.org/10.1007/s12033-020-00236-0

[3] Lukas Pekar, Michael Busch, Bernhard Valldorf, Steffen C. Hinz, Lars Toleikis, Simon Krah & Stefan Zielonka (2020) Biophysical and biochemical characterization of a VHH-based IgG-like bi- and trispecific antibody platform, mAbs, 12:1, DOI: 10.1080/19420862.2020.1812210

[4] Pekar L. et al. Affinity maturation of B7-H6 translates into enhanced NK cell-mediated tumor cell lysis and improved proinflammatory cytokine release of bispecific immunoligands via NKp30 engagement (Eingereicht zur Begutachtung am 30. August 2020)

[5] Janina Klemm*, Lukas Pekar*, Simon Krah and Stefan Zielonka. Antibody Display Systems (zur Veröffentlichung in Introduction to Antibody Engineering 2020 angenommen)

[6] Roth L, Krah S, Klemm J, et al. Isolation of Antigen-Specific VHH Single-Domain Antibodies by Combining Animal Immunization with Yeast Surface Display. Methods Mol Biol. 2020;2070:173-189. doi:10.1007/978-1-4939-9853-1_10

3.9.20

(Datum)

Referent (Prof. Dr. Harald Kolmar)

03.09.2020

(Datum)

Siegfried Neumann

Koreferent (Prof. Dr. Siegfried Neumann)

Erklärung zum Eigenanteil an den Veröffentlichungen

Im Folgenden ist aufgelistet, mit welchem Anteil ich an den Veröffentlichungen beteiligt war.

Mein Anteil an der folgenden Veröffentlichung beträgt 40 %

[1] Facile generation of antibody heavy and light chain diversities for yeast surface display by Golden Gate Cloning

Mein Anteil an der folgenden Veröffentlichung beträgt 40 %

[2] A One-Step Process for the Construction of Phage Display scFv and VHH Libraries

Mein Anteil an der folgenden Veröffentlichung beträgt 80 %

[3] Biophysical and biochemical characterization of a VHH-based IgG-like bi- and trispecific antibody platform

Mein Anteil an der folgenden Veröffentlichung beträgt 40 %

[4] Affinity maturation of B7-H6 translates into enhanced NK cell-mediated tumor cell lysis and improved proinflammatory cytokine release of bispecific immunoligands via NKp30 engagement (Eingereicht zur Begutachtung am 30. August 2020)

Mein Anteil an der folgenden Veröffentlichung beträgt 35 %

[5] Antibody Display Systems (zur Veröffentlichung angenommen)

Mein Anteil an der folgenden Veröffentlichung beträgt 80 %

[6] Isolation of Antigen-Specific VHH Single-Domain Antibodies by Combining Animal Immunization with Yeast Surface Display.

05.09.2020

(Datum)

(Unterschrift Antragsteller Lukas Pekar)